Melanin's surprising role in mutagenesis *pp. 824 & 842*

A designed protein traps a transition state *pp. 829 & 863*

Coping with quakes induced by injections *p. 830*

Science

$10
20 FEBRUARY 2015
sciencemag.org

AAAS



Gordon Research Conferences

Diverse program includes neurobiology of model organisms

p. 888

CONTENTS

20 FEBRUARY 2015 • VOLUME 347 • ISSUE 6224



818



828 & 857

Clocking light in the slow lane

NEWS

IN BRIEF

808 Roundup of the week's news

IN DEPTH

812 **DROUGHT TRIGGERS ALARMS IN BRAZIL'S BIGGEST METROPOLIS**
Water shortages blamed on climate anomaly, tardy response *By H. Escobar*

813 **DAWN PROBE TO LOOK FOR A HABITABLE OCEAN ON CERES**
Asteroid belt's largest body to yield its icy secrets to NASA orbiter, due to arrive next month *By E. Hand*

814 **INDO-EUROPEAN LANGUAGES TIED TO HERDERS**
Ancient migration from the east shaped European genome and language *By M. Balter and A. Gibbons*

817 **NIH PLOTS MILLION-PERSON MEGASTUDY**
Questions abound as researchers discuss personalized medicine project *By J. Kaiser*

FEATURE

818 **ARCTIC IMPACT**
Is the melting Arctic really bringing frigid winters to North America and Eurasia? Scientists struggle to piece together an atmospheric puzzle
By C. Gramling

821 **The Siberian snow connection**
By C. Gramling

INSIGHTS

PERSPECTIVES

822 **MOTHERS SHAPE ECOLOGICAL COMMUNITIES**
Individual hormonal responses affect the distributions and abundances of bird species *By B. Dantzer*
▸ REPORT P. 875

824 **THE DARK SIDE OF SUNLIGHT AND MELANOMA**
UV-initiated DNA photodamage in melanocytes is found to continue in the dark *By J.-S. Taylor*
▸ RESEARCH ARTICLE P. 842

825 **CAN OXYTOCIN TREAT AUTISM?**
We are still at an early stage of assessing oxytocin-based therapy for autism spectrum disorders
By L. J. Young and C. E. Barrett

826 **PANCREAS MICROMANAGES AUTOPHAGY**
Nutrient-sensing β cells degrade insulin when blood glucose is low
By G. A. Rutter
▸ REPORT P. 878

828 **STRUCTURED PHOTONS TAKE IT SLOW**
Specially prepared single photons travel below the "speed of light," even in vacuum *By J. R. Sambles*
▸ REPORT P. 857

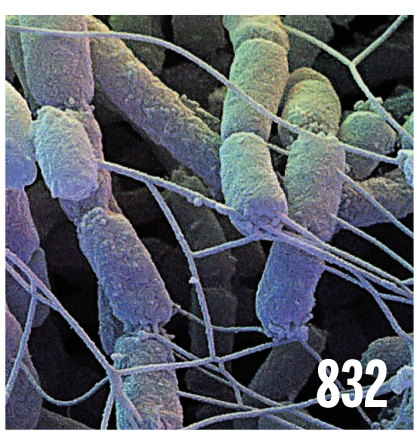
829 **CLIMBING JACOB'S LADDER**
Protein design enables the stabilization of a transient molecular state *By D. K. Romney and S. J. Miller*
▸ REPORT P. 863

830 **COPING WITH EARTHQUAKES INDUCED BY FLUID INJECTION**
Hazard may be reduced by managing injection activities
By A. McGarr et al.

BOOKS *ET AL.*

832 **PHILOSOPHY OF MICROBIOLOGY**
By M. A. O'Malley, reviewed by A. Woolfson

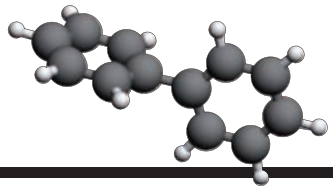
833 **HALF-LIFE**
By F. Close, reviewed by A. Wellerstein



832

Science Staff 806
New Products 887
Gordon Research Conferences 888
Science Careers 913

Published by AAAS



829 & 863
Setting a trap for a transition state



840
Leveraging DNA for materials design

LETTERS

834 EDITORIAL RETRACTION
By M. McNutt

834 PETA FUELS ANIMAL LAB IMPROVEMENTS
By J. Pawlowski

834 PETA UNDERMINES SCIENCE AND SCIENTISTS
By F. L. Trull

834 ENFORCEMENT KEY TO CHINA'S ENVIRONMENT
By H. Yang et al.

835 TECHNICAL COMMENT ABSTRACTS

RESEARCH

IN BRIEF

836 From *Science* and other journals

REVIEW

840 NANOMATERIALS
Programmable materials and the nature of the DNA bond *M. R. Jones* et al.
REVIEW SUMMARY; FOR FULL TEXT:
dx.doi.org/10.1126/science.1260901

RESEARCH ARTICLES

841 DISEASE NETWORKS
Uncovering disease-disease relationships through the incomplete interactome *J. Menche* et al.
RESEARCH ARTICLE SUMMARY; FOR FULL TEXT:
dx.doi.org/10.1126/science.1257601

842 PHOTOCHEMISTRY
Chemiexcitation of melanin derivatives induces DNA photoproducts long after UV exposure *S. Premi* et al.
▸ PERSPECTIVE P. 824

847 STRUCTURAL BIOLOGY
Structural basis for Notch1 engagement of Delta-like 4 *V. C. Luca* et al.

REPORTS

853 QUANTUM ENGINEERING
Confining the state of light to a quantum manifold by engineered two-photon loss *Z. Leghtas* et al.

857 OPTICS
Spatially structured photons that travel in free space slower than the speed of light
D. Giovannini et al.
▸ PERSPECTIVE P. 828

860 GALAXY EVOLUTION
Black hole feedback in the luminous quasar PDS 456 *E. Nardini* et al.

863 TRANSITION STATES
Trapping a transition state in a computationally designed protein bottle *A. D. Pearson* et al.
▸ PERSPECTIVE P. 829

867 ANIMAL EVOLUTION
Cope's rule in the evolution of marine animals *N. A. Heim* et al.



870 SPATIAL NAVIGATION
Disruption of the head direction cell network impairs the parahippocampal grid cell signal *S. S. Winter* et al.

875 EVOLUTIONARY ECOLOGY
Cycles of species replacement emerge from locally induced maternal effects on offspring behavior in a passerine bird *R. A. Duckworth* et al.
▸ PERSPECTIVE P. 822; PODCAST

878 INSULIN GRANULES
Insulin secretory granules control autophagy in pancreatic β cells
A. Goginashvili et al.
▸ PERSPECTIVE P. 826

882 KINASE DYNAMICS
Using ancient protein kinases to unravel a modern cancer drug's mechanism
C. Wilson et al.

DEPARTMENTS

807 EDITORIAL
Why science? Why AAAS?
By Rush D. Holt

918 WORKING LIFE
A career's twisting road
By Richard Dasheiff

ON THE COVER



Sea slugs like the Spanish shawl nudibranch (*Flabellina iodinea*) are model systems for helping us to understand neural circuits, cellular properties of neurons, neuromodulation, learning, memory, and behavioral evolution. The Gordon Research Seminar (GRS) on Neuroethology will be held 28 June to 3 July 2015 in Barga, Italy. See page 888 for the Gordon Research Conference schedule and preliminary programs. *Photo: Charuni Gunaratne, Chair, 2015 Neuroethology: Behavior, Evolution & Neurobiology GRS; and Georgia State University*

PHOTO: ALEXANDER BADYAEV

SCIENCE (ISSN 0036-8075) is published weekly on Friday, except the last week in December, by the American Association for the Advancement of Science, 1200 New York Avenue, NW, Washington, DC 20005. Periodicals mail postage (publication No. 484460) paid at Washington, DC, and additional mailing offices. Copyright © 2015 by the American Association for the Advancement of Science. The title SCIENCE is a registered trademark of the AAAS. Domestic individual membership and subscription (51 issues): $153 ($74 allocated to subscription). Domestic institutional subscription (51 issues): $1282; Foreign postage extra: Mexico, Caribbean (surface mail) $55; other countries (air assist delivery) $85. First class, airmail, student, and emeritus rates on request. Canadian rates with GST available upon request, GST #1254 88122. Publications Mail Agreement Number 1069624. **Printed in the U.S.A.**
Change of address: Allow 4 weeks, giving old and new addresses and 8-digit account number. **Postmaster:** Send change of address to AAAS, P.O. Box 96178, Washington, DC 20090–6178. **Single-copy sales:** $10.00 current issue, $15.00 back issue prepaid includes surface postage; bulk rates on request. **Authorization to photocopy** material for internal or personal use under circumstances not falling within the fair use provisions of the Copyright Act is granted by AAAS to libraries and other users registered with the Copyright Clearance Center (CCC) Transactional Reporting Service, provided that $30.00 per article is paid directly to CCC, 222 Rosewood Drive, Danvers, MA 01923. The identification code for *Science* is 0036-8075. *Science* is indexed in the *Reader's Guide to Periodical Literature* and in several specialized indexes.

Published by AAAS

Science
AAAS
1200 New York Avenue, NW, Washington, DC 20005
Bateman House, 82-88 Hills Road, Cambridge, UK CB2 1LQ

Editor-in-Chief Marcia McNutt
Executive Editor Monica M. Bradford **News Editor** Tim Appenzeller
Managing Editor, Research Journals Katrina L. Kelner
Deputy Editors Barbara R. Jasny, Andrew M. Sugden(UK), Valda J. Vinson, Jake S. Yeston

Research and Insights

SR. EDITORS Caroline Ash(UK), Gilbert J. Chin, Lisa D. Chong, Maria Cruz(UK), Julia Fahrenkamp-Uppenbrink(UK), Pamela J. Hines, Stella M. Hurtley(UK), Paula A. Kiberstis, Marc S. Lavine(Canada), Kristen L. Mueller, Ian S. Osborne(UK), Beverly A. Purnell, L. Bryan Ray, Guy Riddihough, H. Jesse Smith, Jelena Stajic, Peter Stern(UK), Phillip D. Szuromi, Brad Wible, Nicholas S. Wigginton, Laura M. Zahn **ASSOCIATE EDITORS** Brent Grocholski, Melissa R. McCartney, Margaret M. Moerchen, Sacha Vignieri **ASSOCIATE BOOK REVIEW EDITOR** Valerie B. Thompson **ASSOCIATE LETTERS EDITOR** Jennifer Sills **CHIEF CONTENT PRODUCTION EDITOR** Cara Tate **SR. CONTENT PRODUCTION EDITORS** Harry Jach, Trista Wagoner **CONTENT PRODUCTION EDITORS** Jeffrey E. Cook, Chris Filiatreau, Cynthia Howe, Lauren Kmec, Barbara P. Ordway **SR. EDITORIAL COORDINATORS** Carolyn Kyle, Beverly Shields **EDITORIAL COORDINATORS** Ramatoulaye Diop, Joi S. Granger, Lisa Johnson, Anita Wynn **PUBLICATIONS ASSISTANTS** Aneera Dobbins, Jeffrey Hearn, Dona Mathieu, Le-Toya Mayne Flood, Shannon McMahon, Scott Miller, Jerry Richardson, Rachel Roberts(UK), Alice Whaley(UK), Brian White **EXECUTIVE ASSISTANT** Anna Bashkirova **ADMINISTRATIVE SUPPORT** Janet Clements(UK), Michael Crabtree(UK, Intern), Lizanne Newton(UK), Maryrose Madrid, John Wood(UK)

News

NEWS MANAGING EDITOR John Travis **INTERNATIONAL EDITOR** Richard Stone **DEPUTY NEWS EDITORS** Daniel Clery(UK), Robert Coontz, Elizabeth Culotta, David Grimm, David Malakoff, Leslie Roberts **CONTRIBUING EDITORS** Martin Enserink(Europe), Mara Hvistendahl **SR. CORRESPONDENTS** Jeffrey Mervis, Elizabeth Pennisi **NEWS WRITERS** Adrian Cho, Jon Cohen, Jennifer Couzin-Frankel, Carolyn Gramling, Eric Hand, Jocelyn Kaiser, Kelly Servick, Robert F. Service, Erik Stokstad(Cambridge, UK), Emily Underwood **INTERNS** Emily Conover, David Shultz, Jia You **CONTRIBUTING CORRESPONDENTS** Pallava Bagla(South Asia), Michael Balter(Paris), John Bohannon, Ann Gibbons, Sam Kean, Richard A. Kerr, Eli Kintisch, Kai Kupferschmidt(Berlin), Andrew Lawler, Christina Larson(Beijing), Mitch Leslie, Charles C. Mann, Eliot Marshall, Virginia Morell, Dennis Normile(Tokyo), Heather Pringle, Tania Rabesandratana(Brussels), Gretchen Vogel(Berlin), Lizzie Wade(Mexico City) **CAREERS** Jim Austin(Editor), Donisha Adams, Rachel Bernstein **COPY EDITORS** Kara Estelle, Nora Kelly, Jennifer Levin **ADMINISTRATIVE SUPPORT** Scherraine Mack

Executive Publisher Alan I. Leshner
Publisher Kent R. Anderson **Chief Digital Media Officer** Rob Covey

BUSINESS OPERATIONS AND ADMINISTRATION DIRECTOR Deborah Rivera-Wienhold **BUSINESS SYSTEMS AND FINANCIAL ANALYSIS DIRECTOR** Randy Yi **MANAGER OF FULFILLMENT SYSTEMS** Neal Hawkins **SYSTEMS ANALYST** Nicole Mehmedovich **ASSISTANT DIRECTOR, BUSINESS OPERATIONS** Eric Knott **MANAGER, BUSINESS OPERATIONS** Jessica Tierney **BUSINESS ANALYSTS** Cory Lipman, Cooper Tilton, Celeste Troxler **FINANCIAL ANALYST** Jeremy Clay **RIGHTS AND PERMISSIONS ASSISTANT DIRECTOR** Emilie David **PERMISSIONS ASSOCIATE** Elizabeth Sandler **RIGHTS, CONTRACTS, AND LICENSING ASSOCIATE** Lili Kiser

MARKETING DIRECTOR Ian King **MARKETING MANAGER** Julianne Wielga **MARKETING ASSOCIATE** Elizabeth Sattler **SR. MARKETING EXECUTIVE** Jennifer Reeves **SR. ART ASSOCIATE, PROJECT MANAGER** Tzeitel Sorrosa **ART ASSOCIATE** Seil Lee **ASSISTANT COMMERCIAL EDITOR** Selby Frame **MARKETING PROJECT MANAGER** Angelissa McArthur **SR. WRITER** Bill Zimmer **PROGRAM DIRECTOR, AAAS MEMBER CENTRAL** Peggy Mihelich **FULFILLMENT SYSTEMS AND OPERATIONS** membership@aaas.org **MANAGER, MEMBER SERVICES** Pat Butler **SPECIALISTS** LaToya Casteel, Javia Flemmings, Latasha Russell **MANAGER, DATA ENTRY** Mickie Napoleoni **DATA ENTRY SPECIALISTS** JJ Regan, Jaimee Wise, Fiona Giblin

DIRECTOR, SITE LICENSING Tom Ryan **DIRECTOR, CORPORATE RELATIONS** Eileen Bernadette Moran **SR. PUBLISHER RELATIONS SPECIALIST** Kiki Forsythe **PUBLISHER RELATIONS MANAGER** Catherine Holland **PUBLISHER RELATIONS, EASTERN REGION** Keith Layson **PUBLISHER RELATIONS, WESTERN REGION** Ryan Rexroth **MANAGER, SITE LICENSE OPERATIONS** Iquo Edim **FULFILLMENT ANALYST** Lana Guz **ASSOCIATE DIRECTOR, MARKETING** Christina Schlecht **MARKETING ASSOCIATES** Thomas Landreth, Minah Kim

DIRECTOR OF WEB TECHNOLOGIES Ahmed Khadr **SR. DEVELOPER** Chris Coleman **DEVELOPERS** Dan Berger, Jimmy Marks **SR. PROJECT MANAGER** Trista Smith **SYSTEMS ENGINEER** Luke Johnson **PRODUCT MANAGER** Walter Jones

CREATIVE DIRECTOR, MULTIMEDIA Martyn Green **DIRECTOR OF ANALYTICS** Enrique Gonzales **SR. WEB PRODUCER** Sarah Crespi **WEB PRODUCER** Alison Crawford **VIDEO PRODUCER** Nguyen Nguyen **SOCIAL MEDIA PRODUCER** Meghna Sachdev

DIRECTOR OF OPERATIONS PRINT AND ONLINE Lizabeth Harman **DIGITAL/PRINT STRATEGY MANAGER** Jason Hillman **QUALITY TECHNICAL MANAGER** Marcus Spiegler **DIGITAL PRODUCTION MANAGER** Lisa Stanford **ASSISTANT MANAGER DIGITAL/PRINT** Rebecca Doshi **DIGITAL MEDIA SPECIALIST** Tara Kelly **SENIOR CONTENT SPECIALISTS** Steve Forrester, Antoinette Hodal, Lori Murphy, Anthony Rosen **CONTENT SPECIALISTS** Jacob Hedrick, Kimberley Oster

DESIGN DIRECTOR Beth Rakouskas **DESIGN EDITOR** Marcy Atarod **SENIOR SCIENTIFIC ILLUSTRATORS** Chris Bickel, Katharine Sutliff **SCIENTIFIC ILLUSTRATOR** Valerie Altounian **SENIOR ART ASSOCIATES** Holly Bishop, Preston Huey **SENIOR DESIGNER** Garvin Grullón **DESIGNER** Chrystal Smith **SENIOR PHOTO EDITOR** William Douthitt **PHOTO EDITOR** Leslie Blizard

DIRECTOR, GLOBAL COLLABORATION, CUSTOM PUBLICATIONS, ADVERTISING Bill Moran **EDITOR, CUSTOM PUBLISHING** Sean Sanders: 202-326-6430 **ASSISTANT EDITOR, CUSTOM PUBLISHING** Tianna Hicklin: 202-326-6463 **ADVERTISING MARKETING MANAGER** Justin Sawyers: 202-326-7061 science_advertising@aaas.org **ADVERTISING MARKETING ASSOCIATE** Javia Flemmings **ADVERTISING SUPPORT MANAGER** Karen Foote: 202-326-6740 **ADVERTISING PRODUCTION OPERATIONS MANAGER** Deborah Tompkins **SR. PRODUCTION SPECIALIST/GRAPHIC DESIGNER** Amy Hardcastle **PRODUCTION SPECIALIST** Yuse Lajiminmuhip **SR. TRAFFIC ASSOCIATE** Christine Hall **SALES COORDINATOR** Shirley Young **ASSOCIATE DIRECTOR, COLLABORATION, CUSTOM PUBLICATIONS/CHINA/TAIWAN/KOREA/SINGAPORE** Ruolei Wu: +86-186 0822 9345, rwu@aaas.org **COLLABORATION/CUSTOM PUBLICATIONS/JAPAN** Adarsh Sandhu + 81532-81-5142 asandhu@aaas.org **EAST COAST/E. CANADA** Laurie Faraday: 508-747-9395, FAX 617-507-8189 **WEST COAST/W. CANADA** Lynne Stickrod: 415-931-9782, FAX 415-520-6940 **MIDWEST** Jeffrey Dembksi: 847-498-4520 x3005, Steven Loerch: 847-498-4520 x3006 **UK EUROPE/ASIA** Roger Goncalves: TEL/FAX +41 43 243 1358 **JAPAN** Katsuyoshi Fukamizu(Tokyo): +81-3-3219-5777 kfukamizu@aaas.org **CHINA/TAIWAN** Ruolei Wu: +186-0082-9345

WORLDWIDE ASSOCIATE DIRECTOR OF SCIENCE CAREERS Tracy Holmes: +44 (0) 1223 326525, FAX +44 (0) 1223 326532 tholmes@science-int.co.uk **CLASSIFIED** advertise@sciencecareers.org **U.S. SALES** Tina Burks: 202-326-6577, Nancy Toema: 202-326-6578 **SALES ADMINISTRATOR** Marci Gallun **EUROPE/ROW SALES** Axel Gesatzki, Sarah Lelarge **SALES ASSISTANT** Kelly Grace **JAPAN** Hiroyuki Mashiki(Kyoto): +81-75-823-1109 hmashiki@aaas.org **CHINA/TAIWAN** Ruolei Wu: +86-186 0082 9345 rwu@aaas.org **MARKETING MANAGER** Allison Pritchard **MARKETING ASSOCIATE** Aimee Aponte

AAAS BOARD OF DIRECTORS RETIRING PRESIDENT, CHAIR Phillip A. Sharp **PRESIDENT** Gerald R. Fink **PRESIDENT-ELECT** Geraldine (Geri) Richmond **TREASURER** David Evans Shaw **CHIEF EXECUTIVE OFFICER** Alan I. Leshner **BOARD** Bonnie L. Bassler, May R. Berenbaum, Carlos J. Bustamante, Claire M. Fraser, Laura H. Greene, Elizabeth Loftus, Raymond Orbach, Inder M. Verma

SUBSCRIPTION SERVICES For change of address, missing issues, new orders and renewals, and payment questions: 866-434-AAAS (2227) or 202-326-6417, FAX 202-842-1065. Mailing addresses: AAAS, P.O. Box 96178, Washington, DC 20090-6178 or AAAS Member Services, 1200 New York Avenue, NW, Washington, DC 20005

INSTITUTIONAL SITE LICENSES 202-326-6755 **REPRINTS:** Author Inquiries 800-635-7181 **COMMERCIAL INQUIRIES** 803-359-4578 **PERMISSIONS** 202-326-6765, permissions@aaas.org **AAAS Member Services** 202-326-6417 or http://membercentral.aaas.org/discounts

Science serves as a forum for discussion of important issues related to the advancement of science by publishing material on which a consensus has been reached as well as including the presentation of minority of conflicting points of view. Accordingly, all articles published in *Science*—including editorials, news and comment, and books reviews—are signed and reflect the individual views of the authors and not official points of view adopted by AAAS or the institutions with which the authors are affiliated.

INFORMATION FOR AUTHORS See pages 678 and 679 of the 6 February 2015 issue or access www.sciencemag.org/about/authors

SENIOR EDITORIAL BOARD

A. Paul Alivisatos, *Lawrence Berkeley Nat'l. Laboratory,* **Ernst Fehr,** *U. of Zürich*
Susan M. Rosenberg, *Baylor College of Medicine,* **Ali Shilatifard,** *Northwestern University Feinberg School of Medicine,* **Michael S. Turner,** *U. of Chicago*

BOARD OF REVIEWING EDITORS (Statistics board members indicated with **(S)**)

Adriano Aguzzi, *U. Hospital Zürich*
Takuzo Aida, *U. of Tokyo*
Leslie Aiello, *Wenner-Gren Foundation*
Judith Allen, *U. of Edinburgh*
Sonia Altizer, *U. of Georgia*
Sebastian Amigorena, *Institut Curie*
Kathryn Anderson, *Memorial Sloan-Kettering Cancer Center*
Meinrat O. Andreae, *Max-Planck Inst. Mainz*
Paola Arlotta, *Harvard U.*
Johan Auwerx, *EPFL*
David Awschalom, *U. of Chicago*
Jordi Bascompte, *Estación Biológica de Doñana CSIC*
Facundo Batista, *London Research Inst.*
Ray H. Baughman, *U. of Texas, Dallas*
David Baum, *U. of Wisconsin*
Carlo Beenakker, *Leiden U.*
Kamran Behnia, *ESPCI-ParisTech*
Yasmine Belkaid, *NIAID, NIH*
Philip Benfey, *Duke U.*
Stephen J. Benkovic, *Penn State U.*
May Berenbaum, *U. of Illinois*
Gabriele Bergers, *U. of California, San Francisco*
Bradley Bernstein, *Massachusettes General Hospital*
Peer Bork, *EMBL*
Bernard Bourdon, *Ecole Normale Supérieure de Lyon*
Chris Bowler, *École Normale Supérieure*
Ian Boyd, *U. of St. Andrews*
Emily Brodsky, *U. of California, Santa Cruz*
Ron Brookmeyer, *U. of California Los Angeles* **(S)**
Christian Büchel, *U. Hamburg-Eppendorf*
Joseph A. Burns, *Cornell U.*
Gyorgy Buzsaki, *New York U. School of Medicine*
Blanche Capel, *Duke U.*
Mats Carlsson, *U. of Oslo*
David Clapham, *Children's Hospital Boston*
David Clary, *U. of Oxford*
Joel Cohen, *Rockefeller U., Columbia U.*
Jonathan D. Cohen, *Princeton U.*
James Collins, *Boston U.*
Robert Cook-Deegan, *Duke U.*
Alan Cowman, *Walter & Eliza Hall Inst.*
Robert H. Crabtree, *Yale U.*
Roberta Croce, *Vrije Universiteit*
Janet Currie, *Princeton U.*
Jeff L. Dangl, *U. of North Carolina*
Tom Daniel, *U. of Washington*
Frans de Waal, *Emory U.*
Stanislas Dehaene, *Collège de France*
Robert Desimone, *MIT*
Claude Desplan, *New York U.*
Ap Dijksterhuis, *Radboud U. of Nijmegen*
Dennis Discher, *U. of Pennsylvania*
Gerald W. Dorn II, *Washington U. School of Medicine*
Jennifer A. Doudna, *U. of California, Berkeley*
Bruce Dunn, *U. of California, Los Angeles*
Christopher Dye, *WHO*
Todd Ehlers, *U. of Tuebingen*
David Ehrhardt, *Carnegie Inst. of Washington*
Tim Elston, *U. of North Carolina at Chapel Hill*
Gerhard Ertl, *Fritz-Haber-Institut, Berlin*
Barry Everitt, *U. of Cambridge*
Ernst Fehr, *U. of Zurich*
Anne C. Ferguson-Smith, *U. of Cambridge*
Michael Feuer, *The George Washington U.*
Kate Fitzgerald, *U. of Massachusetts*
Peter Fratzl, *Max-Planck Inst.*
Elaine Fuchs, *Rockefeller U.*
Daniel Geschwind, *UCLA*
Andrew Gewirth, *U. of Illinois*
Karl-Heinz Glassmeier, *TU Braunschweig*
Ramon Gonzalez, *Rice U.*
Julia R. Greer, *Caltech*
Elizabeth Grove, *U. of Chicago*
Nicolas Gruber, *ETH Zurich*
Kip Guy, *St. Jude's Children's Research Hospital*
Taekjip Ha, *U. of Illinois at Urbana-Champaign*
Christian Haass, *Ludwig Maximilians U.*
Steven Hahn, *Fred Hutchinson Cancer Research Center*
Michael Hasselmo, *Boston U.*
Martin Heimann, *Max-Planck Inst. Jena*
Yka Helariutta, *U. of Cambridge*
James A. Hendler, *Rensselaer Polytechnic Inst.*
Janet G. Hering, *Swiss Fed. Inst. of Aquatic Science & Technology*
Kai-Uwe Hinrichs, *U. of Bremen*
Kei Hirose, *Tokyo Inst. of Technology*
David Hodell, *U. of Cambridge*
David Holden, *Imperial College*
Lora Hooper, *UT Southwestern Medical Ctr. at Dallas*
Raymond Huey, *U. of Washington*
Steven Jacobsen, *U. of California, Los Angeles*
Kai Johnsson, *EPFL Lausanne*
Peter Jonas, *Inst. of Science & Technology (IST) Austria*
Matt Kaeberlein, *U. of Washington*
William Kaelin Jr., *Dana-Farber Cancer Inst.*
Daniel Kahne, *Harvard U.*
Daniel Kammen, *U. of California, Berkeley*
Masashi Kawasaki, *U. of Tokyo*
Joel Kingsolver, *U. of North Carolina at Chapel Hill*
Robert Kingston, *Harvard Medical School*
Etienne Koechlin, *Ecole Normale Supérieure*
Alexander Kolodkin, *Johns Hopkins U.*
Alberto R. Kornblihtt, *U. of Buenos Aires*
Leonid Kruglyak, *UCLA*
Thomas Langer, *U. of Cologne*
Mitchell A. Lazar, *U. of Pennsylvania*
David Lazer, *Harvard U.*
Thomas Lecuit, *IBDM*
Virginia Lee, *U. of Pennsylvania*
Stanley Lemon, *U. of North Carolina at Chapel Hill*
Ottoline Leyser, *Cambridge U.*
Marcia C. Linn, *U. of California, Berkeley*
Jianguo Liu, *Michigan State U.*
Luis Liz-Marzan, *CIC biomaGUNE*
Jonathan Losos, *Harvard U.*
Ke Lu, *Chinese Acad. of Sciences*
Christian Lüscher, *U. of Geneva*
Laura Machesky, *CRUK Beatson Inst. for Cancer Research*
Anne Magurran, *U. of St. Andrews*
Oscar Marin, *CSIC & U. Miguel Hernández*
Charles Marshall, *U. of California, Berkeley*
C. Robertson McClung, *Dartmouth College*
Graham Medley, *U. of Warwick*
Yasushi Miyashita, *U. of Tokyo*
Mary Ann Moran, *U. of Georgia*
Richard Morris, *U. of Edinburgh*
Alison Motsinger-Reif, *NC State U.* **(S)**
Sean Munro, *MRC Lab. of Molecular Biology*
Thomas Murray, *The Hastings Center*
James Nelson, *Stanford U. School of Med.*
Daniel Neumark, *U. of California, Berkeley*
Timothy W. Nilsen, *Case Western Reserve U.*
Pär Nordlund, *Karolinska Inst.*
Helga Nowotny, *European Research Advisory Board*
Ben Olken, *MIT*
Joe Orenstein, *U. of California Berkeley & Lawrence Berkeley National Lab*
Harry Orr, *U. of Minnesota*
Andrew Oswald, *U. of Warwick*
Steve Palumbi, *Stanford U.*
Jane Parker, *Max-Planck Inst. of Plant Breeding Research*
Giovanni Parmigiani, *Dana-Farber Cancer Inst.* **(S)**
Donald R. Paul, *U. of Texas, Austin*
John H. J. Petrini, *Memorial Sloan-Kettering Cancer Center*
Joshua Plotkin, *U. of Pennsylvania*
Albert Polman, *FOM Institute AMOLF*
Philippe Poulin, *CNRS*
Jonathan Pritchard, *Stanford U.*
David Randall, *Colorado State U.*
Colin Renfrew, *U. of Cambridge*
Felix Rey, *Institut Pasteur*
Trevor Robbins, *U. of Cambridge*
Jim Roberts, *Fred Hutchinson Cancer Research Ctr.*
Barbara A. Romanowicz, *U. of California, Berkeley*
Jens Rostrup-Nielsen, *Haldor Topsoe*
Mike Ryan, *U. of Texas, Austin*
Mitinori Saitou, *Kyoto U.*
Shimon Sakaguchi, *Kyoto U.*
Miquel Salmeron, *Lawrence Berkeley National Lab*
Jürgen Sandkühler, *Medical U. of Vienna*
Alexander Schier, *Harvard U.*
Randy Seeley, *U. of Cincinnati*
Vladimir Shalaev, *Purdue U.*
Robert Siliciano, *Johns Hopkins School of Medicine*
Joseph Silk, *Institut d'Astrophysique de Paris*
Denis Simon, *Arizona State U.*
Alison Smith, *John Innes Centre*
Richard Smith, *U. of North Carolina* **(S)**
John Speakman, *U. of Aberdeen*
Allan C. Spradling, *Carnegie Institution of Washington*
Jonathan Sprent, *Garvan Inst. of Medical Research*
Eric Steig, *U. of Washington*
Paula Stephan, *Georgia State U. and National Bureau of Economic Research*
Molly Stevens, *Imperial College London*
V. S. Subrahmanian, *U. of Maryland*
Ira Tabas, *Columbia U.*
Sarah Teichmann, *Cambridge U.*
John Thomas, *North Carolina State U.*
Shubha Tole, *Tata Institute of Fundamental Research*
Christopher Tyler-Smith, *The Wellcome Trust Sanger Inst.*
Herbert Virgin, *Washington U.*
Bert Vogelstein, *Johns Hopkins U.*
Cynthia Volkert, *U. of Göttingen*
Douglas Wallace, *Dalhousie U.*
David Wallach, *Weizmann Inst. of Science*
Ian Walmsley, *U. of Oxford*
David A. Wardle, *Swedish U. of Agric. Sciences*
David Waxman, *Fudan U.*
Jonathan Weissman, *U. of California, San Francisco*
Chris Wikle, *U. of Missouri* **(S)**
Ian A. Wilson, *The Scripps Res. Inst.* **(S)**
Timothy D. Wilson, *U. of Virginia*
Rosemary Wyse, *Johns Hopkins U.*
Jan Zaanen, *Leiden U.*
Kenneth Zaret, *U. of Pennsylvania School of Medicine*
Jonathan Zehr, *U. of California, Santa Cruz*
Len Zon, *Children's Hospital Boston*
Maria Zuber, *MIT*

BOOK REVIEW BOARD

David Bloom, *Harvard U.,* **Samuel Bowring,** *MIT,* **Angela Creager,** *Princeton U.,* **Richard Shweder,** *U. of Chicago,* **Ed Wasserman,** *DuPont*

Published by AAAS

EDITORIAL

Why science? Why AAAS?

Among the various ways of thinking and knowing about the universe and ourselves, science is special. Asking questions that can be answered empirically and engaging in open communication so that others can collectively review and verify possible answers lead to the most reliable knowledge—a knowledge that is powerfully applicable in daily life. Science is, as physician and essayist Lewis Thomas wrote, the "shrewdest maneuver" for discovering the world. This grand and clever enterprise, while surely not removing all worldly woes, brings beauty, wonderfully fulfilling intellectual pleasure, and cultural enrichment. It can lead to improved human interaction, more constructive commerce, and a better quality of life. Science helps bring what I think is a deep human need—a sense of progress.

That progress is not assured. To thrive, science needs the support of the society it serves, and that support must be cultivated. In 1848, a forward-looking group of scientists and advocates formed the American Association for the Advancement of Science (AAAS) to promote cooperation across various scientific and technical fields and create an encouraging environment for the practice of science. They saw in America a widespread appreciation of science, as reflected in the country's founding political documents and in the habits of mind of even their nonscientific fellow citizens. From this general appreciation, they fostered robust support for a scientific research and educational enterprise that has remained strong for a century and a half. AAAS became the principal voice for science and grew in many ways, including a realization that efforts to strengthen science must extend worldwide.

Today, however, in many places the appreciation, respect, and support for science need attention and renewal. Even as the practice of science becomes ever more advanced, the observations more precise, and the applications more prevalent, there are signs of public misapprehension, distrust, and eroding support. Who better to address this looming problem than AAAS? AAAS should remain the force for science.



"AAAS should remain the force for science."

For the past 14 years, AAAS has been led by Dr. Alan Leshner, whose wisdom, skill, and industry have left it in a strong and influential position. The association now has about 110,000 individual members and 252 affiliated organizations across the globe, thousands of honored fellows and alumni of its various programs, and a variety of publications of the highest quality and reputation (including the one you are reading now). This is a strong foundation from which to move ahead, and this week, I am honored and excited to join AAAS as its Chief Executive Officer and Executive Publisher of *Science*. As a former professor of physics and public policy, and a former member of the U.S. Congress for the past 16 years, I deeply appreciate the importance of advancing science for the benefit of society and am sensitive to the many challenges ahead in accomplishing this. AAAS must continue to enhance science and engineering for the well-being of all people. The organization must defend openness and integrity in the practice of science. Communication and education among scientists, engineers, and the public must improve. AAAS must be even more inclusive of all who can contribute to the scientific enterprise. And AAAS must be persistent in promoting the responsible use of science in society and in public and international affairs.

To do these things, and following the changes begun under Dr. Leshner, AAAS will seek to further strengthen its membership, in both numbers and engagement. The organization will build its publications and communications ability to meet the modern needs of the scientific community and the general public. AAAS will enhance its programs in public affairs, education, law, and international relations, and continue to explore constructive relationships between science and religion, art, history, and other disciplines. I am committed to raising the necessary resources to do these things. Especially, AAAS intends to remain the world's most effective advocate for science.

– **Rush D. Holt**



Rush D. Holt is Chief Executive Officer of AAAS and Executive Publisher of Science.

10.1126/science.aaa9126

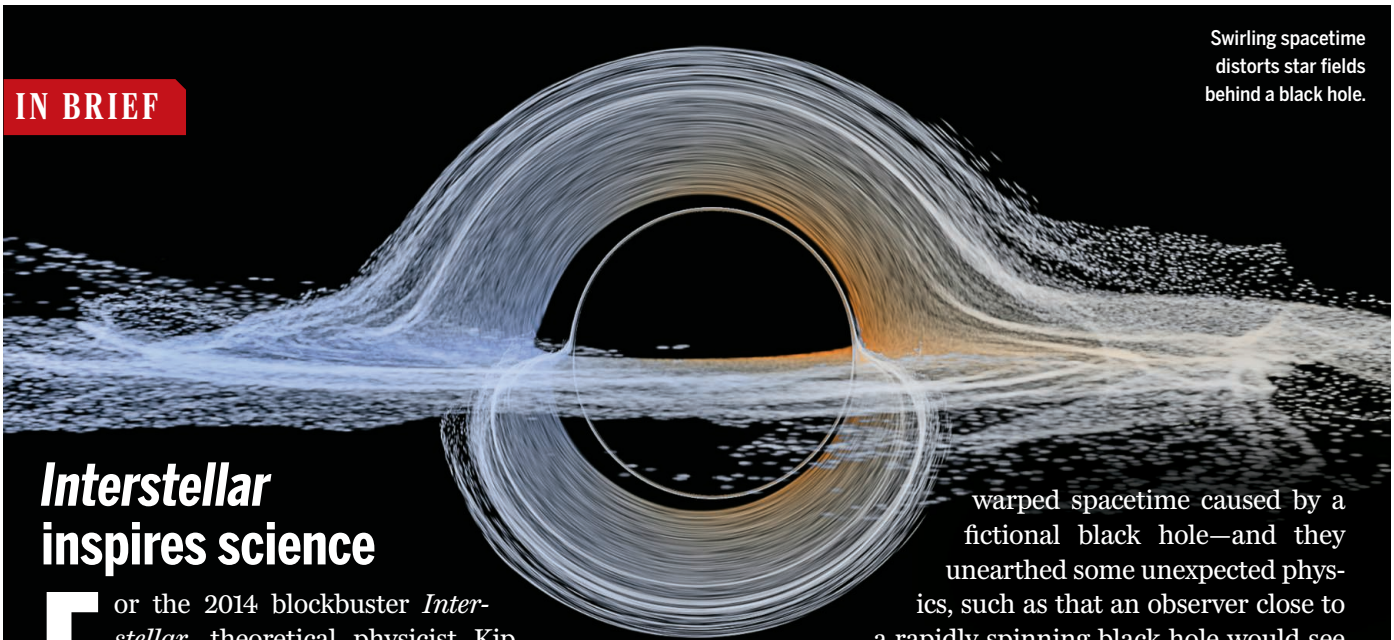
PHOTO: (TOP RIGHT) ANNASTEW/FLICKR; (INSET) INCOMIBLE/ISTOCKPHOTO.COM

Downloaded from www.sciencemag.org on February 21, 2015

Published by AAAS

NEWS

> "Arctic apples ... are likely the most tested apples on the planet."
>
> **Statement by Okanagan Specialty Fruits** about its genetically modified "nonbrowning" apples, approved by the U.S. Department of Agriculture on 13 February.



Swirling spacetime distorts star fields behind a black hole.

IN BRIEF

Interstellar inspires science

For the 2014 blockbuster *Interstellar*, theoretical physicist Kip Thorne of the California Institute of Technology in Pasadena worked closely with London-based special effects company Double Negative to ensure that the wormhole and black hole shown were as realistic as possible. Now, their efforts have spawned an academic paper in *Classical and Quantum Gravity*. Using physics equations provided by Thorne, the company's computers mapped the paths of millions of rays of light through the warped spacetime caused by a fictional black hole—and they unearthed some unexpected physics, such as that an observer close to a rapidly spinning black hole would see more than a dozen images of individual stars just outside one edge of the black hole's "shadow." These multiple images are caused by the spinning mass dragging spacetime into a whirlpool that bends the light rays around itself. The multiple-image effect was observed only on the side of the black hole where spacetime is being dragged toward the observer, which the team concluded was because some light was being "flung" outward. http://scim.ag/Interstellsci

AROUND THE WORLD

Fracking moves ahead in U.K.

LONDON | Parliament has approved a controversial bill that will facilitate the use of hydraulic fracturing technologies to recover shale gas in England and Wales. Last month politicians in the Labour Party added more than a dozen environmental constraints, such as prohibiting drilling beneath national parks, protected groundwater sources, and sites of special scientific interest. But last week lawmakers removed the safeguards, including obligating companies to conduct environmental impact assessments at drill sites. The new law will "boost our energy security ... and help us tackle climate change, all within one of the most robust regulatory regimes in the world," several agencies said in a joint statement. The law does not apply to Scotland, which has a fracking moratorium. Environmental safeguards will be clarified in a separate bill in July.

Comeback wolf confirmed dead

TUSHAR MOUNTAINS, UTAH | New genetic analyses reveal that the endangered female gray wolf seen on the north rim of the Grand Canyon in fall 2014 is the same animal killed by an authorized coyote bounty hunter in Utah later that year. DNA from the dead wolf's tissue samples matched DNA from wolf scat collected near the canyon in November, the U.S. Fish and Wildlife Service (FWS) announced on 11 February. The wolf, identified by FWS as 914F, was given a radio collar near Cody, Wyoming, on 8 January 2014, but by the time she reached Arizona it had stopped working. She was the first wolf in northern Arizona since the animals were exterminated there 70 years ago. http://scim.ag/wolfcons



A wolf hailed as a conservation comeback was shot by a hunter.

IMAGES: (TOP TO BOTTOM) © *CLASSICAL AND QUANTUM GRAVITY*, 2015, REPRODUCED BY PERMISSION OF IOP PUBLISHING; AP PHOTO/ARIZONA GAME AND FISH DEPARTMENT

Downloaded from www.sciencemag.org on February 21, 2015

Published by AAAS

STAP scandal punishments

TOKYO | RIKEN, Japan's network of national laboratories, on 10 February announced punishments for staff involved in a stem cell scandal (*Science*, 20 June 2014, p. 1324). It centered on two 2014 papers in *Nature*, since retracted, that described a cell creation technique called stimulus-triggered acquisition of pluripotency, or STAP. Masatoshi Takeichi, former head of RIKEN's Center for Developmental Biology, and Hitoshi Niwa, a co-author of the papers, received reprimands; Takeichi will also voluntarily return some salary. Officials said they would have suspended Teruhiko Wakayama, a co-author who left RIKEN before publication; they revoked his appointment as an associate. RIKEN had already found lead author Haruko Obokata, who has resigned, guilty of misconduct. RIKEN is still investigating whether it should return related research money to funders and withdraw pending STAP patent applications.
http://scim.ag/RIKENpen

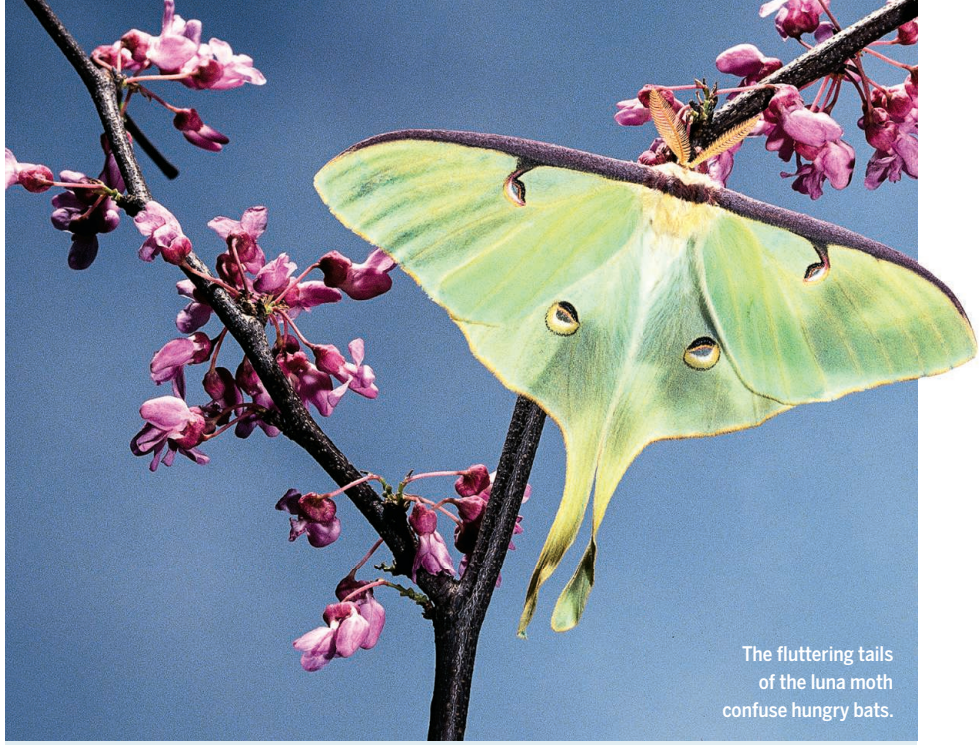
Weather sat gap still looms

WASHINGTON, D.C. | Launch delays for the first of two planned next-generation weather satellites could lead to a data-supply gap for the United States that will last anywhere from 3 to 15 months, federal officials said last week. The National Oceanic and Atmospheric Administration (NOAA) plans to launch a new satellite in March 2017, but a report last week by the Government Accountability Office (GAO)—Congress's investigative arm—suggested that NOAA's most recent projection of a 3-month coverage gap is likely optimistic. Cost overruns, new launch delays, and the uncertain life spans of aging satellites (in part due to possible collisions with space debris) all mean the gap could grow, says GAO, which since 2013 has said the government faces a "high risk" of a gap.

NEWSMAKERS

Lawsuit over retractions

Arguing his university has cleared him of misconduct, Brazil-based researcher **Mario Saad** filed a lawsuit against the American Diabetes Association on 5 February. He demanded that the association, which publishes the journal *Diabetes*, remove expressions of concern posted on four of his papers and be prevented from retracting them. According to the suit, the journal informed Saad in March 2014 that two of his articles "appear to contain instances of image manipulation and duplication." Saad's employer, the State University of Campinas in São Paulo, investigated and, the lawsuit says, "found no evidence of dishonesty," concluding that although "mistakes had occurred in the treatment of the digital images," they did not compromise the papers' conclusions. But on 2 February the journal attached an expression of concern to the four papers. This, and the potential retractions, the lawsuit argues, "have and will continue to severely damage Dr. Saad's professional reputation." Saad is seeking unspecified damages and a jury trial.



The fluttering tails of the luna moth confuse hungry bats.

Luna moth's tails fool bat sonar

The green wings of the luna moth, with their elegant, long tails, aren't just about style—they can also confound hungry bats. The fluttering tails appear to create an acoustic signal that attracts echolocating bats, causing the predators to zero in on the wings rather than the moth's more vital body parts, researchers report this week in the *Proceedings of the National Academy of Sciences*. Scientists pinned down the tails' lifesaving role by taking 162 moths and plucking the tails off 75 of them. They used fishing line to tether two moths—one with tails, the other without—to the ceiling of a darkened room. Then, they let loose a big brown bat. The bats caught 81% of the tailless moths, but just 35% of those with fully intact wings—and high-speed cameras revealed that in more than half of the attacks on moths with tails, the bats went after the tails, often missing the body.

Three Q's

The U.S. National Academies has taken on a thorny issue, launching a study of federal regulations affecting research universities. Academics hope it will pave the way toward easing the burden on scientists. The panel's chair, University of Texas, Austin, President Emeritus **Larry Faulkner**, discussed the issue at the group's first meeting last week in Washington, D.C.

Q: Why did you sign on?
A: It's a congressionally chartered effort … and unless you have Congress or the White House involved, your opportunity to influence the overall picture is limited.

Q: How bad is the situation?
A: My sense is that there's vastly more demands for accountability than when I was a researcher. But it would be a mistake to think that the only purpose of this study is to lighten the regulatory burden on universities. We would like to see regulations made sensible enough that investigators have more time to do research.

Q: There have been many such studies. What can you add?
A: Yes, a lot of useful work has been done. But we've also been asked to create a framework that provides the intellectual structure against which regulations, old and new, would be tested. If we can succeed, I think it would be of great value.

PHOTO: © ROBERT MARIEN/CORBIS

Published by AAAS

AAAS | 2015 ANNUAL MEETING

The AAAS (which publishes *Science*) annual meeting, held in San Jose, California, from 12 to 16 February, drew thousands of participants, including scientists, journalists, and visitors to Family Science Days activities. Here are some highlights from the meeting; for more AAAS coverage, including reports from sessions, live chats, and responses to "What message would you send into space?" visit http://scim.ag/2015AAAS.

A dissection of dissection

Human dissection: It's better than it used to be. That's the conclusion Jenna Dittmar of the University of Cambridge in the United Kingdom came to after studying skeletons excavated from a hospital graveyard in England, as well as those stored by universities and medical museums. Using scanning electron microscopes to examine the cut marks medical students and other dissectors left behind on the bones of their subjects, Dittmar tracked the change in dissection practices from 1650 to 1900. Before 1700, surgical instruments were more like "woodworking tools," but over time, the saws got thinner and the cuts—and techniques—more refined. For example, early dissectors simply sawed off the top of the skull horizontally, which often damaged the brain, but beginning in the late 1880s, dissectors began cutting a delicate arc across the back of the skull, a technique that protected the fragile organ. http://scim.ag/earlydissect



Vertical cuts to a skull were rare; this 19th century dissection, from the University of Cambridge's collection, was likely a teaching tool.

Spotted from space: Lost cities

Remote sensing technology is revealing traces of past civilizations that have been hiding in plain sight. "Although [the Amazon rainforest and the Sahara desert] seem so different, a lot of the questions are actually very similar," says David Mattingly, an archaeologist at the University of Leicester in the United Kingdom. Both are inhospitable environments that were thought to be devoid of large-scale human settlements. But, Mattingly says, satellite images covering 2500 square kilometers of southern Libya have revealed with "stunning" detail 158 major settlements of the Garamantes, a people who began building cities, forts, and farmland in the region around 1000 B.C.E. Satellites are less helpful at peering through the thick vegetation of the Amazon rainforest, says José Iriarte, an archaeologist at the University of Exeter in the United Kingdom, so he opts for drones outfitted with LiDAR to map the ground through the trees and sensors to analyze the distribution of plants, which may reveal ancient farming sites. http://scim.ag/lostcivs

What's your Twitter dialect?

It's legit: The language you use on Twitter reflects your geography. By analyzing roughly 100 million tweets and accompanying GPS data, computational linguist Jacob Eisenstein of the Georgia Institute of Technology in Atlanta has pieced together and mapped geographical patterns of Twitter slang. A few highlights: The plural pronoun "yinz" (as in, "I'll see yinz later") and the adjective "hella" ("That movie was hella long") occur in tight clumps around Pittsburgh and northern California, respectively. "Legit" pops up along the Northeast Corridor and in major cities such as Chicago and Los Angeles. If you use "frfr" (for real for real), you're probably tweeting from the American South. How region-specific your tweets are may depend on your intended audience, Eisenstein notes: Tweets with a hashtag—a way to reach more readers—are less likely to have "local variables" than those directed at a specific user. Frfr. http://scim.ag/Twitdial

A map of silence

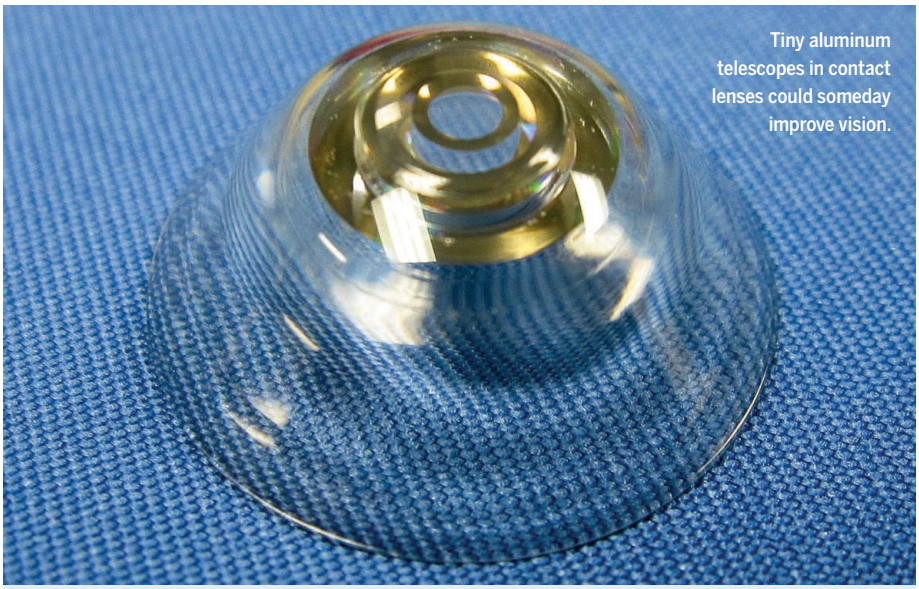
Using 1.5 million hours of acoustical monitoring from places as remote as Dinosaur National Monument in Utah and as urban as New York City, scientists have created a color-coded map of noise levels across the country on an average summer day. Deep blue regions, such as Yellowstone National Park in Wyoming and the Great Sand Dunes National Park in Colorado, have background noise levels lower than 20 decibels—a silence likely as deep as before European colonization, researchers say, and orders of magnitude quieter than most cities, where noise levels average 50 to 60 decibels. The National Park Service is using the map to identify places where humanmade noises are affecting wildlife such as bats and owls, whose ears are up to 20 decibels more sensitive than human ears. The noises drown out the rustles of the insects and rodents they hunt. http://scim.ag/silencemap



Satellite images reveal a fortified citadel at the Garamantian site Qasr ash-Sharraba.

PHOTOS: (TOP TO BOTTOM) JENNA DITTMAR; © DIGITALGLOBE INC.. ALL RIGHTS RESERVED

Published by AAAS



Tiny aluminum telescopes in contact lenses could someday improve vision.

A telescopic contact lens

Wink your right eye to zoom in; wink your left eye to zoom out. Those are the operating instructions for a vision-enhancing system that could be a workaround for certain kinds of vision loss—or a futuristic upgrade to human sight. A new prototype of the technology relies on contact lenses containing tiny aluminum telescopes that interact with a pair of eyeglasses to toggle between normal and 3x magnification. The contact lens telescopes were developed with Defense Advanced Research Projects Agency funding as superthin cameras for aerial drones, then reimagined as an aid for age-related macular degeneration—the loss of light receptors on the inner surface of the eye that blurs the center of the visual field. Now, optical engineer Eric Tremblay of the Swiss Federal Institute of Technology in Lausanne has revealed the latest tweak: zoom-controlling glasses that receive signals from reflectors in the contacts. When a user covers one of the reflectors by winking, the glasses change polarization. Two kinds of polarized light take two different paths through the contact lenses, activating the normal or magnified view. The next major hurdle for the developers: making the lenses breathable for long-term wear. **http://scim.ag/telelens**

NEWSMAKERS

Three Q's

In 2006, South Africa's future president Jacob Zuma said that he showered after sex to avoid HIV. The statement highlighted the country's struggle to accurately communicate science—a situation that **Thandi Mgwebi**, executive director of research chairs and centers of excellence at the South African National Research Foundation, is working to improve. After participating in a meeting panel on improving access to scientific expertise in African countries, Mgwebi chatted with *Science*. **http://scim.ag/MgwebiAAAS**

Q: What's the disconnect between science and the public?
A: We don't have platforms [for communicating science] that are institutionalized. The [scientists] are there and they've got the will, but they don't have the expertise to do it. And then you get false stories [like Zuma's statement]. Those kinds of stories are because of lack of communication and teaching. We don't know why he said it, but it wasn't a joke.

Q: What was the impact of that?
A: Nobody has quantified it. From the learned community of course it's laughable, but you don't know what's happening in a village. It's coming from a head of state. Obviously there must be some bad impact.

Q: How is [this problem] different in South Africa than in the United States?
A: I think the issues are the same, but the scale is different. Indigenous knowledge systems are very important in Africa. With the prevention of HIV, there were a lot of education initiatives, and most of them were aligned with what people believe. You have to look at the belief system, and not just come with your hardcore facts about science.



Should we send messages to alien worlds?

Advocates in the search for extraterrestrial intelligence (SETI) argue yes, but others urge caution (http://scim.ag/msgdebate). *Science* asked attendees: What message would you send?

"I would want to ask an extraterrestrial: What do you care about? What makes you happy?"

Douglas Vakoch, the SETI Institute's director of interstellar message composition

"On behalf of the linguists of Earth: Call us! Let's talk."

Elly Zimmer, University of Arizona Ph.D. student in linguistics

"Please be very careful in how you contact us, or if you do."

Paul Farber, Oregon State University science historian

"We have a beautiful planet and a lot we can teach you."

Linda Spilker, Jet Propulsion Laboratory Cassini project scientist

"How's the food?"

Aidan Cohen, student presenter and future rocket scientist

PHOTOS: (LEFT TO RIGHT) ERIC TREMBLAY AND JOE FORD, COURTESY OF EPFL; ESO

Published by AAAS

PLANETARY SCIENCE

Dawn probe to look for a habitable ocean on Ceres

Asteroid belt's largest body to yield its icy secrets to NASA orbiter, due to arrive next month

By **Eric Hand**

Ceres, the largest object in the asteroid belt, isn't an asteroid. It's not a planet, either; since 2006, this ball of rock and ice some 950 kilometers in diameter has been classed as a dwarf planet, like Pluto. But it is a member of an even more exclusive club: the short list of solar system bodies that may have once been habitable.

Exploring that possibility is a key goal for NASA's Dawn spacecraft, which arrives at Ceres on 6 March for the first-ever close-up of this unusual body. Judging from meteorites, most asteroids either are bone-dry or keep their water content locked up in hydrated minerals. But density measurements suggest Ceres is roughly one-third ice. And although that ice was once thought to be uniformly mixed throughout the orb, planetary scientists now think that as the newly formed Ceres cooled, its constituents separated into layers, including a liquid subsurface ocean that occasionally percolated up to the surface.

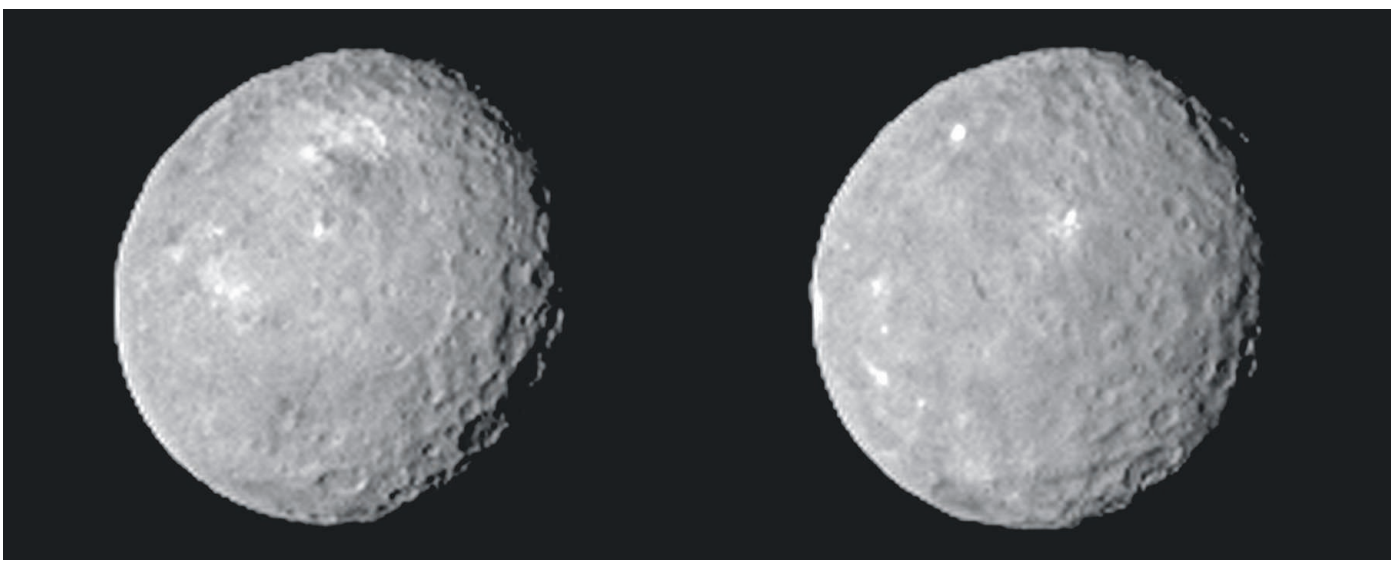
One of Dawn's chief goals is assessing whether that ocean still exists or has frozen solid. Either way, "I think [astrobiologists] should be quite excited, and I think they already are," says Dawn Deputy Principal Investigator Carol Raymond, a planetary scientist at NASA's Jet Propulsion Laboratory (JPL) in Pasadena, California. Ceres, she says, belongs in the same category as Jupiter's moon Europa and Saturn's moon Enceladus—both of which host underground oceans today—but Ceres could be easier to explore. "Importantly, Ceres is a lot easier to get to and it's not in the radiation environment of Jupiter. Landing on Ceres is going to rise to be a priority."

Still millions of kilometers from its destination, Dawn is already sending back tantalizing glimpses. The images, which since January have surpassed those from the Hubble Space Telescope, show a bright feature within a crater, which Raymond says could be subsurface ice exposed by an asteroid impact. And they will continue to improve. By the end of April, Dawn will have settled into a circular orbit at an altitude of 13,500 kilometers. By the end of 2015, it will have dropped as low as 375 kilometers—close enough to get 35-meter resolution with its cameras, says Marc Rayman, Dawn mission director at JPL. "This will show an exquisite level of detail," he says.

Already, the hints of ice indicate that Ceres is a very different world from Vesta, the rocky, parched asteroid 530 kilometers across that Dawn orbited for 14 months in 2011 and 2012. Christopher Russell, Dawn's principal investigator, who is based at the University of California, Los Angeles, attributes the difference to their disparate origins. Both are thought to have formed soon after the birth of the solar system more than 4.5 billion years ago. But Vesta may have taken shape first, Russell says, at a time when the planetary nebula held short-lived radioactive elements that would have generated enough decay heat to vaporize any ice. The coalescence of Ceres may have lagged by a few million years. By then, those radioactive elements would have disappeared, which would explain how its ice survived.

Given its similarities to icy bodies in the outer solar system, some scientists have proposed that Ceres may originally have formed farther from the sun, before the gravity of a migrating Jupiter and Saturn nudged it inward. In that case, Ceres might share more in common with Pluto than just its status as a dwarf planet: They could be twins separated at birth. Dawn will test that possibility by searching for molecules, such as ammonia, that are associated with formation in the colder parts of the solar system, says Andrew Rivkin, a planetary astronomer at the Johns Hopkins University Applied Physics Laboratory in Laurel, Maryland.

Dawn will also try to pin down what lies beneath Ceres's surface. From its density and models of how it cooled with time, scientists have already sketched a basic picture: a rocky, silicate core, surrounded by a layer of water-rich silicates, in turn wrapped in an icy mantle. By making fine measurements of



Ceres, imaged on 12 February at a distance of 80,000 kilometers, displays bright spots that could be icy materials exhumed by impacts.

PHOTO: NASA/JPL-CALTECH/UCLA/MPS/DLR/IDA

Downloaded from www.sciencemag.org on February 21, 2015

Published by AAAS

Ceres's gravity field, the Dawn team will attempt to sort out the dimensions of these layers—and figure out whether any liquid water remains in the ice layer. The Dawn team will also try to determine whether the hundreds of meters of dirt blanketing the surface are debris from impacts, the leftovers after dirty ice has sublimated away, or rocky material somehow exhumed from deep underground.

That third possibility gained support in 2006, when Rivkin and his colleagues, using ground-based telescopes, saw evidence of iron-rich clays and carbonates at the surface. These minerals often form when hot water encounters rock—the conditions that may once have prevailed at the base of the ocean, where it met a hot, rocky core, Rivkin says. Frigid cryovolcanoes perched atop fissures in the ice could have spewed the minerals onto the surface. Now Dawn scientists hope to map those minerals to learn when those volcanoes erupted and how widespread they were.

Last year came a hint that Ceres's ocean may still be liquid. Scientists using Herschel, an infrared space telescope, reported finding faint traces of water vapor escaping from the surface. Few scientists expect to find geysers like the ones that spew from Enceladus—but the wispy plumes could indicate that water is being squeezed from subterranean pockets of melt. On the other hand, Raymond says, they could be due to the sublimation of ice exposed by a recent asteroid impact.

A thrifty ion propulsion system powered Dawn's journey to Ceres. The system, which uses electricity to charge and expel small amounts of xenon, delivers a push so gentle that it would take 9 days for the spacecraft to accelerate from 0 to 100 kilometers per hour, Rayman says. "It's what I like to call acceleration with patience." But the ion engine uses a tenth as much propellant as a chemical rocket. That allowed engineers to keep the thrusters on for nearly two-thirds of the mission and made Dawn's complex trajectory possible.

Another technical component has caused major headaches: the spacecraft's reaction wheels, spinning disks that control where the spacecraft points along three axes. Just before launch, Rayman says, the team was warned that wheels of this type had a checkered history, but it was too late to replace them. (Failures of the same type of wheels later crippled the Kepler exoplanet-hunting spacecraft.) Dawn's first reaction wheel conked out in June 2010, and a second failed in August 2012, as the spacecraft was spiraling away from Vesta. Mission managers turned off the remaining two wheels and shifted to a backup plan, in which they would point the spacecraft with thrusters that rely on a limited 45-kilogram supply of hydrazine.

Rayman says that the team has hoarded the hydrazine carefully. On the trip from Vesta to Ceres, the spacecraft spun to aim its antenna toward Earth for a "check-in" once every 4 weeks rather than once a week as planned. Once in orbit around Ceres, Dawn will spin to send data back to Earth less often than planned, storing more data on board. As a result, the main mission will take longer and won't be completed until June 2016. But Rayman is proud that Dawn won't have to compromise mission goals. He expects to finish with 19 of the 28 kilograms of hydrazine unused.

Rivkin hopes that what Dawn finds will ensure that this won't be the last robotic visitor to Ceres. "We're only now getting to the point where the pieces are starting to fall into place," he says. "It'd be a great place to put a rover." ■

Iced over

Under an icy mantle, Ceres may harbor a thin ocean of liquid water, some of which could spew to the surface in cryovolcanoes.

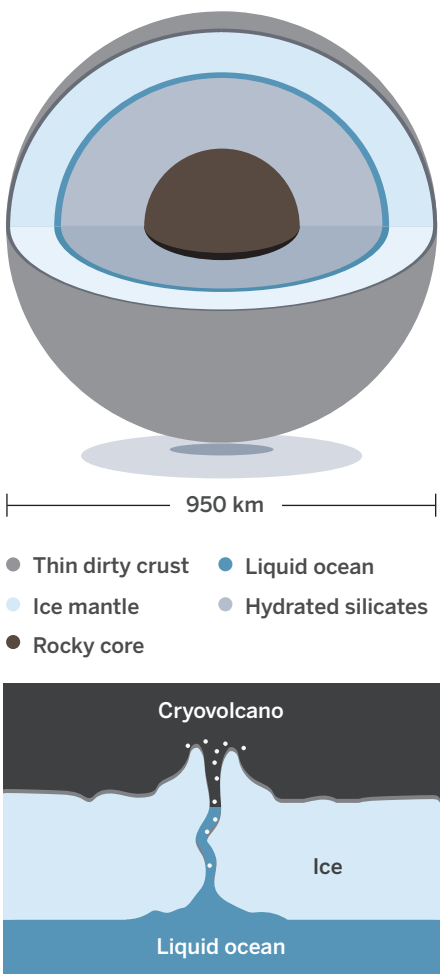


ILLUSTRATION: G. GRULLON/*SCIENCE*

ANCIENT DNA

Indo-European languages tied to herders

Ancient migration from the east shaped European genome and language

By **Michael Balter** *and* **Ann Gibbons**

Despite their allegiances to 47 different nations, 87 ethnic groups, and countless football teams, Europeans have a lot in common. Most speak closely related languages that are members of the great Indo-European language family. Now a new study uses ancient DNA to suggest that a massive migration of herders from the east shaped the genomes of most living Europeans—and that these immigrants may have been the source of Proto-Indo-European (PIE), the mysterious ancestral tongue from which the more than 400 Indo-European languages sprang.

Based on DNA gathered from dozens of ancient skeletons across Europe and Asia, the study, described last week in a preprint posted on the bioRxiv server but not yet published in a journal, reveals when and where different groups of people arrived in Europe and interbred with each other. One surprise is that a migration of herders from the steppes of today's Russia and Ukraine about 4500 years ago significantly shifted the genetic makeup of today's Europeans. "What we know now as 'the European genome' didn't come into existence until the Bronze Age," says evolutionary biologist Greger Larson of the University of Oxford in the United Kingdom. "Lots of people hung out in Europe before then, but their genetic makeup didn't closely mirror modern Europeans."

Almost everyone praises the new genetic data, which include nuclear DNA from twice as many ancient Europeans as all previous analyses combined. But the researchers go further, suggesting that these herders, the Yamnaya people, spoke either PIE or an early form of Indo-European language and brought it to central Europe. Some critics say that connecting populations identified by DNA to any specific language or culture goes too far. The location of the so-called Indo-European homeland where PIE was first spoken, "is not nailed down yet," says ancient

Published by AAAS

DNA specialist Pontus Skoglund.

Up until the 1980s, linguists and archaeologists embraced variations of the steppe hypothesis for the origin of PIE. Then in 1987, archaeologist Colin Renfrew of the University of Cambridge in the United Kingdom proposed that early farmers of Anatolia (present-day Turkey) and the Middle East spoke this ancestral tongue and brought it with them as they expanded both east and west about 8000 years ago. Signs of this mass migration of farmers out of the Middle East show up in the genomes of living and ancient people, boosting the so-called Anatolian hypothesis. But most of this evidence comes from only a few individuals or from maternally inherited mtDNA, making it difficult to know whether the findings represented true population movements.

A group led by geneticist David Reich of Harvard Medical School in Boston recently developed a method to get a genetic fingerprint from ancient skeletons without the time and expense of sequencing their entire genome. His team has now analyzed DNA from 69 Europeans who lived 3000 to 8000 years ago, reading bases at 400,000 positions across the genome that tend to vary among individuals. The DNA revealed patterns of ancestry, and the researchers also knew the culture associated with each skeleton, plus when and where each individual lived. So the team could trace the spread of groups through Europe.

The analysis, which also incorporates some previously published DNA sequences, has produced a new chronology for the peopling of Europe, confirming some earlier studies (*Science*, 5 September 2014, p. 1106) and adding important new details. The researchers found that 8000 to 5000 years ago, two populations of hunter-gatherers in western and eastern Europe evolved along independent paths. Between 8000 and 7000 years ago, closely related people began appearing in Germany, Hungary, and Spain—the influx of the Middle Eastern farmers.

Hunter-gatherers persisted in Russia and eastern Europe until about 6000 years ago when the Yamnaya culture emerged north of the Black Sea. These people herded cattle and other animals and buried their dead in earthen mounds called kurgans. They may have also used wheels, which could explain how they spread quickly through the steppes. Reich's team sampled nine individuals from this Yamnaya culture.

The team also analyzed ancient DNA from four skeletons at one site from the Corded Ware culture of central Europe, known for its distinctive pottery as well as for the skills of its dairy farmers. The four Corded Ware people could trace an astonishing three-quarters of their ancestry to the Yamnaya,



The people who made this ancient Corded Ware pot in central Europe may have descended from herders.

according to the paper. That suggests a massive migration of Yamnaya people from their steppe homeland into eastern Europe about 4500 years ago when the Corded Ware culture began, perhaps carrying an early form of Indo-European language.

The Corded Ware culture then spread rapidly across north and central Europe, carrying the Yamnaya genetic signature as far as today's Scandinavia. The steppe ancestry is "ubiquitous" in most living Europeans, the authors write.

The results are a "smoking gun" for an ancient migration into Europe from the steppes, and boost the odds that PIE emerged there, says Skoglund, who works in Reich's lab but was not a co-author. "The results level the playing field between the steppe hypothesis and the Anatolian hypothesis by showing that the spread of farming was not the only large migration into Europe," he says.

The genetic results complement a study published this week in *Language*. A team led by University of California, Berkeley, linguists Andrew Garrett and Will Chang analyzed all Indo-European languages using methods borrowed from biology for crafting evolutionary trees. They concluded that the origins of PIE date to about 6000 years ago, consistent with the steppe hypothesis but not the earlier Anatolian one (see http://scim.ag/ProtoIndoEuro).

But some researchers remain unconvinced that PIE came from the steppes. Linguist Paul Heggarty of the Max Planck Institute for Evolutionary Anthropology in Leipzig, Germany, criticizes the linguistic analysis for predetermining the relatedness of certain languages, which could bias the result.

The links between genes and language are still weak, Larson adds. "This data is super solid and phenomenally revelatory when thinking about the origin of the modern European genome," he says. "But the whole Indo-European thing is interesting, but a speculative leap away from the raw data."

Meanwhile, Renfrew is holding steady to his Anatolian hypothesis. The movement out of the steppes seen in the ancient DNA data, he says, "may be a secondary migration into central Europe, 3000 to 4000 years later than the spread of farmers which first brought Indo-European speech to Europe." In that case, the Yamnaya people may have spoken not PIE, but an already derived Indo-European tongue ancestral to today's Balto-Slavic languages such as Russian and Polish.

Even Reich and his colleagues seem to be hedging their bets. Their preprint carefully states that the steppe was the source of "at least some," rather than all, of the Indo-European languages. The team suggests that more ancient DNA, especially from east of the steppes, may finally tie our linguistic history with our genes. ■

Influential immigrants from the east

The Corded Ware people, ancestors of many modern Europeans, have genetic links to Yamnaya herders, who swept westward from the steppes about 4500 years ago. The Yamnaya may have spoken the mother tongue of Indo-European languages.

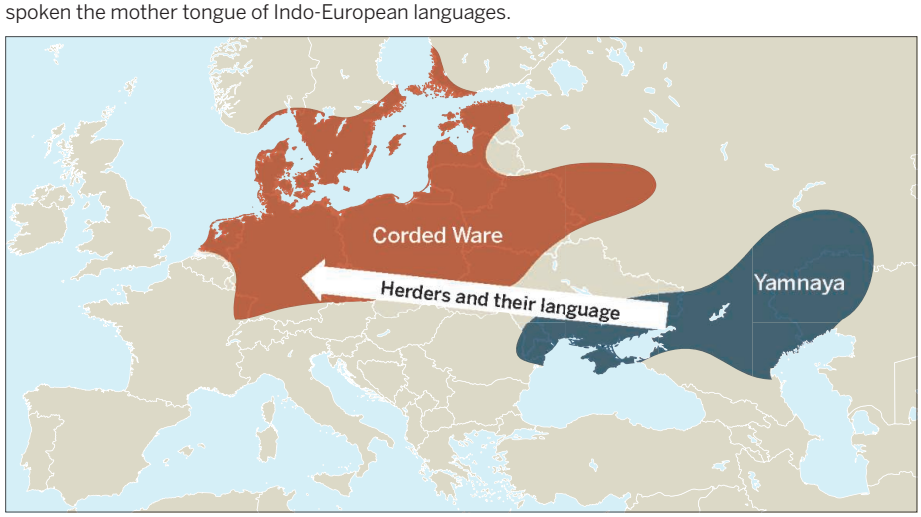


PHOTO: JUG WITH BROAD HANDLE AND INSCIED DECORATION/WERNER FROM AN ARCHIVE/BRIDGEMAN IMAGES

Published by AAAS

BIOMEDICAL RESEARCH

NIH plots million-person megastudy

Questions abound as researchers discuss personalized medicine project

By **Jocelyn Kaiser**

Convince 1 million Americans to wear smart watches that beam their blood pressure, steps walked, and other health information to a central database every hour of every day? Ask them to weigh in on how their genetic data are used by researchers? Those were some of the ideas floated last week at a workshop to flesh out the precision medicine initiative that President Barack Obama proposed last month. To accelerate the development of treatments tailored to individual patients, Obama called for enlisting at least 1 million American volunteers in a long-term study of genes, environment, and health (*Science*, 6 February p. 601).

It may sound straightforward, but not so, concluded the nearly 90 scientists and industry and patient representatives who met at the National Institutes of Health (NIH). Still, by the end of the 2-day meeting, most of the participants seemed enthusiastically on board, if somewhat daunted by the challenges of designing what could be a project costing a billion dollars or more and lasting a decade or longer.

"This absolutely needs to be done. But we need to crisply articulate the goals and design it to optimize success," says cardiologist and human geneticist Sekar Kathiresan of Massachusetts General Hospital in Boston. "Otherwise, we are headed down a rabbit hole of spending lots of money, people questioning it left and right, and it being really wasteful."

The U.S. cohort study, the centerpiece of the precision medicine initiative included in Obama's 2016 budget proposal, is the brainchild of NIH Director Francis Collins. He first broached the idea in 2004, when he was director of NIH's genome institute. At the time, other countries, including the United Kingdom and Estonia, were already moving forward with large population studies. But Collins's plan, deemed impractical and prohibitively expensive, went nowhere.

Now, the situation is different, Collins says, thanks to new technologies that should lower costs. The money-savers include electronic health records, cheaper genome sequencing, and ubiquitous devices such as smartphones and Fitbits that can monitor health.

Still, huge questions loom: Who should be recruited? How can researchers knit together their health data? What should be the study's overall objectives—to find rare disease genes or to test new treatments and devices?

To save money, as an initial step NIH proposes to recruit participants who are already enrolled in ongoing cohort studies, instead of starting from scratch. For example, the precision medicine initiative could piggyback on the Department of Veterans Affairs' Million Veteran Program, which is linking volunteers' DNA samples to its 20-year database of health records. Some participants, however, wondered whether this approach really will be cost-effective. Researchers would have to re-contact the participants to ask if they're willing to participate, and many may decline. Others warned that existing cohort studies may not adequately represent the country's geographic, ethnic, and socioeconomic diversity.

Participants must be involved in the study's design and decisions about how individual data will be used, Collins says. But such inclusion will be a challenge, he concedes. Some ideas could come from existing programs, such as PatientsLikeMe, a commercial Web portal that allows patients to share their health data for disease studies. Another company, 23andMe, has built a genetics research database using information from consenting customers. If older cohort studies had let patients "own" their data, "we could recruit this million person cohort almost instantaneously," said 23andMe CEO Anne Wojcicki.

Others raised additional questions. For example: Should the study enroll children? Including families would strengthen the study's power to find genetic links with disease, some noted. But Rory Collins, a leader of UK Biobank, a cohort study of 500,000 adults, recommended a separate pediatric cohort because recruiting children and studying their diseases is a very different enterprise than dealing with adults. "If you try to do everything, you're likely to fail," he predicted—a problem that contributed to the recent demise of NIH's National Children's Study (*Science*, 19 December 2014, p. 1441).

There was greater agreement that mobile, "mHealth" technologies that can monitor a person's health hold promise, for tracking not just physical activity and heart rate, but also measures such as social interactions and toxic exposures—factors that electronic health records have trouble capturing. Some participants were eager to outfit all 1 million participants with a smart phone and smart watch. But others urged caution, noting it's still not clear how useful such mobile data will be to researchers.

Once it was over, Collins called the workshop "historic"—and concluded that despite the unsettled issues, there are no "big showstoppers." But NIH has a tight deadline to work out the details. The 2016 fiscal year begins in October, and assuming Congress approves a "down payment" of $130 million (which appears likely), NIH will have just 12 months to issue requests for proposals and spend the money. A working group, led by Yale University human geneticist Richard Lifton and NIH policy chief Kathy Hudson, is charged with coming up with an interim plan by September. Before then, Lifton said, "there is an enormous amount of work that remains to be done." ■

Seizing an opportunity

Francis Collins says plummeting sequencing costs and new technologies have made a large U.S. cohort study feasible.

	2004	2014
Cost of sequencing a human genome	$22,000,000	$1000 to $5000
Time to sequence a human genome	2 years	<1 day
Number of smart phones in the United States	1 million (<2% of population)	160 million (58%)
Health providers using electronic records	20% to 30%	>90%
Computing power	n	n x 16

Downloaded from www.sciencemag.org on February 21, 2015

Published by AAAS

FEATURES



ARCTIC IMPACT

Is the melting Arctic really bringing frigid winters to North America and Eurasia? Scientists struggle to piece together an atmospheric puzzle

By **Carolyn Gramling**

Downloaded from www.sciencemag.org on February 21, 2015

Weather experts were on high alert in December 2009. A region of high pressure had settled over Greenland, forming a roadblock in the path of the circumpolar jet stream. Thwarted, the jet stream meandered, bending southward into a large loop and shunting cold Arctic air toward the center of the United States. Meteorologists were familiar with this "Greenland block." It was a climate pattern historically favorable for winter storms—and as if on cue, record snowfalls blanketed the eastern United States over the next few months.

Against the backdrop of "Snowmageddon" and other powerful winter storms that have blasted the United States, Europe, and Asia in the past few years, a different kind of tempest has been swirling within the Arctic science community. Its core is a flurry of recent research proposing that such extreme weather events in the midlatitudes are linked through the atmosphere with the effects of rapid climate change in the Arctic, such as dwindling sea ice. The idea has galvanized the public and even caught the attention of the White House. But some Arctic researchers say the data don't support it or that the jury is at least still out. Even some of its proponents agree that the media hype is premature.

Now, scientists are starting to tackle the issue in earnest. Atmospheric links between the poles and midlatitudes are becoming a marquee topic at Arctic-related conferences. Last December alone it drew researchers to a workshop in Barcelona, Spain, and a dedicated session at the annual American Geophysical Union meeting in San Francisco, California. "A lot of scientists have worked individually, in isolation, pursuing their own ideas," says Judah Cohen, a climate scientist at the Massachusetts Institute of Technology in Cambridge—one of several researchers who hope that a coordinated effort will measure the reach of the north.

THE IDEA THAT THE ARCTIC could have a regional, even hemisphere-scale impact on the atmosphere represents a paradigm shift for climate scientists. "When I was in grad school, [the thinking was that] the tropics are everything," Cohen says. "The tropics, the ocean—that was it, there was no other player."

The Arctic Ocean, after all, is small and cold; the tropical Pacific Ocean is vast and, of course, warmer. To influence the atmosphere on a global scale, very large amounts of heat and moisture must flow from ocean to air. That heat engine is huge in the Pacific and powers the El Niño–Southern Oscillation (ENSO), the planet's dominant interannual climate pattern. ENSO also has a helpful supply chain: Even as heat escapes from the eastern tropical Pacific to the atmosphere, currents flowing in from the western tropical Pacific provide a fresh supply.

But there is a new kind of engine forming in the Arctic. The rapid loss of sea ice in the Arctic Ocean due to global warming—the area of summer ice has shrunk more than 11% per decade since 1979—has created an expanse of dark open water newly available to absorb the sun's energy. This extra energy input and the corresponding flux of moisture and heat to the Arctic atmosphere are helping drive a strong local positive feedback to global warming, called Arctic amplification. As a result, surface temperatures are rising twice as fast in the Arctic as at lower latitudes.

But is the loss of sea ice influencing more than just local warming? In 2012, climatologists Jennifer Francis of Rutgers University, New Brunswick, in New Jersey and Stephen Vavrus of the University of Wisconsin, Madison, proposed that Arctic amplification driven by sea ice loss could significantly affect midlatitude weather by slowing the jet stream (*Science*, 18 April 2014, p. 250). The mechanism they suggested was this: A faster warming Arctic means a reduced temperature gradient between the Arctic and midlatitudes, which in turn weakens west-to-east winds. The result is a slowdown of the jet stream, allowing it to meander more and form elongated waves (called Rossby or planetary waves) that jut to the north or south. Among other effects, Francis and Vavrus proposed, the deep waves in the jet stream could enable a winter storm to push farther south and then linger in one location, possibly dumping record amounts of snow.

A handful of newer studies support one key part of this hypothesis: that large-amplitude Rossby waves in the jet stream are indeed linked, statistically, to extreme weather in the midlatitudes. For example, Vladimir Petoukhov of the Potsdam Institute for Climate Impact Research in Germany and colleagues in 2013 correlated summer heat waves in Europe with instances of slow-moving, high-amplitude Rossby waves. And last year, James Screen, a climate modeler at the University of Exeter in the United Kingdom, and Ian Simmonds of the University of Melbourne in Australia co-authored a paper that reported a strong statistical correlation between amplified, slow Rossby waves and months from 1979 to 2012 with extreme weather events. More waviness, they found, made the western United States more susceptible to heat waves and the eastern United States to extreme cold.

But other parts of the hypothesis remain controversial—particularly the part of the chain that links these changes to Arctic amplification. Some evidence supports Francis and Vavrus's idea that a decreasing temperature gradient between the midlatitudes and the Arctic might slow the jet stream and make it wavier.

Yet climate dynamicist Elizabeth Barnes of Colorado State University, Fort Collins, reported in 2013 that she could find no uptick in the instances of Rossby waves in the last couple of decades, the period encompassing extreme sea ice loss and Arctic warming.



Heavy blizzards that paralyzed Central Europe in February 2012 may have been part of a larger pattern.

PHOTOS: (OPPOSITE) © JENNY E. ROSS/CORBIS; (RIGHT) © BOGDAN CRISTEL/REUTERS/CORBIS

Published by AAAS



As open water replaces ice, Arctic warming accelerates—with unknown consequences.

And in a 2013 study, Screen and Simmonds found no statistically significant changes in these waves from 1979 to 2011, despite a declining north-south temperature gradient.

Some theorists have proposed another mechanism by which dwindling sea ice could shape midlatitude weather: by forcing changes in a multiyear atmospheric cycle called the Arctic Oscillation. In a positive Arctic Oscillation phase, the jet stream is strong and less wavy, and cold air stays in the Arctic. In a negative phase, the jet stream is weaker and wavier, and the cold air spills southward. Some analyses suggest that in the last few decades the Arctic Oscillation has increasingly been in a negative phase, which might drive not just storminess but also longer term cooling in the midlatitudes.

But evidence that the retreat of sea ice has influenced the Arctic Oscillation is scarce. "Since any Arctic effect [on the jet stream] is buried in large random climate [variations], and the record is short," such a link is simply impossible to prove at the moment, says James Overland, an oceanographer at the National Oceanic and Atmospheric Administration's Pacific Marine Environmental Laboratory in Seattle, Washington.

FRANCIS ACKNOWLEDGES the lingering uncertainty about how the changes in the Arctic could drive bouts of extreme weather farther south. But, she says, as the mystery attracts more researchers, they are finding clues. Last year, climate scientist Masato Mori of the University of Tokyo and colleagues modeled how sea ice loss in the Barents and Kara seas north of Russia could increase blocking events—and the resulting severe winters—over Eurasia. And Baek-Min Kim of the Korea Polar Research Institute in Incheon and colleagues showed in a model how changes in sea ice loss in the Barents and Kara seas could set off a chain of events that produced a negative phase of the Arctic Oscillation.

Another paper published last year, this one by Kazutoshi Sato of the Japan Agency for Marine-Earth Science and Technology in Yokosuka and colleagues, suggests that ice loss in the Barents Sea and cold Eurasian winters are actually part of an even bigger climate pattern originating in the North Atlantic Gulf Stream. Recent observations show that the current is pushing warm water farther to the north. That shift, Sato and his colleagues found, may produce planetary waves that both warm the Barents Sea and cause a cold anomaly over Eurasia.

"That's a pretty robust linkage there," Francis says. "It's not going to happen every single year, but it's pretty convincing that there are real physical mechanisms disrupting the jet stream."

> ***"We've put the cart before the horse. We're missing ... the dynamics, the mechanistic understanding."***
>
> **Elizabeth Barnes**, Colorado State University, Fort Collins

IT'S TOO EARLY TO TAKE SIDES about whether the Arctic influence is real, many researchers say. Last December's Barcelona workshop grappled with that "two camps" misconception, Screen says. "I don't like to frame it like that," he says. "The majority [of people] are somewhere in the middle." In fact, a few are in an entirely different camp: blaming changes in Eurasian snow cover, rather than the retreat of Arctic ice, for the midlatitude weather extremes (see sidebar, p. 821).

"We have records of sea ice only going back 30 years, with dramatic losses in the last decade or so," Screen says. A statistical analysis of that brief period of observations, he says, is unlikely to settle the debate. Instead, scientists need to turn to other sources of knowledge, such as models and theory, "to better understand what we might be seeing in the observations."

Overland, for his part, calls this the "preconsensus period." He says meetings such as the workshop in Barcelona (which both he and Screen attended) have shown encouraging signs of progress. For one, researchers plagued by inconsistent definitions of terms such as waviness are finally getting a chance to straighten things out. And he felt that the Barcelona workshop did come to at least one consensus: that if there are links between Arctic amplification and midlatitude weather, they're amplifications of already existing and known climate patterns—Greenland blocking and a region of persistent high pressure called the Siberian high—so there's no need to build brand-new physics into the models.

PHOTO: © STEVEN KAZLOWSKI/SCIENCE FACTION/CORBIS

Published by AAAS

The Siberian snow connection

By **Carolyn Gramling**

Sea ice may have grabbed the headlines, but for nearly 2 decades a team led by climate scientist Judah Cohen of the Massachusetts Institute of Technology in Cambridge has been quietly and persistently chasing an alternative link between the changing Arctic and midlatitude weather: how much snow falls over Siberia each October. Snow cover in Eurasia from year to year can vary dramatically, Cohen says, by as much as a factor of three.

Like the retreat of sea ice, more snow cover would ultimately lead to a wavier jet stream, allowing cold polar air to invade midlatitudes. But whereas sea ice proponents suggest that a rapidly warming Arctic leads directly to a slow, more meandering jet stream, Cohen envisions a series of causal links from Siberian snow via the lower atmosphere to large-amplitude planetary waves that reach into the stratosphere and shape weather patterns in the midlatitudes.

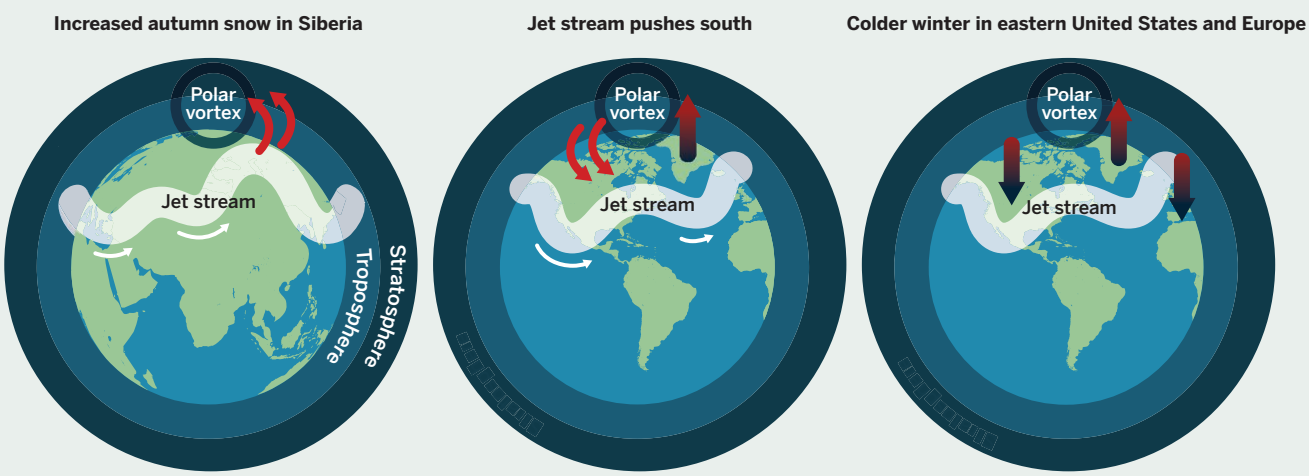
His "six-step" cycle goes like this: With broader snow cover blanketing more of Siberia in October, there is more cold, dense air in the lower atmosphere, and the high-pressure center known as the Siberian high becomes bigger and stronger. By November to December, these atmospheric transformations increase the flow of energy upward, from the troposphere into the stratosphere. The stratosphere suddenly warms, and the stratospheric polar vortex—the mass of cold air that is normally confined to the Arctic—breaks down, creating a more meandering jet stream and allowing cold polar air to penetrate farther south.

In a 2014 paper, Cohen brought sea ice into the picture as well. "We tried to argue how they can all work together," he said. Although melting sea ice warms the lower atmosphere over the Barents and Kara seas, and melting snow cools it to the east, over Siberia, the two effects can actually work in tandem to force the same planetary wave pattern in the atmosphere that promotes the weakening of the polar vortex in wintertime.

But Cohen's hypothesis is far from widely accepted. "His hypothesis that all these things are connected … there are so many steps in that kind of chain" and there's a lot of uncertainty in the data, says James Screen, a climate modeler at the University of Exeter in the United Kingdom. For example, Screen says, Cohen "reports increasing snow cover in Eurasia in October," but other researchers haven't seen that trend.

Cohen, who directs seasonal forecasting efforts at the firm Atmospheric and Environmental Research, a unit of Verisk Climate, has been working not only to understand these links but also to use them to predict changes in the polar vortex and anticipate storms. (They've made their predictions public at https://www.aer.com/science-research/climate-weather/arctic-oscillation.) One recent success: In late November 2014, the team predicted—on the basis of extensive Siberian snow cover last October—that the stratospheric polar vortex would weaken in early January 2015. In mid-January, a blizzard pounded the northeastern United States.

"This is relevant to the whole argument of whether the Arctic can have any influence on midlatitude weather, or [whether] it is all just random noise," Cohen says. "If all we can discern in the system is noise, then it should be impossible to make an accurate prediction of a stratospheric warming 6 weeks in advance." ■



ILLUSTRATIONS: ADAPTED FROM NSF BY G. GRULLÓN/*SCIENCE*

SORTING OUT THOSE "known knowns" is exactly what researchers should be doing, Barnes says. "In my mind, we've put the cart before the horse a bit" by focusing on weather extremes, she says. "We're missing the theory, the dynamics, the mechanistic understanding." She suggests that the community go back to basics to determine how Arctic warming could influence the jet stream dynamics. "It's certainly not sexy like telling you that we're going to have more extreme cold events—but in terms of the science, it's the way forward."

One key to success, she says, is teasing out the effects of the Arctic on the jet stream from those of other atmospheric powerhouses, such as the chaotic atmospheric flow at midlatitudes and the ENSO pattern in the tropics. Indeed, researchers need to look beyond the potential impacts of Arctic change, Overland says, and aim for a better picture of atmospheric dynamics as a whole.

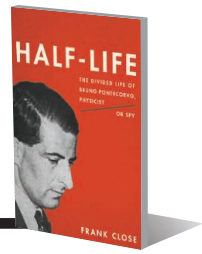
"We're just getting into that time where people get interested," Barnes says. "If you look over the literature in the last 10 years, there's a lot of focus over how tropical warming will influence the jet stream, but not a lot on how Arctic warming will influence it. As a community our eyes were turned to the south, and now we're looking north. That, to me, is what's exciting." ■

Published by AAAS

INSIGHTS

Oxytocin therapy for autism *p. 825*

Scientist or Soviet spy? *p. 833*



PERSPECTIVES

ECOLOGY

Mothers shape ecological communities

Individual hormonal responses affect the distributions and abundances of bird species

By **Ben Dantzer**

The species assemblages that make up ecological communities change over time (*1*), in part as a result of interactions among species such as predation and competition. However, it is often not clear how interactions among individuals scale up to affect broader ecological processes such as changes in species assemblages (*2*, *3*). On page 875 of this issue, Duckworth *et al.* (*4*) provide field evidence for how individual competition between members of different bird species leads to changes in community composition. The key to these observations lies in maternal hormone changes that affect their sons' behavioral characteristics.

In western North America, forest fires create new habitat for passerine birds. Mountain bluebirds colonize these post-fire habitats before their sister species, the western bluebirds (see the photo) (*5*–*7*). These two bluebird species and other bird species compete for access to nest cavities that they need for reproduction but that are created by other species. Duckworth *et al.* use long-term data from multiple post-fire habitats in Montana to show that there is a predictable pattern of bluebird species replacement in post-fire habitats. Mountain bluebirds first colonize post-fire habitats but are eventually replaced by more aggressive western bluebirds that arrive from areas with high western bluebird densities. These more aggressive western bluebirds are eventually joined and then replaced by less aggressive and less dispersive western bluebirds. As western bluebird densities increase in the newly colonized areas, the cycle of species succession resets, and more aggressive dispersive males are again produced.

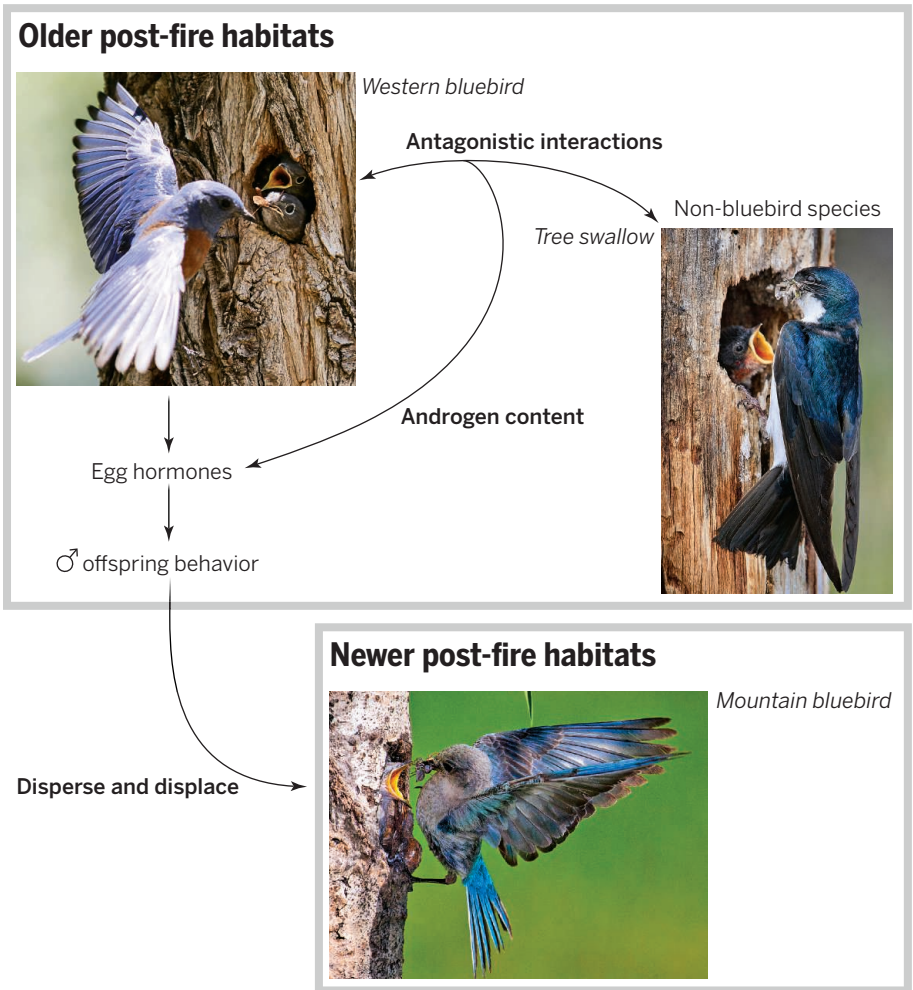


A male western bluebird at his nest.

PHOTO: DONALD M. JONES/CORBIS

Downloaded from www.sciencemag.org on February 21, 2015

Published by AAAS



From individual to large-scale effects. Duckworth *et al.* (*4*) show that female western bluebirds experiencing increased conflict with individuals from non-bluebird species have more androgens in their eggs and produce sons that hatch early. These males are more aggressive and disperse to newer post-fire habitats, where they displace mountain bluebirds. Non-bluebird species thus indirectly affect (*13*) the distribution of mountain bluebirds. This hormone-mediated maternal effect on the behavior of individual male offspring in turn affects higher ecological scales by influencing the distribution and abundance of bluebird species in these communities.

Could maternal effects explain this cycle of bluebird succession? Mothers can induce pronounced changes in offspring characteristics (*8*). Previous work in wild animals has shown that such maternal effects can promote beneficial changes in offspring characteristics in anticipation of competitive environments and alter the evolutionary response to natural selection (*8*–*10*). Maternal effects can also affect population dynamics in laboratory studies (*11*), but evidence that they can influence ecological processes in natural populations has remained elusive.

Duckworth *et al.* now show that maternal effects can indeed have important ecological consequences in the wild (see the figure). In western bluebirds, eggs hatch asynchronously. Males that hatch early tend to be more aggressive and are more likely to disperse to post-fire habitats occupied by mountain bluebirds (*5*–*7*). The aggressive male western bluebirds that first disperse to these habitats acquire large territories by outcompeting mountain bluebirds (*5*–*7*). In Duckworth *et al.*'s study, western bluebird mothers in older populations with high western bluebird densities produced sons earlier in the hatching order, and these sons were more aggressive and likely to disperse.

Same-species population density is often thought to be a cue that induces such maternal effects (*10*). However, in natural populations, limited resources and population density often covary, necessitating experimental manipulations (*10*). Duckworth *et al.* decoupled the relationship between western bluebird density and nest cavity availability by experimentally increasing nest cavity availability for some females but not others. Females in high-density populations that had extra nest cavities on their territory produced fewer males that hatched early. This suggests that nest cavity availability (rather than population density itself) induces this maternal effect.

How do changes in nest cavity availability experienced by the mother translate into alterations in male offspring behavior? Ecological cues affecting maternal physiology can induce adaptive changes in offspring characteristics in preparation for competitive environments (*8*, *10*). As Duckworth *et al.* show, females that experienced more antagonistic interactions produced clutches of eggs containing higher androgen hormone levels; males in these clutches tended to hatch earlier.

Maternal effects are often thought to be induced by competition with members of the same species over limited resources (*8*, *10*). Surprisingly, antagonism from a non-bluebird species appears to trigger this maternal effect in female western bluebirds. The level of conflict with non-bluebird species was highest during egg production, whereas conflict experienced from members of the same species peaks several months prior when nests were being built (*4*). This is important because androgens in bird eggs accumulate during oogenesis (*12*). Non-bluebird species thus have indirect effects (*13*) on bluebird communities by influencing the hormone levels of eggs produced by western bluebird mothers.

The results show how interactions among individuals at a small spatial scale affect the organization of ecological communities at broader spatial scales through the influence of mothers on offspring behavior. The experiments by Duckworth *et al.* (*4*) and others (*8*–*11*) indicate that the influence of mothers on offspring characteristics likely transcends generations and ecological scales. ■

Department of Psychology and Department of Ecology and Evolutionary Biology, University of Michigan, Ann Arbor, MI 48109, USA. E-mail: dantzer@umich.edu

REFERENCES AND NOTES

1. H. C. Cowles, *Bot. Gaz.* **27**, 95 (1899).
2. S. A. Levin, *Ecology* **73**, 1943 (1992).
3. G. A. Wellborn *et al.*, *Annu. Rev. Ecol. Syst.* **27**, 337 (1996).
4. R. A. Duckworth *et al.*, *Science* **347**, 875 (2015).
5. R. A. Duckworth, A. V. Badyaev, *Proc. Natl. Acad. Sci. U.S.A.* **104**, 15017 (2007).
6. R. A. Duckworth, *Am. Nat.* **172** (suppl. 1), S4 (2008).
7. R. A. Duckworth, *Philos. Trans. R. Soc. B* **364**, 1075 (2009).
8. T. A. Mousseau, C. A. Fox, Eds., *Maternal Effects as Adaptations* (Oxford Univ. Press, Oxford, 1998).
9. A. G. McAdam, S. Boutin, *Philos. Trans. R. Soc. B* **271**, 75 (2004).
10. B. Dantzer *et al.*, *Science* **340**, 1215 (2013).
11. S. J. Plaistow, T. G. Benton, *Philos. Trans. R. Soc. B* **364**, 1049 (2009).
12. T. G. G. Groothuis, H. Schwabl, *Philos. Trans. R. Soc. B* **363**, 1647 (2008).
13. E. E. Werner, S. D. Peacor, *Ecology* **84**, 1083 (2003).

ACKNOWLEDGMENTS

I thank Q. E. Fletcher, A. G. McAdam, and E. E. Werner for helpful comments.

10.1126/science.aaa6480

PHOTOS: (TOP TO BOTTOM) NOBUO IWATA/GETTY IMAGES; CONNOR STEFANISON/ALAMY; ALEX BADYAEV/UNIVERSITY OF ARIZONA

Published by AAAS

BIOMOLECULES

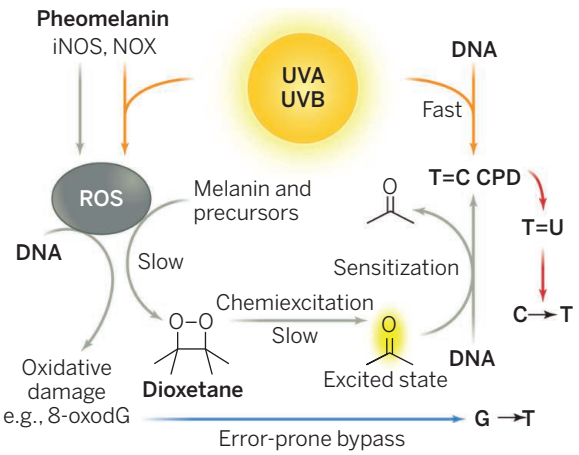
The dark side of sunlight and melanoma

UV-initiated DNA photodamage in melanocytes is found to continue in the dark

By **John-Stephen Taylor**

Skin cancer is the most prevalent form of cancer, with a lifetime risk of 1 in 5 for Americans (*1*). Most skin cancers can be attributed to C→T and CC→TT mutations in DNA resulting from cyclobutane pyrimidine dimers (CPDs) produced by the direct absorption of UVB light (290 to 320 nm) present in sunlight (*2*). The most generally accepted mechanism for the formation of these mutations is that Cs or 5-methyl-Cs in the CPDs rapidly deaminate to Us or Ts, which are then replicated in an error-free manner. One might expect that photodamage would cease once out of the Sun, but Premi *et al.*, on page 842 of this issue, show that this is not the case in melanocytes (*3*). A substantial fraction of UV damage to DNA in these cells may be occurring in the dark, by a novel pathway with important implications for melanoma formation.

Although melanoma accounts for only about 2% of all skin cancers, with a lifetime incidence of 1 in 50, it is the most aggressive type of skin cancer, with about one American dying from melanoma every hour (*1*). Of particular concern is that melanoma has been increasing by about 2% per year and has been correlated with increasing exposure to UVA (320 to 400 nm) from tanning beds and extended time in the Sun encouraged by sunscreens. The role of UVA in melanomagenesis has been controversial, however. One major risk factor for melanoma is a red hair phenotype characterized by a high ratio of red pheomelanin to black eumelanin in the melanin pigment that serves as nature's sunscreen. Whereas eumelanin is considered photoprotective, pheomelanin is thought to be phototoxic owing to its ability to generate superoxide upon irradiation, which leads to reactive oxygen species (ROS) that can damage DNA (*4*). Indeed, melanomagenesis by UVA light was found to require melanin and to be associated with increased amounts of the DNA oxidation product 8-oxodG (8-oxo-7,8-dihydro-2′-deoxyguanosine) (*5*). Mice with a red phenotype containing a cancer-initiating "driver" mutation have also been found to progress to melanoma in the absence of UV light, whereas black and albino mice do so much more slowly (*6*). A higher level of oxidative DNA damage in the red mice suggested that pheomelanin biosynthesis might be either producing ROS or reducing radical scavenging thiols.



Danger in the dark. Light and dark pathways (yellow and gray arrows, respectively) leading to melanoma-inducing mutations involving UV and biochemical-mediated formation of DNA photoproducts and oxidative damage.

The new pathway leading to CPDs discovered by Premi *et al.* also involves melanin and was determined by carefully monitoring the concentration of CPDs after UV irradiation. In doing so, they discovered that CPDs continued to rise for 2 to 3 hours after irradiation of normal melanocytes with both UVA and UVB before decreasing due to repair, whereas CPDs decreased immediately in albino melanocytes. The increase in CPDs was even greater in melanocytes with the red phenotype, underscoring the importance of pheomelanin in this process. The CPDs formed during the dark reaction also had a higher fraction of C-containing CPDs than did those produced by UVA alone, which suggests that this pathway is more mutagenic.

The increase in CPDs could not be explained by a direct photochemical or indirect photosensitization mechanism, both of which take place in a fraction of a second upon absorption of light. Such unusual behavior could only be explained by a chemisensitization mechanism, in which the triplet electronic excited state of a sensitizer is produced slowly from the thermal decomposition of a high-energy precursor molecule (chemiexcitation); the excited molecule then transfers its triplet energy to DNA in a nonradiative manner to produce a CPD. In a prescient experiment carried out more than 40 years ago, Lamola showed that thermal decompression of the highly strained trimethyl dioxetane to an excited carbonyl induces CPD formation in DNA (*7*). He also envisioned that such a chemisensitization process might occur in vivo but was unsure about how such high-energy dioxetanes might arise biochemically.

To answer the latter question, Premi *et al.* carried out a brilliant piece of detective work to elucidate a possible pathway that involves the reaction of superoxide, formed by photoexcitation of pheomelanin or by UV-induced NOX [reduced nicotinamide adenine dinucleotide phosphate (NADPH) oxidase], with nitric oxide generated enzymatically by iNOS (inducible nitric oxide synthase) to form peroxynitrite. The peroxynitrite was shown to react with melanin and melanin precursors to chemosensitize C-containing CPD formation, presumably via dioxetane intermediates.

Researchers have long sought methods to prevent skin cancer induction, and the results of this study indicate that sunscreens should aim to minimize exposure to both UVB and UVA. As suggested by the authors, UV DNA damage arising in the dark might also be reduced by agents that scavenge or interfere with superoxide and nitric oxide production, or that quench the excited triplet-state intermediates. It is intriguing to speculate as to whether oxidatively generated DNA chemisensitizers may also be playing a role in the induction of cancers in tissues not exposed to light, which could thus benefit from similar intervention. ■

Department of Chemistry, Washington University, St. Louis, MO 63130, USA. E-mail: taylor@wustl.edu

REFERENCES

1. www.skincancer.org/skin-cancer-information/skin-cancer-facts (2015).
2. H. Ikehata, T. Ono, *J. Radiat. Res.* **52**, 115 (2011).
3. S. Premi *et al.*, *Science* **347**, 842 (2015).
4. A. Napolitano, L. Panzella, G. Monfrecola, M. d'Ischia, *Pigment Cell Melanoma Res.* **27**, 721 (2014).
5. F. P. Noonan *et al.*, *Nat. Commun.* **3**, 884 (2012).
6. D. Mitra *et al.*, *Nature* **491**, 449 (2012).
7. A. A. Lamola, *Biochem. Biophys. Res. Commun.* **43**, 893 (1971).

10.1126/science.aaa6578

Published by AAAS

Downloaded from www.sciencemag.org on February 21, 2015

NEUROSCIENCE

Can oxytocin treat autism?

We are still at an early stage of assessing oxytocin-based therapy for autism spectrum disorders

By **Larry J. Young**
and **Catherine E. Barrett**

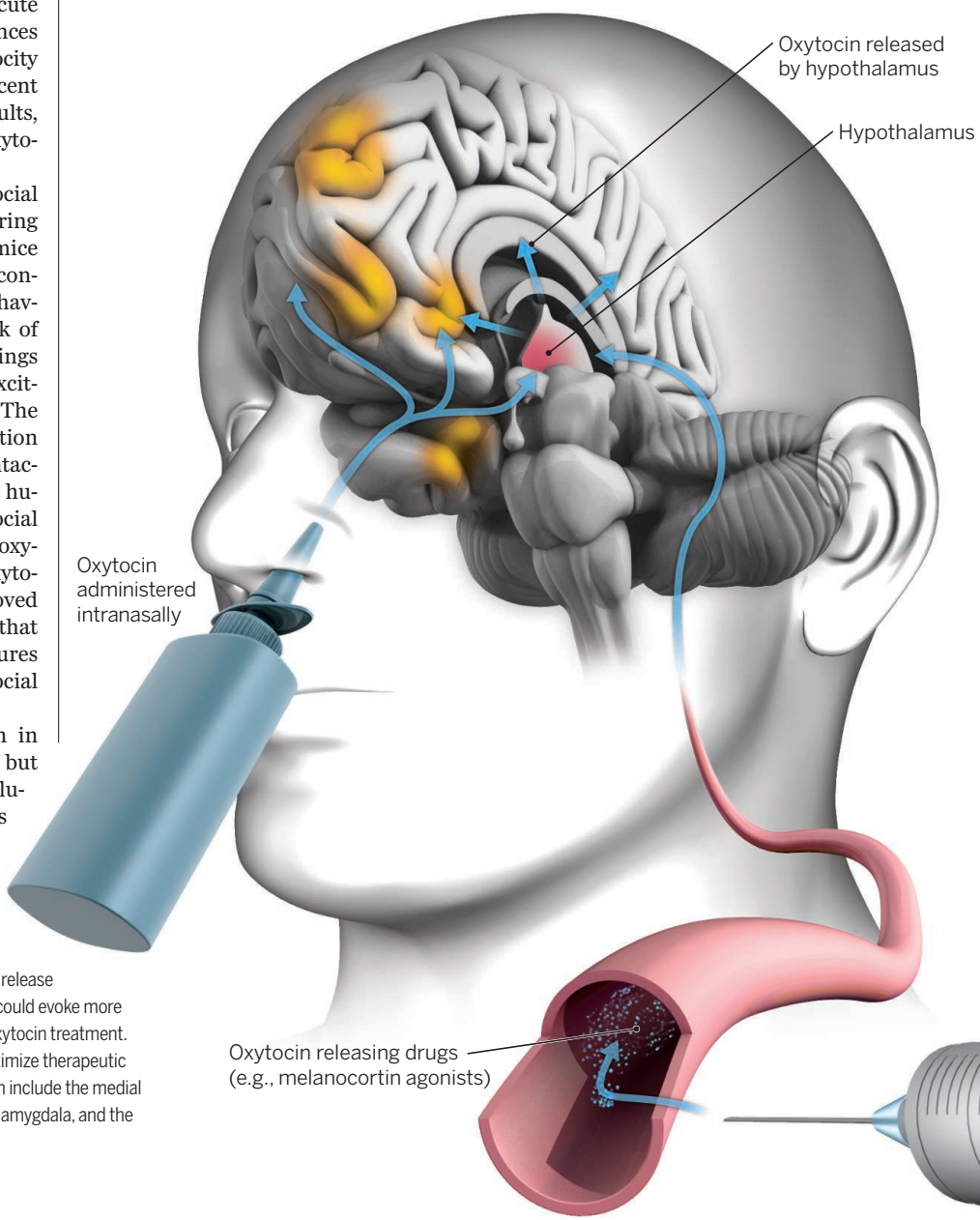
The U.S. Centers for Disease Control and Prevention estimates the prevalence of autism spectrum disorders (ASDs) to be 1 in 68 children in the United States, yet no drugs to treat the debilitating social deficits of ASD are available. Oxytocin, a natural brain peptide produced in the hypothalamus, has received considerable attention as a potential treatment for social deficits in ASD. Acute intranasal oxytocin temporarily enhances social cognition, empathy, and reciprocity in individuals with ASD (*1*). However, recent clinical trials have yielded mixed results, leaving the field questioning whether oxytocin can live up to the hype.

Oxytocin increases the salience of social stimuli and promotes parental nurturing and social bonds. Recent studies in mice and humans have come to conflicting conclusions about its effects on social behaviors associated with autism (e.g., a lack of social interest or reciprocity). The findings of Peñagarikano *et al.* (*2*) have added exciting support for using oxytocin in ASD. The authors observed that mice with a mutation in *Cntnap2* (the gene that encodes contactin-associated protein-like 2), which in humans results in ASD, display robust social deficits and reduced amounts of brain oxytocin. Remarkably, daily intranasal oxytocin treatment over development improved later social engagement, suggesting that early exposure to oxytocin restructures neural circuits to permanently rescue social impairments in this ASD model.

Numerous clinical trials of oxytocin in ASD are ongoing (clinicaltrials.gov), but completed trials have produced inconclusive results (*1*). Several trials in adults and children show modest improvements in social function in response to oxytocin treatment, with no adverse effects. Still, other studies failed to yield positive outcomes (*1*, *3*).

What accounts for the variable findings in human studies? It may be attributed to variation in doses, study duration, age, and small, heterogeneous study samples. Context is likely critical to the success of oxytocin therapies. As oxytocin enhances salience and the reinforcing value of social stimuli, oxytocin therapies should be most effective when combined with behavioral therapies.

To move forward, parallel animal and human studies are needed to elucidate conserved effects of oxytocin on brain communication in response to social stimuli. Animal research is critical for understanding precise mechanisms of action. For example, oxytocin receptors are localized to cholinergic regions in the primate brain that modulate visual and auditory attention, suggesting an important role in social sensory processing (*4*). Oxytocin also regulates the signal-to-noise ratio in the hippocampus to tune attention toward socially relevant stimuli in mice (*5*). Is this a possible mechanism by which intranasal oxytocin enhances neural responses to social stimuli, while suppressing responses to nonsocial stimuli, in ASD (*6*)? Another link to autism is suggested by the developmental switch in the neurotransmitter γ-aminobutyric acid from excitatory to inhibitory neurotransmission at birth in



Oxytocin therapeutic strategies. Next-generation therapies (such as MC4R agonists) that stimulate the release of endogenous oxytocin in the brain (hypothalamus) could evoke more potent and targeted effects compared to intranasal oxytocin treatment. Combining oxytocin with behavioral therapy may maximize therapeutic potential. Brain regions affected by intranasal oxytocin include the medial prefrontal cortex, anterior insula, orbitofrontal cortex, amygdala, and the ventral striatum (orange).

ILLUSTRATION: C. BICKEL/*SCIENCE*

Published by AAAS

Downloaded from www.sciencemag.org on February 21, 2015

mice. This switch is impaired in ASD-like mice, and oxytocin-mediated restoration of this process alleviates social deficits (*7*).

Parallel animal and human studies are also needed to determine the developmental consequences of chronic oxytocin exposure. For these investigations, care must be taken to avoid detrimentally affecting brain maturation, as early chronic intranasal administration apparently reduces oxytocin receptor expression and social behavior in normal mice (*8*). An intermittent oxytocin treatment regimen may be preferable over chronic exposure (*9*).

Whether a compromised oxytocin system contributes to ASDs is unclear. A meta-analysis found that variation in the oxytocin receptor gene associates with ASD (*10*), although individual studies fail to report associations (*11*, *12*). Rather, it appears that variation in the oxytocin system contributes to social phenotypes, regardless of diagnosis. Blood oxytocin concentration and oxytocin receptor genotype strongly associate with social cognition but not with ASD diagnosis, which suggests that circulating oxytocin and oxytocin receptor sequence may be useful biomarkers to identify individuals most responsive to oxytocin therapies (*12*). The heterogeneity of ASD makes identification of therapies based on diagnoses difficult. That oxytocin was effective in *Cntnap2* mutant mice with compromised oxytocin signaling does not imply that oxytocin will be effective for all ASD populations.

"...approaches to target ... oxytocin... will hopefully lead to improving social function in ASD..."

The U.S. National Institute of Mental Health (NIMH) is encouraging a classification system based on Research Domain Criteria, which stratifies clinical populations based on behavioral dimensions and biological mechanisms. NIMH is also requiring evidence of target engagement for clinical trial funding involving oxytocin. As an example, oxytocin improved social emotion detection in ASD males and modulated activity in the brain's insular cortex, thus demonstrating a functional impact on an impaired neural system (*13*). Incorporating these suggestions will likely lead to improved oxytocin-based therapies in ASD.

Silvio O. Conte Center for Oxytocin and Social Cognition, Department of Psychiatry, Yerkes National Primate Research Center, Emory University, Atlanta, GA 30329, USA. E-mail: lyoun03@emory.edu

Efficient brain penetration and activation of oxytocin receptors throughout the social neural network, as occurs after endogenous oxytocin release, is potentially an important limitation to the current oxytocin therapies. The next generation of therapeutics may bypass this obstacle (*14*). Pharmacologically enhancing endogenous oxytocin release, or developing small-molecule agonists and positive allosteric modulators, may be most effective for engaging the brain's natural oxytocin system to improve social cognition. For example, acute melanocortin-4 receptor (MC4R) agonist treatment potentiates oxytocin release in brain reward centers (including the ventral striatum) and facilitates oxytocin-mediated social attachment in voles (*14*). Activating MC4Rs during the first postnatal week enhances later social relationships in these animals as well (*15*). Acute stimulation of MC4R also rescues social deficits in the *Cntnap2* mutant mouse (*2*). Further, social impairment in this mouse model was rescued by a gene therapy strategy involving the expression of designer receptors exclusively activated by designer drugs (DREADDs) in oxytocin neurons, an approach that may one day be feasible in humans.

Oxytocin remains an exciting target for improving social function. However, investigations into its potential therapeutic application are still in the early stages. Some would argue that the therapeutic value of intranasal oxytocin remains tenuous. Indeed, there are insufficient data for physicians to prescribe oxytocin to patients or for parents to seek oxytocin for their autistic child. Nonetheless, increasing information on mechanisms from animal studies, optimizing current therapeutic paradigms, and developing next-generation approaches to target the oxytocin system will hopefully lead to improving social function in ASD and other psychiatric disorders. ■

REFERENCES

1. E. Anagnostou *et al.*, *Brain Res.* **1580**, 188 (2014).
2. O. Peñagarikano *et al.*, *Sci. Transl. Med.* **7**, 271ra8 (2015).
3. A. J. Guastella *et al.*, *J. Child Psychol. Psychiatry* 10.1111/jcpp.12305 (2014).
4. S. M. Freeman, K. Inoue, A. L. Smith, M. M. Goodman, L. J. Young, *Psychoneuroendocrinology* **45**, 128 (2014).
5. S. F. Owen *et al.*, *Nature* **500**, 458 (2013).
6. I. Gordon *et al.*, *Proc. Natl. Acad. Sci. U.S.A.* **110**, 20953 (2013).
7. R. Tyzio *et al.*, *Science* **343**, 675 (2014).
8. H. Huang *et al.*, *Neuropsychopharmacology* **39**, 1102 (2014).
9. B. L. Teng *et al.*, *Neuropharmacology* **72**, 187 (2013).
10. D. LoParo, I. D. Waldman, *Mol. Psychiatry* 10.1038/mp.2014.77 (2014).
11. D. H. Skuse *et al.*, *Proc. Natl. Acad. Sci. U.S.A.* **111**, 1987 (2014).
12. K. J. Parker *et al.*, *Proc. Natl. Acad. Sci. U.S.A.* **111**, 12258 (2014).
13. Y. Aoki *et al.*, *Brain* **137**, 3073 (2014).
14. M. E. Modi *et al.*, *Neuropsychopharmacology* 10.1038/npp.2015.35 (2015).
15. C. E. Barrett *et al.*, *Neuropharmacology* **85**, 357 (2014).

10.1126/science.aaa8120

CELL BIOLOGY

Pancreas micromanages autophagy

Nutrient-sensing β cells degrade insulin when blood glucose is low

By **Guy A. Rutter**

Cells need to find ways of surviving when times are hard. One way of dealing with nutrient scarcity is to digest intracellular constituents, providing a source of amino acids that can be used to synthesize proteins that are essential for survival (*1*). This process of autophagy (*2*), however, poses a problem for the body's specialized fuel-sensing cells. β cells within the pancreatic islet respond to blood glucose concentration—when it rises after a meal, these cells release insulin; otherwise, under basal conditions (between meals), the cells are in a "starvation"-like state (*3*). So how do they maintain a normal turnover of intracellular components during this metabolic deprivation? Why don't they eat themselves as other cells would? At the very least, autophagy under basal conditions could compromise the ability to respond optimally to fluctuations in blood glucose, posing a health risk. On page 878 of this issue, Goginashvili *et al.* (*4*) show how β cells avoid inappropriate autophagy, and describe a form of this process tailored to the needs of these cells.

Classical autophagy is a complex process regulated by multiple mechanisms. In starvation, the ratio of adenosine triphosphate (ATP) to adenosine diphosphate (ADP) falls, as does the ratio of ATP to adenosine monophosphate (AMP). These changes stimulate AMP-activated protein kinase (AMPK) (*5*) and a downstream signaling pathway that eventually inhibits mechanistic target of rapamycin complex 1 (mTORC1) (*6*). The outcome is the activation of autophagy. Most cells, however, usually maintain a high ATP/ADP ratio such that autophagy is suppressed most of the time.

Autophagy has an important role to play in replacing exhausted cellular components, such as mitochondria and other membrane-bound organelles. Previous studies have shown that maintaining minimal levels of autophagy is important

Downloaded from www.sciencemag.org on February 21, 2015

Published by AAAS

in β cells because deletion of the gene encoding autophagy-related 7 (*Atg7*), required for autophagy, in these cells leads to diabetes in the mouse (*7*, *8*). Thus, it has been assumed that β cells, like other cell types, use "classical" autophagy (or "crinophagy") to degrade aging insulin-containing secretory granules, and that this process maintains stable insulin levels (*9*). Goginashvili *et al.* suggest that a separate process—or at least a process that is controlled separately from classical autophagy—plays a dominant role in β cells (see the figure).

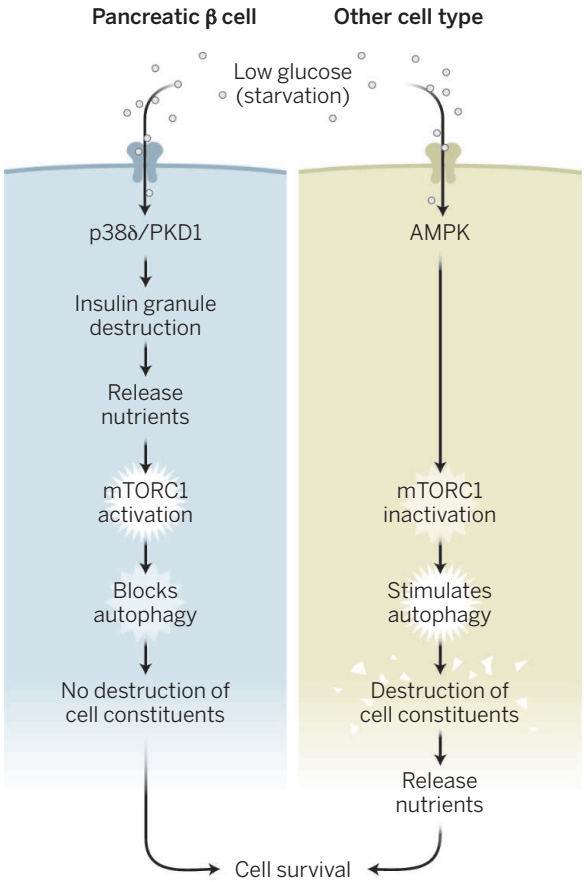
Remarkably, and in contrast to non–nutrient-sensing cells (including human embryonic kidney cells and plasma cells), for β cells, starvation produces a decrease in the usual indices of autophagy, notably the incorporation of microtubule-associated protein 1 light chain 3B into membranes. Instead, Goginashvili *et al.* observed a different form of autophagy by which insulin-containing granules (and not other organelles) are preferentially degraded by lysosomes at low extracellular glucose concentrations. The authors call this process starvation-induced nascent granule degradation (SINGD). Here, the released amino acids resulting from the destruction of insulin granules in the cell's lysosomes activate mTORC1, which translocates to lysosomal membranes and suppresses wmore general cellular autophagy. Thus, a highly localized change in an intracellular metabolic signal, as previously seen in β cells (*10*), controls the ultimate fate of both newly synthesized insulin and other cellular constituents to ensure that insulin granule turnover occurs without jeopardizing other organelles.

This mechanism may also provide a means of ensuring that when blood glucose concentration is low, key fuel sensing systems in the β cell—notably mitochondrial metabolism—are not activated (to synthesize ATP) by the released amino acids. In this way, the closure of ATP-sensitive K^+ channels at the cell surface, membrane depolarization, and the activation of calcium influx into the cell (*3*)—a cascade that triggers insulin release—is avoided.

Given the existence of such a complex and finely balanced system, it should be no surprise that interference with autophagy or SINGD has deleterious consequences for regulated insulin secretion. Indeed, insulin release increased at low glucose concentration in the presence of the mTORC1 inhibitor rapamycin, or an artificial autophagy activator, tat-beclin1. These findings show the importance of suppressing autophagy under starvation conditions.

How is the balance of SINGD and autophagy controlled at the molecular level? Goginashvili *et al.* implicate protein kinase D1 (PKD1) in the control of SINGD. PKD1 is thought to regulate insulin release (*11*). Thus, inactivation of the enzyme p38δ, which phosphorylates and inactivates PKD1, decreased SINGD, but increased classical autophagy in mouse β cells.

How exactly are autophagy and enhanced insulin release related? Using diazoxide, a compound that prevents cell depolarization and calcium influx, Goginashvili *et al.* show that a catastrophic event such as cell death and lysis (which would allow insulin to leach out of the cell) is unlikely to be the explanation for enhanced insulin secretion when autophagy is activated. Likewise, this suggests that insulin is not mistargeted toward the constitutive secretory pathway under these conditions, instead of being packaged into mature secretory granules.



Autophagy or not? Under low glucose conditions (starvation), the degradation of insulin granules in β cells leads to the production of amino acids, the local activation of mTORC1, and suppression of autophagy, which removes a signal for insulin release and ensures cell survival. In non–nutrient-sensing cells, the same condition activates autophagy to ensure survival.

The findings of Goginashvili *et al.* provide an answer to interesting conundrums, including the observation that genetic deletion of AMPK (or the upstream kinase liver kinase B1) has relatively minor effects on autophagy in β cells (*12*). However, that the stimulation of autophagy activates insulin release still leaves many questions to be answered. Is this simply a result of increasing the number of secretory granules, or is their localization with respect to the plasma membrane (where they fuse to release insulin) also changed? Are other "triggering" signals for secretion (e.g., ATP/ADP, intracellular calcium concentration, etc.) also elevated? It is also not clear how p38δ, and therefore PKD1, are regulated by nutrients.

The global health care burden of diabetes is hard to overestimate, with >380 million individuals currently affected worldwide (*13*) and a cost to the taxpayer in the United States alone of ~$250 billion per year (*14*). The incidence of the disease is predicted to rise to >500 million by 2035, with most new cases due to type 2 diabetes. The study of Goginashvili *et al.* suggests that pharmacological activation of classical autophagy in β cells is likely to be problematic or even dangerous, as it is likely to enhance secretion when blood glucose concentration is low and thus run the risk of hypoglycemia. On the other hand, the identification of SINGD and its regulation by PKD1 may provide a useful therapeutic target to improve insulin release in some settings. ■

Section of Cell Biology and Functional Genomics, Division of Diabetes, Endocrinology and Metabolism, Imperial College London, Hammersmith Hospital, London W12 0NN, UK. E-mail: g.rutter@imperial.ac.uk

ILLUSTRATION: V. ALTOUNIAN/*SCIENCE*

REFERENCES

1. D. G. Hardie, *Science* **331**, 410 (2011).
2. S. L. Clark Jr., *J. Biophys. Biochem. Cytol.* **3**, 349 (1957).
3. G. A. Rutter, T. J. Pullen, D. J. Hodson, A. Martinez-Sanchez, *Biochem. J.* **66**, 202 (2015).
4. A. Goginashvili *et al.*, *Science* **347**, 878 (2015).
5. G. A. Rutter, G. da Silva Xavier, I. Leclerc, *Biochem. J.* **375**, 1 (2003).
6. K. Inoki, T. Zhu, K. L. Guan, *Cell* **115**, 577 (2003).
7. C. Ebato *et al.*, *Cell Metab.* **8**, 325 (2008).
8. H. S. Jung *et al.*, *Cell Metab.* **8**, 318 (2008).
9. B. J. Marsh *et al.*, *Mol. Endocrinol.* **21**, 2255 (2007).
10. H. J. Kennedy *et al.*, *J. Biol. Chem.* **274**, 13281 (1999).
11. G. Sumara *et al.*, *Cell* **136**, 235 (2009).
12. M. Kone *et al.*, *FASEB J.* **28**, 4972 (2014).
13. L. Guariguata *et al.*, *Diabetes Res. Clin. Pract.* **103**, 137 (2014).
14. American Diabetes Association, *Diabetes Care* **36**, 1033 (2013).

10.1126/science.aaa6810

Published by AAAS

OPTICS

Structured photons take it slow

Specially prepared single photons travel below the "speed of light," even in vacuum

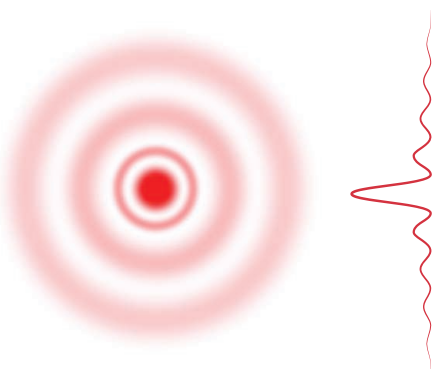
By **J. R. Sambles**

Light may behave both as a particle and as a wave. Newton conjectured the particle aspects and observed wave aspects ("Newton's rings"). Young showed wave interference in his double-slit experiments, and Einstein formulated light as particles (photons) to explain the photoelectric effect. This dual description leads to two different speeds for light: the wave speed, which for a plane wave in vacuum is the now fixed constant, c; and the particle or "group" speed at which energy or information propagates, which can be less than c—even zero, in some cases. On page 857 of this issue, Giovannini *et al.* (*1*) convincingly show that individual photons can have a speed less than c. In order to show this, the individual photons were prepared with transverse structure, so they cannot be represented as truly plane waves.

Although this result is surprising for light at high frequencies (the optical regime), it is known for light at low frequencies (the electromagnetic regime). For example, microwaves in a hollow metallic waveguide can have a group speed that ranges from zero at the cutoff frequency of the waveguide to c as the frequency is raised. Simplistically, one might argue that the photons zigzag along the guide, and their forward progress is slower than if they were simply plane waves traveling along the guide. At the lowest acceptable frequency, they bounce back and forth at right angles to the guide, so the group speed is zero at this cutoff frequency.

An alternative viewpoint is that the zigzagging waves interfere with each other and create a transverse standing wave that has lateral structure and a transverse wave vector. To maintain the total wave vector of the photons, defined by their frequency, the wave vector in the direction along the guide has to decrease or the effective wavelength along the guide has to increase. At the cutoff frequency, the effective wavelength tends to infinity. This increase in wavelength along the guide enhances the effective phase (wave) speed of the photons to infinity at the cutoff. As the frequency is increased, the phase speed reduces to c. The product of the phase speed with the group speed must equal c^2, so the group speed is reduced.

From either viewpoint, this reduced group speed is caused by the photons having lateral structure within the waveguide (quantized lateral wave vector). Thus, any free-space photons with lateral structure should travel slower than c. In the study by Giovannini *et al.*, this lateral structure is in the form of Bessel or Gaussian profile beams, and the photons so structured are slowed. One could reasonably argue that this result is so blatantly obvious that there was no need to undertake the experiment, but it appears that no one had established this with single photons in the optical regime. Subtle changes in speed have been previously studied with Bessel beams (*2*–*5*). However, these studies used light pulses (bundles of photons), and arguments then abound. Where does one measure a pulse? Where does it start and end?



Radial structure. A plane-wave photon travels at c in vacuum, but one with transverse structure, such as a Bessel beam (shown as a radial color map on the left and an intensity cross section on the right), slows down slightly.

The elegant experiment of Giovannini *et al.* avoids such controversy by determining the different times taken for two individual coprepared photons to travel different pathways. One photon is laterally structured, and the other has as little lateral structure as possible. The reduced particle (group) speed of the laterally structured photons can then be well quantified. The nonlinear optical process of down-conversion simultaneously creates pairs of photons of the same frequency at a point in space. One of the photons travels on a path containing a reflective device (a spatial light modulator) that creates lateral structure (either a Bessel beam, shown in the figure, or a Gaussian beam). The other travels with as little lateral structure as possible. The arrival of both photons was determined at a single detector.

By adjusting the path length of one route, the authors establish precisely the condition when the two photons arrive simultaneously using Hong-Ou-Mandel interference (*6*). The spatial precision was better than 0.07 μm, equivalent to a temporal resolution of 0.2 fs. The slowing of the structured photons is precisely established by measuring the required path-length change to bring the two photons into coincidence compared with the distance required when both are largely unstructured. For the Bessel beam having an angle of 0.0045 rad, they measure a distance of the delay of 7.7 μm (26 fs), well beyond any measurement uncertainty, corresponding to a drop in speed of ~0.001%. For the focused photons, they record similar changes.

The consequences of this result are quite broad. First, all photons come from finite-sized sources (often single atoms), so one might ask if photons are ever truly plane waves. Surely they always have lateral structure, and thus can never really travel at c. Second, even plane-wave photons must somehow converge onto detectors of finite extent, so again the measured light speed would be less than c. Only spherical electromagnetic waves or true plane waves can ever travel at c. However, spherical waves cannot be generated from dipolar sources, and because the universe is finite in extent, there can be no true planar waves, so in principle no light ever travels at c. However, the lateral structure is normally so minor that measurements of c will not be significantly in error.

One might wonder if there are any implications for the early universe, when light may have been in highly entangled states with appreciable transverse structure and then may not have traveled at c. Or one might consider a situation where there is simultaneous cocreation of light and low-mass particles. Is it possible for the particles to arrive sooner than the light because they had lateral (Gaussian) character? Finally, if photons with lateral structure travel at less than c, what about gravitons, and are there any implications? ■

School of Physics and Astronomy, University of Exeter, Exeter EX4 4QL UK. E-mail: j.r.Sambles@exeter.ac.uk

REFERENCES

1. D. Giovannini *et al.*, *Science* **347**, 857 (2015).
2. D. Mugnai *et al.*, *Phys. Rev. Lett.* **84**, 4830 (2000).
3. I. Alexeev *et al.*, *Phys. Rev. Lett.* **88**, 073901 (2002).
4. P. W. Milonni, *J. Phys. B* **35**, R31 (2002).
5. K. B. Kuntz *et al.*, *Phys. Rev. A* **79**, 043802 (2009).
6. C. K. Hong *et al.*, *Phys. Rev. Lett.* **59**, 2044 (1987).

10.1126/science.aaa6931

IMAGE: ADAPTED FROM EGMASON/WIKIMEDIA COMMONS

Downloaded from www.sciencemag.org on February 21, 2015

Published by AAAS

CHEMISTRY

Climbing Jacob's ladder

Protein design enables the stabilization of a transient molecular state

By **David K. Romney** *and* **Scott J. Miller**

The description of the potential energy surface of a single bond rotation is a standard concept for understanding chemical reactions and molecular motions (*1*). The energetic progression around a single bond in biphenyl (see the first figure) (*2*) provides an illustration. An entire conformational energy landscape can be captured with a simple reaction coordinate diagram or multidimensional potential energy surface (*3*). On page 863 of this issue, Pearson *et al.* describe a way to trap and observe an otherwise fleeting state at a rarified elevation of the conformational energy landscape (*4*).

It can be very difficult to observe the high-energy states along a complex trajectory. Ultrafast spectroscopy provides one lens with which to see fleeting high-energy states (*5*), but many other techniques require more stable structures. If a molecular host can be made to stabilize a transition state, numerous other analytical techniques, such as x-ray crystallography, become available for detailed observation. Pearson *et al.* now combine different approaches to artificial protein design to stabilize a high-energy state of a simple but dynamic molecule. Their success is attributable to the creative combination of computational design, the use of an amino acid not found in natural proteins, and the iterative synthesis and crystallographic evaluation of candidate structures.

The fundamental question posed by Pearson *et al.* is whether the packing forces of a protein can distort intrinsic bond rotations in a molecule to such an extent that an apparent bond-rotational transition state geometry may be observed. Using biphenyl as the substructure to address this question, the authors show the answer to be a resounding "yes." But several hurdles had to be overcome to reach this conclusion. First, biphenyl is not found in extant proteins. The authors accomplished its incorporation into a host protein through the insertion of the nonproteinogenic amino acid biphenylalanine using the amber suppressor tRNA/aminoacyl-tRNA synthetase pair method (*6*). Second, the choice of a host protein and, perhaps more importantly, its required alteration were not straightforward. The authors used the computational protein design program Rosetta to craft the protein environment surrounding the biphenyl (*7*).

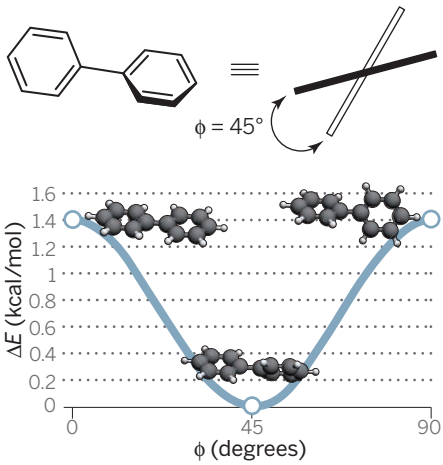
Through several iterative rounds of design and analysis, Pearson *et al.* collected data sets that showed increasingly distorted biphenyl rings, with dihedral angles nearing 0°. Computational design, synthesis, and measurement, informed by visual inspection of the computational and crystallographic output, finally led to the targeted protein. Designated BIF_0, it contains a biphenyl moiety in the recesses of the protein coat, with its two phenyl rings essentially coplanar (see the second figure).

This observation is remarkable. One can certainly mine the Protein Data Bank to capture higher-energy states for rotations about various types of bonds that depart from their lowest-energy minima and approach higher-energy local maxima (*8*), but chemical intuition suggests that the observation of a planar biphenyl requires extraordinary circumstances. The rational design and synthesis of this state in a protein host marks a singular achievement in molecular design.

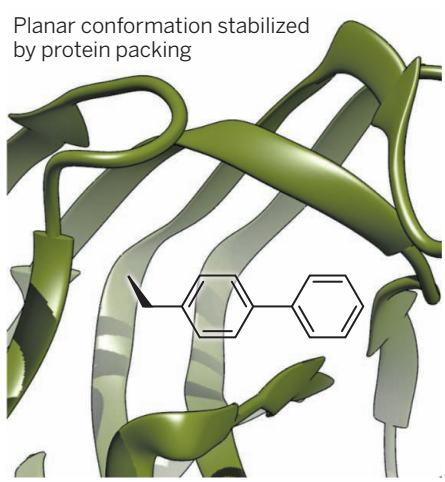
The results illustrate the value of protein hosts for facilitating observation of otherwise fleeting molecular events. The observation of features of catalyst-substrate complex in a carrier protein provides another example (*9*); other studies will surely follow. A particularly notable connection made by Pearson *et al.* is the possible analogy to transition state stabilization in enzyme catalysis. The suggestion recalls the Pauling paradigm for enzymatic rate acceleration, which calls for the complementarity of an enzyme's active site to the transition state structure of the catalyzed reaction (*10*).

There is no doubt that Pearson *et al.* have observed a substructure that exhibits features of the biphenyl bond rotational transition state. A careful energetic balancing act is required to stabilize such a high-energy state in a large molecule. Its persistence is particularly notable given the sum of the energetic compensations required to capture it. However, biphenyl has a relatively low barrier to rotation; one challenge in the future will be to apply the approach to the stabilization of even higher-energy structures.

The present accomplishment illustrates the precision with which proteins may be designed for functional purposes with computational methods. Lessons learned here could well portend applications in protein and enzyme engineering. The assembly of a unique ladder to climb, and the sight to behold at its top rung, tell of much more to see in the future. ■



Transient state. Molecules interconvert between low-energy conformations by passing through transient high-energy states. Biphenyl is at a stable energy minimum when the rings are offset by 45° and a transient energy maximum when the rings are offset by 0° or 90°.



Stabilizing an energy maximum. Pearson *et al.* show that a carefully designed protein environment enables observation of a biphenyl moiety in a conformation with essentially coplanar rings.

Department of Chemistry, Yale University, New Haven, CT 06520, USA. E-mail: scott.miller@yale.edu

REFERENCES

1. J. D. Kemp, K. S. Pitzer, *J. Chem. Phys.* **4**, 749 (1936).
2. A. Almenningen *et al.*, *J. Mol. Struct.* **128**, 59 (1985).
3. E. V. Anslyn, D. A. Dougherty, in *Modern Physical Organic Chemistry*, E. V. Anslyn, D. A. Dougherty, Eds. (University Science Books, Sausalito, CA, 2006), pp. 365–373.
4. A. D. Pearson *et al.*, *Science* **347**, 863 (2015).
5. J. C. Polanyi, A. H. Zewail, *Acc. Chem. Res.* **28**, 119 (1995).
6. L. Wang, A. Brock, B. Herberich, P. G. Schultz, *Science* **292**, 498 (2001).
7. A. Zanghellini *et al.*, *Protein Sci.* **15**, 2785 (2006).
8. A. A. Kossiakoff, S. Shteyn, *Nature* **311**, 582 (1984).
9. S. Han, B. V. Le, H. S. Hajare, R. H. Baxter, S. J. Miller, *J. Org. Chem.* **79**, 8550 (2014).
10. L. Pauling, *Nature* **161**, 707 (1948).

10.1126/science.aaa5623

Published by AAAS

Downloaded from www.sciencemag.org on February 21, 2015

GEOPHYSICS

Coping with earthquakes induced by fluid injection

Hazard may be reduced by managing injection activities

By **A. McGarr,[1]* B. Bekins,[2] N. Burkardt,[3] J. Dewey,[4] P. Earle,[4] W. Ellsworth,[1] S. Ge,[5] S. Hickman,[1] A. Holland,[6] E. Majer,[7] J. Rubinstein,[1] A. Sheehan[5]**

Large areas of the United States long considered geologically stable with little or no detected seismicity have recently become seismically active. The increase in earthquake activity began in the mid-continent starting in 2001 (*1*) and has continued to rise. In 2014, the rate of occurrence of earthquakes with magnitudes (*M*) of 3 and greater in Oklahoma exceeded that in California (see the figure). This elevated activity includes larger earthquakes, several with $M > 5$, that have caused significant damage (*2*, *3*).

POLICY

To a large extent, the increasing rate of earthquakes in the mid-continent is due to fluid-injection activities used in modern energy production (*1*, *4*, *5*). We explore potential avenues for mitigating effects of induced seismicity. Although the United States is our focus here, Canada, China, the UK, and others confront similar problems associated with oil and gas production, whereas quakes induced by geothermal activities affect Switzerland, Germany, and others.

These injection activities include (i) disposal of wastewater by injection into deep formations; (ii) injection of water or CO_2 into depleted reservoirs for enhanced oil recovery (EOR); (iii) hydraulic fracturing (fracking) to enable production of oil and gas from low-permeability reservoirs; (iv) injection of supercritical CO_2 into deep formations for permanent carbon capture and storage (CCS); and (v) injection into geothermal reservoirs to replenish water lost to steam production or to develop enhanced geothermal systems (EGS).

Although only a small fraction of disposal wells have been associated with induced earthquakes large enough to be felt, there are so many disposal wells that this contributes significantly to the total seismic hazard, at least in the mid-continent (*1*, *2*, *6*). EOR has been associated with earthquakes as large as *M*4.5, but felt earthquakes are rare (*7*). For the most part, fracking induces only micro-earthquakes (too small to be felt), although there have been a few felt earthquakes (*8*). CCS may pose future seismic hazards (*9*), but few projects are under way, and the largest earthquakes have been too small to be felt at the surface. Geothermal fields and EGS sites are few in number and, within the United States, limited to western states where earthquakes up to *M*4.6 have been associated with geothermal production (*10*).

Wastewater injection directly into the crystalline basement has induced earthquakes of particular notoriety [e.g., in the Denver region during the 1960s (*11*)]. EGS case histories (e.g., the Deep Heat Mining Project in Basel, Switzerland) show that injection of water into crystalline basement is likely to result in significant earthquake response (*10*, *12*).

> ***"Developing a hazard model for earthquakes induced by industrial activities is key to determining effective ways to mitigate their damaging effects."***

Most disposal wells inject not into basement but into sedimentary layers of high permeability and porosity, targeted because of their ability to accept fluid, with little or no earthquake response (*13*). For some cases, however, effects of fluid injection were not confined to the target formation but were communicated to greater depth along a preexisting fault, as evidenced by earthquake locations in the basement (*14*) and simulated by numerical modeling (*15*).

Large volumes of injected wastewater may be required for an earthquake response that includes events large enough to be felt, or even damaging (*5*). The magnitudes of the largest induced earthquakes in some sequences correlate with the volume of injected fluid. Nonetheless, there is debate as to whether injected volume is the key factor that limits maximum magnitude (*6*) or whether it is controlled by the size of a nearby fault and its relation to the contemporaneous stress state, as is the case for natural earthquakes. Although faults evidently play at least several possible roles that affect the likelihood of inducing felt earthquakes, most of these faults are only detected when they are imaged by well-located induced earthquakes (*3*, *14*).

SEISMIC HAZARD MODELS. The long-term (50-year) model for seismic hazard in the United States, which sets design provisions in building codes, intentionally excludes, as much as possible, contributions from induced earthquakes (*16*). Developing a corresponding model for earthquakes induced by industrial activities is key to determining effective ways to mitigate their damaging effects. But to do so requires taking account of some essential differences between induced and natural seismicity.

Natural seismicity is usually assumed to be independent of time in assessing its hazard. Seismicity induced by fluid injection, in contrast, varies with time, often because of changes in injection rate. When a project is terminated, the rate of induced earthquakes diminishes with time, often in an irregular way (*11*). The spatial distribution of injection also changes as oil and gas production declines in one region and increases in another. These realities rule out simply combining induced and natural earthquake sources to develop a model for setting seismic safety provisions for new construction, the traditional application of the hazard model. Instead, a separate 1-year hazard model for induced earthquakes is being developed and will be updated frequently (*17*).

Thus, it is important to be able to determine whether an earthquake sequence was induced or natural, so as to avoid inappropriate earthquake input to either hazard model. This is not always straightforward. Induced and natural earthquakes appear similar when observed on seismograms. If an injection activity and an earthquake sequence correlate in space and time, with no known previous earthquake activity in the area, the earthquakes were likely induced (*11*, *18*). Some sequences are more challenging. There may be a lengthy delay between the start of injection and the first detected earthquakes or an offset of many kilometers between the injection site and earthquakes (*5*). Adding to the difficulties are enigmatic

[1]U.S. Geological Survey (USGS), Earthquake Science Center, Menlo Park, CA 94025, USA. *E-mail: mcgarr@usgs.gov [2]USGS, National Water Quality Assessment Program, Menlo Park, CA 94025, USA. [3]USGS, Powell Center, Fort Collins, CO 80526, USA. [4]USGS, Geologic Hazards Center, Golden, CO 80225, USA. [5]University of Colorado at Boulder, Boulder, CO 80302, USA. [6]Oklahoma Geological Survey, Norman, OK 73069, USA. [7]Lawrence Berkeley National Laboratory, Berkeley, CA, USA.

Published by AAAS

Downloaded from www.sciencemag.org on February 21, 2015

swarms of natural tectonic earthquakes unrelated to fluid injection (*19*). Novel approaches for addressing these challenges are being tested; for instance, analysis of earthquake rate changes has revealed systematic differences between natural and induced earthquake sequences (*20*).

REDUCING HAZARD, MITIGATING RISK. The general public is the most important stakeholder because they may be exposed to potential injury and damage. Organizations with more specific roles and stakes in mitigating impacts of induced seismicity include (i) oil and gas producers, wastewater disposers, and geothermal energy providers; (ii) land-management, regulatory, and permitting agencies (federal, state, and local); (iii) emergency managers and responders; (iv) building owners, insurers, and mortgage holders; and (v) scientists in the research community investigating induced seismicity.

The U.S. Environmental Protection Agency has federal responsibility for regulating wastewater disposal wells, but in most cases permitting authority has been delegated to state agencies. These agencies, federal and state, work with constituents to add or modify regulations or practices regarding the possibility of induced seismicity from fluid injection. Research agencies such as the U.S. and state geological surveys have operational roles in monitoring seismicity and may also be responsible for assessing associated seismic hazard.

Actions may be directed toward reducing the hazard, which is not possible for natural earthquakes, or reducing the risk (hazard times consequences). For instance, risk can be reduced for new injection projects by siting them away from population centers or critical facilities for which the largest, but lowest-probability, earthquakes are of greatest concern.

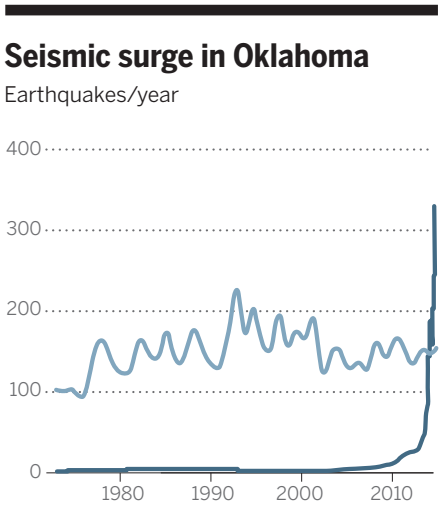
The possibility of reducing the hazard of induced earthquakes has policy implications inasmuch as stakeholders are in a position to balance economic benefits of energy production activities against costs incurred owing to the increase in hazard. This cost-benefit analysis is rarely straightforward because benefits, mostly economic, are geographically diffuse, whereas hazardous effects are localized to the environs of the injection wells. Moreover, if an induced earthquake sequence results in damage, then blame can be assigned with legal implications for liability (*21*). The question of whether an earthquake sequence was induced or natural is of more than academic interest.

The importance of seismic monitoring cannot be overstated. The current detection threshold within most of the contiguous United States is *M*3. For adequate monitoring of the hazard from fluid-induced earthquakes, it would be advisable to augment the national network to detect and locate events with significantly lower magnitudes (e.g., as low as 2 or less) to identify seismic hazards in time to take corrective actions while the problems are still manageable. For instance, a seismic network capable of precise locations of small earthquakes could reveal the presence of a large, possibly dangerous, fault being reactivated due to fluid injection (*14*). Information of this sort might prove invaluable for avoiding a damaging earthquake.

Local seismic networks are the main components of "traffic light" systems (*12*, *22*), which have been useful for reducing the hazard of induced earthquakes. These systems set magnitude thresholds that, if exceeded, result in adjustments to injection operations so as to avoid inducing earthquakes of greater consequence. Such a network was deployed near Greeley, Colorado, in 2014 by seismologists from the University of Colorado, following a felt earthquake in the vicinity of a wastewater disposal well. Based on seismic data from his network, the Colorado Oil and Gas Conservation Commission required the operator to modify disposal rates and depths in response to an earthquake located near the well (*23*).

Traffic light systems, and other approaches to hazard reduction based on seismic network data, are most effective during early stages of an injection project. The possibility of controlling seismic hazard diminishes as the pore pressure effects migrate away from the injection interval and become less amenable to control from the wellhead (*11*).

For purposes of transparency and avoiding public distrust, it is important to put the results of these seismic network operations into the public domain in near real time. Even if a network is owned and operated by industry, regulators must ensure that seismic data are not withheld from the public. Similarly, making injection data, such as daily injection rates, wellhead pressures, depth of the injection interval, and properties of the target formation, publicly accessible can be invaluable for attaining a better understanding of fluid-induced earthquakes. Open sharing of data can benefit all stakeholders, including industry, by enabling the research needed to develop more effective techniques for reducing the seismic hazard. ■



Annual rate of earthquake sequences with at least one $M \geq 3$ earthquake in California (light blue) and Oklahoma (dark blue) since 1973. (Based on USGS earthquake catalog data from http://.earthquake.usgs.gov.)

REFERENCES AND NOTES

1. W. L. Ellsworth, *Science* **341**, 1225942 (2013).
2. K. M. Keranen *et al.*, *Geology* **2013**, G34045 (2013).
3. J. L. Rubinstein, W. L. Ellsworth, A. McGarr, H. M. Benz, *Bull. Seismol. Soc. Am.* **104**, 2162 (2014).
4. C. Frohlich, *Proc. Natl. Acad. Sci. U.S.A.* **109**, 13934 (2012).
5. K. M. Keranen, M. Weingarten, G. A. Abers, B. A. Bekins, S. Ge, *Science* **345**, 448 (2014).
6. A. McGarr, *J. Geophys. Res.* **119**, 1008 (2014).
7. W. Gan, C. Frohlich, *Proc. Natl. Acad. Sci. U.S.A.* **110**, 18786 (2013).
8. A. Holland, *Bull. Seismol. Soc. Am.* **103**, 1784 (2013).
9. M. D. Zoback, S. M. Gorelick, *Proc. Natl. Acad. Sci. U.S.A.* **109**, 10164 (2012).
10. E. L. Majer *et al.*, *Geothermics* **36**, 185 (2007).
11. J. H. Healy, W. W. Rubey, D. T. Griggs, C. B. Raleigh, *Science* **161**, 1301 (1968).
12. N. Deichmann, D. Giardini, *Seismol. Res. Lett.* **80**, 784 (2009).
13. M. K. Hubbert, W. W. Rubey, *Geol. Soc. Am. Bull.* **70**, 115 (1959).
14. S. Horton, *Seismol. Res. Lett.* **83**, 250 (2012).
15. Y. Zhang *et al.*, *Ground Water* **51**, 525 (2013).
16. M. D. Petersen *et al.*, Documentation for the 2014 update of the United States national seismic hazard maps, Open-File Report 2014-1091 (USGS, 2014). http://pubs.usgs.gov/of/2014/1091
17. J. L. Rubinstein *et al.*, Quantifying the Seismic Hazard from Natural and Induced Earthquakes, American Geophysical Union Fall Meeting Abstract (2013). http://abstractsearch.agu.org/meetings/2013/FM/sections/S/sessions/S32C/abstracts/S32C-05.html
18. S. Davis, C. Frohlich, *Seismol. Res. Lett.* **64**, 207 (1993).
19. L. C. Haar *et al.*, *Bull. Seismol. Soc. Am.* **74**, 2463 (1984).
20. A. L. Llenos, A. J. Michael, *Bull. Seismol. Soc. Am.* **103**, 2850 (2013).
21. D. A. Cypser, S. D. Davis, *J. Environ. Law Litigation* **9**, 551 (1994).
22. M. D. Zoback, *Earth Magazine* **57**, 38 (2012).
23. T. Sperry, "After second Greeley earthquake, COGCC orders halt of nearby wastewater injection well," *Greeley Tribune*, 24 June 2014; www.greeleytribune.com/news/11957606-113/injection-cogcc-release-wells

ACKNOWLEDGMENTS

This article is a contribution of the USGS's John Wesley Powell Center Working Group on Understanding Fluid Injection Induced Seismicity. We thank W. Leith, D. W. Duncan, M. Diggles, and K. Knudsen for helpful suggestions.

10.1126/science.aaa0494

Published by AAAS

BOOKS *et al.*

PHILOSOPHY OF SCIENCE

The meaning of microbes

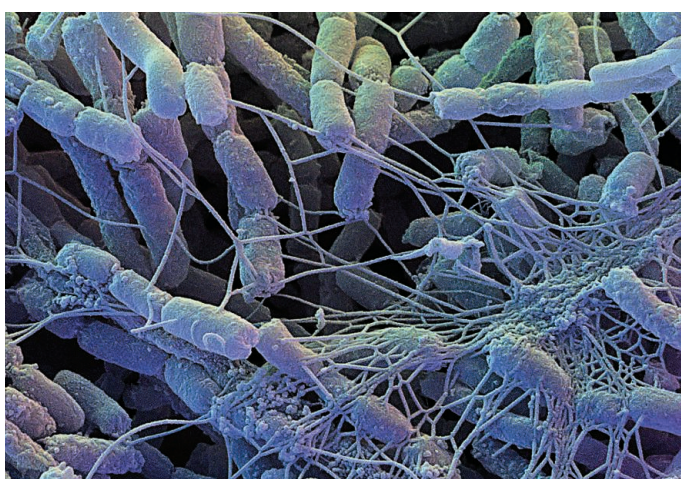
Microorganisms may offer unique insights into the nature and evolution of life

By **Adrian Woolfson**

The American philosopher of popular culture known to the music world as "Madonna" once concluded that "we are living in a material world." In *Philosophy of Microbiology*, Maureen A. O'Malley, a philosopher of biology, authoritatively sets the issue straight, arguing that we are in fact living in a microbial world and that a realization of this will change the way we perceive biological phenomena and the manner in which they are investigated.

To date, the study of microbes has not specifically been identified as having the potential to make unique contributions to the philosophy of biology, but significant advances in this field in recent years may make this a timely moment to consider it as a discrete instrument for empiric philosophical explorations. Laying the ground for her analysis, O'Malley makes a case for the special significance of microbes by describing four of their unique features: their biomass and diversity, ability to impact planetary processes, influence on the major evolutionary transitions, and tendency to coexist in mutually beneficial relationships with other organisms. But while of undeniable importance, will this expanded knowledge of microbes affect the central issues of the philosophy of biology?

From the perspective of prevalence, O'Malley informs us that human life on Earth is an irrelevant detail, thereby debunking another myth of popular culture: that size matters. A mere teaspoon of soil, we learn, contains more microbes than there are humans inhabiting the entire subcontinent of Africa. Microbes account for more than 90% of the biomass of oceans, and upwards of 80 million of them migrate between participants during an intimate kiss. These tenacious critters may be found floating in the stratosphere 50 kilometers above Earth's surface and as uninvited passengers in the capsules we discharge into space. They linger in the depths of oceans, thrive in hot springs, flourish in brine, and vacation at the frozen poles. They live inside us, forming a microbiome, and their mitochondrial endosymbiont remnants power our cells. If there is life on other planets, O'Malley argues, it is likely to be microbial. They unhinge human civilizations through sickness and plagues and generate spores that may lie dormant for millions of years. They facilitated some of the major evolutionary events by oxidizing Earth's atmosphere 2.4 billion years ago and helped form the cellular soup that gave rise to the metazoan body plan. Their protean metabolisms ferment wine, assist with breadmaking, and fix the nitrogen needed to synthesize RNA, DNA, and proteins. Their ubiquitous nature and numerical dominance argue for the importance of their contribution in any overarching philosophical analysis of biological systems.



Known for giving soil its "earthy" odor, *Streptomyces* (shown here) also produce clinically useful antibiotics.

O'Malley begins by outlining some of the core microbiological topics that may inform philosophical debates. These include the role of microbes in photosynthesis, their effects on the major transitions of evolution, and the existence of magnetotactic bacteria that align with Earth's geomagnetic field. The latter have provided philosophy-of-mind debates with a rudimentary example of organismal representation and intentionality.

Microbial classification systems have influenced those of multicellular organisms, and the extensive cooperation between microbes has provided a unique perspective on the "units of selection" debate. Other features, including their generalized capacity for hypermutability and the phenomenon of endosymbiosis, provide some support for O'Malley's assertion that microbes may not always be readily accommodated by the modern evolutionary synthesis.

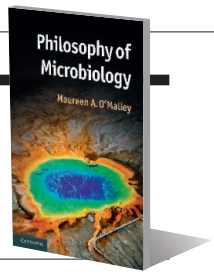
In her strongest and most ambitious moments, O'Malley imaginatively argues that the lateral exchange of genetic material between bacteria implies a communal mode of genetic ownership, suggesting that the historical focus on single organisms has overlooked an ecological, coevolutionary perspective.

The use of microbes to study evolution experimentally has allowed some of the key philosophical conundrums resulting from the incomplete fossil record to be played out on compressed time scales. These artificial replays of the tape of life are the most concrete example of how the study of microbes may affect philosophical issues, as they have shown that rather than being open-ended, the products of evolution are in some instances highly constrained.

It was the informational simplicity of microbes that accelerated the science of genomics, facilitated the sequencing of the first genome, and opened the door for the synthesis of the first artificial one. It is this aspect of microbes that is perhaps the most philosophically compelling, but one to which the book gives scant attention.

In the end, however, O'Malley succeeds in convincing us that the microbial world is a tractable treasure trove of unexplored philosophical potential that may serve as a heuristic for the macroworld we inhabit. Microbes are not the poor cousins of the dazzling multicellular world but key facilitators of biological complexity. It may indeed be time to take these little critters more seriously and to define the steps necessary to safeguard the invisible microbial universe underpinning our tenuous existence.

10.1126/science.aaa3119



Philosophy of Microbiology
Maureen A. O'Malley
Cambridge University Press, 2014. 279 pp.

The reviewer is the author of An Intelligent Person's Guide to Genetics *(Overlook, New York, 2006). E-mail: adrianwoolfson@yahoo.com*

IMAGE: DAVID SCHARF/SCIENCE SOURCE

Published by AAAS

SCIENCE LIVES

Physicist. Defector. Spy?

A closer look at the enigmatic life of Bruno Pontecorvo

By **Alex Wellerstein**

In late July of 1950, the physicist Bruno Pontecorvo and his family left the United Kingdom to take a relaxing, well-deserved vacation through France, Switzerland, and Italy. All seemed well—until suddenly, it didn't. On 24 August, Pontecorvo missed an arranged meeting with his parents and the next day sent a strange, contradictory telegram that made little sense to them. Instead of returning to England, the Pontecorvos took a flight to Sweden, paid for with a large sum of American currency, and then traveled to Helsinki. From there, they vanished without a message or a trace. It would be 5 years before the world learned where they had gone: the Soviet Union.

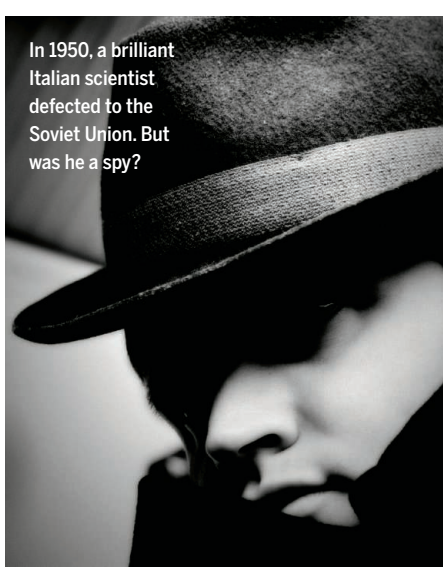
Pontecorvo's defection has long been mentioned in the same breath as known Soviet spies including Klaus Fuchs, Alan Nunn May, and Kim Philby. And yet, there is still considerable ambiguity about whether he was, in fact, a spy. Until recently, the literature on this has been remarkably thin, consisting mainly of unsubstantiated claims by intelligence officers (both Soviet and Anglo-American).

Published in 2012, Simone Turchetti's *The Pontecorvo Affair* was the first major academic study of Pontecorvo and focused primarily on the reaction of British and American authorities to his defection (*1*). Frank Close's *Half-Life* is more of a general biography of Pontecorvo, one simultaneously personal, political, and scientific. Close, a physicist and historian, has taken full advantage of the work of Turchetti and pushed it into some further, deeper areas as well, anchoring the narrative in archival discoveries, personal connections, and interviews.

Bruno Pontecorvo was the youngest member of the Italian physicist Enrico Fermi's famous "Via Panisperna Boys," whose experiments in the 1930s served as the foundation for many of the advances in nuclear physics that eventually led to the development of the atomic bomb. Fermi was not generally heavy on praise, but he once described Pontecorvo as "scientifically one of the brightest men with whom I have come in contact in my scientific career" (*2*).

Displaced from Italy during World War II, Pontecorvo found employment in Europe and North America, working with the physicist Frédéric Joliot-Curie in France, helping to develop a novel means of oil prospecting in the United States, and contributing to the design of the NRX heavy-water reactor in Montreal as part of the Anglo-Canadian portion of the Manhattan Project. He made major contributions to the study of neutrinos, and their possible detection, among other work. Close argues that he could have been one of the great scientists of the 20th century—had he not fled to the USSR, where his work and personal life were strongly constrained.

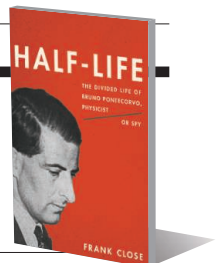
There is no concrete evidence that Pontecorvo was ever a clandestine Soviet agent. At most, it has been established that he had long been a card-carrying Communist who had joined the party immediately after the Nazi-Soviet Nonaggression Pact was established—a sign of a true believer. He does not appear in any decrypted documents or messages in the U.S. counterintelligence "Venona Project," and no other spies ever persuasively named him as a collaborator. (Some memoirs of ex-KGB members have lumped him in with other spies, but these have a feeling of unreliability about them. In one, his code name is listed as MLAD, but we now know definitively that this was a different scientist spy, Theodore Hall.)



In 1950, a brilliant Italian scientist defected to the Soviet Union. But was he a spy?

PHOTO: DUNCAN1890/ISTOCKPHOTO.COM

The reviewer is at the College of Arts and Letters, Stevens Institute of Technology, Hoboken, NJ 07030, USA. E-mail: wellerstein@gmail.com



Half-Life
The Divided Life of Bruno Pontecorvo, Physicist or Spy
Frank Close
Basic Books, 2015. 398 pp.

Despite the lack of definitive proof, Close ultimately concludes that Pontecorvo was, in all likelihood, some kind of spy, citing the fact that someone gave the Soviets the blueprints for the NRX reactor and offering reasons to exclude other, known spies. Pontecorvo himself was conspicuously quiet about the topic, even when he was allowed to speak publicly. Although it is not possible to say for certain whether Pontecorvo committed explicit acts of espionage, Close has found some evidence that he was probably of value to the Soviets, in particular with regard to prospecting (the Soviets were low on uranium reserves) and reactor shielding.

As for the timing of Pontecorvo's defection, Close makes a plausible case that Kim Philby—a high-ranking member of the British intelligence agency MI6 and double agent—may have interpreted some vague inquiries from the FBI as evidence that Pontecorvo was about to be outed as a Soviet spy. In reality, the FBI had almost nothing on Pontecorvo, but Philby would not have known that. Close speculates that someone got in touch with Pontecorvo midvacation, and, fearing imminent arrest, he made the decision to defect. Given his convictions about communism, it is possible that he could have been convinced to defect even if he hadn't yet committed any acts of espionage.

In the end, Close argues that if Pontecorvo was a spy, he paid dearly for it. On arrival, he found himself under house arrest, not even able to be referred to by his true name (he was known only as "the professor" for years). His scientific work suffered, and even after he was allowed to reveal his location, his travel (and that of his family) was harshly constricted, and he found that his old colleagues in the West regarded him icily.

Pontecorvo's mystery and tragic arc bring to mind several protagonists from the novels of John le Carré. Like Pontecorvo, le Carré's spies have nothing of James Bond to them, are riddled with all-too-human character flaws, and always inadvertently seal their own melancholic fates.

REFERENCES

1. S. Turchetti, *The Pontecorvo Affair* (University of Chicago, Chicago, 2012).
2. Enrico Fermi to Brien McMahon (13 March 1951), National Archives and Records Administration, Records of the Joint Committee on Atomic Energy, RG 128, Unclassified General Subjects, Box 316.

10.1126/science.aaa3654

Downloaded from www.sciencemag.org on February 21, 2015

Published by AAAS

LETTERS

Edited by **Jennifer Sills**

Editorial retraction

ON 27 JUNE 2014, *Science* published an Editorial Expression of Concern about the Report "Unclicking the click: Mechanically facilitated 1,3-dipolar cycloreversions" by J. N. Brantley *et al.* (*1*). After concerns were raised in an e-mail to the editors from a reader, the corresponding author supervised a comprehensive evaluation of all data presented in the original manuscript by tracing all figures back to their raw data files. In over 50% of the figure parts, the authors deemed the data unreliable due to uncertainty regarding the origin of data or the manner in which the data were processed. The University of Texas at Austin conducted a confidential investigation and shared the conclusion that scientific misconduct had occurred, but provided no further detail of the nature of the misconduct. After the conclusion of the investigation, authors Bielawski and Brantley volunteered to withdraw the paper; it has not been possible to contact author Wiggins. *Science* is therefore retracting the paper.

Marcia McNutt

Editor-in-Chief

REFERENCE

1. J. N. Brantley, K. M. Wiggins, C. W. Bielawski, *Science* **333**, 1606 (2011).

PETA fuels animal lab improvements

I READ D. GRIMM'S News Feature about People for the Ethical Treatment of Animals' (PETA's) campaigns to expose and end animal research ("The insurgent," 23 January, p. 366) with interest. Since its inception in 1980, PETA has decried animal research based on its cruelty, as well as its inapplicability to human illnesses. Thirty-five years later, there is overwhelming scientific evidence showing how much animals suffer in labs, that the results generally fail to translate to people, and that alternatives are often more effective. This has helped move PETA's criticism of animal research from the street, to the boardroom, to Capitol Hill, and even to AAAS's own annual conference.

In my work, the important shift we've seen from crude animal-based labs to sophisticated simulation for medical training has certainly been fueled in part by



Targeting animal research, for better or worse.

animal welfare concerns from PETA and others. I applaud *Science* for giving voice to a group that deserves credit from the biomedical research community for its successful work to improve the lives of animals and push science forward. I look forward to a time when both community scientists and PETA researchers can share a collective conversation about the best ways to advance knowledge in a responsible manner.

John Pawlowski

Division of Thoracic Anesthesia, Beth Israel Deaconess Medical Center, Boston, MA 02215, USA; and Principles of Pharmacology, Harvard Medical School, Boston, MA 02215, USA. E-mail: jpawlows@bidmc.harvard.edu

PETA undermines science and scientists

ON BEHALF OF THE National Association for Biomedical Research and our more than 360 institutional members nationwide, I write to express concerns regarding the News Feature "The insurgent" (23 January, p. 366), in which D. Grimm profiled Justin Goodman of People for the Ethical Treatment of Animals (PETA). The article devotes the majority of its space to what easily could be interpreted as an endorsement of Goodman and PETA.

PETA is an organization that has long been publicly opposed to the use of animals in biomedical research. Goodman, a well-known animal rights activist, has made clear his personal mission of vilifying research. An online article by PETA promoting Goodman's actions refers to biomedical research facilities as "torture chambers" and notes that he has organized campaigns to end research with nonhuman primates, even going so far as to chain himself to an iron fence at the University of Connecticut's 125th anniversary celebration in protest (*1*). Goodman and PETA were also permitted to present a poster at last year's AAAS Annual Meeting in Chicago, where they cited data that the number of Americans believing that ethical animal research is "morally wrong" was on the rise (*2*).

For years, many biomedical researchers, their staff, and their families have been egregiously targeted by PETA and understandably are demoralized. It is shocking that *Science* would take the time and effort to highlight and chronicle the sentiments of someone whose sole mission is to derail biomedical research that is dependent on animal models.

Frankie L. Trull

National Association for Biomedical Research, Washington, DC 20005, USA. E-mail: ftrull@nabr.org

REFERENCES

1. Peta2, Justin Goodman: Exposing the Torture Chamber (www.peta2.com/heroes/justin-goodman/).
2. EurekAlert, "New study shows growing opposition to animal tests" (www.eurekalert.org/pub_releases/2014-02/pfte-nss021314.php).

Enforcement key to China's environment

ON 1 JANUARY 2015, China formally began implementing its revised Environmental Protection Law (EPL). The new EPL offers some hope for sustainable development in China, but its potential may be limited if local governments continue to focus on the economy.

Since the first EPL in 1989, China has become the largest emitter of carbon dioxide (*1*). After many calls for its revision (*2*), the new EPL, which was finalized in April 2014 (*3*), includes substantial amendments (*4*). Caps on penalties have been lifted, the "per day calculation" for pollution fines should increase punishments, and some NGOs will be able to bring lawsuits against polluters. An ecological "red line" will define areas requiring special protection from, for example, urban smog.

The new EPL looks good on paper, but it remains to be seen how local environmental protection bureaus will use it. Local bureaus have often attempted to reconcile conflicting goals of economic development and environmental protection (*5*). The situation is exacerbated by overlapping responsibilities of local governments and the Ministry of Environmental Protection. Environmental responsibilities scattered across different ministries and agencies further weaken EPL enforcement (*6*).

Application of environmental laws in rural, less developed areas has been much weaker than in cities (*5*). Because of protests by middle-class city dwellers, factories have relocated to rural middle and western China (*7*, *8*), causing serious

PHOTO: © ZOO ATLANTA/SPLASH NEWS/CORBIS

Downloaded from www.sciencemag.org on February 21, 2015

Published by AAAS

environmental degradation. This includes major water pollution within Inner Mongolia's deserts (*9*). Strengthening EPL enforcement in these areas is essential to avoid the spread of contamination.

The potential for environmental litigation is still limited. Only the largest NGOs will be able to initiate lawsuits, with only around 300 qualifying (*10*). Provisions for lawsuits against environmental enforcement authorities remain unclear.

The Chinese Premier has declared "war on pollution." The new EPL provides weapons for this war, but their effectiveness will depend on enforcement, particularly in China's developing regions.

Hong Yang,[1]* Xianjin Huang,[2]* Julian R. Thompson,[3] Roger J. Flower[3]

[1]CEES, Department of Biosciences, University of Oslo, Blindern, 0316, Oslo, Norway. [2]School of Geographic and Oceanographic Science, Xianlin Campus, Nanjing University, Nanjing, 210023, China. [3]Wetland Research Unit/Environmental Change Research Centre, UCL Department of Geography, University College London, London, WC1E 6BT, UK.

*Corresponding authors. E-mail: hongyanghy@gmail.com (H.Y.); hxj369@nju.edu.cn (X.H.)

REFERENCES

1. PBL Netherlands Environmental Assessment Agency, Trends in Global CO_2 Emissions 2013 Report (2014); http://edgar.jrc.ec.europa.eu/news_docs/pbl-2013-trends-in-global-co2-emissions-2013-report-1148.pdf
2. G. Z. He, L. Zhang, A. P. J. Mol, Y. L. Lu, J. G. Liu, *Science* **341**, 133 (2013).
3. H. Yang, *Nature* **509**, 535 (2014).
4. The National People's Congress of the People's Republic of China, Environmental Protection Law of the People's Republic of China (2014); www.npc.gov.cn/huiyi/lfzt/hjbhfxzaca/2014-04/25/content_1861320.htm [in Chinese].
5. G. Kostka, "Barriers to the implementation of environmental policies at the local level in China," World Bank Policy Research Working Paper (World Bank, Berlin, 2014).
6. J. G. Liu, W. Yang, *Science* **337**, 649 (2012).
7. H. Yang, R. J. Flower, J. R. Thompson, *Nature* **490**, 342 (2012).
8. H. Yang, X. Huang, J. R. Thompson, R. J. Flower, *Science* **344**, 691 (2014).
9. S. Huan, Water pollution in N. China desert kills thousands of birds (2014); www.ecns.cn/cns-wire/2014/09-12/134208.shtml.
10. J. Y. Hsu, *Geogr. Compass* **8**, 98 (2014).

TECHNICAL COMMENT ABSTRACTS

Comment on "Late Pleistocene human skeleton and mtDNA link Paleoamericans and modern Native Americans"

Kay Prüfer and Matthias Meyer

Chatters *et al.* (Reports, 16 May 2014, p. 750) reported the retrieval of DNA sequences from a 12,000- to 13,000-year-old human tooth discovered in an underwater cave in Mexico's Yucatan peninsula. They propose that this ancient human individual's mitochondrial DNA (mtDNA) belongs to haplogroup D1. However, our analysis of postmortem damage patterns finds no evidence for an ancient origin of these sequences.

Full text at http://dx.doi.org/10.1126/science.1260617

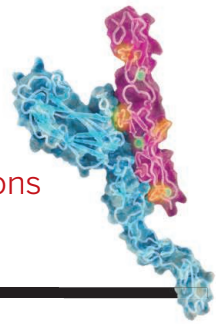
Response to Comment on "Late Pleistocene human skeleton and mtDNA link Paleoamericans and modern Native Americans"

Brian M. Kemp, John Lindo, Deborah A. Bolnick, Ripan S. Malhi, James C. Chatters

Prüfer and Meyer raise concerns over the mitochondrial DNA (mtDNA) results we reported for the Hoyo Negro individual, citing failure of a portion of these data to conform to their expectations of ancient DNA (aDNA). Because damage patterns in aDNA vary, outright rejection of our findings on this basis is unwarranted, especially in light of our other observations.

Full text at http://dx.doi.org/10.1126/science.1261188

RESEARCH



Bound sugars increase the flexibility of Notch interactions

Luca et al., *p. 847*

IN *SCIENCE* JOURNALS

Edited by **Stella Hurtley**



Marine mammals such as this manatee have evolved to be larger over time

ANIMAL EVOLUTION

Getting bigger all the time

In today's world, many animal species are large, with even larger species only recently extinct, but the first animals to evolve were tiny. Was this increase in size due to active selection or to some more random process? Heim *et al.* test the classic hypothesis known as Cope's rule, which posits that there is selection for increasing body size. They analyzed a data set that spans over 500 million years and includes more than 17,000 marine animal species. In support of Cope's rule, body volumes have increased by over five orders of magnitude since the first animals evolved. Furthermore, modeling suggests that such a massive increase could not have emerged from a random process. — SNV

Science, this issue p. 867

SPATIAL NAVIGATION

Are we heading in the right direction?

Some neurons, called grid cells, discharge at multiple locations to form a regular pattern that represents the animal's environment. These cells use information about the animal's running speed and direction of movement to constantly update its location. The so-called head direction cells provide the direction-of-movement signal. Winter *et al.* recorded neuronal activity in awake behaving rats. When they disabled the input from the head direction cells, the grid cells lost their normal function. These findings provide experimental confirmation of theoretical predictions that grid cells will no longer exhibit their characteristic firing pattern when the head direction signal is disturbed. — PRS

Science, this issue p. 870

GLOBAL FOOD SECURITY

China addresses food and environment security

Chinese leaders are addressing the difficult challenge of meeting growing demands to produce more food in sustainable ways. Lu *et al.* describe current air, water, and soil conditions in China, along with changing food security demands. They argue that national policies must rely on a science-based "ecological red line" that balances food security and safety with sustainable management of soil, air, water, and biodiversity resources. The scientific community will need to work with policy-makers to ensure that national, provincial, and local land-use practices are data-driven. Land-use programs should be created and enforced with long-term consequences in mind. — GEM

Science Advances 10.1126/sciadv.1400039 (2015).

KINASE DYNAMICS

Evolution of dynamics affects function

The drug Gleevac inhibits Abl kinases and is used to treat multiple cancers. The closely related Src kinases also play a role in cancer but are not inhibited effectively by Gleevac. Nevertheless, Gleevac-bound structures of Src and Abl are nearly identical. Based on this structural information and protein sequence data, Wilson *et al*. reconstructed the common ancestor of Src and Abl. Mutations that affected conformational dynamics caused Gleevac affinity to be gained on the evolutionary trajectory toward Abl and lost on the trajectory toward Src. — VV

Science, this issue p. 882

OPTICS

Slowing down light with added structure

We are taught that the speed of light in free space is one of the universal physical constants: *c*. Giovannini *et al*. now show that there are certain conditions under which such certainty can be broken (see the Perspective by Sambles). Adding spatial structure to an optical beam of single photons reduced the speed of light. The magnitude of the decrease depended on

Downloaded from www.sciencemag.org on February 21, 2015

CREDITS: (TOP TO BOTTOM) ERIC SMITH AND CHRIS GARCIA; © STEPHEN FRINK COLLECTION/ALAMY

Published by AAAS

the complexity of the structure imprinted onto the photons. — ISO

Science, this issue p. 857; see also p. 828

GALAXY EVOLUTION

Finding the necessary negative feedback

The evolution of galaxies seems to be tied to the growth of the supermassive black holes at their centers, but it's not entirely clear why. Models have suggested a mechanism in which the growth of the black hole results in an outflow of gas that interrupts star formation. However, evidence for enough of this negative feedback has been lacking. Nardini *et al*. now see a signature in x-ray spectra of a strong persistent outflow in the quasar PDS 456. They estimate a broad solid angle spanned by the wind that enables a far greater impact on the host galaxy than narrower jet outflows. — MMM

Science, this issue p. 860

PHOTOCHEMISTRY

The dark side of melanin exposed

Sun worshippers may have more to worry about than the DNA damage that occurs while they're relaxing on the beach. It seems that the DNA photoproducts responsible for cancer-causing mutations in skin cells continue to be generated for hours after sunlight exposure. Premi *et al*. find that a key mediator of this delayed damage is melanin, a pigment thought to protect against cancer (see the Perspective by Taylor). They propose a "chemiexcitation" model in which reactive oxygen and nitrogen species induced by ultraviolet light excite an electron in melanin fragments. This energy is then transferred to DNA, inducing the same damage as ultraviolet light, but in the dark. Conceivably, this energy could be dissipated by adding quenchers to sunscreens. — PAK

Science, this issue p. 842; see also p. 824

TRANSITION STATES

A transition state holds a pose

The transition state of a chemical transformation is inherently fleeting because the structure is high in energy. Nonetheless, Pearson *et al*. trapped a classical example of a bond rotation transition state using a modified protein (see the Perspective by Romney and Miller). The biphenyl molecule passes through an energy maximum when its rings rotate through a parallel position. A pocket within the editing domain of threonyl–transfer RNA synthetase was modified to stabilize parallel biphenyl rings, allowing further characterization of this normally transient structure. — PDS

Science, this issue p. 863; see also p. 829

CANCER

How Pez dispenses with metastasis

Tumor cells have greater numbers of growth-promoting receptors on their surface and release factors that promote metastasis. Belle *et al*. found that the protein tyrosine phosphatase PTPN14 (also called Pez) prevented receptors from moving to the cell surface and pro-metastatic factors from being released. Mice with breast cancer xenografts that lacked Pez had larger tumors and more metastases. — LKF

Sci. Signal. **8**, ra18 (2015).

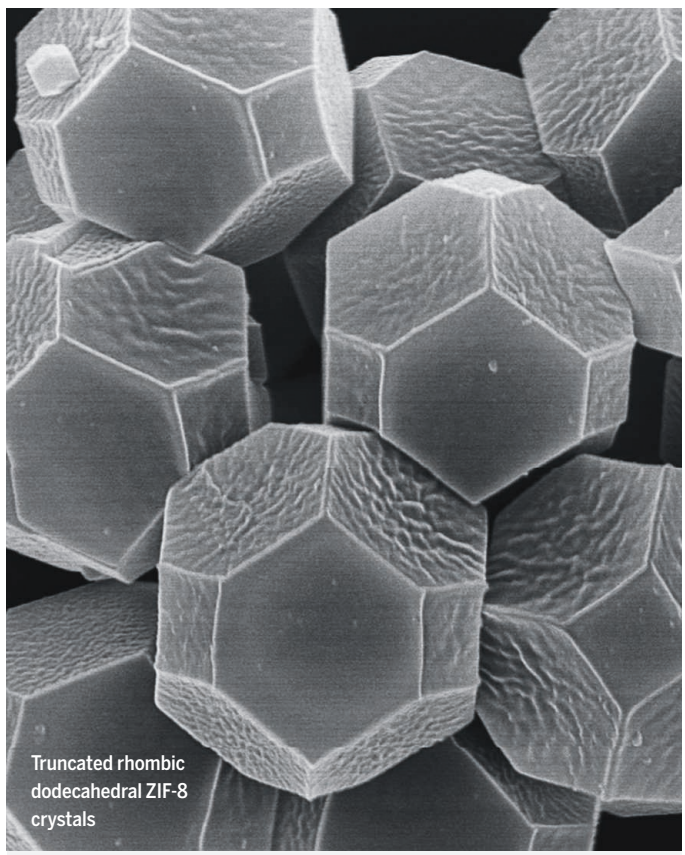


DNA damage can continue after sun exposure has ended

PHOTOS: (LEFT TO RIGHT) © KUTTIG - PEOPLE - 2/ALAMY; SU *ET AL. JOURNAL OF THE AMERICAN CHEMICAL SOCIETY* **137**, 5 (29 JANUARY 2015) © 2015 AMERICAN CHEMICAL SOCIETY

IN OTHER JOURNALS

Edited by **Sacha Vignieri** *and* **Jesse Smith**



Truncated rhombic dodecahedral ZIF-8 crystals

MATERIALS SCIENCE

Microporous mechanics

Metal-organic framework (MOF) materials, in which metal ions or inorganic clusters are linked together by organic ligands to form cages, are highly porous and potentially useful for gas storage. However, repeated cycles of adsorption and desorption mechanically stress these materials and reduce their functionality. With transmission electron microscopy, Su *et al*. examined the effects of compression on individual micrometer- and submicrometer-scale crystals of a zinc zeolitic-imidazolate framework compound. The presence of methanol in the pores made the crystals much more rigid; they shattered when similar forces would have caused only plastic deformation of the empty framework. — PDS

J. Am. Chem. Soc. 10.1021/ja5113436 (2015).

T CELL METABOLISM

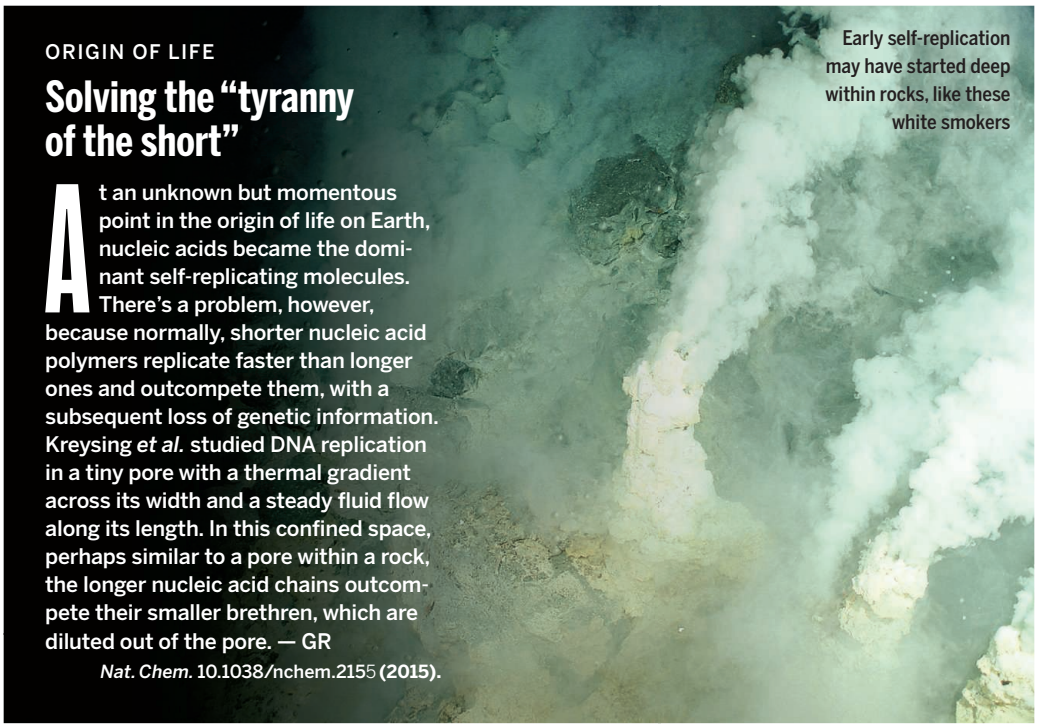
Flexibility lets activated T cells thrive

For T cells, fighting infections is demanding work. They must proliferate many times over and quickly produce a myriad of antimicrobial factors. T cells do this by switching from mitochondrial to glycolytic metabolism, but what happens when nutrients are scarce, such as in infected tissues or tumors? Blagih *et al*. examined this question by starving

Published by AAAS

ORIGIN OF LIFE

Solving the "tyranny of the short"



Early self-replication may have started deep within rocks, like these white smokers

At an unknown but momentous point in the origin of life on Earth, nucleic acids became the dominant self-replicating molecules. There's a problem, however, because normally, shorter nucleic acid polymers replicate faster than longer ones and outcompete them, with a subsequent loss of genetic information. Kreysing *et al.* studied DNA replication in a tiny pore with a thermal gradient across its width and a steady fluid flow along its length. In this confined space, perhaps similar to a pore within a rock, the longer nucleic acid chains outcompete their smaller brethren, which are diluted out of the pore. — GR

***Nat. Chem.* 10.1038/nchem.2155 (2015).**

mouse T cells of glucose. They found that T cells are highly adaptable—they pulled back on protein translation, used glutamine as an energy source, and relied more on mitochondrial metabolism. The enzyme AMPK, an evolutionarily conserved energy sensor, facilitated these changes. — KLM

Immunity **42**, 41 (2015).

GENOMICS

What are the genomic requirements for life?

To promote identification and understanding of the minimal set of genomic elements required for life, Lluch-Senar *et al*. studied *M. pneumonia*. This small bacterium has an 816-kb genome with about 700 open reading frames; about a third of the genome appeared to be essential. Small open reading frames, of less than 100 residues, made up slightly more than half of the essential components, and they appeared to encode components of larger protein, DNA, or RNA complexes. Protein domains, rather than complete proteins, were often the essential elements of larger proteins, whereas regulatory elements—5′ untranslated regions and noncoding RNAs—were also fundamental components. — LBR

Mol. Syst. Biol. 10.15252/msb.20145558 (2015).

CROWD SCIENCE

Wisdom of the crowd, waning

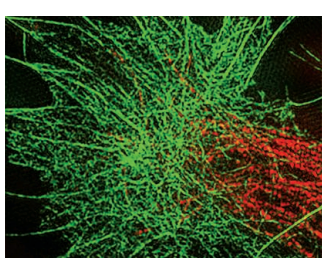
Many researchers, agencies, and companies are turning to "the crowd" for help with data collection and analysis, but we lack systematic understanding of who those volunteers are and how they perform. Such insights might help expand and improve crowd sourcing for research. Sauermann and Franzoni draw on over 12 million daily observations of more than 100,000 users across seven projects on the Zooniverse platform. They estimate that the average project received volunteer labor worth roughly $220,000 during the first 180 days. But 79% of the effort, on average, was provided by the most productive 10% of users. Roughly 75% of users failed to participate in a project after their first session, and even those who returned multiple times did so with increasingly long breaks between visits. Significant effort is expended by new users who join over time, but this does not offset the loss of effort from original users. — BW

Proc. Natl. Acad. Sci. U.S.A. 10.1073/pnas.1408907112 (2014).

NEURODEVELOPMENT

Growth cones carve a path through tissues

A growth cone leading a neuron's development needs more than muscle to push its way through tissues and across boundaries. Santiago-Medina *et al.* found features on neuronal growth cones that are like the invadosomes of immune and metastatic cancer cells, which themselves have a knack for squeezing through existing tissues. These invadosomes, fingers that poke out into the surrounding tissue, are packed with cytoskeleton and exude proteases that degrade the extracellular matrix. The invadosomes were key for Xenopus motoneurons trying to find a path out of the spinal cord and into the developing musculature. — PJH



Neural growth cones use invadopodia-like fingers to push through tissues

Development 10.1242/dev.108266 (2015).

PLANETARY SCIENCE

Why the "Y" in the Venusian sky?

Venus has its own version of Jupiter's Great Red Spot, an enormous Y-shaped feature which comes and goes on a monthly cycle. The origin and stability of the atmospheric feature, visible only in ultraviolet photographs, have perplexed observers for decades. Peralta *et al*. take a fresh look at this persistent structure with an updated analytic atmospheric model. A wind-distorted equatorial wave reproduces the morphology, darkness, and time evolution of the "Y." The model should be applicable to the atmospheres of other slowly rotating bodies, in our solar system and beyond. — BG

Geophys. Res. Lett. 10.1002/2014GL062280 (2014).

EVOLUTIONARY BIOLOGY

Finch genomes and human face shapes

The beak shapes of 15 Galápagos finch species, each optimized for its island's most ample food source, helped shape Charles Darwin's ideas on evolution. Now, scientists have a genetic link: Lamichhaney ***et al.*** sequenced the genomes of 120 individual birds and found a gene, *ALX1*, which varies between species with large or small, pointy or dull beaks. In humans, mutations in this gene are linked to frontonasal dysplasia, a birth defect ranging in severity from a cleft palate to skull malformations. Smaller variations in *ALX1* could be behind the diversity of our face shapes. — SW

Nature 10.1038/nature14181 (2015).

PHOTOS: (TOP TO BOTTOM) NOAA; TIMOTHY GOMEZ

Published by AAAS

ALSO IN *SCIENCE* JOURNALS

Edited by **Stella Hurtley**

NANOMATERIALS

Valency and bonding on a larger scale

In molecular systems, valency describes the number of bonds an atom can make with its neighbors. Larger objects such as colloids can be linked together to make connected structures in which the number of connections, or valency, is controlled by the central object. Jones *et al*. review the two main approaches to creating stiff bonds, based on DNA-based materials synthesis. These approaches allow the construction of molecular-like objects from building blocks much larger than single atoms. — MSL

Science, this issue p. 840

DISEASE NETWORKS

A network approach to finding disease modules

Shared genes represent a powerful but limited representation of the mechanistic relationship between two diseases. However, the analysis of protein-protein interactions has been hampered by the incompleteness of interactome maps. Menche *et al*. formulated the mathematical conditions needed to allow a disease module (a localized region of connections between disease-related proteins) to be observed. Only diseases with data coverage that exceeds a specific threshold have identifiable disease modules. The network-based distance between two disease modules revealed that disease pairs that are predicted to have overlapping modules had statistically significant molecular similarity. These similarities encompassed their protein components, gene expression, symptoms, and morbidity. Molecular-level links between diseases lacking shared disease genes could also be identified. — BJ

Science, this issue p. 841

STRUCTURAL BIOLOGY

An interaction that guides cell fate

Notch signaling is important in cell fate determination in mammals. Signaling is initiated when the extracellular domain of the transmembrane Notch protein on one cell binds to a surface ligand on another cell. Luca *et al*. report the crystal structure of the interacting regions of Notch and the Delta-like ligand DLL-4. The Notch protein is modified by O-linked glycan addition, and this is required for signaling. The structure shows two interaction interfaces. A glycan anchors the less conserved interface, which potentially provides a flexible way of regulating Notch interactions during development. — VV

Science, this issue p. 847

QUANTUM ENGINEERING

A way to induce quantum stability

Dynamical systems, whether classical or quantum, usually require a method to stabilize performance and maintain the required state. For instance, communication between computers requires error correction codes to ensure that information is transferred correctly. In a quantum system, however, the very act of measuring it can perturb it. Leghtas *et al*. show that engineering the interaction between a quantum system and its environment can induce stability for the delicate quantum states, a process that could simplify quantum information processing. — ISO

Science, this issue p. 853

INSULIN GRANULES

Too hungry to eat, too hungry not to eat

Pancreatic beta cells, the source of insulin in response to food, employ an unusual mechanism to adapt to nutrient depletion. Goginashvili *et al*. found that starvation of beta cells induced selective degradation of newly formed insulin granules through their fusion with lysosomes, the cell's garbage disposal units (see the Perspective by Rutter). The nutrient sensor mTOR is recruited to these lysosomes, leading to its local activation and the suppression of autophagy—a process by which cells "eat" their own constituents. Protein kinase D, a major regulator of insulin granule biogenesis, controls this granule degradation in response to nutrient availability. Thus, unlike most other cells, autophagy is not the strategy of choice in beta cells to adapt to starvation. — SMH

Science, this issue p. 878; see also p. 826

DRUG MECHANISM

Drugs can compete for vitamin K

Patients on warfarin—a commonly prescribed anticoagulant—are warned against eating leafy greens because they harbor loads of vitamin K, which interferes with the drug's activity. Takada *et al.* now show that Niemann-Pick C1-like 1 (NPC1L1), a cholesterol transporter, complicates this picture even further through its role in vitamin K absorption. Warfarin activity was enhanced in animals taking the cholesterol-lowering drug ezetimibe, which acts on NPC1L1, because vitamin K was not absorbed properly. Giving the animals vitamin K returned warfarin activity to normal levels. In patients, too, the warfarin action was boosted when it was taken with ezetimibe. This drug-drug interaction is an important consideration when warfarin is prescribed to patients taking ezetimibe (or similar drugs that alter vitamin uptake). — MLF

Sci. Transl. Med. **7**, 275ra23 (2015).

EVOLUTIONARY ECOLOGY

Mother knows best

Dynamic natural environments are challenging places to start life. In many species, however, the environment the mother lives in can actually shape the environment in which her offspring grow. Such maternal effects facilitate the exchange of important environmental information across generations. Duckworth *et al*. show that a mother's physiological responses to her environment can convey more complex information than we thought (see the Perspective by Dantzer). Female western bluebirds deposit more androgens in their eggs when competition for nest sites increases. This results in more-aggressive male chicks that are more likely to move on and colonize new, less crowded habitats. — SNV

Science, this issue p. 875; see also p. 822

Published by AAAS

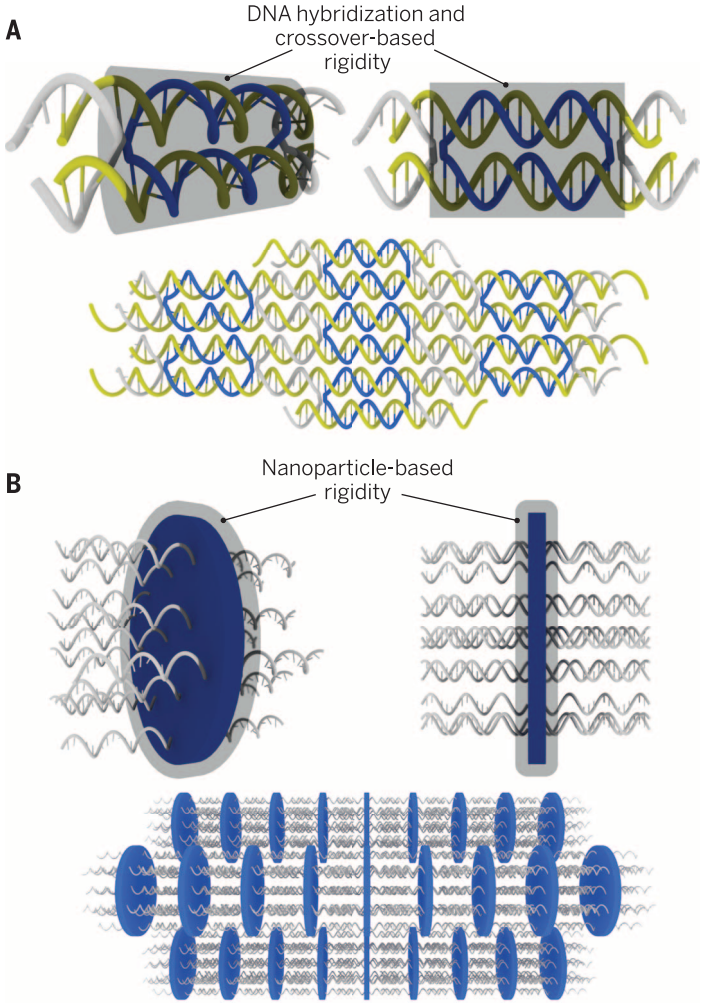
REVIEW SUMMARY

NANOMATERIALS

Programmable materials and the nature of the DNA bond

Matthew R. Jones, Nadrian C. Seeman,* Chad A. Mirkin*

BACKGROUND: Nucleic acids are ubiquitous in biology because of their ability to encode vast amounts of information via canonical Watson-Crick base-pairing interactions. With the advent of chemical methods to make synthetic oligonucleotides of an arbitrary sequence, researchers can program entire libraries of molecules with orthogonal interactions, directed to assemble in highly specific arrangements. Early attempts to use DNA to make nanostructures led to topologically defined architectures, but ones that were too conformationally flexible to be used to guide the construction of well-defined nanoscale materials from the bottom up. In this Review, we discuss the key discoveries that have overcome this limitation and distill common design principles that have since led to a revolution in materials sophistication based on DNA-directed assembly.



Differentiating nanoscale DNA bonds. (**A**) Multiple strand crossover events and DNA hybridization produce a conformationally constrained molecule with a rigid core. (**B**) A rigid nanoparticle acts as a scaffold for the immobilization and organization of DNA strands in a surface-normal direction.

ADVANCES: The experimental realization of DNA-based constructs that are sufficiently rigid so as to impart directionality to hybridization interactions marks a major milestone in the development of programmable materials assembly. This feat was accomplished simultaneously by the Mirkin Group and Seeman Group in 1996, but through chemically and conceptually distinct pathways. In one approach, rigidity is derived from multiple strand crossover events and the hybridization that stabilizes them to create a conformationally restricted DNA tile. In the other approach, a rigid non-nucleic acid–based nanoparticle (inorganic or organic) core acts as a template to organize functionalized DNA strands in a surface-normal orientation. It is appealing to draw the analogy between DNA-based constructs of this sort with the concepts of "bonds" and "valency" found in atomic systems. Just as understanding the nature of atomic bonding is crucial for chemists to manipulate the formation of molecular and supramolecular species, so too is an understanding of the nature of these DNA bonding modes necessary for nanoscientists to build complex and functional architectures to address materials needs.

ON OUR WEB SITE

Read the full article at http://dx.doi.org/10.1126/science.1260901

OUTLOOK: The interest in nanoscale materials constructed by using DNA bonds has continued to grow steadily, but has seen a noteworthy explosion in relevance over the past several years. This is due in large part to the development of methods to move beyond simple clusters and crystals to more sophisticated nanostructured materials that are dynamic and stimuli responsive, are macroscopic in spatial extent, and exhibit emergent physical properties that arise from specific arrangements of matter. These techniques offer perhaps the most versatile way of organizing optically active materials into architectures that exhibit unusual and deliberately tailorable plasmonic and photonic properties. In addition, prospects include the use of these materials in biological settings, being that they are constructed, in large measure, from nucleic acid precursors. The ability to manipulate gene expression, deliver molecular payloads via DNA-based binding events, and detect relevant markers of disease with nanoscale spatial resolution represent some of the most fruitful avenues of future research. ■

The list of author affiliations is available in the full article online.
*Corresponding author. E-mail: chadnano@northwestern.edu (C.A.M.); ned.seeman@nyu.edu (N.C.S.)
Cite this article as M. R. Jones *et al.*, *Science* **347**, 1260901 (2015). DOI: 10.1126/science.1260901

Downloaded from www.sciencemag.org on February 21, 2015

REVIEW

NANOMATERIALS

Programmable materials and the nature of the DNA bond

Matthew R. Jones,[1] Nadrian C. Seeman,[2]* Chad A. Mirkin[1,3]*

For over half a century, the biological roles of nucleic acids as catalytic enzymes, intracellular regulatory molecules, and the carriers of genetic information have been studied extensively. More recently, the sequence-specific binding properties of DNA have been exploited to direct the assembly of materials at the nanoscale. Integral to any methodology focused on assembling matter from smaller pieces is the idea that final structures have well-defined spacings, orientations, and stereo-relationships. This requirement can be met by using DNA-based constructs that present oriented nanoscale bonding elements from rigid core units. Here, we draw analogy between such building blocks and the familiar chemical concepts of "bonds" and "valency" and review two distinct but related strategies that have used this design principle in constructing new configurations of matter.

A grand challenge in the fields of chemistry and materials science is the ability to construct materials with absolute control over the placement of each component in order to tailor properties for a given application. Synthetic chemists regularly wield this degree of control over atoms by manipulating the formation of covalent bonds, and supramolecular chemists control the organization of larger molecular species through the manipulation of noncovalent interactions. A key requirement for these bonds is that their interactions be sufficiently directional so that the final arrangement and orientation of molecules may be predicted with reasonable accuracy (*1*, *2*). When this condition is not met—when interactions are conformationally flexible—it is difficult for a system to arrive at a singular thermodynamic product that is well-defined (for example, inherent nonuniformity found in polymer systems), and rational control over the final material is greatly diminished. The synthesis of nanomaterials and their assembly into larger well-defined architectures has conceptually similar goals. We foresee the recent advances in nanomaterials synthesis facilitated by DNA-based assembly processes as capable of one day producing a synthetic methodology that may rival, and in certain cases exceed, at the nanoscale what small-molecule chemists have achieved at the molecular scale (*3*, *4*). Therefore, we find it useful to explore the concepts of "valency" and the "bond" when applied to nanoscale building blocks whose interactions are governed by DNA hybridization.

Aside from their obvious role as carriers of genetic information, nucleic acids have also been used by biological systems to generate natural nanostructures such as ribozymes (*5*) and Holliday junctions (*6*) that serve crucial roles in a variety of cellular processes. Perhaps the most salient feature of DNA that can explain its versatility in biological settings is the specificity of canonical Watson-Crick base-pairing interactions (A-T and G-C). Permutation of the nucleobase sequence of particular DNA strands, even those that are relatively short, results in an enormous library of orthogonal interactions that can direct hybridization to occur with high selectivity and specificity.

The concept of controlled valency or directional DNA bonding in programmable materials synthesis can be traced to two seminal papers (*7*, *8*) and several patents (acknowledgements, this paper) published circa 1996 (Fig. 1). These examples were the first to use rigid nanoscale building materials that retained the tailorability of DNA-mediated interactions, as opposed to structures defined only by topology that were explored in early efforts to gain structural control with DNA (*9*). Although rigidity of a central building block is essential to the valency control in both of these approaches, they differ in how such rigidity is attained and the types of architectures one can envision and construct. The first methodology uses branched DNA architectures (molecules containing multiple crossover junctions between double helical domains) (*8*), which results in constructs that lacked the flexibility seen previously with only a single crossover junction (*2*, *10*, *11*) and form much of the basis for what is called "structural DNA nanotechnology" [Summary figure, (A)] (*12*). In this approach, carefully designed hybridization and intertwining of DNA strands create a rigid building block with programmable bonding characteristics and allow one to make functional architectures with well-defined geometries. Although these molecules, commonly known as DX tiles, were intriguing for a variety of fundamental reasons (*13*), it was the demonstration of their conformational rigidity (*8*) and later their assembly into large crystals (*14*) that proved their ability to function as two-dimensional (2D) nanoscale building blocks with programmable bonds.

The second approach introduced the concept of a programmable atom equivalent comprised of a rigid non-nucleic acid core, densely functionalized with a layer of highly oriented single strands of DNA (*7*). The valency in these structures, now termed spherical nucleic acids (SNAs) (*15*), is dictated by both the central particle and the dense loading of oligonucleotides on the surface of the structure [Summary figure, (B)]; crowding directs the oligonucleotide bonding elements and provides subnanometer control with respect to particle-particle binding events. They do not require hybridization to create a functional building block, and they permit building hybrid materials not attainable via the approaches that rely on nucleic acids to attain valency. Although the prototypical example was a spherical gold particle chemically functionalized with alkylthiol-modified DNA (*7*), there is now a large table of element equivalents consisting of particles that vary in size, composition, shape, and type of functionalized nucleic acid (*3*). With this approach, a number of assembled structures, first with short-range order (*16*, *17*) and ultimately with extended 3D periodicity (*18*, *19*), demonstrated the power of this nanoparticle building block to imbue DNA with bonding properties.

Contemporaneous with these aforementioned contributions to DNA valency, a more complete fundamental understanding of the thermodynamics of DNA hybridization allowed for quantitative predictions of duplex melting temperatures that included empirically relevant conditions such as sequence and salt dependencies (*20*). In addition, a number of important materials possessing only topological order were reported that used DNA to assemble proteins (*21*) and nanoparticles on discrete molecular templates (*22*). This approach was expanded by using organic molecules or transition metal complexes whose inherently well-defined bonding geometries allow for DNA hybridization events to be somewhat oriented in space (*23*, *24*). Although these structures do not present rigid DNA bonds and are not useful for programming the formation of macroscopic materials, they are valuable for labeling nucleic acid architectures and building certain molecular analogs to the 3D materials that are the focus of this manuscript.

The field of nucleic acid–guided programmable materials has been bifurcated into two subdivisions that achieve the goal of rigid, directional, DNA-based bonds through different fundamental chemical interactions: (i) the use of intricately woven oligonucleotides participating in hybridization to produce rigid architectures such as tiles and scaffolds, and (ii) the use of rigid nanoparticle cores, which act to template directional interactions on the basis of the core geometry (Fig. 1). We will commonly differentiate these methodologies by referring to each as "hybridization-based DNA bonds" or "nanoparticle-templated DNA bonds," respectively. These methods

[1]Department of Materials Science and Engineering, Northwestern University, Evanston, IL 60208, USA. [2]Department of Chemistry, New York University, New York, NY 10003, USA. [3]Department of Chemistry and International Institute for Nanotechnology, Northwestern University, Evanston, IL 60208, USA.
*Corresponding author. E-mail: chadnano@northwestern.edu (C.A.M.); ned.seeman@nyu.edu (N.C.S.)

represent contrasting but powerful approaches at manipulating matter at the nanoscale through DNA bonds and the principle of valency. Just as the character of different atomic bonds dictates the types of materials that can be constructed from atoms, each type of nanoscale building block presented here has distinct properties that allow access to different materials that are constructed using DNA.

Hybridization-based DNA bonds: Tiles

Some of the first DNA hybridization-based nanostructures used the principle of multiple crossover junctions to impart sufficient rigidity to achieve directional interactions [Summary figure, (A)]. Typically in these molecules, coplanar double helices—often called helical domains—contain two or more locations at which the component single strands switch their connectivity from one helix to the other (Fig. 2A) (*12*). Although there are numerous forms of these molecules, those used for construction typically have their crossovers formed between strands of opposite polarity. These crossover events between helical domains impart substantial structural rigidity by greatly reducing the number of possible conformations that still produce a hybridization-driven topology. Structures that have two helical domains and two crossover junctions between them are known as DX (double crossover) (*12*), and those that have three helical domains (often, but not necessarily coplanar) with two crossover junctions between each are known as TX (triple crossover) (*12*, *25*). The rigidity imparted by this strategy has been quantified through measurement of the persistence length of these molecules; DX structures have a persistence length that is roughly double that of an ordinary DNA duplex (*26*), whereas more complex analogs built of six helices surrounding a central vacancy rotated 120° from each other (*27*) have even larger values (*28*). Although the antiparallel and coplanar arrangement of DNA helices in these molecules roughly mimics a linear coordination geometry, because each helical domain can be terminated in a different sticky-end sequence, multicomponent systems of two to eight DX or TX molecules have been designed to tile in an alternating brickwork-like

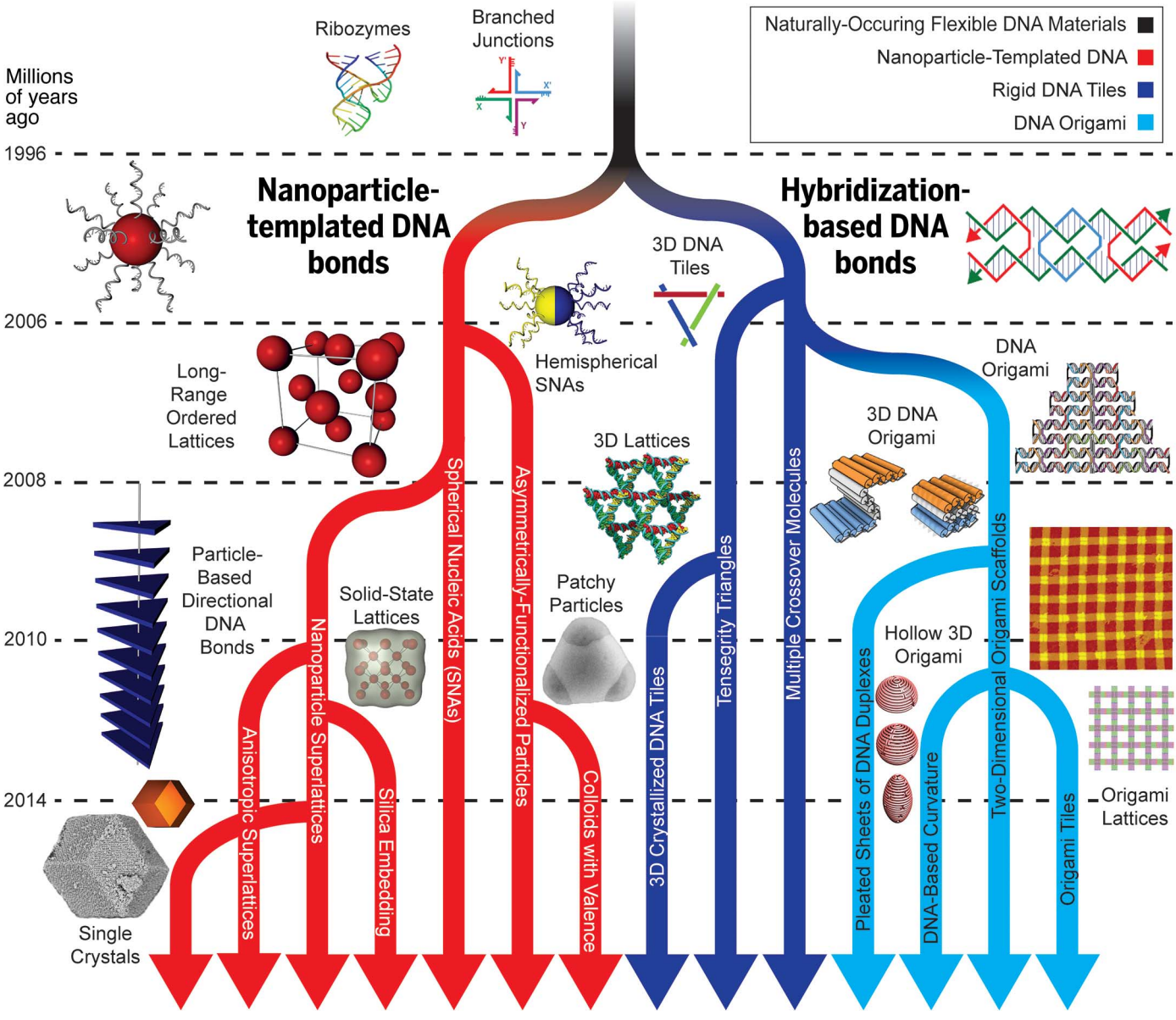


Fig. 1. The development of nanoscale DNA bonds. Although nature has provided several examples of evolutionarily selected DNA nanostructures, they are conformationally flexible and often do not result in well-defined thermodynamic products when used as building blocks for materials assembly. The development of rigid nanoscale constructs that present directional DNA hybridization interactions via two contrasting approaches in 1996 is largely responsible for the diversity of DNA-programmable materials available to researchers today. [Modified from (*12*, *41*, *47*, *58*, *60*, *64*, *81*, *82*, *91*), with permission]

pattern to produce 2D crystalline lattices (Fig. 2A) (*14*, *25*).

This ability to rationally assemble synthetic DNA-based tiles has enabled a number of important advances in both the construction of scaffolds for the immobilization of other nanoobjects and for the development of dynamic nanoscale materials. Slight modifications to the DNA design allow for DX and TX tiles in which hairpin loops or sticky-end sequences protrude approximately perpendicular to the plane of the molecule (*25*). In addition to being useful as a topographical marker in atomic force microscopy (AFM) characterization, these strands can be used to capture proteins or nanoparticles and organize them on the 2D lattice assembled from these tiles (*29*, *30*). By linking two DX molecules with a DNA sequence capable of undergoing a rotational structural transition, the concept of using rigid DNA tiles in the formation of nanomechanical devices was introduced (*31*). This work marks the start of the field of nanorobotics, which has made extensive use of rigid DNA bonds to create dynamic systems that can carry out physical tasks of impressive sophistication (*32*–*35*). One tile design that has become particularly useful in systems requiring DNA-based rotary motion is the PX molecule (paranemic crossover) (*34*, *35*), in which crossover events occur at every possible location where the major or minor grooves of the antiparallel helical domains meet (*36*).

Although many of the early tile-based structures presented linear or pseudolinear bonding modes, more advanced tessellating structures constructed by using DNA hybridization have expanded directional assembly interactions to include more complex symmetries. This concept was first explored by combining several four-arm branched junction molecules into a single parallelogram-shaped structure (*37*). Although individually too flexible to be considered bonds (*38*), when these DNA junctions are combined into larger well-defined molecules, it was shown that they could assemble into 1D ribbons or 2D lattices, depending on the placement of sticky-end groups, each with a rhombus-shaped repeat unit. Yan, Reif, and coworkers later showed a cross-shaped DNA structure, known as the 4 by 4 tile, that presented four coplanar arms oriented 90° to one another (Fig. 2B) (*39*). Each arm in this structure consists of two helical domains, much like the DX molecules, the antiparallel orientation of which imparts sufficient rigidity to maintain the orientational relationship between each of the four arms. When sticky-end sequences are placed on the ends of each arm, these structures are able to assemble into 1D rolled-up tubes or periodic 2D square lattices, depending on the number of helical turns of DNA that are in each arm (Fig. 2B). Because the central strand in this tile can be readily modified to present capture sequences or protein binding domains (such as biotin), these tiles have been used extensively to organize proteins and nanoparticles into single-component and alternating 2D arrays (*40*).

Mao and coworkers presented directional binding domains in three dimensions using structures known as tensegrity triangles (Fig. 3A) (*41*). Like the parallelogram structures discussed previously, these constructs derive their rigidity from the linking of several four-arm branch junctions and conceptually consist of three double-helical domains oriented to form a triangular-shaped tile. However, unlike previous structures, the arms of this tile are not all coplanar and point in three separate directions in 3D space like the axes of a rhombohedral coordinate system. Thus when two of the three arms of the tensegrity triangle are assembled via sticky-end hybridization, 2D arrays form with the third arm pointing at a noncoplanar angle. In later work, a more rigid version of this molecule was synthesized in which each arm consisted of a DX molecule, rather than a single linear duplex, which allowed for the generation of ordered 2D arrays of nanoparticles (*42*). Recently, tensegrity triangles have been assembled into macroscopic 3D crystalline materials with considerable long-range order so as to be characterized by means of x-ray diffraction, demonstrating their power as DNA-bonds (Fig. 3A) (*43*). Mao and coworkers have shown an alternative method using DNA tile-based building blocks to construct 3D wireframe polyhedral structures (Fig. 3B) (*44*). In this work, they use a single, versatile structure known as the three-point-star motif, which consists of three DX tile arms linked via a central cyclic strand. The presence of hairpin loops on this central strand imparts intrinsic curvature to the tile and allows one to tailor the flexibility of the structure via the length of the loop. When these tiles were designed to present sticky-end sequences on each arm, it was found that the tile concentration and arm flexibility (controlled through loop length) dictated the morphology of the assembled structure; tetrahedra were observed with flexible tiles at low concentrations, and dodecahedra and truncated icosahedra were observed with more rigid tiles at low and high concentrations, respectively (Fig. 3B). The yield of each structure is considerable (69, 76, and 90% for the truncated icosahedra, dodecahedra, and tetrahedra, respectively), and it is likely that more complex 3D objects can be made with a more diverse library of tiles from which to build. With added sophistication, however, comes an increased likelihood of undesirable side-products, suggesting that methods to mitigate error propagation must go hand-in-hand with increases in structural complexity.

In an interesting departure from the usual rigid tile approach, Yin and coworkers demonstrated in 2012 extremely complex discrete 2D and 3D objects using single-stranded DNA units (Fig. 3C) (*45*, *46*). In this case, a library of oligonucleotides that are conceptually split into four sequence domains are designed to hybridize to four independent neighbors. This forms a rigid bricklike building block that serves the crucial purpose of enabling directional hybridization interactions. Because of the well-defined helical twist of a DNA duplex, the number of bases in a domain determines the dihedral angle between adjacent hybridized segments. Consequently, strands can be designed to form a 2D (*45*) or 3D (*46*) brickwork pattern. Conceptually, one then imagines selectively removing pixels or voxels from this molecular canvas to create an arbitrary 2D (*45*) or 3D (*46*) object, respectively. A computer program then considers a number of important design rules and generates a set of thousands of single-stranded oligonucleotides that, when combined and annealed for a day or more, form extremely complex aperiodic patterns, including 2D symbols and images and 3D block letters and shapes (Fig. 3C) (*45*, *46*). Although the relative yield of these nanoscale objects is low, the technique is comparable with DNA origami and uses a modular approach by computationally selecting the desired tiles from a master set. This method does not seem to require a tight control over the stoichiometry of the strands; like other large multicomponent systems, including DNA origami and crystals, failures to include an individual component results in a flaw, sometimes not detectable, rather than complete failure to make the target.

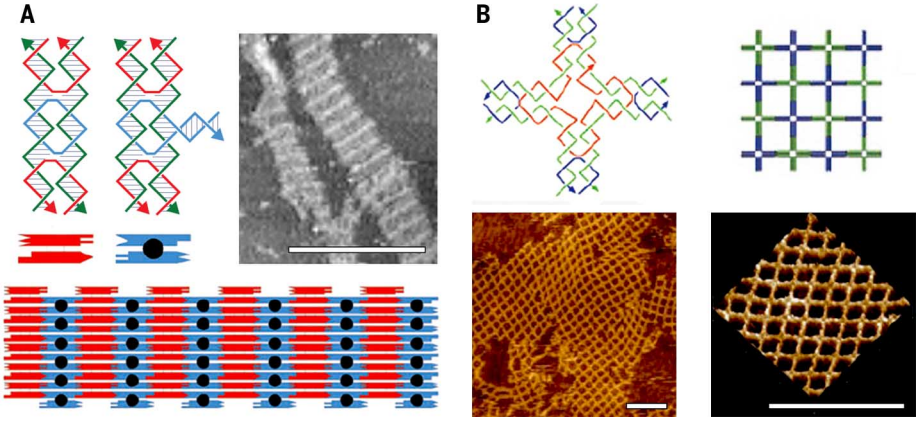


Fig. 2. 2D DNA hybridization-based tiles. (**A**) The DX and DX+J tiles assembled into a brickwork 2D lattice. Scale bar, 300 nm. [Modified from (*12*, *14*), with permission] (**B**) The 4 by 4 tile assembled into a 2D alternating square lattice. Scale bars, 100 nm. [Modified from (*39*), with permission]

Hybridization-based DNA bonds: Origami

The premise of DNA origami is to fold a multithousand-base circular single-stranded DNA

"scaffold," obtained from a viral genome, by using short helper or "staple" oligonucleotides into a desired nanoscale shape (Fig. 4A) (*47*). Because each staple strand is different, some can be designed to present DNA sticky ends at programmed locations on the periphery of the final assembled object, allowing these structures to act as scaffolds with spatially prescribed DNA bonds that capture and organize other nano-objects. These materials, therefore, derive the structural rigidity of their DNA bonds from the same chemical source as DNA tiles: numerous crossover events between neighboring duplexes and the hydrogen bonds that link them. However, this approach differs in that it is less focused on the development of a small number of building blocks that can arrange themselves into large periodic structures, and is more interested in constructing discrete nanoscale objects whose size and shape is well-defined. The advantage over tile-based assembly is that hybridization occurs frequently via intramolecular interactions on the scaffold strand, resulting in a high local concentration of complementary oligonucleotides that drives the system toward the intended sequence-specific thermodynamic product (*48*). This allows for relatively high yields of particularly complex objects and obviates the need for a precise stoichiometry of all components in the system. As in all these systems, one must be extremely careful to control the sequences of the staple oligonucleotides to fold the scaffold strand into a desired shape, necessitating computational methods to be applied for the design of each structure that is to be synthesized. To address this problem, a number of open-source software packages are now available that aid researchers in developing the strands and sequences required for a particular DNA origami structure (*49*, *50*).

Although this principle was experimentally demonstrated with barcode arrays (*51*) and in the construction of a nanoscale wireframe octahedron (*52*), the power of the technique was best illustrated with the formation of numerous 2D shapes of impressive complexity (*47*). Conceptually, these patterns are generated by imaging the scaffold strand being rastered back and forth to fill an arbitrarily shaped 2D area (Fig. 4A). Computational methods are then used to select the appropriate staple strands so that the desired folding path is stabilized by DNA hybridization and numerous crossover junctions. The method requires that several important design parameters be considered, including the number of helical twists of DNA between crossover points and the elimination of strain, nicks, and seams. Although the majority of structures formed in greater than 60% yield, two alternate strategies for forming similar triangular patterns resulted in vastly different yields of ~1 and 88%, highlighting the need to carefully design and optimize sequences because the number of potential undesired interactions is quite large.

DNA origami has become a powerful tool for building discrete nanoscale materials, generating a variety of complex and dynamic structures, including a box with a sequence-specific opening lid (*53*) and a barrel-shaped structure that can carry molecular payloads and release them based on intracellular logic-gated aptamer binding events (*54*). Origami methods have found particular utility in constructing 2D scaffold materials because individual sticky-ends and other DNA-based features can be placed in nearly any arrangement. This has facilitated the demonstration of DNA walkers that can pick up nanoscale cargo (*35*), studies of distance-dependent bivalent ligand-protein binding (*55*), and the controlled placement of nanoparticles for plasmonic applications (*56*, *57*).

A conceptual leap in DNA origami was made in 2009 when these principles were extended from building 2D objects to those that fill 3D space (*58*, *59*). This was accomplished by imagining the scaffold strand being rastered into an elongated 2D sheet, which is then encouraged to fold back and forth onto itself via the interactions of staple strands to form pleated sheets of antiparallel double helices (Fig. 4B) (*58*). Because of the helical twist of DNA, crossover events between helical domains are selected to occur at 120° dihedral angles, as in the six-helix bundle (*27*), resulting in a dense honeycomb lattice of DNA helices that fill a 3D volume. From this block of DNA, one must imagine removing segments in order to "carve out" the desired nanoscale object, a

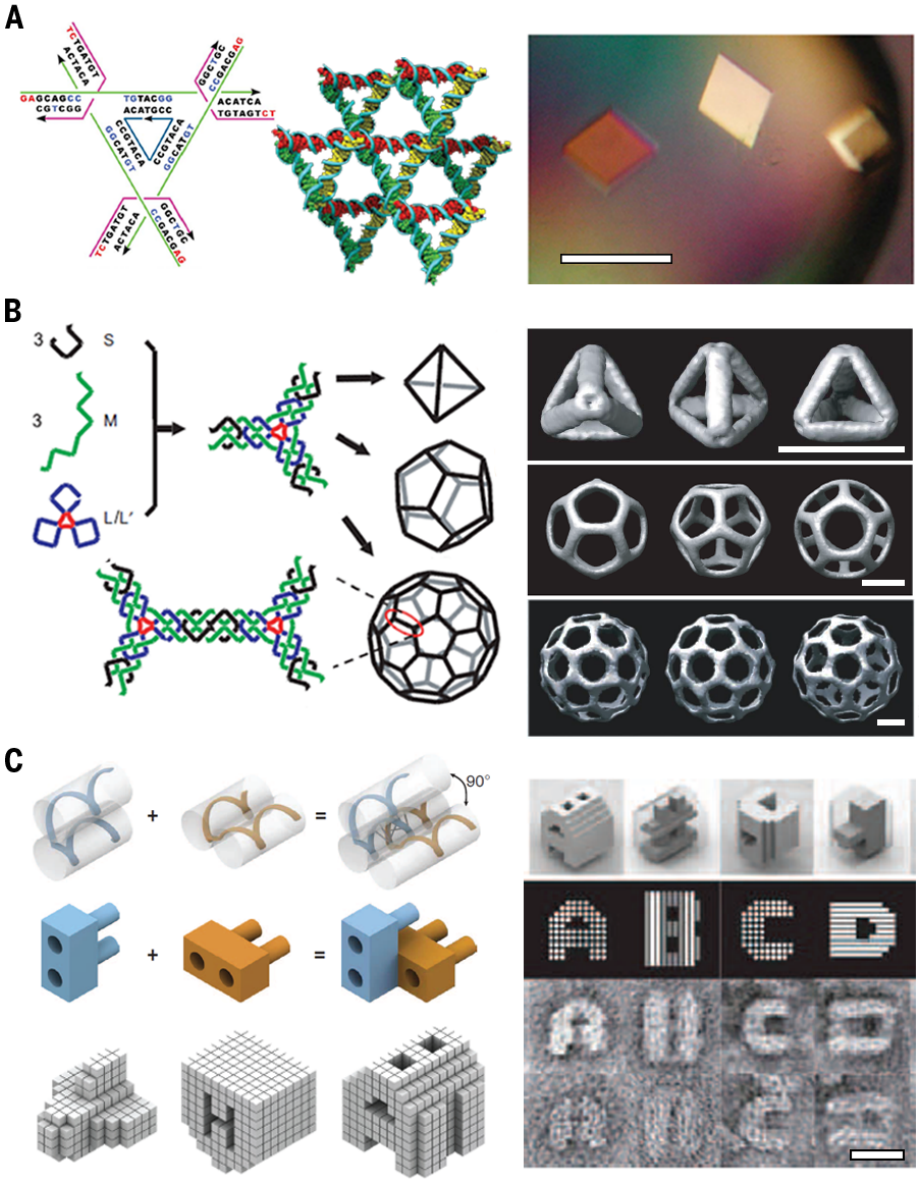


Fig. 3. 3D DNA hybridization-based tiles. (**A**) The tensegrity triangle assembled into a macroscopic 3D rhombohedral lattice. Scale bar, 500 μm. [Modified from (*12*, *43*), with permission] (**B**) The three-point star motif assembled into a variety of wireframe polyhedra based on the intrinsic curvature of the tile and its concentration. Scale bars, 20 nm. [Modified from (*44*), with permission] (**C**) Single-stranded DNA assembled into arbitrary 3D brickworklike nanoscale objects. Scale bar, 20 nm. [Modified from (*46*), with permission]

process that requires careful attention to a variety of design considerations but is now simplified by computer-aided design (CAD) software (*49*). Using this approach, a variety of complex 3D shapes were synthesized, including a monolith, a square cross, and a genie bottle (Fig. 4B); in some cases, these objects could even be assembled hierarchically into larger structures, such as a wireframe icosahedron approximately 100 nm in size (*58*). A second enhancement introduced the concept that insertion or deletion of bases in a block of honeycomb duplexes creates local regions of strain because of underwinding or overwinding of the helix, respectively (Fig. 4C) (*59*). This strain is accommodated by the system through simultaneous global twists and global bends of the origami structure. By properly selecting the insertion or deletion sites in a block of duplexes, one can isolate a single deformation mode and create structures that either twist or bend in a controllable manner. This approach greatly expands the types of materials available to origami methods because structures no longer need to be imagined as comprising voxel-type, stepwise components but instead can experience smooth spatial transitions from one feature to another. To demonstrate the power of this approach, a variety of impressive structures were formed, including twisted ribbons of both chiralities, bent arms with a full range of internal angles, notched gears of different sizes, and 3D spherical wireframe objects.

In a conceptually similar approach, one imagines folding a scaffold strand in such a way as to create a series of concentric circular rings of DNA duplexes that are coplanar (Fig. 4D) (*60*). Through appropriate design of crossover points and staple sequences, each ring can then be positioned at non-coplanar dihedral angles with respect to its neighboring rings. In the simplest case, this has the effect of pulling the concentric circular rings out of their coplanar arrangement to generate a hemisphere or bowl-shaped object (Fig. 4D). Additional designs for incorporating gradual curvature allow for hollow sphere and vase-shaped objects to be formed.

In all of these examples, such a high degree of structural complexity comes at a price: Mixtures of scaffold and staple strands require precise recipes for counterion concentrations (Na^+ and Mg^{2+}) and long annealing times of up to a week for equilibrium materials to be formed (*58*). Even under these ideal and optimized conditions, scaffold strands are estimated to incorporate into the desired monomeric species at between 7 and 44% yield and therefore necessitate a gel purification step to isolate (*58*). Conversely, Dietz and coworkers have demonstrated non-equilibrium folding of complex origami structures with near quantitative yield in minutes, suggesting that kinetic routes to idealized materials may be an

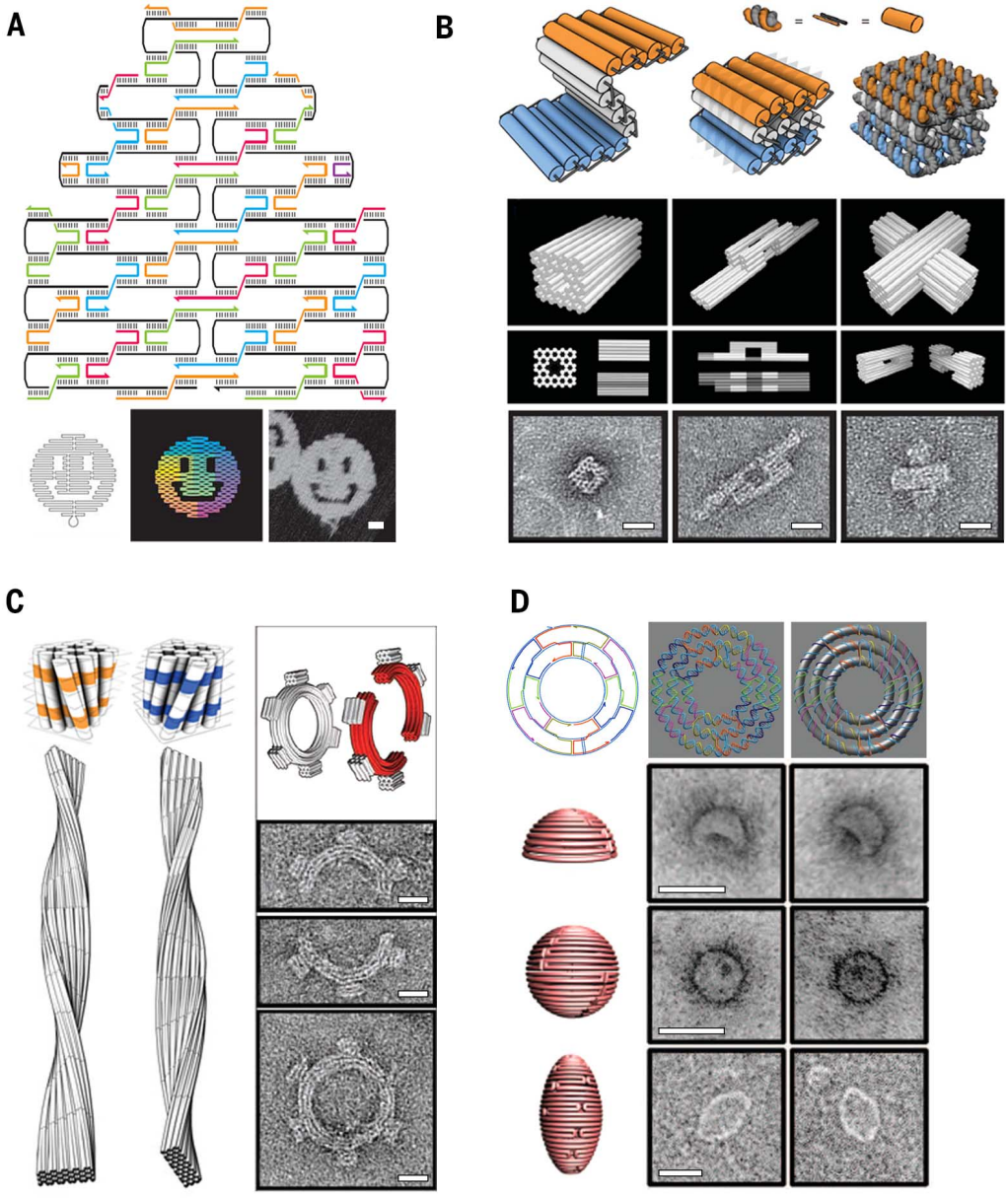


Fig. 4. DNA hybridization-based origami structures. (**A**) Illustration of the rasterlike pattern of the scaffold strand folded by staple strands, which are collectively used to generate arbitrary 2D patterns. Scale bar, 20 nm. [Modified from (*47*), with permission] (**B**) Extension of the origami principle to 3D by using staple strands which promote the formation of pleated sheets of duplexes, which ultimately pack into a honeycomb lattice. Scale bars, 20 nm. [Modified from (*58*), with permission] (**C**) Insertion or deletion of bases at specific sites in a block of honeycomb duplexes can be used to selectively create regions of local twisting or curvature. Scale bars, 20 nm. [Modified from (*59*), with permission] (**D**) Concentric rings of duplexes can be encouraged to extrude out into the third dimension to form hollow spherical and pseudospherical objects. Scale bars, 50 nm. [Modified from (*60*), with permission]

important synthetic tool for future research (61). Nonetheless, these objects have already been used by other groups to generate DNA bonds that facilitate the construction of interesting plasmonic (62) and metamaterial (63) architectures.

Both brick structures and origami structures are objects and not periodic lattices. Although both can fill large areas (about 10^4 nm^2) in two dimensions, they are finite. Both of these types of structures have been facilitated by the drop in effective DNA cost, largely because the methods used to analyze structures require much less material.

There is another phenomenon that has been revealed when using both simple tiles and DNA origami structures as building blocks to construct larger periodic (or perhaps aperiodic) arrays: The success of an assembly depends on the presence of helix axes pointing in the direction of crystal propagation. The first 2D crystals formed from DX or TX tiles tended to be long and narrow (14, 25) but certainly passed for crystals. The assembly algorithm was diagonal complementarity along the tile. When this approach was applied to forming larger crystals from origami building blocks, the arrays were even thinner, relative to the size of the tiles (64). Only when the helix axes pointed in the direction of propagation were substantially isotropic crystals of origami tiles produced (64). The same is true of 3D crystals from small tiles: The six-helix bundle and the TX tile are capable of forming 3D-ordered materials (65) but fail to produce crystals that diffract adequately. Only the tensegrity triangle (41), with three linearly independent helix axes, has produced substantial 3D crystals thus far (43). However, although the rule of connecting objects along the direction of the helix axis is a necessary condition, it is not a sufficient condition. Numerous examples of very small arrays have been found in systems that ought to have done better (65). This is an avenue of investigation that needs to be explored further.

Nanoparticle-templated DNA bonds

A fundamentally different approach to generating nanoscale DNA bonds is to use nanoparticles as templates for the immobilization and orientation of surface-bound oligonucleotides [Summary figure, (B)] (66). Rather than use hybridization and intertwining of DNA strands, it is most often the metallic or ionic bonds that form the crystalline lattice of an inorganic core material that provide the necessary rigidity for these species to generate directional interactions. Thus, many of the design considerations for DNA hybridization-based systems, like the helical twist of a DNA duplex or the necessity of several crossover junctions, become unimportant so long as the inorganic material can be functionalized with a dense shell of the desired oligonucleotide ligands. One of the more notable differences of this approach is that nanoparticle-templated DNA bonds typically hybridize with other constructs through the collective interactions of tens to hundreds of individual, densely packed DNA strands. The result of spatially confining these strands is profound; enormous changes to the thermodynamics of hybridization lead to sharper melting transitions (67), enhanced binding constants (68), and elevated thermal stability (69), the enthalpic and entropic underpinnings of which remain the subject of continuing research effort. This focus on engineering individually weak but multivalent DNA hybridization interactions results in substantial differences in how these constructs participate in bonding, the symmetries of their interactions, and ultimately the materials that can be constructed from them.

Nanoparticle-based structures using DNA hybridization to govern their association were developed by using oligonucleotides presenting 3′ or 5′ terminal alkyl-thiol moieties that were added to solutions of colloidal gold nanoparticles ~13 nm in diameter (7). By gradually increasing the ionic strength of the solution, the negatively charged phosphate backbone of the DNA strands could be effectively screened, facilitating the formation of extremely dense monolayers of oligonucleotides on the gold nanoparticle scaffolds (70). Because the DNA nucleobases themselves have a considerable affinity for gold surfaces (71), ordinary oligonucleotides are able to lie down and wrap around gold nanoparticles in a random and nondirectional manner. Therefore, the presence of the thiol moiety as a robust anchoring group on one end of the DNA strands (either 3′ or 5′, depending on synthetic details) serves the nontrivial role of orienting all of the oligonucleotides in a common surface-normal direction, making them available for hybridization to their complements. Initial work focused on exploring the use of linker oligonucleotides that contained regions complementary to the strands anchored to the particles to hybridize them into macroscopic networks (7, 72). It was found that these materials exhibited considerable short-range order, with interparticle distances proportional to the length of DNA used to link them (16, 17). Significant correlation between the particle positions was only observed when the DNA linking them was primarily double-stranded; introduction of single-stranded regions resulted in significant a loss of ordering (17). These results demonstrate that it is a combination of the rigidity of the inorganic core, coupled with a dense, oriented monolayer of primarily duplexed oligonucleotide ligands that create the conditions necessary for these constructs to generate directional DNA bonds.

These building blocks can be crystallized into well-ordered superlattices with considerable long-range periodicity (Fig. 5A) (18, 19). The key advance was the use of a thermal annealing step at temperatures just below the particle-particle dehybridization transition and the design of short DNA sticky ends that are strong enough to hold the particles together but weak enough to allow for rapid equilibration (18). The implication is that the thermodynamic state of the system is one in which the particles are assembled into ordered superlattices that maximize the number of DNA hybridization events, and the network structures observed initially represent kinetically trapped, metastable states (73). This hypothesis was tested and confirmed in numerous subsequent investigations and now forms the basis for a series of design rules that guide and explain the formation of dozens of different superlattice symmetries (3, 74, 75). In order to determine the thermodynamic stability of an arbitrary arrangement of particles, one can simply account for the surface-area contact between spherical particles baring complementary linkers as a proxy for counting the number of hybridization events (74). This formalism, known as the complementary contact model (CCM), explains the effects of experimental parameters such as linker sequence, DNA flexibility, linker number ratio, and particle size ratio and has even been used in the a priori design of more complex three-component nanoparticle superlattices (76).

Although understanding the fundamental properties of these nanoparticle-templated DNA bonds was crucial, the technique presented several limitations: Lattices had only been constructed from gold nanoparticles, were only stable in buffered solution conditions amenable to DNA hybridization, and were polycrystalline in nature. Because the only requirement for these DNA bonds is that they derive their structural rigidity from a solid material core, inorganic nanoparticles with a variety of different compositions—including catalytic noble metals, semiconductors, and magnetic oxides—were subsequently functionalized with DNA and assembled by use of this technique (77–79). In addition, lattices have since been grown from substrates with a preferred crystallographic direction (Fig. 5B) and encapsulated in glass by using a molecule that provides an initiation site for silica growth (80, 81). These advances have allowed DNA-nanoparticle superlattices to become solid-state materials, greatly expanding their potential use in a variety of applications. It may be possible to use similar approaches to create solid-state analogs of the tile- and origami-based structures. Last, these programmable atom equivalents, when cooled slowly, have been shown to form large single crystals with a well-defined crystal habit (a rhombic dodecahedron) indicative of the minimum-energy Wulff polyhedron of the parent superlattice (Fig. 5A) (82). When these faceted microcrystals are assembled from plasmonic nanoparticles, they interact strongly with light through hybrid plasmonic-photonic modes, demonstrating the importance of using nanoparticle-templated DNA bonds that can assemble materials that are approaching macroscopic length scales (83).

Although these spherical nanoparticle-based DNA bonds allow for regularly spaced network structures and extremely well-ordered superlattices to be assembled via fairly isotropic interactions that mimic metallic or ionic bonding, considerable effort has been applied to develop methods to break the spherical symmetry and achieve a greater directionality of the DNA interactions that more closely mimic covalent bonding (Fig. 6A). One conceptually straightforward, albeit experimentally challenging, way to achieve this is to dictate an asymmetric spatial distribution of oligonucleotide ligands on the surface of a spherical nanoparticle. Two alternate strategies have been demonstrated for achieving DNA-functionalized gold nanoparticles having one hemisphere hybridized

with linker strands to make them asymmetric (*84*, *85*). Both methods rely on the hybridization of small DNA–gold nanoparticles (AuNPs) to larger DNA-coated colloidal particles in order to "capture" new oligonucleotide functionality at the hemispherical interface between the two particles. In one case, the strands of the smaller particle are enzymatically ligated to short oligonucleotides, extending their length and sequence (*84*), and in the other case, the smaller particle hybridizes and acquires linker oligonucleotides that offer new binding functionality (*85*). An alternative method has been used to produce the same asymmetric DNA functionality by hybridizing small DNA-AuNPs to larger DNA-modified particles that act to sterically and electrostatically block access to the hemisphere nearest the larger particle while allowing hybridization of linker strands to the hemisphere exposed to solution (*86*). Building blocks of this variety resemble linear or unidirectional bonding modes and therefore assemble into discrete dimer clusters or can be combined with particles of differing size to create hierarchically assembled core-satellite structures.

Although asymmetrically functionalized particles are appealing for achieving nanoparticle-based DNA bonds, reliable methods for moving beyond simple linear geometries have proved elusive. One approach to overcome this hurdle has been to use anisotropic nanostructures that present regions of greater chemical reactivity that can be functionalized selectively with DNA. It is thought that the native surfactant coating required for the synthesis of these structures is less dense at regions of high curvature (tips and edges) and can therefore be replaced by alkylthiol-functionalized DNA ligands more readily. This has been experimentally demonstrated by the selective incorporation of DNA at the tips and edges of platelike triangular nanoprisms (*87*), or at the tips of gold nanorods (*88*), resulting in anisotropic core-satellite clusters (Fig. 6A). Several reports have demonstrated dynamic forms of asymmetric bonding in which large colloids or emulsions are functionalized with DNA ligands that are mobile around the particle surface and can pool together at bridge points between complementary structures, forming valence clusters (*89*, *90*). One impressive alternative strategy generates micrometer-sized colloidal particles with between 1 and 7 DNA patches arranged in highly symmetric geometries that mimic the multivalent bonding modes of atomic orbitals (Fig. 6B) (*91*, *92*). The process starts by creating clusters with different numbers of amine-modified polystyrene spheres packed into highly symmetric arrangements. A chemically distinct polymer is then spherically grown from the center of any cluster by using a swelling and cross-linking process to the extent that only small islands or patches remain from the original amine-modified spheres. DNA strands can then be selectively conjugated to these amine-terminated domains, resulting in spherical colloids with sequence-selective patches oriented in well-defined geometries (*91*). Combinations of particles with different bonding coordination modes allow for the assembly of colloidal analogs to common molecules, including linear CO_2, triangular BF_3, and tetrahedral CH_4, to name a few (Fig. 6B) (*92*). It remains a challenge to extend these principles of selective DNA functionalization to rigid nanoparticles of smaller size or with interesting compositions.

One interesting feature that differentiates particle-templated DNA bonds is that the role of the DNA in mediating sequence-specific interactions is conceptually decoupled from the role that the nanoparticle plays as the rigid scaffold necessary for the formation of well-defined products. Consequently, one can imagine an alternative strategy for accessing directional oligonucleotide interactions that adopt nonspherical geometries: Replace the typically spherical nanoparticle cores with those that are anisotropic, leaving the DNA design and functionalization unchanged (Fig. 6C).

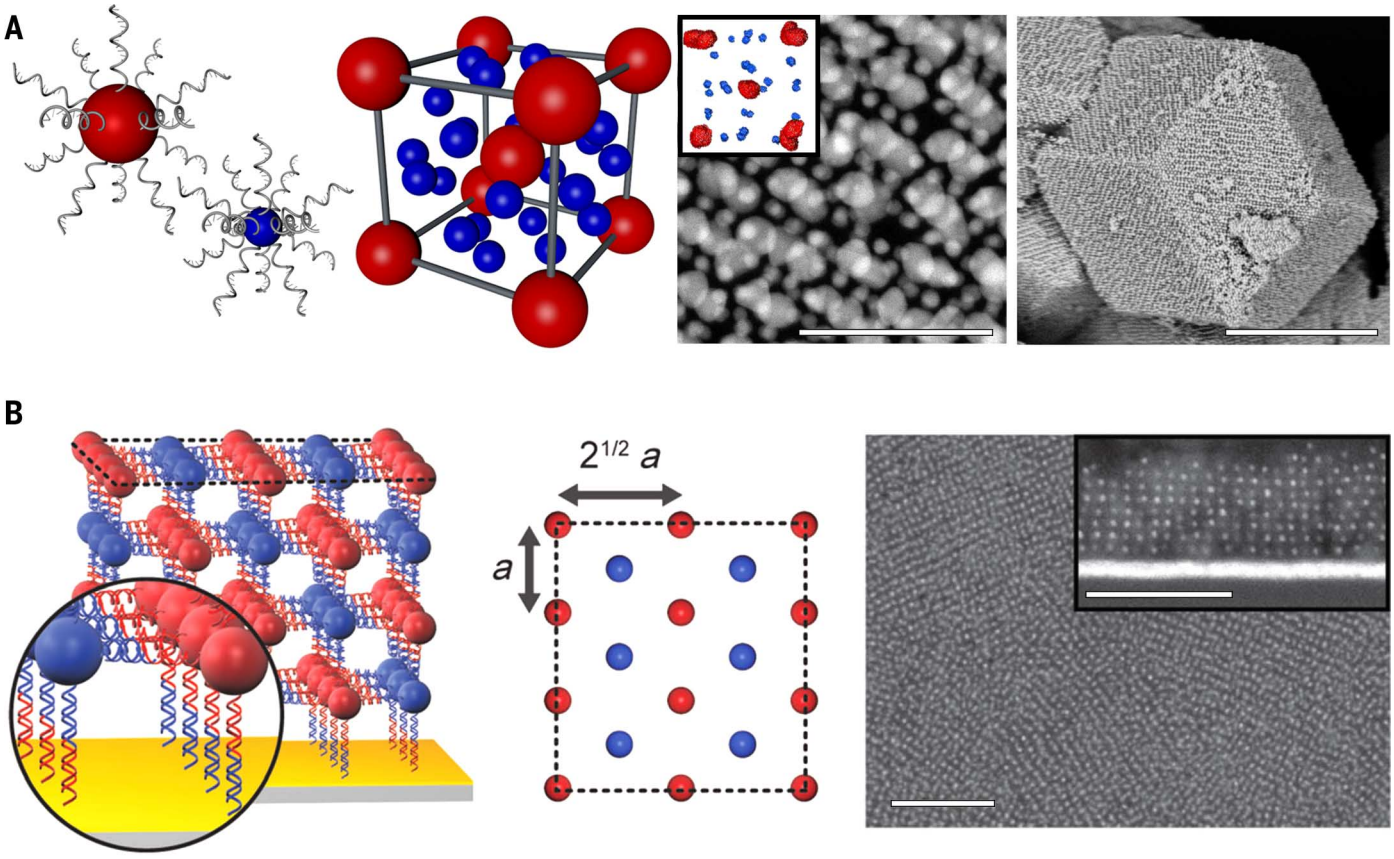


Fig. 5. Nanoparticle-templated spherical DNA constructs. (**A**) Spherical nanoparticles functionalized with the appropriate DNA strands can assemble into a variety of superlattices (AB_6-type structure shown in the scheme and transmission electron microscopy (TEM) image with tomographic reconstruction, inset), some of which form large faceted single crystals. Scale bars, TEM image, 100 nm; scanning electron microscopy image, 1 μm. [Modified from (*74*, *82*), with permission] (**B**) Superlattices can be grown from a substrate with a preferred crystal orientation, allowing for textured nanoparticle films. Scale bars, 200 nm. [Modified from (*80*), with permission]

This modular approach uses several different anisotropic gold nanostructures (rods, triangular prisms, rhombic dodecahedra, and octahedra) uniformly functionalized with oligonucleotides and allowed to assemble via DNA-linker–mediated hybridization (93). In each case, it was found that nanoparticle superlattices formed whose symmetry and dimensionality were dictated by the geometry of the particle used in their construction. In particular, regions of each nanoparticle shape with the least curvature (flat facets) showed strong preferences for interacting such that rods formed 2D hexagonal close-packed lattices, triangular plates (prisms) formed 1D columnar stacks, and rhombic dodecahedra and octahedra formed face-centered-cubic (FCC) and body-centered-cubic (BCC) superlattices with face-to-face orientational correlations, respectively (Fig. 6C). It was later shown that the collective interaction of numerous oligonucleotide ligands oriented perpendicular to these flat surfaces could exhibit binding constants six orders of magnitude larger than similarly functionalized curved surfaces (94). The implication of this work is that when bundles of densely packed DNA strands are collectively oriented in conformations ideal for binding (such as flat face-to-face interactions), the shape of the

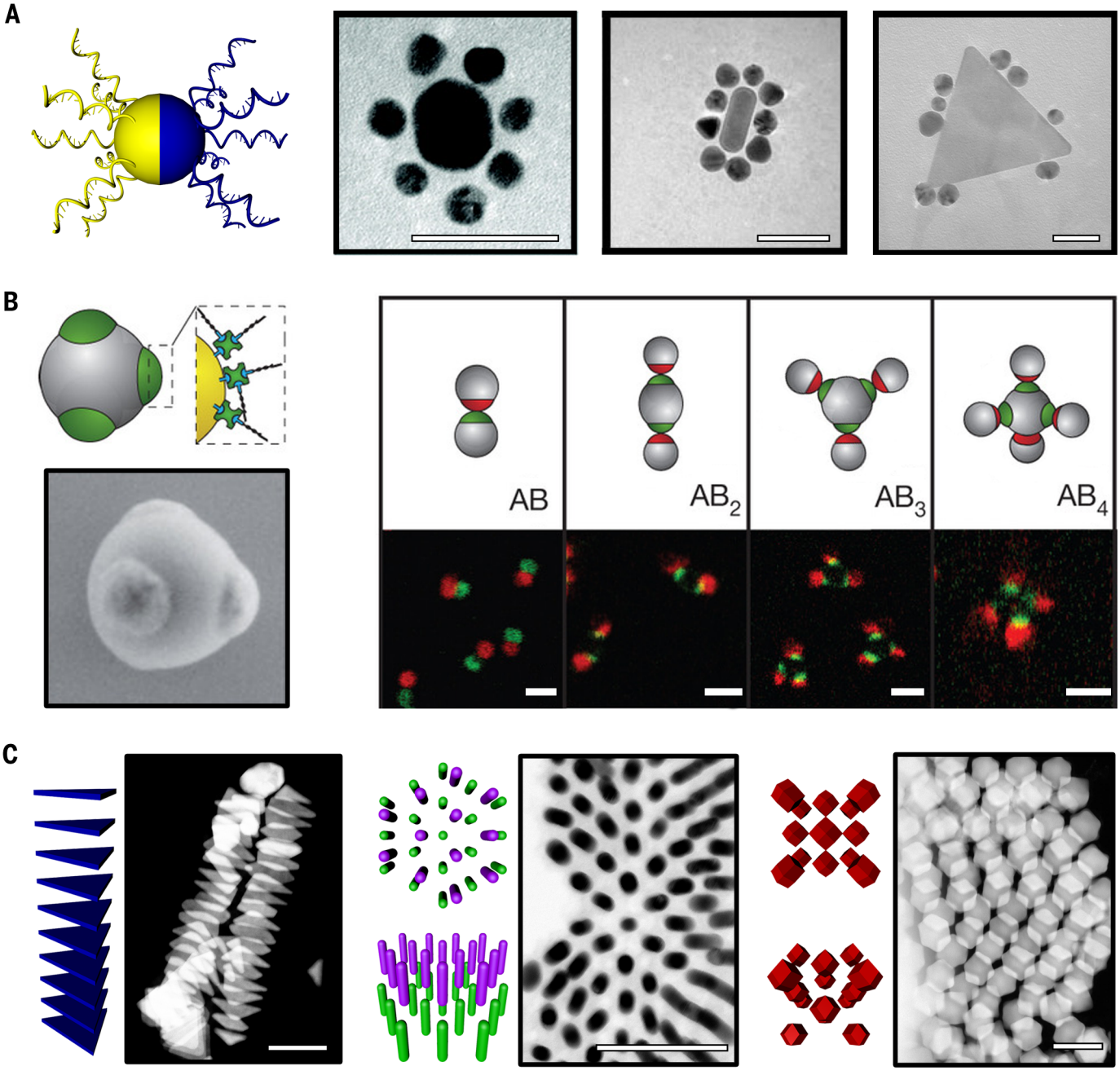


Fig. 6. Nanoparticle-templated anisotropic and asymmetric DNA constructs. (**A**) Control over the spatial distribution of surface-bound DNA strands allows for particles that are asymmetric and can form core-satellite clusters. Scale bars, 50 nm. [Modified from (84, 87, 88), with permission] (**B**) The formation of DNA patches at symmetrically arranged positions on spherical colloids allows for particle analogs of certain molecular species. Scale bars, 2 μm. [Modified from (91), with permission] (**C**) By using core nanoparticles that are anisotropic (triangular prisms, rods, and rhombic dodecahedra), while leaving the DNA design unchanged, directional interactions that mimic the symmetry of the underlying particle facilitate the formation of different superlattice architectures. Scale bars, 100 nm. [Modified from (93), with permission]

underlying inorganic nanoparticle can play an enormous role in dictating the directionality of interparticle interactions (*95*). Consistent with results from Chaikin and others (*96*, *97*), this highlights the importance of considering the entropic consequences of tethering and otherwise conformationally restricting particle-bound strands when using particle-based DNA bonds. Indeed, when loosely packed single-stranded oligonucleotides (*78*) or extremely long duplexed linker strands (*93*) are used to direct anisotropic particle association, assemblies that indicate isotropic interactions are observed because the DNA is too conformationally flexible to retain the symmetry of the rigid scaffold to which it is anchored; these conditions do not favor the use of anisotropic particles to create directional nanoscale bonds.

Conclusions

Although DNA-based nanoscale construction continues to produce materials with an impressive degree of control, the hybridization-based and nanoparticle-templated subfields remain relatively isolated, with very few examples of overlap between disciplines (*98*). It is likely that there are fruitful areas of research that make use of the advantages of each approach. For example, DNA nanotechnology and DNA origami have been used extensively in the creation of dynamic nanostructures such as DNA machines (*31*, *32*), walkers (*33*), a nanoscale assembly line (*35*), and complex hybridization-based amplification or reaction networks (*99*–*101*). Although some of these concepts have recently been applied to nanoparticle-based bonds to create superlattices that are dynamically tunable or have programmable phase behavior (*102*–*104*), there is considerable room for improvement in the creation of reconfigurable particle-based structures. On the other hand, although nanoparticle-based structures have been used in a number of biological applications as tools for gene regulation (*105*) and as probes in more than 2000 medical diagnostic products available worldwide (*106*–*109*), tile- or origami-based DNA structures are only now being used for cellular applications, including drug delivery (*54*) and biological imaging (*110*). Last, it remains a considerable research challenge to mimic the complexity and versatility of discrete DNA origami structures with inorganic materials such as noble metal and semiconductor nanostructures.

Although periodic structures assembled efficiently by using tile- and nanoparticle-based DNA bonds and have allowed the rational design of large, faceted single crystals of each (*43*, *82*), more robust methods at generating discrete DNA objects in high yield with techniques such as origami are necessary. This advance may be accomplished through methods that allow for synthetic oligonucleotides whose sequence and chemical structure are more pure, or perhaps there are alternative methods that are superior at creating large objects that challenge conventional thoughts in DNA origami (*45*, *46*). Improvements in understanding the complex thermodynamic and kinetic influences of various counterions and thermal cycling may also aid in allowing these systems to arrive at the desired product.

Historically, this field has been driven primarily by the control of matter at the smallest length scales, with functional applications being demonstrated only after materials can be constructed in high-yield and in a well-defined manner. This notion persists today, and consequently, an enormous focus still rests on the development of DNA bonds that are versatile and powerful tools for programming the construction of sophisticated nanoscale materials. Although enormous progress has been made in the short time that these building blocks have been available, the field is still in its infancy and has much more to offer the scientific community. Just as chemists have learned to manipulate atomic bonds to synthesize astonishingly complex and functional molecules, an understanding of the nature of these DNA bonds and an ability to control them may one day allow nanoscientists to create similarly complex and functional nanoscale materials.

REFERENCES AND NOTES

1. G. R. Desiraju, Supramolecular synthons in crystal engineering—A new organic synthesis. *Angew. Chem. Int. Ed. Engl.* **34**, 2311–2327 (1995). doi: 10.1002/anie.199523111
2. B. Liu, N. B. Leontis, N. C. Seeman, Bulged 3-arm DNA branched junctions as components for nanoconstruction. *Nanobiology* **3**, 177–188 (1994).
3. R. J. Macfarlane, M. N. O'Brien, S. H. Petrosko, C. A. Mirkin, Nucleic acid-modified nanostructures as programmable atom equivalents: Forging a new "table of elements". *Angew. Chem. Int. Ed. Engl.* **52**, 5688–5698 (2013). doi: 10.1002/anie.201209336; pmid: 23640804
4. F. A. Aldaye, A. L. Palmer, H. F. Sleiman, Assembling materials with DNA as the guide. *Science* **321**, 1795–1799 (2008). doi: 10.1126/science.1154533; pmid: 18818351
5. K. Kruger *et al*., Self-splicing RNA: Autoexcision and autocyclization of the ribosomal RNA intervening sequence of *Tetrahymena*. *Cell* **31**, 147–157 (1982). doi: 10.1016/0092-8674(82)90414-7; pmid: 6297745
6. R. Holliday, A mechanism for gene conversion in fungi. *Genet. Res.* **5**, 282–304 (1964). doi: 10.1017/S0016672300001233; pmid: 18976517
7. C. A. Mirkin, R. L. Letsinger, R. C. Mucic, J. J. Storhoff, A DNA-based method for rationally assembling nanoparticles into macroscopic materials. *Nature* **382**, 607–609 (1996). doi: 10.1038/382607a0; pmid: 8757129
8. X. Li, X. Yang, J. Qi, N. C. Seeman, Antiparallel DNA double crossover molecules as components for nanoconstruction. *J. Am. Chem. Soc.* **118**, 6131–6140 (1996). doi: 10.1021/ja960162o
9. J. H. Chen, N. C. Seeman, Synthesis from DNA of a molecule with the connectivity of a cube. *Nature* **350**, 631–633 (1991). doi: 10.1038/350631a0; pmid: 2017259
10. N. C. Seeman, Nucleic acid junctions and lattices. *J. Theor. Biol.* **99**, 237–247 (1982). doi: 10.1016/0022-5193(82)90002-9; pmid: 6188926
11. N. R. Kallenbach, R.-I. Ma, N. C. Seeman, An immobile nucleic acid junction constructed from oligonucleotides. *Nature* **305**, 829–831 (1983). doi: 10.1038/305829a0
12. N. C. Seeman, Nanomaterials based on DNA. *Annu. Rev. Biochem.* **79**, 65–87 (2010). doi: 10.1146/annurev-biochem-060308-102244; pmid: 20222824
13. T. J. Fu, N. C. Seeman, DNA double-crossover molecules. *Biochemistry* **32**, 3211–3220 (1993). doi: 10.1021/bi00064a003; pmid: 8461289
14. E. Winfree, F. Liu, L. A. Wenzler, N. C. Seeman, Design and self-assembly of two-dimensional DNA crystals. *Nature* **394**, 539–544 (1998). doi: 10.1038/28998; pmid: 9707114
15. J. I. Cutler, E. Auyeung, C. A. Mirkin, Spherical nucleic acids. *J. Am. Chem. Soc.* **134**, 1376–1391 (2012). doi: 10.1021/ja209351u; pmid: 22229439
16. S.-J. Park, A. A. Lazarides, C. A. Mirkin, R. L. Letsinger, Directed assembly of periodic materials from protein and oligonucleotide-modified nanoparticle building blocks. *Angew. Chem. Int. Ed. Engl.* **40**, 2909–2912 (2001). doi: 10.1002/1521-3757(20010803)113:15<2993::AID-ANGE2993>3.0.CO;2-9; pmid: 11500906
17. S.-J. Park, A. A. Lazarides, J. J. Storhoff, L. Pesce, C. A. Mirkin, The structural characterization of oligonucleotide-modified gold nanoparticle networks formed by DNA hybridization. *J. Phys. Chem. B* **108**, 12375–12380 (2004). doi: 10.1021/jp040242b
18. S. Y. Park *et al*., DNA-programmable nanoparticle crystallization. *Nature* **451**, 553–556 (2008). doi: 10.1038/nature06508; pmid: 18235497
19. D. Nykypanchuk, M. M. Maye, D. van der Lelie, O. Gang, DNA-guided crystallization of colloidal nanoparticles. *Nature* **451**, 549–552 (2008). doi: 10.1038/nature06560; pmid: 18235496
20. J. SantaLucia Jr., A unified view of polymer, dumbbell, and oligonucleotide DNA nearest-neighbor thermodynamics. *Proc. Natl. Acad. Sci. U.S.A.* **95**, 1460–1465 (1998). doi: 10.1073/pnas.95.4.1460; pmid: 9465037
21. C. M. Niemeyer, T. Sano, C. L. Smith, C. R. Cantor, Oligonucleotide-directed self-assembly of proteins: Semisynthetic DNA—Streptavidin hybrid molecules as connectors for the generation of macroscopic arrays and the construction of supramolecular bioconjugates. *Nucleic Acids Res.* **22**, 5530–5539 (1994). doi: 10.1093/nar/22.25.5530; pmid: 7530841
22. A. P. Alivisatos *et al*., Organization of 'nanocrystal molecules' using DNA. *Nature* **382**, 609–611 (1996). doi: 10.1038/382609a0; pmid: 8757130
23. F. A. Aldaye, H. F. Sleiman, Sequential self-assembly of a DNA hexagon as a template for the organization of gold nanoparticles. *Angew. Chem. Int. Ed. Engl.* **45**, 2204–2209 (2006). doi: 10.1002/anie.200502481; pmid: 16502437
24. H. Yang, H. F. Sleiman, Templated synthesis of highly stable, electroactive, and dynamic metal-DNA branched junctions. *Angew. Chem. Int. Ed. Engl.* **47**, 2443–2446 (2008). doi: 10.1002/anie.200703741; pmid: 18330865
25. T. H. LaBean *et al*., Construction, Analysis, ligation, and self-assembly of DNA triple crossover complexes. *J. Am. Chem. Soc.* **122**, 1848–1860 (2000). doi: 10.1021/ja993393e
26. P. Sa-Ardyen, A. V. Vologodskii, N. C. Seeman, The flexibility of DNA double crossover molecules. *Biophys. J.* **84**, 3829–3837 (2003). doi: 10.1016/S0006-3495(03)75110-8; pmid: 12770888
27. F. Mathieu *et al*., Six-helix bundles designed from DNA. *Nano Lett.* **5**, 661–665 (2005). doi: 10.1021/nl050084f; pmid: 15826105
28. T. Wang, D. Schiffels, S. Martinez Cuesta, D. K. Fygenson, N. C. Seeman, Design and characterization of 1D nanotubes and 2D periodic arrays self-assembled from DNA multi-helix bundles. *J. Am. Chem. Soc.* **134**, 1606–1616 (2012). doi: 10.1021/ja207976q; pmid: 22239727
29. H. Li, S. H. Park, J. H. Reif, T. H. LaBean, H. Yan, DNA-templated self-assembly of protein and nanoparticle linear arrays. *J. Am. Chem. Soc.* **126**, 418–419 (2004). doi: 10.1021/ja0383367; pmid: 14719910
30. J. D. Le *et al*., DNA-templated self-assembly of metallic nanocomponent arrays on a surface. *Nano Lett.* **4**, 2343–2347 (2004). doi: 10.1021/nl048635+
31. C. Mao, W. Sun, Z. Shen, N. C. Seeman, A nanomechanical device based on the B-Z transition of DNA. *Nature* **397**, 144–146 (1999). doi: 10.1038/16437; pmid: 9923675
32. B. Yurke, A. J. Turberfield, A. P. Mills Jr., F. C. Simmel, J. L. Neumann, A DNA-fuelled molecular machine made of DNA. *Nature* **406**, 605–608 (2000). doi: 10.1038/35020524; pmid: 10949296
33. W. B. Sherman, N. C. Seeman, A precisely controlled DNA biped walking device. *Nano Lett.* **4**, 1203–1207 (2004). doi: 10.1021/nl049527q
34. H. Yan, X. Zhang, Z. Shen, N. C. Seeman, A robust DNA mechanical device controlled by hybridization topology. *Nature* **415**, 62–65 (2002). doi: 10.1038/415062a; pmid: 11780115
35. H. Gu, J. Chao, S.-J. Xiao, N. C. Seeman, A proximity-based programmable DNA nanoscale assembly line. *Nature* **465**, 202–205 (2010). doi: 10.1038/nature09026; pmid: 20463734
36. X. Zhang, H. Yan, Z. Shen, N. C. Seeman, Paranemic cohesion of topologically-closed DNA molecules. *J. Am. Chem. Soc.* **124**, 12940–12941 (2002). doi: 10.1021/ja026973b; pmid: 12405808
37. C. Mao, W. Sun, N. C. Seeman, Designed two-dimensional DNA holliday junction arrays visualized by atomic force

microscopy. *J. Am. Chem. Soc.* **121**, 5437–5443 (1999). doi: 10.1021/ja9900398
38. M. L. Petrillo *et al*., The ligation and flexibility of four-arm DNA junctions. *Biopolymers* **27**, 1337–1352 (1988). doi: 10.1002/bip.360270902; pmid: 3219399
39. H. Yan, S. H. Park, G. Finkelstein, J. H. Reif, T. H. LaBean, DNA-templated self-assembly of protein arrays and highly conductive nanowires. *Science* **301**, 1882–1884 (2003). doi: 10.1126/science.1089389; pmid: 14512621
40. J. Zhang, Y. Liu, Y. Ke, H. Yan, Periodic square-like gold nanoparticle arrays templated by self-assembled 2D DNA Nanogrids on a surface. *Nano Lett.* **6**, 248–251 (2006). doi: 10.1021/nl052210l; pmid: 16464044
41. D. Liu, M. Wang, Z. Deng, R. Walulu, C. Mao, Tensegrity: Construction of rigid DNA triangles with flexible four-arm DNA junctions. *J. Am. Chem. Soc.* **126**, 2324–2325 (2004). doi: 10.1021/ja031754r; pmid: 14982434
42. J. Zheng *et al*., Two-dimensional nanoparticle arrays show the organizational power of robust DNA motifs. *Nano Lett.* **6**, 1502–1504 (2006). doi: 10.1021/nl060994c; pmid: 16834438
43. J. Zheng *et al*., From molecular to macroscopic via the rational design of a self-assembled 3D DNA crystal. *Nature* **461**, 74–77 (2009). doi: 10.1038/nature08274; pmid: 19727196
44. Y. He *et al*., Hierarchical self-assembly of DNA into symmetric supramolecular polyhedra. *Nature* **452**, 198–201 (2008). doi: 10.1038/nature06597; pmid: 18337818
45. B. Wei, M. Dai, P. Yin, Complex shapes self-assembled from single-stranded DNA tiles. *Nature* **485**, 623–626 (2012). doi: 10.1038/nature11075; pmid: 22660323
46. Y. Ke, L. L. Ong, W. M. Shih, P. Yin, Three-dimensional structures self-assembled from DNA bricks. *Science* **338**, 1177–1183 (2012). doi: 10.1126/science.1227268; pmid: 23197527
47. P. W. K. Rothemund, Folding DNA to create nanoscale shapes and patterns. *Nature* **440**, 297–302 (2006). doi: 10.1038/nature04586; pmid: 16541064
48. A. V. Pinheiro, D. Han, W. M. Shih, H. Yan, Challenges and opportunities for structural DNA nanotechnology. *Nat. Nanotechnol.* **6**, 763–772 (2011). doi: 10.1038/nnano.2011.187; pmid: 22056726
49. S. M. Douglas *et al*., Rapid prototyping of 3D DNA-origami shapes with caDNAno. *Nucleic Acids Res.* **37**, 5001–5006 (2009). doi: 10.1093/nar/gkp436; pmid: 19531737
50. C. E. Castro *et al*., A primer to scaffolded DNA origami. *Nat. Methods* **8**, 221–229 (2011). doi: 10.1038/nmeth.1570; pmid: 21358626
51. H. Yan, T. H. LaBean, L. Feng, J. H. Reif, Directed nucleation assembly of DNA tile complexes for barcode-patterned lattices. *Proc. Natl. Acad. Sci. U.S.A.* **100**, 8103–8108 (2003). doi: 10.1073/pnas.1032954100; pmid: 12821776
52. W. M. Shih, J. D. Quispe, G. F. Joyce, A 1.7-kilobase single-stranded DNA that folds into a nanoscale octahedron. *Nature* **427**, 618–621 (2004). doi: 10.1038/nature02307; pmid: 14961116
53. E. S. Andersen *et al*., Self-assembly of a nanoscale DNA box with a controllable lid. *Nature* **459**, 73–76 (2009). doi: 10.1038/nature07971; pmid: 19424153
54. S. M. Douglas, I. Bachelet, G. M. Church, A logic-gated nanorobot for targeted transport of molecular payloads. *Science* **335**, 831–834 (2012). doi: 10.1126/science.1214081; pmid: 22344439
55. S. Rinker, Y. Ke, Y. Liu, R. Chhabra, H. Yan, Self-assembled DNA nanostructures for distance-dependent multivalent ligand-protein binding. *Nat. Nanotechnol.* **3**, 418–422 (2008). doi: 10.1038/nnano.2008.164; pmid: 18654566
56. B. Ding *et al*., Gold nanoparticle self-similar chain structure organized by DNA origami. *J. Am. Chem. Soc.* **132**, 3248–3249 (2010). doi: 10.1021/ja9101198; pmid: 20163139
57. S. Pal *et al*., DNA directed self-assembly of anisotropic plasmonic nanostructures. *J. Am. Chem. Soc.* **133**, 17606–17609 (2011). doi: 10.1021/ja207898r; pmid: 21981707
58. S. M. Douglas *et al*., Self-assembly of DNA into nanoscale three-dimensional shapes. *Nature* **459**, 414–418 (2009). doi: 10.1038/nature08016; pmid: 19458720
59. H. Dietz, S. M. Douglas, W. M. Shih, Folding DNA into twisted and curved nanoscale shapes. *Science* **325**, 725–730 (2009). doi: 10.1126/science.1174251; pmid: 19661424
60. D. Han *et al*., DNA origami with complex curvatures in three-dimensional space. *Science* **332**, 342–346 (2011). doi: 10.1126/science.1202998; pmid: 21493857
61. J.-P. J. Sobczak, T. G. Martin, T. Gerling, H. Dietz, Rapid folding of DNA into nanoscale shapes at constant temperature. *Science* **338**, 1458–1461 (2012). doi: 10.1126/science.1229919; pmid: 23239734
62. G. P. Acuna *et al*., Fluorescence enhancement at docking sites of DNA-directed self-assembled nanoantennas. *Science* **338**, 506–510 (2012). doi: 10.1126/science.1228638; pmid: 23112329
63. A. Kuzyk *et al*., DNA-based self-assembly of chiral plasmonic nanostructures with tailored optical response. *Nature* **483**, 311–314 (2012). doi: 10.1038/nature10889; pmid: 22422265
64. W. Liu, H. Zhong, R. Wang, N. C. Seeman, Crystalline two-dimensional DNA-origami arrays. *Angew. Chem. Int. Ed. Engl.* **50**, 264–267 (2011). doi: 10.1002/anie.201005911; pmid: 21053236
65. P. E. Constantinou *et al*., Double cohesion in structural DNA nanotechnology. *Org. Biomol. Chem.* **4**, 3414–3419 (2006). doi: 10.1039/b605212f; pmid: 17036134
66. M. R. Jones, K. D. Osberg, R. J. Macfarlane, M. R. Langille, C. A. Mirkin, Templated techniques for the synthesis and assembly of plasmonic nanostructures. *Chem. Rev.* **111**, 3736–3827 (2011). doi: 10.1021/cr1004452; pmid: 21648955
67. R. Jin, G. Wu, Z. Li, C. A. Mirkin, G. C. Schatz, What controls the melting properties of DNA-linked gold nanoparticle assemblies? *J. Am. Chem. Soc.* **125**, 1643–1654 (2003). doi: 10.1021/ja021096v; pmid: 12568626
68. A. K. R. Lytton-Jean, C. A. Mirkin, A thermodynamic investigation into the binding properties of DNA functionalized gold nanoparticle probes and molecular fluorophore probes. *J. Am. Chem. Soc.* **127**, 12754–12755 (2005). doi: 10.1021/ja052255o; pmid: 16159241
69. R. Elghanian, J. J. Storhoff, R. C. Mucic, R. L. Letsinger, C. A. Mirkin, Selective colorimetric detection of polynucleotides based on the distance-dependent optical properties of gold nanoparticles. *Science* **277**, 1078–1081 (1997). doi: 10.1126/science.277.5329.1078; pmid: 9262471
70. H. D. Hill, C. A. Mirkin, The bio-barcode assay for the detection of protein and nucleic acid targets using DTT-induced ligand exchange. *Nat. Protoc.* **1**, 324–336 (2006). doi: 10.1038/nprot.2006.51; pmid: 17406253
71. T. M. Herne, M. J. Tarlov, Characterization of DNA probes immobilized on gold surfaces. *J. Am. Chem. Soc.* **119**, 8916–8920 (1997). doi: 10.1021/ja9719586
72. R. C. Mucic, J. J. Storhoff, C. A. Mirkin, R. L. Letsinger, DNA-directed synthesis of binary nanoparticle network materials. *J. Am. Chem. Soc.* **120**, 12674–12675 (1998). doi: 10.1021/ja982721s
73. R. J. Macfarlane *et al*., Assembly and organization processes in DNA-directed colloidal crystallization. *Proc. Natl. Acad. Sci. U.S.A.* **106**, 10493–10498 (2009). doi: 10.1073/pnas.0900630106; pmid: 19549828
74. R. J. Macfarlane *et al*., Nanoparticle superlattice engineering with DNA. *Science* **334**, 204–208 (2011). doi: 10.1126/science.1210493; pmid: 21998382
75. E. Auyeung *et al*., Synthetically programmable nanoparticle superlattices using a hollow three-dimensional spacer approach. *Nat. Nanotechnol.* **7**, 24–28 (2012). doi: 10.1038/nnano.2011.222; pmid: 22157725
76. R. J. Macfarlane, M. R. Jones, B. Lee, E. Auyeung, C. A. Mirkin, Topotactic interconversion of nanoparticle superlattices. *Science* **341**, 1222–1225 (2013). doi: 10.1126/science.1241402; pmid: 23970559
77. C. Zhang *et al*., A general approach to DNA-programmable atom equivalents. *Nat. Mater.* **12**, 741–746 (2013). doi: 10.1038/nmat3647; pmid: 23685863
78. Y. Zhang, F. Lu, K. G. Yager, D. van der Lelie, O. Gang, A general strategy for the DNA-mediated self-assembly of functional nanoparticles into heterogeneous systems. *Nat. Nanotechnol.* **8**, 865–872 (2013). doi: 10.1038/nnano.2013.209; pmid: 24141539
79. D. Sun, O. Gang, Binary heterogeneous superlattices assembled from quantum dots and gold nanoparticles with DNA. *J. Am. Chem. Soc.* **133**, 5252–5254 (2011). doi: 10.1021/ja111542t; pmid: 21425848
80. A. J. Senesi *et al*., Stepwise evolution of DNA-programmable nanoparticle superlattices. *Angew. Chem. Int. Ed. Engl.* **52**, 6624–6628 (2013). doi: 10.1002/anie.201301936; pmid: 23681747
81. E. Auyeung, R. J. Macfarlane, C. H. J. Choi, J. I. Cutler, C. A. Mirkin, Transitioning DNA-engineered nanoparticle superlattices from solution to the solid state. *Adv. Mater.* **24**, 5181–5186 (2012). doi: 10.1002/adma.201202069; pmid: 22810947
82. E. Auyeung *et al*., DNA-mediated nanoparticle crystallization into Wulff polyhedra. *Nature* **505**, 73–77 (2014). doi: 10.1038/nature12739; pmid: 24284632
83. D. J. Park *et al*., Plasmonic photonic crystals realized through DNA-programmable assembly. *Proc. Natl. Acad. Sci. U.S.A.* **112**, 977–981 (2015). doi: 10.1073/pnas.1422649112; pmid: 25548175
84. X. Xu, N. L. Rosi, Y. Wang, F. Huo, C. A. Mirkin, Asymmetric functionalization of gold nanoparticles with oligonucleotides. *J. Am. Chem. Soc.* **128**, 9286–9287 (2006). doi: 10.1021/ja061980b; pmid: 16848436
85. F. Huo, A. K. R. Lytton-Jean, C. A. Mirkin, Asymmetric functionalization of nanoparticles based on thermally addressable DNA interconnects. *Adv. Mater.* **18**, 2304–2306 (2006). doi: 10.1002/adma.200601178
86. M. M. Maye, D. Nykypanchuk, M. Cuisinier, D. van der Lelie, O. Gang, Stepwise surface encoding for high-throughput assembly of nanoclusters. *Nat. Mater.* **8**, 388–391 (2009). doi: 10.1038/nmat2421; pmid: 19329992
87. J. E. Millstone *et al*., DNA-gold triangular nanoprism conjugates. *Small* **4**, 2176–2180 (2008). doi: 10.1002/smll.200800931; pmid: 19016498
88. L. Xu *et al*., Regiospecific plasmonic assemblies for in situ Raman spectroscopy in live cells. *J. Am. Chem. Soc.* **134**, 1699–1709 (2012). doi: 10.1021/ja2088713; pmid: 22192084
89. L. Feng, L.-L. Pontani, R. Dreyfus, P. Chaikin, J. Brujic, Specificity, flexibility and valence of DNA bonds guide emulsion architecture. *Soft Matter* **9**, 9816–9823 (2013). doi: 10.1039/c3sm51586a
90. S. A. J. van der Meulen, M. E. Leunissen, Solid colloids with surface-mobile DNA linkers. *J. Am. Chem. Soc.* **135**, 15129–15134 (2013). doi: 10.1021/ja406226b; pmid: 24040916
91. Y. Wang *et al*., Colloids with valence and specific directional bonding. *Nature* **491**, 51–55 (2012). doi: 10.1038/nature11564; pmid: 23128225
92. M. R. Jones, C. A. Mirkin, Materials science: Self-assembly gets new direction. *Nature* **491**, 42–43 (2012). doi: 10.1038/491042a; pmid: 23128220
93. M. R. Jones *et al*., DNA-nanoparticle superlattices formed from anisotropic building blocks. *Nat. Mater.* **9**, 913–917 (2010). doi: 10.1038/nmat2870; pmid: 20890281
94. M. R. Jones, R. J. Macfarlane, A. E. Prigodich, P. C. Patel, C. A. Mirkin, Nanoparticle shape anisotropy dictates the collective behavior of surface-bound ligands. *J. Am. Chem. Soc.* **133**, 18865–18869 (2011). doi: 10.1021/ja206777k; pmid: 22043984
95. M. R. Jones, C. A. Mirkin, Bypassing the limitations of classical chemical purification with DNA-programmable nanoparticle recrystallization. *Angew. Chem. Int. Ed. Engl.* **52**, 2886–2891 (2013). doi: 10.1002/anie.201209504; pmid: 23404954
96. R. Dreyfus *et al*., Simple quantitative model for the reversible association of DNA coated colloids. *Phys. Rev. Lett.* **102**, 048301 (2009). doi: 10.1103/PhysRevLett.102.048301; pmid: 19257481
97. F. J. Martinez-Veracoechea, M. E. Leunissen, The entropic impact of tethering, multivalency and dynamic recruitment in systems with specific binding groups. *Soft Matter* **9**, 3213–3219 (2013). doi: 10.1039/c3sm27766f
98. R. Schreiber *et al*., Hierarchical assembly of metal nanoparticles, quantum dots and organic dyes using DNA origami scaffolds. *Nat. Nanotechnol.* **9**, 74–78 (2014). doi: 10.1038/nnano.2013.253; pmid: 24292513
99. D. Y. Zhang, A. J. Turberfield, B. Yurke, E. Winfree, Engineering entropy-driven reactions and networks catalyzed by DNA. *Science* **318**, 1121–1125 (2007). doi: 10.1126/science.1148532; pmid: 18006742
100. R. M. Dirks, N. A. Pierce, Triggered amplification by hybridization chain reaction. *Proc. Natl. Acad. Sci. U.S.A.* **101**, 15275–15278 (2004). doi: 10.1073/pnas.0407024101; pmid: 15492210
101. F. Wang, C.-H. Lu, I. Willner, From cascaded catalytic nucleic acids to enzyme-DNA nanostructures: Controlling reactivity, sensing, logic operations, and assembly of complex structures. *Chem. Rev.* **114**, 2881–2941 (2014). doi: 10.1021/cr400354z; pmid: 24576227
102. Y. Kim, R. J. Macfarlane, C. A. Mirkin, Dynamically interchangeable nanoparticle superlattices through the use of nucleic acid-based allosteric effectors. *J. Am. Chem. Soc.* **135**, 10342–10345 (2013). doi: 10.1021/ja405988r; pmid: 23822216
103. M. M. Maye, M. T. Kumara, D. Nykypanchuk, W. B. Sherman, O. Gang, Switching binary states of nanoparticle superlattices and dimer clusters by DNA strands. *Nat. Nanotechnol.* **5**, 116–120 (2010). doi: 10.1038/nnano.2009.378; pmid: 20023646

104. W. B. Rogers, V. N. Manoharan, Programming colloidal phase transitions with DNA strand displacement. *Science* **347** 639 (2015).
105. N. L. Rosi *et al*., Oligonucleotide-modified gold nanoparticles for intracellular gene regulation. *Science* **312**, 1027–1030 (2006). doi: 10.1126/science.1125559; pmid: 16709779
106. T. A. Taton, C. A. Mirkin, R. L. Letsinger, Scanometric DNA array detection with nanoparticle probes. *Science* **289**, 1757–1760 (2000). doi: 10.1126/science.289.5485.1757; pmid: 10976070
107. D. S. Seferos, D. A. Giljohann, H. D. Hill, A. E. Prigodich, C. A. Mirkin, Nano-flares: Probes for transfection and mRNA detection in living cells. *J. Am. Chem. Soc.* **129**, 15477–15479 (2007). doi: 10.1021/ja0776529; pmid: 18034495
108. Nanosphere; www.nanosphere.us.
109. EMD Millipore; www.emdmillipore.com/smartflare.
110. C. Lin *et al*., Submicrometre geometrically encoded fluorescent barcodes self-assembled from DNA. *Nat. Chem.* **4**, 832–839 (2012). doi: 10.1038/nchem.1451; pmid: 23000997

ACKNOWLEDGMENTS

C.A.M. thanks the Air Force Office of Scientific Research under award FA9550-11-1-0275. N.C.S. thanks the following grants: N000141110729 and N000140911118 from the Office of Naval Research; grants CMMI-1120890, EFRI-1332411, and CCF-1117210 from the National Science Foundation (NSF); Multidisciplinary University Research Initiative W911NF-11-1-0024 from the Army Research Office; DE-SC0007991 from the U.S. Department of Energy for partial salary support; and grant 3849 from the Gordon and Betty Moore Foundation. C.A.M. and M.R.J. thank E. Auyeung, J. Cutler, and J. Wu for providing the tomographic reconstruction of the AB_6 nanoparticle superlattice provided in Fig. 5A. M.R.J. thanks NSF for a Graduate Research Fellowship. The authors acknowledge the following patents based on the work described in this document: C.A.M., R. L. Letsinger, R. C. Mucic, J. J. Storhoff, R. Elghanian (Nanosphere), Nanoparticles having oligonucleotides attached thereto and uses therefor, W.O. Patent 1998004740, February 5, 1998; C.A.M., R. L. Letsinger, R. C. Mucic, J. J. Storhoff, R. Elghanian (Nanosphere), Nanoparticles having oligonucleotides attached thereto and uses therefor, U.S. Patent 8,323,888, December 4, 2012; N.C.S., X. Li, X. Yang, J. Qi (New York University), Nanoconstructions of geometrical objects and lattices from antiparallel nucleic acid double crossover molecules, W.O. Patent 1997041142, November 6, 1997; N.C.S., E. Winfree, F. Liu, L. W. Savin (New York University), Polynucleotide lattice for use as tools in genetic engineering, U.S. Patent 6,255,469, July 3, 2001.

10.1126/science.1260901

RESEARCH ARTICLE SUMMARY

DISEASE NETWORKS

Uncovering disease-disease relationships through the incomplete interactome

Jörg Menche, Amitabh Sharma, Maksim Kitsak, Susan Dina Ghiassian, Marc Vidal, Joseph Loscalzo, Albert-László Barabási*

INTRODUCTION: A disease is rarely a straightforward consequence of an abnormality in a single gene, but rather reflects the interplay of multiple molecular processes. The relationships among these processes are encoded in the interactome, a network that integrates all physical interactions within a cell, from protein-protein to regulatory protein–DNA and metabolic interactions. The documented propensity of disease-associated proteins to interact with each other suggests that they tend to cluster in the same neighborhood of the interactome, forming a disease module, a connected subgraph that contains all molecular determinants of a disease. The accurate identification of the corresponding disease module represents the first step toward a systematic understanding of the molecular mechanisms underlying a complex disease. Here, we present a network-based framework to identify the location of disease modules within the interactome and use the overlap between the modules to predict disease-disease relationships.

RATIONALE: Despite impressive advances in high-throughput interactome mapping and disease gene identification, both the interactome and our knowledge of disease-associated genes remain incomplete. This incompleteness prompts us to ask to what extent the current data are sufficient to map out the disease modules, the first step toward an integrated approach toward human disease. To make progress, we must formulate mathematically the impact of network incompleteness on the identifiability of disease modules, quantifying the predictive power and the limitations of the current interactome.

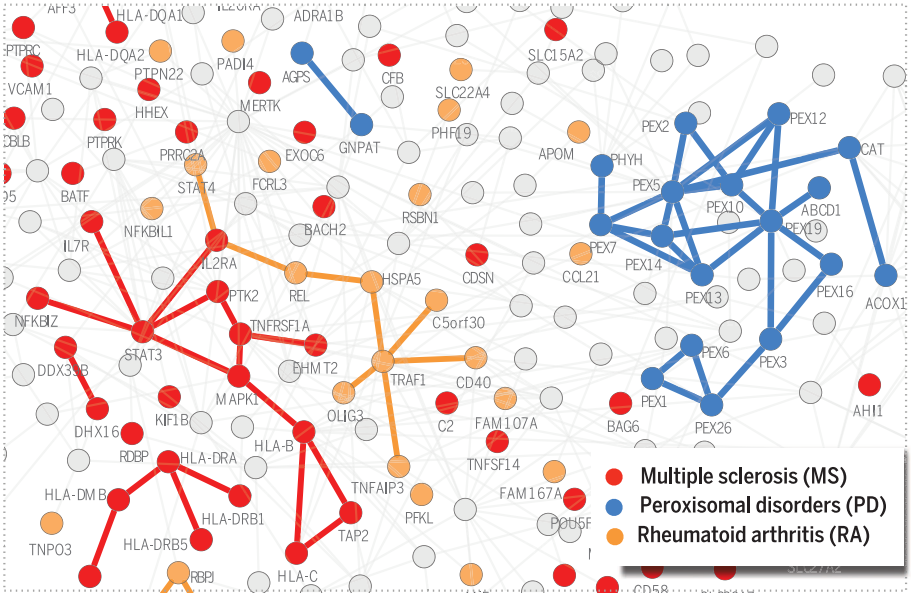
RESULTS: Using the tools of network science, we show that we can only uncover disease modules for diseases whose number of associated genes exceeds a critical threshold determined by the network incompleteness. We find that disease proteins associated with 226 diseases are clustered in the same network neighborhood, displaying a statistically significant tendency to form identifiable disease modules. The higher the degree of agglomeration of the disease proteins within the interactome, the higher the biological and functional similarity of the corresponding genes. These findings indicate that many local neighborhoods of the interactome represent the observable part of the true, larger and denser disease modules.

If two disease modules overlap, local perturbations causing one disease can disrupt pathways of the other disease module as well, resulting in shared clinical and pathobiological characteristics. To test this hypothesis, we measure the network-based separation of each disease pair, observing a direct relation between the pathobiological similarity of diseases and their relative distance in the interactome. We find that disease pairs with overlapping disease modules display significant molecular similarity, elevated coexpression of their associated genes, and similar symptoms and high comorbidity. At the same time, non-overlapping disease pairs lack any detectable pathobiological relationships. The proposed network-based distance allows us to predict the pathobiological relationship even for diseases that do not share genes.

CONCLUSION: Despite its incompleteness, the interactome has reached sufficient coverage to allow the systematic investigation of disease mechanisms and to help uncover the molecular origins of the pathobiological relationships between diseases. The introduced network-based framework can be extended to address numerous questions at the forefront of network medicine, from interpreting genome-wide association study data to drug target identification and repurposing. ■

ON OUR WEB SITE

Read the full article at http://dx.doi.org/10.1126/science.1257601



Diseases within the interactome. The interactome collects all physical interactions between a cell's molecular components. Proteins associated with the same disease form connected subgraphs, called disease modules, shown for multiple sclerosis (MS), peroxisomal disorders (PD), and rheumatoid arthritis (RA). Disease pairs with overlapping modules (MS and RA) have some phenotypic similarities and high comorbidity. Non-overlapping diseases, like MS and PD, lack detectable clinical relationships.

The list of author affiliations is available in the full article online.
*Corresponding author. E-mail: alb@neu.edu
Cite this article as J. Menche *et al.*, *Science* **347**, 1257601 (2015). DOI: 10.1126/science.1257601

Downloaded from www.sciencemag.org on February 21, 2015

RESEARCH ARTICLE

DISEASE NETWORKS

Uncovering disease-disease relationships through the incomplete interactome

Jörg Menche,[1,2,3] Amitabh Sharma,[1,2] Maksim Kitsak,[1,2] Susan Dina Ghiassian,[1,2] Marc Vidal,[2,4] Joseph Loscalzo,[5] Albert-László Barabási[1,2,3,5]*

According to the disease module hypothesis, the cellular components associated with a disease segregate in the same neighborhood of the human interactome, the map of biologically relevant molecular interactions. Yet, given the incompleteness of the interactome and the limited knowledge of disease-associated genes, it is not obvious if the available data have sufficient coverage to map out modules associated with each disease. Here we derive mathematical conditions for the identifiability of disease modules and show that the network-based location of each disease module determines its pathobiological relationship to other diseases. For example, diseases with overlapping network modules show significant coexpression patterns, symptom similarity, and comorbidity, whereas diseases residing in separated network neighborhoods are phenotypically distinct. These tools represent an interactome-based platform to predict molecular commonalities between phenotypically related diseases, even if they do not share primary disease genes.

Identifying sequence variations associated with specific phenotypes represents only the first step of a systematic program toward understanding human disease. Indeed, most phenotypes reflect the interplay of multiple molecular components that interact with each other (*1*–*6*), many of which do not carry disease-associated variations. Hence, we must view disease-associated mutations in the context of the human interactome, a comprehensive map of all biologically relevant molecular interactions (*6*–*12*).

Yet, the predictive power of the current network-based approaches to human disease is limited by several conceptual and methodological issues. First, high-throughput methods cover less than 20% of all potential pairwise protein interactions in the human cell (*11*–*16*), which means that we seek to discover disease mechanisms relying on interactome maps that are 80% incomplete. Second, the genetic roots of a disease are traditionally captured by the list of disease genes whose mutations have a causal effect on the respective phenotype. The disease proteins (the products of disease genes) are not scattered randomly in the interactome, but tend to interact with each other, forming one or several connected subgraphs that we call the disease module (Fig. 1A). This agglomeration of disease proteins is supported by a range of biological and empirical evidence (*7*, *17*, *18*) and has fueled the development of numerous tools to identify new disease genes and prioritize pathways for disease relevance (*8*, *9*, *19*–*28*). Despite its frequent use, however, the disease module hypothesis lacks a solid mathematical basis. Third, the relationships between distinct phenotypes are currently uncovered by identifying shared components like disease genes, single-nucleotide polymorphisms (SNPs), pathways, or differentially expressed genes involved in both diseases. This has resulted in the construction of "disease networks," unveiling the common genetic origins of many disease pairs (*7*, *29*). Yet, shared genes offer only limited information about the relationship between two diseases. Indeed, mechanistic insights are often carried by the molecular networks through which the gene products associated with the two diseases interact with each other.

[1]Center for Complex Networks Research and Department of Physics, Northeastern University, 110 Forsyth Street, 111 Dana Research Center, Boston, MA 02115, USA. [2]Center for Cancer Systems Biology (CCSB) and Department of Cancer Biology, Dana-Farber Cancer Institute, 450 Brookline Avenue, Boston, MA 02215, USA. [3]Center for Network Science, Central European University, Nador u. 9, 1051 Budapest, Hungary. [4]Department of Genetics, Harvard Medical School, 77 Avenue Louis Pasteur, Boston, MA 02115, USA. [5]Department of Medicine, Brigham and Women's Hospital, Harvard Medical School, 75 Francis Street, Boston, MA 02115, USA.
*Corresponding author. E-mail: alb@neu.edu

The fragmentation of disease modules

We started by compiling 141,296 physical interactions between 13,460 proteins experimentally documented in human cells, including protein-protein and regulatory interactions, metabolic pathway interactions, and kinase-substrate interactions [Fig. 1; see also figs. S1 and S2 and supplementary materials (SM) section 1 for a detailed discussion], representing a blueprint of the human interactome (Fig. 1D). We also compiled a corpus of all 299 diseases defined by the Medical Subject Headings (MeSH) ontology that have at least 20 associated genes in the current Online Mendelian Inheritance in Man (OMIM) and genome-wide association study (GWAS) databases (*30*, *31*), involving 2436 disease-associated proteins (Fig. 1, B and C, and SM section 1).

Despite the best curation efforts, both the interactome and the disease gene list remain incomplete (*6*, *11*–*16*) and biased toward much-studied disease genes and disease mechanisms (*32*, *33*). The consequences of this incompleteness are illustrated by multiple sclerosis: Of the 69 genes associated with the disease, only 11 disease proteins form a connected subgraph (observable module, Fig. 1D); the remaining 58 proteins appear to be distributed randomly in the interactome. This pattern holds for all 299 diseases, their observable modules comprising on average only 20% of the respective disease genes (Fig. 1C). Several factors contribute to this fragmentation (Fig. 1A), the main one being data incompleteness: Missing links leave many disease proteins isolated from their disease module (Fig. 1A).

In percolation theory, if only a p fraction of links is available, a connected subgraph (disease module) of m nodes undergoes a phase transition under certain conditions (*34*, *35*): If p is above p_c^m, some fraction of nodes continue to form an observable module; if, however, p is below p_c^m, the module becomes too fragmented to be observable (Fig. 1E; see also fig. S14 and SM section 6). To quantify this phenomenon, we calculated the minimum network coverage p_c^m required to observe a disease module of original size m, finding that $p_c^m \sim 1/m$, valid for an arbitrary degree distribution of the underlying interactome. Figure 1F illustrates a signature of this phenomenon in the interactome: The observable disease module size S_i versus the number of disease genes associated with each disease follows the predicted percolation transition (purple line). Hence, percolation theory predicts that for diseases with fewer than $N_c \approx 25$ genes, the module is too fragmented to be observable in the current interactome; only diseases with $N_d > N_c$ disease genes should have an observable disease module.

To test whether the observed disease modules represent nonrandom disease gene aggregations, for each disease we compared the size S_i of its observable module with the expected S_i^{rand} if the same number of disease proteins were placed randomly on the interactome. For example, for multiple sclerosis, the observed $S_i = 11$ is significantly larger than the random expectation $S_i^{\text{rand}} = 2 \pm 1$ (z score = 5.8, p value = 3.3×10^{-9}, Figs. 1D and 2A); hence, the observed multiple sclerosis module cannot be attributed to a random agglomeration of disease genes. We also determined for each disease protein the network-based distance d_s to the closest other protein associated with the same disease. Again, for multiple sclerosis, $P(d_s)$ is shifted toward smaller d_s compared to the random expectation $P^{\text{rand}}(d_s)$ (p value = 2.6×10^{-6}, Fig. 2B), indicating that the disconnected disease proteins agglomerate in the neighborhood of the observable module. Altogether, disease genes associated with 226

of the 299 diseases show a statistically significant tendency to form disease modules based on both S_i and $P(d_s)$ (fig. S4).

We also asked if there is a relationship between the tendency of disease proteins to agglomerate in the same interactome neighborhood and their biological similarity (*7*, *36*, *37*). We find that as the relative size $s_i \equiv S_i/N_i$ of the observable module increases from 0.1 to 0.8, a sign

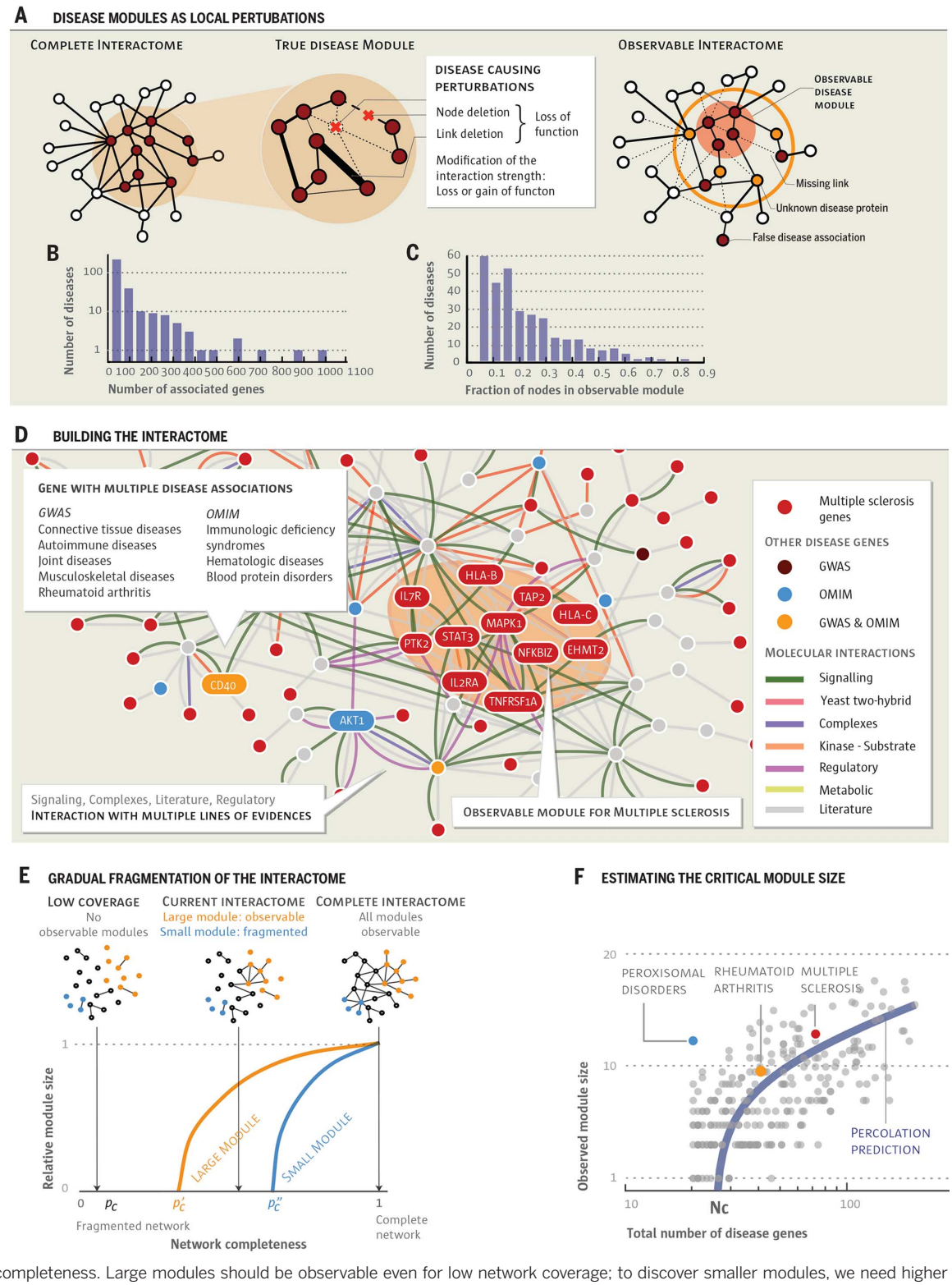


Fig. 1. From the human interactome to disease modules. (**A**) According to the disease module hypothesis, a disease represents a local perturbation of the underlying disease-associated subgraph. Such perturbations could represent the removal of a protein (e.g., by a nonsense mutation), the disruption of a protein-protein interaction, or modifications in the strength of an interaction. The complete disease module can be identified only in a full interactome map; the disease module observable to us captures a subset of this module, owing to data incompleteness. (**B**) Distribution of the number of disease-associated genes for 299 diseases. (**C**) Distribution of the fraction of disease genes within the observable disease module. (**D**) A small neighborhood of the interactome showing the biological nature of each physical interaction and the origin of the disease-gene associations used in our study (see also SM section 1). Genes associated with multiple sclerosis are shown in red, the shaded area indicating their observable module, a connected subgraph consisting of 11 proteins. (**E**) Schematic illustration of the predicted size of the observable disease modules (subgraphs) as a function of network completeness. Large modules should be observable even for low network coverage; to discover smaller modules, we need higher network completeness. (**F**) Size of the observable module as a function of the total number of disease genes. The purple curve corresponds to the percolation-based prediction (SM section 6), indicating that diseases with $N_d < N_c \approx 25$ genes do not have an observable disease module in the current interactome. Each gray point captures one of the 299 diseases.

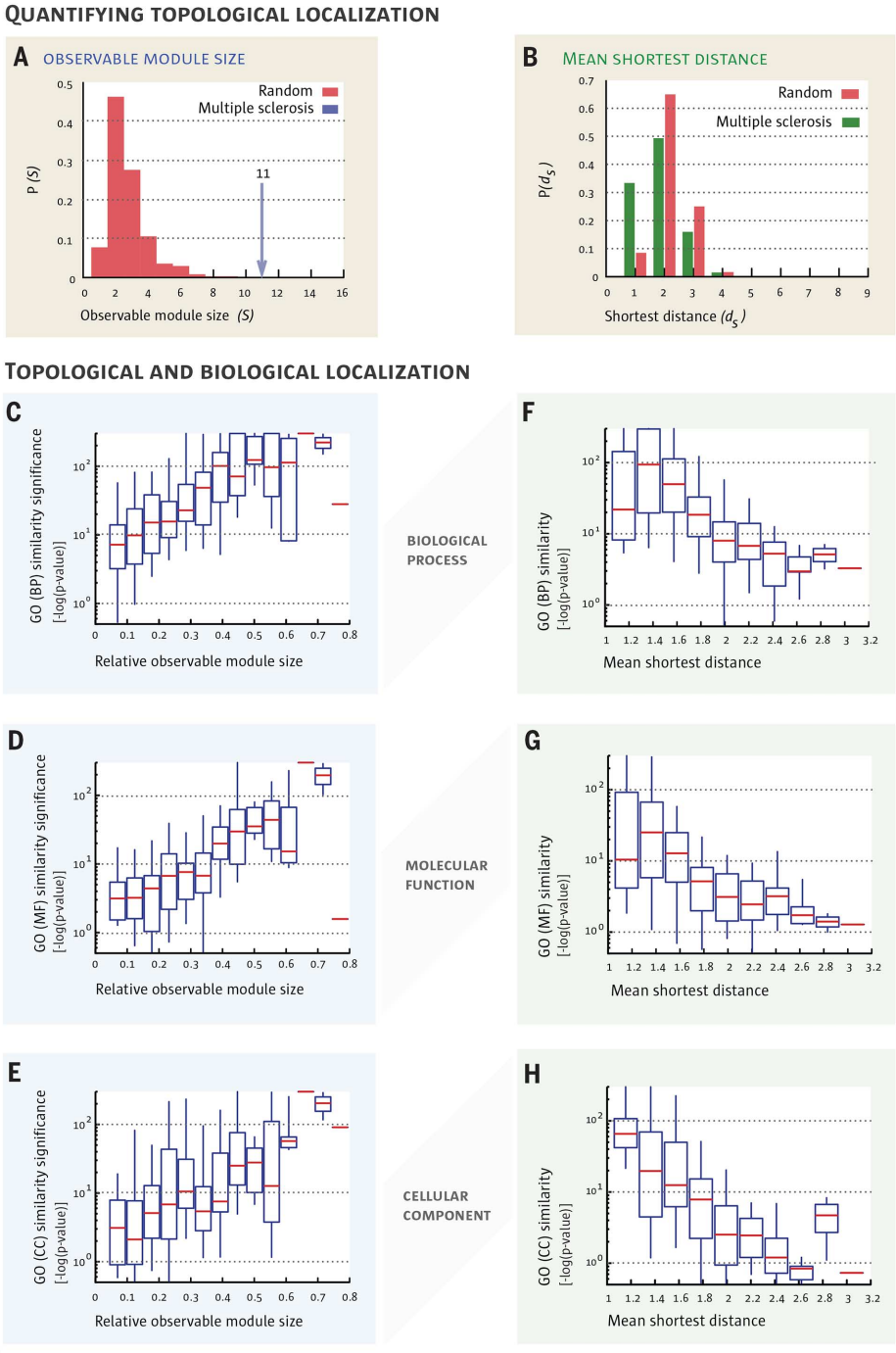


Fig. 2. Topological localization and biological similarity of disease genes. (**A**) The size of the largest connected component S of proteins associated with the same disease shown for multiple sclerosis. The observed module size, $S = 11$, is significantly larger than the random expectation $S^{rand} = 2 \pm 1$. (**B**) The distribution of the shortest distance of each disease protein to the next closest disease protein d_s. For multiple sclerosis, $P(d_s)$ is significantly shifted compared to the random expectation, indicating that disease genes tend to agglomerate in each other's network neighborhood. (**C** to **H**) The degree of the network-based localization of a disease, as measured by the relative size of its observable module $s_i = S_i/N_d$ and the mean shortest distance $\langle d_s \rangle$, correlates strongly with the significance of the biological similarity of the respective disease genes. Using the GO annotations, we determine for each disease how similar its associated genes are in terms of their biological processes (C and F), molecular function (D and G), and cellular component (E and H). Comparing the resulting values with random expectation, we find that the more localized a disease is topologically (i.e., the larger s_i or the shorter $\langle d_s \rangle$), the higher the significance in the similarity of the associated genes.

of increasing agglomeration of the disease genes, the significance of the biological similarity in Gene Ontology (GO) annotations (biological processes, molecular function, and cellular component) increases 10- to 100-fold (Fig. 2, C to E, and fig. S3, a to c), an exceptionally strong effect (see SM sect. 2 for statistical analysis). Similarly, as the mean shortest distance between disease proteins increases from 1 (agglomerated disease proteins) to 3 (scattered disease proteins), we observe a factor of 10 to 100 decrease in the significance of GO term similarity (Fig. 2, F to H, and fig. S3, d to f).

Taken together, we find that genes associated with the same disease tend to agglomerate in the same neighborhood of the interactome. Indeed, although ~80% of the disease proteins are disconnected from the observable module, these isolates tend to be localized in its network vicinity. This result offers quantitative support to the hypothesis that many local neighborhoods of the interactome represent the observable parts of the true, larger and denser disease modules.

Relationship between diseases

If two disease modules overlap, local perturbations leading to one disease will likely disrupt pathways involved in the other disease module as well, resulting in shared clinical characteristics. To test the validity of this hypothesis, we introduce the network-based separation of a disease pair, A and B (Fig. 3A; see also figs. S5 to S7) using

$$s_{AB} \equiv \langle d_{AB} \rangle - \frac{\langle d_{AA} \rangle + \langle d_{BB} \rangle}{2} \qquad (1)$$

s_{AB} compares the shortest distances between proteins within each disease, $\langle d_{AA} \rangle$ and $\langle d_{BB} \rangle$, to the shortest distances $\langle d_{AB} \rangle$ between A-B protein pairs. Proteins associated with both A and B have $d_{AB} = 0$. As discussed in SM section 3.3, the generalization of s_{AB} to account for directed regulatory and signaling interactions does not alter our subsequent findings (fig. S8).

We find that only 7% of disease pairs have overlapping disease neighborhoods with negative s_{AB} (Fig. 3B); the remaining 93% have a positive s_{AB}, indicating that their disease modules are topologically separated (Fig. 3C). Because we lack unambiguous true positive and true negative disease relationships that could be used as a reference, we use two complementary null models to evaluate the statistical significance of each disease pair compared to random expectation (see SM section 2.2). At a global false discovery level of 5%, we find that 75% of all disease pairs exhibit significant s_{AB}. To determine the degree to which this network-based separation of two diseases is predictive for pathobiological manifestations, we rely on four data sets:

1) Biological similarity: We find that the closer two diseases are in the interactome, the higher the GO annotation–based similarity of the proteins associated with them (Fig. 3, D to F). The effect is strong, resulting in a two-order-of-magnitude decrease in GO term similarity as we move from highly overlapping ($s_{AB} \approx -2$) to well-separated disease pairs ($s_{AB} > 0$).

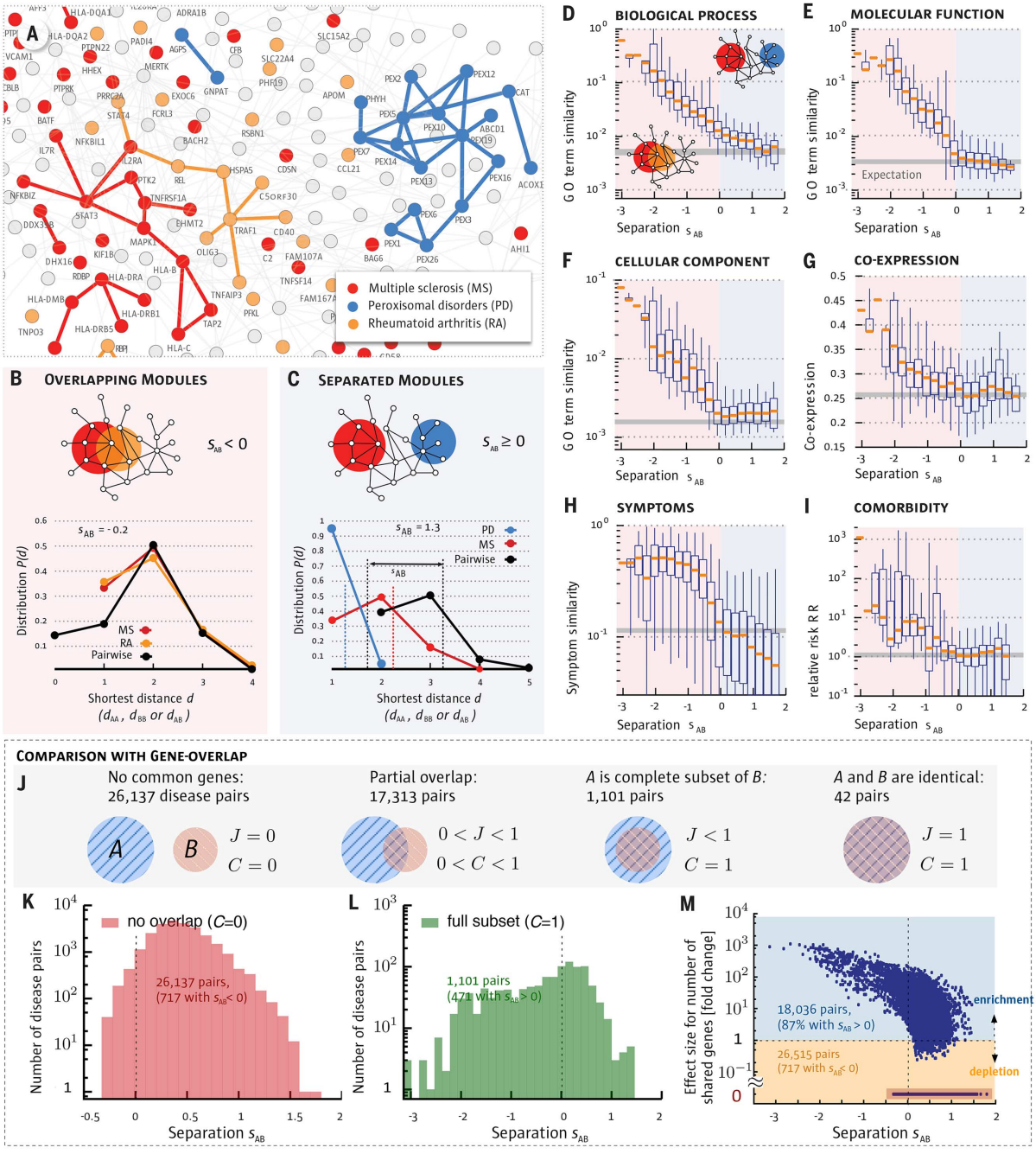


Fig. 3. Network separation and disease similarity. (**A**) A subnetwork of the full interactome highlighting the network-based relationship between disease genes associated with three diseases identified in the legend. (**B** and **C**) Distance distributions for disease pairs that have topologically overlapping modules ($s_{AB} < 0$, B) or topologically separated modules ($s_{AB} > 0$, C). The plots show $P(d)$ for the disease pairs shown in (A). (**D** to **I**) Topological separation versus biomedical similarity. (D to F) GO term similarity; (G) gene coexpression; (H) symptom similarity for all disease pairs in function of their topological separation s_{AB}. The region of overlapping disease pairs is highlighted in red ($s_{AB} < 0$); the region of the separated disease pairs is shown in blue ($s_{AB} > 0$). For symptom similarity, we show the cosine similarity ($c_{AB} = 0$ if there are no shared symptoms between diseases A and B and $c_{AB} = 1$ for diseases with identical symptoms). Comorbidity in (I) is measured by the relative risk *RR* (*40*). Bars in (D) to (I) indicate random expectation (SM section 1): in (D) to (G), the expected value for a randomly chosen protein pair is shown. In (H) and (I), the mean value of all disease pairs is used. (**J** to **M**) The interplay between gene-set overlap and the network-based relationships between disease pairs. (J) The relationship between gene sets *A* and *B* is captured by the overlap coefficient $C = |A \cap B|/\min(|A|, |B|)$ and the Jaccard-index $J = |A \cap B|/|A \cup B|$. More than half (59%) of the disease pairs do not share genes ($J = C = 0$); hence, their relation cannot be uncovered based on shared genes. (K) Distribution of s_{AB} for disease pairs with no gene overlap. We find that despite having disjoint gene sets, 717 diseases pairs have overlapping modules ($s_{AB} < 0$). (L) The distribution of s_{AB} for disease pairs with complete gene overlap ($C = 1$) shows a broad range of network-based relationships, including non-overlapping modules ($s_{AB} > 0$). (M) Fold change of the number of shared genes compared to random expectation versus s_{AB} for all disease pairs. The 59% of all disease pairs without shared genes are highlighted with red background. For 98% of all disease pairs that share at least one gene, the gene-based overlap is larger than expected by chance. Nevertheless, most (87%) of these disease pairs are separated in the network ($s_{AB} > 0$). Conversely, a considerable number of pairs (717) without shared genes exhibit detectable network overlap ($s_{AB} < 0$).

2) Coexpression: We find that the coexpression-based correlation across 70 tissues (*36*) between genes associated with overlapping diseases is almost twice that of well-separated diseases (Fig. 3G), falling to the random expectation for $s_{AB} > 0$.

3) Disease symptoms: We find that symptom similarity, as captured by large-scale medical bibliographic records (*38*), falls about an order of magnitude as we move from overlapping ($s_{AB} < 0$) to separated ($s_{AB} > 0$) diseases (Fig. 3H). Non-overlapping diseases share fewer symptoms than expected by chance.

4) Comorbidity: We used the disease history of 30 million individuals aged 65 and older (U.S. Medicare) to determine for each disease pair the relative risk *RR* of disease comorbidity (*39*) (Fig. 3I), finding that the relative risk drops from $RR \geq 10$ for $s_{AB} < 0$ to the random expectation of $RR \approx 1$ for $s_{AB} > 0$.

Thus, the network-based distance of two diseases indicates their pathobiological and clinical similarity. This result suggests a molecular network model of human disease: Each disease has a well-defined location and a diameter $\langle d_{AA} \rangle$ that captures its network-based size (Fig. 3, A to C). If two disease modules are topologically separated ($s_{AB} > 0$), then the diseases are pathobiologically distinct. If the disease modules topologically overlap ($s_{AB} < 0$), the magnitude of the overlap is indicative of their biological relationship: The higher the overlap, the more significant are the pathobiological similarities between them. We, therefore, represent each disease by a sphere with diameter $\langle d_{AA} \rangle$ in a three-dimensional (3D) disease space such that the physical distance r_{AB} between diseases A and B correlates with the observed network-based distance $\langle d_{AB} \rangle$ (Fig. 4A; see also fig. S15 and SM section 8). Disease modules that do not overlap in Fig. 4A are predicted to be pathobiologically distinct; for those that overlap, the degree of overlap captures their common pathobiology and phenotypic characteristics.

To test the predictive power of this model, we grouped the disease pairs with $s_{AB} < 0$ into the "overlapping" disease category, and those with $s_{AB} > 0$ into the "non-overlapping" disease category. As Fig. 4, B to G, indicates, all biological and clinical characteristics show statistically highly significant similarity for overlapping diseases, whereas the effects vanish for the non-overlapping disease pairs.

The disease separation allows us to identify unexpected overlapping disease pairs, i.e., those that lack overt pathobiological or clinical association (see table S1 for 12 such examples). For example, we find that asthma, a respiratory disease, and celiac disease, an autoimmune disease of the small intestine, are localized in overlapping neighborhoods ($s_{AB} < 0$, Fig. 4N), suggesting shared molecular roots despite their rather different pathobiologies. A closer inspection reveals evidence supporting this prediction: The two diseases share three genes identified via genome-wide associations with genome-wide significance (*HLA-DQA1*, *IL18R1*, *IL1RL1*), and, recently, SNP rs1464510, previously associated with celiac disease, was also found to be associated with asthma (*40*). Although the two diseases have few common phenotypic features, they exhibit a remarkably high comorbidity (*RR* = 6.18) and statistically significant coexpression between their genes ($r = 0.32$, p value = 0.02). Furthermore, the top enriched pathway in the combined gene set of the two diseases is the immune network for immunoglobulin A (IgA) production (p value = 5×10^{-15}, Fig. 4O) with 48 genes, of which seven are associated with asthma and five with celiac disease. Measuring amounts of an IgA antibody subclass against tissue transglutaminase (ATA) is widely used to screen for and diagnose celiac disease (*41*). At the same time, the IgA response to allergens in the respiratory tract of asthma patients plays a pathogenic role through eosinophil activation (*42*).

To determine whether we could have arrived at the same conclusion by identifying diseases with shared genes (*7*), we quantified the predictive power of gene overlap, finding that, indeed, disease pairs with large gene overlap tend to be localized in the same network neighborhood (Fig. 3, L and M). Nevertheless, 59% of disease pairs do not share genes; hence, their relationship cannot be resolved based on the shared gene hypothesis (Fig. 3J; see also figs. S9 and S10). We, therefore, repeated the analysis of Fig. 4, B to G, for all disease pairs without common genes, finding that s_{AB} continues to predict accurately the biological similarity (or distinctness) of these disease pairs (Fig. 4, H to M, and SM section 3). Overall, we find 717 pairs with overlapping disease modules ($s_{AB} < 0$, Fig. 3K), relationships that cannot be predicted based on gene overlap. For example, lymphoma, a cancer, and myocardial infarction, a heart disease, do not share disease genes. Yet, they have strongly overlapping modules ($s_{AB} = -0.24$), indicating that they are located in the same neighborhood of the interactome. Indeed, we find that SMARCA4, a protein associated with myocardial infarction, interacts with ALK, MYC, and NF-κB2, which are lymphoma disease proteins. Cancer cells frequently depend on chromatin regulatory activities to maintain a malignant phenotype. It has been shown that leukemia cells require the SWI/SNF chromatin remodeling complex containing the SMARCA4 protein as the catalytic subunit for their survival and aberrant self-renewal potential (*43*). The relatedness of the two diseases is further supported by a high comorbidity [relative risk (*RR*) = 2.1] and the clinical finding that intravascular large cell lymphoma can affect and obstruct the small vessels of the heart (*44*). Other disease pairs that lack shared genes but are found in the same neighborhood of the interactome include glioma and gout, glioma and myocardial infarction, and myeloproliferative disorders and proteinuria, each pair having high comorbidity (*RR* = 2.43, 6.3, and 2.0, respectively). A detailed discussion of these and other novel disease-disease relationships predicted by our approach is offered in SM section 10.

Summary and discussion

A complete and accurate map of the interactome could have tremendous impact on our ability to understand the molecular underpinnings of human disease. Yet, such a map is at least a decade away, which makes it currently impossible to evaluate precisely how far a given disease module is from completion. Yet, here we showed that despite its incompleteness, the available interactome has sufficient coverage to pursue a systematic network-based approach to human diseases. To be specific, we offer quantitative evidence for the identifiability of some disease modules, while showing that for other diseases the identifiability condition is not yet satisfied at the current level of incompleteness of the interactome. Most important, we demonstrated that the relative interactome-based position of two disease modules is a strong predictor of their biological and phenotypic similarity. Throughout this paper, we focused on the impact of network incompleteness, ignoring another limitation of the interactome: It is prone to notable investigative biases (*12*, *32*, *33*) (see also fig. S13 and SM section 5). We, therefore, repeated our analysis relying only on high-throughput data from yeast two-hybrid screens (*12*) (y2h, SM section 4), finding that the diameter $\langle d_{AA} \rangle$ of the observable modules, the distance $\langle d_{AB} \rangle$ and separation s_{AB} of all disease pairs measured in the full and the unbiased interactome show statistically highly significant correlations. Similarly, OMIM is also prone to selection and investigative biases; hence, we repeated our measurements using only unbiased GWAS-associated disease genes. Comparing gene sets that include OMIM data and those that only contain GWAS associations, we again find highly significant correlations for $\langle d_{AA} \rangle$, $\langle d_{AB} \rangle$, and s_{AB} (figs. S11 and S12). Therefore, the disease modules and the overlap between them can be reproduced in the unbiased data as well, indicating that our key findings cannot be attributed to investigative biases. We estimate the minimal number of associated genes that a disease needs to have in order to be observable to be around 25 for the current interactome. Unbiased high-throughput data alone have not yet reached sufficient coverage to map out putative modules for many diseases; For the y2h network, being a subset of the interactome with a much lower coverage, the respective minimal number is around 350 (N_c^{y2h}); hence, only a few disease modules can be observed (see fig. S14f). However, this approach can provide valuable insights into the properties of the complete interactome (SM section 6). Indeed, as the current y2h data are expected to represent a uniform subset of the complete y2h network (*12*), we can use it to derive the minimum coverage p_c^m of the latter. As the coverage of high-throughput maps improves, they will allow us to use the full power of unbiased approaches for disease module identification.

The true value of the developed interactome-based approach is its open-ended multipurpose nature: It offers a platform that can address numerous fundamental and practical issues pertaining to our understanding of human disease. This platform can be used to improve the interpretation of GWAS data (see fig. S16 and SM section 10 for an application to type II

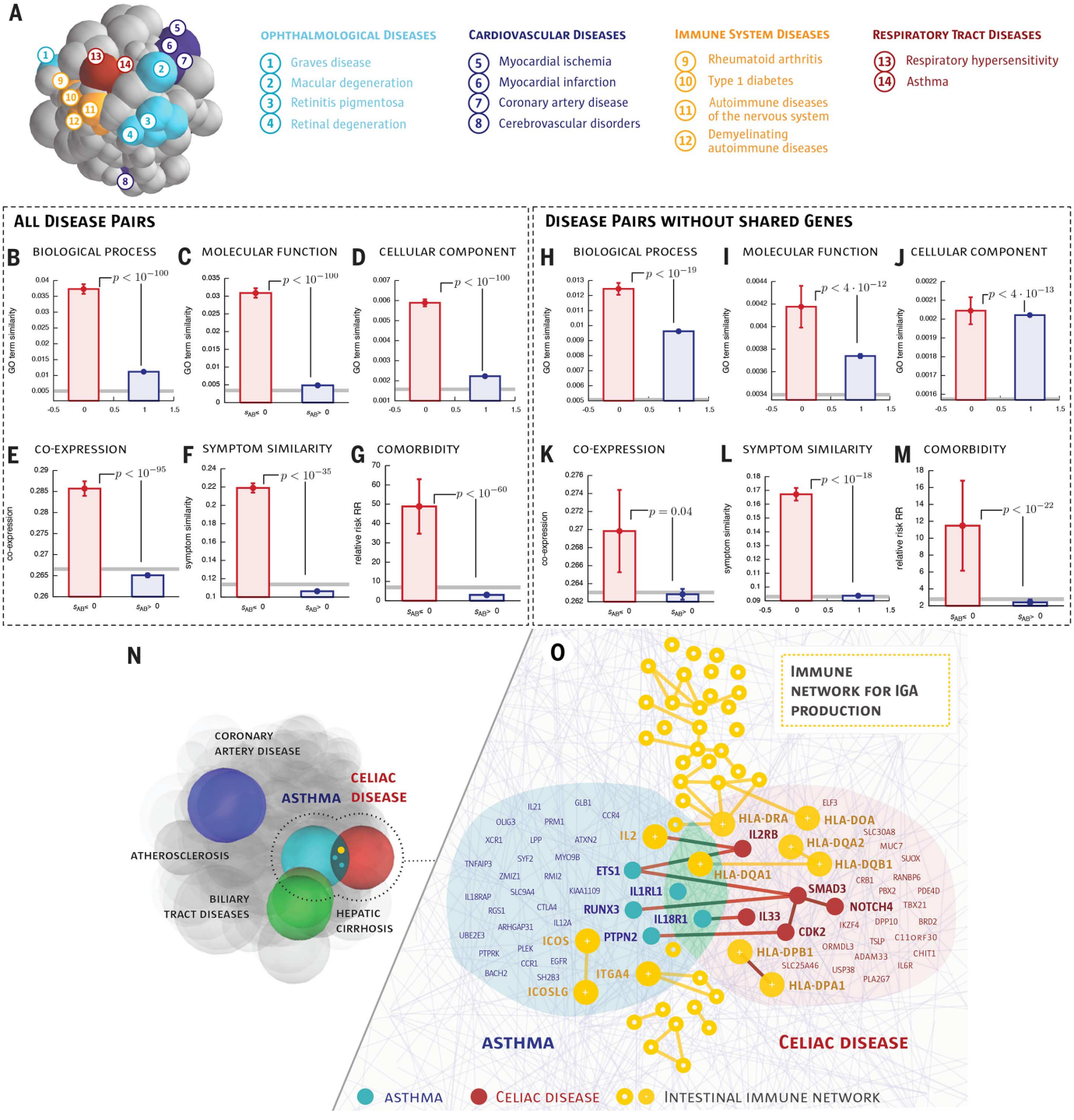


Fig. 4. Network-based model of disease-disease relationship. (**A**) To illustrate the uncovered network-based relationship between diseases, we place each disease in a 3D disease space, such that their physical distance to other diseases is proportional to $\langle d_{AB} \rangle$ predicted by the interactome-based analysis. Diseases whose modules (spheres) overlap are predicted to have common molecular underpinnings. The colors capture several broad disease classes, indicating that typically diseases of the same class are located close to each other. There are exceptions, such as cerebrovascular disease, which is separated from other cardiovascular diseases, suggesting distinct molecular roots. (**B** to **G**) Biological similarity shown separately for the predicted overlapping and non-overlapping disease pairs (see Fig. 3, D to I, for interpretation). Error bars indicate the SEM. Gray lines show random expectation, either for random protein pairs (B to E, H to K) or for a random disease pair (F, G, L, M); p values denote the significance of the difference of the means according to a Mann-Whitney U test. (**H** to **M**) Biological similarity for disease pairs that do not share genes (control set). (**N**) Three overlapping disease pairs in the disease space. Coronary artery diseases and atherosclerosis, as well as hepatic cirrhosis and biliary tract diseases, are diseases with common classification; hence, their disease modules overlap. Our methodology also predicts several overlapping disease modules of apparently unrelated disease pairs (table S1), illustrated by asthma and celiac disease. (**O**) A network-level map of the overlapping asthma–celiac disease network neighborhood; also shown is the IgA production pathway (yellow) that plays a biological role in both diseases. We denote genes that are either shared by the two diseases or by the pathway, or that interact across the modules.

diabetes), help us uncover new uses for existing drugs (repurposing) by identifying the disease modules located in the vicinity of each drug target (*45*–*47*), and facilitate the discovery of the molecular underpinnings of undiagnosed diseases by exploiting the agglomeration of mutations and expression changes in network neighborhoods associated with well-characterized diseases. In the long run, network-based approaches, relying on an increasingly accurate interactome, are poised to become highly useful in interpreting disease-associated genome variations.

Materials and methods

Interactome construction

We combine several sources of protein interactions: (i) regulatory interactions derived from transcription factors binding to regulatory elements; (ii) binary interactions from several yeast two-hybrid high-throughput and literature-curated data sets; (iii) literature-curated interactions derived mostly from low-throughput experiments; (iv) metabolic enzyme-coupled interactions; (v) protein complexes; (vi) kinase-substrate pairs; and (vii) signaling interactions. The union of all interactions from (i) to (vii) yields a network of 13,460 proteins that are interconnected by 141,296 interactions. For more information on the individual data sets and general properties of the interactome, see SM section 1.

Disease-gene associations

We integrate disease-gene annotations from Online Mendelian Inheritance in Man (OMIM; www.ncbi.nlm.nih.gov/omim) (*48*) and UniProtKB/Swiss-Prot as compiled by (*30*) with GWAS data from the Phenotype-Genotype Integrator database (PheGenI; www.ncbi.nlm.nih.gov/gap/PheGenI) (*31*), using a genome-wide significance cutoff of p value $\leq 5 \times 10^{-8}$. To combine the different disease nomenclatures of the two sources into a single standard vocabulary, we use the Medical Subject Headings ontology (MeSH; www.nlm.nih.gov/mesh/) as described in SM section 1. After filtering for diseases with at least 20 associated genes and genes for which we have interaction information, we obtain 299 diseases and 3173 associated genes.

Additional disease and gene annotation data

For the analysis of the similarity between genes and diseases, we use (i) Gene Ontology (GO) annotations (*49*); (ii) tissue-specific gene expression data (*36*); (iii) symptom disease associations (*38*); (iv) comorbidity data (*39*); and (v) pathway annotations from the Molecular Signatures Database (MSigDB) (*50*). Full details on data sources, processing, and analysis are provided in SM section 1.

Network localization

We use two complementary measures to quantify the degree to which disease proteins agglomerate in specific interactome neighborhoods: (i) observable module size S, representing the size of the largest connected subgraph formed by disease proteins; and (ii) shortest distance d_s. For each of the N_d disease proteins, we determine the distance d_s to the next-closest protein associated with the same disease. The average $\langle d_s \rangle$ can be interpreted as the diameter of a disease on the interactome. The network-based overlap between two diseases A and B is measured by comparing the diameters $\langle d_{AA} \rangle$ and $\langle d_{BB} \rangle$ of the respective diseases to the mean shortest distance $\langle d_{AB} \rangle$ between their proteins: $s_{AB} = \langle d_{AB} \rangle - (\langle d_{AA} \rangle + \langle d_{BB} \rangle)/2$. Positive s_{AB} indicates that the two disease modules are separated on the interactome, whereas negative values correspond to overlapping modules. Details on the analysis and the appropriate random controls are presented in SM section 2.

Gene-based disease overlap

The overlap between two gene sets A and B is measured by the overlap coefficient $C = |A \cap B| / \min(|A|,|B|)$ and the Jaccard-index $J = |A \cap B| / |A \cup B|$. The values of both measures lie in the range [0,1] with $J,C = 0$ for no common genes. A Jaccard-index $J = 1$ indicates two identical gene sets, whereas the overlap coefficient $C = 1$ when one set is a complete subset of the other. For a statistical evaluation of the observed overlaps, we use a basic hypergeometric model with the null hypothesis that disease-associated genes are randomly drawn from the space of all N genes in the network (see SM section 3 for full details).

REFERENCES AND NOTES

1. M. Buchanan, G. Caldarelli, P. De Los Rios, *Networks in Cell Biology* (Cambridge Univ. Press, Cambridge, 2010).
2. T. Pawson, R. Linding, Network medicine. *FEBS Lett.* **582**, 1266–1270 (2008). doi: 10.1016/j.febslet.2008.02.011; pmid: 18282479
3. E. E. Schadt, Molecular networks as sensors and drivers of common human diseases. *Nature* **461**, 218–223 (2009). doi: 10.1038/nature08454; pmid: 19741703
4. A. Califano, A. J. Butte, S. Friend, T. Ideker, E. Schadt, Leveraging models of cell regulation and GWAS data in integrative network-based association studies. *Nat. Genet.* **44**, 841–847 (2012). doi: 10.1038/ng.2355; pmid: 22836096
5. A. Zanzoni, M. Soler-López, P. Aloy, A network medicine approach to human disease. *FEBS Lett.* **583**, 1759–1765 (2009). doi: 10.1016/j.febslet.2009.03.001; pmid: 19269289
6. A.-L. Barabási, N. Gulbahce, J. Loscalzo, Network medicine: A network-based approach to human disease. *Nat. Rev. Genet.* **12**, 56–68 (2011). doi: 10.1038/nrg2918; pmid: 21164525
7. K.-I. Goh *et al*., The human disease network. *Proc. Natl. Acad. Sci. U.S.A.* **104**, 8685–8690 (2007). doi: 10.1073/pnas.0701361104; pmid: 17502601
8. M. Oti, B. Snel, M. A. Huynen, H. G. Brunner, Predicting disease genes using protein-protein interactions. *J. Med. Genet.* **43**, 691–698 (2006). doi: 10.1136/jmg.2006.041376; pmid: 16611749
9. K. Lage *et al*., Dissecting spatio-temporal protein networks driving human heart development and related disorders. *Mol. Syst. Biol.* **6**, 381 (2010). doi: 10.1038/msb.2010.36; pmid: 20571530
10. H.-Y. Chuang, E. Lee, Y.-T. Liu, D. Lee, T. Ideker, Network-based classification of breast cancer metastasis. *Mol. Syst. Biol.* **3**, 140 (2007). doi: 10.1038/msb4100180; pmid: 17940530
11. R. Mosca, T. Pons, A. Céol, A. Valencia, P. Aloy, Towards a detailed atlas of protein-protein interactions. *Curr. Opin. Struct. Biol.* **23**, 929–940 (2013). doi: 10.1016/j.sbi.2013.07.005; pmid: 23896349
12. T. Rolland *et al*., A proteome-scale map of the human interactome network. *Cell* **159**, 1212–1226 (2014). doi: 10.1016/j.cell.2014.10.050; pmid: 25416956
13. G. T. Hart, A. K. Ramani, E. M. Marcotte, How complete are current yeast and human protein-interaction networks? *Genome Biol.* **7**, 120 (2006). doi: 10.1186/gb-2006-7-11-120; pmid: 17147767
14. K. Venkatesan *et al*., An empirical framework for binary interactome mapping. *Nat. Methods* **6**, 83–90 (2009). pmid: 19060904
15. M. P. Stumpf *et al*., Estimating the size of the human interactome. *Proc. Natl. Acad. Sci. U.S.A.* **105**, 6959–6964 (2008). doi: 10.1073/pnas.0708078105; pmid: 18474861
16. M. N. Wass, A. David, M. J. Sternberg, Challenges for the prediction of macromolecular interactions. *Curr. Opin. Struct. Biol.* **21**, 382–390 (2011). doi: 10.1016/j.sbi.2011.03.013; pmid: 21497504
17. J. Xu, Y. Li, Discovering disease-genes by topological features in human protein-protein interaction network. *Bioinformatics* **22**, 2800–2805 (2006). doi: 10.1093/bioinformatics/btl467; pmid: 16954137
18. I. Feldman, A. Rzhetsky, D. Vitkup, Network properties of genes harboring inherited disease mutations. *Proc. Natl. Acad. Sci. U.S.A.* **105**, 4323–4328 (2008). doi: 10.1073/pnas.0701722105; pmid: 18326631
19. M. Krauthammer, C. A. Kaufmann, T. C. Gilliam, A. Rzhetsky, Molecular triangulation: Bridging linkage and molecular-network information for identifying candidate genes in Alzheimer's disease. *Proc. Natl. Acad. Sci. U.S.A.* **101**, 15148–15153 (2004). doi: 10.1073/pnas.0404315101; pmid: 15471992
20. L. Franke *et al*., Reconstruction of a functional human gene network, with an application for prioritizing positional candidate genes. *Am. J. Hum. Genet.* **78**, 1011–1025 (2006). doi: 10.1086/504300; pmid: 16685651
21. S. Köhler, S. Bauer, D. Horn, P. N. Robinson, Walking the interactome for prioritization of candidate disease genes. *Am. J. Hum. Genet.* **82**, 949–958 (2008). doi: 10.1016/j.ajhg.2008.02.013; pmid: 18371930
22. Y. Chen *et al*., Variations in DNA elucidate molecular networks that cause disease. *Nature* **452**, 429–435 (2008). doi: 10.1038/nature06757; pmid: 18344982
23. S. E. Baranzini *et al*., Pathway and network-based analysis of genome-wide association studies in multiple sclerosis. *Hum. Mol. Genet.* **18**, 2078–2090 (2009). doi: 10.1093/hmg/ddp120; pmid: 19286671
24. C. E. Wheelock *et al*., Systems biology approaches and pathway tools for investigating cardiovascular disease. *Mol. Biosyst.* **5**, 588–602 (2009). doi: 10.1039/b902356a; pmid: 19462016
25. A. S. Khalil, J. J. Collins, Synthetic biology: Applications come of age. *Nat. Rev. Genet.* **11**, 367–379 (2010). doi: 10.1038/nrg2775; pmid: 20395970
26. S. Wuchty *et al*., Gene pathways and subnetworks distinguish between major glioma subtypes and elucidate potential underlying biology. *J. Biomed. Inform.* **43**, 945–952 (2010). doi: 10.1016/j.jbi.2010.08.011; pmid: 20828632
27. I. Lee, U. M. Blom, P. I. Wang, J. E. Shim, E. M. Marcotte, Prioritizing candidate disease genes by network-based boosting of genome-wide association data. *Genome Res.* **21**, 1109–1121 (2011). doi: 10.1101/gr.118992.110; pmid: 21536720
28. U. M. Singh-Blom *et al*., Prediction and validation of gene-disease associations using methods inspired by social network analyses. *PLOS ONE* **8**, e58977 (2013). doi: 10.1371/journal.pone.0058977; pmid: 23650495
29. A. Rzhetsky, D. Wajngurt, N. Park, T. Zheng, Probing genetic overlap among complex human phenotypes. *Proc. Natl. Acad. Sci. U.S.A.* **104**, 11694–11699 (2007). doi: 10.1073/pnas.0704820104; pmid: 17609372
30. A. Mottaz, Y. L. Yip, P. Ruch, A.-L. Veuthey, Mapping proteins to disease terminologies: From UniProt to MeSH. *BMC Bioinformatics* **9** (suppl. 5), S3 (2008). doi: 10.1186/1471-2105-9-S5-S3; pmid: 18460185
31. E. M. Ramos *et al*., Phenotype-Genotype Integrator (PheGenI): Synthesizing genome-wide association study (GWAS) data with existing genomic resources. *Eur. J. Hum. Genet.* **22**, 144–147 (2014). doi: 10.1038/ejhg.2013.96; pmid: 23695286
32. L. Hakes, J. W. Pinney, D. L. Robertson, S. C. Lovell, Protein-protein interaction networks and biology—What's the connection? *Nat. Biotechnol.* **26**, 69–72 (2008). doi: 10.1038/nbt0108-69
33. M. E. Cusick *et al*., Literature-curated protein interaction datasets. *Nat. Methods* **6**, 39–46 (2009). doi: 10.1038/nmeth.1284; pmid: 19116613
34. R. Cohen, S. Havlin, *Complex Networks. Structure, Robustness and Function* (Cambridge Univ., Cambridge, 2010).
35. S. Bornholdt, H. G. Schuster, Eds., *Handbook of Graphs and Networks* (Wiley Online Library, 2003), vol. 2.
36. A. I. Su *et al*., A gene atlas of the mouse and human protein-encoding transcriptomes. *Proc. Natl. Acad. Sci. U.S.A.* **101**, 6062–6067 (2004). doi: 10.1073/pnas.0400782101; pmid: 15075390
37. T. K. Gandhi *et al*., Analysis of the human protein interactome and comparison with yeast, worm and fly interaction datasets. *Nat. Genet.* **38**, 285–293 (2006). pmid: 16501559

38. X. Zhou, J. Menche, A.-L. Barabási, A. Sharma, Human symptoms-disease network. *Nat. Commun.* **5**, 4212 (2014). doi: 10.1038/ncomms5212; pmid: 24967666
39. C. A. Hidalgo, N. Blumm, A.-L. Barabási, N. A. Christakis, A dynamic network approach for the study of human phenotypes. *PLOS Comput. Biol.* **5**, e1000353 (2009). doi: 10.1371/journal.pcbi.1000353; pmid: 19360091
40. K. A. Hunt *et al*., Newly identified genetic risk variants for celiac disease related to the immune response. *Nat. Genet.* **40**, 395–402 (2008). doi: 10.1038/ng.102; pmid: 18311140
41. D. A. van der Windt, P. Jellema, C. J. Mulder, C. M. Kneepkens, H. E. van der Horst, Diagnostic testing for celiac disease among patients with abdominal symptoms: A systematic review. *JAMA* **303**, 1738–1746 (2010). doi: 10.1001/jama.2010.549; pmid: 20442390
42. C. Pilette, S. R. Durham, J.-P. Vaerman, Y. Sibille, Mucosal immunity in asthma and chronic obstructive pulmonary disease: A role for immunoglobulin A? *Proc. Am. Thorac. Soc.* **1**, 125–135 (2004). doi: 10.1513/pats.2306032
43. J. Shi *et al*., Role of SWI/SNF in acute leukemia maintenance and enhancer-mediated Myc regulation. *Genes Dev.* **27**, 2648–2662 (2013). doi: 10.1101/gad.232710.113; pmid: 24285714
44. A. Bauer, B. Perras, S. Sufke, H.-P. Horny, B. Kreft, Myocardial infarction as an uncommon clinical manifestation of intravascular large cell lymphoma. *Acta Cardiol.* **60**, 551–555 (2005). doi: 10.2143/AC.60.5.2004979; pmid: 16261789
45. A. L. Hopkins, Network pharmacology: The next paradigm in drug discovery. *Nat. Chem. Biol.* **4**, 682–690 (2008). doi: 10.1038/nchembio.118; pmid: 18936753
46. J. Mestres, E. Gregori-Puigjané, S. Valverde, R. V. Solé, The topology of drug-target interaction networks: Implicit dependence on drug properties and target families. *Mol. Biosyst.* **5**, 1051–1057 (2009). doi: 10.1039/b905821b; pmid: 19668871
47. M. Kuhn *et al*., Systematic identification of proteins that elicit drug side effects. *Mol. Syst. Biol.* **9**, 663 (2013). doi: 10.1038/msb.2013.10; pmid: 23632385
48. A. Hamosh, A. F. Scott, J. S. Amberger, C. A. Bocchini, V. A. McKusick, Online Mendelian Inheritance in Man (OMIM), a knowledgebase of human genes and genetic disorders. *Nucleic Acids Res.* **33**, D514–D517 (2005). doi: 10.1093/nar/gki033; pmid: 15608251
49. M. Ashburner *et al*.The Gene Ontology Consortium, Gene ontology: Tool for the unification of biology. *Nat. Genet.* **25**, 25–29 (2000). doi: 10.1038/75556; pmid: 10802651
50. A. Subramanian *et al*., Gene set enrichment analysis: A knowledge-based approach for interpreting genome-wide expression profiles. *Proc. Natl. Acad. Sci. U.S.A.* **102**, 15545–15550 (2005). doi: 10.1073/pnas.0506580102 pmid: 16199517

ACKNOWLEDGMENTS

We thank A.-R. Carvunis, S. Pevzner, and T. Rolland for providing invaluable insights into the y2h data set; J. Bagrow and F. Simini for many discussions on the network methods; and G. Musella for figure design. This work was supported by NIH grants P50-HG004233, U01-HG001715, and U01-HG007690 from NHGRI and PO1-HL083069, R37-HL061795, RC2-HL101543, and U01-HL108630 from NHLBI.

SUPPLEMENTARY MATERIALS

www.sciencemag.org/content/347/6224/1257601/suppl/DC1
Materials and Methods
Figs. S1 to S16
Table S1
External Databases S1 to S4
Source Code
References (*51–107*)

17 June 2014; accepted 15 January 2015
10.1126/science.1257601

RESEARCH ARTICLES

PHOTOCHEMISTRY

Chemiexcitation of melanin derivatives induces DNA photoproducts long after UV exposure

Sanjay Premi,[1] Silvia Wallisch,[1] Camila M. Mano,[1,2] Adam B. Weiner,[1]* Antonella Bacchiocchi,[3] Kazumasa Wakamatsu,[4] Etelvino J. H. Bechara,[2,5]† Ruth Halaban,[3,6] Thierry Douki,[7]† Douglas E. Brash[1,6]‡

Mutations in sunlight-induced melanoma arise from cyclobutane pyrimidine dimers (CPDs), DNA photoproducts that are typically created picoseconds after an ultraviolet (UV) photon is absorbed at thymine or cytosine. We found that in melanocytes, CPDs are generated for >3 hours after exposure to UVA, a major component of the radiation in sunlight and in tanning beds. These "dark CPDs" constitute the majority of CPDs and include the cytosine-containing CPDs that initiate UV-signature C→T mutations. Dark CPDs arise when UV-induced reactive oxygen and nitrogen species combine to excite an electron in fragments of the pigment melanin. This creates a quantum triplet state that has the energy of a UV photon but induces CPDs by energy transfer to DNA in a radiation-independent manner. Melanin may thus be carcinogenic as well as protective against cancer. These findings also validate the long-standing suggestion that chemically generated excited electronic states are relevant to mammalian biology.

The pigment melanin protects against sunlight-induced burns, DNA damage, and skin cancer. These attributes of melanin are due to an unusually broad absorption spectrum and perhaps radical scavenging activity (*1*). Yet paradoxes abound. First, melanin is not solely beneficial: Blondes and redheads, who have a higher ratio of yellow pheomelanin to brown eumelanin in their skin and hair, have a greater risk for melanoma than dark-haired individuals (by a factor of 2 to 4), and the pheomelanin/eumelanin ratio accounts for some of this risk (*2*). UVA-irradiated mice do not develop melanoma if they lack melanin (*3*), and *Braf*-mutant mice develop 10 times as many spontaneous melanomas if they carry the pheomelanin-associated $Mc1r^{e/e}$ allele (*4*). UV-irradiated melanin, especially pheomelanin, triggers apoptosis and production of reactive oxygen species (ROS) and DNA strand breaks (*5*, *6*). Melanin synthesis itself generates ROS, especially synthesis of pheomelanin (*7*).

[1]Department of Therapeutic Radiology, Yale University School of Medicine, New Haven, CT 06520, USA. [2]Departamento de Bioquímica, Instituto de Química, Universidade de São Paulo, São Paulo 05513-970 SP, Brazil. [3]Department of Dermatology, Yale University School of Medicine, New Haven, CT 06520, USA. [4]Department of Chemistry, Fujita Health University School of Health Sciences, Toyoake, Aichi 470-1192, Japan. [5]Departamento de Ciências Exatas e da Terra, Universidade Federal de São Paulo, Diadema, São Paulo 09972-270 SP, Brazil. [6]Yale Comprehensive Cancer Center, Yale University School of Medicine, New Haven, CT 06520, USA. [7]INAC/LCIB UMR-E3 CEA-UJF/Commissariat à l'Energie Atomique (CEA), 38054 Grenoble Cedex 9, France.
*Present address: Pritzker School of Medicine, University of Chicago, Chicago, IL 60637, USA. †These authors contributed equally to this work. ‡Corresponding author. E-mail: douglas.brash@yale.edu

Yet melanin's ROS-generating properties do not explain its role in melanoma development, because most mutations in human melanomas display the UV signature of C→T substitutions at sites of adjacent pyrimidines (*8*, *9*). Such mutations arise from cyclobutane pyrimidine dimers (CPDs), which join adjacent pyrimidines to distort the DNA helix (*10*, *11*); genetic disorders of CPD repair, such as xeroderma pigmentosum, elevate the risk for childhood melanoma by four orders of magnitude. The most energetic component of sunlight, UVB (280 to 315 nm), creates these DNA photoproducts almost instantaneously, so the only obvious effect of melanin is shielding. The lower-energy UVA (315 to 400 nm), which constitutes ~95% of the ultraviolet energy that penetrates the atmosphere, also induces melanoma in mice and in humans who use tanning beds, but it is inefficient at making the cytosine-containing CPDs that cause C→T mutations (*12*, *13*). We provide evidence for an unusual biochemical pathway that resolves these oncological discrepancies by making melanin an active participant in CPD formation.

Delayed cyclobutane pyrimidine dimer induction in melanocytes

As a positive control for an unrelated experiment, we exposed murine fibroblasts and melanocytes to radiation from a UVA lamp, using an enzyme-linked immunosorbent assay (ELISA) to measure the number of CPDs over time. Induction of CPDs by direct UV absorption is complete in one picosecond (*11*). Consistent with this, we found that for fibroblasts and for melanocytes derived from albino mice, the peak of CPD induction was reached immediately upon exposure, followed by slow nucleotide excision repair (Fig. 1A and fig. S1A). (*14*). Unexpectedly, melanin-containing murine melanocytes instead continued to generate CPD for at least 3 hours after UVA exposure, at which point generation was offset by DNA repair (Fig. 1, B and C). The negative result with albino melanocytes implicated melanin in the process and ruled out the involvement of photosensitizing compounds in the growth medium. We confirmed the delayed production of CPDs by using a comet assay for DNA strand breaks after treating lysed cells with a nucleotide excision repair enzyme to induce DNA breaks at CPD sites (fig. S1B). This result also indicated that delayed CPDs resided in nuclear DNA. Delayed CPDs were also visible by immunofluorescence in normal melanocytes, whereas albino melanocytes showed only repair (fig. S1, C and D). We conclude that pigmented melanocytes induce "dark CPDs" after UV exposure ends.

We next examined whether dark CPD induction was masked by concurrent repair and thus might be more extensive than it appeared. Knocking down excision repair of CPDs by means of small interfering RNA (siRNA) against *Xpa* or *Xpc* transcripts (corresponding to genes mutated in xeroderma pigmentosum) revealed that dark CPDs constituted half of all CPDs (Fig. 1D). This factor of 2 increase in DNA photoproducts is substantial because cancer-predisposed individuals in xeroderma pigmentosum complementation group D are only 60% defective in CPD repair (*15*). For the higher-energy UVB, the majority of CPDs in melanocytes were created in the dark, even without repair knockdown (fig. S1, E to H). The UVB process was also dependent on melanin, and thus it differs from the delayed production of CPDs that has been reported occasionally in other cell types after UVC or UVB exposure (*16*–*18*).

Human melanocytes also generated dark CPDs after UVA or UVB exposure (Fig. 1E and fig. S1I), although there was interindividual variation in the response, particularly for UVA. This likely reflects genetic differences between the donors. For human melanocytes in which there was a modest rate of CPD decline after exposure but which showed no obvious dark CPDs, the dark CPDs were revealed by siRNA knockdown of *XPA* or *XPC* transcripts (Fig. 1F). It was not possible to determine whether individual variation was due to variation in melanin type because of privacy restrictions for newborn foreskin tissue.

To examine CPD induction in vivo, we used transgenic mice in which melanocytes remain in the epidermis throughout life because of expression of the Kit ligand in keratinocytes (*K14-Kitl*), thus mimicking human skin. After exposure of these mice to UVA, the level of epidermal CPDs at the 2-hour time point was 3 times the level immediately after exposure (Fig. 1, G and H). Most epidermal cells were keratinocytes, which receive pigment from the melanocytes; this finding suggests that melanin content, rather than synthesis, was the crucial requirement for dark CPD induction. Furthermore, in *K14-Kitl* mice homozygous

Downloaded from www.sciencemag.org on February 21, 2015

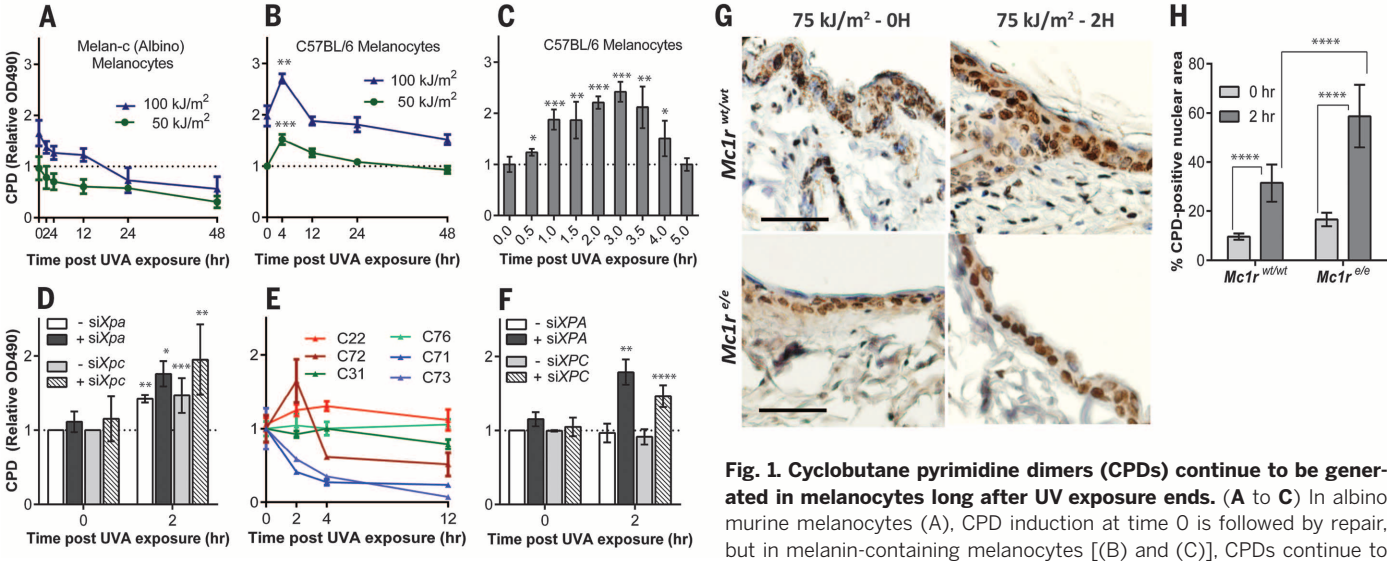


Fig. 1. Cyclobutane pyrimidine dimers (CPDs) continue to be generated in melanocytes long after UV exposure ends. (**A** to **C**) In albino murine melanocytes (A), CPD induction at time 0 is followed by repair, but in melanin-containing melanocytes [(B) and (C)], CPDs continue to increase for 4 hours after UVA exposure ends. CPDs were assayed by DNA ELISA. (**D**) Additional dark CPDs are revealed in melanocytes when excision repair is suppressed by si*Xpa* or si*Xpc*; dark CPDs account for half the total CPDs. (**E**) In melanocytes from humans, the production of dark CPDs after UVA varies between individuals. (**F**) "Nonproducers" are revealed as producers after DNA repair is suppressed in the cells by si*XPA* or si*XPC*. (**G**) Dark CPDs in mouse melanocytes and keratinocytes in vivo. *K14-Kitl* transgenic mice, which have epidermal melanocytes containing eumelanin, were crossed to mice carrying the *Mc1r*$^{e/e}$ allele, which confers epidermal pheomelanin and yellow fur. Scale bar, 50 μm. (**H**) Quantitation of CPDs in epidermal sections. Error bars are SD from four experiments [(A) to (C)], three experiments [(D) to (F)], or two experiments (H). *P* values by *t* test are for the difference between the asterisked time point and 0 hours or as indicated. *$P \le 0.05$, **$P \le 0.005$, ***$P \le 0.0005$, ****$P \le 0.00005$.

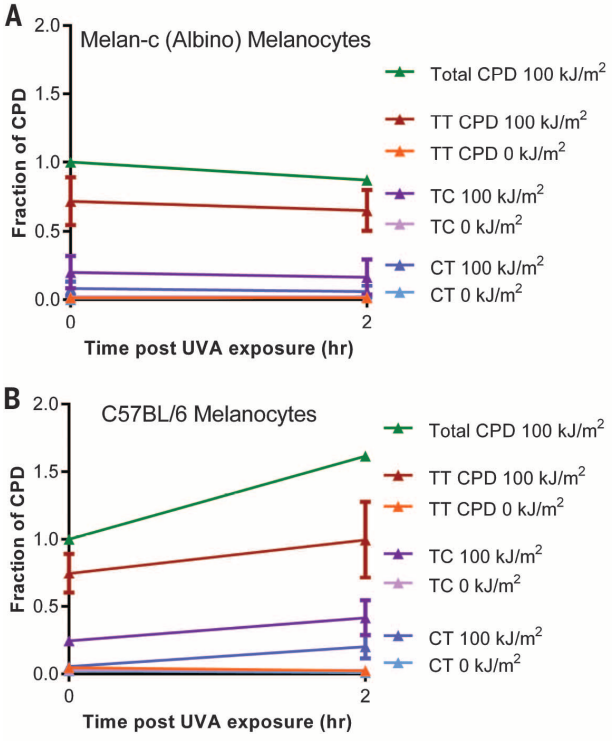


Fig. 2. Mass spectrometry reveals enrichment of dark CPDs for CPDs that contain cytosine. For energetic reasons, direct absorption of UVA generates primarily thymine-containing (TT) cyclobutane pyrimidine dimers. (**A**) There is no dark CPD formation in albino melanocytes after UVA exposure. The slope of post-UVA CPD induction in albino cells is indistinguishable from the slope in unirradiated cells. Data represent the average of three experiments, expressed as a fraction of the total CPDs generated at 0 hours. Hence, the total CPD line has no error bar. The total number of CPDs at 0 hours was 169 CPDs per megabase of DNA. (**B**) Dark CPDs are induced in melanin-containing melanocytes by UVA and include a greater number of cytosine-containing TC and CT dimers, capable of causing UV-signature C→T mutations. Slopes for post-UVA induction of TT, TC, and CT CPDs in melanin-containing cells are greater than those in albino, with $P = 0.01$, 0.05, and 0.03, respectively. The total number of CPDs at 0 hours was 87 CPDs per megabase of DNA, consistent with the shielding function of eumelanin. Data represent the average of five experiments.

for the inactive *Mc1r*$^{e/e}$ allele, in which melanocytes synthesize red-yellow pheomelanin, both initial and dark CPDs were twice as frequent as in black mice. This suggests that pheomelanin is both a poorer shield against normal CPD formation and a more potent dark CPD generator.

Cytosine-containing dark CPDs

We next used mass spectrometry to identify individual CPD species in murine melanocytes. This analysis revealed that the delayed CPDs in melanin-containing melanocytes included the cytosine-containing CPDs that generate UV-signature C→T mutations (Fig. 2, A and B). Unexpectedly, relative to directly induced CPDs, we observed a higher (TC + CT)/TT CPD ratio (by a factor of 4) in the delayed CPDs, which is suggestive of unusual chemistry. UVA generates primarily TT CPDs, with TC and CT CPDs together contributing only 10 to 30% of these three CPD types (*13*). The (TC + CT)/TT CPD ratio in melanin-containing cells increased from the UVA-like 0.37 at 0 hours (directly induced CPDs) to 1.33 in the CPDs arising during the next 2 hours ($P = 0.027$)—a ratio more typical of cells irradiated with the higher-energy UVB. Mass spectrometry ruled out two possibilities: (i) that the ELISA and comet assays cross-reacted with melanin-DNA adducts, and (ii) that the delayed CPD appearance reflected greater access of the antibody or endonuclease due to a change in DNA conformation after UV exposure.

Photochemical pathway

To identify the photochemical pathway that produces dark CPDs, we focused on UVA because it reduces background from CPDs created by direct UVB absorption, reduces photosensitization from aromatic molecules, and is used in indoor tanning beds. We found that kojic acid—an inhibitor of tyrosinase, the rate-limiting enzyme in melanin synthesis—suppressed production of dark CPDs by 85% (Fig. 3A). Because ROS can be produced in cells for long periods after UVA exposure (*19*), we tested the ROS scavengers

N-acetylcysteine and α-tocopherol (vitamin E). The former suppressed production of dark CPDs by 64% and the latter abolished it (fig. S2, A and B). An effect of antioxidants on CPDs detectable immediately after UV has been reported, but was linked to changes in chromatin structure (*20*). Because melanin generates superoxide radical ion ($O_2^{\bullet-}$) while it is being irradiated, we specifically scavenged it with TEMPOL (1-oxyl-2,2,6,6-tetramethyl-4-hydroxypiperidine) and found that this also abolished the production of dark CPDs after UVA (fig. S2C). A longer-lasting source of $O_2^{\bullet-}$ in cells is NOX [reduced nicotinamide adenine dinucleotide phosphate (NADPH) oxidase], which is rapidly induced by UVA (*19*). The NOX inhibitor VAS2870 also abolished production of dark CPDs (Fig. 3B). CPDs were inhibited to a level below that at 0 hours, indicating that dark CPDs were also induced during the irradiation itself.

The $O_2^{\bullet-}$ requirement recalled an old observation (*21*) that CPDs can be generated in the dark by dioxetane, a strained four-member ring peroxide. This moiety undergoes thermolysis to two carbonyls, with one in an electronically excited triplet state having the high energy of a UV photon (>3 eV, 70 kcal/mol, or 35,000 K) and capable of transferring its energy to DNA by a process that is independent of radiation (*21*). One of the few biologically synthesized molecules that can initiate such "photochemistry in the dark" (*22*, *23*) is peroxynitrite ($ONOO^-$) (*24*), which is generated by the reaction of $O_2^{\bullet-}$ with nitric oxide ($NO^{\bullet}$). Peroxynitrite and its precursors are stable enough to diffuse several cell diameters from the site of generation to the target molecule. NOX and the $NO^{\bullet}$ generator iNOS are UV-inducible within minutes and are expressed in melanocytes, including nuclear NOX4 (*25*). To determine whether $NO^{\bullet}$ is required for production of dark CPDs, we inhibited iNOS by treating melanocytes with aminoguanidine. This resulted in complete suppression of dark CPD production (Fig. 3C).

We next investigated whether melanin-containing cells generate peroxynitrite when exposed to UV. Peroxynitrite can be detected by its nitration of tyrosines. Assays for 3-nitrotyrosine revealed that basal nitration activity was present even without UV, that it was located primarily in the nucleus, and that its appearance required melanin (Fig. 3, D and E, and fig. S2D). The melanin requirement suggests that the $NO^{\bullet}$ requirement in melanocytes is distinct from that observed in cultured keratinocytes (*18*). Peroxynitrite's presence in the nucleus without UV exposure is plausible because the synthesis of melanin monomers is a redox reaction that releases $O_2^{\bullet-}$ (*7*) and melanosomes are assembled in the perinuclear space. In support of an additional UV role, we found that exposure of melanin-containing melanocytes to UVA created as much nuclear and cytoplasmic nitrotyrosine in 30 min as had accumulated from basal induction over ~8 days (Fig. 3, D and E, and fig. S2D) (*14*). This represents a factor of ~400 spike in the flux of peroxynitrite per hour.

A diagnostic for excited triplet states is that their energy can also discharge via ultraweak blue or green luminescence (*23*). This signal can be enhanced by several orders of magnitude by diverting the energy to a triplet energy acceptor, sodium 9,10-dibromoanthracene-2-sulfonate (DBAS), which is a more efficient emitter. To allow rapid DBAS entry, we permeabilized melanocytes within a liquid scintillation counter set to single-photon counting mode. UVA-irradiated melanocytes generated DBAS-amplified luminescence for several hours after irradiation, and only in cells containing melanin (Fig. 3, F and G). The lifetime of triplet carbonyls is ~10 μs (*24*), so a signal persistent over the course of hours indicates ongoing creation. To test whether this triplet state is required for dark CPDs, we added ethyl sorbate, a specific quencher of triplet states (*26*), to intact melanocytes after UVA exposure. We found that this treatment prevented production of dark CPDs (Fig. 3H). Because DBAS diverts triplet energy to luminescence, this compound also blocked dark CPDs (fig. S2E). These results provide direct evidence that UV-induced superoxide and nitric oxide lead to a high-energy triplet state moiety, which then creates a dark CPD by energy transfer.

Electronically excited melanin as a molecular vector

Melanin is located in the cytoplasm, yet CPDs were generated in the nucleus, raising the question of what molecule acquired the energetic carbonyl. An $O_2^{\bullet-}$-initiated radical chain reaction in lipids was one possible conduit (*26*), but inducing lipid peroxidation in isolated nuclei by exposure to cumene hydroperoxide did not appear to induce CPDs in nuclear DNA (fig. S3).

Another candidate for the triplet-state carrier was the set of melanin monomers out of which the final melanin polymers are assembled. These monomers are lipophilic and are therefore potentially

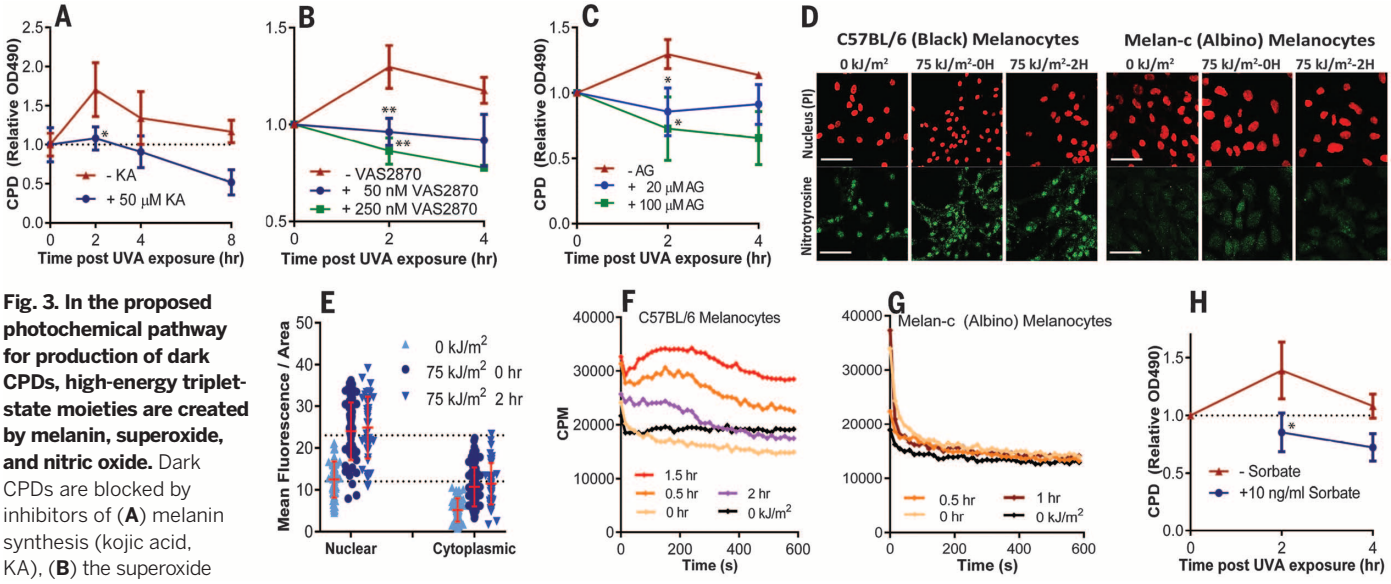


Fig. 3. In the proposed photochemical pathway for production of dark CPDs, high-energy triplet-state moieties are created by melanin, superoxide, and nitric oxide. Dark CPDs are blocked by inhibitors of (**A**) melanin synthesis (kojic acid, KA), (**B**) the superoxide generator NADPH oxidase (VAS2870), and (**C**) the nitric oxide generator iNOS (aminoguanidine). Inhibitors are not expected to reduce CPD levels below those seen at 0 hours, a time when CPDs are generated primarily by direct UV absorption (dotted line). (**D**) The product of superoxide and nitric oxide, peroxynitrite, generates 3-nitrotyrosine–modified proteins in melanocyte nuclei (except in albino melanocytes), and these increase with UVA exposure. (**E**) Quantitation of 3-nitrotyrosine in melanin-containing melanocytes. The increase at 0 hours arises from protein nitration during the 27-min UVA exposure. (**F**) Ultraweak chemiluminescence is generated by permeabilized UVA-irradiated melanized melanocytes that had been incubated with a triplet energy acceptor probe, DBAS. Chemiluminescence was quantified by single-photon counting (cpm, counts per minute). (**G**) Albino melanocytes do not produce chemiluminescence when irradiated. (**H**) A triplet-state quencher, ethyl sorbate, inhibits production of dark CPDs in pigmented mouse melanocytes after they are exposed to UVA. Data are the average of three experiments. (F) and (G) show data from one of three similar experiments. *P* values are for the difference between treated and untreated samples.

able to enter the nucleus, and are concentrated in perinuclear coated vesicles before transfer to melanosomes (*27*). Melanin polymer rapidly solubilizes when exposed to hydrogen peroxide (H_2O_2) (*28*), and its degradation by peroxidation or UV photoionization has been proposed to involve dioxetane and triplet carbonyls (*29*, *30*). We first investigated whether a triplet state could be created in melanin by a cell-free system. Synthetic melanin oxidized with peroxynitrite and incubated with DBAS generated a chemiluminescence signal two orders of magnitude larger than that seen in melanocytes (Fig. 4A and fig. S4A). We found that chemiluminescence began immediately and proceeded for >10 min. To further test melanin's ability to host a triplet state, we oxidized synthetic melanin with horseradish peroxidase in the presence of hydrogen peroxide, which generates dioxetane intermediates by a mechanism similar to that of peroxynitrite (*24*). This produced similar levels of chemiluminescence (Fig. 4A and fig. S4B). The eumelanin monomer 5,6-dihydroxyindole-2-carboxylic acid (DHICA) and the pheomelanin monomer 5-*S*-cysteinyldopa (5SCD) also generated chemiluminescence when oxidized (Fig. 4A).

We found that CPDs were generated in the complete absence of UV when we incubated plasmid DNA and peroxynitrite with melanin, DHICA, or 5SCD (Fig. 4B). We were unable to test whether the triplet quencher ethyl sorbate blocked these reactions because it was insufficiently soluble in the aqueous buffer. However, we found that DBAS, which redirects triplet energy toward luminescence, reduced CPD production by 50 to 90% (Fig. 4C and fig. S4C). The CPDs created by oxidizing melanin or its monomers included the mutagenic cytosine-containing CPDs (fig. S4D). The level of CPDs induced in the absence of UV was approximately equal to that generated in pure DNA by 25 kJ/m^2 of UVA—an exposure about one-quarter of that required to produce a barely perceptible sunburn (the "minimal erythema dose"). On the basis of our mass spectrometry data from albino murine melanocytes (Fig. 2), this value is approximately 1 CPD per 24 kb of DNA created solely by oxidized melanin.

We next explored whether UV exposure overcomes the migration barrier posed by the nuclear membrane. Cell-free experiments revealed that melanin polymer was rapidly solubilized after exposure to UVA or peroxynitrite (Fig. 4D). Because antibodies to melanin monomers do not exist, we were unable to directly monitor melanin migration into the nucleus. We therefore imaged unfixed melanocytes (to avoid artifactually permeabilizing the nuclear membrane), using differential interference contrast microscopy to maintain contrast at high magnification. Unirradiated normal melanocytes, but not albino melanocytes, showed dark granules in the cytoplasm, especially in the perinuclear area (fig. S5). We presume that these are melanin aggregates in melanosomes, coated vesicles, and endoplasmic reticulum because they have the same size and cellular locations as granules seen in melanocytes immunostained for tyrosinase (*31*). After UVA exposure, 3D images reconstructed from serial planar images revealed granules inside the nucleus (movies S1 and S2). We do not know whether these represent melanin-containing organelles that moved into the nucleus or molecular aggregates formed by spontaneous polymerization of melanin precursors, as occurs during normal melanin synthesis. We conclude that in cells exposed to UV, melanin or its constituents are able to enter the nucleus.

Finally, we sought to identify carbonyl-containing DHICA reaction products remaining after the triplet excitation energy discharges. The milder reaction of horseradish peroxidase with hydrogen peroxide was used to avoid complete oxidation and thereby reveal labile reaction intermediates. The DHICA analog of the predicted eumelanin degradation product (*29*) (Fig. 4E, structure **1**) has a molecular weight of 225 daltons and would be highly polar. An alternative reaction is formation of a dioxetane moiety at the pyrrole ring (*32*), also leading to a polar structure of 225 daltons (structure **2**). When we separated reaction

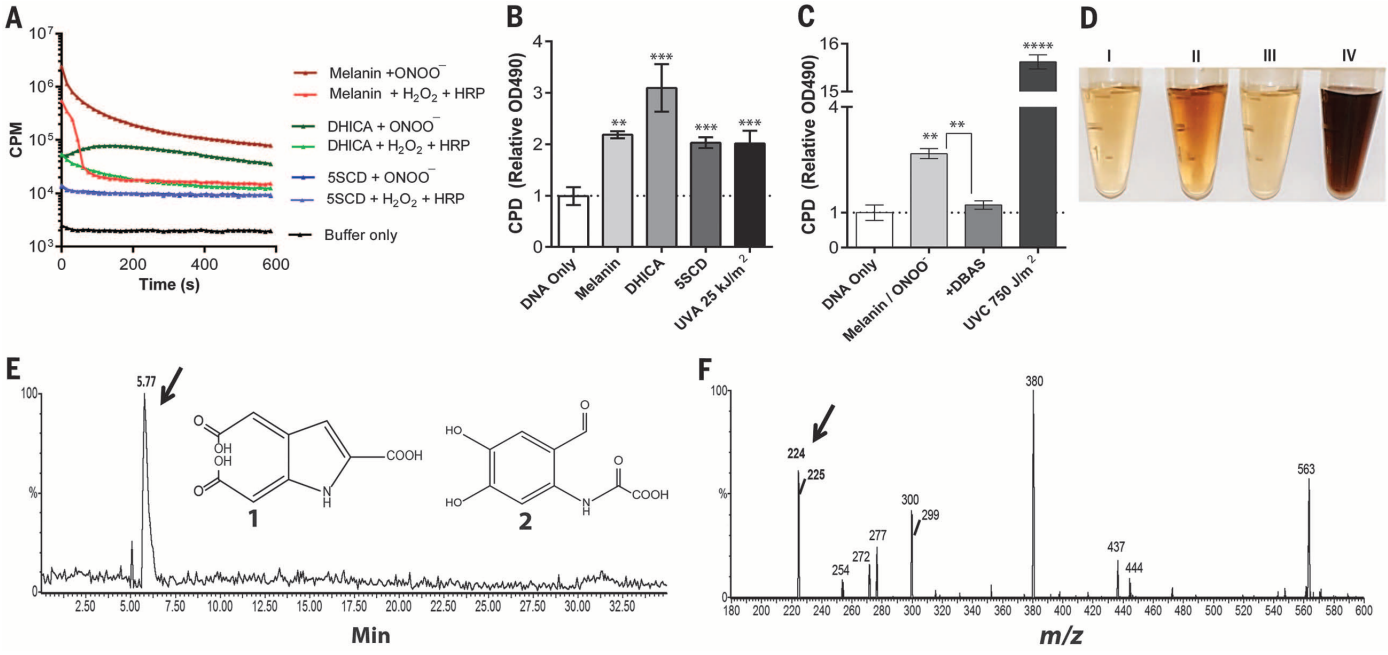


Fig. 4. Excited-state melanin may act as a molecular vector. (**A**) Synthetic melanin, its eumelanin monomer DHICA, and its pheomelanin monomer 5SCD generate ultraweak chemiluminescence when oxidized by peroxynitrite or by horseradish peroxidase plus H_2O_2. DBAS was used as a triplet energy probe, so luminescence indicates the presence of electronically excited triplet states. Data represent one of six experiments. (**B**) CPDs are created in the dark when melanin or its monomers are oxidized with peroxynitrite. The level of CPDs resulting from direct DNA absorption of UVA is shown for comparison. (**C**) Diverting triplet energy to luminescence with DBAS blocks production of CPDs by oxidized melanin. The UVC dose used for comparison is about two orders of magnitude higher than that lethal to 50% of normal cells. In (B) and (C), data represent the average of three experiments. *P* values are for the difference between treated and "DNA only" samples or as indicated. (**D**) Synthetic melanin is rapidly solubilized upon exposure to UV or peroxynitrite. Left to right: Supernatants resulting from untreated melanin or from melanin exposed to UVA (200 kJ/m^2), 7.8 mM NaOH, or peroxynitrite (1 mM in NaOH stabilizer). (**E** and **F**) Identification of a putative triplet-carbonyl carrier. (E) The eumelanin monomer DHICA was oxidized and products were separated by HPLC, monitoring the HPLC output by mass spectrometry in negative ion mode. Monitoring for the 224 *m/z* ion of 225-dalton compounds **1** and **2**, expected for triplet-carbonyl derivatives of dioxetane-adducted DHICA, reveals a single polar peak. (F) Scanning the polar HPLC peak reveals four principal *m/z* peaks, one at 224 *m/z*.

products by high-performance liquid chromatography (HPLC) and scanned the HPLC eluate by mass spectrometry in negative ion mode for the corresponding 224 *m/z* product, we observed a single peak eluting in the highly polar region of the buffer gradient (Fig. 4E). Scanning this fraction of the HPLC eluate across the small-molecule region of the mass spectrometer revealed four principal *m/z* peaks, of which the second largest was 224 daltons (Fig. 4F). Fragmentation of these HPLC fractions generated *m/z* peaks assignable to oxidation products of either structure **1** or **2** created by known oxidation reactions. When we blocked the reactivity of DHICA's six-membered ring by omitting an OH group (5-hydroxyindole-2-carboxylic acid) (fig. S6A), oxidation still produced chemiluminescence (fig. S6, B and C) and CPDs (fig. S6D), which suggests that **2** is the predominant product. Together, these results indicate that melanin and melanin fragments are capable of acting as the molecular vectors that acquire an electronically excited triplet state, probably at a carbonyl arising from a dioxetane intermediate.

Proposed scheme for the participation of melanin in melanoma development

We have shown that exposing melanin-containing cells to UV radiation induces superoxide and nitric oxide, causing a factor of ~400 peroxynitrite spike that degrades melanin, allows melanin-like granules to appear in the nucleus and, for hours after the original UV exposure, excites melanin derivatives to a triplet state that has the high energy of a UV photon (Fig. 5). These evanescent electronically excited products transfer their triplet energy to DNA, creating mutagenic cyclobutane pyrimidine dimers in the dark. We speculate that the degradation of melanin polymer into fragments allows these moieties to closely approach the DNA, and that the peroxynitrite-melanin reaction intermediate is a short-lived dioxetane (fig. S6E) whose triplet energy level lies well above that of the DNA bases. The sustained time course of dark CPD generation can be accounted for by the prolonged steps of UV induction of NOX and iNOS, peroxynitrite-induced solubilization of melanin to fragments (or release of pre-melanin monomers from UV-damaged melanosomes and vesicles), and migration to the nucleus. Still unidentified are the isozymes generating superoxide and nitric oxide, the cell site(s) at which melanin is degraded and its fragments are excited to a triplet state, the full inventory of eumelanin and pheomelanin fragments that can host triplet states, the chemical intermediate through which $ONOO^-$ creates the triplet carbonyl, and the energy transfer process.

A consequence of these events is that melanin may be carcinogenic as well as protective against cancer. This double nature would explain the apparent cancer-facilitating effects of melanin seen in mice and in human epidemiology (*2*–*4*, *6*). Melanin is an unusual polymer whose properties set the stage for the events we have described (*33*). Highly reactive *o*-quinones created by ROS-generating redox transformations of tyrosine polymerize spontaneously into oligomers. The *o*-quinones readily accept an electron to become semiquinone radicals, giving melanin a high concentration of free radicals in stable redox equilibrium and stabilized by metal ions. This macromolecule is a photon trap that also acts as an electron-proton photoconductor. These characteristics give melanin its broad light absorption, radical scavenging, and metal reservoir properties, but at a price. First, melanin synthesis generates $O_2^{\bullet-}$ and H_2O_2. UV exposure additionally excites the rings to an energy that, especially for pheomelanin, ejects an electron that is captured by oxygen to yield more $O_2^{\bullet-}$ (*5*, *34*). Second, the reactive semiquinones allow melanin to be degraded and these fragments to be adducted to create high-energy unstable moieties such as dioxetanes. Although most of the cell's melanin synthesis is safely isolated inside melanosomes, the early steps occur in close proximity to the nucleus.

It was proposed long ago that chemiexcitation—the creation of chemical reaction products containing excited electrons that underlie bioluminescence in lower organisms—has broad importance in biology (*22*, *23*). Our data suggest that this may be the case in human skin. The consequence is that half or more of the CPDs in a melanocyte arise after UV exposure ends. In vivo the same appears to be true of keratinocytes, which receive

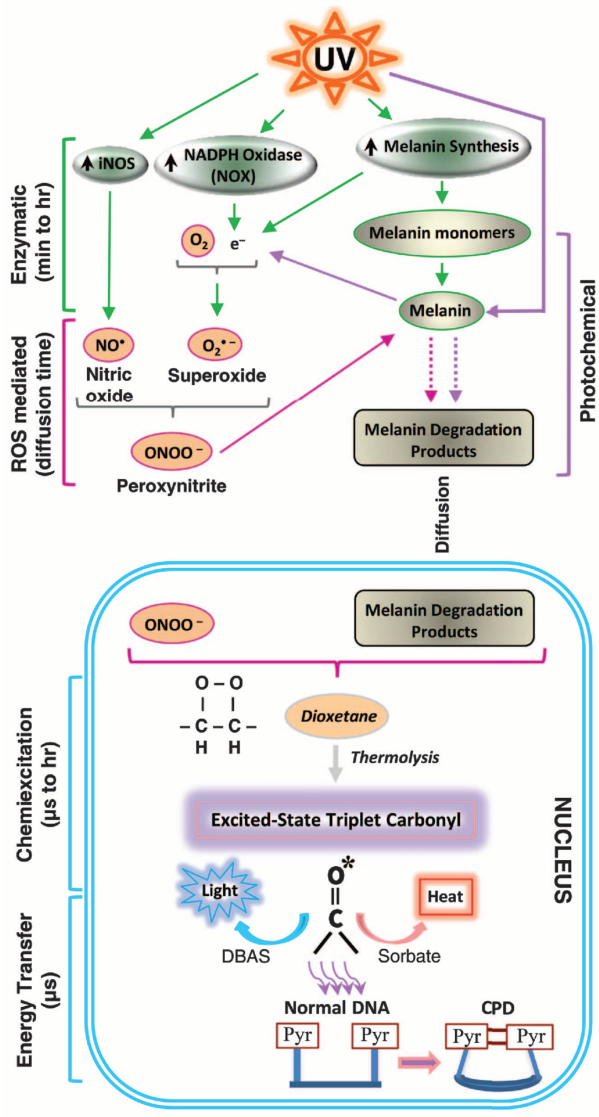


Fig. 5. A mechanistic model for the generation of dark CPD in melanocytes by chemiexcitation, with melanin as an active participant. Exposing cells to UV radiation is known to up-regulate iNOS, NADPH oxidase (NOX), and enzymes of melanin synthesis, presumably causing sustained generation of nitric oxide ($NO^{\bullet}$) and superoxide ($O_2^{\bullet-}$). Cytoplasmic NOS and NOX are indicated on the figure but some isoforms are located in the nucleus. The present experiments show a UV-induced surge in the product of these two radicals, the powerful oxidant peroxynitrite ($ONOO^-$), and show that peroxynitrite degrades melanin polymer to fragments. Melanin or melanin fragments then appear in the nucleus. Peroxynitrite is also one of the few biologically synthesized molecules capable of exciting an electron to a triplet state. The present experiments show that on a faster time scale, peroxynitrite excites an electron in a melanin fragment to a triplet state that has the high energy of a UV photon. The typical triplet-state reaction intermediate, not demonstrated here (hence indicated in italics), is a cycloaddition of –O–O– to create an unstable dioxetane; dioxetanes undergo spontaneous thermolysis to yield two carbonyls, one of which acquires most of the energy and finishes in a high-energy triplet state (*). For the melanin-related triplet, the half-life of the reaction intermediate appeared to be minutes, and a carbonyl consistent with a dioxetane precursor was identified by mass spectrometry. Triplet energy then discharges on a microsecond time scale to generate visible luminescence, or discharges in a radiation-independent manner to DBAS (to be emitted as fluorescence), to sorbate (to be dissipated as isomerization and heat), or evidently to DNA bases (where it makes CPDs). The presence of melanin, activation of iNOS and NOX, and the triplet state were shown to be required for dark CPD formation.

melanosomes donated by melanocytes. If the same holds for human skin, this would mean that past measurements of CPDs immediately after UV exposure have underestimated the consequences of UV exposure.

One benefit of dark photochemistry's slow course is that it allows intervention. A blocker of dark CPDs, α-tocopherol (vitamin E), is not only an antioxidant but also inactivates dioxetanes by converting them to a pair of diols (*35*). The triplet quencher ethyl sorbate is an analog of the widely used food preservative potassium sorbate. Screening for novel triplet quenchers offers the prospect of developing "evening-after" sunscreens that could potentially prevent the carcinogenic processes occurring in the skin hours after sunlight exposure ends.

REFERENCES AND NOTES

1. N. Kollias, R. M. Sayre, L. Zeise, M. R. Chedekel, *J. Photochem. Photobiol. B* **9**, 135–160 (1991).
2. P. F. Williams, C. M. Olsen, N. K. Hayward, D. C. Whiteman, *Int. J. Cancer* **129**, 1730–1740 (2011).
3. F. P. Noonan *et al.*, *Nat. Commun.* **3**, 884 (2012).
4. D. Mitra *et al.*, *Nature* **491**, 449–453 (2012).
5. M. R. Chedekel, S. K. Smith, P. W. Post, A. Pokora, D. L. Vessell, *Proc. Natl. Acad. Sci. U.S.A.* **75**, 5395–5399 (1978).
6. S. Takeuchi *et al.*, *Proc. Natl. Acad. Sci. U.S.A.* **101**, 15076–15081 (2004).
7. J. L. Munoz-Munoz *et al.*, *Biochim. Biophys. Acta* **1794**, 1017–1029 (2009).
8. D. E. Brash, *Photochem. Photobiol.* **91**, 15–26 (2015).
9. M. Krauthammer *et al.*, *Nat. Genet.* **44**, 1006–1014 (2012).
10. D. E. Brash, S. Seetharam, K. H. Kraemer, M. M. Seidman, A. Bredberg, *Proc. Natl. Acad. Sci. U.S.A.* **84**, 3782–3786 (1987).
11. W. J. Schreier *et al.*, *Science* **315**, 625–629 (2007).
12. D. Lazovich *et al.*, *Cancer Epidemiol. Biomarkers Prev.* **19**, 1557–1568 (2010).
13. T. Douki, A. Reynaud-Angelin, J. Cadet, E. Sage, *Biochemistry* **42**, 9221–9226 (2003).
14. See supplementary materials on *Science* Online.
15. K. H. Kraemer *et al.*, *Proc. Natl. Acad. Sci. U.S.A.* **72**, 59–63 (1975).
16. W. Carrier, R. Snyder, J. Regan, in *The Science of Photomedicine*, J. Regan, J. Parrish, Eds. (Plenum, New York, 1982), pp. 91–112.
17. E. J. Beecham, J. F. Mushinski, E. Shacter, M. Potter, V. A. Bohr, *Mol. Cell. Biol.* **11**, 3095–3104 (1991).
18. C. Gordon-Thomson *et al.*, *Photochem. Photobiol. Sci.* **11**, 1837–1847 (2012).
19. A. Valencia, I. E. Kochevar, *J. Invest. Dermatol.* **128**, 214–222 (2008).
20. M. Hochberg, R. Kohen, C. D. Enk, *Biomed. Pharmacother.* **60**, 233–237 (2006).
21. A. A. Lamola, *Biochem. Biophys. Res. Commun.* **43**, 893–898 (1971).
22. E. White, J. Miano, C. Watkins, E. Breaux, *Angew. Chem. Int. Ed. Engl.* **13**, 229–243 (1974).
23. G. Cilento, in *Chemical and Biological Generation of Excited States*, W. Adam, G. Cilento, Eds. (Academic Press, New York, 1982), pp. 277–307.
24. F. S. Knudsen *et al.*, *Chem. Res. Toxicol.* **13**, 317–326 (2000).
25. C. Roméro-Graillet *et al.*, *J. Biol. Chem.* **271**, 28052–28056 (1996).
26. A. C. Velosa, W. J. Baader, C. V. Stevani, C. M. Mano, E. J. Bechara, *Chem. Res. Toxicol.* **20**, 1162–1169 (2007).
27. S. Hatta, Y. Mishima, M. Ichihashi, S. Ito, *J. Invest. Dermatol.* **91**, 181–184 (1988).
28. P. Kayatz *et al.*, *Invest. Ophthalmol. Vis. Sci.* **42**, 241–246 (2001).
29. D. Slawinska, J. Slawinski, *Physiol. Chem. Phys.* **14**, 363–374 (1982).
30. K. Wakamatsu, Y. Nakanishi, N. Miyazaki, L. Kolbe, S. Ito, *Pigment Cell Melanoma Res.* **25**, 434–445 (2012).
31. R. Halaban *et al.*, *Proc. Natl. Acad. Sci. U.S.A.* **97**, 5889–5894 (2000).
32. I. Saito, S. Matsugo, T. Matsuura, *J. Am. Chem. Soc.* **101**, 4757–4759 (1979).
33. P. Meredith, T. Sarna, *Pigment Cell Res.* **19**, 572–594 (2006).
34. T. Ye *et al.*, *Photochem. Photobiol.* **82**, 733–737 (2006).
35. W. Adam, F. Vargas, B. Epe, D. Schiffmann, D. Wild, *Free Radic. Res. Commun.* **5**, 253–258 (1989).

ACKNOWLEDGMENTS

We thank M. Bosenberg and V. Muthusamy for UVA-irradiated mouse skin; the Yale Office of Environmental Health and Safety for the single-photon liquid scintillation counter; A. Bommakanti for photography; and D. Mitchell and A. Mennone for helpful discussions. Supported by Department of Defense CDMRP grants CA093473P1 and CA093473 (D.E.B. and R.H.); NIH grant 2 P50 CA121974 (R.H. and D.E.B.); a postgraduate fellowship from the University of Veterinary Medicine, Vienna (S.W.); Fundação de Amparo a Pesquisa do Estado de São Paulo (FAPESP) doctoral fellowship 09/02062-8 (C.M.M.); and FAPESP grant 06/56530-4 and the INCT–Processos Redox em Biomedicina (E.J.H.B.). Confocal support was provided by NIH grant P30 DK34989 to the Yale Liver Center.

SUPPLEMENTARY MATERIALS

www.sciencemag.org/content/347/6224/842/suppl/DC1
Materials and Methods
Supplementary Text
Figs. S1 to S6
Movies S1 and S2
References (*36*–*39*)

13 May 2014; accepted 2 January 2015
10.1126/science.1256022

STRUCTURAL BIOLOGY

Structural basis for Notch1 engagement of Delta-like 4

Vincent C. Luca,[1,2,3] Kevin M. Jude,[1,2,3] Nathan W. Pierce,[2] Maxence V. Nachury,[2] Suzanne Fischer,[1,2,3] K. Christopher Garcia[1,2,3]*

Notch receptors guide mammalian cell fate decisions by engaging the proteins Jagged and Delta-like (DLL). The 2.3 angstrom resolution crystal structure of the interacting regions of the Notch1-DLL4 complex reveals a two-site, antiparallel binding orientation assisted by Notch1 O-linked glycosylation. Notch1 epidermal growth factor–like repeats 11 and 12 interact with the DLL4 Delta/Serrate/Lag-2 (DSL) domain and module at the N-terminus of Notch ligands (MNNL) domains, respectively. Threonine and serine residues on Notch1 are functionalized with O-fucose and O-glucose, which act as surrogate amino acids by making specific, and essential, contacts to residues on DLL4. The elucidation of a direct chemical role for O-glycans in Notch1 ligand engagement demonstrates how, by relying on posttranslational modifications of their ligand binding sites, Notch proteins have linked their functional capacity to developmentally regulated biosynthetic pathways.

The Notch signaling pathway is essential for cell-fate determination in all metazoan species (*1*). In adult mammals, Notch signaling directs neural and hematopoietic stem cell differentiation and development of many immune cell subsets (*2*–*4*). Mammalian Notch receptor homologs (Notch1 to 4) encode a Notch extracellular domain (NECD) that engages ligands, a transmembrane domain, and a Notch intracellular domain (NICD) that translocates to the nucleus to serve as a transcriptional cofactor (*5*). Signaling is initiated when the NECD binds Jagged1, Jagged2, Delta-like 1 (DLL1), or Delta-like 4 (DLL4) ligands on the surface of an apposing cell, triggering proteolysis of the Notch receptor in a process that is dependent on ligand endocytosis (*6*–*9*). Mutations in Notch and its ligands are associated with a number of inherited and acquired diseases, including Alagille syndrome (AGS) and T cell acute lymphoblastic leukemia (T-ALL) (*10*).

Notch-ligand interactions are apparently dependent on posttranslational modification of Notch receptors with O-glucose (O-Glc) and O-fucose (O-Fuc). The epidermal growth factor (EGF) modules of the NECD are specifically targeted by protein O-glucosyltransferase 1 (Poglut) and protein O-fucosyltransferase 1 (Pofut1) enzymes (*11*, *12*). O-glucosylation and O-fucosylation are both required for Notch activation yet play distinct roles in the signaling pathway. O-glucose modifications indirectly affect signaling by increasing susceptibility to protease processing after ligand engagement, whereas O-fucose modifications directly enhance Notch affinity for Jagged/DLL (*11*–*13*). Elongation of O-fucose to a disaccharide by Fringe N-acetyl-glucosaminyltransferases further influences specificity by facilitating preferential interactions between certain receptor-ligand pairs (*14*–*16*). A long-standing question has been whether O-glycans directly contact ligands or contribute through allosteric effects. There are few examples of posttranslational

[1]Howard Hughes Medical Institute, Stanford University School of Medicine, Stanford, CA 94305, USA. [2]Department of Molecular and Cellular Physiology, Stanford University School of Medicine, Stanford, CA 94305, USA. [3]Department of Structural Biology, Stanford University School of Medicine, Stanford, CA 94305, USA.
***Corresponding author. E-mail: kcgarcia@stanford.edu**

modifications engaging in specific interactions between extracellular signaling proteins, although this has been observed in other ancient developmental pathways, such as the lipid-mediated interaction critical to Wnt-Frizzled recognition (*17*).

There are presently no high-resolution structures describing Notch-ligand complexes, although there are structures of unliganded Notch1 EGF-like repeats 11 to 13 (Notch1(11–13), amino acids 411 to 530) and an unliganded Jagged1 fragment spanning from the N terminus to EGF3 (amino acids 32 to 337) (*18*, *19*). Mammalian NECDs consist of 29 to 36 EGF repeats followed by 3 cysteine-rich LIN repeats. It has been established from many studies that EGF11 and 12 alone are sufficient for binding to Jagged/DLL, and these domains are assumed to represent the core recognition element (*18*, *20*). Additional regions have been implicated in Notch ligand recognition, including EGF domains 6 to 15 (*21*, *22*). Jagged/DLL ECDs, like those of Notch, have a modular extracellular domain architecture consisting of a region termed module at the N-terminus of Notch ligands (MNNL) domain followed by a Delta/Serrate/Lag-2 (DSL) domain, and either 6 (DLL3), 8 (DLL1 and DLL4), or 16 (Jagged1 and Jagged2) EGF repeats (*19*, *23*). Alanine scanning mutagenesis studies have identified conserved residue Phe^{207} of the Jagged1 DSL domain and residues Leu^{468}, Asp^{469}, and Ile^{477} of Notch1 EGF12 as critical to receptor-ligand interactions (*18*, *24*).

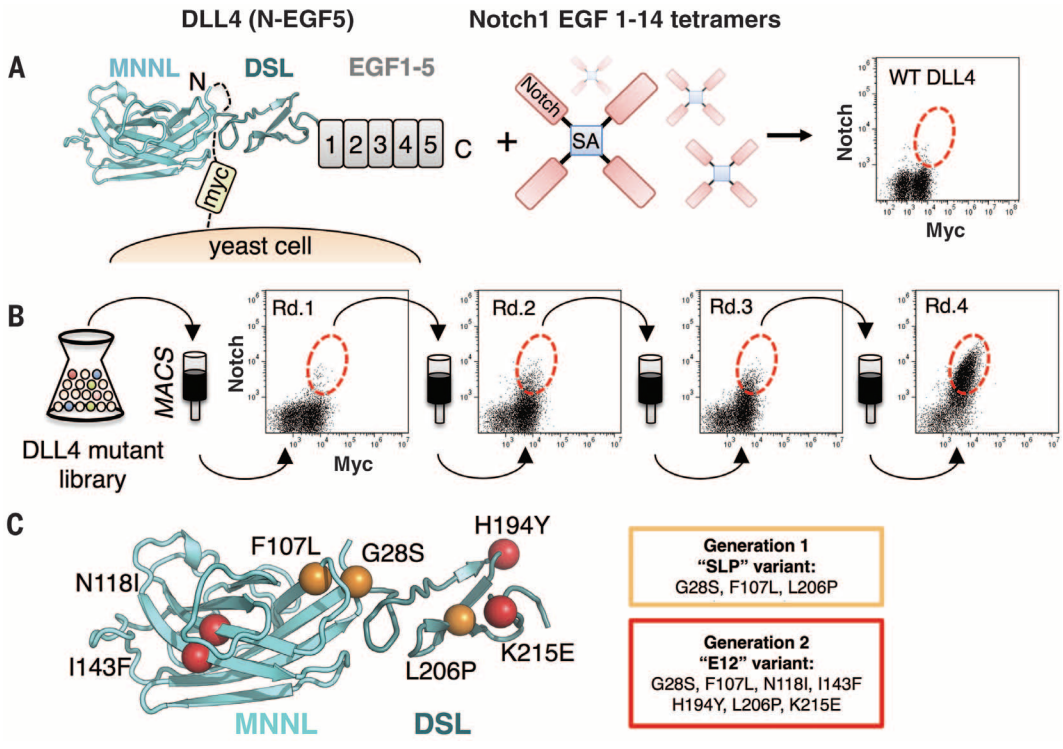
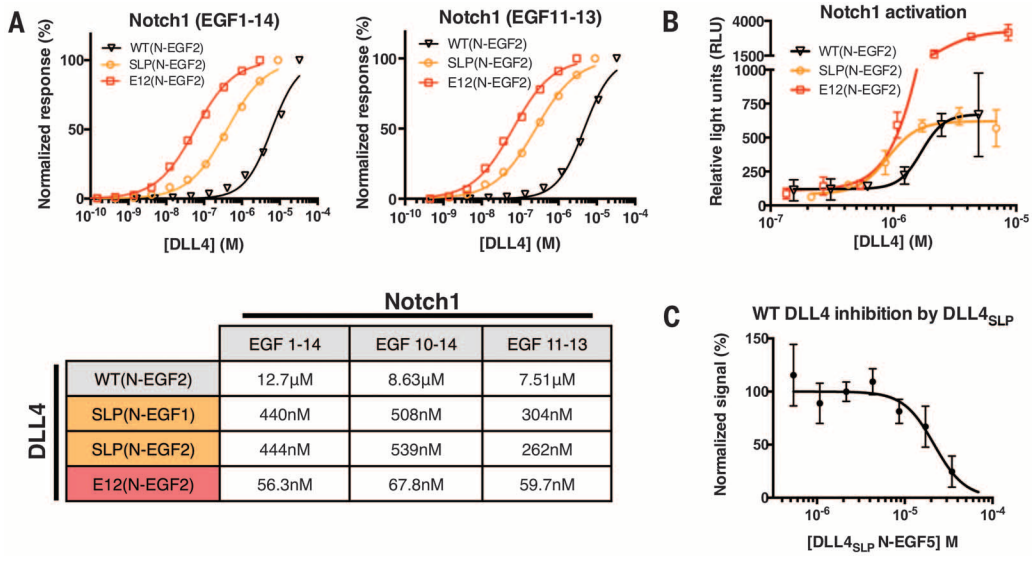


Fig. 1. In vitro evolution of Notch1-DLL4 interactions with yeast surface display. (**A**) Schematic representation of the yeast-displayed DLL4(N-EGF5)construct used for mutant library generation, stained with Notch1(1–14) tetramers. The flow cytometry dot plot shows double staining of DLL4 (N-EGF5) with 50 nM Notch1 tetramer and antibody to c-Myc. (**B**) Four rounds of selection were performed on magnetic-activated cell sorting (MACS) columns using a mutant library of DLL4(N-EGF5). Yeast isolated from selection rounds 1 to 4 (Rd.1 to Rd.4) were each double stained with 50 nM Notch1(1-14) tetramer and antibody to c-Myc. Dot plots for each round are displayed, with enriched populations circled with a red dotted line. (**C**) Affinity-enhancing mutants isolated from generation 1 and generation 2 libraries are mapped onto the surface of MNNL/DSL domains from the DLL4 crystal structure. The first generation SLP mutations are depicted as orange spheres. The second generation E12 variant includes the SLP mutations, plus four additional mutations (colored red).



DLL4	Notch1 EGF 1-14	Notch1 EGF 10-14	Notch1 EGF 11-13
WT(N-EGF2)	12.7μM	8.63μM	7.51μM
SLP(N-EGF1)	440nM	508nM	304nM
SLP(N-EGF2)	444nM	539nM	262nM
E12(N-EGF2)	56.3nM	67.8nM	59.7nM

Fig. 2. Notch1 binding and activation by high-affinity DLL4 variants. (**A**) Binding isotherms were obtained by surface plasmon resonance. Wild-type DLL4(N-EGF2), generation 1 DLL4$_{SLP}$(N-EGF1 and N-EGF2) and generation 2 DLL4$_{E12}$(N-EGF2) constructs were flowed over immobilized Notch1 EGF1–14, 10–14, or 11–13. Curves were fit to a 1:1 binding model to obtain the K_d values indicated in the table. (**B**) Notch1 activation was measured in a luciferase assay using cell lines expressing Notch1 and stably integrated with a luciferase gene under control of a CSL-driven promotor. Plates (96-well) were coated with serial dilutions of wild-type and high-affinity DLL4 variants. High-affinity mutants have increased potency relative to wild type. (**C**) Soluble DLL4$_{SLP}$ (N-EGF5) inhibited Notch1 activation by immobilized, wild-type DLL4(N-EGF5) in the luciferase assay.

Structural information about Notch-Delta/Jagged interactions is absent largely due to several complicating factors that have precluded the reconstitution of Notch receptor-ligand complexes for structural studies. Notch possesses an intrinsically low affinity for its ligands (*25*, *26*). Furthermore, optimal ligand binding requires proper modification by O-glycosyltransferases in the recombinant Notch fragments used for structural analysis (*13*). Finally, the calcium binding by several Notch EGFs is important for folding and ligand engagement (*5*, *18*, *27*). To overcome these obstacles and capture a stable complex for structure determination, we used in vitro evolution to engineer mutations in DLL4 stability and enhance affinity for Notch1.

Affinity maturation of DLL4

We targeted the interaction between Notch1 and DLL4 for affinity maturation because they represent the mammalian receptor-ligand pair with the highest intrinsic affinity (*21*). As a platform for in vitro evolution, we expressed DLL4 comprising the predicted receptor-binding region spanning from the N terminus to EGF2, plus EGFs 3 to 5, on the surface of yeast as a fusion to cell wall protein Aga2 (Fig. 1A). DLL4 was displayed, rather than Notch1, because yeast do not encode for the O-glycosylation enzymes required for modification of Notch EGFs. To isolate higher-affinity DLL4 variants, we generated a mutant library of DLL4(N-EGF5) using unbiased error-prone polymerase chain reaction and performed several rounds of selection on magnetic beads with decreasing concentrations of Notch1(1–14) tetramers or monomers. Wild-type DLL4 did not bind Notch1(1–14) (Fig. 1A) but gradually increased in affinity after each round of selection (Fig. 1B). To further enhance DLL4-Notch1 affinity, the selectants were pooled and subjected to a second cycle of mutagenesis. Clones isolated from the first- and second-generation libraries were sequenced and revealed a series of consensus mutations in only the MNNL and DSL domains (Fig. 1C and fig. S1).

We expressed recombinant forms of wild-type DLL4 and engineered DLL4 variants in insect cells and measured their binding affinities for Notch1 by surface plasmon resonance. Wild-type DLL4(N-EGF2) bound Notch1(1–14), Notch1(10–14), and Notch1(11–13) with dissociation constant (K_d) values of 12.7 μM, 8.6 μM, and 7.5 μM, respectively (Fig. 2A). The similar DLL4 affinity for Notch1(11–13) and Notch1(1–14) is consistent with previous studies suggesting that EGFs 11 and 12 constitute the major binding determinants (*18*, *20*). We next determined the affinity of a variant containing SLP consensus mutations (G28S, F107L, and L206P) named $DLL4_{SLP}$, and the highest-affinity variant from the second-generation library, named $DLL4_{E12}$, containing the three SLP mutations plus four additional substitutions (N118I, I143F, H194Y, and K215E) (Fig. 1C). Minimal binding regions of $DLL4_{SLP}$ (N-EGF1) or $DLL4_{SLP}$(N-EGF2) bound our Notch1 constructs with a K_d of ~260 to 540 nM. $DLL4_{E12}$ (N-EGF2) interacted with an even lower K_d range of ~56 to 68 nM (Fig. 2A), a 125- to 225-fold increase in affinity relative to wild-type DLL4(N-EGF2) (Fig. 2A). The kinetics of the Notch1-DLL4 interactions suggests that affinity-enhancing mutations have slowed the dissociation rate of the complex (fig. S2).

Notch1 activation by DLL4 variants

To ensure that the affinity-enhancing mutations in DLL4 did not diminish function, we assayed the signaling activity of the high-affinity DLL4 variants. We performed a luciferase assay using a stable cell-line expressing Notch1 and a luciferase reporter gene under control of the Notch-driven CBF1, Suppressor of Hairless, Lag-1 (CSL) promoter. Cells incubated with $DLL4_{SLP}$(N-EGF2) gave a similar maximal response (E_{max}) as wild-type DLL4(N-EGF2) (Fig. 2B), but there was a marked left-shift in the dose-response curve for $DLL4_{SLP}$(N-EGF2) as a result of its higher affinity. The highest-affinity variant, $DLL4_{E12}$(N-EGF2), yielded a five-fold increase in E_{max} relative

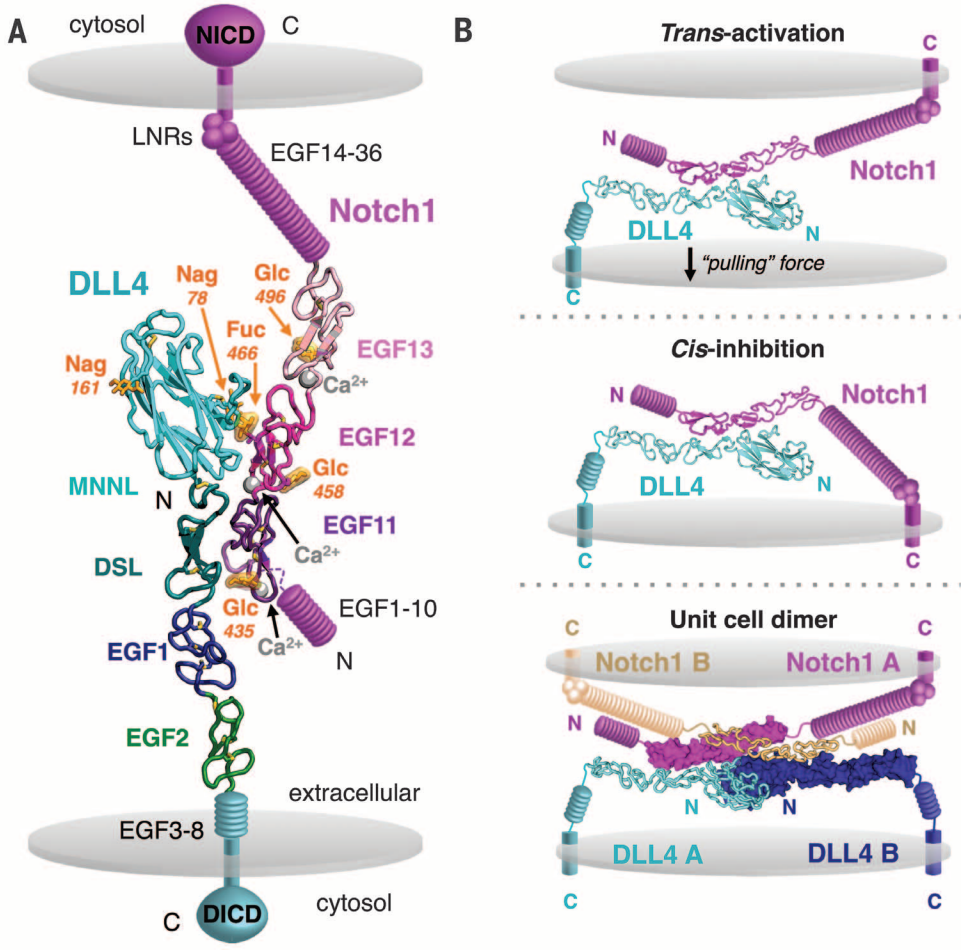


Fig. 3. Structure of the Notch1(11–13)–$DLL4_{SLP}$(N-EGF2) complex. (**A**) The structure of Notch1(11–13) bound to $DLL4_{SLP}$(N-EGF2) is shown in ribbon representation. Calcium ions are represented as gray spheres, Notch1 O-glycans are highlighted in orange, and cell membranes are depicted as gray discs. The remaining domains of the Notch1 or DLL4 receptors are displayed schematically in magenta or teal, respectively. DICD, DLL4 intracellular domain. (**B**) The Notch1-DLL4 crystal structure is modeled as the interaction is predicted to occur in cellular contexts. Notch is trans-activated upon binding to ligands on adjacent cells or cis-inhibited upon binding to ligands on the same cell. In one model for trans-activation, mechanical pulling force resulting from endocytosis of ligand by adjacent cells activates Notch. The 2:2 dimer observed in the crystal asymmetric unit is also displayed as it may occur between two cells. The same dimer organization was observed in crystals of Notch1(11–13)–$DLL4_{SLP}$(N-EGF1) and is further described in fig. S5.

to wild-type DLL4 and $DLL4_{SLP}$ proteins (Fig. 2B). Performing activation assays with longer DLL4(N-EGF5) constructs increased the E_{max} of wild-type DLL4 and the SLP variant, suggesting that EGF3-5 may provide the low and intermediate affinity ligands with sufficient length to access the cellular Notch1 receptors in the plate-based format (fig. S3) (*21*). We also assessed the ability of the first generation SLP variant to compete with immobilized wild-type DLL4 for Notch1 binding. The soluble $DLL4_{SLP}$(N-EGF5) effectively inhibited Notch1 activation (Fig. 2C). Thus, the affinity-enhanced DLL4 variants remain functional in activating Notch signaling.

Crystallization of the Notch1-DLL4 complex

We attempted to make Notch1-DLL4 complexes with a variety of different combinations of DLL4 affinity-matured constructs and Notch1. $DLL4_{SLP}$(N-EGF2) formed biochemically stable complexes with Notch1(11–13) (fig. S4). Heterogeneous N-linked glycans were enzymatically trimmed in $DLL4_{SLP}$(N-EGF2) by sensitizing the insect cells with a mannosidase inhibitor, kifunensine, followed by treatment with endoglycosidase F1 (Endo F1). This strategy digests all but the proximal N-acetyl glucosamine (Nag) from asparagine residues without affecting O-linked sugars. Crystals of Notch1(11–13) bound to the glycan-shaved $DLL4_{SLP}$(N-EGF2) diffracted to a resolution of 3.4 Å (table S1). Crystals of a complex containing a shorter $DLL4_{SLP}$(N-EGF1) construct were obtained by the same strategy and diffracted to a resolution of 2.3 Å (table S1). We determined both structures by molecular replacement using models of unliganded Notch1(11–13) and Jagged1 (*18*, *19*). The electron density maps obtained from the high-resolution Notch1(11–13)–$DLL4_{SLP}$(N-EGF1) structure were used for analysis of atomic contacts, whereas the lower-resolution Notch1(11–13)–$DLL4_{SLP}$(N-EGF2) structure allowed us to model the additional EGF2 domain.

Architecture of the Notch1-DLL4 complex

In the complex of Notch1(11–13) and $DLL4_{SLP}$(N-EGF2), the two proteins form a colinear, antiparallel interaction across a narrow interface that buries ~1100 $Å^2$ of protein and glycan surface area (Fig. 3A). This antiparallel binding orientation is compatible with either a trans cell-cell contact to initiate signaling or a self-inhibited cis interaction, as has also been proposed (Fig. 3B) (*28*, *29*). Notch1 EGFs 11 to 13 assemble into a ~90 Å rod stabilized by three disulfide bonds per EGF and by Ca^{2+} ions coordinated at the inter-EGF junctions. $DLL4_{SLP}$(N-EGF2) MNNL (C2-like), DSL, EGF1, and EGF2 domains stretch 120 Å lengthwise. Notch1 ligand-binding residues localize to a continuous surface of EGF 11 and 12, providing structural validation for long-standing cellular, genetic, and biochemical studies implicating this region in Notch activation (*18*, *20*, *24*, *30*). Although Notch EGF12 and the Delta/Jagged DSL domain are widely regarded as the central interacting nodes, the complex structure indicates that these regions are offset such that EGF11 lies opposite the DSL and EGF12 engages a disulfide-tethered loop at the base of the MNNL (Fig. 3A). Calcium ions did not contribute directly to the interface in the Notch1-DLL4 structure but are coordinated by residues at the N terminus of EGF11 and at the EGF11-12/EGF12-13 junctions and potentiate the interaction by rigidifying the DLL4-binding platform (Fig. 3A) (*31*). Although it has been proposed that Notch activation requires calcium-dependent phospholipid binding by ligand MNNL domains, DLL4 was not bound to any calcium ions, which would suggest that this feature is not essential for signal transduction by all ligands (*19*).

The Notch1-DLL4 complex forms an antiparallel 2:2 dimer in the asymmetric unit of the

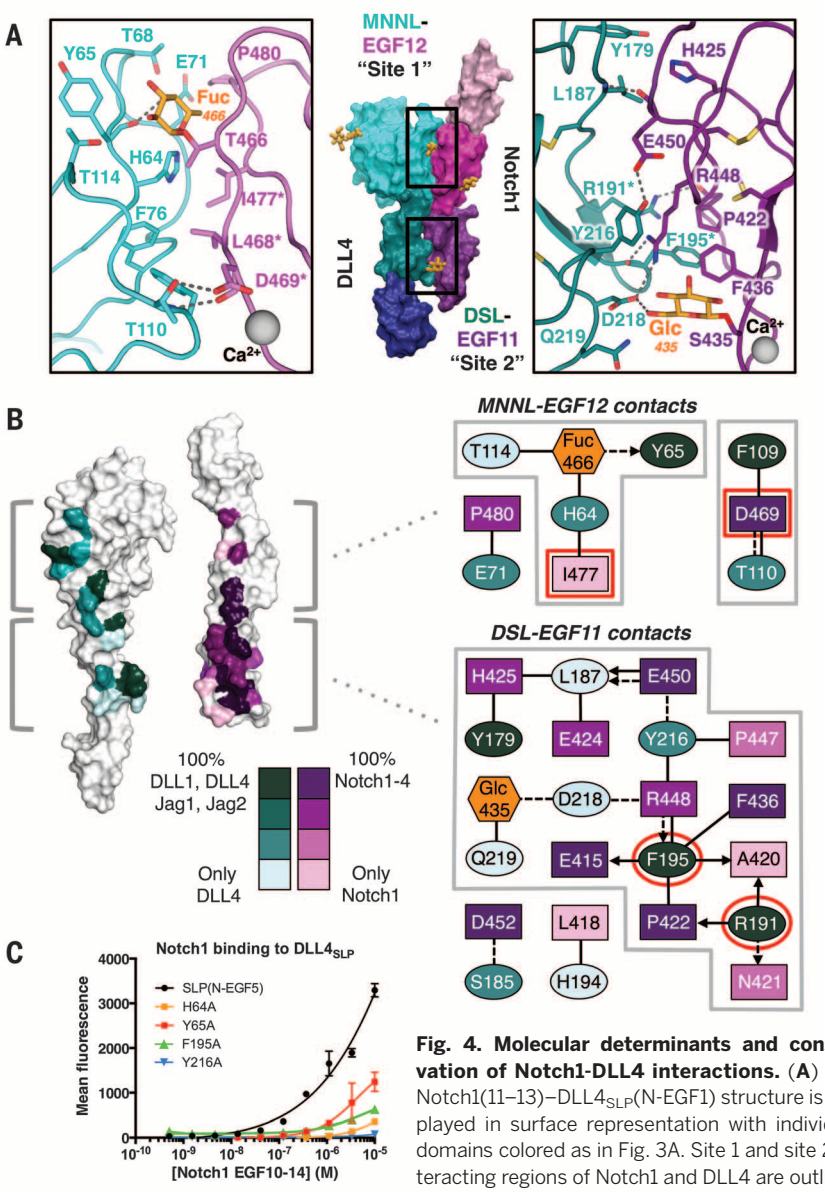


Fig. 4. Molecular determinants and conservation of Notch1-DLL4 interactions. (**A**) The Notch1(11–13)–$DLL4_{SLP}$(N-EGF1) structure is displayed in surface representation with individual domains colored as in Fig. 3A. Site 1 and site 2 interacting regions of Notch1 and DLL4 are outlined in black boxes. In the zoomed panels, dashed gray lines represent H-bonds or salt bridges. (**B**) White surface representations of Notch1 and DLL4 represent an "open-book" view of the contact residues. Conservation of contact residues among mammalian paralogs is indicated by a color gradient painted onto the structures. Jag1, Jagged1. Jag2, Jagged2. The panels to the right serve as an interface contact map. Ovals represent DLL4 residues, rectangles represent Notch1 residues, and hexagons represent O-glycans. Each residue is colored according to conservation, and glycans are colored orange. Dashed lines connecting residues are H-bonds or salt bridges, and solid lines are VDW contacts. Interactions between side chains and backbones are represented as arrows pointing toward the backbone. Red outlines indicate residues that, when mutated, result in null binding or dysfunction in developmental assays (*18*, *24*). (**C**) $DLL4_{SLP}$(N-EGF5) and $DLL4_{SLP}$ (N-EGF5) containing H64A, Y65A, F195A, or Y216A mutations were expressed on yeast and evaluated for binding to biotinylated Notch1(10–14). Binding is indicated as mean fluorescence intensity from SA-647 secondary staining.

crystal (fig. S5A). The same dimer organization was present in crystals of both different Notch1-DLL4 complexes (fig. S5B). Although such a dimer would be feasible to form between two cells, it is unclear whether the dimer observed in the crystal lattices represents a physiologically relevant assembly (Fig. 3B). Multi-angle light-scattering analyses of Notch1(11–13) and $DLL4_{SLP}$(N-2EGF) indicated that the proteins formed a 1:1 complex in solution (fig. S6). It is possible that the high local concentration of proteins in the two-dimensional environment of cell membranes may drive oligomerization in vivo, but this remains to be shown experimentally.

The Notch1-DLL4 interaction is partitioned across two interfaces: a "site 1" between the DLL4 MNNL domain and Notch1 EGF12, and a "site 2" between the DLL4 DSL domain and Notch1 EGF11 (Fig. 4A and table S2). With respect to site 1, mutagenesis studies of Notch1-EGF12 defined a patch of residues—Leu^{468}, Asp^{469}, and Ile^{477}—localized on a single face of EGF12 as critical for Jagged1 recognition, and O-glycosylation of residue Thr^{466} on this same face enhances binding to DLL1, DLL4, and Jagged1 (*13*, *24*). Remarkably, the Notch1(11–13)–$DLL4_{SLP}$(N-EGF1) structure indicates that the Notch1 Thr^{466} O-fucose modification centrally anchors the DLL4-binding interface, essentially acting as a surrogate amino acid (Fig. 4A). O-Fuc^{466} buries more than 80% of its total surface area between Notch1 EGF12 and the surface of the MNNL, where it participates in a network of glycan-protein contacts (Fig. 4, A and B). The MNNL domain presents a fucose-binding platform formed by interstrand loops stabilized by the Cys^{61}-Cys^{74} disulfide bond. The platform accommodates the O-Fuc^{466} ring atop the planar side chains of DLL4 His^{64} and Tyr^{65} (Fig. 4A). A hydroxyl group of O-Fuc^{466} points downward toward the MNNL platform and hydrogen bonds (H-bonds) to the main-chain carbonyl of Tyr^{65} (Fig. 4A). In addition to the Thr^{466} fucose, several Notch1 residues that were previously implicated in Jagged1-binding (Leu^{468}, Asp^{469}, and Ile^{477}) are buried at the MNNL interface (*24*). Leu^{468} and Ile^{477} occupy a hydrophobic cleft of DLL4 composed of His^{64}, Phe^{76}, and Phe^{109}, whereas Asp^{469} accepts H-bonds from the side-chain hydroxyl and backbone amine of Thr^{110} (Fig. 4, A and B).

Although site 2 is dominated by protein-protein contacts, there is an unexpected interaction between an O-glycan attached to Ser^{435} of Notch1 and DLL4 (*21*). DLL4 DSL engages Notch EGF11 with several residues at the apices of disulfide-knotted loops linking Cys^{188}-Cys^{200} and Cys^{208}-Cys^{217} (Fig. 4A). Phe^{195} and Tyr^{216} protrude from these loops to form a clamp sandwiching the side chain of Notch1 Arg^{448}, which serves as the major linchpin for DLL4 engagement. The Notch1 Arg^{448} side chain extends deeply into a DSL groove, burying ~100 $Å^2$ of surface area and forming a salt bridge with the carboxylate head group of DLL4 Asp^{218}, an H-bond with the backbone carbonyl of Phe^{195}, and engaging in aliphatic interactions with Tyr^{216} (Fig. 4, A and B). The O-Glc modification Ser^{435} of Notch1 interacts with DLL4 by donating an H-bond to the carboxylate head group of DLL4 Asp^{218} and participating in a van der Waals (VDW) interaction with the side chain of Gln^{219} (Fig. 4, A and B). We modeled a β1-glucose at this position because recent mass spectroscopy data classified the sugar as a hexose, although we cannot rule out the possibility of other O-linked hexoses such as mannose or galactose (*21*). The role of the Ser^{435} modification is much less clear than that of the well-characterized O-Fuc modification of Thr^{466}. Ser^{435} is only present in Notch1 and Notch4, is part of neither a Poglut nor a Pofut1 consensus motif, and there is no strong evidence for another functionally important O-glycosyltransferase that directly modifies Notch receptors. Additional contacts that stabilize site 2 include the benzene ring of DLL4 Phe^{195} filling a hydrophobic pocket of EGF11, where it participates in a triad of VDW interactions with Pro^{422} and Phe^{436} of Notch1 (Fig. 4, A and B).

To assess the relative importance of key interface residues to binding, we mutated MNNL fucose-binding platform residues His^{64} and Tyr^{65} and DSL residues Phe^{195} and Tyr^{216} to alanine and analyzed cell-surface capture of Notch1(10–14) using a fluorescence-based assay. Mutation of Y216A completely abolished binding to Notch1, whereas H64A, Y65A, and F195A substantially diminished Notch1(10–14) interactions relative to $DLL4_{SLP}$(N-EGF5) (Fig. 4C).

Location of affinity-enhancing mutations

We examined the structural context of our engineered mutations to better understand the molecular basis for affinity enhancement.

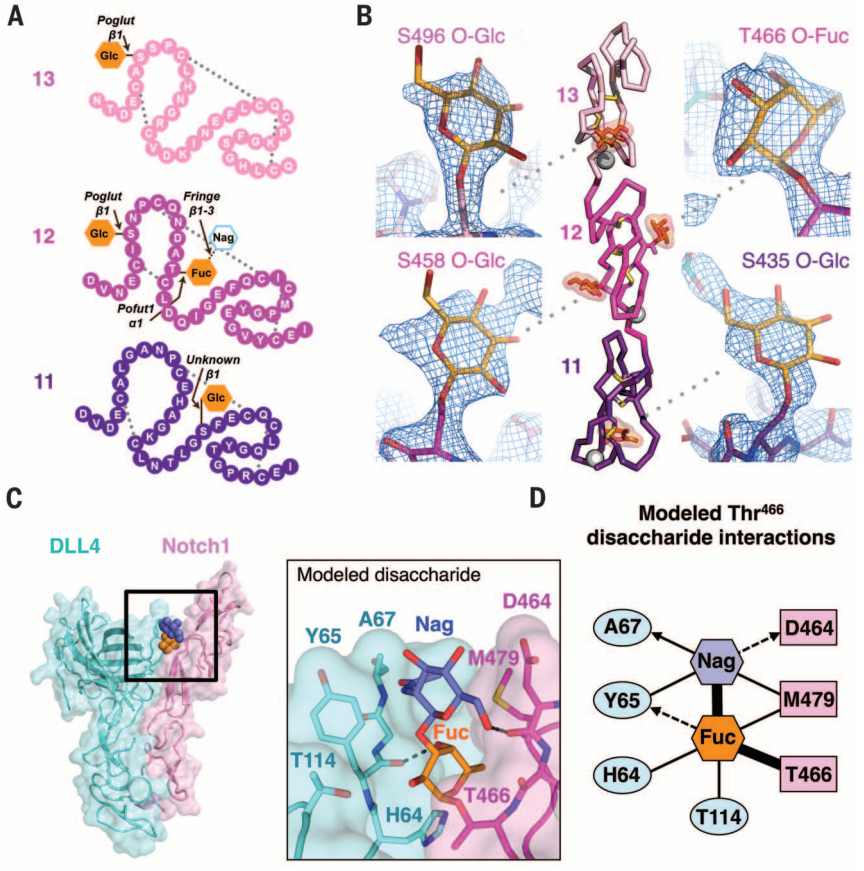


Fig. 5. Basis of affinity tuning by O-fucose modification. (**A**) Schematic diagram of Notch1(11–13) with amino acids depicted as colored spheres and disulfide connectivity as dotted gray lines. The O-linked glycans observed in the structure are shown as filled orange hexagons. The Thr^{466} O-Fuc is elongated by Fringe enzymes to form a disaccharide, represented as an outlined hexagon. Enzymes responsible for each modification, along with the glycosidic linkages, are shown above each O-glycan. (**B**) Ribbon diagram of Notch1(11–13) indicating the position of disulfide bonds (yellow sticks), Ca^{2+} ions (gray spheres), and O-linked glycans (orange highlighted sticks). Simulated annealing composite omit map electron density surrounding each of the four O-glycans is shown in zoomed panels as blue mesh and contoured at 1.5 σ. (**C**) The Notch1 Thr^{466} disaccharide is modeled as spheres in the context of a Notch1-DLL4 complex and are colored as in (A). The zoomed panel depicts Thr^{466} disaccharide interactions with protein side chains, with H-bonds represented as dashed gray lines. (**D**) Contact map describing interactions between the modeled disaccharide and Notch1-DLL4. Sugars, Notch1, and DLL4 residues are colored corresponding to the panels in (C). Thick black lines represent covalent bonds, thin black lines are VDW interactions, and dashed black lines are H-bonds.

Surprisingly, none of the three DLL4 SLP substitutions directly contacted Notch1 (fig. S7A). G28S and F107L mutations are in close spatial proximity within the MNNL and probably strengthen the interaction by stabilizing the MNNL-DSL hinge or the adjacent EGF12-contacting residues Phe^{109} and Thr^{110} (fig. S7A). The L206P mutation lies at the center of a DSL beta strand, where it may indirectly enhance binding (fig. S7A). Modeling of the additional mutations in our second-generation E12 construct revealed that only the H194Y and K215E substitutions occur at DLL4 contact positions. Thus, it is unlikely that the evolved mutations have introduced differences in the manner that Notch1 binds to wild-type DLL4.

Conservation of contact residues

The four mammalian Notch receptor homologs (Notch1 to 4) signal in response to engagement by four different ligands (Jagged1, Jagged2, DLL1, and DLL4). We performed a conservation analysis to assess whether the Notch1(11–13)–DLL4$_{SLP}$(N-EGF1) complex structure is broadly representative of a conserved Notch receptor-ligand interaction mode (Fig. 4B and fig. S8). Along the EGF11 interface, discontinuous Notch1 residues Glu^{415}, Pro^{422}, Phe^{436}, Glu^{450}, and Asp^{452} collectively form a DSL-binding surface that is conserved in Notch1 to 4 (Fig. 4B). The complementary DLL4 DSL surface includes three conserved DLL4 residues: Tyr^{179}, Arg^{191}, and Phe^{195}. The importance of Arg^{191} and Phe^{195} to the interaction is supported by the deleterious functional effects of mutating the equivalent positions in Jagged1 in the *Drosophila melanogaster* ligand Serrate (Fig. 4B) (*18*). Aligning the sequence of Notch ligands to divergent family member DLL3 revealed that only 6 out of 15 Notch1-binding residues are conserved in DLL3 (fig. S8). Because DLL3 has been reported not to bind or activate Notch, it was omitted from our structural analysis of interface conservation (*32*). EGF12 interface contacts are more divergent than those of EGF11: Only the calcium-coordinating Asp^{469} is identical in all four Notch receptors (Fig. 4B and fig. S8). The functionally relevant, O-fucose–bearing Thr^{466} is encoded by Notch1, Notch2, and Notch4 (fig. S8). On the MNNL side, the interacting Phe^{109} and a fucose-binding Tyr^{65} residue are conserved (Fig. 4B). Collectively, we propose that the EGF11-DSL interface is the conserved focal point for ligand binding and the more variable EGF12-MNNL interface facilitates ligand pleiotropy. The limited sequence identity at the MNNL interface may then contribute to diverse surface chemistry important for Fringe-mediated tuning of ligand specificity (discussed below). Taken together, our analyses suggest that the general binding mode observed in the Notch1(11–13)–DLL4$_{SLP}$(N-EGF1) structure is consistent among Notch receptor and ligand paralogs.

Notch1 O-linked glycans

O-glucosylation and O-fucosylation of Notch1 are strictly required for Notch signaling (*11*, *12*). Notch1 EGF11 to 13 contains two Poglut glucosylation consensus sequences at Ser^{458} and Ser^{496}, one Pofut1 fucosylation sequence Thr^{466}, and a Ser^{435} hexose of unknown origin (Fig. 5A) (*21*). We observed clear electron density for the proximal O-glycan at all four predicted positions (Fig. 5B). Neither O-Glc^{458} nor O-Glc^{496} contacted DLL4 in the complex structure; thus, their effect on signaling activity would appear to be indirect (Fig. 3A). O-Glc^{458} lies flat against the surface of EGF12, opposite the DLL4-binding face, where it shields hydrophobic Pro^{460} and Phe^{474} side chains from solvent exposure. Glc^{496} similarly covers the Pro^{494} and Phe^{512} residues at equivalent positions in EGF13. As opposed to O-fucose, which directly influences ligand binding, Poglut-mediated Notch O-glucose modifications enhance signaling by increasing Notch receptor susceptibility to proteolytic processing (*11*, *33*). From a structural perspective, O-glucose may then facilitate efficient proteolysis by protecting hydrophobic surfaces from aggregation as Notch clusters on the cell surface. The newly identified O-glycan modification of S^{435} does not occur at a known O-glycosyltransferase consensus motif but is a salient feature of the structure, given its position at the DLL4 interface (Figs. 3A and 4A). Elongation of O-Glc^{435} has the potential to regulate Notch by enhancing or inhibiting interaction with the opposing DSL domain.

Modeling Thr^{466} fucose elongation

Regulation of ligand specificity by Fringe enzymes is a complex process that involves the coordinated elongation of several Notch1 O-fucose moieties (*34*). Recent biophysical studies have begun to deconvolve this process by determining that O-fucosylation of Thr^{466} of Notch1 substantially enhances binding to Jagged1/DLL1 and moderately enhances binding to DLL4 (*13*). Affinity was further increased in all cases when a β1-3 Nag was added to O-Fuc^{466} by Fringe enzymes. To probe the molecular basis for Fringe-mediated affinity enhancement, we generated a model of the naturally occurring Thr^{466} O-linked disaccharide based on the single O-fucosylation we see in the structure (Fig. 5C). The modeled disaccharide tunnels outward through a crevice at the Notch1-DLL4 interface and adopts a similar conformation to that observed in an unliganded, disaccharide-modified Notch1(11–13) structure (*13*). The elongated Nag glycan appears to facilitate interactions by generating a network of H-bonds and VDW contacts with both Notch1 and DLL4 and acting as a molecular bridge (Fig. 5D). The modeled Nag is sandwiched between hydrophobic side chains presented by Tyr^{65} of DLL4 and Met^{479} of Notch1 and donates a H-bond to the backbone carbonyl of Asp^{464} of Notch1 (Fig. 5C). It is clear from our model that elongated O-glycans are capable of providing substantial additional energetic contributions to Notch-ligand interfaces.

The central chemical and structural role of an O-linked glycan in mediating a receptor-ligand interaction, essentially functionalizing the Notch protein with an expanded capacity for molecular recognition beyond the 20 naturally occurring amino acids, is unusual. It is intriguing that two other key receptor-ligand systems that act as developmental checkpoints in mammals, Wnt/Frizzled and sonic hedgehog (Shh)/patched, also rely on posttranslational modifications for function. Wnt is lipidated, and Shh is cholesterol modified (*17*, *35*). It is possible that these primordial systems took advantage of the biosynthetic modification pathways (e.g., Pofut and fringe) to achieve fine regulation of signaling in a way that would be difficult to achieve through nonpolymorphic amino acid contacts alone. By linking molecular recognition to the O-glycan heterogeneity, the Notch-ligand interaction can be tuned to reflect the developmental and metabolic state of the cell.

Trans- versus cis-interaction

Canonical Notch signaling involves trans-activation by ligands expressed on adjacent cells, though cis-inhibition of Notch by ligands expressed on the same cell is a potential regulatory mechanism (*28*, *29*). The antiparallel orientation observed in our structure could mediate both trans- and cis-interactions because of the interdomain flexibility of regions of Notch receptors and ligands (Fig. 3B) (*36*, *37*). That the same binding site could mediate trans-interactions between opposing cells and cis-interactions on the same cell has been observed in several immune receptors (*38*).

Comparison of Notch1-DLL4 complex with unliganded structures

Notch activation involves ligand-induced conformational changes that render Notch susceptible to proteolytic cleavage. To assess whether conformational changes occur in the interacting regions upon binding, we compared the individual Notch and DLL4 subunits of the complex structure with unliganded structures of Notch1(11–13) and Jagged1. Unliganded Notch1(11–13) superimposed onto the backbone and side chains of complexed Notch1(11–13) with a root mean square deviation of 1.44 Å (fig. S9A), indicating that the protein does not undergo major conformational changes upon binding to DLL4 (*18*). Because there is no available structure of DLL4 alone, we compared Notch1-complexed DLL4$_{SLP}$ to the unliganded structure of homolog Jagged1. The DSL, EGF1, and EGF2 of DLL4 are rotated ~25° about the MNNL domain relative to their position in Jagged1 (fig. S9B), suggesting that ligands may flex at an MNNL-DSL "hinge" to engage Notch. Given that the Notch-interacting residues of DLL4 are well conserved (Fig. 4B and fig. S8) and that many of our affinity-enhancing mutations were at noncontact positions, it is possible that the lower affinity of ligands Jagged1 and DLL1 are due to differences in domain orientations about the MNNL-DSL linker.

AGS disease mutations

AGS is an inherited developmental disease that is frequently caused by mutations in Jagged1 (*10*). We mapped AGS-associated Jagged1 missense mutations onto their equivalent DLL4 positions

in the Notch1(11–13)–DLL4$_{SLP}$(N-EGF2) complex to clarify their effect on receptor binding (fig. S7B) (*39*). The majority of AGS mutations are predicted to disrupt disulfide bond formation, perturb the hydrophobic core of the MNNL domain, or interfere with inter-EGF packing. However, mutations at conserved Thr^{110} and Tyr^{179} residues would directly affect binding, whereas other mutations at Gly^{28}, Pro^{112}, and Val^{151} positions could indirectly influence interactions by distorting the MNNL-DSL linker (fig. S7B). Notably, one AGS patient had a Jagged1 mutation analogous to the DLL4 G28S mutation isolated from our affinity maturation experiments, raising the possibility that the mutation disrupts Notch binding in the context of Jagged1 (fig. S7B) (*40*).

Implications for therapeutic targeting of the Notch pathway

The distinct pathologies linked to Notch receptors and ligands necessitates the development of more precisely targeted therapies. For example, Notch1 mutations are associated with leukemia and aortic valve disease, Notch3 mutations with cerebral autosomal dominant arteriopathy with subcortical infarcts and leukoencephalopathy, and Jagged1/Notch2 mutations with AGS (*39*, *41*–*44*). Physiological processes can also be differentially regulated by ligands, evidenced by the opposing roles of Jagged1 and DLL4 in angiogenesis and the role of the Notch1-DLL4 axis in lymphatic development and the lymphatic system (*45*, *46*). Certain advantages of receptor-specific therapeutics have begun to emerge in studies describing the inhibition of tumor growth by Notch1-antagonist antibodies and the control of graft-versus-host disease by DLL1/4-antagonist antibodies (*47*, *48*). The Notch1(11–13)–DLL4$_{SLP}$(N-EGF1) structure provides new insights toward the development of receptor- and ligand-specific drugs. Antibodies against Notch EGF11 and 12 reportedly have limited effectiveness in cellular assays; based on the structure, this is likely due to occlusion of relevant protein epitopes by the Ser^{435} O-glucose and Thr^{466} O-fucose moieties (*49*). More effective therapeutic targeting of EGF11 and 12 may be achieved with engineered high-affinity ligands such as those presented here, which have coevolved with Notch receptors to accommodate O-glycan binding.

REFERENCES AND NOTES

1. S. Artavanis-Tsakonas, M. D. Rand, R. J. Lake, *Science* **284**, 770–776 (1999).
2. L. A. Milner, A. Bigas, *Blood* **93**, 2431–2448 (1999).
3. Y. Nyfeler *et al.*, *EMBO J.* **24**, 3504–3515 (2005).
4. F. Radtke, H. R. MacDonald, F. Tacchini-Cottier, *Nat. Rev. Immunol.* **13**, 427–437 (2013).
5. R. J. Fleming, *Semin. Cell Dev. Biol.* **9**, 599–607 (1998).
6. G. Struhl, I. Greenwald, *Nature* **398**, 522–525 (1999).
7. B. De Strooper *et al.*, *Nature* **398**, 518–522 (1999).
8. C. Brou *et al.*, *Mol. Cell* **5**, 207–216 (2000).
9. W. R. Gordon *et al.*, *Nat. Struct. Mol. Biol.* **14**, 295–300 (2007).
10. E. M. Hansson, U. Lendahl, G. Chapman, *Semin. Cancer Biol.* **14**, 320–328 (2004).
11. M. Acar *et al.*, *Cell* **132**, 247–258 (2008).
12. T. Okajima, K. D. Irvine, *Cell* **111**, 893–904 (2002).
13. P. Taylor *et al.*, *Proc. Natl. Acad. Sci. U.S.A.* **111**, 7290–7295 (2014).
14. C. Hicks *et al.*, *Nat. Cell Biol.* **2**, 515–520 (2000).
15. V. M. Panin, V. Papayannopoulos, R. Wilson, K. D. Irvine, *Nature* **387**, 908–912 (1997).
16. J. Chen, D. J. Moloney, P. Stanley, *Proc. Natl. Acad. Sci. U.S.A.* **98**, 13716–13721 (2001).
17. C. Y. Janda, D. Waghray, A. M. Levin, C. Thomas, K. C. Garcia, *Science* **337**, 59–64 (2012).
18. J. Cordle *et al.*, *Nat. Struct. Mol. Biol.* **15**, 849–857 (2008).
19. C. R. Chillakuri *et al.*, *Cell Reports* **5**, 861–867 (2013).
20. I. Rebay *et al.*, *Cell* **67**, 687–699 (1991).
21. M. B. Andrawes *et al.*, *J. Biol. Chem.* **288**, 25477–25489 (2013).
22. S. Yamamoto *et al.*, *Science* **338**, 1229–1232 (2012).
23. B. D'Souza, A. Miyamoto, G. Weinmaster, *Oncogene* **27**, 5148–5167 (2008).
24. P. Whiteman *et al.*, *J. Biol. Chem.* **288**, 7305–7312 (2013).
25. C. Hicks *et al.*, *J. Neurosci. Res.* **68**, 655–667 (2002).
26. J. T. Nichols *et al.*, *J. Cell Biol.* **176**, 445–458 (2007).
27. R. G. Fehon *et al.*, *Cell* **61**, 523–534 (1990).
28. J. F. de Celis, S. Bray, *Development* **124**, 3241–3251 (1997).
29. D. Sprinzak *et al.*, *Nature* **465**, 86–90 (2010).
30. J. Cordle *et al.*, *J. Biol. Chem.* **283**, 11785–11793 (2008).
31. S. Hambleton *et al.*, *Structure* **12**, 2173–2183 (2004).
32. E. Ladi *et al.*, *J. Cell Biol.* **170**, 983–992 (2005).
33. N. A. Rana, R. S. Haltiwanger, *Curr. Opin. Struct. Biol.* **21**, 583–589 (2011).
34. R. Rampal, J. F. Arboleda-Velasquez, A. Nita-Lazar, K. S. Kosik, R. S. Haltiwanger, *J. Biol. Chem.* **280**, 32133–32140 (2005).
35. J. A. Porter, K. E. Young, P. A. Beachy, *Science* **274**, 255–259 (1996).
36. A. Xu, L. Lei, K. D. Irvine, *J. Biol. Chem.* **280**, 30158–30165 (2005).
37. W. D. Morgan *et al.*, *J. Mol. Biol.* **289**, 113–122 (1999).
38. W. Held, R. A. Mariuzza, *Nat. Rev. Immunol.* **8**, 269–278 (2008).
39. N. B. Spinner *et al.*, *Hum. Mutat.* **17**, 18–33 (2001).
40. D. M. Warthen *et al.*, *Hum. Mutat.* **27**, 436–443 (2006).
41. A. P. Weng *et al.*, *Science* **306**, 269–271 (2004).
42. V. Garg *et al.*, *Nature* **437**, 270–274 (2005).
43. A. Joutel *et al.*, *Nature* **383**, 707–710 (1996).
44. R. McDaniell *et al.*, *Am. J. Hum. Genet.* **79**, 169–173 (2006).
45. R. Benedito *et al.*, *Cell* **137**, 1124–1135 (2009).
46. K. Niessen *et al.*, *Blood* **118**, 1989–1997 (2011).
47. Y. Wu *et al.*, *Nature* **464**, 1052–1057 (2010).
48. I. T. Tran *et al.*, *J. Clin. Invest.* **123**, 1590–1604 (2013).
49. R. Falk *et al.*, *Methods* **58**, 69–78 (2012).

ACKNOWLEDGMENTS

We thank A. Velasco, D. Waghray, and J. Spangler for assistance. We also thank the staff of the Advanced Photon Source for support and access to the 23-ID-D beamline; the staff of the Advanced Light Source for support and access to the 8.2.2 Howard Hughes Medical Institute (HHMI) beamline; and the staff of the Stanford Synchrotron Radiation Lightsource, which is supported by the U.S. Department of Energy, Office of Science, Office of Basic Energy Sciences under contract DE-AC02-76SF00515. This work was supported by NIH-1RO1-GM097015, Ludwig Cancer Foundation, and the HHMI (K.C.G.). V.C.L. was supported by a Cancer Research Institute postdoctoral fellowship and an NIH-Immunology postdoctoral training grant. M.V.N. was supported by the Stanford Discovery Innovation fund, and N.W.P. was supported by an HHMI fellowship of the Helen Hey Whitney Foundation. K.C.G. and V.L. are inventors on a patent applied for by Stanford University describing high-affinity Notch ligands. Coordinates and structure factors of 1egf DLL4 and 2egf DLL4 have been deposited in the Protein Data Bank with accession codes 4XL1 and 4XLW.

SUPPLEMENTARY MATERIALS

www.sciencemag.org/content/347/6224/847/suppl/DC1
Materials and Methods
Supplementary Text
Figs. S1 to S9
Tables S1 to S2
References (*50*–*65*)

10 September 2014; accepted 14 January 2015
10.1126/science.1261093

REPORTS

QUANTUM ENGINEERING

Confining the state of light to a quantum manifold by engineered two-photon loss

Z. Leghtas,[1]* S. Touzard,[1] I. M. Pop,[1] A. Kou,[1] B. Vlastakis,[1] A. Petrenko,[1] K. M. Sliwa,[1] A. Narla,[1] S. Shankar,[1] M. J. Hatridge,[1] M. Reagor,[1] L. Frunzio,[1] R. J. Schoelkopf,[1] M. Mirrahimi,[2,1] M. H. Devoret[1]

Physical systems usually exhibit quantum behavior, such as superpositions and entanglement, only when they are sufficiently decoupled from a lossy environment. Paradoxically, a specially engineered interaction with the environment can become a resource for the generation and protection of quantum states. This notion can be generalized to the confinement of a system into a manifold of quantum states, consisting of all coherent superpositions of multiple stable steady states. We have confined the state of a superconducting resonator to the quantum manifold spanned by two coherent states of opposite phases and have observed a Schrödinger cat state spontaneously squeeze out of vacuum before decaying into a classical mixture. This experiment points toward robustly encoding quantum information in multidimensional steady-state manifolds.

Stabilizing the state of a system in the vicinity of a predefined state despite the presence of external perturbations plays a central role in science and engineering. On a quantum system, stabilization is a fundamentally more subtle process than on a classical system, as it requires an interaction that, quantum mechanically, is always invasive. The mere act of learning something about a system perturbs it. Carefully designed nondestructive quantum measurements have recently

[1]Department of Applied Physics, Yale University, New Haven, CT 06520, USA. [2]Institut National de Recherche en Informatique et en Automatique (INRIA) Paris-Rocquencourt, Domaine de Voluceau, B.P. 105, 78153 Le Chesnay Cedex, France.
*Corresponding author. E-mail: zaki.leghtas@yale.edu

been incorporated in feedback loops to stabilize a single quantum state (*1*–*4*). Alternatively, adequately engineering an interaction with an auxiliary dissipative system, termed "engineered dissipation," can also stabilize a single quantum state (*5*–*8*).

Can engineered dissipation protect all unknown superpositions of two states, thus protecting quantum information? In fact, the static random access memory of a computer chip dynamically stabilizes the states representing 0 and 1 by combining the energy supply and dissipation, providing fast

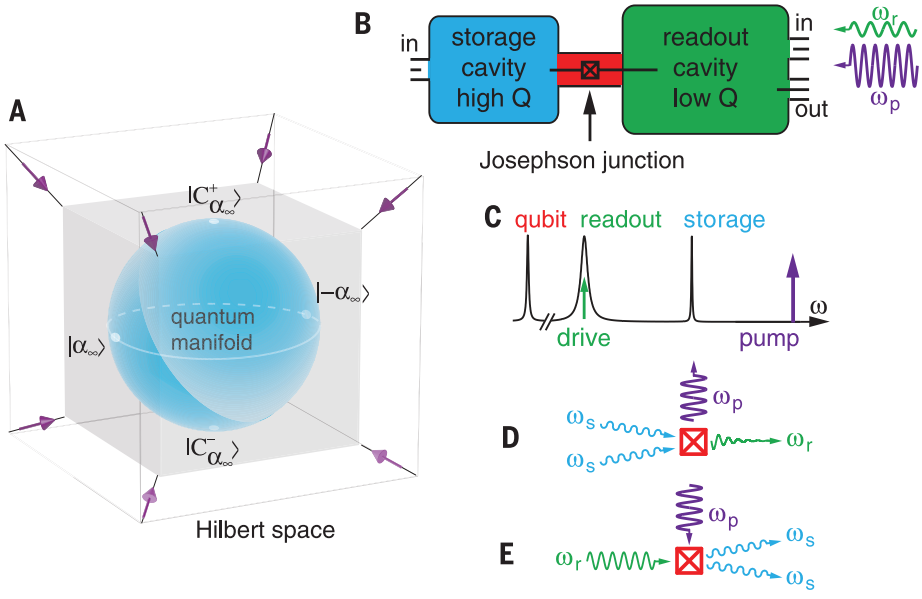


Fig. 1. Schematic of the experiment. (**A**) Confinement of a quantum state belonging to a large Hilbert space into a 2D quantum manifold. The outer and inner cubes form a hypercube representing a multidimensional Hilbert space. The inner blue sphere represents the manifold of states spanned by the two coherent states $|\pm\alpha_\infty\rangle$. Quantum states such as the even and odd Schrödinger cat states $|C^{\pm}_{\alpha_\infty}\rangle = \mathcal{N}(|\alpha_\infty\rangle \pm |-\alpha_\infty\rangle)$ also belong to this manifold, where $\mathcal{N}$ is a normalization factor. Stabilizing forces direct all states toward the inner sphere without inducing any rotation in this subspace, as indicated by the purple arrows. (**B**) Two superconducting cavities are coupled through a Josephson junction. Pump and drive microwave tones are applied to the readout, creating the appropriate nonlinear interaction, which generates a coherent superposition of steady states in the storage. The readout output port is connected to an amplifier chain [(*17*), section 1.2]. Direct Wigner tomography of the storage is performed using its input port and the qubit mode. Q stands for "quality factor." (**C**) Schematic spectrum of different modes involved in the experiment. The pump and drive tones are shown as vertical arrows. (**D** and **E**) Four-wave processes involved in the nonlinear damping and nonlinear drive, respectively, experienced by the storage. In (D), two photons of the storage combine and convert, stimulated by the pump tone, into a readout photon that is irreversibly radiated away by the transmission line. This process is balanced by the conversion of the drive tone, which, in the presence of the pump, creates two photons in the storage (E).

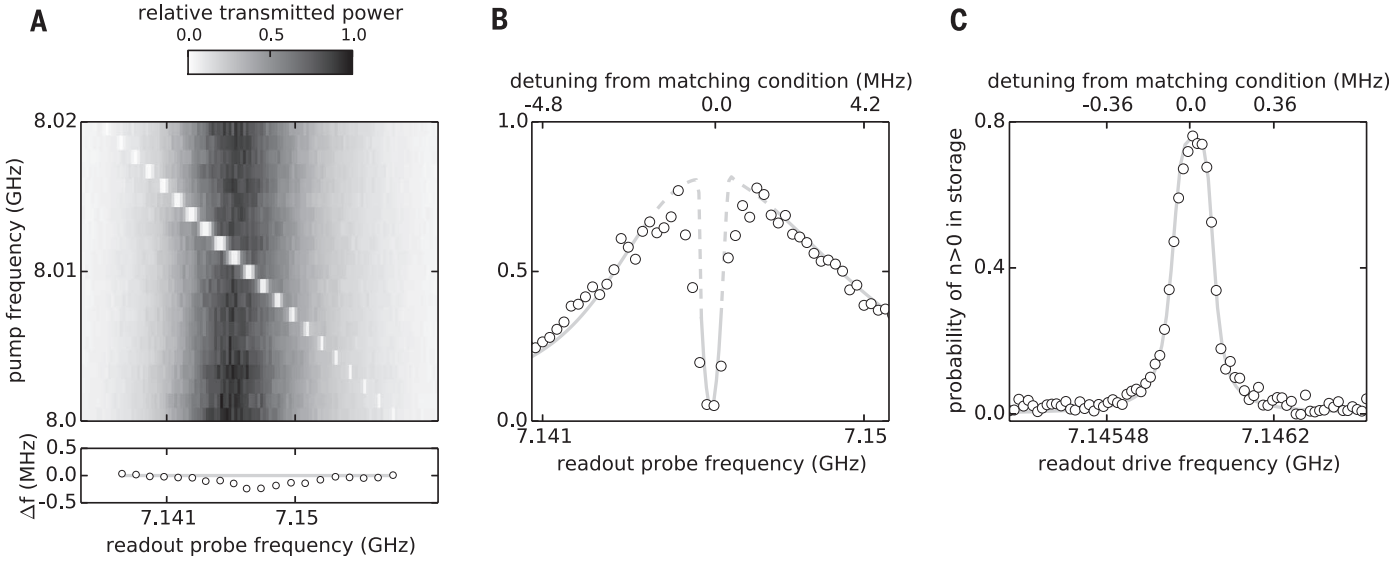


Fig. 2. Conversion of readout photons into pairs of storage photons. (**A** and **B**) CW spectroscopy of the readout in presence of the pump tone. The grayscale represents transmitted power of the probe tone through the readout as a function of probe frequency (horizontal axis) and pump frequency (vertical axis). In the top panel of (A), the usual Lorentzian response develops a sharp and deep dip, signaling conversion of probe photons into storage photons. The dip frequency $\omega_{dip}(\omega_p)$ decreases as the pump frequency increases. In the lower panel of (A), we plot $\Delta f = \omega_{dip}/2\pi - (2\omega_s - \omega_p)/2\pi$ for each dip and see that the deviation of the data (open circles) to the theory (full line: $\Delta f = 0$) is only of the order of 0.24 MHz over a span of 20 MHz. The Stark-shifted value of ω_s due to the pump is used [(*17*), fig. S5]. (B) Cut of the gray-scale map (A) at $\omega_p/2\pi$ = 8.011 GHz. (**C**) Conversion seen from the storage, represented as the probability of not being in the vacuum state, as a function of drive frequency. The dashed and full lines in (B) and (C) are the result of a numerical computation of the steady-state density matrix of the system with Hamiltonian (Eq. 2) and loss operators $\sqrt{\kappa_s}\mathbf{a}_s$, $\sqrt{\kappa_r}\mathbf{a}_r$, sweeping the drive frequency and keeping the pump frequency fixed. All parameters entering in theoretical predictions were measured or estimated independently. However, in (C) the theory was rescaled by a factor of 0.76 to fit the data. We believe that the need for this rescaling is a consequence of the unexplained modified qubit relaxation times when the pump and the drive are on [(*17*), section 1.4.9].

access time and robustness against noise. For a quantum memory, however, the system must not only have one or two stable steady states (SSSs), but rather a whole quantum manifold composed of all coherent superpositions of two SSSs (Fig. 1A). All quantum states are attracted to this manifold and are thus protected against diffusion out of it. However, by construction, such a system does not distinguish between all of its SSSs and hence cannot correct against random transitions within the quantum manifold.

An oscillator that exchanges only pairs of photons with a dissipative auxiliary system (*9*) is a practical example that displays a manifold of SSSs. This two-photon loss will force and confine the state of the oscillator into the quantum manifold spanned by two oscillation states with opposite phases. Uncontrolled energy decay, termed "single-photon loss," causes decoherence within the SSS manifold, and hence quantum superpositions will eventually decay into classical mixtures. Nevertheless, in the regime where pairs of photons are extracted at a rate at least as large as the single-photon decay rate, transient quantum coherence can be observed. This regime requires combining strong nonlinear interactions between modes and low single-photon decay rates.

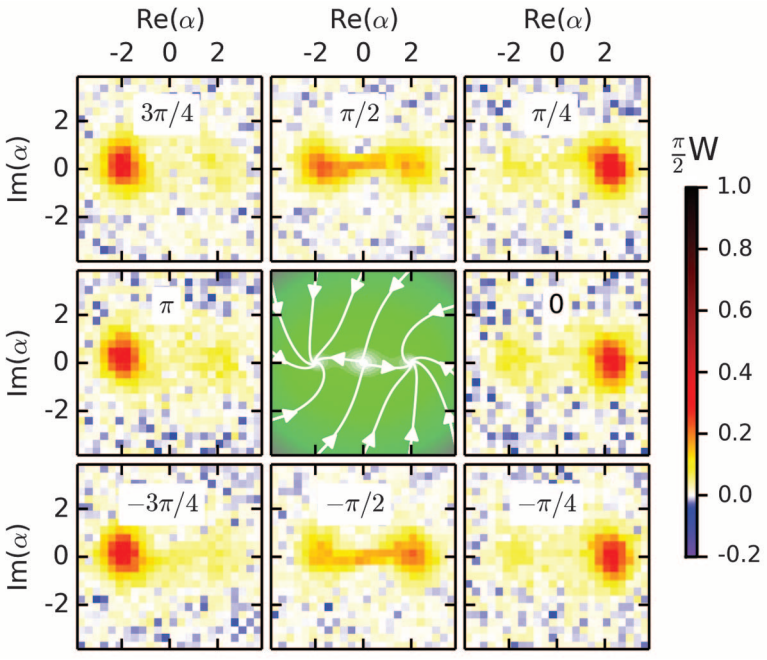


Fig. 3. Bistable behavior of the steady-state manifold of the nonlinearly driven damped storage oscillator. The central panel shows the theoretical classical equivalent of a potential of the storage nonlinear dynamics. The modulus of the velocity (color) has three zeroes corresponding to two SSSs $|\pm\alpha_\infty\rangle$ and the saddle point $|0\rangle$. Trajectories initialized on the panel border converge to one of these two SSSs. These trajectories are curved due to the Kerr effect. The outside panels show the measured Wigner function W(α) of the storage after 10 μs of pumping for different initial states. For each panel, we initialize the storage in a coherent state of amplitude α_k, where $|\alpha_k| = 2.6$ and $\arg(\alpha_k)$ is indicated in each panel. The storage converges to a combination of $|\pm\alpha_\infty\rangle$. The weight of each of these two states and the coherence of their superposition is set by the initial state. For the initial phases $\arg(\alpha_k) = 0, \pm\pi/4$, the storage mainly evolves to $|\alpha_\infty\rangle$, with only a small weight on $|-\alpha_\infty\rangle$. On the other hand, for initial phases $\arg(\alpha_k) = \pm 3\pi/4, \pi$, the state mainly evolves to $|-\alpha_\infty\rangle$, with a small weight on $|\alpha_\infty\rangle$. For the initial phases $\arg(\alpha_k) = \pm\pi/2$, the initial state is almost symmetrically positioned with respect to the two states $|\pm\alpha_\infty\rangle$ and has no definite parity (even and odd photon number states are almost equally populated). Hence, the state evolves to a mixture of $|\pm\alpha_\infty\rangle$. Re(α) and Im(α) denote the real and imaginary part of α, respectively.

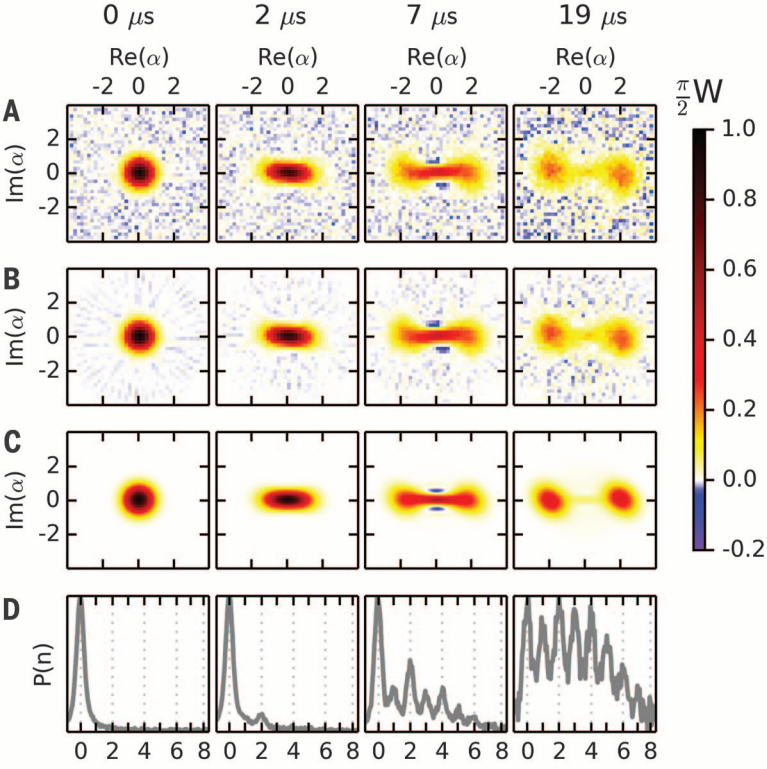


Fig. 4. Time evolution of the storage state in the presence of the nonlinear drive and dissipation processes. The panels correspond to measured data (**A**), reconstructed density matrices (*22*) (**B**), and numerical simulations (**C**). They display the Wigner function after a pumping duration indicated at the top of each column. The storage is initialized in the quantum vacuum state at time $t = 0$ μs. First, the state squeezes in the Q quadrature ($t = 2$ μs). Small but visible negativities appearing at $t = 7$ μs indicate that the superposition of the SSSs shown in Fig. 3 is now coherent and that a continuous evolution from a squeezed state to a quantum state approximating a Schrödinger cat state is taking place. Finally, these negativities disappear as a consequence of the unavoidable storage photon loss, and the state decays into a statistical mixture of the two SSSs ($t = 19$ μs). (**D**) Storage photon number distribution P(n) measured using the photon number splitting of the qubit (*29*). At $t = 2{,}7$ μs, the $n = 2$ population is larger than $n = 1$. A similar population inversion is also present between $n = 4$ and $n = 3$ at $t = 7$ μs. The non-Poissonian character of the photon number distribution at $t = 2{,}7$ μs confirms the nonclassical nature of the dynamical states of the storage for these intermediate times.

Our experiment enters this regime and demonstrates transient quantum states through a circuit quantum electrodynamics architecture (*10*), benefiting from the strong nonlinearity and low loss of a Josephson junction. Our setup (Fig. 1B), based on a recent proposal (*11*), consists of two superconducting microwave oscillators coupled through a Josephson junction in a bridge transmon configuration (*12*). These oscillators are the fundamental modes of two superconducting cavities. One cavity, termed "the storage," holds the manifold of SSSs and is designed to have minimal single-photon dissipation. The other, termed "the readout," is overcoupled to a transmission line, and its role is to evacuate entropy from the storage. In a variety of nonlinear systems, the interaction of a pump tone with relevant degrees of freedom provides cooling (*13*), squeezing (*14*), and amplification (*15*, *16*). Similarly, we use the four-wave mixing capability of the Josephson junction to generate a coupling that exchanges pairs of photons in the storage with single photons in the readout.

By off-resonantly pumping the readout at an angular frequency

$$\omega_p = 2\omega_s - \omega_r \quad (1)$$

where ω_r and ω_s are the readout and storage angular frequencies, respectively, the pump stimulates the conversion of two storage photons into one readout photon and one pump photon. The readout photon then rapidly dissipates through the transmission line, resulting in a loss in photon pairs for the storage (Fig. 1D). This engineered dissipation is the key ingredient in our experiment. The input power that balances this dissipation is provided by the readout drive, a weak resonant irradiation of the readout. Due to the nonlinear mixing with the pump, these input readout photons are converted into pairs of storage photons (Fig. 1E). Unlike the usual linearly driven dissipative oscillator, which adopts only one oscillation state, our nonlinearly driven dissipative system displays a quantum manifold of SSSs corresponding to all superpositions of two oscillation states with opposite phases.

We used a third mode besides the storage and readout: the excitation of the bridge transmon qubit, restricted to its ground and first excited state. It served as a calibration tool for all of the experimental parameters and as a means to directly measure the Wigner function of the storage. Our system is well described by the effective Hamiltonian for the storage and the readout [(*17*), section 2]

$$\mathbf{H}_{sr}/\hbar = g_2^*\mathbf{a}_s^2\mathbf{a}_r^\dagger + g_2(\mathbf{a}_s^\dagger)^2\mathbf{a}_r + \epsilon_d\mathbf{a}_r^\dagger + \epsilon_d^*\mathbf{a}_r - \chi_{rs}\mathbf{a}_r^\dagger\mathbf{a}_r\mathbf{a}_s^\dagger\mathbf{a}_s - \sum_{m=r,s}\frac{\chi_{mm}}{2}(\mathbf{a}_m^\dagger)^2\mathbf{a}_m^2 \quad (2)$$

The readout and storage annihilation operators are denoted $\mathbf{a}_r$ and $\mathbf{a}_s$, respectively, and $\hbar$ is Planck's constant h divided by 2π. The first four terms constitute a microscopic Hamiltonian of the degenerate parametric oscillator [(*18*), section 9.2.4] with

$$g_2 = \chi_{rs}\xi_p^*/2,$$
$$\xi_p \approx -i\epsilon_p/\left[\frac{\kappa_r}{2} + i(\omega_r - \omega_p)\right]$$

where $\chi_{rs}/2\pi$ = 206 kHz is the dispersive coupling between the readout and the storage, κ_r is the decay rate of the readout, and ϵ_p and ϵ_d are the pump and drive amplitudes, respectively. The terms in g_2 correspond to the conversion of pairs of photons in the storage into single photons in the readout (Fig. 1, D and E). The readout and storage have a Kerr nonlinearity: $\chi_{rr}/2\pi$ = 2.14 MHz and $\chi_{ss}/2\pi$ = 4 kHz, respectively. The Kerr interactions can be considered as perturbations that do not substantially disturb the two-photon conversion effects [(*17*), section 2.3]. The storage and readout single-photon lifetimes are, respectively, $1/\kappa_s$ = 20 μs and $1/\kappa_r$ = 25 ns.

The two-photon processes (Fig. 1, D and E) are activated only when the frequency-matching condition (Eq. 1) is met. We satisfy this condition by performing a calibration experiment (Fig. 2). We excited the readout with a weak continuous wave (CW) probe tone (≈one photon) and measured its transmitted power in the presence of the pump tone while sweeping the frequency of both tones. The pump power is kept fixed during this measurement, and its value was chosen as the largest that did not degrade the coherence times of our system [(*17*), fig. S5]. When the frequency-matching condition is met, the probe photons are converted back and forth into pairs of storage photons (Fig. 1, D and E). When equilibrium is reached for this process, the input probe photons interfere destructively with the back-converted storage photons and are now reflected back into the probe input port [(*18*), section 12.1.1]: the readout is in an induced dark state. The dip (Fig. 2, A and B) is a signature of this interference. Its depth indicates that we have achieved a large nonlinear coupling $g_2 \gg \kappa_s$ [(*17*), section 2.2]. For the subsequent experiments, we fixed the pump frequency to $\omega_p/2\pi$ = 8.011 GHz, which makes the dip coincide with the readout resonance frequency.

We demonstrate that photons are inserted in the storage by measuring the probability of having $n > 0$ photons in the storage while sweeping the readout drive frequency (Fig. 2C). A 10-μs square pulse is applied from the pump and drive tones simultaneously, and then the qubit is excited from its ground to its excited state, conditioned on there being $n = 0$ photons in the storage (*19*). Reading out the qubit state then answers the question of whether there are 0 photons in the storage. The peak at zero detuning shows that the readout drive and the pump combine nonlinearly to insert photons into the storage. The drive tone frequency is chosen such that it maximizes the number of photons in the storage, and the drive power is fixed to ensure an equilibrium average photon number in the storage of about four [(*17*), section 1.4.6].

Adiabatically eliminating the readout from Eq. 2 [(*17*), section 2.3.1; (*18*), section 12.1], we obtain a dynamics for the storage governed by the Hamiltonian

$$\mathbf{H}_s/\hbar = \epsilon_2^*\mathbf{a}_s^2 + \epsilon_2(\mathbf{a}_s^\dagger)^2 - \frac{\chi_{ss}}{2}(\mathbf{a}_s^\dagger)^2\mathbf{a}_s^2$$

and loss operators $\sqrt{\kappa_2}\mathbf{a}_s^2$ and $\sqrt{\kappa_s}\mathbf{a}_s$, where

$$\epsilon_2 = -i\frac{\chi_{sr}}{\kappa_r}\xi_p^*\epsilon_d,\ \kappa_2 = \frac{\chi_{sr}^2}{\kappa_r}|\xi_p|^2$$

The ϵ_2 nonlinear drive inserts pairs of photons in the storage (Fig. 1E) and is analogous to the usual squeezing drive of a nonlinear oscillator [(*14*), equation 1.66]. The novel element in this experiment is the nonlinear decay of rate κ_2, which extracts only photons in pairs from the storage (Fig. 1D). In the absence of unavoidable loss κ_s and neglecting the effect of χ_{ss} [(*17*), section 2.3.2], the storage converges into the two-dimensional (2D) quantum manifold spanned by coherent states $|\pm\alpha_\infty\rangle$, where

$$\alpha_\infty\big|_{\chi_{ss}=\kappa_s=0} = i\sqrt{\frac{2\epsilon_d}{\xi_p\chi_{sr}}}$$

In a classical model where quantum noise is just ordinary noise (*20*), our system behaves as a bistable oscillator with two oscillation states of amplitudes $\pm\alpha_\infty$. The storage then evolves to $+\alpha_\infty$ or $-\alpha_\infty$. However, in the full quantum model, the storage must evolve to $+\alpha_\infty$ and $-\alpha_\infty$ when initialized in the vacuum state, thus forming an even Schrödinger cat state: $\mathcal{N}(|\alpha_\infty\rangle + |-\alpha_\infty\rangle) = \mathcal{N}[\sum_{n=0}^{\infty}(\alpha_\infty^{2n}/2n!)|2n\rangle]$, where $\mathcal{N}$ is a normalization constant (*21*–*25*).

We visualize these dynamics by measuring the state of the storage by direct Wigner tomography (*22*, *26*). The Wigner function [(*27*), section 6.5] is a representation of a quantum state defined over the complex plane as $W(\alpha) = \frac{2}{\pi}\langle\mathbf{D}_\alpha\mathbf{P}\mathbf{D}_{-\alpha}\rangle$, the normalized expectation value of the parity operator $\mathbf{P} = e^{i\pi\mathbf{a}_s^\dagger\mathbf{a}_s}$ for the state displaced by the operator $\mathbf{D}_\alpha = e^{\alpha\mathbf{a}_s^\dagger - \alpha^*\mathbf{a}_s}$. This quasi-probability distribution vividly displays the quantum features of a coherent superposition.

The bistable property of our system is demonstrated by initializing the storage in coherent states with a mean photon number of 6.8 with various phases and observing their convergence to the closest equilibrium state (Fig. 3) (displacement angle = {0, ±π/4, ±3π/4,π}). The upper and lower middle panels (Fig. 3) (displacement angle = ±π/2) correspond to states initialized at almost equal distance from $\pm\alpha_\infty$, which randomly evolve to one equilibrium state or the other, thus converging to the statistical mixture of $\pm\alpha_\infty$.

The coherent splitting of the vacuum into the quantum superposition of $|\pm\alpha_\infty\rangle$ is demonstrated in Fig. 4. In the absence of loss in the storage, the pairwise exchange of photons between the storage and the environment conserves parity. Because the vacuum state is an even-parity state, it must transform into the even cat state: the unique even state contained in the manifold of equilibrium states. Similarly, because Fock state $|1\rangle$ is an odd-parity state, it must transform into the odd cat state [(*17*), fig. S8]. In presence of

κ_s, all coherences will ultimately disappear. However, for large enough κ_2, a quantum superposition transient state is observed.

In this experiment, we achieve $|\xi_p|^2 = 1.2$, which implies $g_2/2\pi$ = 111 kHz and κ_2/κ_s = 1.0. The quantum nature of the transient storage state is visible in the negative fringes of the Wigner function (see Fig. 4, A and B; 7 μs) and the non-Poissonian photon number statistics (Fig. 4D; 7 μs). After 7 μs of pumping, we obtain a state with an average photon number $\overline{n} = 2.4$ and a parity of 42%, which is larger than the parity of a thermal state (17%) or a coherent state (0.8%) with equal $\overline{n}$. After 19 μs of pumping, although the negative fringes vanish, the phase and amplitude of the SSSs $|\pm\alpha_\infty\rangle$ are conserved. Our data are in good agreement with numerical simulations (Fig. 4C), indicating that our dominant source of imperfection is single-photon loss. These results illustrate the confinement of the storage state into the manifold of SSSs and how it transits through a quantum superposition of $|\pm\alpha_\infty\rangle$.

We have realized a nonlinearly driven dissipative oscillator that spontaneously evolves toward the quantum manifold spanned by two coherent states. This was achieved by attaining the regime in which the photon-pair exchange rate is of the same order as the single-photon decay rate. The ratio between these two rates can be further improved within the present technology by using an oscillator with a higher quality factor and increasing the oscillator's nonlinear coupling to the bath. Our experiment is an essential step toward a new paradigm for universal quantum computation (*11*). By combining higher-order forms of our nonlinear dissipation with efficient error syndrome measurements (*28*), quantum information can be encoded and manipulated in a protected manifold of quantum states.

REFERENCES AND NOTES

1. C. Sayrin *et al.*, *Nature* **477**, 73–77 (2011).
2. R. Vijay *et al.*, *Nature* **490**, 77–80 (2012).
3. D. Ristè, C. C. Bultink, K. W. Lehnert, L. DiCarlo, *Phys. Rev. Lett.* **109**, 240502 (2012).
4. P. Campagne-Ibarcq *et al.*, *Phys. Rev. X* **3**, 021008 (2013).
5. H. Krauter *et al.*, *Phys. Rev. Lett.* **107**, 080503 (2011).
6. K. W. Murch *et al.*, *Phys. Rev. Lett.* **109**, 183602 (2012).
7. S. Shankar *et al.*, *Nature* **504**, 419–422 (2013).
8. Y. Lin *et al.*, *Nature* **504**, 415–418 (2013).
9. M. Wolinsky, H. J. Carmichael, *Phys. Rev. Lett.* **60**, 1836–1839 (1988).
10. A. Wallraff *et al.*, *Nature* **431**, 162–167 (2004).
11. M. Mirrahimi *et al.*, *New J. Phys.* **16**, 045014 (2014).
12. G. Kirchmair *et al.*, *Nature* **495**, 205–209 (2013).
13. J. D. Teufel *et al.*, *Nature* **475**, 359–363 (2011).
14. P. Drummond, Z. Ficek, Eds., *Quantum Squeezing* (Series on Atomic, Optical, and Plasma Physics, Springer, Berlin, 2004).
15. I. Siddiqi *et al.*, *Phys. Rev. Lett.* **93**, 207002 (2004).
16. M. A. Castellanos-Beltran, K. D. Irwin, G. C. Hilton, L. R. Vale, K. W. Lehnert, *Nat. Phys.* **4**, 929–931 (2008).
17. See the supplementary materials on *Science* Online for details.
18. H. J. Carmichael, *Statistical Methods in Quantum Optics 2* (Series on Theoretical and Mathematical Physics, Springer, Berlin, 2008).
19. B. Johnson *et al.*, *Nat. Phys.* **6**, 663–667 (2010).
20. M. I. Dykman, M. A. Krivoglaz, *Physica A* **104**, 480–494 (1980).
21. A. Ourjoumtsev, H. Jeong, R. Tualle-Brouri, P. Grangier, *Nature* **448**, 784–786 (2007).
22. B. Vlastakis *et al.*, *Science* **342**, 607–610 (2013).
23. S. Deléglise *et al.*, *Nature* **455**, 510–514 (2008).
24. C. Monroe, D. M. Meekhof, B. E. King, D. J. Wineland, *Science* **272**, 1131–1136 (1996).
25. M. Hofheinz *et al.*, *Nature* **459**, 546–549 (2009).
26. L. G. Lutterbach, L. Davidovich, *Phys. Rev. Lett.* **78**, 2547–2550 (1997).
27. S. Haroche, J.-M. Raimond, *Exploring the Quantum: Atoms, Cavities and Photons* (Oxford Univ. Press, Oxford, 2006).
28. L. Sun *et al.*, *Nature* **511**, 444–448 (2014).
29. D. I. Schuster *et al.*, *Nature* **445**, 515–518 (2007).

ACKNOWLEDGMENTS

We thank L. Jiang and V. V. Albert for helpful discussions. Facilities use was supported by the Yale Institute for Nanoscience and Quantum Engineering and NSF Materials Research Science and Engineering Center Division of Material Research award 1119826. This research was supported by the Army Research Office under grant W911NF-14-1-0011. M.M. acknowledges support from the French Agence Nationale de la Recherche under the project EPOQ2 number ANR-09-JCJC-0070. S.T. acknowledges support from ENS Cachan.

SUPPLEMENTARY MATERIALS

www.sciencemag.org/content/347/6224/853/suppl/DC1
Materials and Methods
Supplementary Text
Figs. S1 to S11
Tables S1 and S2
References (*30*–*37*)

31 October 2014; accepted 22 January 2015
10.1126/science.aaa2085

OPTICS

Spatially structured photons that travel in free space slower than the speed of light

Daniel Giovannini,[1]* Jacquiline Romero,[1]* Václav Potoček,[1,2] Gergely Ferenczi,[1] Fiona Speirits,[1] Stephen M. Barnett,[1] Daniele Faccio,[3] Miles J. Padgett[1]†

That the speed of light in free space is constant is a cornerstone of modern physics. However, light beams have finite transverse size, which leads to a modification of their wave vectors resulting in a change to their phase and group velocities. We study the group velocity of single photons by measuring a change in their arrival time that results from changing the beam's transverse spatial structure. Using time-correlated photon pairs, we show a reduction in the group velocity of photons in both a Bessel beam and photons in a focused Gaussian beam. In both cases, the delay is several micrometers over a propagation distance of ~1 meter. Our work highlights that, even in free space, the invariance of the speed of light only applies to plane waves.

The speed of light is trivially given as c/n, where c is the speed of light in free space and n is the refractive index of the medium. In free space, where n = 1, the speed of light is simply c. We show that the introduction of transverse structure to the light beam reduces the group velocity by an amount that depends on the aperture of the optical system. The delay corresponding to this reduction in the group velocity can be greater than the optical wavelength and consequently should not be confused with the ≈π Gouy phase shift (*1*, *2*). To emphasize that this effect is both a linear and intrinsic property of light, we measure the delay as a function of the transverse spatial structure of single photons.

The slowing down of light that we observe in free space should also not be confused with slow, or indeed fast, light associated with propagation in highly nonlinear or structured materials (*3*, *4*). Even in the absence of a medium, the modification of the speed of light has previously been known. For example, within a hollow waveguide, the wave vector along the guide is reduced below the free-space value, leading to a phase velocity v_ϕ greater than c. Within the hollow waveguide, the product of the phase and group velocities is given as $v_\phi v_{g,z} = c^2$, thereby resulting in a group velocity $v_{g,z}$ along the waveguide less than c (*5*).

Although this relation for group and phase velocities is derived for the case of a hollow waveguide, the waveguide material properties are irrelevant. It is the transverse spatial confinement of the field that leads to a modification of the axial component of the wave vector, k_z. In general, for light of wavelength λ, the magnitude of the wave vector, $k_0 = 2\pi/\lambda$, and its Cartesian components $\{k_x, k_y, k_z\}$ are related through (*5*)

$$k_z^2 + k_x^2 + k_y^2 = k_0^2$$

All optical modes of finite x,y spatial extent require nonzero k_x and k_y, which implies $k_z < k_0$, giving a corresponding modification of both the phase and group velocities of the light. In this sense, light beams with nonzero k_x and k_y are naturally dispersive, even in free space.

Extending upon the case of a mode within a hollow waveguide, an example of a structured

[1]School of Physics and Astronomy, Scottish Universities Physics Alliance (SUPA), University of Glasgow, Glasgow G12 8QQ, UK. [2]Faculty of Nuclear Sciences and Physical Engineering, Czech Technical University in Prague, Břehová 7, 115 19 Praha 1, Czech Republic. [3]School of Engineering and Physical Sciences, SUPA, Heriot-Watt University, Edinburgh EH14 4AS, UK.
*These authors contributed equally to this work. †Corresponding author. E-mail: miles.padgett@glasgow.ac.uk

Downloaded from www.sciencemag.org on February 21, 2015

beam is a Bessel beam (Fig. 1A), which is itself the description of a mode within a circular waveguide (*1*, *6*). In free space, Bessel beams can be created with an axicon, or its diffractive optical equivalent (*7*), that converts a plane wave into conical phase fronts characterized by a single radial component of the wave vector, $k_r = \sqrt{k_x^2 + k_y^2}$ (*8*–*10*). This single value of the radial component gives a unique value of $k_z < k_0$ and hence uniquely defined phase and group velocities (*11*).

To avoid complications arising from the finite thickness of refractive optical elements, we use diffractive optics, idealized as having zero thickness. For a Bessel beam created with a diffractive optic (*7*), characterized by k_r (with $k_r << k_0$), the axial component of the wave vector is given by $k_z = k_0 - k_r^2/2k_0$. The resulting phase velocity and group velocity along z are

$$v_\phi = c\left(1 - \frac{k_r^2}{2k_0^2}\right)^{-1}$$

and

$$v_{g,z} = c\left(1 - \frac{k_r^2}{2k_0^2}\right)$$

This modification of the phase and group velocities of Bessel beams has been examined in the classical, many-photon regime. Subtle changes in velocity have been previously studied with Bessel beams in the microwave (*12*) and optical regimes (*13*–*15*).

We demonstrate the intrinsic and linear nature of this reduction in group velocity by measuring the delay in the arrival time of single photons. Over a propagation distance of L, the reduction in the group velocity compared to the plane-wave case gives a delay of

$$\delta z_{\text{Bessel}} \approx L\frac{k_r^2}{2k_0^2} = \frac{L}{2}\alpha^2 \qquad (1)$$

As an example, for an axicon designed to produce $\alpha = k_r/k_0 = 4.5 \times 10^{-3}$ over a propagation distance of 1 m, we predict a delay of ~30 fs, corresponding to a spatial delay of 10 μm.

To measure the arrival time of single photons with femtosecond precision, we adopt a method relying upon a quantum effect, namely, the Hong-Ou-Mandel (HOM) interference (*16*). A parametric down-conversion source is used to produce photon pairs that are strongly correlated in their wavelengths and their generation time. One photon can then act as a reference, against which the arrival of the other photon can be compared (Fig. 2). This second photon goes through a free-space propagation section, in which a first spatial light modulator (SLM) can be programmed to act as a diffractive optical element implementing axicons or lenses. A second SLM then reverses the structuring introduced by the first. When the arrival times of the two photons incident on a beam splitter are matched to a precision better than their coherence time, both photons emerge from the same output port. Under this matched condition, the coincidence rate for detection at the two output ports of the beam splitter falls to zero, which results in what is known as a HOM dip. The position of the dip is recorded as a function of the spatial shaping of the photon propagating in free space.

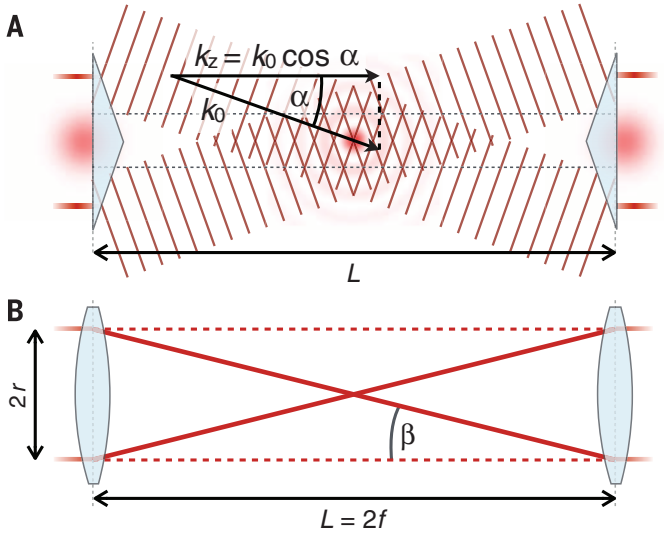


Fig. 1. Adding spatial structure to a light beam. (**A**) A Bessel beam can be created with an axicon, producing conical phase fronts of angle α. (**B**) A ray entering a confocal telescope at radius r will travel an additional distance proportional to $\cos^{-1}\beta$.

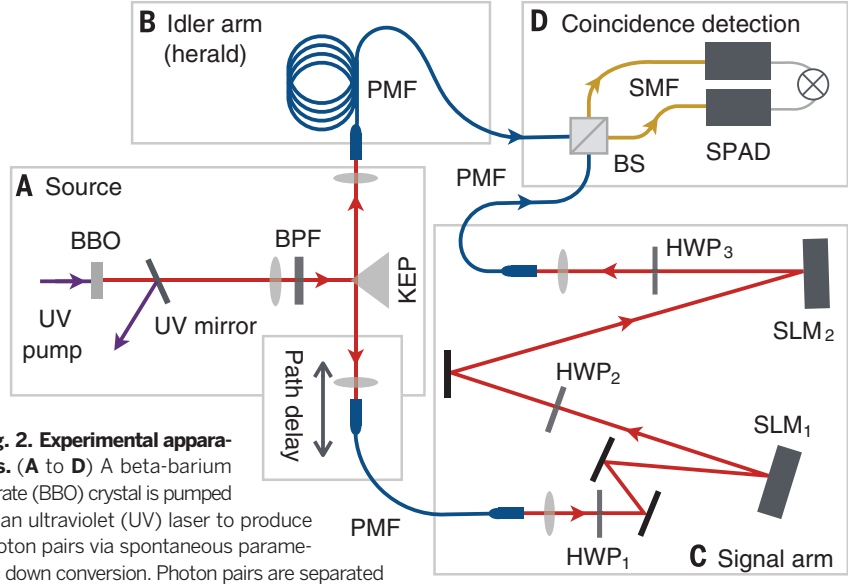


Fig. 2. Experimental apparatus. (**A** to **D**) A beta-barium borate (BBO) crystal is pumped by an ultraviolet (UV) laser to produce photon pairs via spontaneous parametric down conversion. Photon pairs are separated by a knife edge prism (KEP); a band-pass filter (BPF) sets the spectral profile of the down-converted light. Half-wave plates (HWP) are used to maximize the efficiency of the spatial light modulators (SLM) and match the polarization of the polarization-maintaining fibers (PMF). Signal and idler photons enter a fiber-coupled beam splitter (BS) (*21*), whose outputs are single-mode fibers (SMF) connected to avalanche photodiodes (SPAD). The SPADs feed a coincidence counter.

Taking the Bessel beam as our first example, the transverse structuring can be turned on and off for each value of path delay. The corresponding position of the HOM dip can then be directly compared between the two cases. Figure 3A shows the baseline-normalized coincidences for two different values of $\alpha = k_r/k_0$ (where we define the baseline as the coincidence count at path delay far from the dip position). In all cases, the width of the HOM dips is the same, set by the 10-nm spectral bandwidth of the down-converted photons. The key result is that the HOM dip associated with the Bessel beam is delayed with respect to the dip obtained for a collimated beam. We measure a delay of 2.7 ± 0.8 μm for the case of $\alpha_1 = 0.00225$ rad and 7.7 ± 0.8 μm for $\alpha_2 = 0.00450$ rad. These measured values agree with theoretical predictions of 2.0 and 8.1 μm for α_1 and α_2, respectively.

The analytical form of this predicted delay (Eq. 1) suggests a simple geometrical model, where the delay arises from the additional length of the diagonal ray, propagating at an angle α with respect to the optical axis. In Fig. 3B, we compare the measured and predicted values for the delay, showing that Eq. 1 is valid over the range of angles that we tested for the Bessel beam.

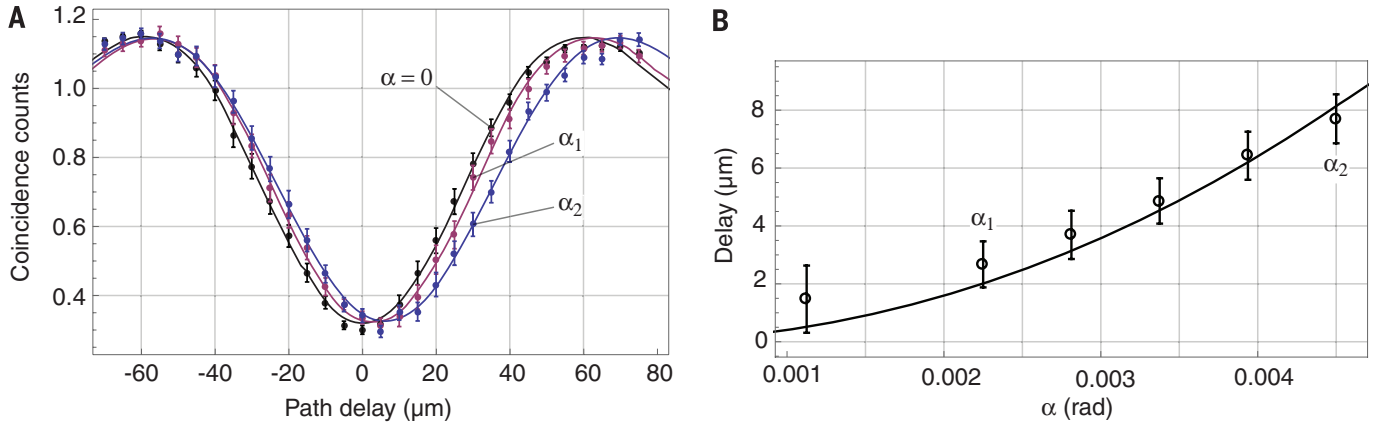


Fig. 3. Experimental results for a Bessel beam. (**A**) Measured HOM dips for two values of α (α_1 = 0.00225, red; α_2 = 0.00450, blue) and the α = 0 case (black), with corresponding best fits (*16*). (**B**) Measured delays (open circles) and theoretical prediction from Eq. 1 (solid line), for different values of α. The delays are expressed with respect to the α = 0 case. corresponding to an unstructured collimated beam.

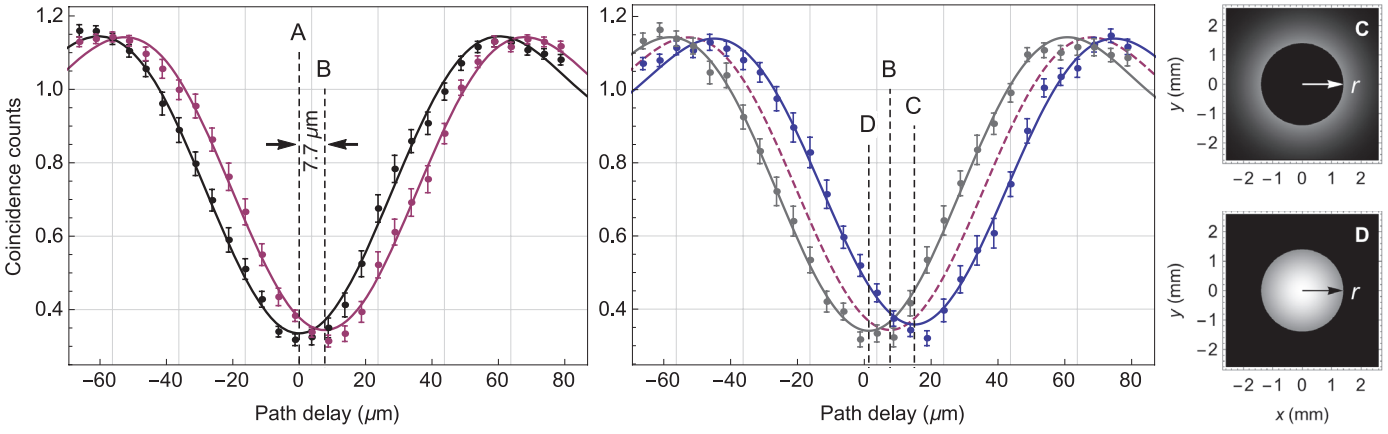


Fig. 4. Measured HOM dips for collimated and focused Gaussian beams. (**Left**) HOM dip comparison for collimated (black) and focused (red) Gaussian beam. Minima are marked by A and B. (**Right**) HOM dip comparison for cases with an r = 1.4 mm center stop (blue, corresponding to inset C), and an edge stop of the same radius (gray, corresponding to inset D). Minima are marked by C and D. The red dashed curve is shown as a reference.

Perhaps the most common form of spatial structuring of a light beam is focusing, which also leads to a modification of the axial component of the wave vector. We consider the propagation of light through a telescope comprising two identical lenses separated by twice their focal length, f (i.e., a confocal telescope). Assuming a ray-optical model, a coaxial ray incident upon the first lens at radius r emerges from the second lens coaxially at the same radius but inverted about the optical axis (Fig. 1B). Comparing the on-axis separation of the lenses to this diagonal distance gives an additional distance traveled of $\delta z = L/\cos\beta - L \approx r^2/f$, where β is the angle between ray and optical axis.

For a beam of Gaussian intensity distribution with $1/e^2$ radius w, the expectation value of r^2 is $\langle r^2 \rangle = w^2/2$. Therefore, the expected delay δz_{Gauss} for a Gaussian beam on transmission through a confocal telescope is

$$\delta z_{\text{Gauss}} = w^2/2f = (w/f)^2 \times f/2 \qquad (2)$$

where w is the waist of the input beam. The delay is a quadratic function of the quantity w/f, which can be considered as a measure of the beam divergence, defined by the numerical aperture of the system. The delay increases with increasing numerical aperture. This geometrical model and a rigorous theoretical calculation provide the same results for both the Bessel and confocal cases, within the same approximations (*17*, *18*). The full theoretical model, however, applies to any arbitrary field. As the delay increases with the square of the numerical aperture, the delay becomes progressively harder to detect at longer distances.

The delay arising from focusing is shown in Fig. 4. Trace A shows the position of the HOM dip for the case of a collimated beam, and trace B shows its position for the case of f = 0.40 m. We measure a delay of 7.7 ± 0.4 μm for the focused case. This is comparable to the predicted delay based on Eq. 2 which, for our beam of w = 2.32 ± 0.09 mm, is 6.7 ± 0.6 μm. The slight difference between our measurement and the predicted value is likely due to residual aberrations and imperfect collimation, leading to an ill-defined beam waist, upon which the delay is quadratically dependent.

We further investigate the dependence of the delay upon the beam structure by introducing aperture restrictions to the beam, in the form of center and edge stops (Fig. 4, insets). Results are shown in traces C and D in Fig. 4, together with the full-aperture focused beam case (red line, trace B). A center stop increases the expectation value of r^2, thereby increasing the delay compared to the full-aperture case. Trace C shows the dip with a center stop of radius 1.4 mm, as shown in inset C. We measure a dip position additionally delayed by 7.3 ± 0.4 μm compared to the full-aperture focused beam, giving a total delay of 15.0 ± 0.6 μm. Next, we introduce an edge stop of the same radius, as shown in inset D. By restricting the aperture, the expectation value of r^2 is decreased, decreasing the delay with respect to the collimated case. Trace D shows the position of the HOM dip, which is now reduced by 6.4 ± 0.4 μm with respect to the full-aperture case, resulting in a total delay compared to the collimated case of 1.3 ± 0.6 μm.

It is important to consider three possible sources of systematic errors. First, the phase values of all the pixels of the SLMs lie between 0 and 2π with an average value of ≈π. Regardless of what optical component is encoded on the SLMs, the effective thickness of the liquid crystal, as averaged over the full aperture, remains the same.

Consequently, the observed delay is not a result of the SLMs themselves. Second, the width of the HOM dip remains compatible with the interference filter used. Therefore, the coherence time of the light is unchanged by the setting of the SLMs and hence the magnitude of the delays cannot be a result of spectral postselection. Third, one must ensure that the delays are not due to misalignment in the optical paths. In aligning the experiment, we used back-projection (*19*). More important, the alignment for the cases that have aperture restrictions remains the same (the coaxial apertures do not change the path of the beam). Hence, the delays that we measure can only result from the transverse structure of the beam and indeed are consistent with our theoretical predictions.

Our measurement of group velocity is strictly a measurement of the difference in propagation speed between a reference photon and a spatially structured photon. No direct measurement of the speed of light is made. Within this manuscript, the velocity that we measure is strictly the group velocity of the photons (*20*).

The speed of light in free-space propagation is a fundamental quantity. It holds a pivotal role in the foundations of relativity and field theory, as well as in technological applications such as time-of-flight measurements. It has previously been experimentally established that single photons travel at the group velocity (*20*). We have now shown that transverse structuring of the photon results in a decrease in the group velocity along the axis of propagation. We emphasize that in our full-aperture experiments, no pre- or post-selection is applied to the spatially structured photons and that the group velocities are always compared over the same propagation distance, much as if they were in a race. The effect can be derived from a simple geometric argument, which is also supported by a rigorous calculation of the harmonic average of the group velocity. Beyond light, the effect observed will have applications to any wave theory, including sound waves.

REFERENCES AND NOTES

1. A. Yariv, *Quantum Electronics* (Wiley, New York, ed. 3, 1989).
2. S. Feng, H. G. Winful, *Opt. Lett.* **26**, 485–487 (2001).
3. R. W. Boyd, D. J. Gauthier, *Science* **326**, 1074–1077 (2009).
4. J. E. Vornehm Jr., R. W. Boyd, in *Tutorials in Complex Photonic Media*, M. A. Noginov, G. Dewar, M. W. McCall, N. I. Zheludev, Eds. (SPIE, Bellingham, WA, 2009), chap. 19.
5. I. S. Grant, W. R. Phillips, *Electromagnetism* (Wiley, New York, 1980).
6. E. R. Nagelberg, J. Shefer, *Bell Syst. Tech. J.* **44**, 1321–1338 (1965).
7. S. Klewitz, S. Sogomonian, M. Woerner, S. Herminghaus, *Opt. Commun.* **154**, 186–190 (1998).
8. R. M. Herman, T. A. Wiggins, *J. Opt. Soc. Am. A* **8**, 932–942 (1991).
9. J. H. McLeod, *J. Opt. Soc. Am.* **44**, 592 (1954).
10. A. Vasara, J. Turunen, A. T. Friberg, *J. Opt. Soc. Am. A* **6**, 1748–1754 (1989).
11. J. T. Lunardi, *Phys. Lett. A* **291**, 66–72 (2001).
12. D. Mugnai, A. Ranfagni, R. Ruggeri, *Phys. Rev. Lett.* **84**, 4830–4833 (2000).
13. K. B. Kuntz *et al.*, *Phys. Rev. A* **79**, 043802 (2009).
14. I. Alexeev, K. Y. Kim, H. M. Milchberg, *Phys. Rev. Lett.* **88**, 073901 (2002).
15. P. W. Milonni, *J. Phys. B* **35**, R31–R56 (2002).
16. C. K. Hong, Z. Y. Ou, L. Mandel, *Phys. Rev. Lett.* **59**, 2044–2046 (1987).
17. Z. L. Horváth, J. Vinko, Zs. Bor, D. von der Linde, *Appl. Phys. B* **63**, 481–484 (1996).
18. Materials and methods are available as supplementary materials on *Science* Online.
19. M. McLaren, J. Romero, M. J. Padgett, F. Roux, A. Forbes, *Phys. Rev. A* **88**, 033818 (2013).
20. A. M. Steinberg, P. G. Kwiat, R. Y. Chiao, *Phys. Rev. Lett.* **68**, 2421–2424 (1992).
21. R. Kaltenbaek, B. Blauensteiner, M. Żukowski, M. Aspelmeyer, A. Zeilinger, *Phys. Rev. Lett.* **96**, 240502 (2006).

ACKNOWLEDGMENTS

We thank S. Franke-Arnold for useful discussions. This work was supported by the Engineering and Physical Sciences Research Council through the COAM program, and by the European Research Council (ERC) through the TWISTS grant; D.F. acknowledges support from ERC through the MOLIGHT project. We thank Hamamatsu for their support. M.J.P. thanks the Royal Society.

M.J.P., D.F. and S.M.B. conceived the experiment and supervised the work; M.J.P., D.G., and J.R. designed the experiment; D.G. and J.R. constructed the experiment, acquired the data, and carried out the data analysis; V.P., J.R., G.F., F.S., and S.M.B. further developed the theoretical model; J.R., D.G., and M.J.P. wrote the text with input from all coauthors.

SUPPLEMENTARY MATERIALS

www.sciencemag.org/content/347/6224/857/suppl/DC1
Materials and Methods
Supplementary Text

14 November 2014; accepted 8 January 2015
Published online 22 January 2015;
10.1126/science.aaa3035

GALAXY EVOLUTION

Black hole feedback in the luminous quasar PDS 456

E. Nardini,[1]* J. N. Reeves,[1,2] J. Gofford,[1,2] F. A. Harrison,[3] G. Risaliti,[4,5] V. Braito,[6] M. T. Costa,[1] G. A. Matzeu,[1] D. J. Walton,[3,7] E. Behar,[8] S. E. Boggs,[9] F. E. Christensen,[10] W. W. Craig,[11] C. J. Hailey,[12] G. Matt,[13] J. M. Miller,[14] P. T. O'Brien,[15] D. Stern,[7] T. J. Turner,[16,17] M. J. Ward[18]

The evolution of galaxies is connected to the growth of supermassive black holes in their centers. During the quasar phase, a huge luminosity is released as matter falls onto the black hole, and radiation-driven winds can transfer most of this energy back to the host galaxy. Over five different epochs, we detected the signatures of a nearly spherical stream of highly ionized gas in the broadband x-ray spectra of the luminous quasar PDS 456. This persistent wind is expelled at relativistic speeds from the inner accretion disk, and its wide aperture suggests an effective coupling with the ambient gas. The outflow's kinetic power larger than 10^{46} ergs per second is enough to provide the feedback required by models of black hole and host galaxy coevolution.

Disk winds are theoretically expected as a natural consequence of highly efficient accretion onto supermassive black holes (*1*), as the energy radiated in this process might easily exceed the local binding energy of the gas. In the past few years, black hole winds with column densities of ~10^{23} cm^{-2} and velocities of ~0.1 times the speed of light (c) have been revealed in a growing number of nearby active galactic nuclei (AGN) through blueshifted x-ray absorption lines (*2*, *3*). Outflows of this kind are commonly believed to affect the dynamical and physical properties of the gas in the host galaxy, and, hence, its star formation history (*4*). However, a complete observational characterization of how this feedback works is still missing. On its own, the detection of narrow, blueshifted features does not convey any information about the opening angle or the ejection site of the wind. This knowledge is critical for measuring the total power carried by the outflow, whose actual influence on galactic scales remains unclear (*5*).

The nearby (z = 0.184) radio-quiet quasar PDS 456 is an established Rosetta stone for studying disk winds (*6*–*8*). With a bolometric luminosity L_{bol} ~ 10^{47} erg/s and a mass of the central black hole on the order of 10^9 solar masses (M_{Sun}) (*9*), it is an exceptionally luminous AGN in the local universe and might be regarded as a counterpart of the accreting supermassive black holes during the peak of quasar activity at high redshift. Since the earliest x-ray observations, PDS 456 has regularly exhibited a deep absorption trough at rest-frame energies above 7 keV (*6*), which was occasionally resolved with high statistical significance into a pair of absorption lines at ~9.09 and 9.64 keV (*7*). Because no strong atomic transitions from cosmically abundant elements correspond to these energies, such lines are most likely associated with resonant K-shell absorption from Fe XXV Heα (6.7 keV) and Fe XXVI Lyα (6.97 keV) in a wind with an outflow velocity of ~0.3 c.

The X-ray Multi-Mirror Mission (XMM)–Newton and Nuclear Spectroscopic Telescope Array (NuSTAR) satellites simultaneously observed PDS 456 on four occasions in 2013, between 27 August and 21 September. A fifth observation was performed several months later, on 26 February 2014 (table S1). The entire campaign caught the quasar in widely different spectral states (Fig. 1). The broad Fe-K absorption trough is conspicuous at all times against a simple baseline continuum, with an equivalent width

increasing in absolute value by a factor of ~4, from 75 ± 45 eV to 350 ± 60 eV (table S2; uncertainties are given at the 90% confidence level). The large blueshift to ~9 keV invariably pushes this broad feature close to the edge of the XMM-Newton energy band, preventing any evaluation of the intrinsic flux blueward of the absorption complex. The addition of the NuSTAR broadband spectra enabled the accurate determination of the intensity and slope of the high-energy continuum that was lacking before. This unveils a broadened Fe Kα emission component, which, combined with the adjacent absorption trough, gives rise to an unmistakable P-Cygni–like profile, as produced by an expanding gaseous envelope.

Despite the overall variability, this characteristic outflow signature is clearly detected in each of the five epochs during the course of the campaign (Fig. 2), demonstrating the persistence of a wide-angle accretion disk wind in PDS 456. For a preliminary evaluation of its basic parameters, we first deconvolved the P-Cygni profile with a pair of Gaussian line shapes. For Doppler broadening relative to a uniform velocity field within a radial outflow, the profile width would suggest an aperture of θ ~ 100 degrees (fig. S1). In reality, this is unlikely to be a simple projection effect, as we might be observing the wind's acceleration region. We therefore applied a custom P-Cygni model to the 2 to 30 keV energy range, only allowing for an absorption-induced continuum curvature (*9*, *10*). The success of this attempt implies that the line's profile is indeed compatible with a quasispherical (fully covering) outflow with terminal velocity of $0.35 \pm 0.02\ c$ (Fig. 3).

We subsequently performed a comprehensive spectral and timing analysis, fitting the ~0.5 to 50 keV spectra from all five observations with a model that includes the standard power-law continuum and self-consistent absorption and emission components from photo-ionized gas (fig. S2). This model provides a very good description of the data, with no obvious residuals over the whole energy range (fig. S3). The main physical parameters obtained from the best fit include the hydrogen column density of the highly ionized absorber, $N_{\rm H} = 6.9^{+0.6}_{-1.2} \times 10^{23}\,{\rm cm}^{-2}$, and its bulk outflow velocity, $v_{\rm out} = 0.25 \pm 0.01\ c$, constant over the five epochs (table S3). Partial covering by less-ionized gas accounts for most of the continuum spectral variability, which indicates clumpy obscuration within the same stream as observed in lower-luminosity active galaxies (*11*).

However, the general validity of the disk wind picture is still disputed. It has been proposed that blueshifted absorption might also arise from corotating optically thick plasma blanketing the accretion flow, which would be seen in x-rays reflected off the disk surface (*12*). Depending on the exact geometry, the extreme velocities inherent to the inner disk could produce a Fe K-shell feature anywhere between 4 and 10 keV through relativistic Doppler shifts. Previously applied to PG 1211+143, another bright quasar where a similar line complex was revealed (*13*), this scenario calls for a reflection-dominated x-ray spectrum. In PDS 456, this model clearly underpredicts the depth of the 9-keV absorption trough, whose energy and profile allow us to rule out this alternative interpretation (figs. S4 and S5).

Even when blueshifted lines can be safely associated with an outflow, the measure of its mass-loss rate and total energetics is subject to large uncertainties. Remarkably, these observations supply a robust estimate of the solid angle Ω filled by the wind, which is computed from the amount of absorbed ionizing radiation that is re-emitted across the spectrum. The average value is $\Omega = 3.2 \pm 0.6\pi$ sr, and each individual observation is consistent with Ω exceeding 2π sr (*9*). No explicit information on Ω for individual sources existed previously, because the absorption components detected in both ultraviolet and x-ray spectra only probe the line of sight. Consequently, this quantity has thus far been assumed rather than directly determined from the data—for example, following the occurrence frequency of outflows amongst local AGN (*14*) or through an a priori selection of a reasonable wind geometry (*15*).

Besides the degree of collimation, critical information is required on the starting point of the wind ($R_{\rm in}$), for which only indirect arguments are usually available (*16*). In PDS 456, the gas location is directly constrained by changes of the wind emission intensity in response to the hard x-ray continuum. The most significant variation, when the Fe K line follows a decrease by a factor of ~3 of the 7- to 30-keV flux, takes place between the first two observations, separated by ~10 days. The corresponding light-crossing time translates into a maximum distance of a few hundreds of gravitational radii ($r_{\rm g} = GM/c^2$, where G is the gravitational constant and M is the black hole's mass) from the illuminating source. This spatial extent is consistent with the degree of ionization of the gas and with predictions of hydrodynamical models of radiation-driven accretion disk winds (*17*). An independent corroboration of the

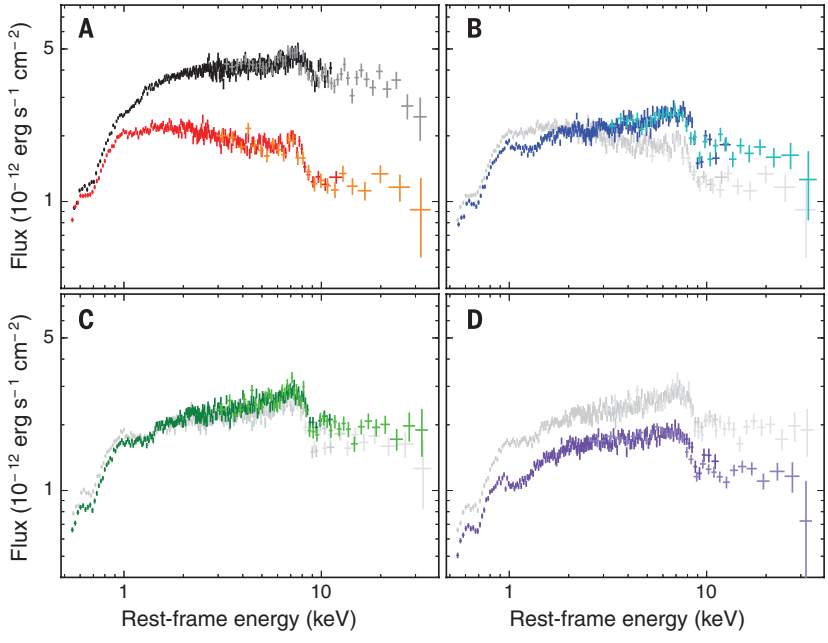


Fig. 1. Broadband x-ray spectra of PDS 456. The spectra of the five XMM-Newton and NuSTAR observations (±1 SD error bars) are plotted in flux density units after factoring out the effects of the instrumental response on the raw photon count rate. All the spectra were rebinned for display purposes only, with the data from the two NuSTAR modules merged and shown in a lighter tone. (**A**) Observation (Obs.). 1 (black) and Obs. 2 (red). (**B**) Obs. 2 (shaded) and Obs. 3 (blue). (**C**) Obs. 3 (shaded) and Obs. 4 (green). (**D**) Obs. 4 (shaded) and Obs. 5 (purple). Each panel also contains the spectrum of the previous observation to highlight the extent of the variability.

[1]Astrophysics Group, School of Physical and Geographical Sciences, Keele University, Keele, Staffordshire ST5 5BG, UK. [2]Center for Space Science and Technology, University of Maryland Baltimore County, 1000 Hilltop Circle, Baltimore, MD 21250, USA. [3]Cahill Center for Astronomy and Astrophysics, California Institute of Technology, Pasadena, CA 91125, USA. [4]Istituto Nazionale di Astrofisica, Osservatorio Astrofisico di Arcetri, Largo Enrico Fermi 5, I-50125 Firenze, Italy. [5]Harvard–Smithsonian Center for Astrophysics, 60 Garden Street, Cambridge, MA 02138, USA. [6]INAF, Osservatorio Astronomico di Brera, Via Bianchi 46, I-23807 Merate (LC), Italy. [7]Jet Propulsion Laboratory, California Institute of Technology, Pasadena, CA 91109, USA. [8]Department of Physics, Technion, Haifa 32000, Israel. [9]Space Science Laboratory, University of California, Berkeley, CA 94720, USA. [10]Danmarks Tekniske Universitet Space–National Space Institute, Technical University of Denmark, Elektrovej 327, 2800 Lyngby, Denmark. [11]Lawrence Livermore National Laboratory, Livermore, CA 94550, USA. [12]Columbia Astrophysics Laboratory, Columbia University, New York, NY 10027, USA. [13]Dipartimento di Matematica e Fisica, Università degli Studi Roma Tre, Via della Vasca Navale 84, I-00146 Roma, Italy. [14]Department of Astronomy, University of Michigan, Ann Arbor, MI 48109, USA. [15]Department of Physics and Astronomy, University of Leicester, University Road, Leicester LE1 7RH, UK. [16]Physics Department, University of Maryland Baltimore County, 1000 Hilltop Circle, Baltimore, MD 21250, USA. [17]Eureka Scientific Inc., 2452 Delmer Street Suite 100, Oakland, CA 94602, USA. [18]Department of Physics, University of Durham, South Road, Durham DH1 3LE, UK.
***Corresponding author. E-mail: e.nardini@keele.ac.uk**

above estimate comes from the variability time scale of ~1 week of the Fe-K absorption feature, probed during the monitoring of PDS 456 by the Suzaku x-ray satellite in early 2013 (*18*). Indeed, the historical behavior of the K-shell absorption line(s) appears to be in keeping with a persistent wind where the gas is in photo-ionization equilibrium with the local radiation field.

We therefore adopt R_{in} = 100 r_g ~ 1000 astronomical units and take conservative values for the other physical and geometrical quantities involved (supplementary text). With all the relevant pieces of information now available, we determine a mass outflow rate at the base of the wind of $\dot{M}_{out}$ ~ 10 M_{Sun}/year, corresponding (for a mass-to-radiation conversion efficiency η ~ 0.1) to about half of the Eddington accretion rate, the limit at which gravitational

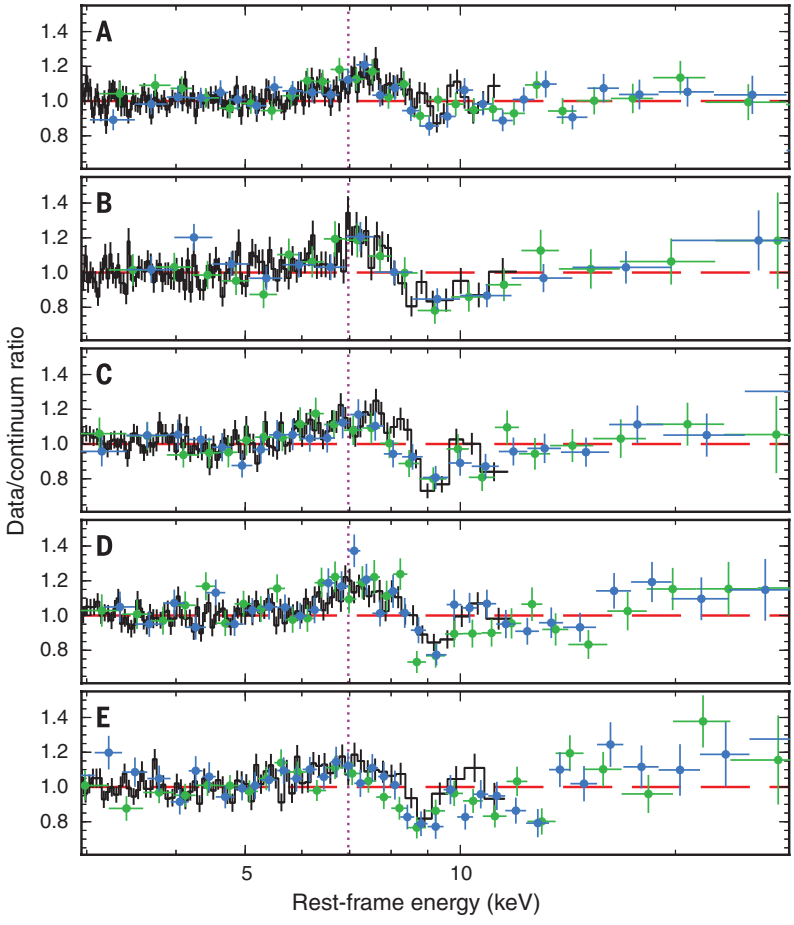


Fig. 2. Persistence of the P-Cygni–like feature. The ratio of the observed emission over the continuum, which was modeled as a partially absorbed power law to reproduce the overall spectral curvature, is shown for XMM-Newton data (in black; ±1 SD error bars) and both NuSTAR modules (superimposed as green and turquoise dots). The P-Cygni–like profile is evident in each snapshot of the campaign, irrespective of the different flux and spectral states of the source. The peak of Fe Kα emission from the wind lies above 7 keV in each observation, and the absorption trough is centered around 9 keV. The line's profile can be resolved independently at any epoch, with a full width at half-maximum for both components of ~900 eV (or 30,000 km/s at 9 keV). The vertical dotted line marks the rest-frame energy (6.97 keV) of the Fe XXVI Kα transition. (**A**) Obs. 1. (**B**) Obs. 2. (**C**) Obs. 3. (**D**) Obs. 4. (**E**) Obs. 5.

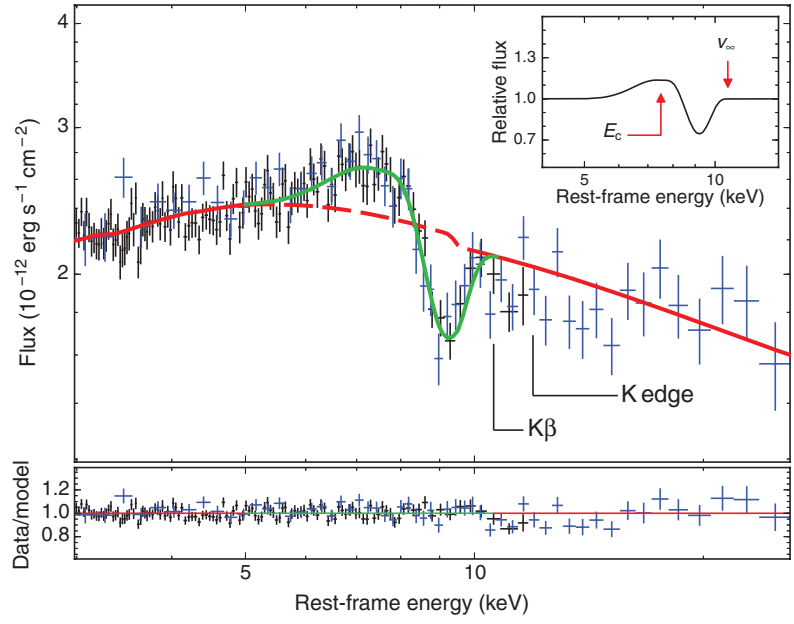


Fig. 3. Fit with a P-Cygni line model. Adopting the same baseline continuum of Fig. 2 (red curve), we fitted the emission and absorption residuals characterizing the Fe-K band by means of a self-consistent P-Cygni profile from a spherically symmetric outflow (green curve). The results are shown for the merged Obs. 3 and Obs. 4, which are separated by only 3 days and are virtually indistinguishable at 2 to 30 keV (Fig. 1). The two NuSTAR modules were combined into a single spectrum (plotted in blue; ±1 SD error bars) for display purposes only. The inset contains a graphical explanation of the key parameters of this model: the characteristic energy E_c, corresponding to the onset of the absorption component, and the wind terminal velocity v_∞ = 0.35 ± 0.02 c, which can be regarded as a measure of the actual outflowing speed of the gas. The bottom panel shows the ratio between the data and the best-fit model. The residual structures above 10 keV are due to the Kβ and K edge absorption features from Fe XXVI. These are not included in the P-Cygni model but are detected with high significance (table S2) and remove any ambiguity in the identification of the ionic species.

infall is balanced by outward radiation pressure. Consequently, the kinetic power of the wind is $P_{kin} \sim 2 \times 10^{46}$ erg/s, or 20% of the bolometric luminosity of the quasar. According to models and simulations (*19*, *20*), the deposition of a few percent of the total radiated energy is sufficient to prompt an appreciable feedback on the host galaxy. Because most of the kinetic output will be ultimately transferred to the surrounding gas (*21*), these conditions are met even if R_{in} is set to the escape radius (~30 r_g for v_{out} = 0.25 c), the minimum plausible starting point of the wind.

The mechanical energy released over a period of 10^7 years (i.e., one-tenth of a typical quasar lifetime) is close to 10^{61} erg, comparable to or exceeding the expected binding energy of the galactic bulge in a system like PDS 456. The large opening angle evinced here suggests that the coupling of the outflow with the gas in the host galaxy will be effective, as required for strong negative feedback. We are then possibly witnessing the initial stage of the sweeping process that leads to molecular mass losses of hundreds to thousands M_{Sun}/year even in sources with no powerful radio jets (*22*). For a commensurate kinetic luminosity, in fact, the observed galaxy-wide outflows entail considerable mass loading and momentum boost.

A fundamental correlation (the so-called $M-\sigma_*$ scaling relation) exists between the mass of the central black holes and the stellar velocity dispersion of galactic bulges on kpc scales (*23*, *24*)—that is, hundreds of times beyond the gravitational sphere of influence of the black holes themselves. It is still debated whether this is the product of a feedback-driven black hole/host galaxy coevolution (*25*) or of a hierarchical assembly through galaxy mergers (*26*). Identifying wide-angle accretion disk winds in the Eddington-limited regime lends weight to the idea that AGN have a substantial impact on the surrounding environment. As a rare, nearby analog of the luminous AGN population at high redshift, PDS 456 shows a flavor of cosmic feedback, believed to have operated at the peak of the quasar epoch about 10 billion years ago. In distant galaxies in a similar activity phase, such powerful winds would have provided the energy and momentum to self-regulate the black hole growth and control the star formation in stellar bulges, leaving the present-day scaling relations as a record of this process (*27*).

REFERENCES AND NOTES

1. A. R. King, *Mon. Not. R. Astron. Soc.* **402**, 1516–1522 (2010).
2. F. Tombesi *et al.*, *Astron. Astrophys.* **521**, A57 (2010).
3. J. Gofford *et al.*, *Mon. Not. R. Astron. Soc.* **430**, 60–80 (2013).
4. J. Silk, M. J. Rees, *Astron. Astrophys.* **331**, L1 (1998).
5. J. Kormendy, L. C. Ho, *Annu. Rev. Astron. Astrophys.* **51**, 511–653 (2013).
6. J. N. Reeves, P. T. O'Brien, M. J. Ward, *Astrophys. J.* **593**, L65–L68 (2003).
7. J. N. Reeves *et al.*, *Astrophys. J.* **701**, 493–507 (2009).
8. J. N. Reeves *et al.*, *Astrophys. J.* **780**, 45 (2014).
9. Materials and methods are available as supplementary materials on *Science* Online.
10. C. Done, M. A. Sobolewska, M. Gierliński, N. J. Schurch, *Mon. Not. R. Astron. Soc.* **374**, L15–L19 (2007).
11. J. S. Kaastra *et al.*, *Science* **345**, 64–68 (2014).
12. L. C. Gallo, A. C. Fabian, *Mon. Not. R. Astron. Soc.* **434**, L66–L69 (2013).
13. K. A. Pounds, J. N. Reeves, *Mon. Not. R. Astron. Soc.* **397**, 249–257 (2009).
14. N. Arav, B. Borguet, C. Chamberlain, D. Edmonds, C. Danforth, *Mon. Not. R. Astron. Soc.* **436**, 3286–3305 (2013).
15. Y. Krongold *et al.*, *Astrophys. J.* **659**, 1022–1039 (2007).
16. F. Tombesi, M. Cappi, J. N. Reeves, V. Braito, *Mon. Not. R. Astron. Soc.* **422**, L1–L5 (2012).
17. D. Proga, J. M. Stone, T. R. Kallman, *Astrophys. J.* **543**, 686–696 (2000).
18. J. Gofford *et al.*, *Astrophys. J.* **784**, 77 (2014).
19. T. Di Matteo, V. Springel, L. Hernquist, *Nature* **433**, 604–607 (2005).
20. P. F. Hopkins, M. Elvis, *Mon. Not. R. Astron. Soc.* **401**, 7–14 (2010).
21. K. Zubovas, A. King, *Astrophys. J.* **745**, L34 (2012).
22. C. Cicone *et al.*, *Astron. Astrophys.* **562**, A21 (2014).
23. L. Ferrarese, D. Merritt, *Astrophys. J.* **539**, L9–L12 (2000).
24. K. Gebhardt *et al.*, *Astrophys. J.* **539**, L13–L16 (2000).
25. A. R. King, *Astrophys. J.* **596**, L27–L29 (2003).
26. K. Jahnke, A. V. Macciò, *Astrophys. J.* **734**, 92 (2011).
27. R. C. McQuillin, D. E. McLaughlin, *Mon. Not. R. Astron. Soc.* **434**, 1332–1338 (2013).

ACKNOWLEDGMENTS

This research was supported under the U.K. Science and Technology Facilities Council grant ST/J001384/1 and is based on x-ray observations obtained with the XMM-Newton and NuSTAR satellites. XMM-Newton is a European Space Agency (ESA) science mission with instruments and contributions directly funded by ESA member states and the National Aeronautics and Space Administration. The NuSTAR mission is a project led by the California Institute of Technology, managed by the Jet Propulsion Laboratory, and funded by NASA. We thank the NuSTAR Operations, Software, and Calibration teams for support with execution and analysis of these observations. We also acknowledge financial support from the Italian Space Agency under grant ASI-INAF I/037/12/0 (G.R. and G.M.); the Italian National Institute for Astrophysics under grant PRIN-INAF 2012 (G.R.); the I-CORE program of the Planning and Budgeting Committee, the Israel Science Foundation under grants 1937/12 and 1163/10, Israel's Ministry of Science and Technology (E.B.); and NASA under grants NNX11AJ57G and NNG08FD60C (T.J.T.). The data are stored in the science archives of the two x-ray observatories involved and will become publicly available on 25 March 2015 (XMM-Newton) and with the upcoming DR6 data release (NuSTAR).

SUPPLEMENTARY MATERIALS

www.sciencemag.org/content/347/6224/860/suppl/DC1
Materials and Methods
Supplementary Text
Figs. S1 to S5
Tables S1 to S3
References (*28*–*63*)

25 July 2014; accepted 20 January 2015
10.1126/science.1259202

TRANSITION STATES

Trapping a transition state in a computationally designed protein bottle

Aaron D. Pearson,[1]* Jeremy H. Mills,[2]* Yifan Song,[2] Fariborz Nasertorabi,[3] Gye Won Han,[3] David Baker,[2,4] Raymond C. Stevens,[3] Peter G. Schultz[1]†

The fleeting lifetimes of the transition states (TSs) of chemical reactions make determination of their three-dimensional structures by diffraction methods a challenge. Here, we used packing interactions within the core of a protein to stabilize the planar TS conformation for rotation around the central carbon-carbon bond of biphenyl so that it could be directly observed by x-ray crystallography. The computational protein design software Rosetta was used to design a pocket within threonyl-transfer RNA synthetase from the thermophile *Pyrococcus abyssi* that forms complementary van der Waals interactions with a planar biphenyl. This latter moiety was introduced biosynthetically as the side chain of the noncanonical amino acid *p*-biphenylalanine. Through iterative rounds of computational design and structural analysis, we identified a protein in which the side chain of *p*-biphenylalanine is trapped in the energetically disfavored, coplanar conformation of the TS of the bond rotation reaction.

The direct observation of the transition state (TS) of a chemical reaction requires highly sensitive spectroscopic techniques with a temporal resolution on the order of 10^{-13} to 10^{-14} s. This milestone was made possible with the advent of ultrafast laser spectroscopy, which allowed the direct observation of the transient species formed as reactants cross an energy barrier to products (*1*, *2*). However, determination of the three-dimensional (3D) structure of a TS requires ultrafast electron or x-ray diffraction techniques with similar temporal resolution and sensitivity (*3*, *4*). An alternative approach is to increase the lifetime of the transition state configuration by trapping it in a free energy (ΔG) well so that it can be directly observed by more conventional spectroscopic methods. In theory, the well-packed interior of a protein could act as a "programmable" solvent to selectively stabilize a TS configuration and thereby make it kinetically persistent and directly observable by conventional x-ray diffraction methods. Indeed, enzymes

[1]Department of Chemistry and Skaggs Institute for Chemical Biology, The Scripps Research Institute, La Jolla, CA 92037, USA. [2]Department of Biochemistry, University of Washington, Seattle, WA 98195, USA. [3]Department of Biological Sciences, Bridge Institute, University of Southern California, Los Angeles, CA 90089, USA. [4]Howard Hughes Medical Institute (HHMI), University of Washington, Seattle, WA 98195, USA.
*These authors contributed equally to this work. †Corresponding author. E-mail: schultz@scripps.edu

Downloaded from www.sciencemag.org on February 21, 2015

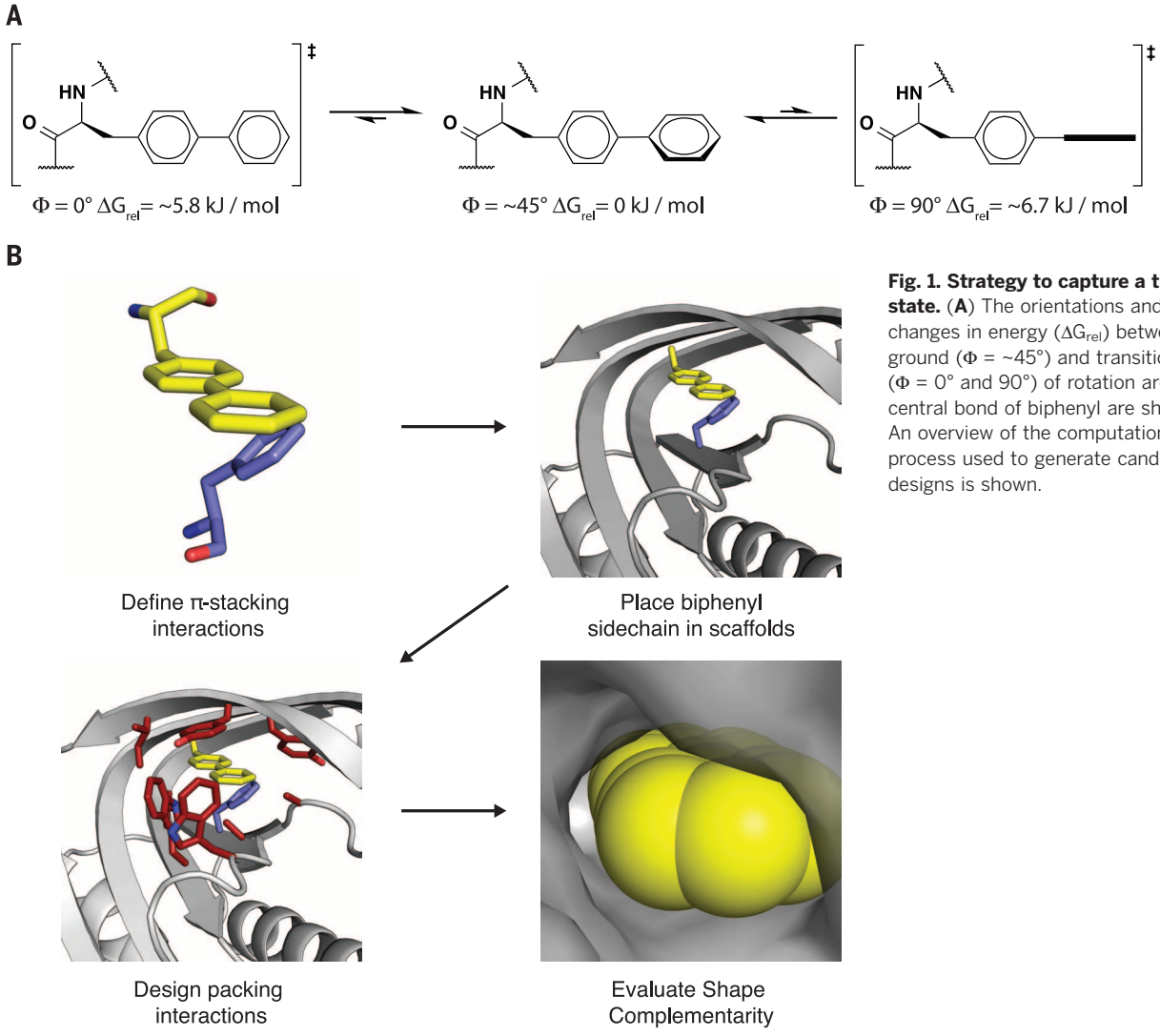


Fig. 1. Strategy to capture a transition state. (**A**) The orientations and relative changes in energy (ΔG_{rel}) between the ground (Φ = ~45°) and transition states (Φ = 0° and 90°) of rotation around the central bond of biphenyl are shown. (**B**) An overview of the computational design process used to generate candidate designs is shown.

catalyze reactions by virtue of their ability to selectively stabilize the rate-limiting TS relative to the ground-state reactants (*5*–*9*). Here, we show the redesign of the interior of the protein threonyl-tRNA synthetase from the thermophile *Pyrococcus abyssi* (*10*) to create a microenvironment that has high complementarity to the planar TS configuration for rotation about the central C–C bond of biphenyl (*11*). Determination of the 3D structure of the designed protein at 2.05 Å resolution by x-ray crystallography revealed a planar biphenyl TS configuration stabilized by van der Waals interactions with side chains in the protein core.

Biphenyl bond rotation is a well-studied reaction, both experimentally and theoretically. In the gas phase, the ground state of biphenyl is twisted, with a dihedral angle of ~45°. Rotation around the central C–C bond connecting the two phenyl rings in biphenyl is estimated to have an energy barrier of 5.8 ± 2.1 and 6.7 ± 2.1 kJ/mol around the 0° (planar) and 90° TSs, respectively, as determined experimentally by electron diffraction studies (Fig. 1A) (*12*). The energy barriers estimated using Raman data (*13*, *14*) and ultraviolet absorption spectroscopy (*15*) are in general agreement with the results from the diffraction studies. Theoretical calculations show that these barriers result from opposing steric and electronic effects of the two phenyl rings but give a range of values depending on the method used (*16*). This simple reaction (which racemizes chiral biphenyls) provides an ideal system to pose the question whether side chain packing interactions in a folded protein can be exploited to make a transition state configuration kinetically persistent so that it can be directly observed by x-ray crystallography.

Table 1. First-round computational designs. Designed protein names, parent scaffolds, and mutations made are listed. Single-letter abbreviations for the amino acid residues are as follows: A, Ala; C, Cys; D, Asp; E, Glu; F, Phe; G, Gly; H, His; I, Ile; K, Lys; L, Leu; M, Met; N, Asn; P, Pro; Q, Gln; R, Arg; S, Ser; T, Thr; V, Val; W, Trp; and Y, Tyr.

Designed protein	Parent scaffold (PDB ID)	Computationally designed mutations
BIF_1	1y2q	$S^{8}A$, I^{11}BiPhe, $F^{42}W$, $Y^{79}A$, $F^{81}W$, $K^{121}I$, $F^{123}Y$
BIF_2	1anu	$V^{20}G$, $F^{22}I$, $C^{33}W$, F^{35}BiPhe, $F^{37}W$, $F^{96}G$
BIF_3	2h2h	$F^{48}L$, F^{60}BiPhe, $Y^{61}W$, $F^{63}W$, $A^{64}M$, $I^{68}G$, $P^{157}G$, $I^{159}A$
BIF_4	1ve0	$I^{21}T$, V^{25}BiPhe, $S^{26}A$, $V^{39}G$, $C^{46}A$, $I^{48}V$

To introduce a biphenyl moiety into a protein core, we used the genetically encoded noncanonical amino acid *p*-biphenylalanine (BiPhe). This amino acid can be introduced site-specifically into a protein in *Escherichia coli* in good yield in response to the amber nonsense codon TAG, with an orthogonal amber suppressor tRNA/aminoacyl-tRNA synthetase (aaRS) pair. The aaRS was evolved from the *Methanococcus jannaschi* tyrosyl-tRNA synthetase to be selective for BiPhe and not incorporate any of the 20 canonical amino acids (*17*, *18*). The rotational barrier around

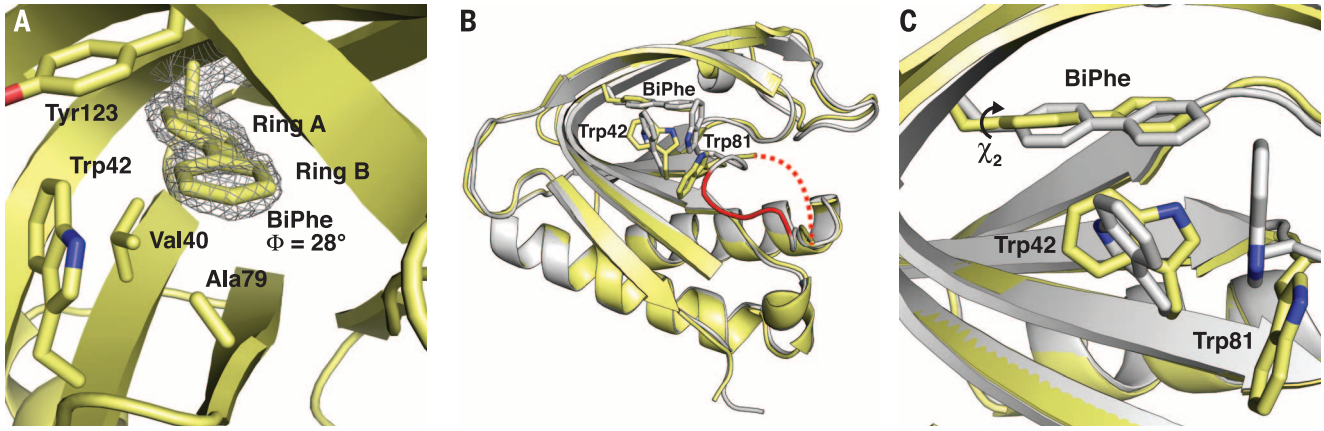


Fig. 2. X-ray crystallographic analysis of BIF_1. (**A**) The x-ray crystal structure of BIF_1 is shown in yellow; BiPhe and surrounding residues are shown in sticks. Rings A and B are those closest to and farthest from the protein backbone, respectively. Electron density around the BiPhe side chain is shown as a $2F_o - F_c$ map contoured to 2σ. (**B**) A comparison of the design model (gray) to the structure (yellow) of BIF_1 is shown; BiPhe, Trp^{42}, and Trp^{81} are shown in sticks. A loop corresponding to residues 81 to 89 of the parent scaffold is shown in red. Missing density in the structure corresponding to residues 83 to 86 of BIF_1 is shown as a dashed red line. (**C**) A comparison of the structure of BIF_1 (yellow) to the design model (gray) is shown. BiPhe, Trp^{42}, and Trp^{81} are shown in sticks. An arrow indicates rotation about χ^2 in the structure relative to the design.

Table 2. Second- and third-round crystallographic analysis. Second-round mutant identities, biphenylalanine dihedral angle, and x-ray crystal structure resolution are listed. Dihedrals listed are averages of those measured on each side of the biphenyl ring.

Scaffold	F^{42}	Y^{79}	F^{123}	BIF Φ (deg.)	Resolution (Å)
BIF_1	W	A	Y	26	1.95
BIF_1.1	F	S	V	35	2.10
BIF_1.2	F	V	V	21	2.50
BIF_1.3	F	S	A	15	2.36
BIF_1.4	F	V	A	20	2.10
BIF_0	F	I	A	0	2.05

the biphenyl C–C bond in BiPhe is not expected to be substantially different from biphenyl itself (*19*).

To identify an appropriate host protein in which to construct a site complementary to the planar biphenyl TS geometry, we first curated a set of ~2300 proteins of known structures from thermophilic organisms [a full description of the computational design process is found in the supplementary materials (*20*)]. Proteins with high thermostabilities have more negative Δ*G*s of folding and are in general more tolerant to mutations; both characteristics are likely to be beneficial when attempting to stabilize a TS configuration through packing interactions in a protein core (*21*, *22*). RosettaMatch (*23*) was then used to identify residues in the core of each protein scaffold where BiPhe could be substituted without creating unfavorable steric interactions with the protein backbone (Fig. 1B), and make π-stacking interactions (*24*) with native Trp, Phe, or Tyr residues. Because the RosettaMatch calculations were carried out with a planar model of the BiPhe, these interactions should stabilize the biphenyl side chain in the desired planar TS conformation. To ensure that the substituted BiPhe side chain was sufficiently buried within a particular protein's core, initial hits were first filtered on the basis of the change in solvent-accessible surface area (ΔSASA) (*25*) that occurs when BiPhe is removed from the substituted site. A ΔSASA cutoff of 0.9 (meaning the BiPhe was >90% buried) removed 35% of the initial matches from further consideration.

RosettaDesign (*26*) was then used to optimize the identities of residues surrounding the BiPhe (excluding residues already participating in π-stacking interactions) such that they packed tightly against the planar BiPhe side chain but did not create unfavorable hydrogen-bonding interactions (Fig. 1B). Candidate designs were ranked by shape complementarity (SC) (*27*) between the designed residues and the BiPhe (Fig. 1B). Ultimately, four designs (BIF_1 to BIF_4) with high SC values were chosen for experimental characterization (Table 1). The computer-modeled proteins containing the BiPhe were reverse-translated and optimized for expression in *E. coli*.

To incorporate BiPhe into these four different protein scaffolds, we used the orthogonal amber suppressor tRNA/BiPheRS pair encoded on the dual-plasmid expression system (pUltra) (*28*). One plasmid contained the tRNA/BiPheRS pair specific for BiPhe, and the other contained the synthetic mutant gene of interest fused to a C-terminal hexa-histidine purification tag. A TAG amber nonsense codon was introduced at the desired site to encode BiPhe (*17*). These plasmids were cotransformed into *E. coli* Bl21(DE3), and protein expression was carried out in the presence of 1 mM BiPhe. Proteins were purified from cell lysate via Ni^{2+}-affinity chromatography followed by size-exclusion chromatography. Mass spectrometric analysis of BIF_1 to BIF_4 indicated successful incorporation of BiPhe in all cases (fig. S1), and SDS–polyacrylamide gel electrophoresis indicated that the purified proteins were of suitable purity (>95%) for crystallographic analysis.

All four designed proteins were subjected to an initial crystallographic screen based on the conditions used to crystallize the wild-type protein (*20*, *29*–*32*). Crystals were obtained only for BIF_1, which has as its parent scaffold threonyl-tRNA synthetase from the thermophile P. *abyssi*, but they were needles and not suitable for x-ray crystallography. An automated high-throughput crystallization system was then used to identify new conditions (0.1 M sodium citrate, 15% polyethylene glycol 6000, pH = 5.5) in which large crystals of BIF_1 grew. The structure of BIF_1 was solved to 1.8 Å resolution by x-ray crystallography using molecular replacement with the parent scaffold (PDB ID 1y2q) serving as a search model. Density for BiPhe was clearly observed in a $2F_o - F_c$ map (Fig. 2A), and the torsion angle between the two phenyl rings was determined to be ~28° (Fig. 2A). This value represented a rotation of ~17° toward the desired planar conformation relative to the dihedral found at the energetic minimum but remained far from the desired value of 0°. To force the BiPhe torsion angle closer to planarity, a second round of computational design was undertaken on the basis of a detailed analysis of the structure of BIF_1.

Globally, the structure of BIF_1 matched the design model quite well (Fig. 2B; root mean square deviation to the design model of ~1.3 Å over all atoms), although differences are apparent in the vicinity of the BiPhe residue. In the model, Trp^{42} and Trp^{81} both form edgewise interactions with the BiPhe side chain. However, in the crystal

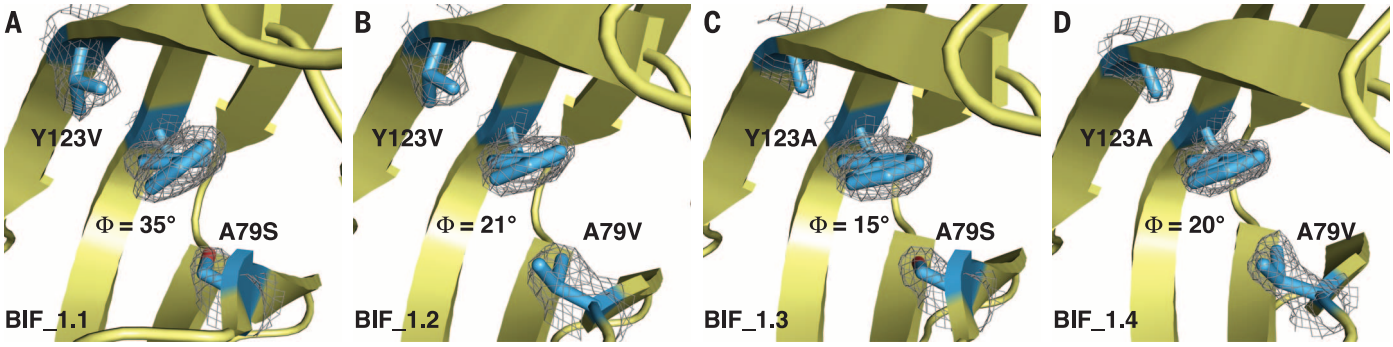


Fig. 3. A comparison of the crystal structures of BIF_1.1 to BIF_1.4. (**A** to **D**) Crystal structures of second-round mutants BIF_1.1 to BIF_1.4 are shown. The side chains of BiPhe, and those at positions 79 and 123, are shown in sticks. Electron density from a $2F_o - F_c$ map contoured to 1.5σ [(A to C)] and 2.0σ (D) is shown for the aforementioned residues. The measured dihedral angle between the two biphenyl rings is shown beneath the biphenyl side chain in each case.

structure, the indole ring of Trp[42] rotates such that it packs lengthwise against the BiPhe side chain in an orientation that would clash with the side-chain orientation of Trp[81] predicted by the design model (Fig. 2C). To avoid this unfavorable steric interaction, a substantial displacement of the loop consisting of residues 81 to 89 likely occurs, as evidenced by the lack of electron density for residues 83 to 86 in the crystal structure (Fig. 2B). In an attempt to return the disordered loop to its native position, we independently mutated each Trp to Phe (the wild-type residue at both positions) in silico. Unconstrained repacking and minimization calculations in the context of each mutation showed that Trp[42]Phe increased SC and scored slightly better than the original design. As a result, this mutation was made standard for the remainder of the computational redesign.

A second focus of the redesign effort was to identify point mutations in residues packing against the biphenyl rings to force the side chain into the desired planar conformation. In the structure of BIF_1, the biphenyl side chain is rotated ~5° about χ_1 and 25° about χ_2, relative to its placement in the design model (Fig. 2C). Although the phenyl ring closest to the backbone (ring A) is out of plane with respect to the model, the ring farthest from the backbone (ring B) is essentially in the plane of the design model (Fig. 2, A and C). Thus, it appears that rotation about χ_2 is the predominant determinant of the 28° deviation from planarity observed in the crystal structure relative to the design model. Because ring A is bounded on one face by the protein backbone, we believed it would be difficult to identify a mutant that would adjust this ring in the desired direction (Fig. 2C). In contrast, ring B is flanked by both Ala[79] and Tyr[123], suggesting that mutagenesis of one or both of these residues could potentially planarize the BiPhe dihedral angle (Fig. 2A). Analysis of the structure of BIF_1 suggested that the phenyl ring of Tyr[123] likely prevents ring B from rotating into the plane of ring A (Fig. 2A); thus, we mutated Tyr[123] in silico to the smaller residues Ala and Val. Concurrently, Ala[79] was mutated to the bulkier residues Cys, Ser, Thr, and Val. Rosetta was then used to analyze these potential sequence alternatives, again by carrying out unconstrained repacking and minimization calculations. The energies for all mutants tested fell within ~6 Rosetta energy units (REU) of one another and gave SC values that differed at most by ~5%. The tight distribution of values for both metrics suggested that no clear preference exists for one mutant over another, so a series of four mutants was examined experimentally.

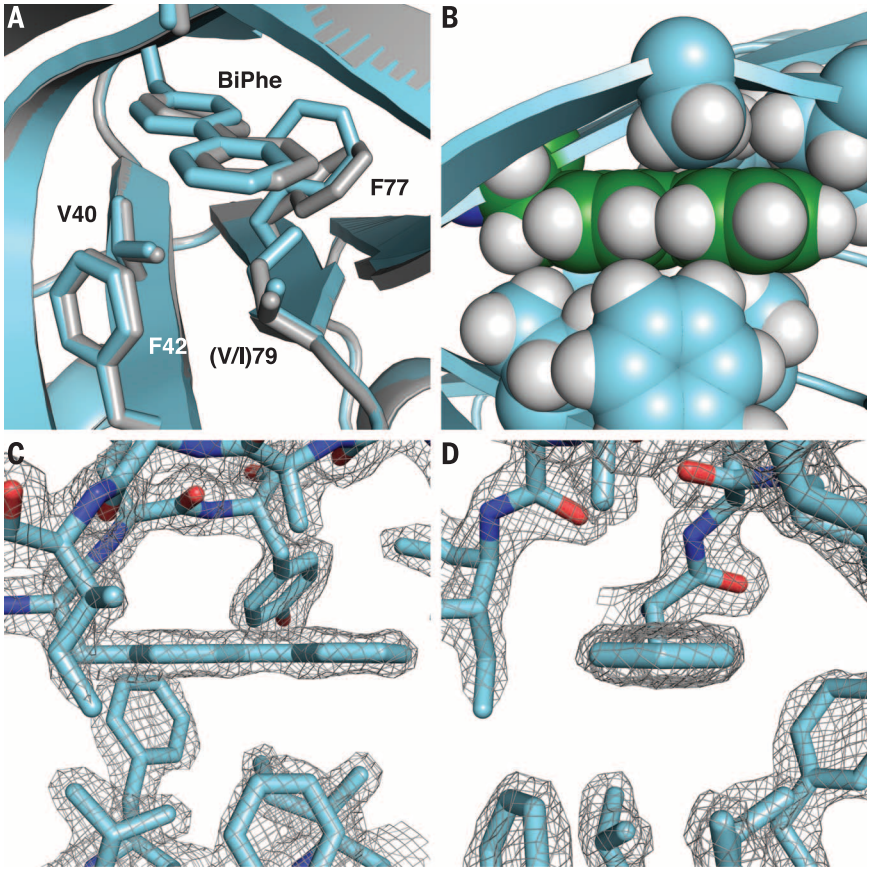


Fig. 4. X-ray crystal structure of BIF_0. (**A**) The crystal structure of BIF_0 is shown in blue, and BIF_1.3 is shown in gray. The BiPhe side chain and surrounding residues are shown in sticks. (**B**) Packing interactions between the designed protein BIF_0 and the BiPhe side are highlighted with space-filling representations of the interacting residues. (**C** and **D**) The structure of BIF_0 is shown, highlighting the BiPhe side chain; views from the front and side are shown. The BiPhe side chain and surrounding residues are shown in sticks, and $2F_o - F_c$ maps are contoured to 2σ in each case.

All four mutants expressed well and afforded diffraction-quality crystals. We solved the structures of BIF_1.1, BIF_1.2, BIF_ 1.3, and BIF_1.4 to 2.10, 2.50, 2.36, and 2.10 Å resolution, respectively, again by molecular replacement. In all cases, the Trp[42]Phe mutation returned the displaced loop to its native position (fig. S2). However, a distribution of BiPhe torsion angles between 35°

and 15° was observed among the four structures (Table 2). In the majority of these cases, the change in the χ_2 angle relative to the original design remained near the value of 25° observed in the initial BIF_1 structure. This result suggested that mutations to Ala^{79} and Trp^{123} have the desired effect of rotating ring B without affecting the absolute orientation of ring A. Unfortunately, substitution of Tyr^{123} with the beta-branched Val and the opposing Ala^{79} with Ser (BIF_1.1) had the effect of rotating ring B even farther out of plane (35°) than in the original structure (Fig. 3A). This undesired rotation was partially remedied in BIF_1.2 (Φ = 21°) (Fig. 3B) by substituting Ala^{79} with a bulkier Val residue and further corrected in BIF_1.3 and BIF_1.4 (Φ = 15° and 20°, respectively) (Fig. 3, C and D) by replacing the opposing Tyr^{123} with a smaller Ala residue and Ala^{79} with Ser (BIF_1.3) or Val (BIF_1.4). This analysis suggested that ring A could potentially be rotated into a coplanar geometry by further increasing the size of the amino acid at position 79 with an Ala^{79}Ile mutation while maintaining Phe^{42} and the Tyr^{123}Ala mutation. The additional methyl group of the isoleucine should force the side of ring A to rotate further in the desired direction.

We next generated the corresponding BIF_0 mutant (S^8A, I^{11}BiPhe, Y^{79}I, F^{81}W, K^{121}I, and F^{123}A), purified the protein, and solved its crystal structure to 2.05 Å resolution (Fig. 4). Analysis of the electron density showed that the two phenyl rings of BiPhe are coplanar, which matches the configuration of the TS for the bond rotation reaction. The structure of BIF_0 shows that, in addition to adding steric bulk beneath ring A, the V^{79}I mutation also forces the side chain of Phe^{77} to adopt a different rotamer than was observed in BIF_1.4, which has the effect of further rotating ring A into the plane of ring B (Fig. 4). The mutations introduced into BIF_0 do not appear to substantially affect the thermal stability of the protein. The melting temperature of this mutant, as determined by differential scanning calorimetry, was ~110°C, consistent with the 3D structure of BIF_0, which shows that the protein core is well packed.

We have shown by iterative computational design, mutagenesis, and protein structure determination that one can design a protein core that stabilizes a simple conformational transition state to such a degree that one can determine its 3D x-ray crystal structure. However, we should note that the biphenyl energy landscape corresponds to a substructure within the protein relative to the energetics of the global protein conformational ensemble. A similar strategy was recently employed to directly observe catalyst-substrate interactions through x-ray crystallographic analysis (*33*). The results described here may not be all that surprising given that enzymes typically stabilize a rate-limiting TS by 8 to 12 kcal/mol. Nonetheless, these experiments underscore the ability of proteins to fold into defined 3D structures in which van der Waals, hydrogen-bonding, and electrostatic interactions can be controlled with exquisite precision.

REFERENCES AND NOTES

1. T. S. Rose, M. J. Rosker, A. H. Zewail, *J. Chem. Phys.* **88**, 6672–6673 (1988).
2. J. C. Polanyi, A. H. Zewail, *Acc. Chem. Res.* **28**, 119–132 (1995).
3. R. Srinivasan, J. S. Feenstra, S. T. Park, S. Xu, A. H. Zewail, *Science* **307**, 558–563 (2005).
4. H. Ihee *et al.*, *Science* **291**, 458–462 (2001).
5. L. Pauling, *Chem. Eng. News* **24**, 1375–1377 (1946).
6. W. P. Jencks, *Catalysis in Chemistry and Enzymology* (Dover, Mineola, NY, 1987).
7. A. Tramontano, K. D. Janda, R. A. Lerner, *Science* **234**, 1566–1570 (1986).
8. S. J. Pollack, J. W. Jacobs, P. G. Schultz, *Science* **234**, 1570–1573 (1986).
9. P. G. Schultz, R. A. Lerner, *Science* **269**, 1835–1842 (1995).
10. S. Dwivedi, S. P. Kruparani, R. Sankaranarayanan, *Nat. Struct. Mol. Biol.* **12**, 556–557 (2005).
11. F. Ceccacci, G. Mancini, P. Mencarelli, C. Villani, *Tetrahedron Asymmetry* **14**, 3117–3122 (2003).
12. A. Almenningen *et al.*, *J. Mol. Struct.* **128**, 59–76 (1985).
13. J. E. Katon, E. R. Lippincott, *Spectrochimica Acta* **15**, 627–650 (1959).
14. L. A. Carreira, T. G. Towns, *J. Mol. Struct.* **41**, 1–9 (1977).
15. H. Suzuki, *Bull. Chem. Soc. Jpn.* **32**, 1340–1350 (1959).
16. O. Bastiansen, S. Samdal, *J. Mol. Struct.* **128**, 115–125 (1985).
17. J. Xie, W. Liu, P. G. Schultz, *Angew. Chem. Int. Ed.* **46**, 9239–9242 (2007).
18. L. Wang, A. Brock, B. Herberich, P. G. Schultz, *Science* **292**, 498–500 (2001).
19. J. K. Eloranta, *Zeitschrift Naturforschung Teil A* **27a**, 1652–1662 (1972).
20. Materials and methods are available as supplementary materials on *Science* Online.
21. A. Razvi, J. M. Scholtz, *Protein Sci.* **15**, 1569–1578 (2006).
22. J. D. Bloom, S. T. Labthavikul, C. R. Otey, F. H. Arnold, *Proc. Natl. Acad. Sci. U.S.A.* **103**, 5869–5874 (2006).
23. A. Zanghellini *et al.*, *Protein Sci.* **15**, 2785–2794 (2006).
24. G. B. McGaughey, M. Gagné, A. K. Rappé, *J. Biol. Chem.* **273**, 15458–15463 (1998).
25. S. M. Le Grand, K. M. Merz, *J. Comput. Chem.* **14**, 349–352 (1993).
26. B. Kuhlman, D. Baker, *Proc. Natl. Acad. Sci. U.S.A.* **97**, 10383–10388 (2000).
27. M. C. Lawrence, P. M. Colman, *J. Mol. Biol.* **234**, 946–950 (1993).
28. A. Chatterjee, M. J. Lajoie, H. Xiao, G. M. Church, P. G. Schultz, *ChemBioChem* **15**, 1782–1786 (2014).
29. L. J. Shimon *et al.*, *Structure* **5**, 381–390 (1997).
30. S. Dwivedi, S. P. Kruparani, R. Sankaranarayanan, *Acta Crystallogr. D Biol. Crystallogr.* **60**, 1662–1664 (2004).
31. Y. Tanaka *et al.*, *Proteins* **61**, 1127–1131 (2005).
32. M. S. Cosgrove *et al.*, *Biochemistry* **45**, 7511–7521 (2006).
33. S. Han, B. V. Le, H. S. Hajare, R. H. G. Baxter, S. J. Miller, *J. Org. Chem.* **79**, 8550–8556 (2014).

ACKNOWLEDGMENTS

The authors thank N. P. King and P.-S. Huang for helpful discussions. D.B and J.H.M. were supported by the Defense Threat Reduction Agency (HDTRA1-11-1-0041). J.H.M. was supported by National Institute of General Medical Science of the National Institutes of Health under award F32GM099210. P.G.S. acknowledges support by the National Institutes of Health under award 2 R01 GM097206-05. The content is solely the responsibility of the authors and does not represent the official views of the National Institutes of Health. Structures of BIF_1, BIF_1.1 to BIF_1.4, and BIF_0 have been deposited in the Protein Data Bank under accession numbers 4S02, 4S0J, 4S0L, 4S0I, 4S0K, and 4S03.

SUPPLEMENTARY MATERIALS

www.sciencemag.org/content/347/6224/863/suppl/DC1
Materials and Methods
Figs. S1 and S2
Tables S1 and S2
References (*34*–*42*)

6 November 2014; accepted 20 January 2015
10.1126/science.aaa2424

ANIMAL EVOLUTION

Cope's rule in the evolution of marine animals

Noel A. Heim,[1]* Matthew L. Knope,[1]† Ellen K. Schaal,[1]‡ Steve C. Wang,[2] Jonathan L. Payne[1]

Cope's rule proposes that animal lineages evolve toward larger body size over time. To test this hypothesis across all marine animals, we compiled a data set of body sizes for 17,208 genera of marine animals spanning the past 542 million years. Mean biovolume across genera has increased by a factor of 150 since the Cambrian, whereas minimum biovolume has decreased by less than a factor of 10, and maximum biovolume has increased by more than a factor of 100,000. Neutral drift from a small initial value cannot explain this pattern. Instead, most of the size increase reflects differential diversification across classes, indicating that the pattern does not reflect a simple scaling-up of widespread and persistent selection for larger size within populations.

Body size constrains key ecological and physiological traits such as generation time, fecundity, metabolic rate, population size, and home range size (*1*, *2*). Because of perceived advantages associated with larger size, there has long been speculation that animals tend to increase in size over evolutionary time (*3*–*8*), a pattern commonly referred to as Cope's rule. Fossil data support size increase in many cases (*6*, *9*–*15*), but numerous counterexamples also exist (*16*–*22*). Moreover, some instances of size increase could simply result from neutral drift away from an initially small size rather than requiring any active selection for size (*17*, *22*).

To determine whether animal sizes have increased since the start of the Cambrian [542 million

[1]Department of Geological and Environmental Sciences, Stanford University, 450 Serra Mall, Stanford, CA 94305, USA. [2]Department of Mathematics and Statistics, Swarthmore College, Swarthmore, PA 19081, USA.
***Corresponding author. E-mail: naheim@stanford.edu** †Present address: Department of Biology, Stanford University, Stanford, CA 94305, USA. ‡Present address: Department of Geology, Lawrence University, Appleton, WI 54911, USA.

years ago (Ma)] and, if so, whether the increase can be accounted for by neutral drift or requires active evolutionary processes, we compiled adult body size measurements for 17,208 genera of marine animals from the phyla Arthropoda, Brachiopoda, Chordata, Echinodermata, and Mollusca, with stratigraphic ranges in the fossil record resolved to stages, the finest temporal units in the global geologic time scale (*23*) (fig. S1A). These phyla together account for 74% of animal diversity in the fossil record (*24*), and our data set covers 75% of total known genus diversity in these phyla. We measured the three major body axes from published images of specimens (typically holotypes of the type species) (*23*) in order to estimate the size of each genus as a simple geometric solid or from known length:mass relationships (*23*). We used linear regressions of biovolume on maximum length for classes and phyla to estimate the biovolume of genera for which fewer than three major axes were illustrated (*23*) (fig. S2 and table S1).

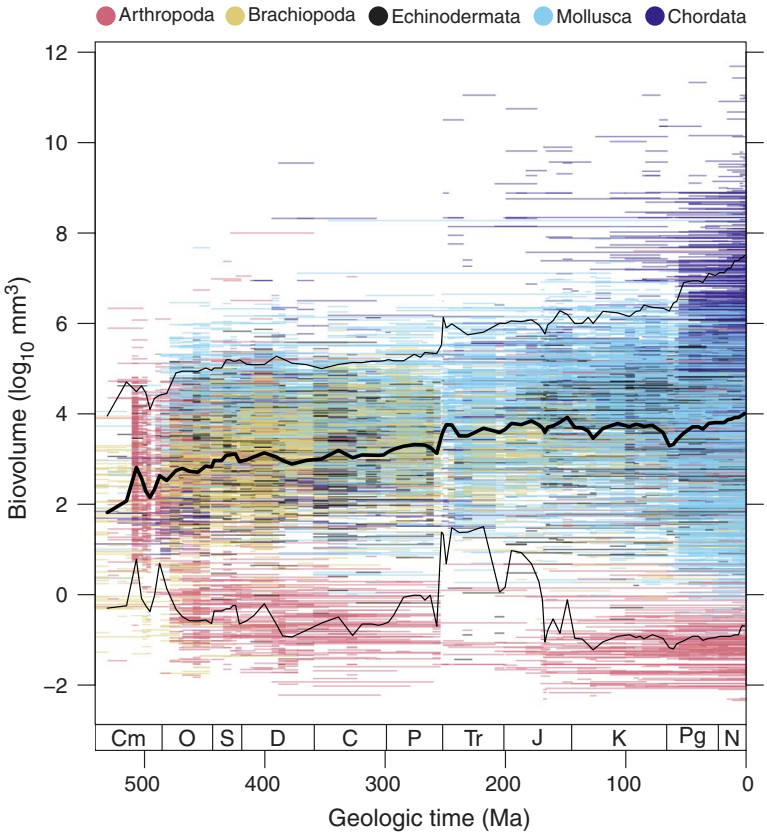


Fig. 1. Body size evolution across the past 542 million years. The distribution of fossil marine animal biovolumes across the Phanerozoic is shown. The colored horizontal lines show genus durations. The thick black line indicates the stage-level mean body size. The thin black lines demarcate the 5th and 95th percentiles. Cm, Cambrian; O, Ordovician; S, Silurian; D, Devonian; C, Carboniferous; P, Permian; Tr, Triassic; J, Jurassic; K, Cretaceous; Pg, Paleogene; N, Neogene.

Figure 1 illustrates the sizes of the marine animal genera in our data set across the past 542 million years. The mean biovolume across genera has increased by more than a factor of 150 (2.18 $\log_{10}$ units; the median increased by 2.35 $\log_{10}$ units) since the earliest Cambrian. Over the same interval, the range in biovolume expanded from 8 orders of magnitude in the Cambrian to 14 orders of magnitude in the Pleistocene (1 Ma). Most of this expansion in size range reflects an increase in the maximum, which climbed by more than three orders of magnitude between the Early Cambrian and Middle Devonian (542 to 385 Ma) and by an additional two orders of magnitude thereafter. In contrast, the overall minimum size decreased by less than one order of magnitude between the Early Cambrian and Middle Devonian and has remained stable ever since.

To test models of neutral change relative to active processes, we compared observed trends in maximum, mean, and minimum size to expectations generated by three evolutionary branching models: an unbiased random walk (i.e., Brownian motion; fig. S3A), a bounded random walk (i.e., Brownian motion with a reflecting lower bound; fig. S3B), and a size-biased random walk (fig. S3C) (*23*). The size-biased model fit observed trends in the minimum, mean, and maximum size better than the neutral and lower-bounded models (Fig. 2 and fig. S4). The observed minimum size is within the predicted range of all three models,

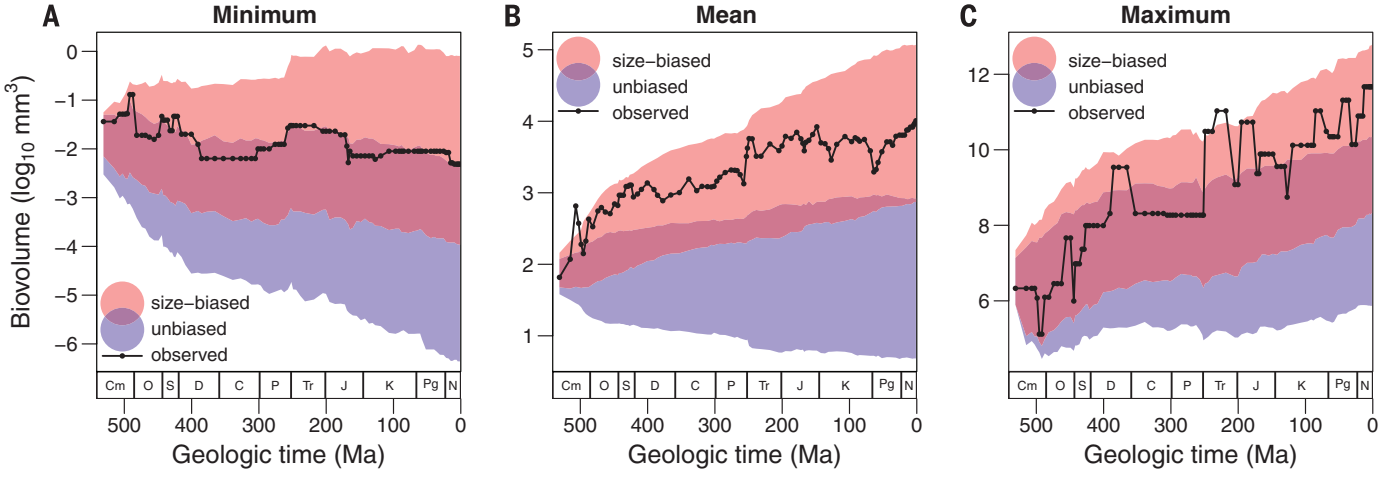


Fig. 2. Comparison of observed biovolume trends to those obtained from stochastic branching models (***23***). The colored regions highlight the size space occupied by 90% of the 1000 model runs. For clarity, only results for the size-biased (red) and unbiased (blue) models are shown; except below the minimum size, the lower-bounded model produced results nearly identical to the unbiased model (fig. S4). (**A**) Minimum, (**B**) mean, and (**C**) maximum sizes. Time scale abbreviations are the same as in Fig. 1.

but the observed mean and maximum sizes trended above the predicted range for the unbiased and lower-bounded models (Fig. 2 and fig. S4). As an additional test of the three models, we compared the observed distribution of biovolumes of all 2280 Pleistocene genera, the most recent and taxonomically diverse time interval in our analyses, to distributions predicted by our branching models and found strong support for the size-biased model over the other two models (table S2) (*23*). Finally, we used an independent, likelihood-based approach to compare support among five models for the trend in mean size over the entire 542 million years (*23*). Three models assumed a single mode of size evolution across the Phanerozoic (driven trend, random walk, or stasis). The best-supported of these models was the driven trend toward larger size (Table 1). However, allowing a shift in model type and parameters at the era-bounding mass extinctions improved the overall model fit, with the best-fit model in the Paleozoic being a driven trend toward larger size, followed by stasis in the Mesozoic, and a reversion to a driven trend in the Cenozoic (*23*) (Table 1). Removing the marine tetrapods, which tend to be very large, did not change this result (table S3). Thus, most of Phanerozoic time has been characterized by a trend toward larger animal sizes.

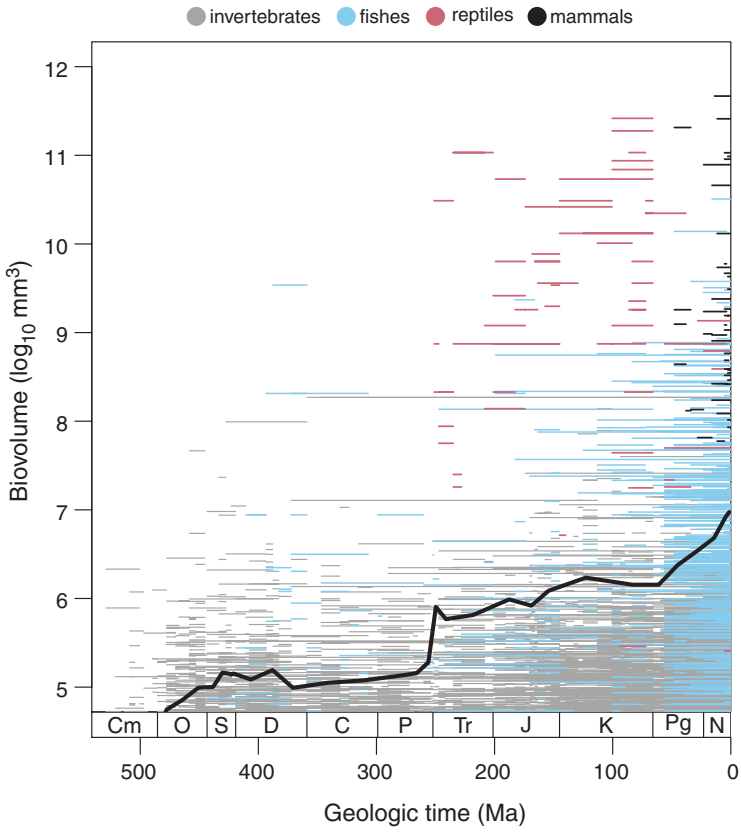


Fig. 3. Taxonomic compositions of the largest genera. Fishes and, later, air-breathing tetrapods, dominate the top of the size distribution. All genera with epoch- or stage-resolved stratigraphic ranges are plotted here, allowing for the inclusion of more large vertebrates. Horizontal lines show genus durations. The heavy black line demarcates the 95th percentile of all genera. Time scale abbreviations are the same as in Fig. 1.

The trends in minimum, mean, and maximum biovolume of marine animals are consistent with actively driven size increase and not consistent with simple neutral drift away from an initially small ancestor. To determine the extent to which this trend reflects size increase at low taxonomic levels across all phyla versus differential diversification of higher taxa with different mean sizes, we compared the observed trend in the mean to the expected trend if size were kept constant as diversity changed within different levels of the Linnaean hierarchy (fig. S5). This comparison demonstrates that much of the observed size increase reflects differential diversification among classes and is consistent with hierarchical size evolution in Paleozoic brachiopods (*15*). This finding also sheds light on the tripartite nature of the Phanerozoic trend in mean biovolume, as there was little differential diversification among classes during Mesozoic time (fig. S1B).

The dominance of differential diversification at the class level in producing the overall trend toward larger animal sizes emphasizes the hierarchical nature of evolutionary processes. In addition, it suggests that the widespread bias toward selection for larger size observed in extant populations (*8*) is unlikely to propagate into large-scale evolutionary trends observed in the fossil record. If the Phanerozoic trend reflected widespread selection for larger size at low taxonomic levels, we would expect to see most of the size trend explained by size increase within families, the lowest taxonomic level at which we can aggregate our data. These findings suggest that the factors favoring the overall trend toward larger size in marine animals relate to basic body plan and ecological life mode rather than competitive advantages associated with size differences within populations. These findings do not rule out an additional, smaller component related to widespread selection for larger size within populations, as there is also a component of size increase that occurs within families (fig. S5).

The taxonomic composition of the smallest and largest genera over time suggests the operation

Table 1. Results of model comparisons for the Phanerozoic trend in mean biovolume. Lower corrected Akaike information criterion (AICc) and higher Akaike weights indicate more support for a given model. logL is the log likelihood, and *K* is the number of free parameters in each model. The two-phase model has a break point at the Permian/Triassic boundary. The three-phase model has break points at the Permian/Triassic and Cretaceous/Paleogene boundaries. The best-fit model for each phase is used in multiphase models. The three-phase model is the best-supported model. See the supporting materials for details of the statistical methods (*23*). n/a, not applicable.

	logL	AICc	*K*	Akaike weight	Akaike weight single-phase model comparison
Random walk	53.7	-103.3	2	0.000	0.305
Driven trend	55.6	-104.9	3	0.000	0.695
Stasis	-63.7	131.5	2	0.000	0.000
Two-phase (driven trend/random walk)	60.5	-110.4	5	0.001	n/a
Three-phase (driven trend/stasis/driven trend)	71.2	-124.8	8	0.999	n/a

of constraints at the size extremes, even if these constraints are not required to model the overall distribution of animal sizes. The size minimum has been populated nearly exclusively by ostracods (a class of exclusively small-bodied crustaceans) since Silurian time (420 Ma). With the exception of the Middle/Late Triassic (235 Ma), where there is a maximum in ostracod size and a minimum in other animals, no other group in our data set comes within a factor of 6 of the smallest ostracod. The size maximum has been populated entirely by chordates since the Early Triassic (252 Ma), with no other genus since then coming within a factor of 2.5 of the largest chordate.

The dominance of a single phylum at each end of the size spectrum could result from simple incumbency effects, but transitions over time in the class affinities of the largest marine chordates suggest that physiology is also an important constraint, at least on the overall maximum size of marine animals. Nearly all of the largest solitary marine bilaterian genera have been reptiles and mammals. Tetrapods first reinvaded the oceans during Late Permian time (260 Ma) and rapidly occupied the size maximum (Fig. 3). Reptiles continued to dominate the top end of the size spectrum during the Mesozoic. Cetaceans were the first mammals to evolve a marine lifestyle and have occupied the largest marine body sizes since they first invaded the oceans during the Eocene (48 Ma) (Fig. 3). Air breathing is an exaptation (*25*) that can explain the rapid and widespread attainment of large size in marine reptiles and mammals. Relative to water, air has 20 to 30 times the concentration of O_2, is up to 100 times less viscous, has diffusion rates of O_2 through membranes that are 300,000 times faster, and is about 1000 times less dense (*26*). Thus, large animals are better able to meet their metabolic needs by breathing air than by breathing water. In fact, O_2 limitation has been proposed as a mechanism for limiting the evolutionary emergence of large, free-swimming, predatory bilateria generally (*27*, *28*).

Synoptic size data show that the average size of marine animals has increased substantially since the Cambrian and that this increase reflects differential diversification of large-bodied classes rather than neutral drift. A remaining question is the extent to which this differential diversification was enabled by intrinsic factors such as physiology, escalatory interactions between predators and prey (*29*), or changes in the physical and non-animal environment, such as oxygen availability (*30*) or the amount and quality of primary production (*7*). Testing among these controls will be critical to understanding how the physical and biological environments combine to shape the evolution of global ecosystems.

REFERENCES AND NOTES

1. R. H. Peters, *The Ecological Implications of Body Size* (Cambridge Univ. Press, Cambridge, 1983).
2. J. H. Brown, *Macroecology* (Univ. of Chicago Press, Chicago, 1995).
3. E. D. Cope, *Am. Nat.* **19**, 234–247 (1885).
4. E. D. Cope, *The Primary Factors of Organic Evolution* (Open Court, London, 1896).
5. C. J. J. Depéret, *The Transformations of the Animal World* (Paul, Trench, Trübner; London, 1909).
6. N. D. Newell, *Evolution* **3**, 103–124 (1949).
7. R. K. Bambach, *Paleobiology* **19**, 372–397 (1993).
8. J. G. Kingsolver, D. W. Pfennig, *Evolution* **58**, 1608–1612 (2004).
9. B. Rensch, *Evolution* **2**, 218–230 (1948).
10. J. Alroy, *Science* **280**, 731–734 (1998).
11. A. J. Arnold, D. C. Kelly, W. C. Parker, *J. Paleontol.* **69**, 203–210 (1995).
12. B. A. Maurer, *Evol. Ecol.* **12**, 925–934 (1998).
13. M. Laurin, *Syst. Biol.* **53**, 594–622 (2004).
14. D. W. E. Hone, T. M. Keesey, D. Pisani, A. Purvis, *J. Evol. Biol.* **18**, 587–595 (2005).
15. P. M. Novack-Gottshall, M. A. Lanier, *Proc. Natl. Acad. Sci. U.S.A.* **105**, 5430–5434 (2008).
16. D. Jablonski, *Nature* **385**, 250–252 (1997).
17. S. J. Gould, *J. Paleontol.* **62**, 319–329 (1988).
18. D. S. Moen, *J. Evol. Biol.* **19**, 1210–1221 (2006).
19. M. J. Monroe, F. Bokma, *J. Evol. Biol.* **23**, 2017–2021 (2010).
20. R. J. Butler, A. Goswami, *J. Evol. Biol.* **21**, 1673–1682 (2008).
21. J. H. Knouft, L. M. Page, *Am. Nat.* **161**, 413–421 (2003).
22. S. M. Stanley, *Evolution* **27**, 1–26 (1973).
23. Materials and methods are available as supplementary materials on *Science* Online.
24. J. J. Sepkoski Jr., *Bull. Am. Paleontol.* **363**, 1–500 (2002).
25. S. J. Gould, E. S. Vrba, *Paleobiology* **8**, 4–15 (1982).
26. D. Pauly, *Gasping Fish and Panting Squids: Oxygen, Temperature and the Growth of Water-Breathing Animals* (International Ecology Institute, Oldendorf, Germany, 2010).
27. T. W. Dahl *et al.*, *Proc. Natl. Acad. Sci. U.S.A.* **107**, 17911–17915 (2010).
28. E. A. Sperling *et al.*, *Proc. Natl. Acad. Sci. U.S.A.* **110**, 13446–13451 (2013).
29. G. J. Vermeij, *Annu. Rev. Ecol. Syst.* **25**, 219–236 (1994).
30. H. D. Holland, *Philos. Trans. R. Soc. London Ser. B* **361**, 903–915 (2006).

ACKNOWLEDGMENTS

We thank G. Griggs, M. Faerber, M. Laws, S. Sanghvi, L. Taylor, and the many undergraduate and high-school students for making body size measurements. J. Saltzman helped recruit high-school students. G. Hunt assisted with time series analysis. A. Clauset and M. A. Etnier kindly made their body size data on extant marine mammals available. Funding was provided by NSF grant EAR-1151022, the Stanford School of Earth Sciences, and the Swarthmore College James Michener Faculty Fellowship. Raw data files used for all analyses are permanently archived in the Stanford Digital Repository (http://purl.stanford.edu/rf761bx8302). This is Paleobiology Database publication 217.

SUPPLEMENTARY MATERIALS

www.sciencemag.org/content/347/6224/867/suppl/DC1
Materials and Methods
Figs. S1 to S6
Tables S1 to S3
Caption for Database S1
References (*31*–*120*)

18 August 2014; accepted 19 December 2014
10.1126/science.1260065

SPATIAL NAVIGATION

Disruption of the head direction cell network impairs the parahippocampal grid cell signal

Shawn S. Winter,* Benjamin J. Clark,*† Jeffrey S. Taube‡

Navigation depends on multiple neural systems that encode the moment-to-moment changes in an animal's direction and location in space. These include head direction (HD) cells representing the orientation of the head and grid cells that fire at multiple locations, forming a repeating hexagonal grid pattern. Computational models hypothesize that generation of the grid cell signal relies upon HD information that ascends to the hippocampal network via the anterior thalamic nuclei (ATN). We inactivated or lesioned the ATN and subsequently recorded single units in the entorhinal cortex and parasubiculum. ATN manipulation significantly disrupted grid and HD cell characteristics while sparing theta rhythmicity in these regions. These results indicate that the HD signal via the ATN is necessary for the generation and function of grid cell activity.

The ability to navigate is critical for survival of all animals and relies on a broad network of hippocampal and limbic brain circuits (*1*, *2*). The parahippocampal cortex contains grid cells, which fire at multiple locations, forming a hexagonal pattern covering the entire environment (*3*, *4*). Computational models explain grid cell generation from combined inputs of distance and direction displacement, which can subsequently be used for path integration (*5*–*7*). Theta rhythm is thought to be necessary for the computation of distance in grid cell models, and disruption of this signal eliminates gridlike firing patterns (*8*, *9*). HD cells fire as a function of an animal's directional orientation in the horizontal plane and are thought to convey the directional heading component to grid cells. However, some models use movement-direction cells, which have yet to be experimentally verified (*10*). The HD cell signal is generated subcortically and then projected rostrally via the anterior thalamic nuclei (ATN) to the parahippocampal cortices (*2*, *11*, *12*). Two nuclei within the ATN are known to contain HD cells—the anterodorsal and anteroventral thalamic nuclei (*13*, *14*). We tested the role of the HD signal in generating grid cell activity in the parahippocampal cortices.

Experiment 1 recorded from parahippocampal cortex, including medial entorhinal cortex (MEC) and parasubiculum, while female Long-Evans rats

Department of Psychological and Brain Sciences, Center for Cognitive Neuroscience, Dartmouth College, Hanover, NH 03755, USA.
*These authors contributed equally to this work. †Present address: Department of Psychology, University of New Mexico, Albuquerque, NM 87131, USA. ‡Corresponding author. E-mail: jeffrey.taube@dartmouth.edu

Downloaded from www.sciencemag.org on February 21, 2015

(n = 3) received infusions of lidocaine bilaterally into the ATN (*15*), which served to inactivate HD cell activity within this region. Lidocaine infusion resulted in a significant reduction of grid scores (Fig. 1G, left) at low doses (n = 55 cells; baseline mean ± SE: 0.746 ± 0.025; low inactivation: 0.502 ± 0.039; $t_{(54)}$ = 6.807, P < 0.001) (Fig. 1B) and high doses of lidocaine (n = 17 cells; baseline: 0.803 ± 0.038; high inactivation: 0.363 ± 0.056; $t_{(16)}$ = 7.112, P < 0.001) (Fig. 1C). For the high-dose group, 10 of 17 cells had reduced grid scores > 60% compared with baseline (>2 SD); the remaining cells all had decreased grid scores, and most of them had no discernible grid pattern during the inactivation session (Figs. 1C and 2C and fig. S6). Recovery of grid scores occurred ~1.5 hours after the infusion [n = 35 cells; low recovery: 0.680 ± 0.041; $t_{(34)}$ = 2.446, not significant (n.s.); n = 17 cells; high recovery: 0.762 ± 0.057; $t_{(16)}$ = 0.793, n.s.]. Grid scores were spared by saline infusions (n = 10 cells; baseline: 0.709 ± 0.084; saline: 0.763 ± 0.074; $t_{(9)}$ = 0.488, n.s.) (Fig. 1A). Lidocaine had the same effect upon peak firing rate (Fig. 1G right), which was significantly decreased by lidocaine infusions at low doses (n = 55 cells; baseline: 9.33 ± 0.46; low inactivation: 5.79 ± 0.37; $t_{(54)}$ = 6.696, P < 0.001) and high doses (n = 17 cells; baseline: 8.71 ± 0.89; high inactivation: 3.01 ± 0.72; $t_{(16)}$ = 7.162, P < 0.001) and recovered within ~1.5 hours (low: n = 35 cells; recovery: 8.28 ± 0.51; $t_{(34)}$ = 2.604, n.s.; high: n = 17 cells; recovery: 9.35 ± 0.95; $t_{(16)}$ = 0.693, n.s.). Decreased firing rates cannot account for the loss of the grid signal observed during inactivation because subsampling firing rates during baseline spared grid scores (fig. S4).

To understand the relationship between the concentration of lidocaine and the time course of inactivation, the inactivation session was divided into four consecutive blocks of 5 min. Saline infusion had no effect on grid scores or peak firing rates

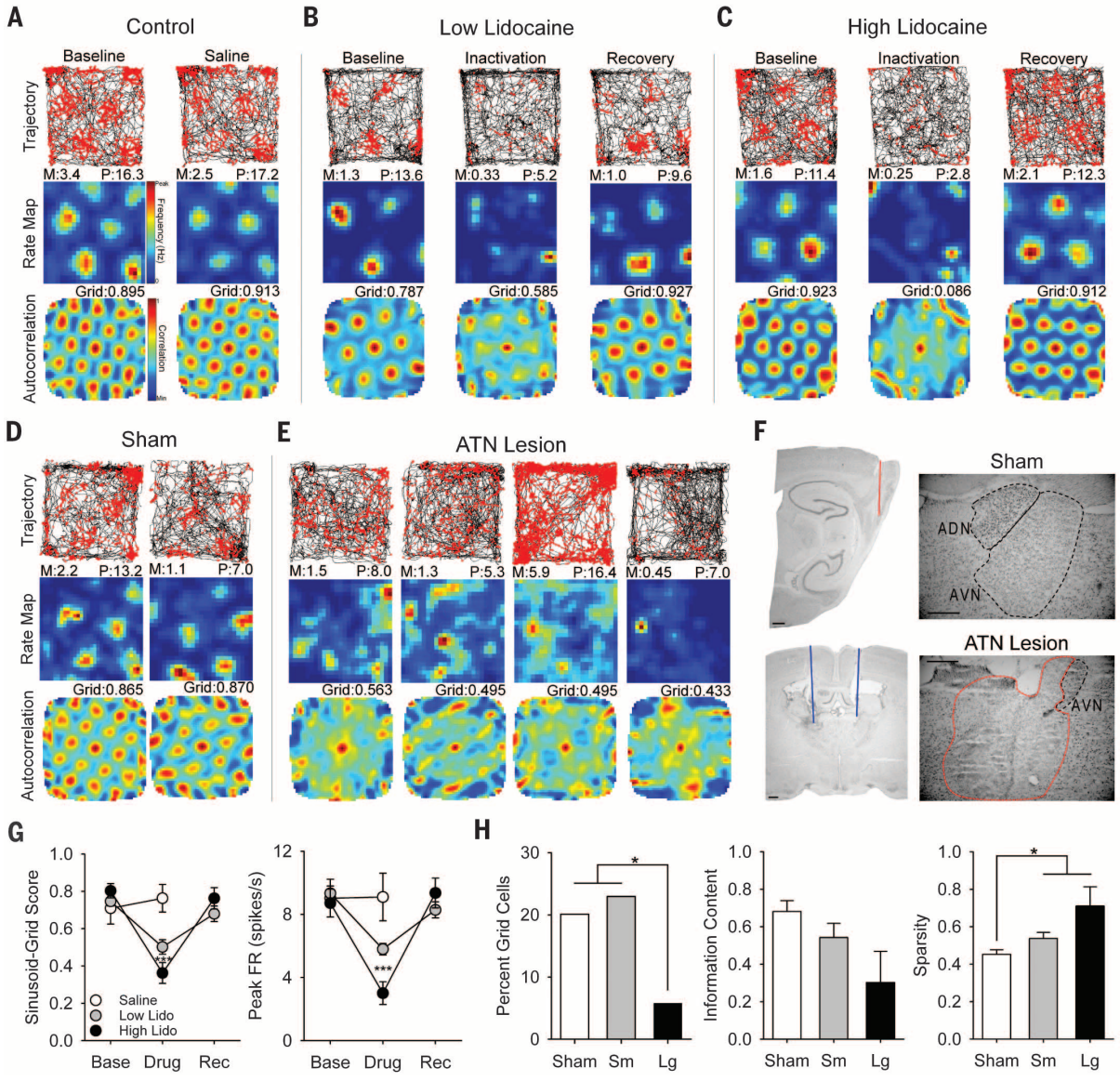


Fig. 1. Effects of ATN manipulation on grid cell activity. Grid cell response to (**A**) saline, (**B**) low-lidocaine, and (**C**) high-lidocaine infusions. Row 1: rat path and individual spikes (red dots). Row 2: smoothed firing rate map. Row 3: autocorrelation map. Column 1: baseline recording. Column 2: recording after infusion. Column 3: recording after ~1.5 hours of recovery. M, mean firing rate in spikes/s; P, peak firing rate in spikes/s, Grid, sinusoid-grid score. (**D**) Two grid cells from sham animals. (**E**) Four highest-scoring grid cells from ATN large-lesion animals. (**F**) Electrode track through the parahippocampal cortex (top left), guide cannulae placement (blue line) within ATN (bottom left), and representative ATN region from sham (top right) and ATN large lesion (bottom right) animals. Minimal healthy ATN tissue [specifically in anteroventral thalamic nucleus (AVN)] was observed in the lesioned group (healthy, black; lesioned, red). Only the right hemisphere is illustrated; however, this example is representative of bilateral damage in animals with ≥85% damage. Scale bars, 0.5 mm. (**G**) Data for sinusoid-grid score (left) and peak firing rate (right) measures, with asterisks indicating significant difference from baseline. (**H**) Data for percentage of grid cell (left), information content (bits/spike) (middle), and sparsity (right) measures. *P < 0.05; ***P < 0.001.

(Fig. 2, A and D). Low doses of lidocaine significantly impaired grid scores for the first three blocks, and scores recovered by the last block (n = 55 cells; baseline 5 min: 0.501 ± 0.034; $F_{(4,216)}$ = 7.647, P < 0.001; low-inactivation block 1: 0.314 ± 0.021, P < 0.001; block 2: 0.349 ± 0.029, P < 0.001; block 3: 0.374 ± 0.036, P < 0.010; block 4: 0.441 ± 0.033, n.s.) (Fig. 2, B and D). High doses significantly impaired grid scores that never recovered within the session (n = 17 cells; baseline 5 min: 0.634 ± 0.073; $F_{(4,64)}$ = 11.389, P < 0.001; high-inactivation block 1: 0.179 ± 0.041, P < 0.001; block 2: 0.200 ± 0.035, P < 0.001; block 3: 0.234 ± 0.047, P < 0.010; block 4: 0.352 ± 0.061, P < 0.010) (Fig. 2, C and D). Low doses significantly impaired peak firing rates for the first three blocks and recovered by the last block (n = 55 cells; baseline 5 min: 11.15 ± 0.50; $F_{(3.061,165.305)}$ = 14.035, P < 0.001; low-inactivation block 1: 6.77 ± 0.65, P < 0.001; block 2: 7.54 ± 0.56, P < 0.001; block 3: 7.54 ± 0.56, P < 0.010; block 4: 10.15 ± 0.58, n.s.). High doses significantly impaired peak firing rates for the first three blocks and recovered by the last block (n = 17 cells; baseline 5 min: 10.88 ± 1.04; $F_{(2.475,39.596)}$ = 30.301, P < 0.001; high inactivation block 1: 2.22 ± 0.65, P < 0.001; block 2: 2.65 ± 0.75, P < 0.001; block 3: 3.32 ± 1.01, P < 0.001; block 4: 7.62 ± 1.05, n.s.). These results are also consistent with mean firing rate (fig. S9) and overall suggest a dissociation between grid-specific firing and peak firing rate.

In experiment 2, we investigated whether permanent bilateral damage to the ATN disrupts grid cell generation. Short-term inactivation could impair network processing necessary for grid cell expression while sparing the mechanisms for generation. Recovery after permanent damage may allow for a compensatory mechanism to provide input suitable for grid cell generation. Sham and small (including <85% loss) ATN-lesioned animals had comparable numbers of grid cells exceeding the 95th percentile of a shuffled distribution (criterion = 0.439) of grid scores (sham, 48 of 239 = 20.8%; small lesion, 31 of 135 = 23.0%); however, large ATN lesions (including ≥85% loss) had significantly fewer cells pass the grid score criterion [large lesion, 3 of 52 = 5.8%; $\chi^2(1)$ = 4.62, P < 0.05] (Fig. 1, E and H, left). The effect was even more pronounced when using the 99th-percentile criterion (fig. S3). Overall, grid cells recorded in lesioned animals displayed appreciably lower information content (bits per spike) measures (sham: 0.682 ± 0.058; small lesion: 0.542 ± 0.076, W = 1067, P = 0.087; large lesion: 0.302 ± 0.166, W = 36, P = 0.097) (Fig. 1H, middle) and significantly higher sparsity scores (sham: 0.452 ± 0.025; small lesion: 0.537 ± 0.033, W = 1469, P < 0.05; large lesion: 0.710 ± 0.103, W = 132, P < 0.05) (Fig. 1H, right), suggesting that these cells fired across a broader range of spatial locations relative to sham animals. In addition, we failed to detect significant differences in the peak firing rates of grid cells between groups (sham: 5.78 ± 0.583; small lesion:

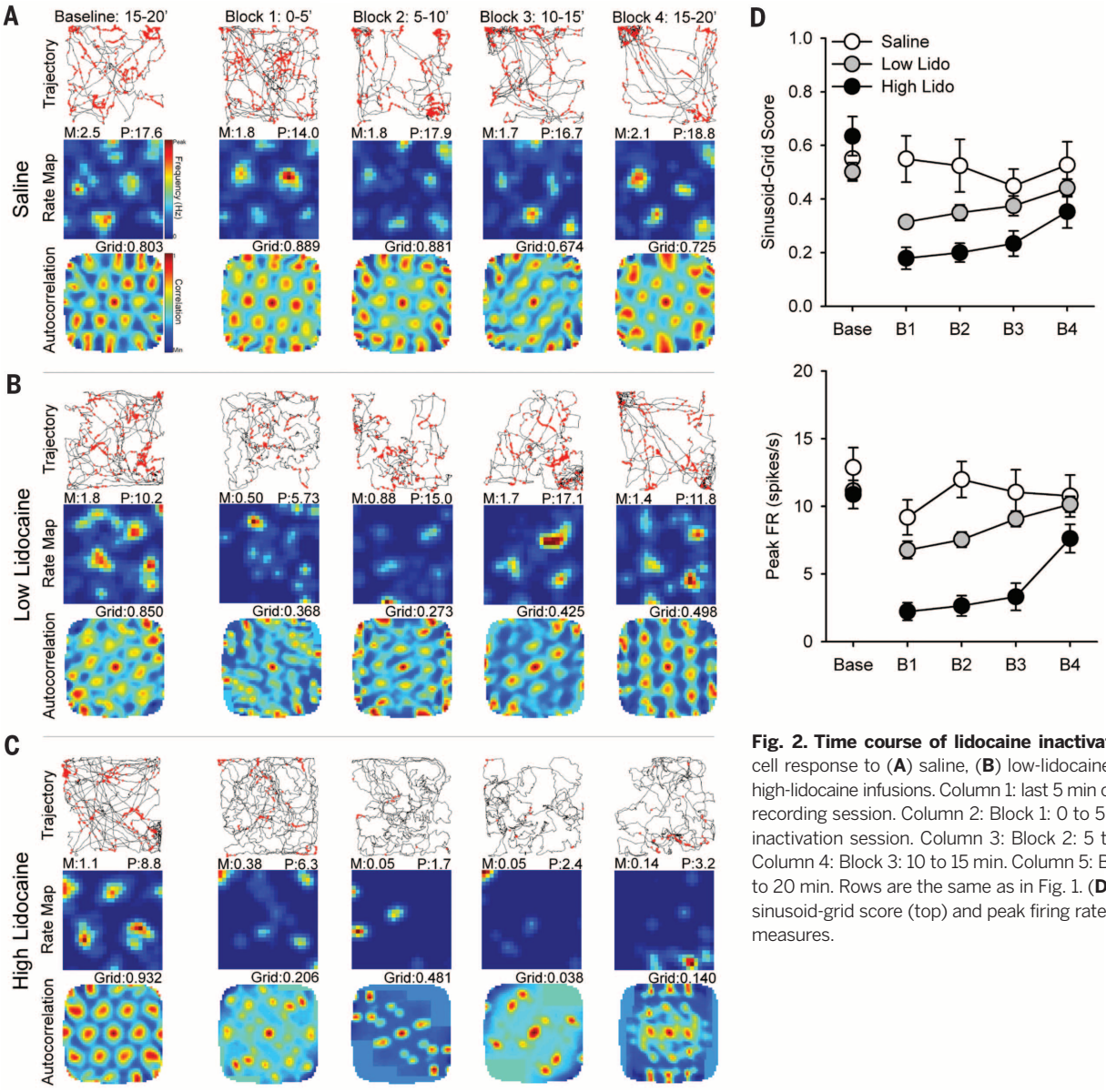


Fig. 2. Time course of lidocaine inactivation. Grid cell response to (**A**) saline, (**B**) low-lidocaine, and (**C**) high-lidocaine infusions. Column 1: last 5 min of baseline recording session. Column 2: Block 1: 0 to 5 min from inactivation session. Column 3: Block 2: 5 to 10 min. Column 4: Block 3: 10 to 15 min. Column 5: Block 4: 15 to 20 min. Rows are the same as in Fig. 1. (**D**) Data for sinusoid-grid score (top) and peak firing rate (bottom) measures.

5.21 ± 0.533; W = 1226, P = 0.892; large lesion: 9.89 ± 3.33; W = 115, P = 0.144).

We additionally recorded from cells that contained directional tuning (*16*). Most of these cells are better considered directionally modulated rather than "classic" HD cells because of their low peak firing rate and broad tuning curve. Experiment 1 lidocaine infusions produced a similar pattern of results on HD cells as they did on grid cells; however, a small sample size did not provide the power necessary to produce significant effects with an adjusted alpha, but there was a significance below $P < 0.05$. Mean vector length of HD cells was nonsignificantly reduced at low doses (n = 12 cells; baseline: 0.461 ± 0.041; low inactivation: 0.364 ± 0.063; $t_{(11)}$ = 1.730, n.s.) (Fig. 3, A and C, left) but was significantly reduced at high doses of lidocaine (n = 5 cells; baseline: 0.378 ± 0.036; high inactivation: 0.244 ± 0.063; $t_{(4)}$ = 4.538, $P < 0.05$) (Fig. 3, B and C, left). Peak firing rate of HD cells was nonsignificantly reduced at low doses (baseline: 7.80 ± 2.37; low inactivation: 4.68 ± 1.19; $t_{(11)}$ = 1.248, n.s.) (Fig. 3C, middle) but was significantly reduced at high doses of lidocaine (baseline: 4.89 ± 1.45; high inactivation: 0.72 ± 0.23; $t_{(4)}$ = 3.006, $P < 0.05$) (Fig. 3C, middle). When analyzed by 5-min blocks across the inactivation session, there was no effect of lidocaine at either concentration on mean vector length. However, there was a tendency for decreased mean vector length during the first block (low inactivation: baseline 5 min: 0.419 ± 0.056; block 1: 0.303 ± 0.065; $F_{(2.308,25.384)}$ = 2.490, n.s.; high inactivation: baseline: 0.394 ± 0.057; block 1: 0.244 ± 0.066; $F_{(4,16)}$ = 1.050, n.s.) (Fig. 3C, left). In contrast, peak firing rate was significantly decreased for the first block with low doses (baseline 5 min: 6.77 ± 1.52; $F_{(2.063,22.696)}$ = 7.091, $P < 0.010$.; block 1: 3.17 ± 0.72, $P < 0.05$; block 2: 5.50 ± 1.25, n.s.; block 3: 6.53 ± 1.38, n.s.; block 4: 8.37 ± 1.72, n.s.) and for three blocks with high doses of lidocaine (baseline: 7.53 ± 2.25; $F_{(4,16)}$ = 5.167, $P < 0.010$; block 1: 0.73 ± 0.13, $P < 0.05$; block 2: 0.60 ± 0.12, $P < 0.05$; block 3: 1.70 ± 0.70, $P < 0.05$; block 4: 3.36 ± 1.65, n. s.) (Fig. 3C, middle). Lidocaine's effect on peak firing rate likely influenced the measure of mean vector length, which is susceptible to reporting high values with few spikes (*17*). Although there were modest effects on HD cell mean vector length, simultaneously recorded cells had changes in mean vector length and grid score that were significantly correlated (r_s = 0.700, $P < 0.05$) (Fig. 3C, far right). Additionally, the effect of inactivation on grid and HD cell peak firing rates was highly correlated across sessions (low: r = 0.933; high: r = 0.976) and blocks (low: r = 0.828; high: r = 0.970). In cases where it was possible to examine the time course of recovery of HD-specific firing for HD cells or conjunctive grid-by-HD cells, the time of recovery generally correlated well with the time of recovery for grid cell characteristics (fig. S11).

Experiment 2 also observed a disruption in HD cell activity in parahippocampal cortices after ATN lesions. In lesioned rats, the number of cells that passed the 95th-percentile criterion of a shuffled distribution (criterion = 0.292) of mean vector length was not reduced for small lesions but was significantly reduced for large lesions [sham: 35 of 102 = 34.3%; small lesion: 6 of 31 = 19.4%; n.s.; large lesion: 7 of 97 = 7.2%; $\chi^2(1) = 14.55$, $P < 0.001$] (Fig. 3D, left, and E and F). Furthermore, cells that were classified as HD cells in lesioned animals showed significantly lower mean vector length (sham: 0.599 ± 0.030; small lesion: 0.442 ± 0.045, W = 206, $P < 0.001$; large lesion: 0.421 ± 0.067, W = 89, $P < 0.05$) (Fig. 3D, middle). HD cell peak firing rates were significantly reduced after large but not small lesions (sham: 3.13 ± 0.47; small lesion: 4.34 ± 1.41, n.s.; large lesion: 1.33 ± 0.39, W = 85, $P < 0.05$) (Fig. 3D, right).

Theta rhythm oscillations (6 to 10 Hz) in the MEC play a critical role in grid cell generation (*8*, *9*). Experiment 1 assessed theta rhythmicity in

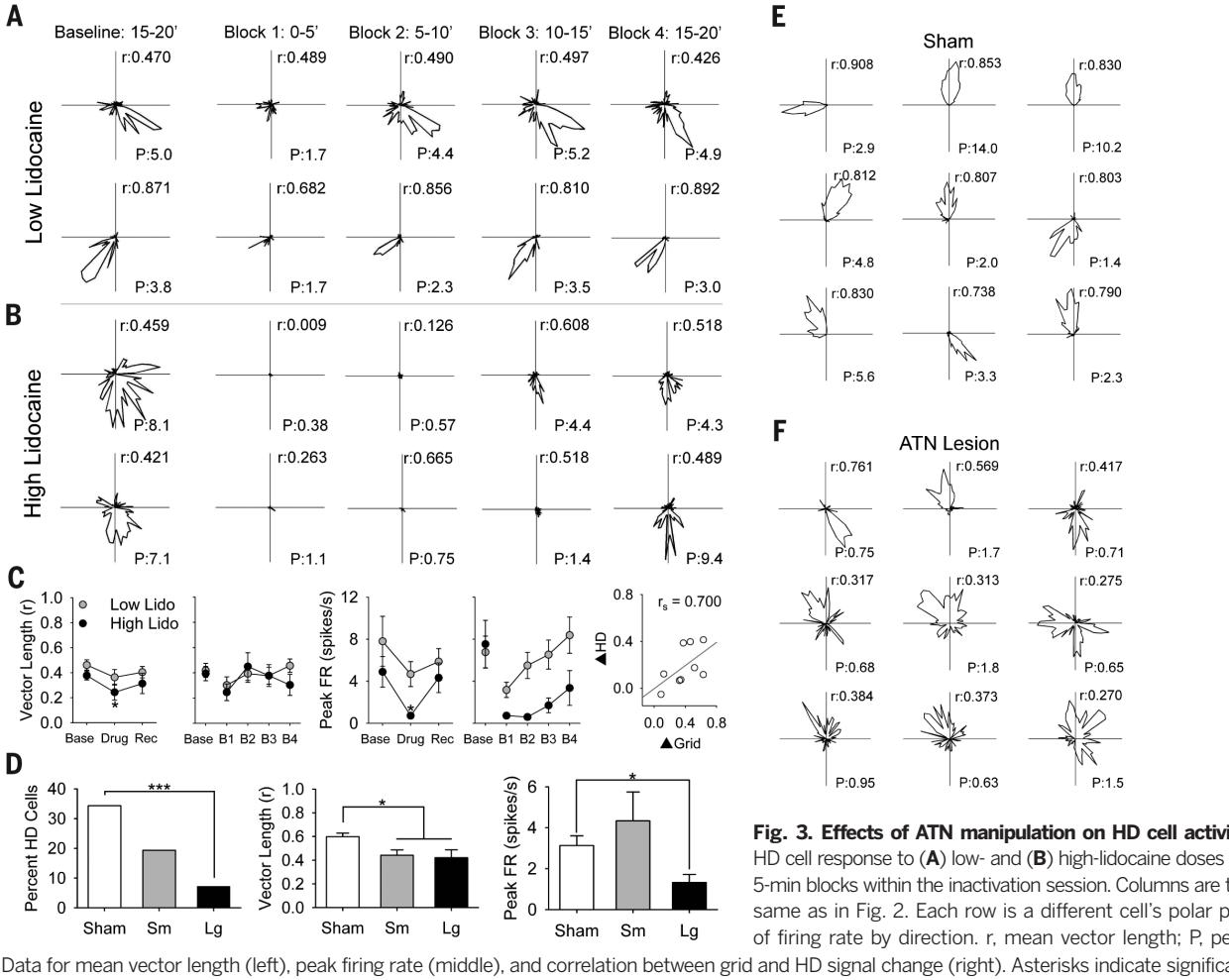


Fig. 3. Effects of ATN manipulation on HD cell activity. HD cell response to (**A**) low- and (**B**) high-lidocaine doses for 5-min blocks within the inactivation session. Columns are the same as in Fig. 2. Each row is a different cell's polar plot of firing rate by direction. r, mean vector length; P, peak firing rate. (**C**) Data for mean vector length (left), peak firing rate (middle), and correlation between grid and HD signal change (right). Asterisks indicate significant difference from baseline. (**D**) Data for percentage of HD cells (left), mean vector length (middle), and peak firing rate (right) measures. Examples of nine HD cells from sham (**E**) and ATN large lesion (**F**) animals. HD cells from ATN lesion animals have less robust polar plots, with lower r and P. *$P < 0.05$; ***$P < 0.001$.

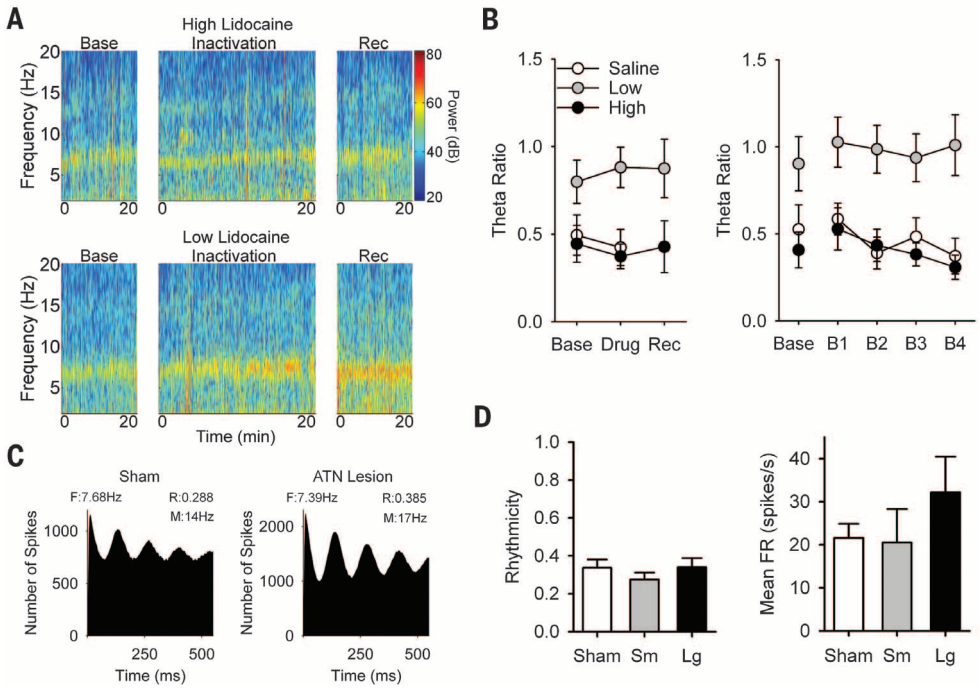


Fig. 4. Effects of ATN manipulation on theta rhythmicity. (**A**) Local field potential displaying theta rhythmicity from high (top) and low (bottom) doses of lidocaine. (**B**) Data for the measure of theta ratio. (**C**) Autocorrelation of spike timing from interneurons of sham (left) and large ATN lesion (right) animals. F, Frequency (Hz); R, rhythmicity; M, mean firing rate. (**D**) Data for rhythmicity (left) and mean firing rate (right) measures. Inactivation or lesion of ATN did not disrupt theta rhythmicity in parahippocampal cortices.

the local field potential by computing a theta ratio (theta power/delta power) (*8*, *18*). There was no significant effect of lidocaine on theta ratio at low doses across sessions (low baseline: 0.799 ± 0.123; low inactivation: 0.881 ± 0.114; $t_{(17)}$ = 0.860, n.s.) (Fig. 4, A and B, saline illustrated) or blocks (low baseline: 0.903 ± 0.156; $F_{(2.424,41.201)}$ = 0.194, n.s.; low block 1: 1.027 ± 0.144; low block 2: 0.987 ± 0.137; low block 3: 0.937 ± 0.138; low block 4: 1.010 ± 0.175). There was no significant effect of lidocaine on theta ratio at high doses across sessions (high baseline: 0.445 ± 0.105; high inactivation: 0.373 ± 0.071; $t_{(6)}$ = 1.453, n.s.) or blocks (high baseline: 0.408 ± 0.103; $F_{(1.446,8.677)}$ = 1.666, n.s.; high block 1: 0.529 ± 0.121; high block 2: 0.434 ± 0.093; high block 3: 0.382 ± 0.067; high block 4: 0.308 ± 0.069). Experiment 2 assessed theta rhythmicity in interneurons (firing rate > 10Hz) by computing the depth of modulation within spike timing autocorrelograms. There was no significant effect of ATN lesion on interneuron rhythmicity (sham: 0.336 ± 0.044; small lesion: 0.275 ± 0.036, n.s.; large lesion: 0.339 ± 0.048, n.s.) (Fig. 4, C and D, left). There was no effect of lesion on interneuron mean firing rate (sham: 21.59 ± 3.26; small lesion: 20.51 ± 7.82, n.s.; large lesion: 32.17 ± 8.30, n.s.) (Fig. 4D, right).

The present study supports three conclusions. First, manipulation of ATN significantly reduced the spatial periodicity of grid cells. High concentrations of lidocaine abolished gridlike firing patterns, and large lesions significantly reduced the number of grid cells. Second, manipulation of ATN significantly influenced the HD signal. Inactivation reduced direction-specific firing properties, and lesions significantly reduced the number of HD cells and their characteristics. Third, ATN manipulation spared theta modulation. These effects cannot be attributed to nearby damage from the injections or lesions because the ATN is more than 10 mm away from the grid cell areas recorded. Our findings are consistent with the hypothesis that HD cell inputs from the ATN are involved in parahippocampal grid cell generation; these data are also consistent with the hypothesis that cosine directionally tuned theta cells in the ATN are necessary for grid cell generation (*19*). In addition to HD and theta inputs, hippocampal projections from CA1 are necessary for grid cell expression in the MEC (*17*). HD cells in anterodorsal thalamic nucleus (ADN) (*20*) or MEC (*17*) remained unaffected by CA1 disruption, and many grid cells developed directional tuning even when no HD preference was identified before inactivation. This observation suggests that CA1 input likely does not contribute directional information to grid cells but instead conveys some other type of information. Behavioral studies provide support for the importance of these signals and brain regions in navigation. Lesions of the ATN produce significant deficits on spatial tasks dependent on either environmental (*21*) or self-movement cues (*22*). Similarly, lesions of the grid cell region of MEC produce significant spatial deficits (*23*, *24*); however, self-movement cues appear to be selectively impaired in distance processing (*25*). In contrast, hippocampal lesions produce significant impairments in both distance and direction processing (*25*–*27*). These results suggest that the functional role of grid cell activity may be related to providing a distance metric whose computations are dependent on direction inputs rather than supporting path integration, as some models posit.

REFERENCES AND NOTES

1. E. I. Moser, E. Kropff, M.-B. Moser, *Annu. Rev. Neurosci.* **31**, 69–89 (2008).
2. J. S. Taube, *Annu. Rev. Neurosci.* **30**, 181–207 (2007).
3. C. N. Boccara *et al.*, *Nat. Neurosci.* **13**, 987–994 (2010).
4. T. Hafting, M. Fyhn, S. Molden, M.-B. Moser, E. I. Moser, *Nature* **436**, 801–806 (2005).
5. N. Burgess, C. Barry, J. O'Keefe, *Hippocampus* **17**, 801–812 (2007).
6. M. E. Hasselmo, L. M. Giocomo, E. A. Zilli, *Hippocampus* **17**, 1252–1271 (2007).
7. B. L. McNaughton, F. P. Battaglia, O. Jensen, E. I. Moser, M.-B. Moser, *Nat. Rev. Neurosci.* **7**, 663–678 (2006).
8. M. P. Brandon *et al.*, *Science* **332**, 595–599 (2011).
9. J. Koenig, A. N. Linder, J. K. Leutgeb, S. Leutgeb, *Science* **332**, 592–595 (2011).
10. F. Raudies, M. P. Brandon, G. William Chapman, M. E. Hasselmo, *Brain Res.* (2014).
11. J. P. Bassett, M. L. Tullman, J. S. Taube, *J. Neurosci.* **27**, 7564–7577 (2007).
12. J. P. Goodridge, J. S. Taube, *J. Neurosci.* **17**, 9315–9330 (1997).
13. J. S. Taube, *J. Neurosci.* **15**, 70–86 (1995).
14. M. Tsanov *et al.*, *J. Neurosci.* **31**, 9489–9502 (2011).
15. Materials and methods are available as supporting materials on *Science* Online.
16. A. Burgalossi *et al.*, *Neuron* **70**, 773–786 (2011).
17. T. Bonnevie *et al.*, *Nat. Neurosci.* **16**, 309–317 (2013).
18. A. Terrazas *et al.*, *J. Neurosci.* **25**, 8085–8096 (2005).
19. A. C. Welday, I. G. Shlifer, M. L. Bloom, K. Zhang, H. T. Blair, *J. Neurosci.* **31**, 16157–16176 (2011).
20. E. J. Golob, J. S. Taube, *Proc. Natl. Acad. Sci. U.S.A.* **94**, 7645–7650 (1997).
21. E. C. Warburton, J. P. Aggleton, *Behav. Brain Res.* **98**, 27–38 (1999).
22. R. J. Frohardt, J. P. Bassett, J. S. Taube, *Behav. Neurosci.* **120**, 135–149 (2006).
23. C. Parron, B. Poucet, E. Save, *Behav. Brain Res.* **154**, 345–352 (2004).
24. C. Parron, E. Save, *Exp. Brain Res.* **159**, 349–359 (2004).
25. S. S. Winter, J. R. Köppen, T. B. N. Ebert, D. G. Wallace, *Hippocampus* **23**, 139–152 (2013).
26. E. J. Golob, J. S. Taube, *J. Neurosci.* **19**, 7198–7211 (1999).
27. H. Maaswinkel, I. Q. Whishaw, *Behav. Brain Res.* **99**, 143–152 (1999).

ACKNOWLEDGMENTS

The authors thank J. Marcroft, S. Valerio, and J. Barry for technical support. This research was supported through the National Institutes of Health grant NS053907 (J.S.T.), a Postgraduate Scholarship–Doctoral program (PGS-D) from the Natural Sciences and Engineering Research Council of Canada (B.J.C.), and an American Psychological Association Dissertation Research Award (B.J.C.). Data will be made available upon request.

SUPPLEMENTARY MATERIALS

www.sciencemag.org/content/347/6224/870/suppl/DC1
Materials and Methods
Figs. S1 to S12
Table S1
References (28–37)

4 August 2014; accepted 26 January 2015
Published online 5 February 2015;
10.1126/science.1259591

EVOLUTIONARY ECOLOGY

Cycles of species replacement emerge from locally induced maternal effects on offspring behavior in a passerine bird

Renée A. Duckworth,[1]* Virginia Belloni,[1,2] Samantha R. Anderson[1]

An important question in ecology is how mechanistic processes occurring among individuals drive large-scale patterns of community formation and change. Here we show that in two species of bluebirds, cycles of replacement of one by the other emerge as an indirect consequence of maternal influence on offspring behavior in response to local resource availability. Sampling across broad temporal and spatial scales, we found that western bluebirds, the more competitive species, bias the birth order of offspring by sex in a way that influences offspring aggression and dispersal, setting the stage for rapid increases in population density that ultimately result in the replacement of their sister species. Our results provide insight into how predictable community dynamics can occur despite the contingency of local behavioral interactions.

Interactions among individuals often drive population- and community-level patterns (*1*, *2*), and in turn, community dynamics and species interactions can affect individual variation in traits (*3*). Understanding these reciprocal feedbacks requires knowledge of the mechanisms underlying trait variation (*4*, *5*). Maternal effects can link phenotypic changes and environmental conditions across generations, making them a potentially important driver of population dynamics (*6*–*9*). In particular, offspring dispersal and competitive ability often depend on conditions experienced by the mother (*10*, *11*) and adaptively track changes in population density and resource abundance (*12*–*15*). The evolution of such adaptive responses requires a reliable link between the cue that induces the response and the environment in which the induced phenotype functions (*16*–*18*). Yet it is not clear how environmental variation can predictably trigger appropriate changes in phenotype.

Here we show that successional replacement of mountain bluebirds (*Sialia currucoides*) by their sister species, western bluebirds (*S. mexicana*), emerges as an indirect consequence of changes in competition experienced by western bluebird females and its impact on levels of aggression and dispersal in their offspring. The two species' ranges overlap in the northwestern United States, where they aggressively compete for nest cavities in successional post-fire habitat (*19*). Mountain bluebirds, the more dispersive species, colonize newly created habitat patches first but are eventually replaced by the slower to arrive (*20*–*22*), but more aggressive, western bluebirds (Fig. 1) (*23*). Differences in competitive ability and dispersal propensity produce cycles of species replacement that result in predictable changes in breeding density and competition for nest sites (Fig. 1) (*24*). An important part of this cycle is changes in western bluebird behavior over time: New habitat is colonized by aggressive dispersing males, and the proportion of nonaggressive-philopatric males increases over time (*24*). Maternal effects adaptively influence aggression and dispersal in western bluebirds, because the birth order of male offspring is negatively correlated with aggression and dispersal in adulthood (fig. S1) (*25*), and females produce a greater proportion of sons late in a clutch, when nest cavities on their territories are abundant, and a greater proportion of sons early in a clutch, when nest cavities are scarce (*25*). However, it is unclear how these maternal effects are induced and whether they mediate changes in aggression and dispersal during the process of colonization. To investigate this, we measured sex-biased birth order within and across populations that varied in colonization stage, experimentally manipulated nest cavity density to determine its effects on female behavior, and assessed the maternal allocation of androgens to eggs.

If maternal effects are driving changes in competitive ability and dispersal over time, then females breeding in newly colonized populations should produce a higher proportion of males later in a clutch as compared to females breeding in older populations. Comparison of sex-biased birth order (percentage of males laid in fourth to seventh position) of clutches (N = 106) across six populations (*26*) that varied in colonization stage (Fig. 2) revealed that, in populations with a low density of breeding western bluebirds, females produced more sons late in a clutch as compared to populations with a high density [Spearman's rank correlation (r_s) = –1.0,

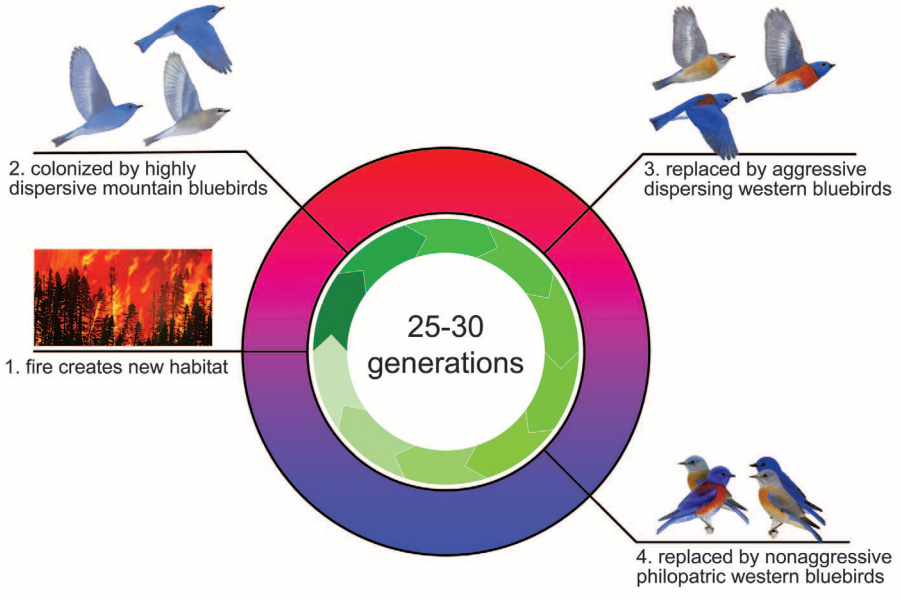


Fig. 1. Cycles of bluebird species replacement in post-fire habitat. New habitat is produced by fire (1) and colonized first by mountain bluebirds (2). Mountain bluebirds are replaced by aggressive dispersing western bluebirds (3), which in turn are replaced by nonaggressive philopatric individuals (4). Shading from red to purple indicates changes from high (early stages) to low (late stages) western bluebird aggression that are associated with increases in breeding density (*24*). The inner green ring indicates the predictable decrease in nest cavity availability as breeding density increases; darker arrows indicate greater resource availability. Post-fire forests provide habitat for up to 30 years. These cycles can be experimentally induced by creating new habitat, using nest boxes placed in open meadows where there are no natural nest cavities (*24*).

[1]Department of Ecology and Evolutionary Biology, University of Arizona, Tucson, AZ 85721, USA. [2]Department of Tropical Medicine, School of Public Health and Tropical Medicine, Tulane University, New Orleans, LA 70112, USA.
*Corresponding author. E-mail: rad3@email.arizona.edu

Downloaded from www.sciencemag.org on February 21, 2015

$P < 0.01$; Fig. 3A]. Across populations, the breeding density of western bluebirds was negatively correlated with the proportion of breeding mountain bluebird pairs ($r_s = -0.83$, $P = 0.04$), leading to a positive correlation between sex-biased birth order and mountain bluebird presence ($r_s = 0.82$, $P < 0.02$; Fig. 3A).

From among-population patterns, the cue that induces females to modify sex-biased birth order is unclear because multiple factors vary with population age. To disentangle these factors, we measured sex-biased birth order over 10 years in a population from which mountain bluebirds had already been excluded (*26*). At this site, the typical association of nest cavity availability and breeding density was reversed through the addition of nest boxes (fig. S2). Whereas under natural conditions the number of available nest cavities decreases as western bluebird population density increases, we increased nest cavity availability as western bluebird density increased (fig. S2). In contrast to the among-population pattern, in years of high conspecific density, females produced a higher proportion of sons late in a clutch [$F = 8.54$, standardized regression coefficient (b_{ST}) = 0.72, $P = 0.01$, $n = 10$ years, 190 nests]. However, this correlation was driven by an association of nest box density and sex-biased birth order ($F = 24.59$, $b_{ST} = 0.89$, $P = 0.001$; Fig. 3B): In years of high nest box density, females produced more sons late in a clutch, making nest box density a better predictor of sex-biased birth order ($t = 5.21$, $b_{ST} = 1.25$, $P = 0.001$) than conspecific density [t statistic (t) = −1.54, $b_{ST} = -0.36$, $P = 0.17$]. These patterns suggest that cues related to nest cavity availability, rather than the number of bluebirds in an area, induce the maternal effect.

How could the simple presence of unoccupied nest cavities trigger the adaptive adjustment of offspring phenotype? Western and mountain bluebirds defend exclusive territories, and the majority of competitive interactions among bluebirds occur in March and April, well before the onset of oogenesis, making them rare during the period when effects on sex-biased birth order are most likely (fig. S3). However, bluebirds defend their primary cavity throughout the breeding period from other species, and the peak of these non-bluebird intrusions overlaps with oogenesis (fig. S3). Thus, we hypothesized that females on territories with extra nest cavities experience differential competition from non-bluebird nest site competitors.

We tested this by experimentally creating territories of high and low nest cavity availability and recording female behavior during oogenesis (*26*). Females breeding on territories where nest cavity abundance was increased experienced fewer attempted takeovers of their primary nest cavity by competitors (0.65 ± 0.11/hour) than females

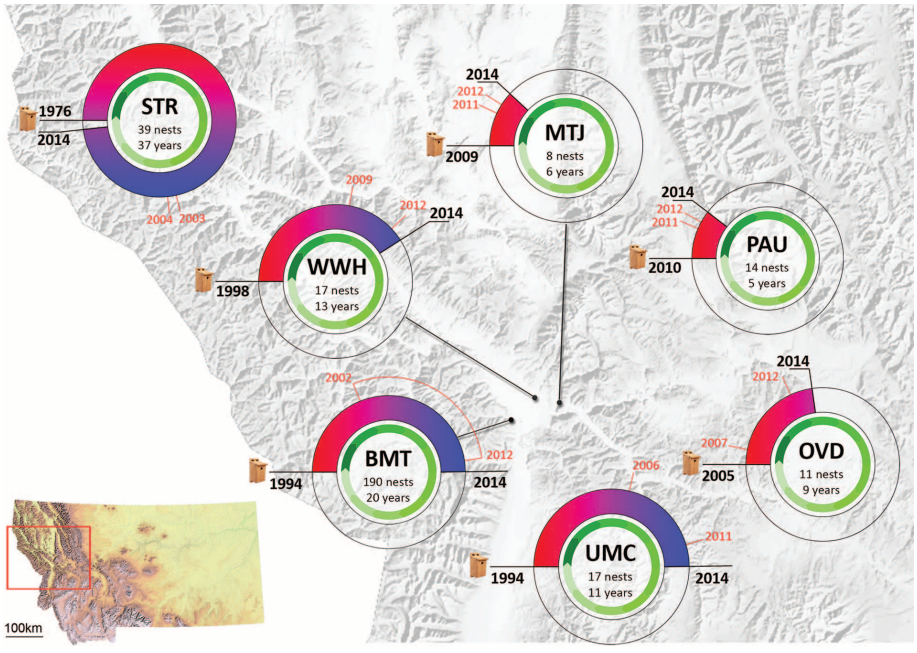


Fig. 2. Colonization stages of study populations in western Montana. The shading of the outer circle shows the start of new habitat (nest box symbol) and the population's current cycle stage (Fig. 1). Red lines transecting the outer ring indicate sampling time. The text in a circle shows population name (OVD, UMC, PAU, WWH, MTJ, and STR), sample size, and time since western bluebirds' colonization.

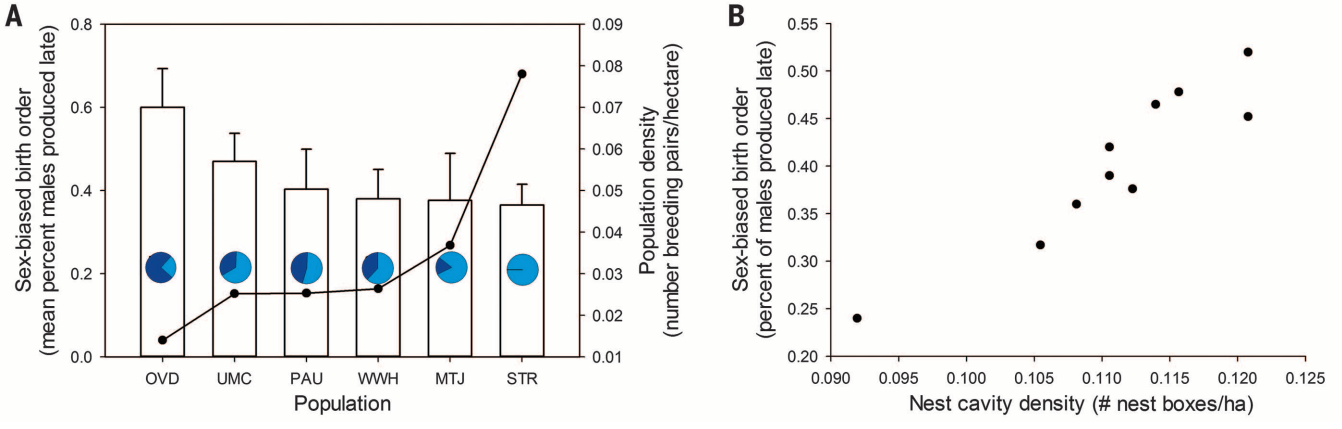


Fig. 3. Among- and within-population variation in sex-biased birth order. (**A**) Sex-biased birth order (bars with standard errors) was negatively correlated with conspecific density (dotted line) and positively correlated with the presence of mountain bluebirds (pie charts). Dark and light blue indicate the percent of territories occupied by mountain and western bluebirds, respectively. (**B**) In years of high nest cavity density, in which nest sites were abundant, females produced sons later in the clutch as compared to years of low nest cavity density ($n = 10$ years).

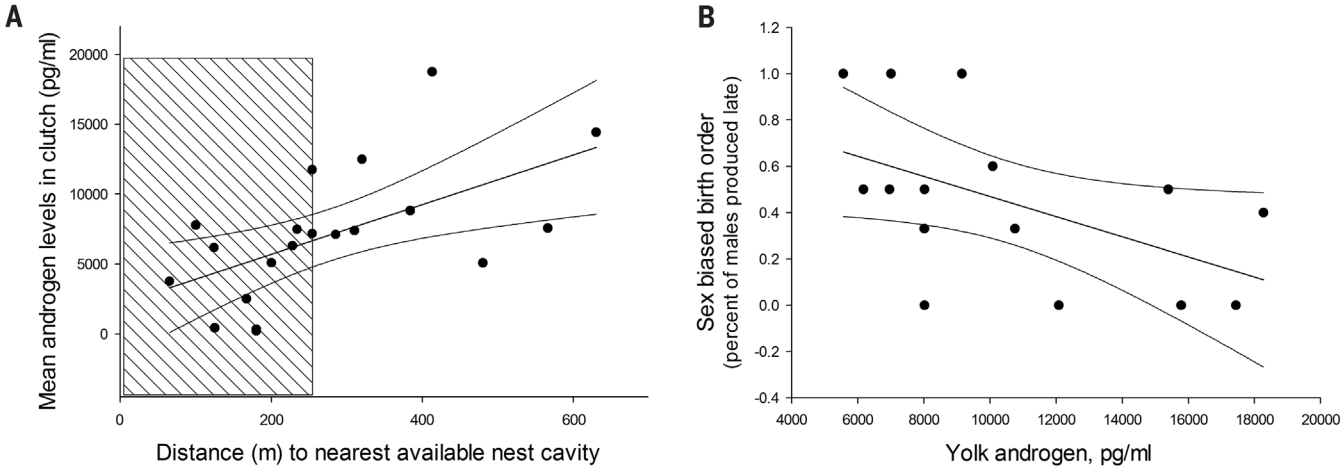


Fig. 4. Androgen allocation to a clutch is a key link between sex-biased birth order and resource availability. (**A**) Mean androgen levels were positively related to the distance to the nearest unoccupied nest cavity. The hatched area indicates distances within a typical bluebird territory. (**B**) Clutches in which females produced sons late in the birth order contained less androgen than did clutches in which females produced sons early. Shown are 95% confidence intervals.

on control territories, which had only a single nest cavity (1.75 ± 0.42/hour; $t_{52} = -2.50$, $P < 0.02$). Intrusion rates of competitor species and female aggressive response rates were correlated ($r = 0.90$, $P < 0.0001$), so that females on multicavity territories engaged in fewer aggressive interactions (0.73 ± 0.15/hour) than did females on single-cavity territories (1.70 ± 0.42/hour, $t_{52} = -2.17$, $P < 0.05$). In vertebrates, engaging in aggressive interactions influences physiology, such as the concentration of circulating steroid hormones (*27*, *28*), which can influence both sex-biased birth order and maternal allocation of hormones to eggs (*29*, *30*).

To determine whether variation in the local competitive environment influenced females' deposition of hormones in eggs, we used enzyme immunoassays to measure yolk androgens (*26*)—which are known to have both short- and long-term effects on offspring competitive behavior (*31*, *32*)—from 20 clutches of eggs collected from a population in which nest cavity density was highly variable. Androgen allocation to eggs differed significantly among clutches (fig S4), and females with extra nest cavities allocated less androgen to their clutches than did females without extra nest cavities on their territories ($F = 9.04$, $b_{ST} = 0.58$, $P < 0.01$; Fig. 4A). To determine whether androgen variation among clutches was linked to sex-biased birth order, we biopsied yolk samples from 15 additional clutches, allowed offspring to develop normally, and determined their sex (*26*). Clutches with a higher percentage of males early had higher androgen levels than clutches with a higher percentage of males in later positions ($r_s = -0.54$, $P < 0.05$, $n = 15$ clutches; Fig. 4B). These results suggest that hormone allocation to egg yolk is a key link between resource abundance, sex-biased birth order, and changes in offspring behavior.

Maternally induced variation in western bluebird behavior ultimately results in the displacement of mountain bluebirds, as females from crowded populations produce aggressive sons that colonize new areas. However, the cue that induces the maternal effect has no direct connection to this larger-scale pattern. Instead, the process of colonization itself sets the stage for rapid changes in aggression over time. By dominating mountain bluebirds and acquiring large resource-rich territories (*19*), the colonizing generation creates the environment that induces rapid changes in offspring aggression and population growth. As habitat patches become crowded, females then produce aggressive sons, which disperse and colonize new areas, restarting the cycle. The extreme limitation of nest cavities for secondary cavity-nesting species means that there will always be competitor species intruding on bluebird territories, making competitive interactions over nest sites a reliable cue of the availability of parental resources. Thus, our results provide insight into how predictable community dynamics can occur despite the contingent nature of local-scale behavioral interactions.

REFERENCES AND NOTES

1. S. A. Levin, *Ecology* **73**, 1943–1967 (1992).
2. M. A. Leibold *et al.*, *Ecol. Lett.* **7**, 601–613 (2004).
3. L. Ginzburg, M. Colyvan, *Ecological Orbits: How Planets Move and Populations Grow* (Oxford Univ. Press, New York, 2004).
4. E. E. Werner, *Am. Nat.* **140**, S5–S32 (1992).
5. D. E. Bowler, T. G. Benton, *Biol. Rev. Camb. Philos. Soc.* **80**, 205–225 (2005).
6. A. V. Badyaev, R. L. Young, G. E. Hill, R. A. Duckworth, *J. Evol. Biol.* **21**, 449–460 (2008).
7. M. Rossiter, *Annu. Rev. Ecol. Syst.* **27**, 451–476 (1996).
8. J. Bernardo, *Am. Zool.* **36**, 83–105 (1996).
9. L. R. Ginzburg, D. E. Taneyhill, *J. Anim. Ecol.* **63**, 79–92 (1994).
10. A. J. Zera, R. F. Denno, *Annu. Rev. Entomol.* **42**, 207–230 (1997).
11. M. Massot, J. Clobert, *J. Evol. Biol.* **13**, 707–719 (2000).
12. K. Donohue, *Am. Nat.* **154**, 674–689 (1999).
13. R. F. Denno, G. K. Roderick, K. L. Olmstead, H. Döbel, *Am. Nat.* **138**, 1513–1541 (1991).
14. R. G. Harrison, *Annu. Rev. Ecol. Syst.* **11**, 95–118 (1980).
15. B. Dantzer *et al.*, *Science* **340**, 1215–1217 (2013).
16. T. J. DeWitt, A. Sih, D. S. Wilson, *Trends Ecol. Evol.* **13**, 77–81 (1998).
17. T. Getty, *Am. Nat.* **148**, 378–385 (1996).
18. A. V. Badyaev, T. Uller, *Philos. Trans. R. Soc. London Ser. B* **364**, 1169–1177 (2009).
19. R. A. Duckworth, in *Avian Urban Ecology: Behavioural and Physiological Adaptations*, D. Gil, H. Brumm, Eds. (Oxford Univ. Press, Oxford, 2013), pp. 181–191.
20. R. L. Hutto, *Conserv. Biol.* **9**, 1041–1058 (1995).
21. N. B. Kotliar, P. L. Kennedy, K. Ferree, *Ecol. Appl.* **17**, 491–507 (2007).
22. V. A. Saab, R. E. Russell, J. G. Dudley, *Condor* **109**, 97–108 (2007).
23. R. A. Duckworth, A. V. Badyaev, *Proc. Natl. Acad. Sci. U.S.A.* **104**, 15017–15022 (2007).
24. R. A. Duckworth, *Am. Nat.* **172**, S4–S17 (2008).
25. R. A. Duckworth, *Philos. Trans. R. Soc. London Ser. B* **364**, 1075–1086 (2009).
26. Materials and methods available as supplementary materials on *Science* Online.
27. J. C. Wingfield, *Horm. Behav.* **48**, 253–255, discussion 256–258 (2005).
28. B. Silverin, *Anim. Behav.* **56**, 811–818 (1998).
29. O. P. Love, E. H. Chin, K. E. Wynne-Edwards, T. D. Williams, *Am. Nat.* **166**, 751–766 (2005).
30. T. W. Pike, M. Petrie, *Biol. Rev. Camb. Philos. Soc.* **78**, 553–574 (2003).
31. H. Schwabl, *Proc. Natl. Acad. Sci. U.S.A.* **90**, 11446–11450 (1993).
32. C. M. Eising, W. Müller, T. G. Groothuis, *Biol. Lett.* **2**, 20–22 (2006).

ACKNOWLEDGMENTS

We thank Mountain Bluebird Trails members for access to trails. A. Badyaev, D. Higginson, C. Gurguis, E. Morrison, S. Aguillon, J. Padway, and two anonymous reviewers provided helpful comments on a draft of this manuscript. This work was funded by NSF (grant DEB-918095). Data are available in the supplementary materials.

SUPPLEMENTARY MATERIALS

www.sciencemag.org/content/347/6224/875/suppl/DC1
Materials and Methods
Figs. S1 to S5
References (*33*–*44*)

19 August 2014; accepted 16 January 2015
10.1126/science.1260154

INSULIN GRANULES

Insulin secretory granules control autophagy in pancreatic β cells

Alexander Goginashvili,[1] Zhirong Zhang,[1] Eric Erbs,[1] Coralie Spiegelhalter,[1] Pascal Kessler,[1] Michael Mihlan,[1] Adrien Pasquier,[1] Ksenia Krupina,[1] Nicole Schieber,[2] Laura Cinque,[3] Joëlle Morvan,[1] Izabela Sumara,[1] Yannick Schwab,[2] Carmine Settembre,[3,4] Romeo Ricci[1,5]*

Pancreatic β cells lower insulin release in response to nutrient depletion. The question of whether starved β cells induce macroautophagy, a predominant mechanism maintaining energy homeostasis, remains poorly explored. We found that, in contrast to many mammalian cells, macroautophagy in pancreatic β cells was suppressed upon starvation. Instead, starved β cells induced lysosomal degradation of nascent secretory insulin granules, which was controlled by protein kinase D (PKD), a key player in secretory granule biogenesis. Starvation-induced nascent granule degradation triggered lysosomal recruitment and activation of mechanistic target of rapamycin that suppressed macroautophagy. Switching from macroautophagy to insulin granule degradation was important to keep insulin secretion low upon fasting. Thus, β cells use a PKD-dependent mechanism to adapt to nutrient availability and couple autophagy flux to secretory function.

Upon feeding, the pancreatic β cell catabolizes nutrients to secrete insulin. Conversely, insulin secretion decreases upon fasting (*1*). A shortage of nutrients also induces macroautophagy (hereafter referred to as "autophagy"). During autophagy, cellular components are sequestered into autophagosomes and degraded upon targeting to lysosomes (autolysosomes). Resulting catabolites maintain cells in a metabolically active state and ensure cell survival (*2*). However, catabolism of nutrients could also trigger insulin release, which should be avoided during fasting. Autophagy might thus be a bad strategy for a β cell to cope with nutrient deprivation. Both induction and lack of induction of autophagy have been reported in fasted β cells (*3*, *4*). We thus wanted to assess the importance of autophagy in fasted β cells.

Microtubule-associated protein 1 light chain 3 B (LC3B) incorporates into membranes of autophagosomes (*5*). Unexpectedly, INS1 cells (a rat insulinoma–derived β cell line) exogenously expressing LC3B tagged with green fluorescent protein (GFP) (LC3B-GFP) deprived of serum and amino acids or glucose (Glc), but not of serum alone, decreased LC3B-GFP puncta (fig. S1, A to C). Conversely, starved human embryonic kidney (HEK) 293 cells increased LC3B-GFP puncta (fig. S1, D and E) (*6*). INS1 cells endogenously expressing LC3B-GFP (INS1$^{LC3B\text{-}GFPendo}$ cells) (fig. S2, A to C) treated without or with bafilomycin A1 (BafA1), which blocks autolysosomal degradation of LC3B (*7*), decreased LC3B-GFP puncta upon starvation (Fig. 1A and fig. S2, D to F). Tandem RFP-GFP–tagged LC3 (ptfLC3; RFP, red fluorescent protein) allows for discrimination of yellow fluorescent autophagosomes and red fluorescent autolysosomes (*8*). Multiple RFP-GFP puncta were converted into RFP-only puncta upon the onset of starvation. A reduction in RFP puncta and no reappearance of RFP-GFP puncta were observed over time (fig. S3, A and B). Correlative light and electron microscopy (CLEM) confirmed their autophagic origin (Fig. 1B). Moreover, lipidated autophagosomal LC3B (LC3B-II) decreased in starved INS1 cells in the absence and presence of BafA1 (Fig. 1C). In contrast, starvation increased LC3B-II in HEK293 cells (fig. S4). p62 binds polyubiquitinylated substrates for targeting to autophagosomes (*9*). p62 was moderately increased during starvation, independent of BafA1 (Fig. 1C). p62 puncta clustered and increased in size (fig. S5A). Accordingly, p62/LC3B-GFP colocalization was decreased, indicating suppressed autophagy-dependent clearance of p62. ATG16L1 binds to preautophagosomes (*10*). ATG16L1- and ATG16L1/LC3B-GFP–positive puncta moderately decreased upon starvation (fig. S5B). Quantitative electron microscopy (QEM) confirmed reduced autophagic compartments in β cells of starved murine primary islets (fig. S6). Moreover, in LC3B-GFP–expressing mice (*11*), autophagosomes decreased in β cells upon fasting (Fig. 1D and fig. S7). What about other secretory cells, in which nutrients do not act as secretagogues? In contrast to β cells, primary murine plasma cells induced autophagy upon starvation, whereas secretion of immunoglobulin G was reduced (fig. S8, A and B). Thus, nutrient-sensing β cells appear to use a distinct mechanism to overcome shortage of nutrients.

Targeting of secretory granules (SGs) to lysosomes might be an alternative strategy (*12*). Lysosomal Lamp1 and SG protein Phogrin colocalized close to the Golgi upon starvation in INS1 cells. Lysosomal inhibitors (LIs) increased their colocalization (fig. S9, A to C). QEM, immunogold labeling, and CLEM revealed abundant granule-containing lysosomes (GCLs) (fig. S10, A to D). We next used density gradients to purify GCLs (see supplementary materials and methods). Upon starvation, Phogrin- and lysosomal Lamp2-positive signals shifted to heavier fractions containing GCLs. LC3B was almost undetectable in shifted fractions, suggesting independence of GCLs from autophagy (Fig. 2A). Accordingly, starvation did not increase LC3B-GFP/Phogrin colocalization (fig. S11). Moreover, inactivation of autophagy did not change the amount of GCLs in starved cells (fig. S12, A and B).

Secretory granules are generated at the Golgi. Proinsulin, a marker for nascent SGs (*13*), markedly decreased upon starvation (Fig. 2B). Its reduction was partially restored by LIs. Abundant GCLs were confirmed ex vivo by QEM of starved primary murine islets (Fig. 2C and fig. S13A). In fasted GFP-LC3B–expressing mice, Lamp2 and proinsulin/insulin [(Pro)insulin] colocalization increased, whereas there was no increase in LC3B-GFP/(Pro)insulin colocalization (Fig. 2D and fig. S13, B and C). Thus, β cells employ starvation-induced nascent granule degradation (SINGD) instead of autophagy during fasting.

Lysosome-derived amino acids induce translocation of mechanistic target of rapamycin (mTOR) complex 1 (mTORC1) to lysosomal membranes, mTORC1 activation (*14*, *15*), and subsequent suppression of autophagy (*16*–*18*). The mTOR inhibitors rapamycin and torin 1 increased the number of LC3B-GFP puncta in starved INS1 cells (Fig. 3A). Moreover, starvation localized mTOR to Phogrin/Lamp1-positive puncta close to the Golgi (Fig. 3B). mTORC1 suppresses starvation-induced autophagy through phosphorylation of Unc-51–like kinase 1 (ULK1) (*19*). Indeed, phospho-ULK1 remained high upon starvation and was abolished by rapamycin, whereas mTORC1-mediated phosphorylation of S6K1 (*20*) diminished during starvation (Fig. 3C). Accordingly, S6K1 phosphorylation was shown to require higher mTOR activity than ULK1 phosphorylation (*21*). Moreover, starvation led to formation of large phospho-ULK1 puncta that colocalized with Lamp1/Phogrin (fig. S14, A and B). Thus, nutrient depletion leads to induction of SINGD that locally activates mTOR to suppress autophagy.

Fasting suppresses both insulin secretion and autophagy. Would insulin secretion increase if autophagy is induced upon starvation? Keeping autophagy high by rapamycin precluded suppression of insulin secretion in INS1 cells (fig. S15). We next used tat-beclin1 (*22*) to specifically trigger autophagy in β cells of murine primary islets upon nonstimulatory Glc (fig. S16, A and B). Tat-beclin1 increased insulin secretion

[1]Institut de Génétique et de Biologie Moléculaire et Cellulaire (IGBMC), INSERM, CNRS, Université de Strasbourg, 67404 Illkirch, France. [2]Cell Biology and Biophysics Unit, European Molecular Biology Laboratory (EMBL), 69117 Heidelberg, Germany. [3]Dulbecco Telethon Institute and Telethon Institute of Genetics and Medicine (TIGEM), 80131 Naples, Italy. [4]Medical Genetics, Department of Medical and Translational Science Unit, Federico II University, Via Pansini 5, 80131 Naples, Italy. [5]Nouvel Hôpital Civil, Laboratoire de Biochimie et de Biologie Moléculaire, Université de Strasbourg, 67091 Strasbourg, France.
*Corresponding author. E-mail: romeo.ricci@igbmc.fr

Downloaded from www.sciencemag.org on February 21, 2015

to levels comparable with those observed upon stimulatory Glc (fig. S16C). Potassium channel closure that evokes calcium influx and exocytosis of SGs (*1*) was required, as the potassium channel activator diazoxide abolished this effect (fig. S16D). Insulin secretion was also potentiated by tat-beclin1 in murine islets at stimulatory Glc, which was blocked by diazoxide (fig. S16, E and F). Tat-beclin1 also increased insulin secretion from ex vivo fasted human islets (Fig. 3D and fig. S17, A and B). Thus, SINGD-mediated suppression of autophagy is important to keep insulin secretion low during fasting.

Protein kinase D (PKD) controls insulin SG biogenesis at the Golgi (*23*, *24*). Thus, PKD inactivation could have an effect on the turnover of nascent SGs. Indeed, inhibition of PKD decreased the amount of proinsulin (Fig. 4A). Proinsulin biosynthesis was unchanged in PKD1-depleted cells (fig. S18, A and B). However, accumulation of newly formed insulin was decreased, suggesting enhanced degradation of de novo synthesized insulin (fig. S18C). QEM and immunogold analyses revealed abundant GCLs in the Golgi area (Fig. 4B and fig. S19, A and B), which was further corroborated by subcellular fractionation (fig. S19C). PKD inhibition increased Phogrin/Lamp1 colocalization, which was more prominent upon LI treatment (fig S19, D to F). Phogrin/LC3B-GFP colocalization remained unchanged (fig. S20). mTOR largely colocalized with Lamp1 (Fig. 4C), and phospho-ULK1 was increased (Fig. 4D) in PKD1-depleted cells. PKD1 knockdown decreased accumulation of LC3B-II in the presence of BafA1 (fig. S21A). Moreover, PKD inhibition decreased LC3B-GFP puncta in absence and presence of BafA1 (fig. S21B).

If PKD controls SINGD, its activity should be regulated by nutrients. PKD activity at the Golgi decreased upon starvation (fig. S22, A and B). Loss of the p38δ kinase leads to activation of PKD in β cells (*23*). GCLs were markedly decreased in β cells of ex vivo fasted *p38δ* knockout ($p38\delta^{-/-}$) islets (Fig. 4E and fig. S23A). Accordingly, (Pro)insulin/Lamp2 colocalized to a lesser extent in β cells of fasted $p38\delta^{-/-}$ mice (fig. S23, C and D), suggesting that high PKD activity prevents SINGD. In contrast, autophagic compartments were increased in fasted $p38\delta^{-/-}$ β cells, indicating that SINGD-dependent suppression of autophagy was diminished (Fig. 4E and fig. S23B). Thus, PKD is a major regulator of SINGD and autophagy in β cells.

Altogether, inactivation of PKD evokes SINGD, localized activation of mTOR, and suppression of autophagy, which is critical to prevent insulin release during fasting. On the other hand, PKD activity is required for SG biogenesis (Fig. 4F). Because the nascent SGs are preferentially secreted (*25*), SINGD-mediated suppression of autophagy may represent an optimal strategy to counteract insulin secretion, at the same time providing sufficient nutrients. Because SINGD-mediated suppression of autophagy depends on abundant nascent SGs, their depletion will probably derepress autophagy without increasing insulin release. Timing when depletion occurs may vary substantially depending on the models and protocols used and may thus explain previously

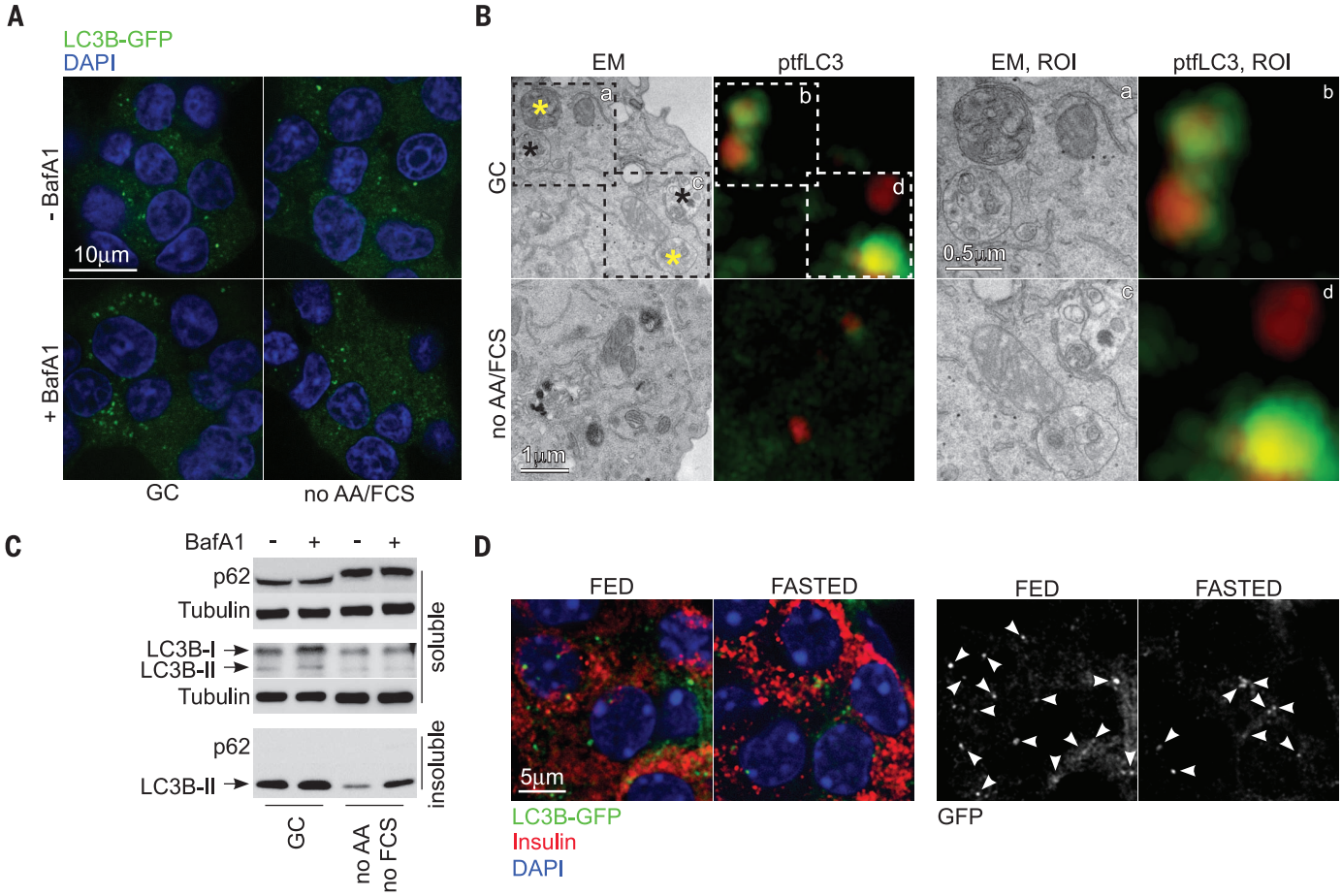


Fig. 1. Nutrient depletion suppresses autophagy in β cells. (**A**) LC3B-GFP puncta in INS1$^{LC3B\text{-}GFPendo}$ cells under growing culture (GC) and no amino acids and fetal calf serum (AA/FCS) for 1 hour in the absence and presence of BafA1 (10 nM). DAPI, 4′,6-diamidino-2-phenylindole. (**B**) CLEM of ptfLC3-expressing INS1 cells under GC and no AA/FCS for 2 hours. Regions of interest (ROI) are indicated with labeled dashed squares. Yellow and black asterisks indicate autophagosomes and autolysosomes, respectively. EM, electron microscopy. (**C**) Immunoblot of LC3B and p62 using soluble and insoluble fractions of lysates of INS1 cells under GC and no AA/FCS for 1.5 hours, nontreated or treated with 1 nM BafA1 for the last hour of incubation. Glyceraldehyde-3-phosphate dehydrogenase (GAPDH) served as a loading control. (**D**) Immunofluorescence (IF) of LC3B-GFP puncta (white arrowheads) and insulin (red) in β cells in islets of fed and fasted LC3B-GFP–expressing mice. The nuclei were stained with DAPI.

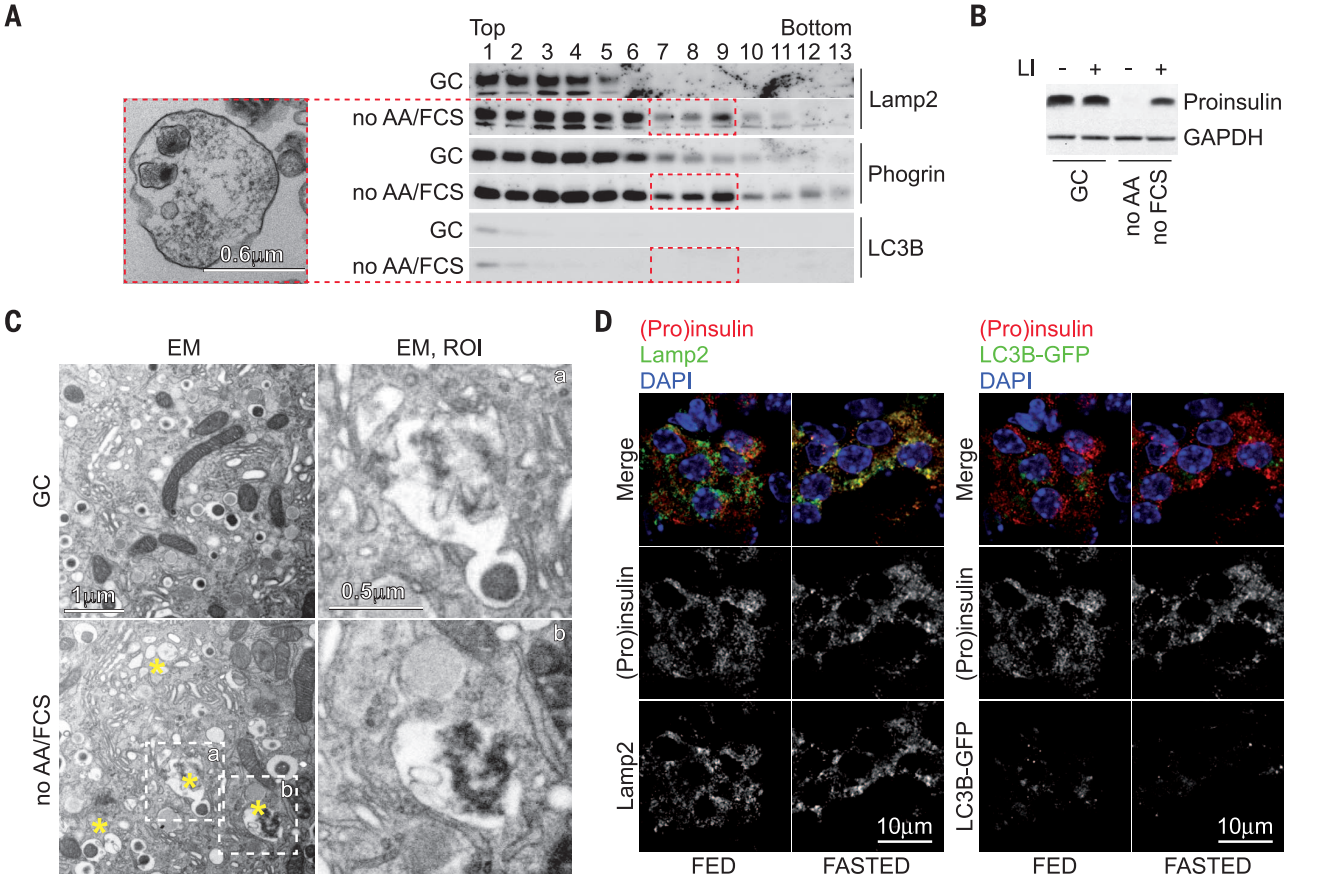


Fig. 2. Nutrient depletion induces SINGD in β cells. (**A**) Immunoblot of Lamp2, Phogrin, and LC3B using lysates of indicated fractions from INS1 cells under GC and no AA/FCS for 30 min. EM of GCLs in shifted fractions is indicated by red dashed boxes. (**B**) Immunoblot of proinsulin using lysates of INS1 cells treated or not with LIs under GC and no AA/FCS for 6 hours. GAPDH was served a loading control. (**C**) EM of Golgi areas in primary murine islets under GC and no AA/FCS for 2 hours. Yellow asterisks indicate GCLs. ROI are indicated with dashed squares. (**D**) IF of (Pro)insulin and Lamp2 (left) and (Pro)insulin and LC3B-GFP (right) in β cells in islets of fed and fasted LC3B-GFP expressing mice. The nuclei were stained with DAPI.

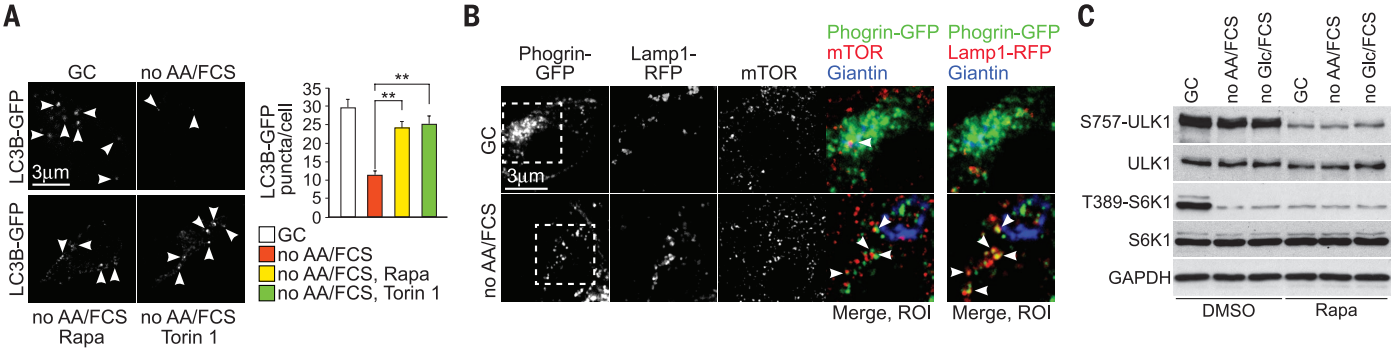


Fig. 3. SINGD suppresses autophagy in a mTOR-dependent manner to prevent insulin release. (**A**) IF of LC3B-GFP puncta (white arrowheads) in INS1 cells under GC and no AA/FCS for 2 hours treated or not with 100 nM rapamycin or 250 nM torin 1, as indicated. Quantification of LC3B-GFP puncta per cell (error bars denote mean ± SEM). $^{**}P < 0.01$. (**B**) IF of mTOR in INS1 cells coexpressing Phogrin-GFP and Lamp1-RFP under GC and no AA/FCS for 2 hours. White arrowheads in ROI (dashed squares) indicate colocalization of Phogrin-GFP with mTOR and Phogrin-GFP with Lamp1-RFP. A Golgi marker (Giantin) was used. (**C**) Immunoblot of indicated proteins using lysates of INS1 cells treated or not with 100 nM rapamycin under GC, no AA/FCS, or no Glc/FCS for 2 hours. GAPDH served as a loading control. DMSO, dimethyl sulfoxide. (**D**) Insulin in supernatants of human islets treated as indicated. Insulin concentrations are expressed as a percentage of insulin upon 16.7 mM stimulatory Glc (mean ± SEM). $^{***}P < 0.001$.

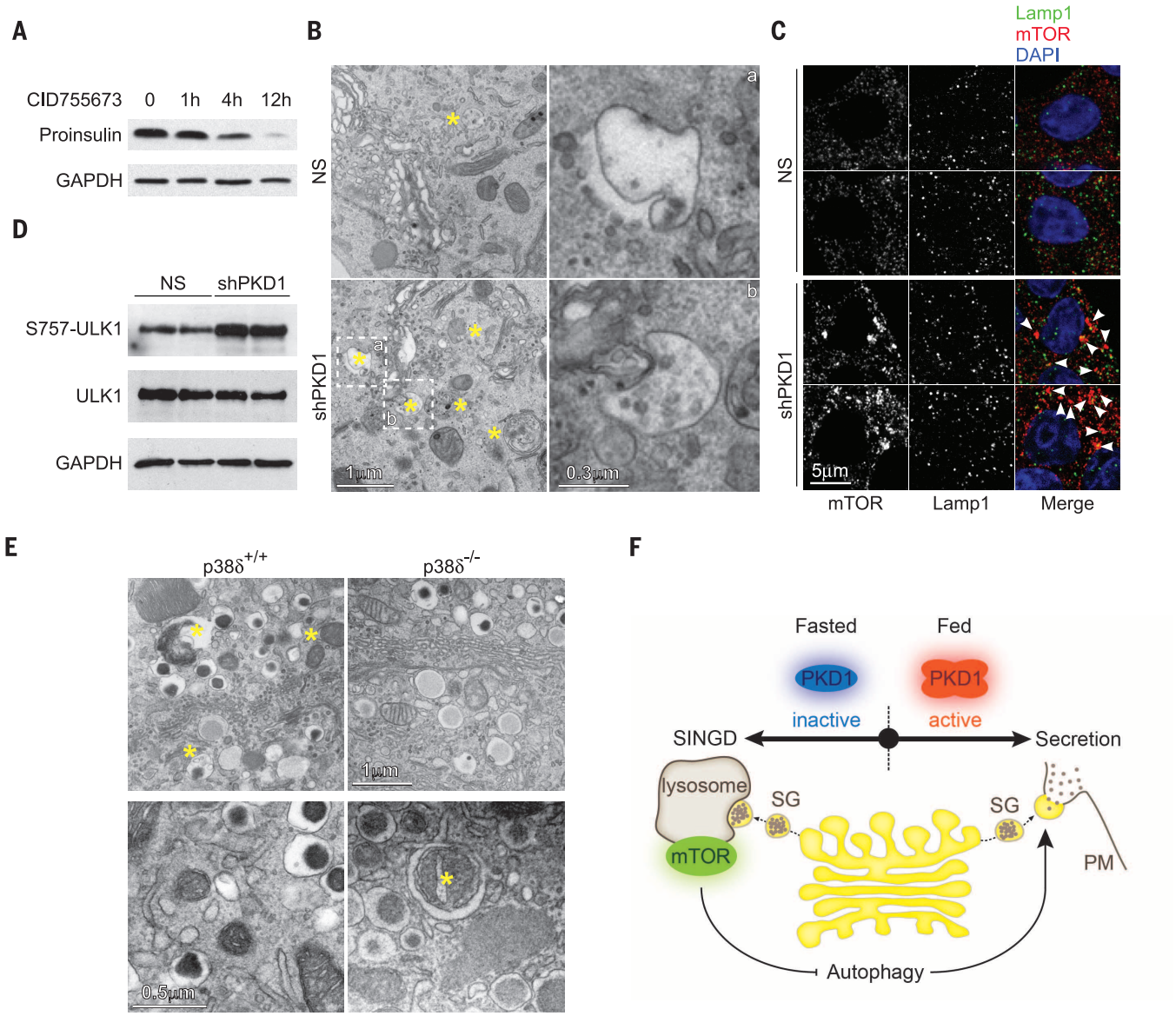


Fig. 4. PKD controls SINGD. (**A**) Immunoblot of proinsulin using lysates of INS1 cells treated with CID755673 for the indicated times. GAPDH served as a loading control. (**B**) EM of Golgi areas in nonsilenced (NS) and PKD1-depleted (shPKD1) INS1 cells. Yellow asterisks indicate GCLs. ROI are indicated with dashed squares. (**C**) IF of mTOR and Lamp1 in nonsilenced and PKD1-depleted INS1 cells. White arrowheads indicate colocalization of mTOR with Lamp1. Nuclei were stained with DAPI. (**D**) Immunoblot of indicated proteins using lysates of nonsilenced and PKD1-depleted INS1 cells. GAPDH served as a loading control. (**E**) (Top) EM of Golgi areas of fasted β cells in primary islets of $p38\delta^{+/+}$ and $p38\delta^{-/-}$ mice. Yellow asterisks indicate GCLs. (Bottom) EM of cytoplasm of fasted β cells in primary islets of $p38\delta^{+/+}$ and $p38\delta^{-/-}$ mice. The yellow asterisk indicates an autophagosome. (**F**) Model linking SINGD, secretion, and autophagy. PM, plasma membrane.

described inconsistencies (*3*). Accordingly, prolonged fasting of mice can induce autophagy in β cells (*26*). Our model could also explain the regulation of autophagy despite constitutively high adenosine monophosphate–activated protein kinase activity in β cells (*27*).

Our data show that triggering autophagy results in increased secretion of insulin. Although this should be avoided during fasting, it may be beneficial when insulin demands are high; for example, after a meal or in diabetes (*28*). The positive correlation between autophagy and insulin secretion may suggest an involvement of autophagy in postprandial insulin release, probably going beyond the widely established housekeeping role of autophagy.

REFERENCES AND NOTES

1. P. Rorsman, M. Braun, *Annu. Rev. Physiol.* **75**, 155–179 (2013).
2. J. D. Rabinowitz, E. White, *Science* **330**, 1344–1348 (2010).
3. C. Ebato *et al.*, *Cell Metab.* **8**, 325–332 (2008).
4. R. Singh, A. M. Cuervo, *Cell Metab.* **13**, 495–504 (2011).
5. I. Tanida, T. Ueno, E. Kominami, *Int. J. Biochem. Cell Biol.* **36**, 2503–2518 (2004).
6. Y. Kabeya *et al.*, *EMBO J.* **19**, 5720–5728 (2000).
7. A. Yamamoto *et al.*, *Cell Struct. Funct.* **23**, 33–42 (1998).
8. S. Kimura, T. Noda, T. Yoshimori, *Autophagy* **3**, 452–460 (2007).
9. G. Bjørkøy *et al.*, *J. Cell Biol.* **171**, 603–614 (2005).
10. N. Fujita *et al.*, *Mol. Biol. Cell* **19**, 2092–2100 (2008).
11. N. Mizushima, A. Yamamoto, M. Matsui, T. Yoshimori, Y. Ohsumi, *Mol. Biol. Cell* **15**, 1101–1111 (2004).
12. R. E. Smith, M. G. Farquhar, *J. Cell Biol.* **31**, 319–347 (1966).
13. D. F. Steiner, D. Cunningham, L. Spigelman, B. Aten, *Science* **157**, 697–700 (1967).
14. R. Zoncu *et al.*, *Science* **334**, 678–683 (2011).
15. Y. Sancak *et al.*, *Science* **320**, 1496–1501 (2008).
16. L. Yu *et al.*, *Nature* **465**, 942–946 (2010).
17. C. Betz, M. N. Hall, *J. Cell Biol.* **203**, 563–574 (2013).
18. S. G. Kim, G. R. Buel, J. Blenis, *Mol. Cells* **35**, 463–473 (2013).
19. J. Kim, M. Kundu, B. Viollet, K. L. Guan, *Nat. Cell Biol.* **13**, 132–141 (2011).

20. R. B. Pearson *et al.*, *EMBO J.* **14**, 5279–5287 (1995).
21. S. A. Kang *et al.*, *Science* **341**, 1236566 (2013).
22. S. Shoji-Kawata *et al.*, *Nature* **494**, 201–206 (2013).
23. G. Sumara *et al.*, *Cell* **136**, 235–248 (2009).
24. H. Gehart *et al.*, *Dev. Cell* **23**, 756–768 (2012).
25. G. Gold, M. L. Gishizky, G. M. Grodsky, *Science* **218**, 56–58 (1982).
26. K. Fujimoto *et al.*, *J. Biol. Chem.* **284**, 27664–27673 (2009).
27. G. A. Rutter, G. Da Silva Xavier, I. Leclerc, *Biochem. J.* **375**, 1–16 (2003).
28. M.-S. Lee, *Trends Endocrinol. Metab.* **25**, 620–627 (2014).

ACKNOWLEDGMENTS

We thank H. de F. Magliarelli, H. Gehart, O. Sumara, G. Sumara, N. Djouder, E. Hafen, R. J. Loewith, J. Klumperman, E. Polishchuk, R. Polishchuk, and all current members of the Ricci laboratory for critical scientific inputs. We thank A. Hausser for providing G-PKDrep-live, G. Rutter for providing Phogrin-GFP, J. Hutton (deceased) and H. Davidson for an antibody against Phogrin, and J. Klumperman for an antibody against Lamp1. We thank M. Koch, N. Messaddeq, and C. Ruhlmann for support in imaging; N. Mizushima for providing GFP-LC3 transgenic mice; and P. Halban and J.-I. Miyazaki for sharing the MIN6B1 cell line. This work was supported by a European Research Council (ERC) starting grant (ERC-2011-StG, 281271-STRESSMETABOL) and a European Foundation for the Study of Diabetes/Lilly European Diabetes Research Programme grant. A.G. and Z.Z. were supported by the ERC grant, M.M. was supported by a fellowship of the Deutsche Forschungsgemeinschaft, A.P. was supported by an IGBMC Ph.D. fellowship, K.K. was supported by a fellowship (Bourse Régionale de Recherche from region Alsace and INSERM), I.S. was supported by the Action Thématique et Incitative sur Programme (ATIP)–Avenir program, L.C. and C. Spiegelhalter were supported by a Telethon Grant, and N.S. and Y.S. were supported by EMBL internal funding. A.G. and R.R. have applied for a patent that protects autophagy-inducing molecules to increase insulin release.

SUPPLEMENTARY MATERIALS

www.sciencemag.org/content/347/6224/878/suppl/DC1
Materials and Methods
Figs. S1 to S23
References (*29*–*36*)

9 November 2014; accepted 5 January 2015
10.1126/science.aaa2628

KINASE DYNAMICS

Using ancient protein kinases to unravel a modern cancer drug's mechanism

C. Wilson,[1]* R. V. Agafonov,[1]* M. Hoemberger,[1] S. Kutter,[1] A. Zorba,[1] J. Halpin,[1] V. Buosi,[1] R. Otten,[1] D. Waterman,[1] D. L. Theobald,[2] D. Kern[1]†

Macromolecular function is rooted in energy landscapes, where sequence determines not a single structure but an ensemble of conformations. Hence, evolution modifies a protein's function by altering its energy landscape. Here, we recreate the evolutionary pathway between two modern human oncogenes, Src and Abl, by reconstructing their common ancestors. Our evolutionary reconstruction combined with x-ray structures of the common ancestor and pre–steady-state kinetics reveals a detailed atomistic mechanism for selectivity of the successful cancer drug Gleevec. Gleevec affinity is gained during the evolutionary trajectory toward Abl and lost toward Src, primarily by shifting an induced-fit equilibrium that is also disrupted in the clinical T315I resistance mutation. This work reveals the mechanism of Gleevec specificity while offering insights into how energy landscapes evolve.

The evolution of protein kinases is a key event in the origin of multicellularity (*1*), which enabled the development of more complex signaling cascades essential for the evolution of higher organisms. The key role of protein kinases in the cell cycle has placed them at the center of cancer drug research. Despite an explosion in diversity in the kinome (*2*), the catalytic kinase domains have maintained nearly identical structures (*2*–*5*). It is therefore surprising that the clinically successful cancer drug Gleevec has such strong selectivity toward Abl versus other tyrosine kinases, including the closely related Src. This is puzzling because the Gleevec-bound structures of Abl and Src are nearly identical, including the N- and C-terminal lobes and the drug-binding pocket (Fig. 1A) (*3*). Extensive work led to a frequently cited but controversial model where Gleevec selectivity is rooted in a pre-existing equilibrium between two alternative conformations of the DFG-motif (for Asp-Phe-Gly), a conserved segment of the activation loop (*3*, *6*–*12*). A number of x-ray structures have revealed the sampling of a Gleevec-binding–competent DFG-out position and a binding-incompetent DFG-in position in free kinases (Figs. 1A and 2A). Recently reported data rule out the predominant role of the DFG-in/out equilibrium (conformational selection) in Gleevec selectivity. It led to a different binding scheme (Scheme 1) that accounts for the 3000-fold difference in Gleevec affinity between Src and Abl (*11*) due to a global conformational change after drug binding (induced fit, Scheme 1).

However, the molecular mechanism of this selectivity remains unknown. Based on x-ray crystal structures, specific point mutations have been made in attempts to convert Abl to Src-like specificity and vice versa. Despite two decades of efforts, such sequence swaps in modern kinases have failed to illuminate the atomistic determinants of selectivity (*3*, *6*). The differences between Src, Abl, and other homologous kinases have evolved over a billion years from their common ancestor—not via residue swaps from one modern kinase to another. Sequence-swap experiments using modern enzymes have a fundamental shortcoming by neglecting epistasis (the effect of the surrounding amino acid background) (*13*). However, evolution has already navigated the complex epistatic protein space by producing functional proteins at each stage despite large numbers of accumulated mutations. We therefore examined the evolution of Src and Abl along their phylogenetic branches using ancestral reconstruction to understand differences not only in their equilibrium structures but also in their energy landscapes.

Ancestral reconstruction has provided a way to achieve mechanistic insight into protein function (*14*–*19*). Here, we elucidate the basis of modern kinase specificity toward Gleevec with atomic resolution by recapitulating the evolution of the Src and Abl catalytic domain from their last common ancestor. Analysis of the ancestral kinases allows us to track the evolution of the protein energy landscape (*20*, *21*). We define "energy landscape" as a set of free energy and kinetic parameters linking kinetically distinct states that are relevant to biological processes.

Seventy-six modern-day sequences spanning the cytosolic tyrosine kinase family (Src/Abl/Tec families) were used in a Bayesian phylogenetic analysis with receptor tyrosine kinases as the out-group (Fig. 1B). Because the quality of the ancestral reconstruction strongly depends on the alignment, we estimated the tree and alignments simultaneously. The most probable sequences were inferred for four key ancestral proteins between modern Src and Abl and their last common ancestor (Fig. 1B and figs. S1 and S2), and their corresponding proteins were expressed, purified, and characterized.

We denote the reconstructed protein corresponding to the last common ancestor of Src and Abl as ANC-AS. Similarly, on the lineage leading from ANC-AS to modern Abl, ANC-A1 represents the common ancestor between humans and colonial choanoflagellates, and ANC-A2 corresponds to the common ancestor between humans and *Caenorhabditis elegans*. On the lineage leading to modern Src, ANC-S1 is the last common ancestor between humans and colonial choanoflagellates/sponges. Despite the fact that ANC-AS differs by 96 residues from any modern cytosolic tyrosine kinase, all ancestral kinases reconstructed here are fully active and thermostable (Fig. 1C and fig. S3). We evaluated the specificity of Gleevec toward the ancestral kinases by measuring inhibition (Fig. 1D) and dissociation constants (fig. S4). The inhibition of ANC-AS is intermediate between

[1]Howard Hughes Medical Institute and Department of Biochemistry, Brandeis University, Waltham, MA 02452, USA. [2]Department of Biochemistry, Brandeis University, Waltham, MA 02452, USA.
*These authors contributed equally to the work. †Corresponding author. E-mail: dkern@brandeis.edu

Downloaded from www.sciencemag.org on February 21, 2015

modern Src and Abl. Gleevec affinity increases gradually toward Abl along the evolutionary pathway, whereas it drastically decreases toward Src.

Src and Abl differ by 146 amino acids, and experiments with the modern kinases could not identify the subset of residues responsible for the changes in dynamics (*11*). Because our reconstructed kinase ancestors have intermediate Gleevec affinities, we can now explore the evolution of these dynamical changes. To this end, we characterized the changes in the energy landscape from ANC-AS to modern Src and Abl by comparing the kinetics of Gleevec binding. All ancestors follow the same kinetic scheme as modern Src and Abl (Scheme 1), but with differences in individual conformational steps. As detailed in (*11*) and (*22*), the double exponential binding kinetics (Fig. 1E and fig. S5) reflect the faster physical binding step (identified by the linear dependence of the observed rate on Gleevec concentration) (Fig. 1G), followed by the slower induced-fit step, with the observed rate approaching a maximum at Gleevec saturation (Fig. 1H).

The gradual change in these kinetic parameters (k_{fast} and k_{slow}) from the weak binders to the tight binders is clearly visible, and the physical off rates (k_{off}), identified by the intercept in Fig. 1G, remain similarly fast. In contrast, the observed overall dissociation of the inhibitor-enzyme complex is extremely slow for ancestors ANC-AS, ANC-A1, and ANC-A2, and much faster for ANC-S1 (Fig. 1F), revealing that the rate-limiting step in Gleevec release is a conformational change before dissociation (E*.I→E.I) (Scheme 1 and Fig. 1F). To summarize (Fig. 2), we detect a systematic shift in the conformational equilibrium from E*.I to E.I when traversing the evolutionary tree from Abl to Src, caused by a gradual decrease in the forward rate (k_{conf+}) and a more dramatic increase in the reverse rate (k_{conf-}) (Fig. 2C). This conformational step, independently validated previously by a direct visualization of the E.I and E*.I conformers by nuclear magnetic resonance (NMR) on the enzyme-drug complex (*11*), accounts for the major difference in binding energy between different ancestors and modern Src and Abl, whereas changes in the drug's binding/dissociation step are nearly negligible (Fig. 2).

Our data reveal the evolution of the induced-fit step that is essential for Gleevec selectivity. It additionally provides experimental estimates of the relative populations of the DFG -in and -out conformations and reinforces that this equilibrium plays only a minor role in Gleevec affinity (Fig. 2, A and D). In the past, quantification of the equilibrium between these two alternative states has proven elusive, despite direct observation of both states in crystal structures (*3*). This new opportunity arises from the time-resolved

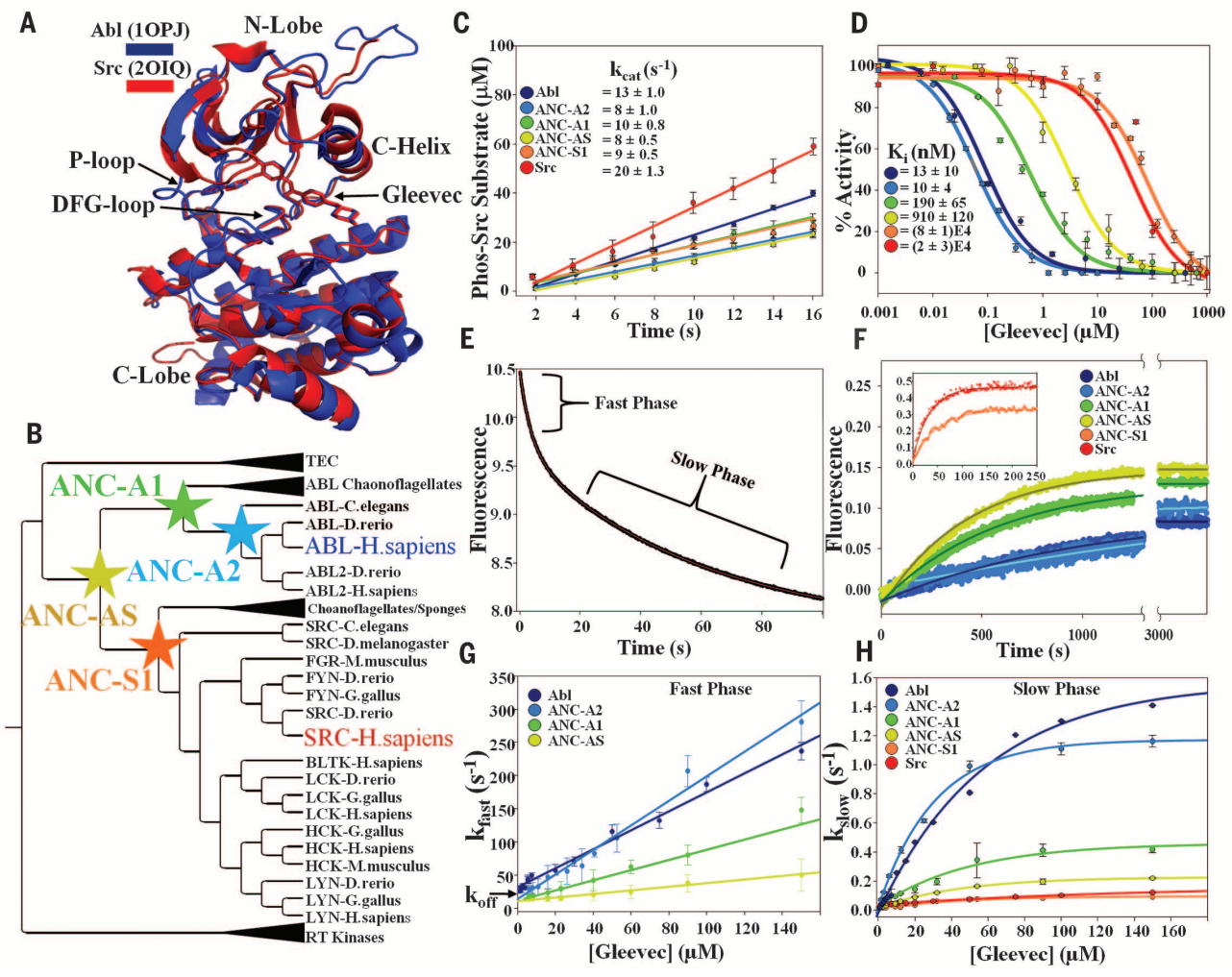


Fig. 1. Reconstructing ancestors of the cytosolic tyrosine kinase family to probe the energy landscape of Gleevec selectivity. (**A**) Structures of Abl (*33*) and Src (*3*) bound to Gleevec. (**B**) Phylogenetic tree constructed with Bali-Phy (*34*). Reconstructed nodes (stars) and human Abl and Src are marked with the colors used throughout the manuscript. For the full tree, including reconstruction posteriors, see fig. S1. (**C**) Kinase activity measured by phosphorylating the target peptide. (**D**) Gleevec inhibition constants (K_i) at 25°C. Kinetics of Gleevec binding (**E**) and dissociation (**F**) were measured by stopped-flow fluorescence at 5°C. (E) Mixing 50 nM of kinase with Gleevec displays double-exponential kinetics with the fast phase reporting on the binding step (**G**) and the slow step monitoring the induced fit (**H**). (F) Rate of dissociation, measured by dilution of the kinase-Gleevec complex, is dominated by E*.I to E.I transition (Scheme 1), whereas k_{off} is much faster [intercept in G)]. Uncertainties in all figures are ±SEM from three experiments.

detection of the binding step. The relative amplitude of the fast binding step (Fig. 2A, bottom) reflects the propensity to populate the DFG-out conformation ($p_{DFG\text{-}out}$). As apparent from Fig. 2A, one can indeed "watch" this flip in population from mainly being in a DFG-in state for modern Src and ANC-S1 to increasing DFG-out population in ANC-AS as an intermediate, and to even higher DFG-out populations for ANC-A1, ANC-A2, and Abl (large amplitudes). The DFG-out population is also an intrinsic component of the observed binding rate constant, $k_{on}^{obs} = k_{on} \times p_{DFG\text{-}out}$. Notably, the increase in $p_{DFG\text{-}out}$ measured from the amplitudes (Fig. 2A) is mirrored in the gradual increase in k_{on}^{obs} (Fig. 2B), implying that the true k_{on} rate constants are very similar. The populations of DFG-out in ANC-S1 and Src are too small to allow a quantitative analysis of the fast binding step (Fig. 2, A and D). The overall equilibrium dissociation constant K_d agrees well with the K_d calculated from all microscopic rate constants (figs. S4 and S6) (*11*, *22*), which corroborates the kinetic scheme and the accuracy of the fitted values.

During the evolution of the energy landscape from the last common ancestor, ANC-AS, to the modern tight-binding Abl and the weak-binding Src, the major contribution to increased affinity arose from an induced-fit mechanism (up to 5 kcal/mol) (Fig. 2E) with a minor contribution from the pre-existing DFG-in/out flip in the free enzymes (Fig. 2D) (*11*) arising from a depletion of the binding competent DFG-out conformation for the weaker binders. The actual binding/unbinding step, which is commonly used in structure-guided rational drug design (e.g., docking analyses), is very similar between the weak and strong binders.

What are the sequence differences responsible for the two major changes in the energy landscape, the DFG loop equilibrium, and the E.I⇔E*.I equilibrium? The ancestral reconstruction narrows down the regions responsible for these changes. Modern Abl and Src differ at 146 amino acids, yet only 70 differences separate ANC-AS and ANC-A2 and only 42 differences separate ANC-AS and ANC-S1 (fig. S2). These sequence changes are located throughout the protein, in agreement with globally distributed NMR chemical shift changes upon Gleevec binding (*11*).

X-ray crystal structures of ANC-AS bound to phosphomethylphosphonic acid adenylate ester (AMPPCP) (fig. S7) and Gleevec (Fig. 3) illustrate the structural consequences of sequence evolution. As expected, the overall structure of ANC-AS is highly similar to modern Src and Abl with subtle differences in the P-loop, C-helix and β4-β5 loop (Fig. 3C and figs. S7 and S8). Ancestral reconstruction identified a subset of 70 mutations potentially responsible for the dramatic shift of the E.I⇔E*.I conformational equilibrium between ANC-AS and ANC-A2, but not all of them are necessarily important for the increased affinity. To pinpoint the essential differences, we analyzed the ANC-AS-Gleevec structure and divided these 70 mutations into four groups (fig. S9). Constructs containing subgroups of mutations were then tested for activity and Gleevec binding (fig. S9). Remarkably, changing only 15 amino acids in the core of the ANC-AS N-terminal lobe to the Abl sequence [named AS(+15)] drastically increased Gleevec affinity to a level similar to Abl (Fig. 3B and fig. S10). Therefore, a small subset of mutations located only in the N-terminal lobe are responsible for the majority of the change in the E.I⇔E*.I equilibrium (fig. S11).

With the importance of these 15 residues clearly established, we can attempt to rationalize the changes in the energy landscape at an atomistic level using the ANC-AS x-ray structures. Most of these 15 amino acids are distant from the drug-binding pocket and are part of a hydrogen-bonding network in both the AMPPCP- and Gleevec-bound conformations in ANC-AS and Src. In contrast,

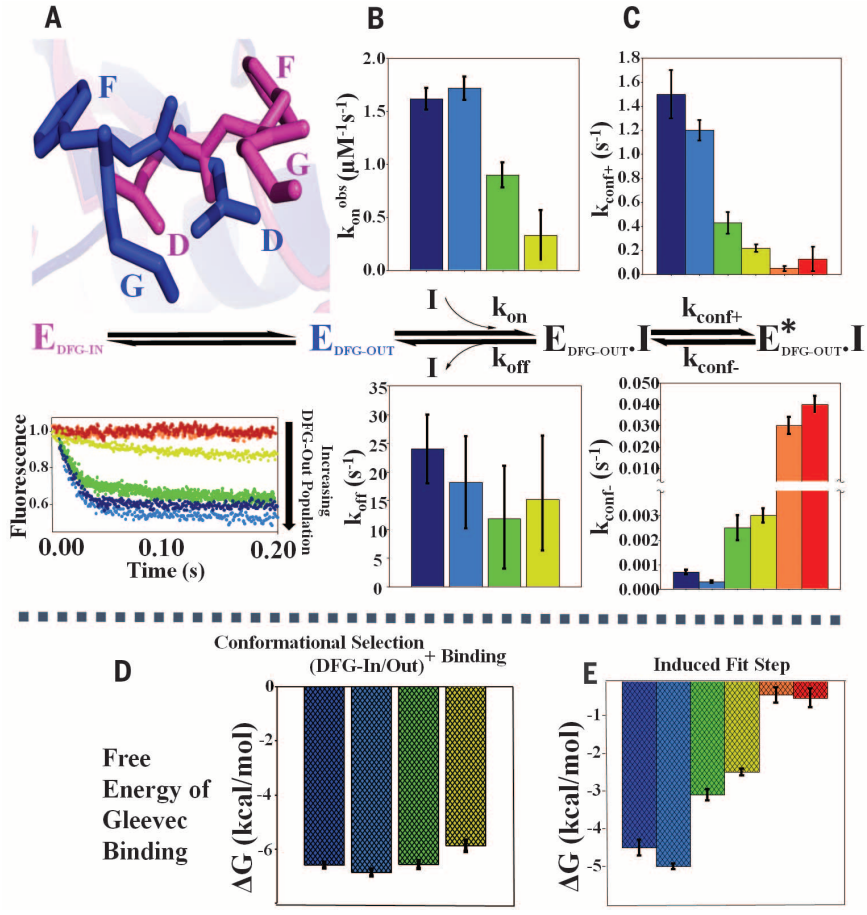
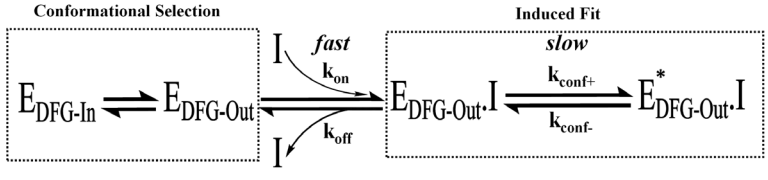


Fig. 2. Evolution of the free-energy landscape in tyrosine kinases based on data in Fig. 1. (**A**) Evolution of the DFG-in/DFG-out equilibrium, (**B**) Gleevec binding step, and (**C**) induced fit step. (A) The gradual population shift between DFG-out (blue, 4CSV) and DFG-in (pink, 4UEU, top) is reflected in the differences in amplitude of the fast phase (bottom). (B) The k_{on}^{obs}, the product of the true k_{on} and the population of DFG-out, increases from ANC-AS to Abl in parallel with the increase in the DFG-out population seen in (A). The measured microscopic k_{off}'s for Gleevec are equivalent. (C) For the induced-fit step, a gradual decrease in the forward rate constant (k_{conf+}, top) and a drastic increase in the reverse rate constant (k_{conf-}, bottom) from Abl via the common ancestor to ANC-S1 and Src are apparent. (**D** and **E**) Free-energy contributions of conformational selection plus binding (D) and the induced-fit step (E) to the overall binding energy.



Scheme 1. Proposed Gleevec binding scheme to human Src and Abl (*11*) and the ancestors (see the supplementary materials). E and E.I correspond to free and inhibitor-bound kinase; E*.I corresponds to inhibitor-bound kinase in a distinct conformational state; DFG-in and DFG-out subscripts specify the conformation of the DFG loop (Fig. 2A).

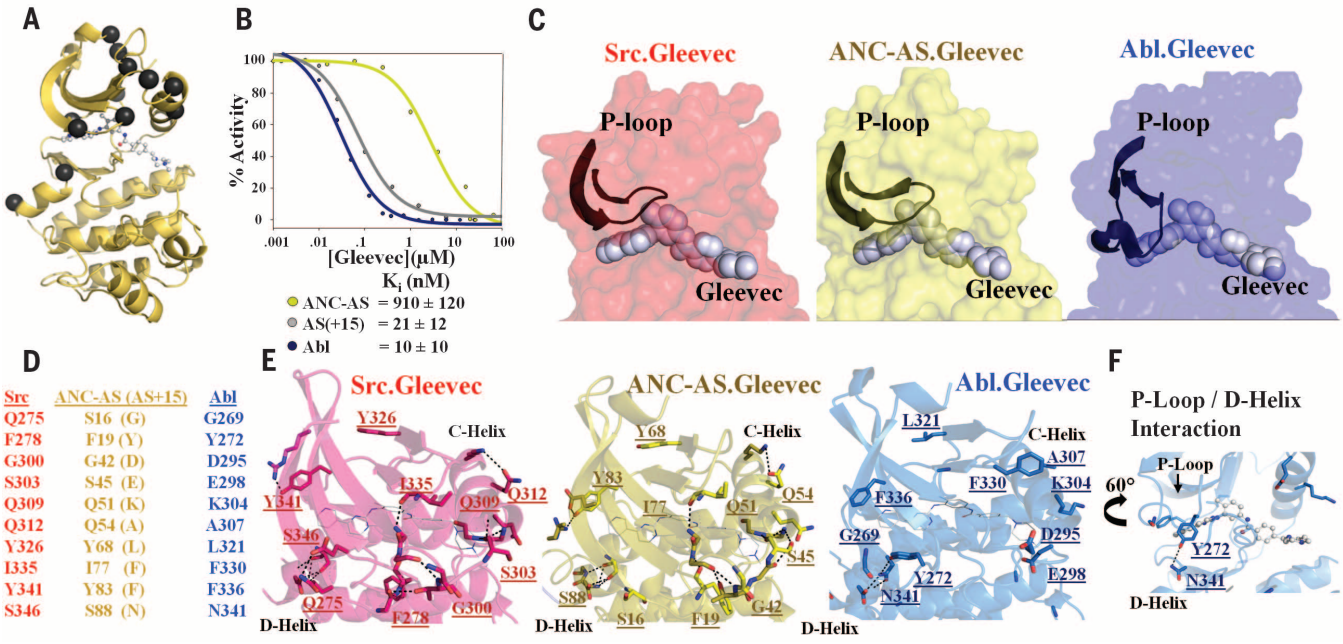


Fig. 3. Atomistic mechanism for Gleevec selectivity. (**A**) Mutations between ANC-AS and AS(+15) are mapped on the ANC-AS structure bound to Gleevec (4CSV) as black spheres. (**B**) Gleevec inhibition constants (K_i) at 25°C. (**C**) Structural comparison of Src (2OIQ), ANC-AS (4CSV), and Abl (1OPJ) bound to Gleevec highlighting the different P-loop conformations. (**D**) Ten out of the 15 identified mutations that are visible in all three x-ray structures are listed and (**E**) shown in the corresponding structures, illustrating how mutations in AS(+15) disrupt the hydrogen bond network (dotted lines) that are present in weak binders Src and ANC-AS. (**F**) Abl.Gleevec structure close-up showing the additional stabilizing interactions between the P-loop and the D-helix.

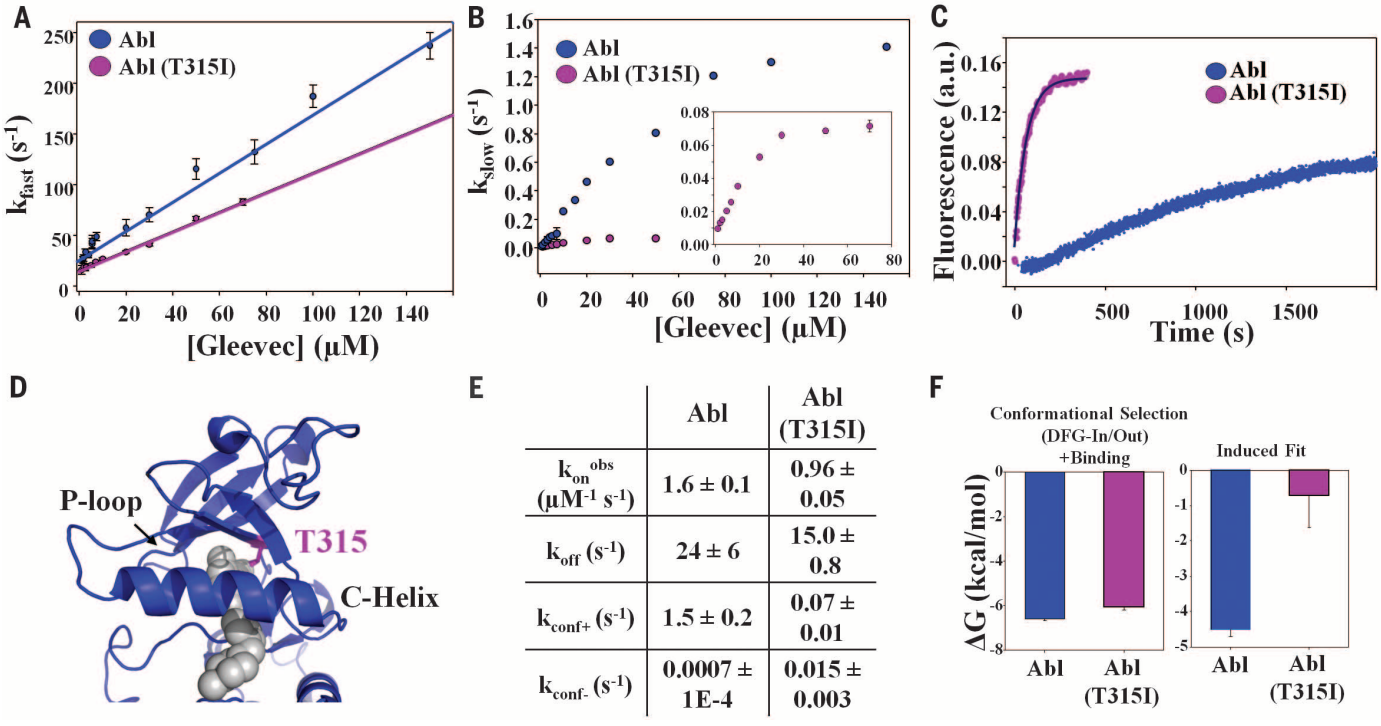


Fig. 4. Mechanism of Gleevec-evolved resistance in Abl(T315I). (**A** and **B**) Mixing 50 nM of kinase with Gleevec displays double-exponential kinetics (fig. S12) with the fast-phase reporting on the binding step (A) and the slow step monitoring the induced fit (B). (**C**) Rate of dissociation measured by rapid dilution of the kinase-Gleevec complex is dominated by E*.I to E.I conversion. (**D**) Site of mutation T315I is plotted onto the x-ray structure of Abl bound to Gleevec (gray) (1OPJ). (**E**) Individual rate constants for binding and induced-fit step and (**F**) the corresponding free-energy contributions.

the corresponding residues in AS(+15) and Abl prohibit such hydrogen-bonding networks (Fig. 3, D and E). We hypothesize that the lack of these hydrogen bonds allow the P-loop (another conserved element of kinases) (Fig. 1A) to close over Gleevec in a kinked conformation (Fig. 3C), whereas in Src and ANC-AS, the identified hydrogen bonds prohibit such a conformational change. A stabilizing role of the N-lobe hydrogen bond networks for the P-loop is consistent with the clear P-loop electron density in Src (3DQW) and ANC-AS (4UEU) bound to nucleotide, in contrast to missing P-loop electron density in the corresponding Abl structures (2G2I).

We note that the difference in P-loop conformation for kinase-Gleevec structures has been discussed previously as a potential basis for differential affinity (*23*). However, a sequence swap of the two P-loop differences placing Abl residues into Src, F278Y, and Q275G failed to increase Src's affinity toward Gleevec (*3*). Our data suggest that an additional mutation, N341, is needed for stabilization of the kinked P-loop, enabling a hydrogen bond between Y272 in the P-loop and N341 in the D-helix (Fig. 3F). This kinked P-loop conformation results in additional favorable interaction between the kinase and the drug; however, they are only possible in the absence of the restricting hydrogen bonds in the N-lobe identified above (Fig. 3E).

A long-standing problem in molecular biology is how to establish the sequence determinants for specificity within protein families. As a modern anthropogenic creation, Gleevec could not have provided evolutionary pressure for the divergence of the Src and Abl kinase families. However, the ancestral kinases deliver a deeper understanding of the molecular mechanism underlying the impressive selectivity of a modern cancer drug. Surprisingly, Gleevec takes advantage of the evolutionary differences in the Src and Abl energy landscapes. In addition, Gleevec binding serves as an experimental readout for the natural evolution of the DFG in/out equilibrium, which is widely considered to be a key element for differential regulation in the protein kinase kingdom, although the corresponding mechanism has been elusive (*3*, *4*, *6*–*8*). We hypothesize that the gradual evolution of both the DFG in/out equilibrium and kinase plasticity responsible for differences in the induced-fit step was driven by evolutionary pressure for differential regulation.

Currently, natural evolutionary selection is in play in the development of Gleevec resistance. During the therapeutic use of Gleevec in chronic myelogenous leukemia patients, a number of clinically relevant resistance mutations have evolved, including the most common Abl(T315I) mutation (*24*) (Fig. 4). This mutation drastically decreases the affinity for Gleevec (K_d of 12 ± 5 μM at 25°C) and has been called the "gatekeeper" mutation because of the hypothesis that the Ile residue obstructs binding due to steric hindrance (*25*, *26*). Surprisingly, we find that the binding step is unaltered by the T315I mutation but that the subsequent induced-fit step is severely hampered (Fig. 4). As described before, this latter step of conformational dynamics after drug binding is the key for high affinity in the wild-type protein, and it is the same step that is compromised under the evolutionary pressure of Gleevec treatment of cancer cells.

Previous ancestral reconstructions investigated highly conserved protein families that remain relatively unchanged in function and sequence over a vast period of time (up to 4 billion years) (*27*–*30*) and metazoan lineages (within the past 600 million years) with large functional divergence caused by a small number of mutations (*31*, *32*). Our system differed in the number of residues involved and focused mainly on revealing the atomistic mechanism of a modern cancer drug for modern kinases. The observed gradual change in energy landscape from the common ancestor to modern kinases, and the mechanism for the resistance mutant that evolved under natural pressure, advocate that altering conformational dynamics, and hence energy landscapes, may be a crucial driving force in evolution.

REFERENCES AND NOTES

1. D. J. Richter, N. King, *Annu. Rev. Genet.* **47**, 509–537 (2013).
2. G. Manning, G. D. Plowman, T. Hunter, S. Sudarsanam, *Trends Biochem. Sci.* **27**, 514–520 (2002).
3. M. A. Seeliger *et al.*, *Structure* **15**, 299–311 (2007).
4. S. S. Taylor, A. P. Kornev, *Trends Biochem. Sci.* **36**, 65–77 (2011).
5. A. P. Kornev, S. S. Taylor, *Biochim. Biophys. Acta* **1804**, 440–444 (2010).
6. Y.-L. Lin, Y. Meng, W. Jiang, B. Roux, *Proc. Natl. Acad. Sci. U.S.A.* **110**, 1664–1669 (2013).
7. A. Aleksandrov, T. Simonson, *J. Biol. Chem.* **285**, 13807–13815 (2010).
8. S. Lovera *et al.*, *J. Am. Chem. Soc.* **134**, 2496–2499 (2012).
9. S. W. Cowan-Jacob *et al.*, *Structure* **13**, 861–871 (2005).
10. A. C. Dar, K. M. Shokat, *Annu. Rev. Biochem.* **80**, 769–795 (2011).
11. R. V. Agafonov, C. Wilson, R. Otten, V. Buosi, D. Kern, *Nat. Struct. Mol. Biol.* **21**, 848–853 (2014).
12. Y. Shan *et al.*, *Proc. Natl. Acad. Sci. U.S.A.* **106**, 139–144 (2009).
13. M. A. DePristo, D. M. Weinreich, D. L. Hartl, *Nat. Rev. Genet.* **6**, 678–687 (2005).
14. M. J. Harms, J. W. Thornton, *Nat. Rev. Genet.* **14**, 559–571 (2013).
15. L. Pauling, E. Zuckerkandl, *Acta Chem. Scand.* **17**, S9–S16 (1963).
16. A. M. Dean, J. W. Thornton, *Nat. Rev. Genet.* **8**, 675–688 (2007).
17. D. A. Liberles, *Ancestral Sequence Reconstruction* (Oxford Univ. Press, Oxford, 2007).
18. P. D. Williams, D. D. Pollock, B. P. Blackburne, R. A. Goldstein, *PLOS Comput. Biol.* **2**, e69 (2006).
19. N. M. Krishnan, H. Seligmann, C. B. Stewart, A. P. De Koning, D. D. Pollock, *Mol. Biol. Evol.* **21**, 1871–1883 (2004).
20. T. Hunter, *Curr. Opin. Cell Biol.* **21**, 140–146 (2009).
21. W. Eckhart, M. A. Hutchinson, T. Hunter, *Cell* **18**, 925–933 (1979).
22. Materials and methods are available as supplementary materials on *Science* Online.
23. M. A. Seeliger *et al.*, *Cancer Res.* **69**, 2384–2392 (2009).
24. M. E. Gorre *et al.*, *Science* **293**, 876–880 (2001).
25. M. Modugno *et al.*, *Cancer Res.* **67**, 7987–7990 (2007).
26. H. Daub, K. Specht, A. Ullrich, *Nat. Rev. Drug Discov.* **3**, 1001–1010 (2004).
27. A. Ingles-Prieto *et al.*, *Structure* **21**, 1690–1697 (2013).
28. R. Perez-Jimenez *et al.*, *Nat. Struct. Mol. Biol.* **18**, 592–596 (2011).
29. E. A. Gaucher, S. Govindarajan, O. K. Ganesh, *Nature* **451**, 704–707 (2008).
30. E. A. Gaucher, J. M. Thomson, M. F. Burgan, S. A. Benner, *Nature* **425**, 285–288 (2003).
31. M. J. Harms, J. W. Thornton, *Curr. Opin. Struct. Biol.* **20**, 360–366 (2010).
32. S. F. Field, M. V. Matz, *Mol. Biol. Evol.* **27**, 225–233 (2010).
33. B. Nagar *et al.*, *Cancer Res.* **62**, 4236–4243 (2002).
34. B. D. Redelings, M. A. Suchard, *Syst. Biol.* **54**, 401–418 (2005).

ACKNOWLEDGMENTS

This work was supported by the Howard Hughes Medical Institute (HHMI), the Office of Basic Energy Sciences, Catalysis Science Program, U.S. Dept. of Energy, award DE-FG02-05ER15699, and NIH (GM100966-01) to D.K and NIH (GM096053 and GM094468) to D.L.T. R.O. is an HHMI Fellow of the Damon Runyon Cancer Research Foundation, DRG-2114-12. We thank the Advanced Light Source (ALS), Berkeley, CA, USA, for access to beamline BL8.2.2. The Berkeley Center for Structural Biology is supported in part by the National Institutes of Health, National Institute of General Medical Sciences, and the HHMI. The ALS is supported by the Director, Office of Science, Office of Basic Energy Sciences, of the U.S. Department of Energy under contract DE-AC02-05CH11231. D.K. is the inventor on a patent applied for by Brandeis University that describes a biophysical platform for drug development based on energy landscapes The Protein Data Bank accession codes are 4CSV (ANC-AS.Gleevec) and 4UEU (ANC-AS.AMPPCP).

SUPPLEMENTARY MATERIALS

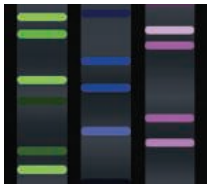
www.sciencemag.org/content/347/6224/882/suppl/DC1
Material and Methods
Supplementary Text
Figs. S1 to S12
Tables S1 and S2
References (*35*–*48*)

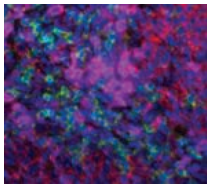
29 October 2014; accepted 30 December 2014
10.1126/science.aaa1823

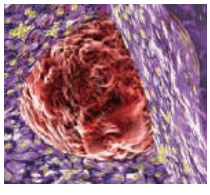
want new technologies?

antibodies
apoptosis
biomarkers
cancer
cytometry
data
diseases
DNA
epigenetics
genomics
immunotherapies
medicine
microbiomics
microfluidics
microscopy
neuroscience
proteomics
sequencing
toxicology
transcriptomics









watch our webinars

Learn about the latest breakthroughs, new technologies, and ground-breaking research in a variety of fields. Our expert speakers explain their quality research to you and answer questions submitted by live viewers.

VIEW NOW!
webinar.sciencemag.org

Science
AAAS

Brought to you by the *Science*/AAAS Custom Publishing Office

@SciMagWebinars



***Science Advances,* the new open-access journal from AAAS, is now available online.** Featuring innovative, multidisciplinary articles, *Science Advances* offers the high quality, peer-reviewed research you expect from the publishers of *Science*–in an open, digital-only format. Read the latest findings and submit your research at **scienceadvances.org.**

Science Advances
AAAS

eppendorf & Science

PRIZE FOR NEURO BIOLOGY



2014 Winner
Eiman Azim, Ph.D.
Columbia University
For research on skilled limb movement

Application Deadline
June 15, 2015

Call for Entries

Eppendorf & Science Prize for Neurobiology
The annual Eppendorf & Science Prize for Neurobiology is an international award which honors young scientists for their outstanding contributions to neurobiological research based on methods of molecular and cell biology. The winner and finalists are selected by a committee of independent scientists, chaired by Science's Senior Editor, Dr. Peter Stern. To be eligible, you must be 35 years of age or younger.

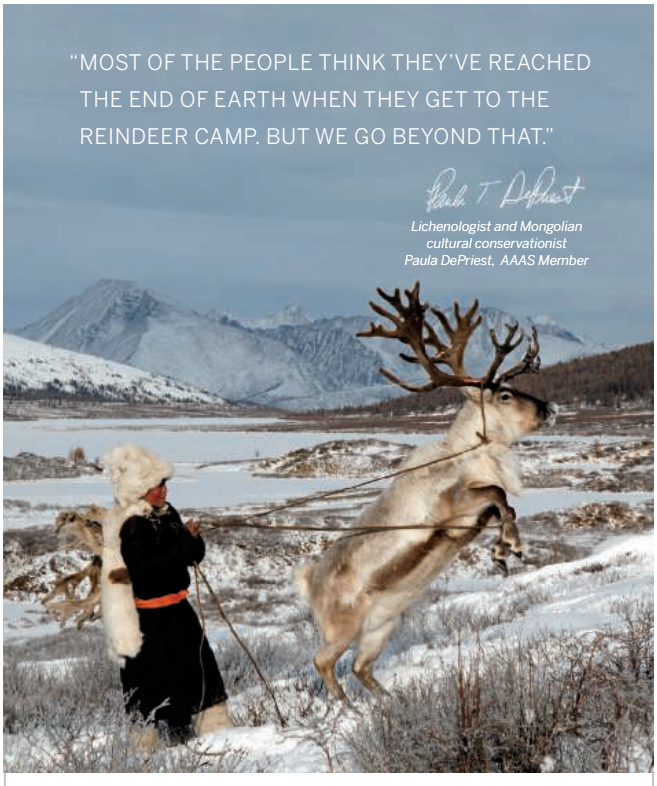
You could be next to win this prize and to receive
> Prize money of US$25,000
> Publication of your work in Science
> Full support to attend the Prize Ceremony held in conjunction with the Annual Meeting of the Society for Neuroscience in the USA
> An invitation to visit Eppendorf in Hamburg, Germany

It's easy to apply!

Learn more at: www.eppendorf.com/prize

eppendorf Science AAAS

AAAS® and Science® are registered trademarks of the American Association for the Advancement of Science, USA. Eppendorf® and the Eppendorf logo are registered trademarks of Eppendorf AG Germany. U.S. Design Patents are listed on www.eppendorf.com/ip. All rights reserved, including graphics and images. Copyright © 2015 by Eppendorf AG. Kurstin Roe Photography.



Every scientist has a *story*

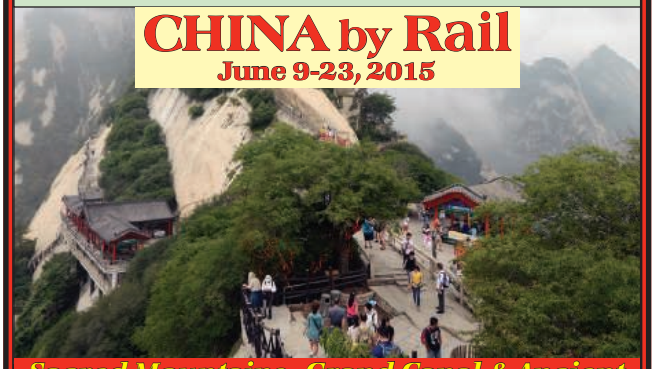
Read her story at membercentral.aaas.org

AAAS MEMBERCENTRAL

AAAS *Travels*

CHINA by Rail

June 9-23, 2015



Sacred Mountains, Grand Canal & Ancient Cities including seven World Heritage sites!

China's high speed rail network offers a terrific and innovative way to explore the Middle Kingdom, making sacred mountain ranges and ancient cities accessible and amazing to behold, including the Terra Cotta Warriors! Discover a China that is off the beaten path with our superb leader team while exploring many fantastic sites! $3,995 pp + air

For a detailed brochure, call (800) 252-4910

All prices are per person twin share + air

BETCHART EXPEDITIONS INC.
17050 Montebello Rd, Cupertino, CA 95014
Email: AAASInfo@betchartexpeditions.com
www.betchartexpeditions.com

ONLINE CAREER FAIR

March 4, 2015 | 10:00 AM – 4 PM EST



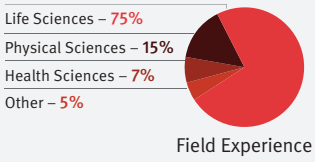
Register now for this exciting virtual career fair and engage, screen, and recruit hundreds of targeted candidates.

HOW THE EVENT WILL WORK

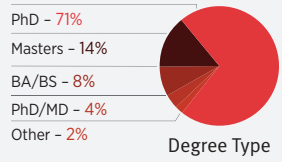
Employers receive a fully customized "booth" tailored to meet their recruiting needs. This landing page can include open positions, company information, testimonials and branding videos.

During the live event, candidates browse your booth and then choose to chat one-on-one. The conversations are timed to allow companies to meet as many candidates as possible.

ATTENDEE DEMOGRAPHICS



Field Experience



Degree Type

Over 3,000 pre-registrants; over 900 live participants

Book your booth today!

For more information, please visit:
ScienceCareers.org/onlinecareerfairemployers

ScienceCareers
FROM THE JOURNAL SCIENCE AAAS

SCIENCECAREERS.ORG

Chromatography Systems

Two new NGC Medium-Pressure Chromatography Systems, the NGC Discover and NGC Discover Pro Systems, have automated capabilities that make them ideal for advanced purification applications such as method optimization and multistep and tandem protein purification. These systems are available with a 10 mL/min pump module or with the recently released next-generation chromatography (NGC) 100 mL/min pump module, which enables flow rates up to 200 mL/min when used in combination with a mixer module. The Discover Systems further increase throughput by being able to load multiple samples and run up to 15 columns sequentially. In addition, the Discover Pro System can collect 12 large-volume fractions via its outlet valve. The Discover Systems' best feature, however, may be their ease of use, a hallmark of the NGC family of chromatography instruments. All NGC Systems feature the same modular design with interchangeable plug-and-play modules that allow researchers to scale the system according to their throughput needs.

Bio-Rad Laboratories
For info: 800-424-6723
www.bio-rad.com/ngcpr

Colony Identification System

The new software module for the ProtoCOL 3 automated colony counter makes the system the first commercial automatic microbial identification and counter of colonies cultured on CHROMagar plates. With minimal training, microbiologists can use the system to rapidly identify and enumerate all key clinical, water, and foodborne pathogens. The new ProtoCOL 3 software module ensures that the ProtoCOL 3 system can accurately identify any bacteria or yeast cultured on a CHROMagar plate in less than a minute, saving microbiologists hours of visually inspecting colonies, and manually recording results. The ProtoCOL 3 system performs these tasks by utilizing unique, patented red, blue, and green lighting to capture a life-like color image of the colonies on the plates. The new software module analyzes the image and is so sophisticated that it can distinguish between rose pink and dusty pink as well as turquoise from steel blue.

Synbiosis
For info: +44-(0)-1223-727125
www.synbiosis.com/chromogenic-id



Compound Management

The new Fluent Laboratory Automation Solution is designed to offer greater throughput and flexibility for compound management workflows. Building on the success of the Fluent cell-based assay workstation, this second application-oriented system introduces a number of new hardware and software options that simplify and improve the productivity of compound management and assay plate generation activities. The compound management workstation is ideally suited to drug discovery laboratories and centralized compound library facilities, offering a host of features intended to streamline day-to-day activities such as daughter plate generation, plate reformatting, and hit picking. Liquid handling versatility has been increased with the introduction of washable fixed tips for the instrument's Flexible Channel Arm. Complementing the existing disposable tip options to provide cost-effective reagent and compound distribution—as well as cap piercing capabilities—the new fixed tips are also available in a low-volume option, offering reliable pipetting below 0.5 µL to help minimize compound consumption and enable effective serial dilutions.

Tecan
For info: +41-44-922-81-11
www.tecan.com/fluent

Serial Sectioning

The ATUMtome (Automatic Tape-collecting Ultramicrotome) opens the door to efficient sectioning and handling of thousands of sections that permit 3-D reconstruction of large volumes of biological materials. It also provides a unique tape collecting method that allows sections to be stored for later processing and examination. The instrument is in its early adopter phase in which scientists are helping to advance the technology with their feedback. The ATUMtome operates with an ultramicrotome and diamond knife included in the system. Typically, researchers mount resin-embedded specimens on the ultramicrotome, cutting serial sections that then float on a water surface in the diamond knife trough. The ATUMtome moves a continuous ribbon of tape through this water trough, automatically removing the serial sections in sequential order. After the sections are collected, researchers mount the tape strips onto substrates like silicon wafers or glass slides. The populated wafers are now ready for imaging with a scanning electron microscope.

RMC Products
For info: 520-745-0001
www.rmcproducts.com/atumtome

Sample Storage

The Hamilton Verso is a truly modular automated storage platform which is easily configured to meet the needs of the most demanding sample management applications. The system can be scaled to fit sample capacities ranging from 100,000 to over 5 million tubes at temperatures from ambient to -20°C. Verso is capable of storing and processing up to 1,500 tubes and plates per hour, and allows loading and unloading of up to 70 sample racks at a time. To complete a fully automated workflow, Verso can integrate with Hamilton automated liquid handling workstations. The intuitive system allows users to easily perform most jobs in three clicks or less. Features include one-touch loading, and a job queue manager which allows users to prioritize jobs and set jobs to process overnight. Every sample is tracked at all times to maintain a complete audit trail, including their temperature logs, who accessed the sample and what function was completed.

Hamilton Storage Technologies
For info: 800-310-5866
www.hamilton-storage.com

Electronically submit your new product description or product literature information! Go to www.sciencemag.org/products/newproducts.dtl for more information.

Newly offered instrumentation, apparatus, and laboratory materials of interest to researchers in all disciplines in academic, industrial, and governmental organizations are featured in this space. Emphasis is given to purpose, chief characteristics, and availability of products and materials. Endorsement by *Science* or AAAS of any products or materials mentioned is not implied. Additional information may be obtained from the manufacturer or supplier.

THE Welch FOUNDATION

Advancing Chemistry. Improving Life.

Next Generation Medicine

59th Annual Conference on Chemical Research



Joseph L. Goldstein,
University of Texas Southwestern Medical Center

The 2015 Welch Conference on Chemical Research, "Next Generation Medicine," is organized to provide a broad perspective on recent genetic, biochemical, and pharmacological advances that will have a major impact on the future understanding and therapy of human diseases.

An all-star cast of 17 Speakers will present their latest discoveries covering diverse areas of contemporary biomedical science that deal with genome sequencing, mapping the brain, new signaling pathways, molecular pathogenesis of common diseases, and modern approaches to drug therapy.

In addition to the 17 Speakers, 4 prominent scientists will act as Session Leaders who will comment critically on the 17 talks.

2015 Conference on Chemical Research:
Next Generation Medicine
October 26-27 in Houston

Conference complimentary with registration.
Program and registration:
www.welch1.org/chemical-conference























David Botstein, *Calico Life Sciences*

Michael Brown, *University of Texas Southwestern Medical Center*

Zhijian (James) Chen, *University of Texas Southwestern Medical Center*

Titia De Lange, *Rockefeller University*

Karl Deisseroth, *Stanford University*

Hal Dietz, *Johns Hopkins University School of Medicine*

Jennifer Doudna, *University of California, Berkeley*

Helen Hobbs, *University of Texas Southwestern Medical Center*

Tasuku Honjo, *Kyoto University*

Rudolf Jaenisch, *Whitehead Institute for Biomedical Research and MIT*

William Kaelin, *Dana-Farber Cancer Institute, Harvard Medical School*

Eric Lander, *Broad Institute and MIT*

Richard Lifton, *Yale University School of Medicine*

Steven McKnight, *University of Texas Southwestern Medical Center*

Vamsi K. Mootha, *Massachusetts General Hosptial, Harvard Medical School*

Eric Olson, *University of Texas Southwestern Medical Center*

Stanley Prusiner, *University of California, San Francisco*

Gerald Rubin, *Janelia Farm Research Campus, HHMI*

Charles Sawyers, *Memorial Sloan Kettering Cancer Center*

Kevan M. Shokat, *University of California, San Francisco*

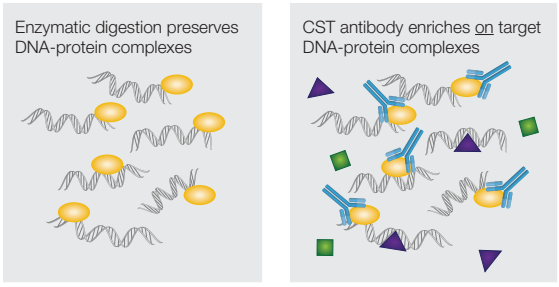
Huda Zoghbi, *Baylor College of Medicine*

Every step matters.



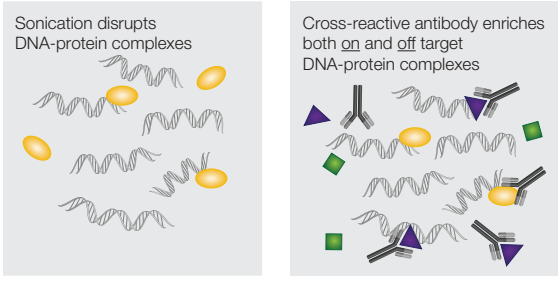
SimpleChIP® Kits + CST Validated Antibodies

CST™ SimpleChIP® Kit

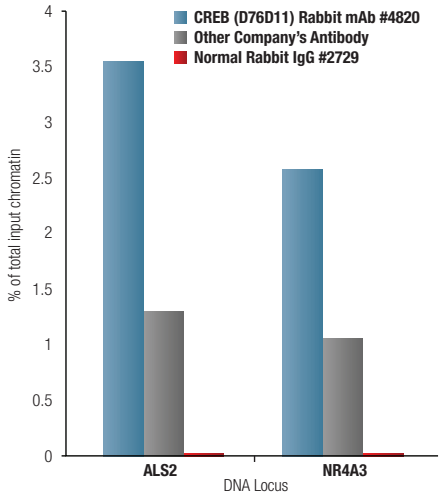


High Signal + **Low Noise** = **Strong, Consistent Results**

Other Company's ChIP Kit



Low Signal + **High Noise** = **Weak, Variable Results**



= Strong, Reliable Results



Learn more about the SimpleChIP® advantage:
www.cellsignal.com/chipscience

WB IP IHC IF F ChIP

For Research Use Only. Not For Use In Diagnostic Procedures.

© 2014 Cell Signaling Technology, Inc. Cell Signaling Technology®, CST™, and SimpleChIP® are trademarks of Cell Signaling Technology, Inc.

14PADCHIPNONE0153ENG_03

Cell Signaling TECHNOLOGY®

Gordon Research Conferences

frontiers of science

2015 "Session II" Meetings will be held between June and August in New England in the United States, and internationally in Italy, Spain and Hong Kong, China. A list of preliminary programs appears on the following 25 pages. For detailed programs, fees, site/travel information and online application, visit our web site at **www.grc.org**.

A Gordon Research Seminar delivers exactly what you expect from a GRC: Cutting-edge science, rich discussion, and a great value. It's no wonder this program grows each year. It's an experience no graduate student or post-doc should miss.

(John Kozarich, Chairman and President of ActivX Biosciences)

Image: *Close-up of ES-cell derived neuroepithelium, immunostained with cytoskeletal and neuronal antibodies.* Courtesy of Nick Love (RIKEN Center for Developmental Biology, Japan). Submitted by Enrique Amaya, Chair, Tissue Repair & Regeneration GRC. The Tissue Repair & Regeneration GRC will take place June 7-12, 2015 at Colby-Sawyer College in New London, NH.

Downloaded from www.sciencemag.org on February 21, 2015

2015 "Session II" Preliminary Programs

The list of meetings, session topics and speakers begins below. Discussion leaders are noted in italics.

Note: Gordon Research Seminars (GRS) are listed below their associated Gordon Research Conference. GRSs are 2-day meetings that precede an associated GRC, designed for graduate students, post-docs, and other young scientists to present and exchange new data and cutting-edge ideas. Seed funding for new Gordon Research Seminars is provided by the Kenan Institute for Engineering, Technology & Science at North Carolina State University and Merck & Co., Inc.

Adhesion, Science of

Emphasizing Soft Materials and Bio-Adhesion
Jul 26-31, 2015
Mount Holyoke College, South Hadley, MA
Chair: Anand Jagota
Vice Chair: Costantino Creton

- **Soft Materials**
  (*Chung-Yuen Hui* / Monica Olvera De La Cruz / Zhigang Suo)
- **Friction and Adhesion**
  (*Manoj Chaudhury* / Robert McMeeking / Lars Pastewka / G. Ravichandran)
- **New Chemistries and Materials**
  (*Timothy Long* / Aranzazu Del Campo / Scott Phillips)
- **Wetting and Contact**
  (*Tian Tang* / Joelle Frechette / Martin Shanahan / Kripa Varanasi)
- **Elastocapillarity**
  (*Eric Dufresne* / Jacco Snoeijer / Robert Style)
- **Biomolecular Adhesion**
  (*Wendy Thomas* / Maria Bykhovskaia / Dennis Discher / Wesley Wong)
- **Biomimetics**
  (*Stanislav Gorb* / David Hu / Timothy Lu)
- **Bioadhesion**
  (*Kevin Turner* / Maithreyi Narasimha / Krystyn Van Vliet / Reinhold Dauskardt)
- **Keynote Session: Cancer Biology and Adhesion**
  (*Costantino Creton* / Mina Bissell)

GRS **Adhesion, Science of**
Emphasizing Soft Materials and Bio-Adhesion
Jul 25-26, 2015
Chair: Nicole Fortoul
Associate Chair: Helen K. Minsky

Aging, Biology of

The Translational Science of Aging: From Functional Pathways to Interventions
Jul 19-24, 2015
Sunday River Resort, Newry, ME
Chairs: John M. Sedivy & Yousin Suh
Vice Chairs: Adam Antebi & Shin-Ichiro Imai

- **Keynote Session: The Translational Science of Aging**
  (*John Sedivy*, *Yousin Suh* / Linda Partridge / Luigi Ferucci / Felipe Sierra)
- **Epigenetics and Genome Stability**
  (*Jan Vijg* / Peter Adams / Bruce Yankner / Vera Gorbunova / Sylvia Lee / Stephen Helfand)
- **Genetics of Aging**
  (*Anne Brunet* / Matt Kaeberlein / Eline Slagboom)
- **Telomeres and Cellular Senescence**
  (*Sandy Chang* / Mary Armanios / Jan Van Deursen / M. Geoffrey Rosenfeld / Janet Lord)
- **Stem Cells and Rejuvenation**
  (*Amy Wagers* / Thomas Rando / Henri Jasper / Joan Mannick)
- **Protein Homeostasis and Autophagy**
  (*Andrew Dillin* / Malene Hansen / Daniel Gottschling / Jodi Nunnari)
- **Neuroendocrine Regulation**
  (*Marc Tatar* / Jens Bruning / Cynthia Kenyon / Akiko Satoh)
- **Metabolic Regulation and Mitochondria**
  (*Shin-Ichiro Imai*, *Adam Antebi* / Marcia Haigis / Peter Rabinovitch / Rozalyn Anderson / Julie Mattison / Luigi Fontana / Rafa De Cabo)
- **Developing Therapeutic Strategies for Aging and Age-Associated Diseases**
  (*Nir Barzilai* / Ana Maria Cuervo / Brian Kennedy / James Kirkland / Valter Longo / Richard Miller / David Sinclair)

GRS **Aging, Biology of**
Mentoring in the Translational Science of Aging: From Functional Pathways to Interventions
Jul 18-19, 2015
Chair: Marco De Cecco
Associate Chair: Cagdas Tazearslan

Amygdala in Health & Disease

Classical Fear/Threat Conditioning and Beyond
Aug 2-7, 2015
Stonehill College, Easton, MA
Chair: Sheena Josselyn
Vice Chair: Andrew Holmes

- **Keynote Session: New Tools from Rodents to Humans**
  (*Stephen Maren* / Barry Everitt / Elizabeth Phelps / AMC Lecturer: Karl Deisseroth)
- **The Amygdala and Cognition**
  (*Mark Baxter* / Daniel Salzman / Rony Paz / Denis Pare / Satish Nair)
- **The Amygdala and Reward**
  (*Michael Fanselow* / Jane Taylor / Yavin Shaham / Kay Tye / Yan Dong)
- **Regulation of Fear: Circuit and Network Interactions**
  (*Punkaj Sah* / Josh Gordon / Adam Carter / Josh Johanson / Vadim Bolshakov / David Anderson)
- **The Amygdala and Social Behaviour**
  (*Regina Sullivan* / Elisabeth Murray / Katalin Gothard / Steve Chang)

Gordon Research Conferences: 2015 "Session II" Meeting Schedule and Preliminary Programs

- **The Amygdala, Appetitive Behaviour, Addiction and Action**
  (*Gregory Quirk* / Susumu Tonegawa / Bernard Balleine / Geoff Shoenbaum)
- **The Amygdala and Stress**
  (*Hans-Christian Pape* / Matthew Hill / Danny Winder / Bo Li / Stan Floresco)
- **Inhibitory Circuits in the Amygdala: Structure and Function**
  (*Donald Rainnie* / Andreas Luthi / Haruhiko Bito / Jin-Hee Han / Ofer Yizhar)
- **The Amygdala and Disease: From Autism to PTSD**
  (*Aleksandra Vicentic* / Sumantra Chattarji / Ted Abel / Kafui Dzirasa / Kerry Ressler)

GRS Amygdala in Health & Disease
New Frontiers in Amygdala Research: From Rodent to Man
Aug 1-2, 2015
Chair: Caitlin A. Orsini
Associate Chair: Jose Rodriguez-Romaguera

Angiogenesis
New Mechanisms in Vascular Patterning and Specialization: From Cells to Functional Networks
Aug 2-7, 2015
Salve Regina University, Newport, RI
Chair: Holger Gerhardt
Vice Chair: Shahin Rafii

- **Keynote Session: Vascular Networks in Development and Disease**
  (*Holger Gerhardt* / Kari Alitalo)
- **Building Tubular Networks - Morphogenic Principles**
  (*Markus Affolter* / Arndt Siekmann / Christer Betsholtz)
- **Vascular Network Specialization and Endothelial Heterogeneity**
  (*Shahin Rafii* / Ralf Adams / Stefan Schulte-Merker / Hellmut Augustin / Shahin Rafii)
- **Endothelial Homeostasis and Metabolism**
  (*Peter Carmeliet* / Peter Carmeliet / Massimo Santoro)
- **Genetic, Molecular and Cellular Mechanisms in Vascular Plasticity**
  (*Elisabetta Dejana* / Anne Eichmann / Douglas Marchuk / Luisa Iruela-Arispe)
- **Endothelial Signaling - Complexity and Integration**
  (*Victoria Bautch* / Chenghua Gu / Lena Claessen-Welsh)
- **Biophysics of Functional Vascular Patterning**
  (*Christopher Hughes* / Julien Vermot / David Beech)
- **New Concepts Through Integrated Experimentation and Computational Modeling**
  (*Katie Bentley* / Shayn Peirce)
- **Clinical Challenges and Approaches in Angiogenesis - New Tools and Avenues**
  (*Gavin Thurston*)

GRS Angiogenesis
Mechanisms Driving Vessel Morphogenesis
Aug 1-2, 2015
Chair: Li-Kun Phng
Associate Chair: Véronique Gebala

Animal-Microbe Symbioses NEW!
Identifying the Common Language of Host-Microbe Associations
Jun 21-26, 2015
Waterville Valley Resort, Waterville Valley, NH
Chair: Nicole Dubilier
Vice Chair: Edward G. Ruby

- **Becoming Small: Genome Reduction in Microbial Symbionts**
  (*Colin Dale* / Christian Kost / John McCutcheon)
- **Alliance, Cooperation and Conflict**
  (*Dieter Ebert* / Monika Bright / Matthias Horn / Stuart West)
- **Overlooked Partners: Viruses and Fungi**
  (*Mya Breitbart* / Michael Poulsen / Forest Rohwer)
- **Hooking up Underwater: Symbiosis in the Sea**
  (*Ute Hentschel* / Silvia Bulgheresi / Todd LaJeunesse / Tim Miyashiro)
- **Learning from Plant-Microbe Symbioses**
  (*R. Ford Denison* / Ann Hirsch / Peter Mergaert)
- **Insects: The Great Experimenters in Symbiosis**
  (*Alex Wilson* / Angela Douglas / Takema Fukatsu / Martin Kaltenpoth)
- **New Approaches in Symbiosis Research**
  (*Robert Hettich* / Pieter Dorrestein / Jeroen Raes)
- **Microbial Effects on Animal Life History Strategies**
  (*Thomas Bosch* / Rosie Alegado / Seth Bordenstein / Denise Dearing)
- **Close to Home: The Human Microbiota**
  (*Sarkis Mazmanian* / Wendy Garrett / Rob Knight)

Apoptotic Cell Recognition & Clearance
Physiological Significance and Pathological Consequences
Jun 14-19, 2015
University of New England, Biddeford, ME
Chairs: David S. Ucker
Vice Chairs: Peter Henson & Kirsten Lauber

- **Apoptosis in the Larger Physiological Context**
  (*Kodi Ravichandran* / Peter Vandenabeele)
- **Lipid Alterations in Apoptotic Cells and in Other Cells, Too**
  (*Peter Henson* / Xiaoping Du / Shigekazu Nagata)
- **Consequences of Lipid Alterations for Apoptotic Cell Clearance**
  (*Christopher Gregory* / Raymond Birge / Ian Dransfield / Xianming Huang)
- **Physiological and Pathological Consequences of Clearance Mechanisms**
  (*Raymond Birge* / Rebecca Cook)
- **Other Apoptotic Signals in Recognition and Clearance**
  (*Zheng Zhou* / Kirstin Lauber / Kodi Ravichandran)
- **Immune Effects of Apoptotic Cells**
  (*Kirsten Lauber* / Philip Cohen / Carla Rothlin)
- **Pathogenic Subversion of Apoptotic Processes**
  (*Nathalie Franc* / Marcello Barcinski / Kouki Morizono / Joao Luiz Wanderley)
- **Evolutionary Insights from Model Organisms**
  (*Marcello Barcinski* / Nathalie Franc / Zheng Zhou / Chun Han)
- **Insights from the Diversity of Cell Death Mechanisms**
  (*Peter Vandenabeele* / Kenneth Bayles / Moritz Nowack / Martin Herrmann)

GRS Apoptotic Cell Recognition & Clearance
Responses to Apoptotic Cells Leading to Inflammatory Resolution and Pathogenesis
Jun 13-14, 2015
Chair: Goutham Pattabiraman

Applied & Environmental Microbiology
Microbes that Influence, Sustain and Protect Our Planet
Jul 12-17, 2015
Mount Holyoke College, South Hadley, MA
Chair: J. Colin Murrell
Vice Chair: Yuri A. Gorby

- **Synthetic Microbiology**
  (*Gregg Whited* / Mary Lidstrom / Louise Horsfall)
- **Microbial Cycling of Nitrogen and Sulfur**
  (*Thomas Hanson* / Josh Neufeld / Levente Bodrossy / Gerard Muyzer / Kim Heylen)
- **New Approaches in Biocatalysis and Biodegradation**
  (*Rebecca Parales* / Lawrence Wackett / Tillmann Lueders / Rams Ramaswamy)
- **Microbial Symbioses**
  (*Joy Watts* / David Bourne / Andreas Brune / Nicole Dubilier / Ryuichi Koga)
- **Electrobiology**
  (*Yuri Gorby* / Lars Nielsen / Mo El Naggar / Gemma Reguera)
- **Marine Biogeochemical Cycles**
  (*Peter Girguis* / Mandy Joye / Julie Huber / Osvaldo Ulloa / Jon Todd)
- **Microbes and Humans: Interactions and Interventions**
  (*Michael Sadowsky* / Andrew Holmes / Christine Salomon / Liping Zhao)
- **Emerging Techniques in Microbial Ecology**
  (*Jennifer Pett-Ridge* / Marja Tiirola / Anne Kaster / Ann Pearson / Michael Wagner)
- **Biogeochemical Cycles in the Terrestrial and Freshwater Environment**
  (*Paul Bodelier* / Kirsten Kusel / Lise Ovreas / Harold Drake)

GRS Applied & Environmental Microbiology
Solving Important Microbiological Questions in the "Omics" Era
Jul 11-12, 2015
Chair: Anne K. Kaster
Associate Chair: Jennifer Hiras

Archaea: Ecology, Metabolism & Molecular Biology
Archaeal Biology Nearly Two Decades After the First Genome: Transforming Our Understanding of Life by Leveraging Tools of the Post-Genomic Age
Jul 26-31, 2015
Sunday River Resort, Newry, ME
Chairs: Todd Lowe & Ruth A. Schmitz-Streit
Vice Chairs: Thomas J. Santangelo & Nick Robinson

- **Keynote Session: Archaeal Biology Nearly Two Decades After the First Genome**
  (*Eugene Koonin* / Gerhard Gottschalk / Anna-Louise Reysenbach)
- **Replication, Recombination, and Repair**
  (*Zvi Kelman* / Nick Robinson / Thorsten Allers / Stephen Bell / Andrew Gardner)
- **Transcription**
  (*Finn Werner* / Thomas Santangelo / Eveline Peeters)
- **CRISPR and Viruses**
  (*Michael Terns* / Patrick Forterre / Eugene Koonin / David Prangishvili / Lennart Randau / Rachel Whitaker / Malcolm White)
- **Cell Biology and Metabolism**
  (*Robert Gunsalus* / Sonja-Verena Albers / Jose del la Torre)
- **Non-Coding RNAs**
  (*Joerg Soppa* / Beatrice Clouet D'Orval / Cameron Mura / Joerg Soppa)
- **Posttranslational Modifications**
  (*Bettina Siebers* / Haruyuki Atomi / Julie Maupin-Furlow)
- **Genomics and Evolution**
  (*Patrick Forterre* / Thijs Ettema / Kira Makarova / William Martin / Laurence Prunetti)
- **Biotechnology Applications**
  (*Frank Robb* / Paul Blum / Frank Robb)

Artificial Molecular Switches & Motors NEW!
Towards Molecules Performing Useful Work
Jun 7-12, 2015
Stonehill College, Easton, MA
Chairs: Rafal Klajn & Christoph A. Schalley
Vice Chair: Amar H. Flood

- **Development of New Switches**
  (*Christoph Schalley* / Jiro Abe / Ivan Aprahamian / A.P. de Silva)
- **Integration with Polymers**
  (*Rachel O'Reilly* / Stefan Hecht / Christopher J. Barrett / Nicolas Giuseppone / Nathalie Katsonis)
- **Switching in the Solid State**
  (*John A. Gladysz* / Miguel A. Garcia-Garibay / Masahiro Irie / Pance Naumov)
- **Emerging Applications in Bioimaging**
  (*Zbigniew Pianowski* / Francisco M. Raymo / Alexander D.Q. Li / Rainer Herges / Angelique Y. Louie)
- **Integration with Solid-State Materials**
  (*Wesley R. Browne* / Paul S. Weiss / Martin Weinelt / Stephen J. Loeb)

- **Emerging Biomedical Applications**
  (*Rafal Klajn* / G. Andrew Woolley / Ben L. Feringa / Dirk Trauner / Jeffrey I. Zink)
- **Supramolecular Switches**
  (*Jovica Badjic* / He Tian / Feihe Huang / Akira Harada)
- **Towards Molecular Machines**
  (*Frederic Coutrot* / Takuzo Aida / R. Dean Astumian / David A. Leigh / Itamar Willner)
- **Mechanically Interlocked Switches**
  (*Gwenael Rapenne* / Alberto Credi / Edith Sevick / J. Fraser Stoddart)

Assisted Circulation

Advancing the Science of Mechanically Assisted Circulatory Support Through Collaboration and Innovation
Jun 14-19, 2015
Renaissance Tuscany Il Ciocco Resort, Lucca (Barga), Italy
Chairs: Joseph G. Rogers & Heinrich Schima
Vice Chairs: Mark S. Slaughter & Karen D. May-Newman

- **Mechanically Assisted Circulation: Past, Present and Future**
  (*O.H. Frazier*, *John Watson* / Michael Acker / George Wieselthaler)
- **Improving Device Performance: Enhancing Durability and Reducing Blood Trauma**
  (*Ulrich Steinseifer*, *Monica Colvin-Adams* / Hardean Achneck / David Ku / William Wagner)
- **The Challenges of Mechanically Assisted Circulation in Special Populations**
  (*Pascal Leprince*, *Stephan Schueler* / Daniel Burkhof / Bartley Griffith)
- **Innovative Circulatory Support Device Designs and Operating Modes**
  (*Karen May-Newman*, *Mark Slaughter* / Andreas Arndt / Walter Dembitsky / William Cohen)
- **New Approaches to Manufacturing and Managing Therapies for Advanced Heart Failure**
  (*Timothy Baldwin*, *Mariell Jessup* / Trevor Snyder)
- **Adverse Events in Assisted Circulation: Developing a Structured Framework for Identification and Mitigation**
  (*Robert Kormos*, *Victor Poirier* / Gregory Lanza / Natasha Loghmonpour / Tim Kelley)
- **Engineering Adverse Events out of Mechanical Blood Pumps**
  (*Paul Mohacsi*, *Cumaraswamy Sivathasan*, / Marcus Granegger / Bart Meyns)
- **Myocardial Recovery: Fundamental Mechanisms and Facilitated Functional Improvement**
  (*Emma Birks*, *Stavros Drakos* / Deborah Ascheim / Michael Dandel / Craig Selzman / Douglas Mann)
- **Moving MCS Forward in the Next 5 Years**
  (*Francesco Moscato*, *Lynne Warner-Stevenson* / Annetine Gelijns)

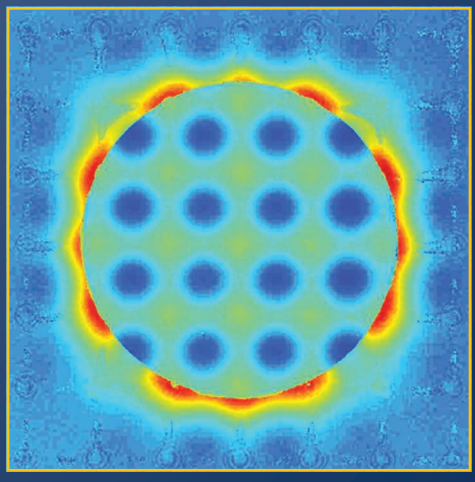
GFS Assisted Circulation
Collaborative Advancements in Technology and Practice to Improve Outcomes During Mechanical Circulatory Support
Jun 13-14, 2015
Chair: Salim E. Olia
Associate Chair: William Cornwell

Atherosclerosis

Mechanisms and Modifiers
Jun 21-26, 2015
Sunday River Resort, Newry, ME
Chairs: Klaus Ley & Stanley L. Hazen
Vice Chairs: Matthias Nahrendorf & Stefanie Dimmeler

- **Microbiota and Cardiometabolic Diseases**
  (*Stephen Nicholls* / Stanley Hazen / Max Nieuwdorp / Mark Brown / Sean Davies)
- **High Density Lipoproteins**
  (*Peter Libby* / John Parks / Mary Sorci-Thomas / Gwendalyn Randolph / Lynn Hedrick)
- **IL1 and Atherosclerosis**
  (*Lynn Hedrick* / Charles Dinarello / Eicke Latz / Peter Libby)
- **Post-MI Myocardial Inflammation**
  (*Stanley Hazen* / Matthias Nahrendorf / Edward Thorp / Filip Swirski / Ziad Mallat / Slava Epelman)
- **Shear Stress and Atherosclerosis**
  (*Matthias Nahrendorf* / Eleni Tzima / Martin Schwartz / Mukesh Jain)
- **Imaging Atherosclerosis / Non-Coding RNAs in Atherosclerosis**
  (*Martin Schwartz, Filip Swirski* / Farouc Jaffer / Robin Choudhury / Zahi Fayad / Carlos Fernandez-Hernando / Christian Weber / Stefanie Dimmeler)
- **Genetics of Cardiovascular Disease**
  (*Carlos Fernandez-Hernando* / Ruth McPherson / Christopher Glass / Jake Lusis / Kenneth Walsh)
- **Innate Immunity and Atherosclerosis**
  (*Ruth McPherson* / Daniel Simon / Esther Lutgens / Masanori Aikawa / Paul Fox / Edward Fisher)
- **New Clinical Targets**
  (*Paul Fox* / Sergio Fazio / Stephen Nicholls / Sam Tsimikas / Bill Sasiela)

GFS Atherosclerosis
Complex Interactions in Atherosclerosis
Jun 20-21, 2015
Chair: Mete Civelek
Associate Chair: Jie Li



Visualized deformation of a compliant substrate due to surface tension of a drop. Courtesy of Dr. Nichole Nadermann. Submitted by Anand Jagota, Chair, Science of Adhesion GRC.

Atmospheric Chemistry

Multiphase Processes: Observations and Fundamentals
Aug 2-7, 2015
Waterville Valley Resort, Waterville Valley, NH
Chair: Paul B. Shepson
Vice Chair: Kim Prather

- **Keynote Session: Atmospheric Chemistry of Metals**
  (*Cort Anastasio* / Mark Taylor / Parisa Ariya / Vicki Grassian)
- **BVOC - Ecosystem Interactions**
  (*Gunnar Schade* / Jose Fuentes / James Tumlinson)
- **Organic Chemistry in the Particle Phase**
  (*Sally Ng* / Sergey Nizkorodov / Faye McNeill / Jason Surratt)
- **Halogens in the Troposphere**
  (*Roland Von Glasow* / Markus Ammann / Urich Platt / Kerri Pratt)
- **Satellite Observations - From Global to Megacities**
  (*Gregory Frost* / David Crisp / John Burrows / Eric Kort)
- **BVOC Oxidation Mechanisms: New Perspectives**
  (*John Orlando* / John Crounse)
- **BVOC Oxidation Mechanisms: Connecting the Laboratory and the Field**
  (*John Orlando* / Frank Keutsch / Delphine Farmer)
- **Ozonolysis and Criegee Radical Chemistry**
  (*Dylan Millet* / Marsha Lester / Dudley Shallcross)
- **Keynote Session: Multiphase Atmospheric Chemistry and Models**
  (*Annmarie Carlton* / Andreas Wahner / James Donaldson / Barbara Finlayson-Pitts)

Atomic Physics

From Ultracold to Strongly Interacting Quantum Systems
Jun 14-19, 2015
Salve Regina University, Newport, RI
Chair: Vladan Vuletic
Vice Chair: Marianna Safronova

- **Fundamental Constants and Tests of Basic Laws**
  (*Joachim Ullrich* / Guglielmo Tino / Peter Graham)
- **Cold Ions**
  (*Dietrich Leibfried* / Hartmut Haeffner / Brian Odom / Jose Lopez-Urrutia)
- **Ultrafast Spectroscopy and Applications**
  (*Kenji Ohmori* / Mette Gaarde / Anne Marie March)
- **Precision Measurements**
  (*Eric Cornell* / Hidetoshi Katori / Jun Ye / Markus Aspelmeyer)
- **Quantum Gases**
  (*Wolfgang Ketterle* / Monika Schleier-Smith / Joseph Thywissen)
- **Quantum Simulation and Computation**
  (*Thad Walker* / Markus Greiner / Benjamin Lev / Alexey Gorshkov)
- **Bose and Fermi Gases**
  (*Maciej Lewenstein* / Hanns-Christoph Naegerl / Chris Vale)
- **Collective Dynamics**
  (*Deborah Jin* / Trey Porto / Wonho Jhe / Eugene Polzik)
- **Quantum Information and Networks**
  (*Mikhail Lukin* / Ronald Hanson / Jelena Vuckovic)

Barrier Function of Mammalian Skin

Defining, Investigating and Surmounting the Barrier
Aug 16-21, 2015
Waterville Valley Resort, Waterville Valley, NH
Chairs: Dennis R. Roop & Reinhard H.H. Neubert
Vice Chairs: Samir S. Mitragotri & Joachim W. Fluhr

- **Keynote Session: Progress in Defining, Investigating and Surmounting the Barrier**
  (*Theodora Mauro*, *Philip Wertz* / Peter Elias / Richard Guy / Lars Norlen)
- **Normal and Pathological Responses to Barrier Disruption**
  (*Steven Hoath*, *Maria Morasso* / Allan Balmain / Irwin McLean / Ralf Paus / Fiona Watt)
- **Overcoming the Barrier in Delivering Therapeutics**
  (*Gerald Kasting*, *Erwin Tschachler* / Adrian Davis / Mike Farwick / Amy Paller / Samir Mitragotri)
- **Regulating Barrier Formation and Maintenance**
  (*Nava Dayan*, *Cristina De Guzman Strong* / Masayuki Amagai / Thomas Magin / Carien Niessen / Sabine Werner)
- **New Technology for Investigating / Penetrating the Barrier**
  (*Marek Haftek*, *Michael Roberts* / Roger Kaspar / Kevin Mills / Xiao-Jing Wang / Gabriel Wittum)
- **Itch and the Epidermal Barrier**
  (*Lisa Beck*, *Ellen Lumpkin* / Ethan Lerner / Sarah Ross / Gil Yosipovitch / Rox Anderson)
- **Late-Breaking Topics / Young Investigator Presentations**
  (*Joachim Fluhr*, *Reinhard H. Neubert*)
- **Stratum Corneum Structure and Function: What Is New?**
  (*Joke Bouwstra*, *Juergen Lademann* / Gerald Brezesinski / Alain Hovnanian / Daniel Huster / Andrzej Slominski)
- **Skin Barrier in Health and Disease / *In Vitro* vs *In Vivo* Models of Barrier Function**
  (*Heidi Kong*, *Birgit Lane*, *Walter Holleran*, *Gopinathan Menon* / Matthew Hardman / Johannes Wohlrab / Jonathan Garlick / Spiro Getsios / Arup Indra / Jerrold Turner)

Gordon Research Conferences are different from other scientific conferences because. . .

...they contain one high caliber presentation after another, complemented by robust discussions of important scientific topics in our field, day after day. It's truly a unique experience. *(David E. Watson, Chair, 2014 Drug Safety GRC)*

Bioenergetics

Structures, Mechanisms and Targets of Human Disease
Jun 21-26, 2015
Proctor Academy, Andover, NH
Chair: Karlett J. Parra
Vice Chair: Judy Hirst

- **ATP Synthase Structures and Mechanisms** (*Wayne Frasch* / John Walker / Masasuke Yoshida)
- **Approaches to Bioenergetics Research** (*Michael Borsch* / Jianhua Zhao / Petra Fromme / Karin Busch)
- **V/A-Type ATPase Motors at Work** (*Stephan Wilkens* / Takeshi Murata / Patricia Kane)
- **Drug Targets in Bioenergetics** (*Dirk Bald* / Markus Huss / Thomas Meier / Gregory Cook / Hazel Szeto)
- **Respiratory Complexes and Supercomplexes** (*Robert Gennis* / Hartmut Michel / Ulrich Brandt / Karen Davies)
- **At the Crossroads Between Health and Disease** (*Susanne Arnold* / Sylvie Breton / Michael Forgac / Vanessa Morais)
- **Mitochondrial Function and Regulation** (*David Nicholls* / Roberto Screaton / Douglas Wallace / David Chan)
- **Young Investigator Presentations** (*Jose Garcia-Trejo, Judy Hirst*)
- **Emerging Concepts in Bioenergetics** (*Heidi McBride* / Roberto Zoncu / Paolo Bernardi)

Biomaterials & Tissue Engineering

Regenerative Engineering and Functional Materials Integration
Jul 19-24, 2015
Melia Golf Vichy Catalan Business and Convention Center, Girona, Spain
Chair: Edward A. Botchwey
Vice Chairs: Horst Von Recum & Joel H. Collier

- **Keynote Session: Immuno-Engineering** (*Joel Collier* / M.G. Finn / Ron Germaine)
- **Harnessing Inflammation for Tissue Repair** (*Edward Botchwey* / Nadia Rosenthal / David Mooney / Shayn Peirce)
- **Strategies to Direct Neural Regeneration** (*Rachel Pearson* / Randolph Ashton / Rachel Pearson)
- **Therapeutic Neovascularization** (*Mary Dickinson* / Mary Dickinson / Steven George / Timothy Hla)
- **Stimulus Response Biomaterials** (*Horst Von Recum* / Arancha del Campo / Cassandra Fraser)
- **Harnessing Niche Concepts for Regenerative Medicine** (*Brendan Harley* / Brendan Harley / Shahin Rafii)
- **Translational Biomaterials** (*Cato Laurencin* / Cato Laurencin / Marc Prausnitz)
- **Hydrogels in Regenerative Medicine** (*Ali Khademhousseini* / Jason Burdick / Ali Khademhousseini / Jennifer West)
- **Selected Poster Presentations** (*Edward Botchwey*)

GRS Biomaterials & Tissue Engineering
Regenerative Engineering and Functional Materials Integration
Jul 18-19, 2015
Chair: Jagannath Padmanabhan

Bioorganic Chemistry

Chemical Tools for Decoding Biology and Advancing Medicine
Jun 7-12, 2015
Proctor Academy, Andover, NH
Chairs: Michelle Arkin & Violeta L. Marin
Vice Chairs: Carole A. Bewley & Douglas S. Johnson

- **Structural Evaluation of Protein-Molecule Interactions** (*Jason Gestwicki* / Derek Lowe / Dorothee Kern / Jolanta Grembecka)
- **Design of New Cellular Tools for Biology** (*Brian Callahan* / Stephen Miller / Jennifer Prescher / Keith Wood)
- **Proteins and Peptides with Novel Functions** (*Joshua Kritzer* / Paramjit Arora / Samuel Gellman)
- **Chemical Biology of Post-Translational Modification** (*Lindsey Ingerman* / Danica Fujimori / Ingrid Wertz / Pauline Rudd)
- **Harnessing the Immune System for Cancer** (*Gregory Weiss* / Ho Sung Cho / David Rabuka / Jane Grogan)
- **Improving on Nature** (*Michelle Arkin* / Roger Linington / Floyd Romesberg / Patrick Brown)
- **Strategies for Drug Discovery's Most Difficult Targets** (*Samy Meroueh* / Eric Olson / Nick Terrett / Lee Rubin)
- **Forward and Reverse Chemical Genetics** (*Milka Kostic* / Matthew Bogyo / Craig Thomas / Bryan Roth)
- **Keynote Session: Beyond the Base-Pair: Molecular Recognition of Nucleic Acids** (*Bruce Armitage* / Jacqueline Barton / Danith Ly / Deborah Wuttke)

CAG Triplet Repeat Disorders

CAG Repeat Expansion Diseases: From Basic Biology to Therapeutics
May 31 - Jun 5, 2015
Renaissance Tuscany Il Ciocco Resort, Lucca (Barga), Italy
Chair: Beverly L. Davidson
Vice Chair: Erich E. Wanker

- **Keynote Session: RNA – New Keys to Pathogenesis?** (*Thomas Cooper, David Housman* / Susan Ackerman / Laura Ranum)
- **Images – Beyond the Eye of the Beholder. What Does the Natural History Data Tell Us?** (*Richard Meyers, Richard Faull* / Steve Rao / Alexandra Durr / Sarah Tabrizi / Gary Egan)
- **Modeling Pathogenesis** (*William Yang, Jenny Morton* / Anthony Chan / Lisa Ellerby / Chris Rogers)
- **Designing Therapies for Brain Diseases** (*Jang-Ho Cha, Hao Wang* / Isabel Perez-Otano / Susan Slaugenhaupt / Joy Yu Zuchero / Bradley Hyman)
- **Emerging Therapies for the Triplet Repeat Disorders** (*Kurt Fischbeck, Bernhard Landwehrmeyer* / Frank Bennett / Helen Puccio)
- **Pathogenesis – Emerging Mechanisms** (*Richard Morimoto, Christopher Pearson* / Gino Cortipassi / Peng Jin / Vikram Shakkottai / Robert Friedlander)
- **Young Investigator Presentations Selected from the GRS: From Molecules to Humans** (*Harry Orr, Sarah Tabrizi*)
- **Pathogenic Mechanisms in Disease Models** (*Elena Cattaneo, Christopher Ross* / Aaron Gitler / Diane Merry / Harry Orr / Leslie Thompson)
- **Beyond the Neuron** (*Michael Hayden, Gillian Bates* / Marija Cvetanovic / Andrew Lieberman / Jodi McBride)

GRS CAG Triplet Repeat Disorders
From Molecular Mechanisms to Therapeutics
May 30-31, 2015
Chair: Emily J. Sontag
Associate Chair: Andreas Neueder

Calcium Signalling

Molecular and Cellular Mechanisms in Health and Disease
Jun 7-12, 2015
Sunday River Resort, Newry, ME
Chair: David I. Yule
Vice Chair: Anant B. Parekh

- **Calcium and Cell Function: Cells, Organs and Organisms** (*Tullio Pozzan* / Baljit Khakh / Silvia Moreno / Andrew Miller)
- **New Insights into Calcium Stores and Intracellular Calcium Channels** (*Katsuhiko Mikoshiba* / Filip Van Petegem / Jonathan Marchant / Andrew Thomas / Rouslan Efremov)
- **Disordered Calcium Release and Disease** (*Ole Petersen* / Donald Bers / Barbara Ehrlich / Haoxing Xu)
- **Plasma Membrane Calcium Channels: Orais, TRPs and VOCCs** (*James Putney* / Henry Colecraft / Arthur Konnerth / Christoph Romanin)
- **Calcium Influx and Disease** (*Donald Gill* / Joost Hoenderop / Shmuel Muallem)
- **Mitochondrial Calcium Handling** (*Aldebaran Hofer* / Gyorgy Hajnoczky / Sarino Rizzuto / Mootha Vamsi / Kevin Foskett)
- **Calcium Signaling and Cell Fate** (*Jan Parys* / Jason Bruce / Ira Tabas / Zhaoxia Sun)
- **Calcium Signaling in Inflammatory and Immunological Disease** (*Alexei Tepikin* / Indu Ambudkar / Stefan Feske / Nicolas Demaurex / Ricardo Dolmetsch)
- **Keynote Session: Signaling to and from IP3R / Late-Breaking Topics** (*Anant Parekh, David Yule* / Colin Taylor)

GRS Calcium Signalling
Insights into Molecular Signaling, Cellular Function and Disease
Jun 6-7, 2015
Chair: Ivana Y. Kuo
Associate Chair: Kamil J. Alzayady

Cancer Nanotechnology

Nanomedicines from Laboratory to Clinical Reality
Jun 28 - Jul 3, 2015
Mount Snow Resort, West Dover, VT
Chair: Leaf Huang
Vice Chair: Alexander V. Kabanov

- **Cancer Microenvironment** (*Leaf Huang* / Douglas Fearon / Biana Godin Vilentchouk)
- **Chemo Drugs** (*Biana Godin Vilentchouk* / Kazunori Kataoka / Puja Sapra / Yuliang Zhao)
- **Stealth Nanoparticles and Tumor Penetrating Peptides** (*Kazunori Kataoka* / Shaoyi Jiang / Samuel Lai)
- **Vector/Host Interaction** (*Carlos Rinaldi* / Suzie Pun / Ronit Satchi-Fainaro)
- **New Nanomaterials** (*Suzie Pun* / David Weiner / Liangfang Zhang)
- **Immunology and Vaccine** (*Shawn Chen* / Peixuan Guo / Carlos Rinaldi)

- **Early Diagnosis and Imaging**
  (*Liangfang Zhang* / Shawn Chen / Dmitri Lapotko)
- **Genes and siRNA**
  (*David Weiner* / Muthiah Manoharan)
- **Selected Poster Presentations**
  (*Alexander Kabanov*)

Carbohydrates
Frontiers in Basic and Translational Glycosciences
Jun 14-19, 2015
Mount Snow Resort, West Dover, VT
Chairs: Jeffery C. Gildersleeve & Alexei V. Demchenko
Vice Chair: Lai-Xi Wang

- **Defining and Understanding Glycomes**
  (*Dan Ratner* / Carlito Lebrilla / Hans Lin / Lara Mahal)
- **Advances in Chemical Glycosylation**
  (*Shang-Cheng Hung* / David Crich / Cristina De Meo / Kieth Stine / Biao Yu)
- **Chemical Glycobiology**
  (*Danielle Dube* / Geert-Jan Boons / Carmen Galan / Suzanne Walker)
- **Frontiers in Carbohydrate Synthesis**
  (*Zhongwu Guo* / Srinivas Hotha / Shino Manabe / George O'Doherty)
- **Wonders of the Bacterial World**
  (*Nikki Pohl* / Robert Field / Daniel Kahne / Christine Szymanski)
- **Design and Synthesis of Carbohydrates**
  (*Steve Kolodziej* / Jeroen Codee / Matthiew Sollogoub / Daniel Varon Silva)
- **Translational Carbohydrate Chemistry**
  (*Robert Woods* / Michael Gelb / Vern Schramm / Mark Von Itzstein)
- **Anti-Glycan Immunity**
  (*Lai-Xi Wang* / Joseph Barchi / Nicolai Bovin / Luigi Panza / Peng George Wang)
- **Carbohydrates and Immunology: Partners for Life**
  (*Jeffery Gildersleeve* / Xuefei Huang / AMC Lecturer: Laura Kiessling)

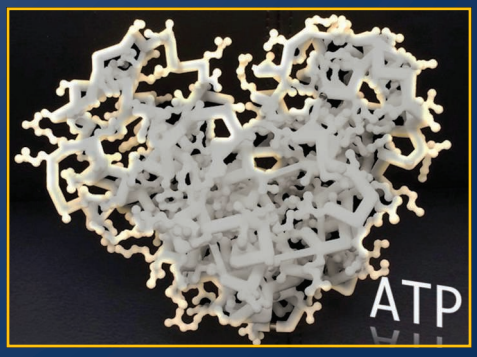
Carbon Capture, Utilization & Storage
NEW!
Defining the Frontiers
May 31 - Jun 5, 2015
Stonehill College, Easton, MA
Chair: Berend Smit
Vice Chair: Ah-Hyung (Alissa) Park

- **Energy Policies and Carbon Capture Utilization and Storage**
  (*Jeffrey Reimer* / Robert Socolow / Jeffrey Sachs)
- **Engineering and Scientific Challenges in Carbon Capture**
  (*George Richards* / Olav Bolland / Liang-Shih Fan / Klaus Lackner)
- **Fundamentals and Challenges of Geological Storage**
  (*Roger Aines* / Sally Benson / Juerg Matter)
- **Fundamentals and Challenges on CO_2 Utilization**
  (*Herve Toulhoat* / Paul Kenis / Martin Saar / Suojiang Zhang)
- **Novel Materials for Carbon Capture**
  (*Paul Fennell* / Jennifer Wilcox / Krista Walton)
- **Barriers Towards Large-Scale CCUS**
  (*Herve Toulhoat* / Julio Friedmann / Sarah Forbes / Jon Gibbins)
- **Emerging Technologies for Carbon Capture**
  (*Jeffrey Reimer* / Sasha Mackler / Marco Mazotti)
- **Technical Challenges in Large-Scale Geological Storage**
  (*Jan Brouwer* / Joshua White / Andrew Cavanagh)
- **Novel Routes to Use CO_2**
  (*G. Tayhas Palmore* / John Hansen / Amin Salehi)

Catchment Science: Interactions of Hydrology, Biology & Geochemistry
Thresholds in Time and Space
Jun 14-19, 2015
Proctor Academy, Andover, NH
Chairs: Kathleen C. Weathers & Jan Seibert
Vice Chair: Kevin J. McGuire

- **Thresholds in Time and Space: Exploring at the Big Picture**
  (*Erika Marin-Spiotta*, *John Stoddard* / Irena Creed)
- **Conceptual Frameworks: Are Thresholds and Resilience Useful Frameworks for Understanding Catchment Behavior?**
  (*Vazken Andreassian*, *Patricia Soranno* / Kathryn Cottingham / Brian McGlynn / Tim Peterson / Richard Pouyat)
- **Dynamical Thresholds in Water Quality**
  (*Vazken Andreassian*, *Patricia Soranno* / James Kirchner)
- **Observations: What's To Be Learned from Catchment Experiments and Models?**
  (*Gary Lovett*, *Ilja van Meerveld* / Christine Alewell / Louise Bracken / Klement Tockner)
- **Where Observations Fall Short**
  (*Gary Lovett*, *Ilja van Meerveld* / Emily Stanley)
- **Predicting Thresholds Under the Wings of Change**
  (*Stacey Archfield, Daniele Penna* / Jill Baron / Markus Hrachowitz / Hilary McMillan / Stefan Gerber)
- **Is It Possible to Predict Surprises?**
  (*Stacey Archfield, Daniele Penna* / Michael Pace)
- **From Vertical to Horizontal Frontiers: Exploring Resilience and Elasticity in Catchments**
  (*Diane McKnight, Tom Harmon* / Jan Fleckenstein / Alberto Montanari / Stephen Sebestyen / Beverley Wemple)
- **Frontiers in Time and Space: Practical Applications of Thresholds**
  (*Diane McKnight, Tom Harmon* / Jennifer Tank)

GRS **Catchment Science: Interactions of Hydrology, Biology & Geochemistry**
Thresholds in Time and Space
Jun 13-14, 2015
Chair: Rachel S. Gabor
Associate Chair: Ingo Heidbuechel



V-ATPase proton pumps are ATP-dependent energy converting molecular motors emerging as important drug targets. Shown is the structural model of the yeast V-ATPase subunit d built in nylon using 3D printing technology based upon the coordinates of the homologous subunit found in Archaea (PBD ID code 1R5Z). Submitted by Karlett J. Parra, Chair, Bioenergetics GRC.

Catecholamines
Frontiers in Catecholamine Function from Synapses to Disease
Aug 9-14, 2015
Sunday River Resort, Newry, ME
Chair: Paul E. Phillips
Vice Chair: David Weinshenker

- **Keynote Session: Neurotransmitter Transporters in the Regulation of Catecholamine Function**
  (*David Weinshenker* / Susan Amara)
- **From Molecules to Circuits**
  (*Howard Fields* / Aurelio Galli / Robert Edwards / Garret Stuber / Patricia Janak / Ann Graybiel / Michael Bruchas)
- **Neuroendocrinology and Development**
  (*Donita Robinson* / Patricia Jensen / Rajeshwar Awatramani / Jill Becker / Larry Zweifel)
- **Cognition**
  (*Anthony Grace* / Antonieta Lavin / Craig Berridge / Susan Sara / Matthew Carter / Joseph Cheer / Patricio O'Donnell)
- **Decision Making**
  (*Stan Floresco* / Yael Niv / Michael Frank / Charlotte Boettiger / Molly Crockett)
- **Stress, and Mood Disorders**
  (*Rita Valentino* / Carmen Sandi / Vidita Vaidya / Mary Kay Lobo / Elisabeth Van Bockstaele / Colleen McClung / Charles Chavkin)
- **Neurodegenerative Disorders**
  (*Marie-Francoise Chesselet* / D. James Surmeier / Louis-Eric Trudeau / Anatol Kreitzer / Jones Parker)
- **Substance Abuse**
  (*Regina Carelli* / Yan Dong / Antonello Bonci / Christian Luscher / Sara Jones / Jeremy Clark / Janet Neisewander)
- **Keynote Session: Regulation of Behavior and Cognition by the Locus Coeruleus / Young Investigator Presentations**
  (*Paul Phillips* / Gary Aston-Jones)

GRS **Catecholamines**
Frontiers in Catecholamine Function from Synapses to Disease
Aug 8-9, 2015
Chair: J. Andrew Hardaway
Associate Chair: Lauren M. Burgeno

Cell Biology of Metals
Mechanisms from Microbes to Humans
Jul 26-31, 2015
Mount Snow Resort, West Dover, VT
Chairs: Dennis J. Thiele & Amy E. Palmer
Vice Chairs: Michael Petris & Roland Lill

- **Keynote Session: Copper in Development and Disease**
  (*Dennis Thiele* / Jonathan Gitlin / Svetlana Lutsenko)
- **Metals, Reactivity and the Environment**
  (*James Imlay* / Eric Boyd / Jennifer Dubois / Mary Lou Guerinot / Mak Saito)
- **Structural Biology of Metalloproteins**
  (*Daniel Kosman* / Pontus Gourdon / Megan McEvoy / Amy Rosenzweig / Yoshitsugu Shiro)
- **Metal Homeostasis**
  (*Amanda Bird* / Tomas Ganz / Taiho Kambe / Byung-Eun Kim / Martina Muckenthaler)
- **Assembly and Localization of Metals**
  (*Emily Que* / Roland Lill / Iqbal Hamza / Ralf Mendel / Wayne Outten / Caroline Philpott)
- **Metals in Signaling**
  (*Daniela Buccela* / Scot Leary / Samantha Pitt / Roman Polishchuck / Michael Petris)
- **Metals at the Host Pathogen Axis**
  (*Shelley Payne* / Valeria Culotta / John Helmann / James Kronstad / Elizabeth Nolan)
- **Tools and Technologies for Metals in Biology**
  (*Christopher Chang* / Peng Chen / Christoph Fahrni / Katherine Franz / Martina Ralle)
- **Metal Homeostasis from Yeast to Mammals**
  (*Amy Palmer* / David Eide / Dennis Winge)

Cell Contact & Adhesion
Collective Behaviors and Mechanics in Health and Disease
Jun 28 - Jul 3, 2015
Proctor Academy, Andover, NH
Chair: Cara J. Gottardi
Vice Chair: Andrea McClatchey

- **Keynote Session: State of the Field: Integrating Cell Contact and Adhesion with Tissue Organization**
  (*Cara Gottardi* / Marino Zerial / Denise Montell / Christopher Chen)
- **Adhesion in Cell and Tissue Polarization**
  (*Andrea McClatchey* / Adam Martin / Jeff Hardin / Carien Niessen / Jennifer Zallen / Daniel Fletcher)

- **Actin Regulation and Organization at Cell Contacts** (*Adam Kwiatkowski* / Mark Peifer / Alpha Yap / William Brieher / Nicolas Plachta)
- **Adhesion Regulation and Collective Cell Behaviors** (*Johan De Rooij* / Francois Fagotto / Sean Sun / Barry Gumbiner / Darren Gilmour / Asako Shindo / Jeffrey Fredberg)
- **Generating and Bearing Force at Cell-Cell Junctions** (*Martin Schwartz* / Douglas Desimone / Kathleen Green / Deborah Leckband / William Weis / Margaret Gardel)
- **Barrier and Signaling Functions of Tight and Other Junctions** (*Vivian Tang* / James Anderson / Sandra Citi / Jerrold Turner / Kris DeMali / Barry Thompson)
- **Cell Contact Regulation in Disease** (*Rachel Hazan* / Andrew Ewald / Greg Longmore / Albert Reynolds / Andrew Kowalczyk / Valeri Vasioukhin)
- **Novel Adhesion Signaling Mechanisms** (*Juliet Daniel* / Helen McNeill / Pierre McCrea / Martin Schwartz / Voula Mili)
- **Adhesion in Developmental Morphogenesis** (*Jennifer Zallen* / Masatoshi Takeichi / Ulrich Tepass)

Cell Contact & Adhesion
Collective Behaviors and Mechanics in Health and Disease
Jun 27-28, 2015
Chair: Stephen S. Folmsbee
Associate Chair: Adi D. Dubash

Cell Growth & Proliferation
New Discoveries and Approaches to the Study of Cell Proliferation, with an Emphasis on Cancers
Jul 12-17, 2015
Mount Snow Resort, West Dover, VT
Chair: Anindya Dutta
Vice Chair: Peter Sicinski

- **Keynote Session: Telomerase and Genomics of Cancer** (*Anindya Dutta* / Carol Greider / Elaine Mardis)
- **Ubiquitination and Its Regulation** (*Jeanette Cook*, *David Pellman* / Vishva Dixit / Michele Pagano / Michael Rape)
- **Cancer** (*Peter Sicinski*, *Thomas Gingeras* / Robert Weinberg / Cristian Tomasetti / Jacqueline Lees)
- **DNA Replication and S-Phase** (*Jacqueline Lees*, *Todd Stukenberg* / Stephen Bell / Jeanette Cook / David Cortez)
- **Mitosis and Aneuploidy** (*Michael Rape*, *Jan Skotheim* / David Pellman / Arshad Desai / Todd Stukenberg)
- **Noncoding RNAs and Epigenetics** (*Maria Blasco* / Thomas Gingeras / Chuan He / John Rinn)
- **Cell Cycle and Telomerase** (*Carol Greider* / Maria Blasco / Jan Skotheim / Peter Sicinski)
- **Drug Targets and New Approaches** (*Elaine Mardis*, *Karlene Cimprich* / Nicholas Keen / Nicholas Navin / Mazhar Adli)
- **DNA Damage** (*David Cortez* / Karlene Cimprich / Lee Zou)

Cell Growth & Proliferation
Linking Cell Growth and Cell Cycle to Cancer Biology
Jul 11-12, 2015
Chair: Gabriel E. Neurohr
Associate Chair: Deepak K. Jha

Cellular & Molecular Mechanisms of Toxicity
Mechanistic Toxicology: The Path Forward
Aug 9-14, 2015
Proctor Academy, Andover, NH
Chair: Dana C. Dolinoy
Vice Chair: Yanan Tian

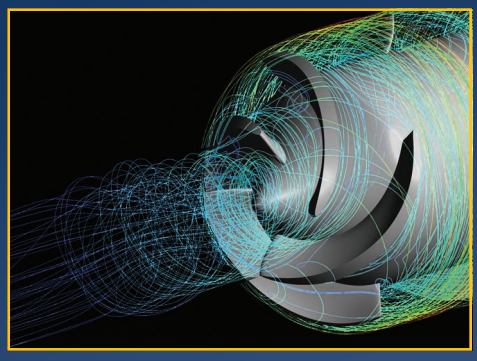
- **Keynote Session: Mechanistic and Personalized Approaches to Evaluating Toxicity and the Microbiome** (*Charlene McQueen* / Nathan Price / Robin Knight)
- **What's in Your Toolbox: Emerging Technologies for Mechanistic Toxicology** (*John Richburg* / Joanna Burdette / Robert Chapin / Serrine Lau)
- **Computational Models in Toxicology** (*Ronald Hines* / John Wambaugh / Thomas Knudsen / Rudy Richardson)
- **Incorporating the Inflammasome into Mechanistic Toxicology Research** (*Jose Manautou* / Arti Shukla / Thirumala-Devi Kannegant)
- **What's in Your Toolbox: Novel *In Vivo* Model Systems in Mechanistic Toxicology** (*Patrick Allard* / Alicia Timme-Largay / Jyotshna Kanungo / Chris Vulpe)
- **Systems Pharmacology Approaches to Mechanisms of Drug Efficacy and Toxicity** (*Donna Mendrick* / Weida Tong / James Stevens)
- **Transgenerational Considerations in Toxicological Sciences** (*Alvaro Puga* / Marisa Bartolomei / Margaret Bell / Toshi Shioda)
- **Microphysiological Systems or Animals? The Present and Future of Safety and Efficacy Testing** (*Ruth Roberts* / Sally Robinson / Andries van der Meer / Uwe Marx)
- **Keynote Session: Communicating Science and Risk / Genetic and Epigenetic Mechanisms of Toxicology** (*Yanan Tian*, *Jason Richardson* / Andrew Maynard / Quan Lu / Richard Paules)

Cellular & Molecular Mechanisms of Toxicity
Advanced *In Vitro* Models in Mechanistic Toxicology
Aug 8-9, 2015
Chair: Rhiannon N. Hardwick
Associate Chair: Alessandro Venosa

Cellulosomes, Cellulases & Other Carbohydrate Modifying Enzymes
A New Era of Research on Carbohydrate-Active Enzymes: Their Reaction Mechanisms and Evolution
Aug 2-7, 2015
Proctor Academy, Andover, NH
Chair: Kiyohiko Igarashi
Vice Chair: Bernard P. Henrissat

- **Keynote Session: Evolution and Reaction Mechanisms of Carbohydrate-Active Enzymes** (*Edward Bayer* / David Hibbett / Jerry Stahlberg)
- **Evolution of Carbohydrate-Active Enzymes and Their Substrates** (*Harry Brumer* / Mary Berbee / Mark Morrison / Steven Ball)
- **Synthesis and Modification of Carbohydrates in Plant Cell Walls** (*Harry Gilbert* / Toshihisa Kotake / Debra Mohnen)
- **Redox Enzyme(s) Boosting Polysaccharide Degradation** (*Leila Lo Leggio* / Michael Marletta / Paul Walton / Bjorge Westereng)
- **Visualization of Cellulase Action** (*Satoshi Kaneko* / Douglas Clark / Shigeru Deguchi)
- **Hydrolytic Mechanisms of Glycosidic Bonds** (*Stephen Withers* / Peter Westh / Gregg Beckham / Shino Manabe)
- **Regulation of Enzyme Production for Biofuel and Biorefinery** (*Merja Penttila* / Louise Glass)
- **Protein-Protein and/or Protein-Carbohydrate Interaction in Carbohydrate-Active Enzymes** (*Alisdair Boraston* / Christina Payne / Henri-Pierre Fierobe / Michelle O'Malley)
- **Utilization of Cellulosic Biomass for Future Renewable Society** (*Mike Himmel* / Ken Tokuyasu)

Cellulosomes, Cellulases & Other Carbohydrate Modifying Enzymes
A New Era of Research on Carbohydrate-Active Enzymes: Their Reaction Mechanisms and Evolution
Aug 1-2, 2015
Chair: Lauren S. McKee



Computational fluid dynamics (CFD) -modeled flow streamlines of a prototype two-stage impeller for an implantable, fully magnetically levitated, rotodynamic, pediatric ventricular assist device (VAD). Courtesy of the PediaFlow(R) Consortium and Advanced Design Optimization LLC. Submitted by Salim E. Olia, Chair, Assisted Circulation GRS.

Cerebellum
Circuit Physiology, Computation and Disease
Aug 9-14, 2015
Bates College, Lewiston, ME
Chair: Michael D. Mauk
Vice Chairs: Thomas S. Otis & Amy Bastian

- **Human Cerebellar Function** (*Reza Shadmehr* / Pablo Celnik / Julie Fiez / Rich Ivry)
- **Synaptic Physiology of the Cerebellum** (*George Augustine* / Michael Hausser / Court Hull / Indira Raman)
- **Mechanisms of Cerebellar Learning** (*Tom Otis* / Sascha Du Lac / Steve Lisberger / Nate Sawtell)
- **Computations of the Cerebellum** (*Dieter Jaeger* / Dora Angelaki / Erik De Schutter / Maurice Smith)
- **Disorders of the Cerebellum** (*Amy Bastian* / Christopher Gomez / Ellen Hess / Joanna Jen)
- **Plasticity and Learning in the Cerebellum** (*Steve Lisberger* / Javier Medina / Jennifer Raymond / Reza Shadmehr)
- **Mechanisms of Cerebellar Development** (*Susan Ackerman* / Susan Ackerman / Kathleen Millen / Roy Sillitoe)
- **Cerebellar Physiology** (*David Linden* / Egidio D'Angelo / David Digregorio / George Augustine)
- **Keynote Session: What Have We Learned About Cerebellar Function from Cellular Electrophysiological Experiments?** (*Michael Mauk* / David Linden)

Chemical Oceanography
Processes at Interfaces: Bridging Spatial, Temporal and Disciplinary Divides from Micro- to Global Scales
Jul 26-31, 2015
Holderness School, Holderness, NH
Chair: Kathleen C. Ruttenberg
Vice Chair: Karen L. Casciotti

- **Processes and Cycling at the Land-Sea Interface** (*Steven Smith* / Fred Mackenzie)

- **Reactions and Fluxes at the Air-Sea Interface** (*Christopher Sabine*)
- **Biogeochemical Cycling at the Seabed-Water Column Interface** (*Robert Aller*)
- **Phosphorus: The Interface Between Geochemistry, Biology, and Geology** (*Albert Colman* / Simon Poulton)
- **Biogeochemical Processes in Oxygen Deficient Environments: Metal, Sulfur and Nitrogen Cycling** (*Mark Altabet*)
- **Nutrient-Trace Metal Interactions: Cycling at the Particle-Seawater Interface** (*Benjamin Twining* / Tristan Horner)
- **Biogeochemistry at Deep-Sea Vents: Thermal and Redox Transition Zones** (*Simon Poulton*)
- **Microbe-Organic Matter Interactions and Transformations** (*Carol Arnosti* / Elizabeth Kujawinski / Rudi Amann / Hilary Close)
- **The Ocean's Role in Climate Change** (*Fred Mackenzie* / Andy Ridgwell / Timothy Lyons)

GFS Chemical Oceanography
Processes at Interfaces: Bridging Spatial, Temporal and Disciplinary Divides from Micro- to Global Scales
Jul 25-26, 2015
Chair: Angelos K. Hannides
Associate Chair: Jessica N. Fitzsimmons

- **Views of Chromosomes** (*Dhruba Chattoraj* / Wendy Bickmore / Nancy Kleckner / Terumi Kohwi-Shigematsu / Francois Cornet / Angelika Amon)
- **Genome Structure and Evolution** (*Aaron Straight* / Douglas Koshland / Houra Merrikh / David Pellman)
- **Chromosome Interactions** (*Abby Dernburg* / Geeta Narlikar / Richard Gourse / Marc Gartenberg / David Shechter / Suckjoon Jun)
- **Chromosome Repair and Recombination** (*Barbara Funnell* / Daniel Durocher / Susan Lovett / Lorraine Symington)
- **Chromosome Architecture** (*John Marko* / Toshio Tsukiyama / Frederic Boccard / Asifa Akhtar / Jeff Errington / Hironori Funabiki)
- **Chromosome Replication** (*Scott Keeney* / Mike O'Donnell / Steve Bell / James Berger)
- **Chromosome Segregation** (*Gary Karpen* / David Sherratt / Sue Biggins / Melissa Gardner / Daniela Barilla / Anne Villeneuve)
- **Centromeres and Telomeres** (*Patrick Higgins* / Beth Sullivan / Christine Jacobs-Wagner / Agnel Sfeir)

GFS Chromosome Dynamics
From Nucleotides to Genomes: Chromosome Biology in the Three Domains of Life
Jun 27-28, 2015
Chair: Ofer Rog
Associate Chair: Andrew B. Lane

Clusters & Nanostructures

Bridging the Gap from Free Clusters to Functional Nanostructures
Jul 5-10, 2015
Melia Golf Vichy Catalan Business and Convention Center, Girona, Spain
Chair: Wolfgang Harbich
Vice Chair: Paolo Milani

- **Keynote Session: Nanocatalysis, Nanofabrication** (*Richard Palmer* / Ueli Heiz / Klaus Kern)
- **Magnetism: Fundamentals** (*Tobias Lau* / Harald Brune / Olle Eriksson)
- **Electronic Structure / Thermodynamics** (*Gerd Gantefoer* / Hannu Haekkinen / Vitaly Kresin / Bernd Von Issendorff)
- **Structure / Alloys** (*Riccardo Ferrando* / Stefan Bromley / Atsushi Nakajima / Peter Lievens)
- **Magnetism: Applications** (*Wolfgang Harbich* / Carlos Balbas / Veronique Dupuis)
- **Optical Properties** (*Vlasta Bonacic-Koutecky* / Marco Potenza / Hans Christian Weissker / Rodolphe Antoine)
- **Clusters in Strong Fields** (*Karl-Heinz Meiwes-Broer* / Thomas Fennel / M. Krishnamurty)
- **Reactivity** (*Scott Anderson* / Thorsten Bernhardt / Stefan Vajda / Alessandro Fortunelli)
- **Cluster Applications** (*Paolo Milani* / Franz Faupel / Simon Brown / Mansoo Choi)

Chemistry Education Research & Practice

Chemistry Education as an Agent in Global Progress
Jun 21-26, 2015
Bates College, Lewiston, ME
Chair: Hannah M. Sevian
Vice Chair: Gabriela C. Weaver

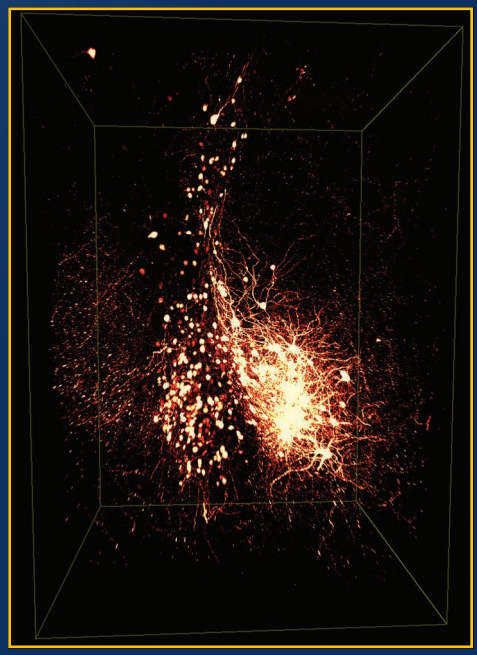
- **Physical and Conceptual Threats to Our Students' Chemistry Learning** (*Rachel Mamlok-Naaman* / Rafael Moure-Eraso / Eduardo Mortimer)
- **Chemical Literacy and Consequence** (*Samuel Pazicni* / Stephen Matlin / Mei-Hung Chiu / Astrid Bulte)
- **Interest, Motivation, and Disciplinary Identity in Chemistry** (*Ellen Yezierski* / Jack Barbera / K. Ann Renninger)
- **Appetite and Agency in Chemistry** (*Renee Cole* / Deborah Corrigan / MJ Morse / Marietjie Potgieter)
- **Reasoning Using Chemistry Knowledge and Common Sense** (*Vicente Talanquer* / Resa Kelly / Tina Grotzer)
- **Navigating Education in Chemistry** (*Maria Oliver-Hoyo* / Fatuma Chege / Imelda Cossette / Scott Lewis)
- **Learning to Practice Chemistry in Meaningful Contexts** (*Yehudit Judy Dori* / Sascha Bernholt)
- **Equipping Chemistry Education to Facilitate Global Progress** (*James Hamos* / Erika Offerdahl / Andoni Garritz / Pamela Mills)
- **What a More Chemically Literate World Would Mean** (*Gabriela Weaver* / Jonathan Forman / Jorge Ibanez)

Chronobiology

Biological Rhythms: Mechanisms – Functions – Implications for Health
Jun 28 - Jul 3, 2015
Melia Golf Vichy Catalan Business and Convention Center, Girona, Spain
Chair: Achim Kramer
Vice Chair: Amita Sehgal

- **Systems and Concepts: Rhythms, Oscillators and Clocks** (*Hiroki Ueda* / Craig Montell / Matthew Bennett / James Locke)
- **Clock Mechanisms: Inputs and Outputs** (*Steven Brown* / Michael Brunner / David Gatfield / Joanna Chiu / Carl Johnson)
- **The Clock in the Cell: Transcriptional Regulation and Beyond** (*Paolo Sassone-Corsi* / Takao Kondo / Charles Weitz / Joseph Takahashi)
- **Timing Is Everywhere: Non-Circadian Rhythms** (*Charalambos Kyriacou* / Helge Grosshans / Takashi Yoshimura / Alexander Aulehla / Florian Storch)
- **Clocks in the Brain: Neuronal Control of Circadian Rhythms** (*Johanna Meijer* / Orie Shafer / Michael Rosbash / Erik Herzog)
- **Timely Defense: Circadian Control of Immune Functions** (*Andrew Loudon* / Janet Braam / Mimi Shirasu-Hiza / Christoph Scheiermann / Pierre Chambon)
- **Growth, Cancer and the Clock** (*Marina Antoch* / Carla Finkielstein / Katja Lamia / Stacey Harmer)
- **Entrainment and Sleep** (*Martha Merrow* / Amita Sehgal / David Prober / Samer Hattar / Till Roenneberg)
- **Metabolism and Aging: The Role of the Clock** (*Fernanda Ceriani* / Carla Green / Pankaj Kapahi / Ueli Schibler)

GFS Chronobiology
Biological Rhythms: Mechanisms – Functions – Implications for Health
Jun 27-28, 2015
Chair: Jennifer Mohawk



Lateral amygdala neurons infected by viral vector. Using CLARITY to optically clear brain chunk (roughly 1 mm-thick coronal section) and examine the pattern and extent of viral infection (viral GFP expression, pseudocolored) in three dimensions. Microinjecting a viral vector infects a small, random population of neurons that are largely restricted to the lateral amygdala. Courtesy of Jonathan Epp. Submitted by Sheena Josselyn, Chair, Amygdala in Health & Disease GRC.

Chromosome Dynamics

From Nucleotides to Genomes: Chromosome Biology in the Three Domains of Life
Jun 28 - Jul 3, 2015
Waterville Valley Resort, Waterville Valley, NH
Chair: David Z. Rudner
Vice Chair: Rebecca Heald

- **Keynote Session: Chromosome Dynamics: From Nucleotides to Chromosomes** (*Ginger Zakian* / Frank Uhlmann / Jeanne Lawrence / Michael Laub)

Coastal Ocean Modeling

Modeling Coastal Marine Circulation and Physics and the Environmental Processes that They Influence
Jun 7-12, 2015
University of New England, Biddeford, ME
Chair: John L. Wilkin
Vice Chair: Ruoying He

- **Boundary Layer Dynamics** (*Erika McPhee-Shaw* / Isaac Ginis / James Girton)

Without the Gordon Research Conferences. . .

...science would progress more slowly. *(Keith Watson, Chair, 2014 Inorganic Chemistry GRC)*

- **Sub-Mesoscale Processes and Internal Waves**
  (*Robert Hetland* / Baylor Fox-Kemper / Weifeng (Gordon) Zhang / Annalisa Bracco)
- **Probabilistic Approaches and Risk Assessment**
  (*Pierre De Mey* / Jean-Marie Beckers / Michael Dowd)
- **Advanced Numerical Methods**
  (*Hans Burchard* / Alastair Adcroft / Mike Herzfeld / Joseph Zhang)
- **State Estimation and Data Assimilation**
  (*Brian Powell* / Hans Ngodock / Peter Oke)
- **Near-Shore and Estuarine Processes**
  (*Jacqueline McSweeney* / Neil Ganju / Sarah Giddings / Henk Schuttelaars)
- **Ice Shelf and Sea Ice Modeling**
  (*John Wilkin* / Ben Galton-Fenzi / Jean-Francois Lemieux)
- **Physics / Ecosystem Interactions**
  (*Parker MacCready* / Jorn Bruggeman / Samantha Siedlecki / Claire Paris)
- **Climate Change in the Coastal Ocean**
  (*Ruoying He* / Markus Meier / Samantha Stevenson)

GRS **Coastal Ocean Modeling**
Modeling the Physics and Circulation of Coastal and Estuarine Environments
Jun 6-7, 2015
Chair: Jacqueline McSweeney
Associate Chair: Sally J. Warner

Collagen

The Collagen Superfamily: From Genes to Organism Physiology
Jul 12-17, 2015
Colby-Sawyer College, New London, NH
Chair: Sergey Leikin
Vice Chair: Florence P. Ruggiero

- **Expression and Regulation of Collagen Genes and Gene Network**
  (*Barbara Smith* / George Bou-Gharios / Barbara Smith)
- **Structure and Function of Different Domains in Collagen Molecules**
  (*Barbara Brodsky* / Jean Baum / Joshua Sakon / Barbara Brodsky)
- **Collagen Homeostasis**
  (*Karl Kadler* / Johanna Myllyharju / Alberto Luini / Karl Kadler)
- **Collagens in Basement Membranes**
  (*Taina Pihlajaniemi* / Leena Bruckner-Tuderman / Cristina Nogueira / Sally Horne-Badovinac / Taina Pihlajaniemi)
- **Collagens in Cell Niche and Cell Signaling**
  (*Valerie Weaver* / Paolo Bonaldo / Valerie Weaver)
- **Collagens in Organism Physiology**
  (*Daniel Greenspan* / Tomoko Wakabayashi / Michael Fox / Marion Gordon / Daniel Greenspan)
- **Collagens in Pathology**
  (*Bjorn Olsen* / Shireen Lamande / Bjorn Olsen)
- **Collagen Based Materials and Bioengineering**
  (*Rocky Tuan* / Jean Chmielewski / Ronald Raines / Rocky Tuan)
- **Keynote Session: Collagenopathies of Skeletal Muscle / Late-Breaking Topics**
  (*Shireen Lamande* / Carsten Bonnemann)

GRS **Collagen**
The Collagen Superfamily: Lessons from Biochemistry, Development and Inflammation
Jul 11-12, 2015
Chair: Jessica M. Trombetta-Esilva
Associate Chair: Pauline Nauroy

Computational Aspects - Biomolecular NMR

Exploring the Frontiers of NMR, Computations and Complementary Biophysical Methods
Jun 7-12, 2015
Renaissance Tuscany Il Ciocco Resort, Lucca (Barga), Italy
Chair: Alexandre Bonvin
Vice Chair: Valerie Daggett

- **Keynote Session: Advances in Integrative Structural Biology**
  (*Antonio Rosato* / Andrej Sali / Adam Lange)
- **Conformational Variability and Dynamics**
  (*Andrew Baldwin* / Christian Griesinger / Claudio Luchinat / Arthur Palmer / David Fushman)
- **NMR and Computations in Industry**
  (*Ben Davis* / Eiso Ab / Michael Schaefer / Chun-Wa Chung)
- **Ligand Interactions and Metabolomics**
  (*Giovanna Musco* / Robert Konrat / James Prestergard / Rafael Bruschweiler / David Wishart)
- **Signal Processing**
  (*Christina Redfield* / Jeffrey Hoch / Tatyana Polenova / Vladislav Orekhov)
- **Pushing the Limits of Solid State NMR**
  (*Tatyana Polenova* / Marc Baldus / Mei Hong / Lyndon Emsley / Anne Ulrich)
- **Frontiers of NMR: Complementary Methods**
  (*Alexandre Bonvin* / Pau Bernardo / Alexander Leitner / Holger Stark)
- **Challenges in Structure Determination**
  (*Torsten Herrmann* / Ad Bax / Tobias Madl / Chad Rienstra / Angela Gronenborn)
- **Intrinsically Disordered Systems and Interactions**
  (*Valerie Daggett* / Frans Mulder / Carine Van Heijenoort / Martin Blackledge)

GRS **Computational Aspects - Biomolecular NMR**
Molecular Simulation for the Interpretation of NMR Data
Jun 6-7, 2015
Chair: Paul Guerry

Computer Aided Drug Design

New Frontiers in Computer-Aided Drug Design
Jul 19-24, 2015
Mount Snow Resort, West Dover, VT
Chair: Anthony Nicholls
Vice Chair: Patrick Walters

- **Designing for Polypharmacology**
  (*Rajarshi Guha* / Andrew Hopkins / Lei Xie / Shuixing Zhang)
- **Tales from the Trenches – Practical Applications of Computer-Aided Drug Design**
  (*Kate Holloway, Veerabahu Shanmugasundaram* / Bernd Kuhn / Ben Sellers / John Sanders / Celia Schiffer / Adrian Whitty)
- **Using Kinetics in Drug Design**
  (*Jose Duca* / Andrea Bortolato / Xavier Barril)
- **Open Source and Open Science**
  (*Greg Landrum* / John Overington / Matthias Rarey / Jon Weiss)
- **Integrating CADD with Phenotypic Screening**
  (*Georgia McGaughey* / Anne Carpenter / Brenda Eustace / Jeremy Jenkins / Paula Petrone / Stephan Reilly / Bridget Wagner)
- **Biophysical Data in Drug Design: Limits and Opportunities for Producers, Consumers, and Developers**
  (*Ajay Jain* / Paul Czodrowski / James Fraser / Neysa Nevins / Gregory Warren / Lance Westerhoff)
- **Applications of CADD in the Design of Biologics**
  (*David Pearlman* / Sandor Vajda / Anne deGroot / Andreas Plueckthun)
- **Applications of Big Data in CADD**
  (*Curt Breneman* / Al Dossetter / Marti Head / Kathryn Loving / Jed Pitera)
- **Keynote Session: Future Directions in CADD**
  (*Patrick Walters* / Mark Murcko)

GRS **Computer Aided Drug Design**
From Big Data to Smart Data
Jul 18-19, 2015
Chair: Christian Kramer
Associate Chair: Felix Terwesten

Crystal Growth & Assembly

Fundamental Mechanisms of Ordering from the Atomic to the Mesoscale
Jun 28 - Jul 3, 2015
University of New England, Biddeford, ME
Chair: Lara A. Estroff
Vice Chair: Elias Vlieg

- **Keynote Session: Assembly Mechanisms**
  (*Peter Vekilov* / Daan Frenkel / Zvonimir Dogic)
- **Surfaces and Interfaces**
  (*Alexander Chernov* / Ulrike Diebold / Joanna Millunchick / David Srolovitz)
- **Nanoparticles**
  (*Tobias Hanrath* / Hongyuan Chen / Yu Huang)
- ***In Situ* Characterization of Growth**
  (*Haimei Zheng* / Mingwei Chen / Gen Sazaki / Eli Sutter)
- **Bio-Inspired Crystallization**
  (*Yael Politi* / Boaz Pokroy / Jeffrey Rimer)
- **Nanowires**
  (*Frances Ross* / Ritesh Agarwal / Jerry Tersoff / Erik Bakkers)
- **Crystals for Energy Production**
  (*Aram Amassian* / Alberto Salleo / Richard Lunt)
- **Molecular Assembly and Crystallization**
  (*Michael McBride* / Bart Kahr / Michele Parrinello / Boris Rybtchinksi)
- **Quasicrystals and Colloids**
  (*Sharon Glotzer* / Clemens Bechinger / Ulrich Wiesner)

Developmental Biology

The Patterns that Shape Our Bodies, from Cellular Organization to Transgenerational Inheritance
Jun 21-26, 2015
Mount Holyoke College, South Hadley, MA
Chair: Susan E. Mango
Vice Chair: Jean-Paul Vincent

- **Morphogenesis**
  (*Roberto Mayor* / Alexander Schier / Cara Gottardi / Darren Gillmour)
- **Epigenetic Control of Development**
  (*Michael Levine* / Bradley Cairns / Sharon Dent / Jason Lieb / Marja Timmermans)
- **Cellular Polarity**
  (*Cliff Brangwynne* / Kathryn Anderson / Dominique Bergmann / Jessica Feldman)
- **Stem Cell Biology**
  (*Nancy Papalopulu* / David Bilder / Cassandra Extavour / Judith Kimble)
- **Small ncRNAs in Development**
  (*Julie Claycomb* / Victor Ambros / Oliver Hobert / Ann Rougvie / Gary Rukun)
- **Intercellular Signaling**
  (*Anne Brunet* / Roberto Mayor / Francesca Peri)
- **Self Assembly Within Cells**
  (*Jessica Feldman* / Cliff Brangwynne / Vladimir Denic / John Rinn)
- **Transgenerational Inheritance**
  (*Jean-Paul Vincent* / Anne Brunet / Julie Claycomb / Oliver Rando)
- **Transcription and Patterning**
  (*Vladimir Denic* / Michael Levine / Nancy Papalopulu)

Drinking Water Disinfection By-Products

Charting the Horizons of Interdisciplinary Research and Application in Water Disinfection, By-Products, Water Reuse and Public Health
Aug 9-14, 2015
Mount Holyoke College, South Hadley, MA
Chair: Michael Plewa
Vice Chair: William A. Mitch

- **Water Disinfection in an Era of Water Scarcity** (*Benito Marinas* / David Sedlak / Benjamin Stanford)
- **Chemistry: Analytical Approaches on the Formation and Detection of Emerging DBPs** (*Lynn Roberts* / Susan Richardson / Xiangru Zhang / Thomas Ternes / Urs Von Gunten)
- **DBP Toxicity: Molecular Mechanisms** (*Frederic Leusch* / Xingfang Li / Beate Escher)
- **Integration of Analytical Chemistry, Quantitative Toxicology and Epidemiology of DBPs** (*Emmanouil (Manolis) Kogevinas* / Weidong Qu / Cristina Villanueva / Jane Simmons)
- **Water Energy Nexus** (*Jeanne Vanbriesen* / Djanette Khiari / William Mitch)
- **Wastewater Reuse and Desalination** (*Jean-Philippe Croue* / Eric Dickinson / Paul Westerhoff / Kathryn Linge)
- **Water Disinfection Challenges and DBP Research in China** (*Yuefeng Xie* / Hong-Ying Hu / Hailin Wang / Jun Ma / Jiang Guibin)
- **Engineering Options on DBP Control** (*Chao Chen* / Stuart Krasner / Tanju Karanfil / Leo Zappa)
- **The Way Forward, Future DBP Research and Regulation** (*Stuart Krasner* / Rex Pegram / Stig Regli)

GRS Drinking Water Disinfection By-Products
Rethinking the Future of Water Treatment Through the Integration of Science, Engineering and Public Health
Aug 8-9, 2015
Chair: Matias Attene Ramos
Associate Chair: Ning Dai

Drug Metabolism

Solving Knowledge Gaps in Drug Metabolism and Pharmacokinetic Prediction, Improving Translational Medicine
Jul 12-17, 2015
Holderness School, Holderness, NH
Chair: Michael A. Zientek
Vice Chair: Kim L. Brouwer

- **Keynote Session: Improving Drug Properties Through Mechanistic Modeling of Drug Disposition** (*Michael Zientek* / Stephen Hall)
- **PK Prediction: From Test Tube to Human** (*Karen Rowland-Yeo* / Christopher Gibson / Hannah Jones / Steven Leeder / Karen Rowland-Yeo)
- **Personalized Medicine: Pharmacogenomics and Disease States on Prediction of Drug Disposition** (*Erica Woodahl* / Steven Scherer / Rachel Tyndale / Erica Woodahl)
- **Oxidative Metabolism: The Advances and Challenges of *In Silico, In Vitro* and Prediction Sciences** (*Jane Kenny* / Gabriele Cruciani / Bernard Murray / Cyrus Khojasteh / Nina Isoherranen)
- **Advances in Conjugative Metabolism: From Molecules to Populations** (*Michael Coughtrie* / Chantal Guillemette / Catherijne Knibbe / Thomas Leyh)
- **Understanding and Predicting the Metabolism and Pharmacokinetics of Biologics** (*Dhavalkumar Shah* / E. Sally Ward / Eric EzanHonghui Zhou / Dhavalkumar Shah)
- **Young Investigator Presentations** (*Henry Strobel*)
- **Transporter Sciences: Evolving to a New Realm of Understanding Drug Interactions from a Victim Perspective** (*Caroline Lee* / Harma Ellens / Katherine Fenner / Mitchell Taub / Maciej Zamek-Gliszczynski)
- **Role of Proteomics and Mass Spectrometry in Drug Metabolism and Pharmacokinetic Prediction** (*Deepak Dalvie* / Philip Smith / Stephen Castellino / Paul Hollenberg)

Dynamics at Surfaces

Reaction Dynamics, Scattering Dynamics, and Molecular and Structural Dynamics at Surfaces and Interfaces
Aug 9-14, 2015
Salve Regina University, Newport, RI
Chair: Alec Wodtke
Vice Chair: Eckart Hasselbrink

- **Single Molecule Forces and Dynamics** (*Klaus Kern* / Harald Brune / Roy Sharani)
- **Dynamics of Chemical Reactions at Surfaces** (*Greg Sitz* / Donghui Zhang / Rainer Beck / Hua Guo)
- **From Surface Dynamics to Heterogeneous Catalysis** (*Scott Anderson* / Ulrich Heiz / Swetlana Schauermann)
- **Dynamics at Liquid, Polymer, Membrane, and Biological Interfaces** (*Bruce Kay* / William Hase / Gilbert Nathanson / Ellen Backhus)
- **Dynamics of Adsorbate Self-Assembly and Motorics** (*Andrew Gellmann* / E. Charles H. Sykes / Karl-Heinz Ernst)
- **Surface Dynamics of Energy Conversion Processes** (*Daniel Auerbach* / Xueming Yang / Natalia Garcia Rey / Jan Rossmeisl)
- **Time-Resolved Dynamics at Surfaces** (*Martin Wolf* / Claus Ropers / Sylvie Rokie)
- **Electron Dynamics at Surfaces and Non-Adiabaticity** (*John Tully* / Oliver Buenermann / Maite Aldcin Ochoa / Reinhard Maurer)
- **Computational Dynamics and Surface Chemistry** (*Matthias Scheffler* / Axel Gross / Alexander Tkatchenko)

GRS Dynamics at Surfaces
Exploring Interactions at Surfaces, from Scattering Dynamics to Heterogeneous Catalysis
Aug 8-9, 2015
Chair: Helen Chadwick
Associate Chair: Vanessa Murray

Ecological & Evolutionary Genomics

From Genomes to Biomes: Using Biodiversity to Explore Biocomplexity
Jul 12-17, 2015
University of New England, Biddeford, ME
Chairs: Michael A. Herman & John H. Werren
Vice Chairs: Michael E. Pfrender & Felicity Jones

- **Population Genomics, Adaptation and Speciation** (*Felicity Jones* / Andrew Clark / Asher Cutter / Elodie Ghedin / Josephine Pemberton)
- **Symbiosis and Interacting Organisms** (*Todd Schlenke* / Siv G. Andersson / Angela Douglas / Takema Fukatsu / Wayne Potts)
- **Behavioral Ecology Meets Genomics** (*John Werren* / Laurent Keller / Amy Toth / Todd Schlenke)
- **Networks: From Genes to Ecosystems** (*Joseph Shaw* / Karoline Faust / Cedric Feschotte / Alvaro Sanchez / Patricia Wittkopp)
- **Applications of Ecological and Evolutionary Genomics** (*Elodie Ghedin* / John Colbourne / Sherry Flint-Garcia / Joseph Shaw)
- **Advances in Computational and Genomic Approaches to Non-Model Organisms** (*John Colbourne* / Steven Salzberg / Wes Warren / Beth Shapiro)
- **Biodiversity and Phylogenomics** (*Wes Warren* / Holly Bik / Casey Dunn / Davide Pisani)
- **Community and Ecosystem Genomics** (*Michael Pfrender* / Jack Gilbert / Blake Matthews / Jenn Schweitzer)
- **Young Investigator Presentations: Advances in Ecological and Evolutionary Genomics** (*Michael Herman*)

Elastin, Elastic Fibers & Microfibrils

Structure, Mechanisms, and Applications in Health and Disease
Jul 26-31, 2015
University of New England, Biddeford, ME
Chair: Zsolt Urban
Vice Chair: Clair Baldock

- **Structure and Assembly of Elastin** (*Elaine Davis* / Robert Mecham / Tomoyuki Nakamura / Anthony Weiss)
- **Microfibrils and Related Molecules** (*Lynn Sakai* / Dieter Reinhardt / Penny Handford / Francesco Ramirez)
- **Enzymatic Modification of Elastic Fibers** (*Suneel Apte* / Jack Dixon / Christian Schmelzer / Philip Trackman)
- **Regulation of Cell Signaling by Elastic Fibers** (*Daniel Rifkin* / Gerhard Sengle / Timothy Springer / Anja Sterner-Kock)
- **Molecular and Functional Modifications of Elastic Fibers** (*Cay Kielty* / Branka Dabovic / Dirk Hubmacher / Brian Varisco)
- **Elastic Fibers in Cardiovascular and Pulmonary Disease** (*Hiromi Yanagisawa* / Jeroen Essers / Bart Loeys / Enid Neptune)
- **Translational Research and Genetics of Elastic Fibers** (*Beth Kozel* / Bert Callewaert / Robert Hinton / Dianna Milewicz)
- **Regenerative Medicine and Engineering of Elastic Materials** (*Ashutosh Chilkoti* / Frederick Keeley / Katja Schenke-Layland / Yadong Wang)
- **New Directions in Elastic Fiber Research** (*Clair Bladock* / Piet Borst / Daniel Greif / Jiangyu Li)

GRS Elastin, Elastic Fibers & Microfibrils
Structure, Mechanisms and Applications in Health and Disease
Jul 25-26, 2015
Chair: Christina L. Papke
Associate Chair: Sacha A. Jensen

Environmental Nanotechnology

Steps for Environmentally Safe Implementation of Nanotechnology
Jun 21-26, 2015
Mount Snow Resort, West Dover, VT
Chair: Paul Westerhoff
Vice Chair: Sharon L. Walker

- **New Challenges of Nanotechnology** (*Rebecca Klaper* / Mark Wiesner / Jonathan Posner / Elijah Petersen / Antonia Praetorius / Gregory Lowry)
- **Safe Development and Manufacturing of Green Nano-Enabled Products** (*Ahmed Busnaina* / Seth Coe-Sullivan / Mark Banash / Jacqueline Isaacs)
- **Challenges of Reporting Null Results - A Race to the Top and Bottom** (*Richard Canady* / Tom van Teuenbroek / Paul Anastas)
- **Finding and Detecting Nanomaterials Released from Products into the Environment** (*Ian Illuminato* / Chris Szakal / Frank van der Kammer / Wendel Wohlleben)
- **Understanding the Reliability and Reproducibility of Nano-Analytics** (*Dave Holbrook* / Rudolf Ruether / Steven Oldenburg / Douglas Gilliland / Zeljka Krpetic)
- **Validity in Using Model Nanomaterials to Predict Fate and Transport of More Complex Nanomaterials and Nano-Enabled Systems** (*Rebecca Klaper* / Robert Hamers / Stacy Harper / Yoram Cohen)
- **Assessing and Using Release Rates from Nano-Enabled Products** (*Ahmed Busnaina* / Denise Mitrano / Jeffery Steevens)

- **Solving Pollution Problems Using Nanotechnology, Without Causing More Pollution**
  (*John Fortner*, *Nora Savage* / Angela Violi / Qilin Li / Jeffrey C.S. Wu)
- **Future Directions: Identifying New Environmental Science Required to Assess Risks and Harness Benefits from Nanotechnology**
  (*Nora Savage* / Tara Sabo-Attwood / Steven Diamond)

GRS Environmental Nanotechnology
Novel Techniques for Synthesizing, Characterizing, and Tracking Engineered Nanomaterials for Sustainable Application of Nanotechnology
Jun 20-21, 2015
Chair: Jacob Lanphere
Associate Chair: Natalia Hoogesteijn

Enzymes, Coenzymes & Metabolic Pathways

Enzymology: Innovations in Understanding and Impact in Application
Jul 12-17, 2015
Waterville Valley Resort, Waterville Valley, NH
Chairs: Giovanni Gadda & Mark S. Hixon
Vice Chairs: Adrian T. Keatinge-Clay & Audrey L. Lamb

- **Enzymology in Drug Development**
  (*Robert Copeland* / Thomas Meek / Erica Pierce / Michael Shultz)
- **Flavoenzymology**
  (*Holly Ellis* / Pimchai Chaiyen / Bruce Palfey / Anne-Frances Miller / Andrea Mattevi)
- **New Analytical Approaches**
  (*Kenneth Johnson* / John Quinn / Rommie Amaro / Wolf-Dieter Fessner)
- **Mechanisms of Electron Transfer**
  (*Andrew Murkin* / Victor Davidson / Jennifer Dubois / Thomas Poulos)
- **The Circe Effect**
  (*Ruma Banerjee* / Patricia Babbitt / Charles Carter / Dan Herschlag)
- **Applications of Enzyme Inhibition**
  (*Jessica Schneck* / Kay Ahn / Rex Pratt / Pascal Fortin)
- **Applications of Metabolic Pathways**
  (*Fan Fan* / Craig Behnke / Christopher White / Kenny Wong)
- **Case Studies in Enzymology**
  (*Audrey Lamb* / Aimin Liu / Ellen Moomaw / Colin Thorpe / Emily Weinhart)
- **Keynote Session: Perspectives on the State of Enzymology and Metabolomics**
  (*Gregory Reinhart* / Frank Raushel / Stephen Benkovic)

GRS Enzymes, Coenzymes & Metabolic Pathways
New Concepts and Methods in Enzymology: From Molecular Mechanisms to Industrial Applications
Jul 11-12, 2015
Chair: Randy Kipp
Associate Chair: Zhen Wang

Epigenetics

Epigenetic Dynamics: Roles in Development, Inheritance, and Responses to the Environment
Aug 2-7, 2015
Bentley University, Waltham, MA
Chairs: William G. Kelly & Ortrun Mittelsten Scheid
Vice Chairs: Pamela K. Geyer & Frederic Berger

- **New Epigenetic Phenomena**
  (*Eric Richards* / Ueli Grossniklaus / Ross Waller)
- **Dynamics of Epigenetic States**
  (*Steven Jacobsen* / David Katz / Bradley Cairns / Frederic Berger)
- **Targeted Epigenetic Modifications**
  (*Robert Martienssen* / Bradley Bernstein / Pamela Silver)
- **Epigenetic Control of Development and Dosage**
  (*Marisa Bartolomei* / Rickard Sandberg / Susan Strome / Doris Wagner)
- **Inheritance of Epigenetic States**
  (*Vincent Colot* / Scott Kennedy / Erica Watson)
- **RNA-Dependent Modes of Epigenetic Regulation**
  (*Craig Pikaard* / David Baulcombe / Chuan He / Jeanne Lawrence)
- **Epigenetics and Nuclear Organization**
  (*Edith Heard* / Susan Gasser / Karen Hayden-Miga / Pamela Geyer)
- **Epigenetic Control of Genome Integrity**
  (*Avraham Levy* / Gaelle Legube / Todd Macfarlan / Kazufumi Mochizuki / Yijun Qi)
- **Epigenetics and Disease**
  (*Anne Ferguson-Smith* / Samie Jaffrey / Heather True / Olivier Voinnet)

GRS Epigenetics
Mechanisms of Mitotic and Meiotic Epigenetic Inheritance
Aug 1-2, 2015
Chair: Shannon Torres
Associate Chair: Sabine K. Dhir



Single melanopsin (Opn4) expressing intrinsically photosensitive retinal ganglion cell (M1) labeled by alkaline phosphatase from Opn4CREert2/+; Z/AP animal. The concentration of the inducer tamoxiphen was adjusted to visualize a single cell. Note the dendrites and the single axon from this cell. Courtesy of Samer Hattar (Johns Hopkins University). Submitted by Achim Kramer, Chair, Chronobiology GRC.

Epithelial Differentiation & Keratinization

Novel Concepts in Epithelial Function and Therapeutics
Jul 12-17, 2015
Sunday River Resort, Newry, ME
Chair: Anthony Oro
Vice Chair: Carien M. Niessen

- **Keynote Session: New Concepts in Genetic and Epigenetic Regulation of Epithelia**
  (*Anthony Oro* / Elaine Fuchs / Pier Paolo Pandolfi)
- **Mechanisms of Epithelial Carcinogenesis**
  (*Andrzej Dlugosz* / Cedric Blanpain / Paul Khavari / Paolo Dotto / Kornelia Polyak)
- **Innovative Techniques in Epithelial Biology**
  (*Vladimir Botchkarev* / Valentina Greco / David Clapham / Howard Chang / Feng Zhang)
- **Advances in Epithelial Homeostasis and Regeneration**
  (*Pritendur Kaur* / George Cotsarelis / Mayumi Ito / Fiona Watt / Michael Rendl / Lorenz Studer)
- **Current Ideas in Epithelial Interactions with the Environment**
  (*Raphael Kopan* / Masayuki Amagai / Valerie Horsley / Diana Bautista)
- **Emerging Concepts in Epithelial Adhesion and Polarity**
  (*Terry Lechler* / Pierre Coulombe / Reinhard Fassler / Kathleen Green / Jurgen Knoblich / Carien Niessen)
- **New Insights in Epithelial Aging and Metabolism**
  (*Birgit Lane* / Jan Hoeijmakers / Amy Wagers / Salvador Aznar-Benitah)
- **Conceptual Advances in Epithelial Evolution and Morphogenesis**
  (*Bruce Morgan* / Sarah Millar / Marja Mikkola / Hopi Hoekstra / Ellen Lumpkin / Cheng-Ming Chuong)
- **Novel Epithelial Based Therapies**
  (*Dennis Roop* / James Bradner / Angela Christiano / Masayo Takahashi)

GRS Epithelial Differentiation & Keratinization
Emerging Themes in Epithelial Signaling
Jul 11-12, 2015
Chair: Scott Atwood
Associate Chair: Yanne S. Doucet

Excitatory Synapses & Brain Function

From Activity- and Experience-Dependent Glutamate Receptor Organization, Function and Trafficking to Synapses and Neural Circuitry in Health and Disease
Jun 7-12, 2015
Salve Regina University, Newport, RI
Chairs: Suzanne Zukin & Daniel Choquet
Vice Chairs: Kang Shen & Christian Luscher

- **Keynote Session: From Synapses to Circuits**
  (*Susumu Tomita* / Cornelia Bargmann / Richard Tsien)
- **Glutamate Receptor Structure and Function**
  (*Yael Stern-Bach* / Eric Gouaux / Ingo Greger / Pierre Paoletti / Gabriela Popescu / Stephen Traynelis)
- **Synapse Organization and Excitatory Synaptic Complexes**
  (*Kang Shen* / Mark Dell'Acqua / William Green / August Smit)
- **Synapse Organization and Dynamics**
  (*Pietro De Camilli* / Jean-Claude Beique / Jonathan Hanley / Stephan Sigrist / Xiaowei Zhuang / Laurent Groc)
- **Synaptic Plasticity: Signaling and Synaptic Strength**
  (*Andres Barria* / Michael Higley / Richard Huganir / Hey-Kyoung Lee / Christophe Mulle)
- **Glutamate Receptor Trafficking and Signaling**
  (*Laurent Groc* / Yukiko Goda / Johannes Hell / Casper Hoogenraad / June Liu / Andres Villu Maricq)
- **Synaptic Plasticity: Spines to Networks**
  (*Katherine Roche* / Pablo Castillo / Roger Nicoll / Bernardo Sabatini / Gina Turrigiano)
- **Plasticity, Networks and Addiction**
  (*Edward Ziff* / Christian Luscher / Julie Kauer / Camilla Bellone / Marina Wolf / Robert Malenka)
- **Next Frontier: Signal Complexes and Networks in Development and Disease**
  (*Richard Huganir* / Claudia Bagni / Kurt Haas / Kimberly Huber / Isabel Perez-Otano / Peter Scheiffele)

GRS Excitatory Synapses & Brain Function
Mechanistic Insights into the Development and Modulation of Excitatory Synaptic Function
Jun 6-7, 2015
Chair: Alma I. Rodenas-Ruano
Associate Chair: Anne-Sophie Hafner

Eye Movements
Integrating Perception and Action for Optimal Vision
Jul 26-31, 2015
Bentley University, Waltham, MA
Chairs: Terrence Stanford & John Van Opstal
Vice Chairs: Marc A. Sommer & Douglas Crawford

- **Keynote Session: On the Nexus Between Sensory and Oculomotor Function** (*Emilio Salinas* / Jennifer Groh / Tirin Moore)
- **Evolving Perspectives on Gaze Control** (*Robert Wurtz* / Brian Corneil / Henrietta Galiana / Douglas Munoz / Daniel Guitton)
- **Oculomotor Biomarkers for Psychiatric Disorders** (*David Zee* / John Sweeney / Chrystalina Antoniades / Jennifer McDowell)
- **The Why and Where of Looking: Eye Movements for Natural Vision** (*Mary Hayhoe* / Brian White / Susana Martinez-Conde / Laurent Itti / Daniel Wood)
- **Eye Fields in Humans and Nonhuman Primates** (*Jeffrey Schall* / Stefan Everling / Sabine Kastner)
- **Anticipatory Visual Analysis Before Saccades** (*Michael Goldberg* / Julie Golomb / Kenji Kawano / Concetta Morrone / David Melcher)
- **Hering or Helmholtz? Probing the Interactions Between Conjugate and Disconjugate Gaze** (*Paul May* / Kathleen Cullen / Paul Gamlin / Michael Mustari)
- **Vision, Efference Copy, and Probabilistic Inference: Insights into Vestibular Function and Development** (*Pierre-Paul Vidal* / Julie Carcaud / Jerome Carriot / Xaq Pitkow / Matthieu Robert / Hans Straka)
- **Optogenetics for Studying Primate Vision and Eye Movements: What Have We Learned, What Can We Learn?** (*Xue Han* / Mehrdad Jazayeri / David Sheinberg)

GFS Eye Movements
Integrating Perception and Action for Optimal Vision
Jul 25-26, 2015
Chair: Jaime Kaminer
Associate Chair: Martin O. Bohlen

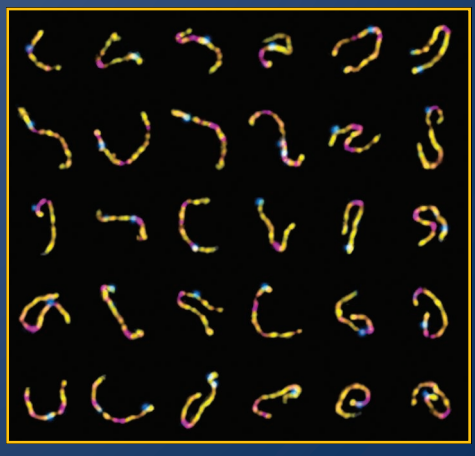
Fertilization & Activation of Development
Where Basic Meets Clinical Meets Mechanism
Jul 19-24, 2015
Holderness School, Holderness, NH
Chair: Gary Wessel
Vice Chair: Mariana F. Wolfner

- **Transgenerational Effects in Reproduction** (*Carmen Williams* / Katsuhiko Hayashi / Isabelle Mansuy)
- **Molecular Mechanisms of Male Gamete Function** (*Pablo Visconti* / David Clapham / Joel Drivet / Martin Matzuk)
- **Meiosis Resumption in the Oocyte** (*Laurinda Jaffe* / Rong Li / Teresa Woodruff)
- **Influences of the Reproductive Tract in Fertilization** (*Harvey Florman* / Sylvie Breton / Michael Miller)
- **Sperm Egg Interactions** (*Janice Evans* / Christine Gourier / Ueli Grossniklaus / Andrew Singson / William Snell / Stefanie Sprunck / Gavin Wright)
- **The Egg-to-Embryo Transition** (*Karl Swann* / Antonio Giraldez / Tim Weil)
- **Late-Breaking Topics / Selected Poster Presentations** (*Mariana Wolfner*)
- **Sperm Competition and Evolution** (*Willie Swanson* / Tim Birkhead / Heidi Fisher / Willie Swanson)
- **Keynote Session: Using Synthetic Biological Approaches to Answer Biological Questions** (*Gary Wessel* / Ron Weiss)

GFS Fertilization & Activation of Development
Unraveling the Molecular Mechanisms
Jul 18-19, 2015
Chair: Matteo A. Avella
Associate Chair: Melissa R. Miller

Genome Architecture in Cell Fate & Disease
NEW!
Unraveling the Form and Function of the Nucleus
Jun 7-12, 2015
The Chinese University of Hong Kong, Hong Kong, China
Chairs: Duanqing Pei & Thomas Misteli
Vice Chair: Wange Lu

- **The Complex Genome** (*Thomas Misteli* / Andrew Feinberg / Bing Ren)
- **Nuclear Architecture in Disease** (*David Gilbert* / Vicente Andres / Brian Burke / Martin Hetzer)
- **Epigenetics in Cancer** (*Andrew Feinberg* / Jonathan Licht / Paola Scaffidi)
- **Transcription and Genome Organization** (*Kathryn Song Eng Cheah* / Karen Reddy / Yijun Ruan / Rui-Ming Xu)
- **Stem Cells** (*Azim Surani* / David Gilbert / Jennifer Philips)
- **Reprogramming** (*Wai-Yee Chan* / Huck Hui Ng / Wolf Reik / Guoliang Xu)
- **Differentiation** (*Wolf Reik* / Philippe Collas / Hongkui Deng / Azim Surani)
- **Development** (*Bing Ren* / Kathryn Song Eng Cheah / Patrick Tam / Dahai Zhu)
- **Selected Poster Presentations** (*Duanqing Pei*)



Computationally isolated meiotic chromosome axes, imaged in 3D and shown here as projections, are colored yellow in regions of low axis curvature and pink in regions of high curvature. A crossover marker, in blue, illustrates that every chromosome in the nematode C. elegans undergoes one and only one crossover during meiosis, and that these crossovers occur in regions of both high and low curvature. Courtesy of Keith C. Cheveralls and Abby F. Dernburg. Submitted by Ofer Rog, Chair, Chromosome Dynamics GRS.

Germinal Stem Cell Biology
Genetics, Niche Development, Transdifferentiation and Reproductive Diseases
May 31 - Jun 5, 2015
The Chinese University of Hong Kong, Hong Kong, China
Chair: Yun-Fai Chris Lau
Vice Chair: Peter Koopman

- **Y Chromosome and Male Germ Cell Biology** (*Peter Koopman* / Jennifer Hughes / Julie Cocquet / Monika Ward)
- **Sex Determination and Gonad Differentiation** (*Robin Lovell-Badge* / Andy Greenfield / Peter Koopman / David Zarkower / Kenneth McElreavey)
- **Fetal Germinal Stem – Cross Talk with the Environment** (*Kyle Orwig* / Blanche Capel / Josephine Bowles / Shinichiro Chuma)
- **Spermatogonial Stem Cells and Niche** (*Wai-Yee Chan* / Jon Oatley / Robin Hobbs / C. Yan Cheng / Robert Braun)
- **Germline Stem Cells – Transdifferentiation** (*John Schimenti* / Renee Reijo Pera / Zuping He / Kehkooi Kee)
- **Female Germinal Stem Cells** (*Jon Oatley* / Lei Lei / Ji Wu / Hua Zhang)
- **Epigenetic Programming** (*Duanqing Pei* / Azim Surani / Hubert Schorle)
- **Germ Cell Tumors** (*Ewa Rajpert-De Meyts* / James Amatruda / Kristian Almstrup / Rolf Skotheim / Anne Goriely / Ina Dobrinski)
- **Technologies in Germ Cell Manipulations and Transgenesis** (*Zijiang Chen* / Jinsong Li / Chengzu Long / Haoyi Wang)

Heterocyclic Compounds
Ascendancy and Transformative Dimensions
Jun 21-26, 2015
Salve Regina University, Newport, RI
Chair: Tadeusz F. Molinski
Vice Chair: Scott C. Sutton

- **Natural Product Synthesis** (*James Leahy* / James Panek / Daniel Romo)
- **Heterocyclic Reactions and Catalysis** (*James Stambuli* / Laszlo Kurti / Janis Louie / David Lupton)
- **Synthesis of Heterocyclic Drugs** (*Corinna Schindler* / Patrick Harran / Minoru Isobe)
- **Innovative Solutions** (*Catharine Larsen* / Jeffrey Katz / Michael Sherburn)
- **Discovery: Marine-Derived Heterocycles** (*Frank Fang* / Carmen Cuevas / Kirk Gustafson)
- **Heterocycles and Contemporary Therapeutics** (*Colin Skepper* / Eric Voight / Frank Fang / Michael Kernan)
- **Synthetic Methodology** (*Kami Hull* / Robert Knowles / Pavel Nagorny / Jennifer Stockdill)
- **Heterocyclic Bioorganic Chemistry** (*Yi-Yin Ku* / Qiu Wang)
- **Synthesis of Heterocyclic Natural Products** (*Jared Shaw* / Viresh Rawal / Robert Williams)

High Temperature Corrosion
Pioneering Protection in Aggressive Environments
Jul 26-31, 2015
Colby-Sawyer College, New London, NH
Chair: Gordon J. Tatlock
Vice Chair: Daniel E. Monceau

- **Fundamental Studies of Oxidation Mechanisms and Lifetime Issues** (*Brian Gleeson* / Willem Quadakkers / Mike Finnis)
- **Oxidation in Steam and Water Vapour Containing Atmospheres** (*Gerald Meier* / Tony Fry / Gordon Holcomb)
- **Corrosion in Aggressive Environments** (*Rachel Pettersson* / Thomas Gheno / Carlos Levi / Luciana Intiso)
- **Oxidation of Chromia Formers in Complex Atmospheres** (*Toshio Maruyama* / Jianqiang Zhang / Sebastien Chevalier)
- **The Development and Degradation of Alloys for Use at Ultra-High Temperatures** (*Elizabeth Opila* / Stephane Mathieu / James Smialek)
- ***In-Situ* Studies of Corrosion and Oxidation Mechanisms** (*Yves Wouters* / Mats Halvarsson / Shigenari Hayashi)
- **Internal Oxidation by Design – The Production and Performance of Oxide Dispersion Strengthened (ODS) Alloys** (*David Young* / Sebastien Dryepondt / Iver Anderson)
- **Stress Development During Oxidation and Its Influence on Oxidation Behaviour** (*John Nicholls* / Barbara Shollock / Michael Scheutze)
- **The Intriguing Properties of Water at Low Temperatures** (*Peter Tortorelli* / Ian Baker)

GFS High Temperature Corrosion
High Temperature Corrosion Processes: From Single Oxidants to Complex Environments
Jul 25-26, 2015
Chair: Thomas Gheno
Associate Chair: Christine Geers

Gordon Research Conferences are different from other scientific conferences because. . .

...they are small and intimate and allow for scientists at every stage of their career to connect and collaborate. *(Laura Sanchez, Chair, 2014 Marine Natural Products GRC)*

High Throughput Chemistry & Chemical Biology

Innovations in Chemistry and Applications to Biological and Medical Discovery
Jun 14-19, 2015
Colby-Sawyer College, New London, NH
Chair: Scott E. Wolkenberg
Vice Chair: Andrew J. Phillips

- **Frontiers in Chemical Biology**
  (*Lyn Jones* / Danica Fujimori / Mark Fishman)
- **New Reactions, Designs, and Libraries**
  (*Scott Wolkenberg* / Jeffrey Bode / Matthew Disney / Frederick Goldberg / Jeremy Jenkins / Ralph Mazitschek)
- **Discovery and Application of New Synthetic Methods**
  (*Andrew Phillips* / Elizabeth Jarvo / Jin-Quan Yu / Timothy Cernak)
- **Novel Approaches to Ligand Discovery and Optimization**
  (*Milana Maletic* / Cullen Cavallaro / William Pomerantz / Steffen Renner / Craig Thomas / Hilmar Weinmann / Richard Payne)
- **Chemistry and Chemical Biology of Natural Products**
  (*Jiyong Hong* / Seth Herzon / Michael Fischbach / Erick Carreira)
- **Frontiers in Synthetic Chemistry**
  (*Scott Wolkenberg* / Phil Baran / Olafs Daugulis)
- **New Targets for Therapeutic Intervention**
  (*Ivan Cornella-Taracido* / Hua Xu / Deborah Hung / Benjamin Cravatt)
- **Profiling and Perturbation with Small Molecule Probes**
  (*Andrew Phillips* / Kate Carroll / Matthew Bogyo / Eranthie Weerapana)
- **Biological Discovery Using Chemical Tools**
  (*M.G. Finn* / Hiroaki Suga / Kimberly Stegmaier / Jack Taunton)

GRS **High Throughput Chemistry & Chemical Biology**
Synthetic and Analytical Methods Enabling a New Frontier in Chemical Biology
Jun 13-14, 2015
Chair: Justin Rettenmaier
Associate Chair: Elizabeth I. Parkinson

Hormone-Dependent Cancers

Mechanisms to Tailored Therapeutics
Aug 16-21, 2015
Sunday River Resort, Newry, ME
Chair: Wayne Tilley
Vice Chair: Jason Carroll

- **Keynote Session: Novel Approaches for Cancer Treatment**
  (*Jason Carroll*, *Wayne Tilley* / William Hahn / Peter Jones)
- **Functional Genomics and Epigenomics: Informing Biology and Defining Novel Targets**
  (*Lisa Butler*, *Steffi Oesterreich* / X. Shirley Liu / Sohrab Shah / Scott Tomlins)
- **Signaling Cross Talk: Driving Disease Progression and Treatment Resistance**
  (*Charlotte Bevan*, *Frank Claessens* / Patricia Elizalde / Lori Friedman)
- **Hormone Receptor Structure and Mutations in Endocrine Resistance**
  (*Geoffrey Greene*, *Jennifer Richer* / Sarat Chandarlapaty / Scott Dehm / Matthew Ellis)
- **Metastasis: Models and Mechanisms**
  (*Daniel Frigo*, *Christopher Ormandy* / Ingunn Holen / Alana Welm)
- **Patient Derived Models of Cancer Initiation and Treatment Resistance**
  (*Theresa Hickey*, *Ganesh Raj* / Alex Swarbrick / Renea Taylor / Valerie Weaver)
- **Tumor Heterogeneity and Evolution**
  (*Scott Cramer*, *Gail Prins* / Senthil Muthuswamy / Kornelia Polyack)
- **Novel Targets and Agents: Advancement to the Clinic**
  (*Felix Feng*, *Carol Lange* / Suzanne Conzen / Naomi Laing / Donald McDonnell)
- **Keynote Session: Future of Cancer Research – Challenges and Solutions**
  (*Robert Clarke*, *Gail Risbridger* / Myles Brown / Carlo Palmieri / Chris Sweeney)

GRS **Hormone-Dependent Cancers**
Bridging Research in Hormone Response and Resistance in Cancer
Aug 15-16, 2015
Chair: Matthew J. Sikora
Associate Chair: Renée de Leeuw

Human Genetics & Genomics

State-of-the-Art Human Genome Science: Illuminating Past and Shaping Future Controversies
Jul 19-24, 2015
Salve Regina University, Newport, RI
Chair: Nancy Cox
Vice Chair: Carlos Bustamante

- **Keynote Session: From Genome Discovery to Translation**
  (*Nancy Cox* / Nicholas Katsanis / Jay Shendure)
- **Population Genetics: Demography, Selection, and Disease**
  (*David Goldstein* / Nelson Freimer / Molly Przeworski / Carlos Bustamante)
- **Sex, Context, and Controversy**
  (*Molly Przeworski* / Magdalena Skipper / Barbara Stranger / David Page)
- **Getting from Discovery to Understanding: Molecular Methods and Progress**
  (*Nelson Freimer* / Bruce Conklin / Len Pennacchio)
- **Getting from Discovery to Understanding: Statistical Methods and Progress**
  (*Eleazar Eskin* / Anna Gloyn / Benjamin Neale)
- **How Do We Get Enough Data?**
  (*Benjamin Neale* / Eleazar Eskin / Nancy Cox)
- **Conundrums at the Clinical and Translational Interface**
  (*Bruce Conklin* / Heidi Rehm / Mary Relling)
- **Progress in Precision Medicine**
  (*Mary Relling* / David Goldstein / Susan Slaugenhaupt)
- **Discoveries in Maintaining Genome Integrity**
  (*Carlos Bustamante* / Haig Kazazian / James Lupski)

GRS **Human Genetics & Genomics**
Genome Beyond Genes: When the Exome Is Negative, Where to Next?
Jul 18-19, 2015
Chair: Anne H. O'Donnell
Associate Chair: Slave Petrovski

Hydrogen-Metal Systems

Fundamental Aspects of Hydrogen Interaction with Materials and Novel Energy Applications
Jul 12-17, 2015
Stonehill College, Easton, MA
Chairs: Ragaiy Zidan & Bjorn C. Hauback
Vice Chairs: Jacques Huot & Bernard Dam

- **Physisorption**
  (*George Froudakis* / Michael Hirscher / Channing Ahn)
- **Reaction Mechanisms / Pathways in Complex Hydrides**
  (*Ewa Ronnebro* / Craig Jensen / Claudia Weidenthaler)
- **Surface Phenomena and Finite Size Effects**
  (*Astrid Pundt* / Claudia Zlotea / Puru Jena / Andrea Baldi)
- **Novel High Capacity Hydrogen Storage Materials**
  (*Andreas Zuttel* / Torben Jensen / Xuebin Yu / Yaroslav Filinchuk)
- **Transport Phenomena in Hydrides (Ionic Conduction in Metal Hydrides)**
  (*Rana Mohtadi* / Shin-ichi Orimo / Alexander Skripov)
- **Hydrogen in Energy Storage Applications**
  (*Richard Chahine* / Akihiro Nakano / Bart Van Hassel)
- **Recent Advances on Hydrides Based on Metals and Alloys**
  (*Etsuo Akiba* / Jean-Louis Bobet / David Sholl)
- **Hydrogenation / Dehydrogenation of Hydride Composites**
  (*Young Whan Cho* / Gavin Walker / Martin Dornheim)
- **Novel Methods and New Characterization Techniques (of Hydrogen Interaction)**
  (*Bjorgvin Hjorvarsson* / Hyunjeong Kim / Andreas Borgschulte / Kazutoshi Miwa)

GRS **Hydrogen-Metal Systems**
Hydrogen: From Production to Applications
Jul 11-12, 2015
Chair: Terry D. Humphries
Associate Chair: Elsa Callini

Infections of the Nervous System

Pathogenesis and Worldwide Impact
Jun 14-19, 2015
The Chinese University of Hong Kong, Hong Kong, China
Chair: Lisa F.P. Ng
Vice Chair: Tom Solomon

- **Challenges in Infections of the Nervous System**
  (*Xavier de Lamballarie* / Christina Marra / Alexandre Alcais / Xavier de Lamballarie)
- **Pathogen Discovery in Infections of the Nervous System**
  (*Linfa Wang* / Michael Katze / Guo-Dong Liang / Paul Kellam / Linfa Wang)
- **Ways of Invading the Nervous System**
  (*Lynn Enquist* / Matteo Caleo / Ignacio Romero / Sara Salinas / Lynn Enquist)
- **Cellular Tropism of the Nervous System and Host-Pathogen Interactions**
  (*Guillaume Dumenil* / Christian Engwerda / Lai Guan Ng / Hans Christian Klein / Guillaume Dumenil)
- **Immune Responses of the CNS to Invasion by Pathogens**
  (*Hans-Gustaf Ljunggren* / Sonja Best / Shen-Ying Zhang / Hans-Gustaf Ljunggren)
- **Mechanisms of Pathogenesis: Clinical Features**
  (*Tom Harrison* / P. Satish Chandra / Peter Kennedy / Rob Heyderman / Mong-How Ooi / Tom Harrison)
- **Mechanisms of Pathogenesis: Cellular Features**
  (*Soren Paludan* / Aras Kadioglu / Daniel Paris / Soren Paludan)
- **Experimental Models of Infections of the Nervous System**
  (*Susan Ross* / Alistair Craig / Shie-Liang Hsieh / Thomas Morrison / Susan Ross)
- **Ways to Control Infections of the Nervous System: From Field to Bench to Bed**
  (*Jane Cardosa* / Tony Wyss-Coray / Gregory Smith / Alain Bouckenooghe / Jane Cardosa)

Inhibition in the CNS
Inhibitory Synapses and Circuits
Aug 16-21, 2015
Bates College, Lewiston, ME
Chair: Linda S. Overstreet-Wadiche
Vice Chair: Jean-Marc Fritschy

- **Keynote Session: Inhibitory Synapses and Circuits** (*Linda Overstreet-Wadiche* / Zoltan Nusser / Hannah Monyer)
- **Mechanisms of Inhibitory Synaptic Function** (*Istvan Mody* / Pablo Castillo / Afia Ali / Cheng-Chang Lien / Larry Trussell)
- **Plasticity of Inhibitory Circuits** (*Chris McBain* / Marlene Bartos / Arianna Maffei / Daniel Feldman)
- **GABA and Interneurons in Developing Circuits** (*Hongjun Song* / Juan Song / Alejandro Schinder / Laszlo Vutkits / Helen Scharfman / Josef Bischofberger)
- **Interneuron Development and Diversity** (*Carolyn Houser* / Gordon Fishell / Pico Caroni / Beatriz Rico)
- **Mechanisms of Inhibitory Synapse Formation** (*Jean-Marc Fritschy* / Jasmina Jovanovic / Shiva Tyagarajan / Suzanne Paradis / Guenter Schwarz)
- **GABA Signaling in Health and Disease** (*Marco Capogna* / Jamie Maguire / Bernhard Bettler / Laura Cancedda)
- **Inhibition in Intact Circuits** (*Ivan Soltesz* / Takao Hensch / Thomas Klausberger)
- **$GABA_A$ Receptors as Therapeutic Targets** (*Zoltan Nusser* / Elif Engin / Bernhard Luscher / Hanns Ulrich Zeilhofer)

Inhibition in the CNS
Inhibitory Neuron Specialization and Function
Aug 15-16, 2015
Chair: Scott F. Owen
Associate Chair: Jaclyn I. Wamsteeker Cusulin

Interior of the Earth
Surface Connections
Jun 7-12, 2015
Mount Holyoke College, South Hadley, MA
Chair: Marc M. Hirschmann
Vice Chair: Ed Garnero

- **Rifting and the Tectonics of Passive Margins** (*Cynthia Ebinger* / Jolante van Wijk / Timothy Minshull)
- **Volcanoes: Mass, Energy, and Information from the Crust and Mantle** (*Kari Cooper* / Terry Plank / Diana Roman / Josef Dufek)
- **Subduction: Fluids, and Melts** (*Craig Manning* / Ronit Kessel / Marc Spiegelman)
- **Deep Earth Volatile Cycles** (*Rajdeep Dasgupta* / Daniel Frost / Anne Pommier / Pierre Cartigny)
- **Upper Mantle Seismic Discontinuities: Melts / Volatiles / Phase Transitions / Anisotropy?** (*Donald Forsyth* / Nick Schmerr / Yasuko Takei)
- **Origin of Plate Tectonics** (*Robert Stern* / Mark Harrison / Taras Gerya / Jeroen Van Hunen)
- **Deforming the Continental Lithosphere** (*Karen Fischer* / Whitney Behr / Robert Van Der Hilst)
- **From Grains to Plates** (*Laurent Montesi* / Andrea Tommasi / Lars Hansen / Julie Castillo-Rogez)
- **Unresolved Questions / Young Investigator Presentations** (*Louise Kellogg* / Roberta Rudnick)

Interior of the Earth
The Structure, Properties and Evolution of Plate Boundaries
Jun 6-7, 2015
Chair: Heather A. Ford

Laser Diagnostics in Combustion
Expanding the Limits in Space and Time
Aug 9-14, 2015
Waterville Valley Resort, Waterville Valley, NH
Chair: Mark A. Linne
Vice Chair: Hope A. Michelsen

- **Keynote Session: Mid-Infrared Spectroscopic Studies of Free Radicals and Their Chemistry / Late-Breaking Topics** (*Hope Michelsen* / Grant Ritchie)
- **Time-Resolved Diagnostics for Reactive, Turbulent Flows** (*Brian Petersen* / Isaac Boxx / Carson Slabaugh / Benjamin Boehm)
- **Coupling Between Modeling and Experiment** (*Margaret Wooldridge* / Heinz Pitsch / Simone Hichgreb)
- **Ultra-Short Nonlinear Interactions** (*Johannes Kiefer* / Hans Stauffer / Christopher Kliewer / Marcus Motzkus)
- **Thermographic Phosphors in Flowfields** (*Marcus Alden* / David Rothamer / Frank Beyrau)
- **Sensing in Multiphase, Mixing, and Reacting Flows** (*Caroline Genzale* / Daniel Guildenbecher / Christof Schulz / Mark Musculus)
- **Advances in Sources and Sensors** (*Jacqueline O'Connor* / James Gord / Brian Thurow)
- **Soot Particle Detection** (*Stefan Will* / Graham Nathan / Patrizia Minutolo / Joshua Schwarz)
- **Novel Signal Processing** (*Edouard Berrocal* / Christopher Goldenstein / Elias Kristensson)

Laser Diagnostics in Combustion
Challenges and Recent Developments in Laser-Based Combustion Diagnostics and Their Applications
Aug 8-9, 2015
Chair: Julia Krueger
Associate Chair: Fahed J. Abou Nada



Participants at the 2014 Transglutaminases in Human Disease Processes GRC enjoy a wine show at the Renaissance Tuscany Il Ciocco Resort and Spa in Lucca (Barga), Italy.

Lipids, Molecular & Cellular Biology of
Lipid Dynamics and Lipidomics
Jul 26-31, 2015
Waterville Valley Resort, Waterville Valley, NH
Chair: Suzanne Jackowski
Vice Chair: David A. Bernlohr

- **Keynote Session: Lipid Dynamics and Lipidomics** (*Suzanne Jackowski* / Todd Graham / Daniel Nomura)
- **Cellular Trafficking of Lipids** (*George Carman* / Thomas Langer / Will Prinz / Symeon Siniossoglou)
- **Lipid Responses to Challenge** (*Daniel Raben* / Nan Chiang / Frank Gonzalez)
- **Lipid Signaling** (*Dennis Voelker* / Richard Proia / Rahat Rohatgi / Lois Weisman)
- **Responses to Lipid Challenge** (*Vytas Bankaitis* / Clay Semenkovich / Tobias Walther)
- **Disease Mechanisms** (*Rosalind Coleman* / Noa Noy / Michael Schlame / Michael Wolfgang)
- **Targeting Lipid Metabolism** (*Judith Storch* / Alex Brown / Michael Wakelam)
- **Microbial Interaction with Host Lipid Metabolism** (*James Ntambi* / Hubert F. Hilbi / Charles Rock / Andrew Tai)
- **Technological Advances in Lipid Biology** (*David Bernlohr* / Arthur Laganowsky / Peter Watson)

Liquid Crystals
Liquid Crystallinity in Soft Matter at and Beyond Equilibrium
Jun 21-26, 2015
University of New England, Biddeford, ME
Chair: Nicholas L. Abbott
Vice Chairs: Linda S. Hirst & Torsten Hegmann

- **Active and Living Systems** (*Tom Lubensky* / Julia Yeomans / Zvonimir Dogic / Igor Aronson)
- **Vesicles and Shells** (*Seth Fraden* / David Weitz / Jan Lagerwall / Robin Selinger / Yan-Yeung Luk)
- **Supramolecular and Functional Materials** (*Juan De Pablo* / Takashi Kato / Dirk Broer / Hiroshi Yokoyama)
- **Defects and Topology** (*Noel Clark* / Emmanuelle Lacaze / Randall Kamien / Alberto Fernandez / Miha Ravnik)
- **Liquid Crystals and Biology** (*Elda Hegmann* / Daniel Schwartz / David Lynn / Cyrus Safinya)
- **Young Investigator Presentations** (*Nicholas Abbott*)
- **Photons and Devices** (*Mohan Srinivasarao* / Igor Musevic / Timothy Bunning / Nelson Tabiryan)
- **Colloids and Interfaces** (*Slobodan Zumer* / Kathleen Stebe / Claudio Zannoni / Christian Bahr / Alejandro Rey)
- **Hierarchical Self-Assembly and New Phases** (*Oleg Lavrentovich* / Robert Lemieux / David Walba / Dong Ki Yoon)

Liquid Crystals
Soft Matter in Liquid Crystals and Liquid Crystals in Soft Matter
Jun 20-21, 2015
Chair: Zoey S. Davidson
Associate Chair: Xiaoguang Wang

Liquids, Chemistry & Physics of
Basic Principles, Complex Consequences
Aug 2-7, 2015
Holderness School, Holderness, NH
Chair: Phillip L. Geissler
Vice Chair: Bruce D. Kay

- **Interfaces** (*Christopher Mundy* / Shekhar Garde / Gilbert Nathanson)
- **Active Matter** (*Steve Granick* / Wilson Poon / Thomas Speck / Daniel Needleman)
- **Protons in Water** (*Xueyu Song* / Andrei Tokmakoff / Mark Johnson)
- **Glassy Dynamics** (*Juan Garrahan* / Zahra Fakhraai / Laura Kaufman / Robert Jack)
- **Phase Transitions** (*Valeria Molinero* / Christoph Dellago / Benjamin Rotenberg)
- **Membranes and Protein Assemblies** (*Sarah Keller* / Ka Yee Lee / Joan-Emma Shea / Douglas Tobias)
- **Hydrophobicity** (*Amish Patel* / Hans-Juergen Butt / Joel Eaves)
- **Ultrafast Liquid Dynamics** (*Nancy Levinger* / Peter Hamm / Poul Petersen)
- **Self-Assembly** (*Steve Whitelam* / Jasna Brujic / Vinothan Manoharan)

Liquids, Chemistry & Physics of
Exploring Liquid Interfaces, Phases and Dynamics
Aug 1-2, 2015
Chair: Martin L. McDermott
Associate Chair: Aleksandra Biedron

Lung Development, Injury & Repair
Translating Lung Biology to Respiratory Medicine
Aug 16-21, 2015
Proctor Academy, Andover, NH
Chair: Thomas Mariani
Vice Chairs: Andreas Guenther & Jason Rock

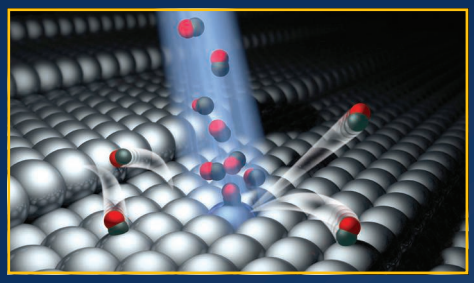
- **The State of Lung Science and Opportunities in Respiratory Medicine**
  (*Thomas Mariani* / Jim Kiley)
- **Early Developmental Mechanisms and Related Disease**
  (*David Ornitz* / Ed Morrissey / Larry Nogee / Xin Sun)
- **Perinatal Developmental Mechanisms and Chronic Pediatric Disease**
  (*Susan Guttentag* / Jeffrey Whitsett / Tom Ferkol)
- **Injury from Respiratory Pathogens**
  (*Joseph Mizgerd* / Susanne Herold / Richard O'Malley / Albert Osterhaus)
- **Inflammation and Immunity**
  (*Bethany Moore* / Pyong Woo Park / Anurada Ray / David Wilkes)
- **Chronic Injury and Progressive Disease**
  (*Andreas Guenther* / Jeanine D'Armiento / Naftali Kaminsky / Ed Silverman)
- **Cancer and Personalized Medicine**
  (*Tomoko Betsuyaku* / Kwok-Kin Wong)
- **Injury Resolution and Tissue Repair**
  (*Lynn Schnapp* / Bruce Levy / Barry Stripp / Irina Petrache)
- **Therapeutic Tissue Engineering and Regeneration**
  (*Jason Rock* / Laura Niklason / Emma Rawlins)

Lung Development, Injury & Repair
From Basic Science to Translational Research
Aug 15-16, 2015
Chair: Jin-Ah Park
Associate Chair: Sarah Utley

Malaria
Translating Malaria Research to the Field
Jul 26-31, 2015
Melia Golf Vichy Catalan Business and Convention Center, Girona, Spain
Chair: Robert Sauerwein
Vice Chair: Maria Mota

- **Drug Development and Resistance**
  (*Sirima Sodiomon Bienvenu* / Thierry Diagana / Arjen Dondorp / Abdoulaye Djimde)
- **Vaccines Tested in Controlled Human Malaria Infections and in the Field**
  (*Salim Abdulla* / Adrian Hill / Johan Vekemans / Stephen Hoffman / Simon Draper / Miguel Prudencio)
- **Immunology in the Lab and in the Field**
  (*Kevin Marsh* / James Beeson / Peter Crompton / Laurant Renia)
- **Models in Animals and Humans**
  (*Jean Langhorne* / Else Bijker / Stefan Kappe / Clemens Kocken / James McCarthy / Philip Spence)
- **Pregnancy Associated Malaria**
  (*Patrick Duffy* / Feiko Ter Kuile)
- **(Molecular) Biology of Asexual and Sexual Stages Parasites**
  (*Andy Waters* / Tania De Koning-Ward / Matthias Marti / Alexandra Rowe / Pietro Alano)
- **Severe Malaria and Pathophysiology**
  (*Nick Anstey* / Marcus Lacerda / Mats Wahlgren)
- **Transmission Stages in Humans and Mosquito**
  (*Chris Drakeley* / Teun Bousema / Azra Ghani / Elena Levashina / Alassane Dicko / Ingrid Felger)
- **Biology of Sporozoites and Liverstages**
  (*Maria Mota* / John Harty / Dominique Mazier)

Malaria
Translating Malaria Research to the Field
Jul 25-26, 2015
Chair: Anja Scholzen
Associate Chair: Janet T. Midega



An artist's conception of Carbon Monoxide (CO) molecules adsorbing at a Platinum (Pt) surface. CO on Pt is to surface science as the fruit fly is to genetics. Recent studies have shown clearly that adsorption involves both attack at flat terraces as well as diffusion to steps, where binding is stronger. Courtesy of the Max Planck Institute for Biophysical Chemistry. Submitted by Alec Wodtke, Chair, Dynamics at Surfaces GRC.

Mammary Gland Biology
Mammary Epithelial Cell Interactions: Actions and Reactions
Jun 7-12, 2015
Mount Snow Resort, West Dover, VT
Chairs: Caroline M. Alexander & Victoria Seewaldt
Vice Chair: Geoffrey J. Lindeman

- **Keynote Session: Immune Regulation of Tumor Development**
  (*Caroline Alexander* / Bob Schreiber)
- **Stressing Out: Checkpoints and Instability**
  (*Jeffrey Rosen* / Beth Weaver / Shridar Ganesan / Alan Diehl)
- **Functional Imaging of the Mammary Gland**
  (*Traci Lyons* / Patricia Keely / John Condeelis)
- **Molecular Risk, Early Detection, and Prevention of Breast Cancer**
  (*Robert Clarke* / Ginger Borges / Priscilla Furth / Elizabeth Repasky)
- **Growing Breasts / Signaling Pathways**
  (*John Wysolomerski* / Connie Eaves / Hallger Rui)
- **Adipose Connections**
  (*Terri Wood* / Liza Makowski / Claudia Fischbach-Tesch / Valerie Horsley)
- **Mammary Circulatory Systems and Metastasis**
  (*Cyrus Ghajar* / Heide Ford / Judith Varner)
- **Metabolism and Epigenetic Regulation of Development and Tumorigenesis**
  (*Steffi Oesterrich* / Leslie Shaw / Richard Cerione / Jayanta Debnath)
- **Keynote Session: Modeling Breast Development and Tumorigenesis**
  (*William Muller* / Robert Cardiff)

Mammary Gland Biology
Finding Your Pathway: Breast Development and Breast Cancer
Jun 6-7, 2015
Chair: Lara Lacerda
Associate Chair: Jessica Finlay-Schultz

Marine Molecular Ecology
Linking Molecular Mechanisms with Ecological Outcomes
Aug 2-7, 2015
The Hong Kong University of Science and Technology, Hong Kong, China
Chairs: Hongbin Liu & Peter D. Steinberg
Vice Chairs: Stanley Lau & Curtis Suttle

- **Connecting Molecular and Cellular Processes to Ecosystem Functions and Biogechemical Cycling**
  (*Curtis Suttle* / Nianzhi Jiao / Birgitta Bergman)
- **Microbial Diversity and Process in Deep Ocean and Other Extreme Environments**
  (*Virginia Edgcomb* / Steve Pointing / Pei-Yuan Qian)
- **Role of Virus in Marine Ecosystems**
  (*Qinglu Zeng* / Feng Chen / Jennifer Brum)
- **Exploring the Bacterial Biodiversity and Ecological Functioning in a Global Oceanographic Context**
  (*Jonathan Zehr* / Silvia Acinas / Alexandra Worden)
- **Molecular Response and Adaptation to Climate Change and Anthropogenic Stressors**
  (*Peter Steinberg* / Gretchen Hofmann / Grieg Steward)
- **Photosynthetic Eukaryotes and Prokaryotes**
  (*Lisa Campbell* / Laurence Garczarek / Ian Paulsen / Daniel Vaulot)
- **Microbial Diversity and Biogeochemical Cycling in Oxygen Minimum Zone and Other Anaerobic Environments**
  (*Hongbin Liu* / Steve Hallam / Osvaldo Ulloa)
- **Marine Holobionts**
  (*Stanley Lau* / Torsten Thomas / Madeleine van Oppen)
- **Genomic and Proteomic Study of Marine Invertebrates and Vertebrates**
  (*Ka Hou Chu* / Benny Chan / Junya Hirai / Jian-Wen Qiu)

Marine Molecular Ecology
Recent Developments in Marine Microbial Interactions: New Approaches and Techniques
Aug 1-2, 2015
Chair: Emma Rocke
Associate Chair: Ezequiel Marzinelli

Matrix Metalloproteinases
From the Organism to the Atom: An Interdisciplinary Exploration of Metalloproteinase Regulation in Development and Disease
Aug 2-7, 2015
Sunday River Resort, Newry, ME
Chair: M. Sharon Stack
Vice Chair: Howard C. Crawford

- **Keynote Session: Metalloproteinases and Mechanobiology**
  (*Alexander Dunn*, *Elizabeth Gardiner* / Valerie Weaver / Alexander Dunn / Elizabeth Gardiner)
- **Developing Roles for Matrix Metalloproteinases**
  (*Andrea Page-McCaw*, *David Sherwood* / Suneel Apte / Bryan Crawford / Andrea Page-McCaw / David Sherwood)
- **Regeneration, Remodeling and Repair**
  (*Ulrich Auf Dem Keller*, *Amanda Fosang* / Kenn Holmbeck / Rama Khokha / Ulrich Auf Dem Keller / Amanda Fosang)
- **Metalloproteinase Control of Effector Cell Function**
  (*William Parks*, *Anne Manicone* / Thomas Bugge / Vincent Dive / Athan Kuliopulos / William Parks / Anne Manicone)
- **Metalloproteolysis in the Tumor Microenvironment**
  (*Elena Deryugina*, *Laurie Littlepage* / Shoukat Dedhar / Elena Deryugina / Laurie Littlepage)
- **Metalloproteinase Regulation in the Intra-, Peri-, and Extracellular Space**
  (*Kaisa Lehti*, *Christopher Overall* / Philippe Chavrier / John Tarbell / Stephen Weiss / Kaisa Lehti / Christopher Overall)
- **Visualization and Control of Metalloproteinases**
  (*Gregg Fields*, *Wiltrum Lederle* / Olga Vasiljeva / Kazuhiro Yamamoto / Gregg Fields / Wiltrum Lederle)
- **Substrate Cleavage**
  (*Yoshi Itoh*, *Katarina Wolf* / Carl Blobel / Christoffer Goth / Yoshi Itoh / Katarina Wolf)
- **Metalloproteinase Biophysics**
  (*Irit Sagi*, *Steven Van Doren* / David Weitz / Irit Sagi / Steven Van Doren)

Matrix Metalloproteinases
The Future of Matrix Metalloproteinases Beyond Proteolysis of Matrix
Aug 1-2, 2015
Chair: Anna Juncker-Jensen
Associate Chair: Trista K. Robichaud

Mechanisms of Membrane Transport
Integrating Structure, Function and Dynamics
Jun 28 - Jul 3, 2015
Bates College, Lewiston, ME
Chair: Lucy R. Forrest
Vice Chair: Hassane S. Mchaourab

- **ABC Transporters**
  (*Heather Pinkett* / Clemens Glaubitz)
- **Emerging Methods in Membrane Transport Research**
  (*Simon Newstead* / William Degrado / Edmund Kunji / Debora Marks / Joseph Mindell)
- **Ion-Motive ATPases**
  (*Miguel Holmgren* / Karen Davies / Benoit Roux / Rajini Rao)
- **Symporters**
  (*Gary Rudnick* / Olga Boudker / Michael Grabe)
- **Integral Roles of Lipids in Transport**
  (*Todd Graham* / William Dowhan / Kaspar Locher / Robert Molday)
- **Ion Exchangers**
  (*Jose Faraldo-Gomez* / Merritt Maduke / Carola Hunte)
- **Channels**
  (*Baron Chanda* / Crina Nimigean / Eduardo Perozo)
- **Ligand-Gated and Calcium-Activated Channels**
  (*Alessio Accardi* / Criss Hartzell / Andrew Marks / Andrew Plested / Paul Shaffer)
- **Late-Breaking Topics in Transport**
  (*Hassane Mchaourab* / Dirk Jan Slotboom / Randy Stockbridge)

GRS Mechanisms of Membrane Transport
Excelling in Scientific and Social Skills While Navigating Complex Career Choices
Jun 27-28, 2015
Chair: Shruti Sharma
Associate Chair: Benjamin C. McIlwain

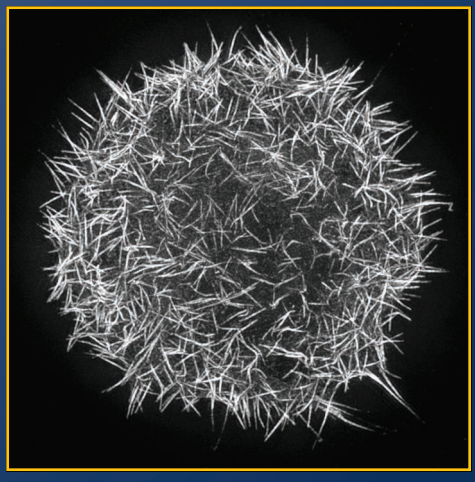
Medicinal Chemistry
Recent Advances in Drug Discovery: Pathways, Targets and Molecules
Aug 2-7, 2015
Colby-Sawyer College, New London, NH
Chair: Lori K. Gavrin
Vice Chair: Bradley Tait

- **Kinase Targets for CNS Disorders**
  (*Brock Shireman* / Carolyn Dzierba / Anthony Estrada / Travis Wager)
- **Challenges and Successes Targeting Rheumatoid Arthritis**
  (*Janeta Popovici-Muller* / Christopher Smith / Stefan Laufer / Brian Safina / Alan Northrup)
- **Advances in Oncology**
  (*Peter Dragovich* / Barry Touré / Chris De Savi / Alessandro Boezio)
- **Ion Channel Drug Discovery for Cardiovascular and Pain**
  (*Sharan Bagal* / Brian Marron / Jeff Zablocki / Patrick Stoy / Alexander Pasternak)
- **Advances in the Treatment of Schizophrenia**
  (*James Barrow* / Carol Tamminga / Matthew Volgraf / Giles Brown)
- **Advances in Antibiotic Research: Porins, Natural Products and Boron Inhibitors**
  (*Blaise Lippa* / David Sherman / Jef De Brabander / Ruben Tommasi / Scott Hecker)
- **Ubiquitin Proteasome System: Untapped Source of New Therapeutic Opportunities**
  (*Shelli McAlpine* / David Wustrow / Jeff Ciavarri)
- **Late-Breaking Topics**
  (*Sabine Hadida*)
- **Keynote Session: New Approaches in Discovery Science, New Challenges for the Biopharmaceutical Industry**
  (*Lori Gavrin* / John LaMattina)

GRS Medicinal Chemistry
Application of *In Vitro* and *In Vivo* Methodologies to Drug Discovery Projects
Aug 1-2, 2015
Chair: Robert T. Jacobs

Membrane Protein Folding
NEW!
Biology, Disease, Design and Theory
Jun 21-26, 2015
Bentley University, Waltham, MA
Chair: Karen Fleming
Vice Chair: James U. Bowie

- **How Do Membrane Proteins Insert into the Membrane?**
  (*James Bowie* / Thomas Miller / Tomoya Tsukazaki / Alexey Ladokhin)
- **Folding in the Periplasm**
  (*Karen Fleming* / David Brockwell / Xinsheng Zhao / Marcelo Sousa / Sebastian Hiller)
- **Principles of Membrane Protein Design**
  (*Ann Dixon* / Patrick Barth / Sarel Fleishman / Tetsuya Yomo)
- **Topology Determination**
  (*Patrick Barth* / William Dowhan / Joanna Slusky / Gunnar Von Heijne / Douglas Theobald)
- **Structure Prediction of Membrane Proteins**
  (*Joanna Slusky* / Charlotte Deane / Alessandro Senes / Debora Marks / Chris Sander)
- **Folding and Dynamics**
  (*Charlotte Deane* / Wonpil Im / Martin Ulmschneider / Francis Valiyaveetil / Tae-Young Yoon)
- **Membrane Protein Folding and Disease**
  (*Martin Ulmschneider* / Amit Chattopadhyay / John Riordan / Charles Sanders)
- **Membrane Protein Structural Stability Determinants**
  (*Charles Sanders* / Isaiah Arkin / Dieter Langosch / Janice Robertson / Peter Tieleman)
- **Paths of Membrane Protein Folding**
  (*Janice Robertson* / Ann Dixon / Daniel Otzen / Shu-Ou Shan)



Super-resolution image of a melanoma cell engineered to assemble cell surface microvilli and labeled with phalloidin to visualize F-actin. Courtesy of Nathan Grega-Larson and Matthew Tyska. Submitted by Fred Chang, Chair, Motile & Contractile Systems GRC.

Microbial Adhesion & Signal Transduction
The Forefront of Microbial Communication, Colonization and Pathogenesis Research
Jul 26-31, 2015
Salve Regina University, Newport, RI
Chairs: Matthew R. Parsek & Joerg Vogel
Vice Chairs: Nina R. Salama & Christoph Dehio

- **Signal Transduction Mechanisms Controlling Microbial Community Behavior**
  (*Daniel Lopez* / Karine Gibbs / Pete Greenberg / Kimberly Kline)
- **Surface Interactions and Their Impact on Cellular Physiology**
  (*Tracy Raivio* / Jean-Marc Ghigo / Tracy Raivio)
- **Signaling Between the Host and Pathogen**
  (*Joerg Vogel* / Andreas Baumler / Jeffery Cox / Craig Roy)
- **Bacterial Regulatory Networks**
  (*Matthew Parsek* / Petra Dersch / Nassos Typas / Michael Gilmore)
- **Composition of the Interface**
  (*Nina Salama* / Staffan Normark / Hank Steven Seifert / Samuel Miller)
- **New Strategies for Antibiotics and Anti-Infectives**
  (*Kimberly Kline* / Dirk Bumann / Daniel Lopez / Jan-Willem Veening)
- **New Technologies and Genome-Wide Approaches**
  (*Christoph Dehio* / Luciano Marraffini / Feng Shao / Nathalie Balaban)
- **Bacterial and Eukaryotic Cell Biology**
  (*Karine Gibbs* / Pascale Cossart / David Holden / Ralph Isberg)
- **Model Systems for Studying Signal Transduction Networks**
  (*Fitnat Yildiz* / Roberto Kolter / Fitnat Yildiz)

GRS Microbial Adhesion & Signal Transduction
The Forefront of Microbial Communication, Colonization and Pathogenesis Research
Jul 25-26, 2015
Chair: Melissa J. Martin
Associate Chair: Sandy R. Pernitzsch

Microbial Population Biology
Disentangling Causes and Consequences
Jul 19-24, 2015
Proctor Academy, Andover, NH
Chair: Michael Travisano
Vice Chairs: Eva M. Top & Larry Forney

- **Astrobiology and Extremes**
  (*Michael Travisano* / Frank Rosenzweig)
- **Microbial Community Ecology**
  (*Eva Top* / Diana Nemergut / Ashley Shade / Marilyn Roossinck)
- **Holobionts and Microbiomes**
  (*Larry Forney* / Maureen O'Malley / Seth Bordenstein / David Guttman)
- **Microbial Predation and Parasitism**
  (*R. Ford Denison* / Katy Heath / Catherine Putonti / Joanna Masel)
- **Microbial Competition**
  (*Duncan Greig* / Kevin Foster / Wenying Shou / Paul Rainey)
- **Understanding Molecular Networks / Genes, Genomes and Microbial Evolution**
  (*Gavin Sherlock* / Gabriela Olmedo / Gerda Saxer)
- **Microbes Go to Work - Industrial Applications**
  (*Kazufumi Hosoda* / Candice Landry)
- **The Material Basis of Microbial Evolution / Proximate Mechanisms of Evolution**
  (*Elizabeth Ostrowski* / Andrew Ellington / Joshua Mell)
- **New Advances in Microbial Population Biology / Late-Breaking Topics**
  (*Lindi Wahl* / Tony Dean / Lone Simonsen)

GRS Microbial Population Biology
Ecology, Evolution and Applications in Microbial Population Biology
Jul 18-19, 2015
Chair: Pleuni S. Pennings
Associate Chair: Krishna B. S. Swamy

Microfluidics, Physics & Chemistry of
Microscale Technology for Advancing and Translating Discovery
May 31 - Jun 5, 2015
Mount Snow Resort, West Dover, VT
Chairs: Shelley L. Anna & Jonathan D. Posner
Vice Chairs: Catherine M. Klapperich & Dino Dicarlo

- **Rare Cell Capture and Analysis**
  (*Jonathan Posner* / Brian Kirby / Mehmet Toner)
- **Tools for Biological Discovery**
  (*Hang Lu* / Cullen Buie / Sarah Koester)

Without the Gordon Research Conferences. . .

...our field would lose its major venue of exchange. *(Andre Kessler, Chair, 2014 Plant Volatiles GRC)*

- **Point of Care Technologies**
  (*Catherine Klapperich, Dino Dicarlo* / Helene Andersson Svahn / Rustem Ismagilov / Scott Phillips)
- **Water Filtration and Desalination**
  (*Juan Santiago* / Maarten Biesheuvel / Rohit Karnik)
- **Energy and Carbon Management**
  (*Patrick Tabeling* / Jan Eijkel / David Sinton)
- **Single Molecule Analysis and Manipulation**
  (*Eric Shaqfeh* / Kevin Dorfman / Susan Muller / Charles Schroeder)
- **Droplet Microfluidics**
  (*Shelley Anna* / Andrew De Mello / Stephan Herminghaus)
- **Concentrated Suspensions in Confined Systems**
  (*Roy Bar-Ziv* / Michael Graham / William Ristenpart / Sindy Tang)
- **Microfluidic Biotechnology**
  (*Jorg Kutter* / Sung-Hoon Kwon / Shoji Takeuchi)

Microfluidics, Physics & Chemistry of
Interfaces, Molecules, and Assays at the Microscale
May 30-31, 2015
Chair: Mark D. Borysiak
Associate Chair: Chris Nelson

Modulation of Neural Circuits & Behavior

NEW!

Neuromodulatory Signaling Pathways that Modify the Function of Circuits
Jun 21-26, 2015
The Hong Kong University of Science and Technology, Hong Kong, China
Chairs: Andres Villu Maricq & Yun Zhang
Vice Chairs: Chun-Fang Wu & Joy A. Alcedo

- **Keynote Session: Neuromodulation: An Emerging Dimension of the Nervous System**
  (*Andres Villu Maricq* / Karl Deisseroth / Larry Young)
- **Functional Organization of Neuromodulatory Circuits**
  (*Yun Zhang* / Mauro Costa-Mattioli / Scott Waddell / Eric Huang)
- **Development and Assembly of Local Circuits**
  (*Chun-Fang Wu* / Nancy Ip / Yi Rao)
- **Novel Strategies for Imaging and Recording Circuit Activity**
  (*Karl Deisseroth* / Rainer Friedrich / Glenn Turner)
- **Perturbation Analysis of Modulatory Circuits**
  (*Joy Alcedo* / Guosong Liu / Gero Miesenboeck)
- **Behavioral Effects of Modulators**
  (*Yi Rao* / Suresh Jesuthasan / Gene Robinson)
- **Mechanisms Shaping Circuit Connectivity and Behavior**
  (*Larry Young* / Randy Bruno / Mandyam Srinivasan)
- **Circuit Homeostasis**
  (*Eve Marder* / Graeme Davis / Yukiko Goda)
- **Keynote Session: Modulation and Experience-Dependent Plasticity**
  (*Guosong Liu* / Ulrike Heberlein / Gilles Laurent / Eve Marder)

Molecular Mechanisms in Evolution

Using Evolutionary Perspectives to Inform Molecular Biology and Medicine, and Molecular Biology to Elucidate Evolutionary History and Mechanisms
Jun 28 - Jul 3, 2015
Stonehill College, Easton, MA
Chair: Christine Queitsch
Vice Chair: Ivan Matic

- **Keynote Session: Advances in Understanding the Mechanistic Underpinnings of Evolution**
  (*Christine Queitsch* / Susan Rosenberg / Stanislas Leibler)
- **Genome Architecture and Evolvability**
  (*Lilach Hadany* / Evan Eichler / Doris Bachtrog / Detlef Weigel / Harmit Malik)
- **Insights from Laboratory Evolution**
  (*Benjamin Kerr* / Jeffrey Barrick / Christopher Marx / Andrew Murray)
- **Physical Constraints and Stochasticity**
  (*Arjun Raj* / Julien Ayroles / Ido Golding / Sophie Martin / Peter Sims)
- **Non-Traditional Mechanisms of Inheritance**
  (*Daniel Jarosz* / Susan Lindquist / Mary Gehring / Oliver Rando)
- **Predicting and Arresting Evolution**
  (*Anna Barker* / Jesse Bloom / Maitreya Dunham / Kevin Esvelt / Franziska Michor)
- **Mechanisms and Consequences of Stress-Inducible Genetic Variation**
  (*Ivan Matic* / Didier Mazel / Reuben Harris / Houra Merrikh)
- **Mechanisms of Coding and Regulatory Evolution**
  (*Christophe Herman* / Joe Thornton / Gunter Wagner / Patricia Wittkopp / Diethard Tautz)
- **Evolution of Complexity**
  (*Joanna Masel* / Michael Lynch / Nicole King / Chris Adami)

Molecular Membrane Biology

Investigating the Inner Life of the Cell
Jul 12-17, 2015
Proctor Academy, Andover, NH
Chair: Frederick M. Hughson
Vice Chair: Anne Spang

- **Keynote Session: Organelle Crosstalk**
  (*Frederick Hughson, Anne Spang* / Pietro De Camilli / Jennifer Lippincott-Schwartz)
- **Organelle Identity and Dynamics**
  (*Scott Emr* / Deborah Fass / Chris Fromme / Randy Schekman / William Shih / Alice Ting)
- **Translocation and Membrane Assembly**
  (*Tom Rapoport* / Daniel Kahne / Shu-Ou Shan / Jonathan Weissman)
- **Membrane Dynamics: Shaping and Fission**
  (*Charlie Barlowe* / John Briggs / Adam Frost / Britta Qualmann / Margaret Robinson / Sandra Schmid)
- **Membrane Dynamics: Fusion and Its Regulation**
  (*Suzanne Pfeffer* / Francis Barr / Alexey Merz / James Rothman)
- **Lipids in Signaling and Disease**
  (*Sean Munro* / Bruno Antonny / Tobias Walther / Xiaochen Wang / Lois Weisman)
- **Quality Control of Membrane Proteins**
  (*Gia Voeltz* / Pedro Carvalho / Russell Debose-Boyd / Ramanujan Hegde)
- **Metabolism and Autophagy**
  (*Maya Schuldiner* / Vladimir Denic / Aimee Edinger / Robbie Loewith / Tamotsu Yoshimori / Roberto Zoncu)
- **Late-Breaking Topics**
  (*Benjamin Glick*)

Molecular Membrane Biology
Investigating the Inner Life of the Cell
Jul 11-12, 2015
Chair: Tina Liu
Associate Chair: Tslil Ast

Motile & Contractile Systems

Physical Biology of Cell Shape, Movement and Division
Jul 19-24, 2015
Colby-Sawyer College, New London, NH
Chair: Fred Chang
Vice Chair: William M. Bement

- **Keynote Session: Regulation of Microtubule Dynamics**
  (*Fred Chang* / Joe Howard / Gary Brouhard / Ekaterina Grishchuk)
- **Actin Filament Regulation and Organization**
  (*Thomas Pollard* / David Kovar / Michael Murrell / Alphee Michelot / Bruce Goode)
- **Assembly of Cytoskeletal Structures**
  (*Amy Gladfelter* / David Ehrhart / Peter Lenart / Daniel Needleman)
- **Design of Cell Shape**
  (*Jennifer Zallen* / Ewa Paluch / K.C. Huang / Amy Gladfelter)
- **Moving Chromosomes**
  (*Daniel Needleman* / Bungo Akiyoshi / Alexey Khodjakov / Phong Tran / Kerry Bloom)
- **Cell Locomotion**
  (*Ewa Paluch* / Margaret Gardel / Tam Mignot / Alexander Verkhovsky / Clare Waterman)
- **Cell Division**
  (*David Burgess* / Julie Canman / Ann Miller / Thomas Pollard)
- **Control of Cellular Motors**
  (*William Bement* / Erika Holtzbaur / Lukas Kapitein / Thomas Surrey)
- **Mechanical Crosstalk Between Cells**
  (*Clare Waterman* / Otger Campas / Olivier Hamant / Matthew Tyska / Jennifer Zallen)

Muscle: Excitation-Contraction Coupling

Advancing Research and Leadership in EC Coupling
May 31 - Jun 5, 2015
Sunday River Resort, Newry, ME
Chairs: Robert T. Dirksen & Susan Treves
Vice Chair: Isaac N. Pessah

- **Keynote Session: Structural Studies of the EC Coupling Apparatus**
  (*Clara Franzini-Armstrong* / Montserrat Samso / Gerhard Meissner / Andrew Marks)
- **New Insights into the Molecular Mechanism of Muscle EC Coupling**
  (*Manfred Grabner* / Roger Bannister / Angela Dulhunty / Symeon Papadopoulos / Bernhard Flucher / John Kuwada)
- **Molecular Mechanisms of Junction Formation and Maintenance**
  (*Isabelle Marty* / Vincenzo Sorrentino / Jocelyn Laporte / Feliciano Protasi)
- **Cardiac EC Coupling Disorders: Pathophysiology and Therapeutics**
  (*Sandor Gyorke* / Nagomi Kurebayashi / Wayne Chen / Hector Valdivia / Long-Sheng Song / Xander Wehrens)
- **Regulation of Cardiac EC Coupling**
  (*Heping Cheng* / Henry Colecraft / Bjorn Knollmann / Donald Bers)
- **Skeletal Muscle EC Coupling Disorders and Therapeutic Interventions**
  (*Paul Allen* / Hua Zhu / Jingsong Zhou / Andrew Voss / James Dowling / Anna Buj Bello)
- **ROS and RNS Regulation of EC Coupling**
  (*Cecilia Hidalgo* / Natalia Shirokova / Christopher Ward / Ana Ferreiro)
- **Impact of EC Coupling on Muscle Metabolism**
  (*Martin Schneider* / Wang Wang / Johanna Lanner / Muthu Periasamy / Susan Hamilton / Karyn Esser)
- **Keynote Session: Mechanisms of Muscle Fatigue and Sarcopenia**
  (*Graham Lamb* / Bradley Launikonis / Laszlo Csernoch / David Glass)

Muscle: Excitation-Contraction Coupling
New Frontiers in EC Coupling
May 30-31, 2015
Chair: Erick O. Hernandez-Ochoa
Associate Chair: John D. Lueck

Mycotoxins & Phycotoxins

The Biology, Chemistry and Ecology of Naturally Occurring Fungal and Algal Toxins with Public Health and Economic Impacts
Jun 14-19, 2015
Stonehill College, Easton, MA
Chairs: Gregory L. Boyer & Genevieve Bondy
Vice Chairs: Kathi A. Lefebvre & Paul Turner

- **Mycotoxin and Phycotoxin Ecology: Changing World, Changing Problems**
  (*Genevieve Bondy, Gregory Boyer* / Daniel Cook / Stephanie Moore)
- **Mycotoxin and Phycotoxin Mode of Action**
  (*Paul Jennings, Wayne Carmichael* / Sven Daenicke / Elaine Faustman / Isabelle Oswald / Michael Janech)
- **Biomarkers in Mycotoxin and Phycotoxin Epidemiology**
  (*Chidozie Amuzie, Ann Abraham* / Luis Botana / Richard Lewis / Richard Manderville)
- **Analytical Chemistry: Challenges for Biotoxin Detection and Quantitation in Biological Matrices**
  (*Maria De Rosa, Kevin James* / Benedikt Cramer / Franz Berthiller / Schonna Manning / Joerg Stroka)
- **Strategies for Mycotoxin and Phycotoxin Prevention and Mitigation**
  (*Gary Payne, Allen Place* / Fiona Doohan / Kathryn Coyne / Marilyn Warburton)
- **Novel and Emerging Toxins and Toxigenic Organisms**
  (*Susan Watson, Kenneth Voss* / Jane Burns / Romulo Araoz / John Pitt / Leopold Ilag)
- **Mycotoxin and Phycotoxin Risk Assessment and Management**
  (*Brian Belliveau, Elizabeth Hamelin* / John Kough / Stacey Degrasse / Wentzel Gelderblom)
- **The Future Is Now: Fungal and Algal Toxin "Omics"**
  (*Steven Wilhelm, Mark Sumarah* / Linda Harris / Morgan Steffen / Ahmad Fakhoury / Olivier Ploux)
- **Keynote Session: Future Perspectives and Directions in Mycotoxin and Phycotoxin Research**
  (*Kathi Lefebvre, Paul Turner* / Donald Anderson)

Mycotoxins & Phycotoxins
Harmful Biotoxins: Their Chemistry, Ecological Role and Associated Risks
Jun 13-14, 2015
Chair: Asha D. Jaja-Chimedza
Associate Chair: Elisabeth Varga

Myogenesis

Molecular and Cellular Networks
Jun 21-26, 2015
Renaissance Tuscany Il Ciocco Resort, Lucca (Barga), Italy
Chair: Gabrielle Kardon
Vice Chair: Denis C. Guttridge

- **Keynote Session: Muscle: From Snakes to Humans**
  (*Helen Blau* / Giulio Cossu / Leslie Leinwand)
- **Development of Muscle**
  (*Gabrielle Kardon* / Peter Currie / Clarissa Henry / Simon Hughes / Robert Krauss / Christophe Marcelle / Frederic Relaix / Shahragim Tajbakhsh)
- **Cellular Interactions in Development of Muscle**
  (*Peter Currie* / Steven Burden / Dennis Discher / Ronen Schweitzer / Eli Zelzer)
- **Cellular Interactions in Adult Muscle Regeneration**
  (*Bradley Olwin* / Benedicte Chazaud / Dawn Cornelison / Pura Munoz-Canoves / Grace Pavlath / Fabio Rossi / David Sassoon / James Tidball)
- **Muscle Fiber Type Specification and Metabolism**
  (*Denis Guttridge* / Zoltan Arany / Carlos Moraes / Markus Ruegg / Frank Schnorrer)
- **Role of Transcription, Epigenetics, and Non-Coding RNAs in Myogenesis**
  (*Michael Rudnicki* / Colin Crist / Jeffrey Dilworth / Graziella Messina / Lorenzo Puri / Vittorio Sartorelli / Stephen Tapscott / Huating Wang)
- **Muscle Cell Biology**
  (*Shahragim Tajbakhsh* / Mary Baylies / Elizabeth Chen / Douglas Millay / Talila Volk)
- **Muscle Stem Cells and Regeneration**
  (*Pura Munoz-Canoves* / Helen Blau / Thomas Braun / David Goldhamer / Christoph Lepper / Bradley Olwin / Thomas Rando / Michael Rudnicki)
- **Muscle Growth, Homeostasis, and Sarcopenia**
  (*Grace Pavlath* / Andrew Brack / Fabio Demontis / David Glass / Russell Hepple)

Myogenesis
Dissecting Molecular and Cellular Networks
Jun 20-21, 2015
Chair: Martin G. Guess
Associate Chair: Mary Colasanto

Nano-Mechanical Interfaces

Theory, Computations and Experiments
Jul 19-24, 2015
The Hong Kong University of Science and Technology, Hong Kong, China
Chair: Narayan R. Aluru
Vice Chairs: Julia R. Greer & Yuan Lin

- **Nanomechanical Interfaces: Advanced Mechanics**
  (*Qing Ping Sun* / Huajian Gao / Yonggang Huang)
- **Nanofluidic Interfaces: Fundamentals**
  (*Zhigang Li* / Paul Bohn / Lyderic Bocquet / Steffen Hardt)
- **Nanomechanical Interfaces: Experiments and Simulations**
  (*Mingxin Huang* / Horacio Espinosa / Yujie Wei)
- **Biointerfaces: Mechano-Biology**
  (*Xinrui Niu* / Chwee Teck Lim / Alfonso Ngan / Vivek Shenoy)
- **Nanofluidic Interfaces: Experiments and Simulations**
  (*Wenjing Ye* / Alberto Striolo / Constantine Megaridis / Suman Chakraborty)
- **Interfacial Science and Engineering**
  (*Baoling Huang* / Michael Strano / Steven Koester / Slaven Garaj)
- **Nanomechanical Interfaces: New Phenomena**
  (*Yang Lu* / Robert Carpick / Pradeep Guduru)
- **Thermal Interfaces**
  (*Gang Li* / Gang Chen / Paddy Kwok Leung Chan / Shuhuai Yao)
- **Biointerfaces: Coupled Phenomena**
  (*William Lu* / Arthur Mak / Anderson H.C. Shum)

Nanoporous Materials & Their Applications

Established Materials and Emerging Opportunities
Aug 9-14, 2015
Holderness School, Holderness, NH
Chair: David Sholl
Vice Chair: Guang Cao

- **New Applications of Zeolites**
  (*Seth Cohen* / Enrique Iglesia / Jeffrey Rimer)
- **Conducting Materials**
  (*Christian Doonan* / Mircea Dinca / Deanna D'Allessandro)
- **Adsorption and Diffusion in Zeolites**
  (*Laura Gagliardi* / Paul Webley / Preeti Kamakoti)
- **Advances in Synthesis and Characterization**
  (*Satoshi Horike* / Christian Doonan / Matthias Thommes)
- **New Applications of MOFs**
  (*Enrique Iglesia* / Seth Cohen / Satoshi Horike)
- **New Frontiers in Modeling and Simulation**
  (*Deanna D'Allessandro* / Laura Gagliardi)
- **New Materials**
  (*Preeti Kamakoti* / Norbert Stock / Mike Zawarotko)
- **Towards Commercial Applications of MOFs**
  (*Alex Katz* / Praveen K. Thallapally)
- **Catalysis and Separations**
  (*Jeffrey Rimer* / Christine Kirschhock)

Nanoporous Materials & Their Applications
Advances in Synthesis, Separations and Environmental Applications
Aug 8-9, 2015
Chair: Jason Gee
Associate Chair: Nicholas C. Burtch

Nanoscale Science and Engineering for Agriculture & Food Systems

NEW!

Advancing Food Security and Safety, Nutrition and Health, Agricultural Productivity and Environmental Sustainability
Jun 7-12, 2015
Bentley University, Waltham, MA
Chairs: Norman Scott & Hongda Chen
Vice Chairs: Cristina Sabliov & David W. Britt

- **Nanotechnology and Its Relevance to Future Agriculture and Food Systems**
  (*Hongda Chen* / Mihail Roco / Norman Scott)
- **Is Nano Safe to Eat?**
  (*Andrew Maynard* / William Hallman / Jennifer Kuzma / Jose Miguel Aguilera)
- **Nanoscale Materials and Sensors for Rapid Detection**
  (*Jose Rivas* / Antje Baeumner / Sunny Shah)
- **Nanoscale Delivery Systems**
  (*Ricky Yada* / D. Julan McClements / Timothy Duncan / Cristina Sabliov)
- **Risk Assessment, Policy and Regulations**
  (*Frans Kampers* / Diana Bowman / Jason Kirby)
- **Intervention Strategies for Food Safety and Agricultural Biosecurity**
  (*Carmen Moraru* / Philip Demokritou / Maria Rubino / Stephen Ebbs)
- **Nanotechnology for Plant Production**
  (*David Britt* / Mariya Khodakovskaya / Jason White)
- **Nanotechnology and Biomaterials**
  (*Melanie Kah* / Dan Luo / Gannon Jennings / Graciela Padua)
- **Nanotechnogy Approaches for Improved Livestock Systems**
  (*Matthew Wheeler* / Peter Sutovsky / Yanbin Li)

Natural Products

The Wide-Ranging Influence of Natural Products Research on Medicine and the Physical Sciences
Jul 26-31, 2015
Proctor Academy, Andover, NH
Chair: Steven H. Olson
Vice Chair: Richard E. Taylor

- **Methods and Strategies for Natural Products Synthesis**
  (*Sarah Wengryniuk* / Jujiro Hayashi / James Leighton)
- **Pharmaceutical Process Chemistry**
  (*Eric Bercot* / Sebastien Caille / Steven Wittenberger)
- **Innovations in Drug Discovery**
  (*David Uehling* / Gregg Keaney / Harold Wood)
- **Natural Product Biosynthesis, Isolation, and Structure Determination**
  (*Amber Onorato* / Sesselja Omarsdottir / William Wuest)
- **Catalysis and Synthetic Methodology**
  (*Steven Mennen* / Vy Dong / Robert Knowles)
- **Natural Products Synthesis and Its Application to Improving Human Health**
  (*William Wuest* / Minji Dai)
- **Synthesis of Natural Products and Other Complex Molecules**
  (*Sergey Pronin* / John Porco / Jeffrey Johnston)
- **Innovations in the Synthesis of Biologically Active Natural Products**
  (*Matthew Lamarche* / Edmund Graziani / Martin Lear)
- **Selected Poster Presentations**
  (*Minji Dai*)

Neural Crest & Cranial Placodes

Development, Malformations and Cancers
Jul 19-24, 2015
Bentley University, Waltham, MA
Chair: Carole LaBonne
Vice Chair: Sally A. Moody

- **Neural Crest and Placode Formation** (*Jean-Pierre Saint Jeannet* / Tatjana Piotrowski / Anne-Helene Monsuro-Burq)
- **Cell Lineage Determination** (*Laura Gammill* / Chaya Kalcheim / David Raible)
- **Morphogenesis and Migration** (*Roberto Mayor* / Eric Theveneau / Philippe Soriano)
- **Congenital Malformations** (*Paul Trainor* / Ralph Marcucio / Karen Liu / Heather Young)
- **Genomics and Proteomics** (*Richard Harland* / Robert Kelsh / Tatjana Sauka-Spengler)
- **Stem Cells and Tissue Regeneration** (*Lukas Sommer* / Lorenz Studer / Maya Sieber-Blum / Ruchi Bajpai)
- **Focus on Disease: Cancers of the Neural Crest** (*Marianne Bronner* / William Weiss)
- **Cell Plasticity** (*Andrea Streit* / Raj Ladher / Tanya Whitfield)
- **Evolutionary Perspectives** (*Clare Baker* / Richard Schneider / Craig Miller)

Neuroethology: Behavior, Evolution & Neurobiology

The Future Is Now: Innovative Concepts in Neuroethology and New Technologies
Jun 28 - Jul 3, 2015
Renaissance Tuscany Il Ciocco Resort, Lucca (Barga), Italy
Chairs: Karen A. Mesce & Eric Warrant
Vice Chairs: Melissa Coleman & Annemarie Surlykke

- **Biomimetics and New Technologies** (*Roy Ritzmann* / Joseph Ayers / Barbara Mazzolai)
- **Animals and Machines Take Flight** (*Emily Baird, Marie Dacke* / Tom Daniel / Dario Floreano / Mark Frye / Graham Taylor)
- **Innovations in Computational Neuroscience** (*Claire Wyart* / Ronald Calabrese / Adrienne Fairhall)
- **Animal Olfaction and Olfactory Guidance in Robots** (*John Hildebrand* / Cornelia Bargmann / Robyn Hudson / Ryohei Kanzaki / Tim Pearce)
- **Plasticity and Circuits** (*Keith Sillar* / Catharine Rankin / David Glanzman)
- **Novel Mechanisms for Signaling and Sensing** (*Justin Marshall* / Roger Hanlon / Sonke Johnsen / Daniel Robert / Dan-Eric Nilsson)
- **Innovative Concepts in Evolution and Development** (*Jessica Fox* / Harvey Karten / Nicholas Strausfeld)
- **Navigation by Animals and Robots** (*Paul Graham, Andrew Philippides* / Henrik Mouritsen / Nachum Ulanovsky / Barbara Webb / Jochen Zeil)
- **Encoding the Outside World: New Tools and Approaches** (*Melissa Coleman, Annemarie Surlykke* / Andre Fenton / Cynthia Moss)

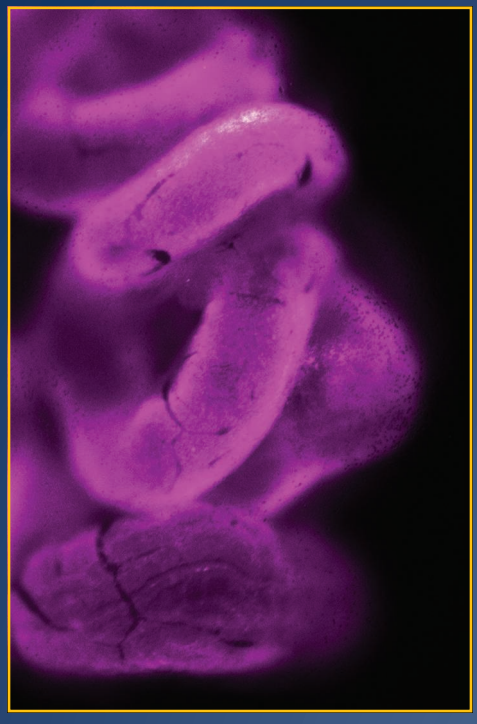
GRS Neuroethology: Behavior, Evolution & Neurobiology

In the Light of Evolution: Technology and the Evolutionary Approach
Jun 27-28, 2015
Chair: Charuni Gunaratne
Associate Chair: Ian C. Hall

Neurotrophic Factors

From Basic Biology to Therapeutic Insights
May 31 - Jun 5, 2015
Salve Regina University, Newport, RI
Chair: Freda Miller
Vice Chair: Wilma J. Friedman

- **Growth Factors and Neural Stem Cell Biology** (*Yves Barde* / Vittorio Gallo / Kate Storey)
- **Neurotrophic Factor Signaling** (*Moses Chao* / Francisca Bronfman / Barbara Hempstead / Alicia Hidalgo / Carlos Ibanez / Ruediger Klein)
- **Retrograde Signaling** (*William Mobley* / Christopher Deppmann / Brian Pierchala / Rosalind Segal)
- **Neurotrophic Factors in the Central Nervous System** (*Mark Bothwell* / Wenbiao Gan / Michael Greenberg / Nancy Ip / Liliana Minichiello / Beatriz Rico)
- **Translational Regulation in the Nervous System** (*David Kaplan* / Claudia Bagni / Nahum Sonenberg)
- **Neurotrophic Factors in Disease and Repair** (*Elizabeth Coulson* / Frank Longo / Michelle Monje / Eric Morrow / Michael Sendtner / David Shelton)
- **Neurotrophins and Metabolic Regulation** (*Lloyd Greene* / Katerina Akassoglou / Maribel Rios)
- **Neurotrophins and Development** (*Susan Birren* / Alun Davies / Patrik Ernfors / David Ginty / Julie Lefebvre)
- **Axon Degeneration and Regeneration** (*Mike Fainzilber* / Marc Hammarlund / Joseph Lewcock)



Fluorescent image of mouse oviduct expressing dsRed with a mitochondria import signal. Courtesy of Melissa R. Miller and Liliya Gabelev. Submitted by Melissa R. Miller, Associate Chair, Fertilization & Activation of Development GRS.

Neutron Scattering

NEW!

Effect of Disorder and Disordered Materials
Jun 21-26, 2015
The Chinese University of Hong Kong, Hong Kong, China
Chair: Xun-Li Wang
Vice Chair: Bruce D. Gaulin

- **Keynote Session: Neutrons and Society** (*Xun-Li Wang* / Thom Mason)
- **Superconductivity and Correlated Electrons** (*Jeffrey Lynn* / Bernhard Keimer / Yuan Li / Despina Louca / John Tranquada)
- **Structure of Liquids and Soft Matter** (*Sung-min Choi* / Sung-min Choi / Kenneth Kelton / Toshiji Kenaya)
- **Dynamics of Liquids and Soft Matter** (*Sow-Hsin Chen* / Sow-Hsin Chen / Takeishi Egami / Andreas Meyer / Hajime Tanaka)
- **Frustrated and Exotic Magnets** (*Bruce Gaulin* / Michel Kenzelmann / Kate Ross)
- **Application of Neutron Scattering** (*Cev Noyan* / Kaoru Sato / Janna Maranas / Dong Ma / Anna Paradowska)
- **Jamming and Glass Transition** (*Peter Harrowell* / Peter Harrowell / Alan Soper / Sunil Sinha)
- **New Materials and Developments** (*Paul Attfield* / Paul Attfield / Michael Crawford)
- **Novel Instrumentation** (*Robert Robinson* / Hesheng Chen / Masatoshi Arai)

Nuclear Chemistry

Confluence of Structure and Reactions
May 31 - Jun 5, 2015
Colby-Sawyer College, New London, NH
Chair: Umesh Garg
Vice Chair: Michael P. Carpenter

- **Heaven and Earth: Constraining the EOS of Neutron-Rich Matter** (*Jorge Piekarewicz, Bao-An Li* / Farrooh Fattoyev / Sebestian Guillot / Yivonne Leifels / Seamus Riordan / Andre Schneider)
- **Emergence of Clusters / Nuclear Astrophysics** (*Martin Freer, Yoshiko Kanada-En'Yo, Manoel Couder, Rebecca Surman* / Dean Lee / Tzany Kokalova / Grigory Rogachev / Masaaki Kimura / James deBoer / Iris Dillman / Fernando Montes / Liliana Caballero)
- **Landscape of Spin and Isospin** (*Alexandra Gade, Augusto Macchiavelli* / Paul Fallon / Brian Bucher / Navin Alahari / Ingo Wiedenhoever / Francesco Recchia)
- **Prospectives of Shell Evolution / Challenge and Prospects in Nuclear Density Functional Theory** (*Takaharu Otsuka, Richard Furnstahl, Witold Nazarewicz* / Pieter Doornenbal / Magdalena Gorska / Riccardo Raabe / Yusuke Tsunoda / Scott Bogner / Nobuo Hinohara / Nicolas Schunck / Furong Xu)
- **Giant Resonances in Astro and Neutrino Physics** (*Muhsin Harakeh, Remco Zegers* / Gabriel Martinez Pinedo / Berta Rubio / Hidetoshi Akimune / Natalie Jachowicz / David Radford)
- **Fission, Fusion and Related Phenomena / Complex Decays and the Splicing of Reactions and Structure** (*Mahananda Dasgupta, Sait Umar, Artemis Spyrou* / Cedric Simenel / Andrei Andreyev / Sergio Almaraz-Caledron / Eric Henry / Felix Wamers / Edward Simpson / Zachary Kohley)
- **Coherence and Decoherence in Collectivity** (*Steven Yates, Yang Sun* / Stefan Frauendorf / Paul Garrett / Rudrajyoti Palit / Javid Sheikh / Noritaka Shimizu)
- **Novel Applications of Nuclear Physics / Masses from Traps** (*Angela Bracco, Paddy Regan, Maxime Brodeur, Matthew Redshaw* / Walter Kutschera / David Robertson / Livius Trache / Andy Pearce / Alex Brown / Jason Clark / Ania Kwiatkowski)
- **Search and Discovery / Late-Breaking Topics** (*Michael Carpenter* / Zheng-Tian Lu)

GRS Nuclear Chemistry

Advancing Nuclear Science Through Structure and Reactions
May 30-31, 2015
Chair: Anthony N. Kuchera

Nucleic Acids

DNA and RNA Metabolism: Fundamental Biological Mechanisms with Key Intersections
May 31 - Jun 5, 2015
University of New England, Biddeford, ME
Chairs: Wolf-Dietrich Heyer & Elena Conti
Vice Chairs: Lorena S. Beese & Eric Phizicky

- **Keynote Session: Mechanisms of Homologous Recombination**
  (*Wolf-Dietrich Heyer* / Stephen Kowalczykowski / Roland Kanaar)
- **DNA Replication and Genome Integrity**
  (*Lorena Beese* / Joann Sweasy / Johannes Walter / Kenneth Marians / Ketan Patel / Lorena Beese)
- **RNA/DNA Structure and Dynamics**
  (*Anna Marie Pyle* / Larry Gold / Yamuna Krishnan / Stewart Shuman / Anna Marie Pyle)
- **Chromatin and Transcription**
  (*Peter Fraser* / Song Tan / Genevieve Almouzni / Robert Kingston / Peter Fraser)
- **RNA/DNA in Cellular Defense**
  (*Karl-Peter Hopfner* / Evgeny Nudler / John Moran / Britt Glaunsinger / Karl-Peter Hopfner)
- **Post-Transcriptional Regulation**
  (*Eric Phizicky* / Marina Rodnina / David Bartel / Sean Ryder / Torben Jensen / Eric Phizicky)
- **RNA/DNA Conflicts**
  (*Peter McGlynn* / Frederic Chedin / Andrew Jackson / Peter McGlynn)
- **Non-Coding RNAs**
  (*Elisa Izaurralde* / Gisela Storz / Alexei Aravin / Lingling Chen / Elisa Izaurralde)
- **Keynote Session: All Ends Well at Telomeres**
  (*Elena Conti* / Thomas Cech / Kathleen Collins / Lifeng Xu)

Nucleosides, Nucleotides & Oligonucleotides

Exploring the Interface of Biology, Function, Chemistry and Drug Development
Jun 28 - Jul 3, 2015
Salve Regina University, Newport, RI
Chair: Vern L. Schramm
Vice Chair: Cynthia J. Burrows

- **Keynote Session: Educating the Genome**
  (*Vern Schramm* / Andrew Fire)
- **Nucleic Acid Therapeutics and Diagnostics**
  (*Muthiah Manoharan* / Danzhou Yang / Matthew Disney / Chad Mirkin / David Giljohann)
- **RNA Metabolism**
  (*Robert Reenan* / Chuan He / Squire Booker / Jennifer Heemstra)
- **Purine and Pyrimidine Metabolism and Enzymology**
  (*Karen Anderson* / Lizbeth Hedstrom / William Parker / Bruce Armitage / Jean-Louis Mergny)
- **Nucleotides, Signaling and Probes**
  (*Donald Ronning* / Herman Sintim / Hening Lin / John Kozarich)
- **Nucleic Acid Chemistry and Structure**
  (*Dipankar Sen* / Shankar Balasubramanian / Thomas Carell / Peng Yin / Catherine Drennen)
- **Nucleoside Analog Chemistry and Functions**
  (*Peter Tyler* / Michal Hocek / Gary Evans / Katherine Seley-Radtke)
- **Antiviral and Anticancer Approaches**
  (*Varsha Gandhi* / Travis Warren / Adrian Ray / George Painter / Ronald Raines)
- **Nucleotide Synthesis and Regulation**
  (*Cynthia Burrows* / Brenda Bass / Vahe Bandarian / Joanne Stubbe)

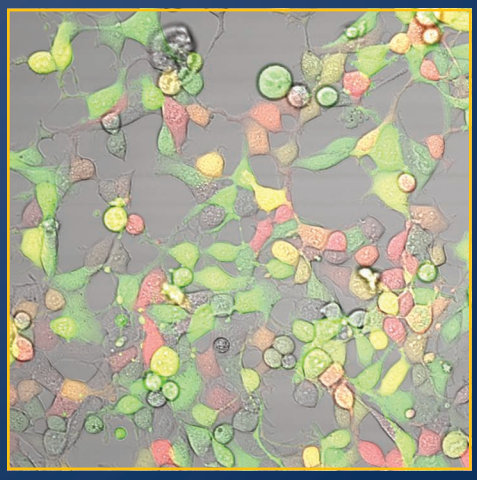
GRS Nucleosides, Nucleotides & Oligonucleotides
Challenges on Research and Career Development
Jun 27-28, 2015
Chair: Rodrigo G. Ducati
Associate Chair: Mindy K. Graham

Organellar Channels & Transporters

NEW!

Breaking Technical Limits: Electrophysiology and Cell Biology of Organellar Channels and Transporters
Jun 14-19, 2015
Bentley University, Waltham, MA
Chairs: Haoxing Xu & Enrico Martinoia
Vice Chair: Ildiko Szabo

- **Ion Transport in Plant Vacuoles**
  (*Cornelia Eisenach* / Eduardo Blumwald / Alexis De Angeli / Ekkehard Neuhaus)
- **Ion/Metabolite Transport in Mitochondria, the Bioenergetic Organelle**
  (*Adam Szewczyk* / Rosario Rizzuto / Yuriy Kirichok)
- **Membrane Transport Proteins Revealed by Organelle Proteomics and Transcriptomics**
  (*Ildiko Szabo* / Daphne Seigneurin-Berny / Vamsi Mootha)
- **Channels/Transporters in Endosomes/Lysosomes**
  (*Michael Pusch* / Robert Edwards / Antony Galione / Juan Marugan)
- **Intracellular Targeting of Ion Channels/Transporters**
  (*Alessandro Vitale* / Inhwan Hwang / Gerhard Thiel)
- **Intracellular Channels and Transporters in Human Disease**
  (*Shmuel Muallem* / Paolo Bernardi / Thomas Jentsch / Rajini Rao / Xiping Cheng)
- **Metabolite Transporters and Chloroplast Channels**
  (*Bruno Gasnier* / Elizabeth Haswell / Andreas Weber)
- **Channels/Transporters of the Endoplasmatic Reticulum and Nucleus**
  (*Barbara Ehrlich* / Youxing Jiang / Kevin Foskett)
- **Keynote Session: New Organellar Channels and Transporters**
  (*Haoxing Xu* / David Clapham)



The induction of IFN-stimulated genes (ISGs) via activation of type I IFN signaling is crucial for the fight against viral invasion. However, how ISGs limit the infection of Chikungunya virus, a re-emerging arbovirus, remain to be deciphered. Viperin, an enigmatic ISG, restricts Chikungunya virus infection and the anti-viral function of Viperin is dependent on its targeting and localization to the ER. HEK 293T cells are transfected with either GFP vector (green) or GFP-tagged N-terminal amphipathic α-helical domain of Viperin (green) before being infected with mCherry-tagged Chikungunya virus (red) and subjected to time-lapse imaging. Submitted by Lisa F.P. Ng, Chair, Infections of the Nervous System GRC.

Organic Reactions & Processes

Innovation in Synthetic Organic Methods and Strategies: Enabling the Processes of Tomorrow
Jul 19-24, 2015
Bates College, Lewiston, ME
Chairs: Jade D. Nelson & Jared L. Piper
Vice Chairs: Neal G. Anderson & Vy Dong

- **New Synthetic Methods**
  (*Kevin Brown* / Paul Knochel / Scott Denmark)
- **Advances in Catalysis**
  (*Mark Biscoe* / Cathleen Crudden / Michael Willis / Guangbin Dong / Neil Garg)
- **Process Development and Structure, Function and Mechanism**
  (*Michael Zacuto, Kami Hull* / Nathan Ide / Kevin Cole / Kendall Houk)
- **New Chemical Technologies**
  (*Jennifer Koviach-Cote* / Emily Balskus / Al Garofalo / Suzanne Blum / Shannon Stahl)
- **Process Development and Catalytic Methods**
  (*Amelie Dion, Jacqueline Milne* / Jonathan Reeves / Richard Fox / Karl Scheidt)
- **Synthetic Methods and Strategies**
  (*Silvia Diez-Gonzalez* / Kenichiro Itami / Cristina Nevado / Daniel Weix / Corey Stephenson)
- **Process Development and Non-Precious Metal Catalysis**
  (*Amy DeBaillie, Shashank Shekhar* / Paul Chirik)
- **Complex Molecular Synthesis / Selected Poster Presentations**
  (*Kenneth Fraunhoffer, Neal Anderson* / Jeremy Wulff / Christopher Vanderwal / Timothy Jamison)
- **Keynote Session: Chemistry: The Central Science**
  (*Vy Dong* / Pascal Dube / Henry Lee)

Organometallic Chemistry

New Challenges and Opportunities for Organometallic Chemistry
Jul 12-17, 2015
Salve Regina University, Newport, RI
Chair: Jerzy Klosin
Vice Chair: Clark R. Landis

- **Energy and Sustainability**
  (*Clark Landis* / Kyoko Nozaki / Douglas Grotjahn)
- **Metals in Organic Synthesis**
  (*Mari Rosen* / Gregory Fu / Michael Krische / Vladimir Gevorgyan)
- **New Reactivity and Transformations**
  (*John Gordon* / Howard Turner / Valentine Ananikov / Alan Goldman)
- **Early Metal and f-Block Chemistry**
  (*Oleg Ozerov* / Lawrence Sita / Michael Mock / Eric Schelter)
- **Polymerization Catalysis**
  (*Mari Rosen* / John Hagadorn / Yann Sarazin / Geoffrey Coates)
- **Transformations with Hydrocarbons**
  (*Glen Alliger* / Timothy Warren / Laurel Schafer / Paul Chirik)
- **Ligand Design and Reactivity**
  (*Morris Bullock* / Shih-Yuan Liu / Katja Heinze / Manuel Alcarazo)
- **Transition Metal Catalysis**
  (*Suzanne Bart* / Joost Reek / Jessica Klinkenberg / Thomas Cundari)
- **Frontiers in Organometallic Chemistry**
  (*Maurice Brookhart* / William Jones / Tobin Marks)

GRS Organometallic Chemistry
Addressing Challenges in Energy Sciences and Materials Development with Organometallic Chemistry
Jul 11-12, 2015
Chair: Alexandra Velian
Associate Chair: Neil C. Tomson

Origins of Solar Systems

The Physics and Chemistry of Building Planets: Recent Advances and Future Prospects
Jun 28 - Jul 3, 2015
Mount Holyoke College, South Hadley, MA
Chair: Fred J. Ciesla
Vice Chair: Edwin A. Bergin

- **The Formation and Early Evolution of Protoplanetary Disks: Processes and Settings**
  (*Lynne Hillenbrand* / Martin Bizzarro / Lee Hartmann)
- **The Chemical Evolution of Protoplanetary Disk Materials**
  (*Geoffrey Blake* / Larry Nittler / Ilaria Pascucci / Ewine Van Dishoeck)

Gordon Research Conferences are different from other scientific conferences because. . .

...I meet the top scientists in my field in a very casual atmosphere, making interactions very meaningful and helpful towards accomplishing my career goals.

(Helena Solo-Gabriele, Chair, 2014 Oceans and Human Health GRC)

- **Pebbles in Protoplanetary Disks**
  (*Andrea Isella* / Cornelius Dullemond / Hal Levison)
- **Planet Migration and Its Collateral Effects**
  (*Rebekah Dawson* / Francesca DeMeo / Richard Nelson / Kevin Walsh)
- **The Nature of Planetesimals and Their Evolution**
  (*Adrian Brearley* / Julie Castillo-Rogez / Thorsten Kleine)
- **Exoplanetary Systems: A Diversity of Outcomes for Planet Formation**
  (*Eliza Kempton* / Jayne Birkby / Eric Ford / Nikku Madhusudhan)
- **Debris Disks and Their Connection to Planet Formation**
  (*Aki Roberge* / Meredith Hughes / Brenda Matthews)
- **The Geophysics and Geochemistry of Planetary Assembly**
  (*Stephen Mojzsis* / Richard Carlson / Tim Elliott / Sarah Stewart)
- **Outer Solar System Record of Planet Formation**
  (*Anita Cochran* / David Minton / Scott Sheppard)

Pancreatic Diseases

Frontiers in Pancreatic Research
Jul 19-24, 2015
Mount Holyoke College, South Hadley, MA
Chair: Michele Solimena
Vice Chair: Diane M. Simeone

- **Autoimmunity in Pancreatic Disorders**
  (*Piero Marchetti* / Decio Eizirik / Suresh Chari)
- **Pancreatic Cell Identity**
  (*Matthias Hebrok* / Lori Sussel / Francesca Spagnoli / Heiko Lickert)
- **Adaption of Beta Cells to Hyperglycemia**
  (*Anke Schulte* / Yuval Dor / Rohit Kulkarni / Domenico Accili)
- **Inflammation in Pancreatic Diseases**
  (*Fred Gorelick* / Minoti Apte / Lisa Coussens / Gregory Beatty)
- **News on Endocrine and Exocrine Secretion**
  (*Susumo Seino* / Herbert Gaisano / Tetsuro Izumi)
- **Genomics and Genetics of Pancreatic Diseases**
  (*Tom Wilkie* / Andrew Biankin / Andrew Hattersley / Teresa Brentnall)
- **Pancreas Development and Pancreatic Diseases**
  (*Christopher Wright* / Steven Leach / Maike Sander / Mike German)
- **Molecular Insight into Pancreatic Cancer**
  (*Dafna Bar-Sagi* / Marco Falasca / Michael Hollingsworth / Andrew Rhim)
- **Novel Approaches for Pancreatic Research**
  (*Howard Crawford* / Anne Grapin-Botton / Maureen Anne Gannon / Sunitha Nagrath)

Parkinson's Disease

NEW!

Emerging Research in the Etiology and Pathogenesis of a Complex Disease
Jun 28 - Jul 3, 2015
Colby-Sawyer College, New London, NH
Chair: David Sulzer
Vice Chair: Andrew Singleton

- **Keynote Session: From Determinants of Selective Neuronal Vulnerability to Possible Neuroprotective Therapy**
  (*Stanley Fahn* / James Surmeier)
- **Neuronal Selectivity and Transmission of Pathology**
  (*Michael Kaplitt* / Aaron Gitler / Jeffrey Kordower / Virginia Lee / Christian Pfil / Dennis Selkoe)
- **Gene Identification: First Steps to Mechanisms**
  (*Matthew Farrer* / Alexis Brice / Mark Cookson / Anthony Cooper)
- **Toxic Dominant Negatives? Gene Functions**
  (*Dennis Dickson* / Jacqueline Burre / Valina Dawson / Robert Edwards / Subhojit Roy / Laura Volpicelli-Daley)
- **Loss of Stress-Induced Protection? Recessive Gene Functions**
  (*Caroline Tanner* / Ted Dawson / Edward Fon / Jie Shen)
- **Disease Mechanisms in Organelle Transport and Turnover**
  (*Karen O'Malley* / Charleen Chu / Erika Holzbaur / Susan Lindquist / Thomas Schwarz / Richard Youle)
- **How Do Aging Processes Fuel Neurodegeneration?**
  (*Luigi Zecca* / Ana Maria Cuervo / Malu Tansey / Zhenyu Yue)
- **Pathological Synaptic Circuitry**
  (*Mahlon DeLong* / Stephanie Cragg / Anatol Kreitzer / Jochen Roeper / Joshua Berke)
- **Compensatory Synaptic Mechanisms**
  (*Un Kang* / Angela Cenci Nilsson / David Eidelberg / Jun Ding)

Particle Physics

NEW!

Prospects of Particle Physics at the 13TeV Large Hadron Collider
Jun 7-12, 2015
The Hong Kong University of Science and Technology, Hong Kong, China
Chair: John Ellis
Vice Chairs: Hitoshi Murayama & Tao Liu

- **QCD and Jets**
  (*Michelangelo Mangano* / Thomas Becher / Matt Schwartz)
- **Top Physics**
  (*Tao Han* / Roberto Tenchini / C.P. Yuan)
- **Neutrino Physics**
  (*Kam-Biu Luk* / Pavel Perez / Yi-Fang Wang)
- **Physics of the SM (or SM-Like) Higgs Boson**
  (*Marcela Carena* / Roberto Contino / Jianming Qian)
- **Dark Matter Physics**
  (*Xiangdong Ji* / Liantao Wang / Daniel Whiteson)
- **Flavor Physics and CP Violation**
  (*Josef Nir* / Tatsuya Nakada / Michael Ramsey-Musolf)
- **Physics of Non-Standard Higgs Bosons**
  (*Christophe Grojean* / Markus Klute / Shufang Su)
- **BSM Physics: Supersymmetry**
  (*Maria Spiropulu* / Joseph Lykken / Andreas Weiler)
- **BSM Physics: Non-Supersymmetry**
  (*Mihoko Nojiri* / Kaustubh Agashe / Erez Etzion)

Phagocytes

The Behaviour and Function of Phagocytes in Health and Disease
May 31 - Jun 5, 2015
Waterville Valley Resort, Waterville Valley, NH
Chair: Paul Kubes
Vice Chair: Dianne Cox

- **Keynote Session: The Signaling Behind Phagocytosis**
  (*John Brumell* / Sergio Grinstein)
- **Formation of Phagosomes**
  (*Sergio Grinstein* / Robin Yates / Mary Dinauer / John Brumell / Kodi Ravichandran)
- **Role of Fc Receptors**
  (*Mary Dinauer* / Marjolein Van Egmond / Jeffrey Ravetch)
- **Monocytes and Macrophage in a Changing Environment**
  (*Dianne Cox* / David Mosser / Gwendalyn Randolph / John Iredale / Catherine Hedrick)
- **Specialized Macrophage**
  (*Gwendalyn Randolph* / Menno van Lookeren Campagn / Ruslan Medzhitov)
- **New Ways of Killing and Dying**
  (*Lee-Ann Allen* / Timo Van Den Berg / William Nauseef / Denisa Wagner / Beth Levine)
- **Leukocyte Dynamic: Relevance to Humans**
  (*Samuel Silverstein* / G. Scott Worthen / Leo Koenderman)
- **Imaging Innate Immunity**
  (*Paul Kubes* / Ronald Germain / Jacco Van Rheenen / Michael Hickey / Mark Miller)
- **Fighting Infections**
  (*Ronald Germain* / Ellen Robey / Bryan Yipp)

GRS **Phagocytes**
Exploring the Spectrum of Phagocyte Function in Inflammation, Infection and Resolution
May 30-31, 2015
Chair: Mallary Greenlee-Wacker
Associate Chair: Laura C. Whitmore

Photochemistry

Photochemistry for the Future: New Approaches, Innovations and Applications
Jul 19-24, 2015
Stonehill College, Easton, MA
Chairs: Malcolm D.E. Forbes & Anna D. Gudmundsdottir
Vice Chairs: Claudia Turro & Daniel E. Falvey

- **Spin Photochemistry**
  (*Dirk Guldi* / Christiane Timmel / Michael Wasielewski)
- **Supramolecular Photochemistry**
  (*Cornelia Bohne* / Peter Ford / Monica Gonzalez / Karen Mulfort / Alexis Ostrowski)
- **Photocatalysis and Synthetic Applications**
  (*Alexander Greer* / Burkhard Koenig / Andrei Kutateladze / Timothy Noel)
- **Phototriggers and Mechanisms**
  (*John Toscano* / Igor Alabugin / Gonzalo Cosa / Maurizio Fagnoni / Martin Schnermann / Pradeep Singh)
- **Spectroscopy and Dynamics**
  (*Jeffrey Rack* / Manabu Abe / Ralf Kaiser / Robert McMahon)
- **Nano/Materials**
  (*Gerald Meyer* / Luis Campos / Bern Kohler / Michael Therien / Emily Weiss / Mikhail Zamkov)
- **Ultrafast Phenomena**
  (*Niels Damrauer* / David Jonas / James McCusker / Jorge Peon / David Lee Philips)
- **Applications in Photobiology and Solar Energy**
  (*Frederick Lewis* / Maria Abrahamsson / Felix Castellano / Jillian Dempsey / Peter Ogilby / Valentine Vullev)
- **Photochemistry for the Future**
  (*Claudia Turro* / Vaidhyanatha Ramamurthy)

GRS **Photochemistry**
Photochemical Applications in Energy Conversion and Sustainability
Jul 18-19, 2015
Chair: John R. Swierk
Associate Chair: Erinn C. Brigham

Photosynthesis

The Dynamics and Regulation of Photosynthesis: From the Origin of Biocatalysis to Innovative Solar Conversion
Jun 28 - Jul 3, 2015
Bentley University, Waltham, MA
Chair: Fabrice Rappaport
Vice Chair: Arthur R. Grossman

- **Photosynthetic Membranes: Structures and Dynamic** (*Toshiharu Shikanai* / Matt Johnson / Ziv Reich)
- **Evolution of Photosynthesis: Functional and Cellular Integration** (*Ziv Reich* / Steven Ball / David Kramer)
- **Light Harvesting: Function and Regulation** (*David Kramer* / Roberto Bassi / Roberta Croce)
- **Light Driven Catalysis of Water Splitting: Oxygen and Hydrogen Evolution** (*Roberto Bassi* / Theodor Agapie / Holger Dau / Rhiannon Evans / Jian-Ren Shen)
- **Structural Aspects of Light Harvesting** (*Holger Dau* / Cheryl Kerfeld / Mei Li)
- **Photosynthesis: Carbon and Nitrogen Metabolism and Rhythm** (*Arthur Grossman* / Arren Bar-Even / Devaki Bhaya / Sabeeha Merchant / Francis-Andre Wollman)
- **Light Driven Catalysis: Charge Separation in Photosynthetic and Man-Made Systems** (*Cheryl Kerfeld* / Anders Hagfeldt / Jennifer Ogilvie)
- **Photosynthetic Electron Transfer and Their Regulation / Late-Breaking Topics** (*Anders Hagfeldt* / Toshiharu Shikanai)
- **Reactive Oxygen Species in Photosynthesis / Late-Breaking Topics** (*Fabrice Rappaport* / Klaus Apel)

GRS **Photosynthesis**
Beyond Steady-State Photosynthesis: Emerging Model Organisms and Technologies
Jun 27-28, 2015
Chair: Alizée Malnoë

Physical Metallurgy

Frontiers in Physical Metallurgy
Jul 19-24, 2015
University of New England, Biddeford, ME
Chairs: Anthony D. Rollett & Roger C. Reed
Vice Chairs: Peter Gumbsch & J.C. Zhao

- **Phase Transformations** (*Diana Farkas* / Lindsay Greer / Michel Rappaz)
- **High Temperature Alloys and Superalloys** (*Dipankar Banerjee* / Akane Suzuki / Christopher Woodward / Rui Yang)
- **Mesoscale** (*Sean Agnew* / Armand Beaudoin / Kaushik Bhattacharya)
- **The Small Scale** (*Nathalie Bozzolo* / Irene Beyerlein / David Srolovitz / Jean-Yves Buffière)
- **Atomistic Resolution** (*Jennifer Carter* / Julie Cairney / Catherine Rae)
- **Imaging in 2D and 3D** (*Tresa Pollock* / Al Hero / Samantha Daly / Philip Withers)
- **Light Metals** (*Ji-Cheng Zhao* / Warren Poole / Timothy Foecke)
- **Data and Data Mining** (*Richard Lesar, Peter Gumbsch* / AMC Lecturer: Gerbrand Ceder / Surya Kalindidi / David McDowell)
- **Advances in Techniques in Physical Metallurgy** (*Peter Collins* / John Lewandowski / Michael Sangid)

Physical Organic Chemistry

Molecule Synthesis, Properties, Theory and Function
Jun 21-26, 2015
Holderness School, Holderness, NH
Chair: Michael M. Haley
Vice Chair: Rik R. Tykwinski

- **Aromaticity and Conjugation - From Theory to Application** (*Lawrence Scott* / Natia Frank / Henrik Ottosson / Amnon Stanger)
- **Polymers in Multiple Dimensions** (*Nancy Goroff* / William Dichtel / Benjamin King / Anne McNeil)
- **Catalysis in the Service of Organic Chemistry** (*Peter Schreiner* / Shawn Collins / Charles Perrin / Steven Wheeler)
- **Supramolecular Interactions and Properties** (*Ognjen Miljanic* / Michael Pittelkow / Rajendra Rathore / Carsten Schmuck)
- **Bio-Inspired Catalysis and Photocatalysis** (*Cornelia Bohne* / Ruth Gschwind / Hermann Wegner / Helma Wennemers)
- **Radicals in Biological Systems** (*Robert Flowers* / Silas Blackstock / Anna Gudmundsdottir / Ryan McCulla / Uta Wille)
- **Radicals and Biradicals - Experimental and Theoretical Considerations** (*Robert McMahon* / Igor Alabugin / Edyta Greer / Takashi Kubo)
- **Cool Tools and Techniques for Organic Chemistry and Chemical Biology** (*Kathleen Kilway* / Eric Anslyn / Jennifer Prescher / Jonathan White)
- **Selected Poster Presentations** (*Rik Tykwinski*)

GRS **Physical Organic Chemistry**
Advances in Understanding - Structure, Function and Reactivity
Jun 20-21, 2015
Chair: Luke F. Gamon
Associate Chair: Conerd Frederickson

Plant Cell Walls

From Genomes to Function
Jul 12-17, 2015
Bentley University, Waltham, MA
Chair: Mary L. Tierney
Vice Chair: Markus Pauly

- **Keynote Session: The Biosynthesis of Structural Polymers in the Plant Cell Wall** (*Mary Tierney* / Geoffrey Fincher / Kenneth Keegstra)
- **Cell Wall Diversity and Evolution** (*Kenneth Keegstra* / David Domozych)
- **Cellulose Biosynthesis** (*Geoffrey Fincher* / Nicholas Carpita / Candace Haigler / Jochen Zimmer)
- **Matrix Glycan Biosynthesis** (*Federica Brandizzi* / Monika Doblin / Debra Mohnen / Breeanna Urbanowicz / Markus Pauly)
- **Cell Walls and Plant Growth** (*Candace Haigler* / Charles Anderson / Daniel Cosgrove / Samuel Hazen)
- **Cell Biology of Wall Biosynthesis** (*Monika Doblin* / Federica Brandizzi / Georgia Drakakaki / Lacey Samuels)
- **Non-Polysaccharide Components of the Cell Wall** (*Markus Pauly* / Clint Chapple / Jocelyn Rose / Allan Showalter)
- **Cell Walls, Signaling and Environmental Interactions** (*Georgia Drakakaki* / Herman Hofte)
- **Bioenergy Model Systems** (*Samuel Hazen* / Henrik Scheller)

GRS **Plant Cell Walls**
Plant Cell Wall Research: From Structure to Sustainability
Jul 11-12, 2015
Chair: Suryatapa Jha
Associate Chair: Miranda J. Meents

Plant Metabolic Engineering

Harnessing Plant Metabolism for the Bio-Based Economy
Jul 19-24, 2015
Waterville Valley Resort, Waterville Valley, NH
Chairs: Richard A. Dixon & Sarah E. O'Connor
Vice Chairs: Andrew D. Hanson & Cathie Martin

- **Keynote Session: Plant Metabolism and Cell Walls – Diversity and Exploitation** (*Andrew Hanson* / Anne Osbourne / Maureen McCann)
- **Specialized Metabolism** (*Eleanore Wurtzel* / Elizabeth Sattely / Reuben Peters / Birgit Draeger)
- **Metabolic Regulation and Signal Transduction** (*Nicole Clay* / Joseph Jez / John Shanklin / Stephen Huber)
- **Metabolism – Spatial and Dynamic** (*Eva Colloakova* / Jonathan Page / Kent Chapman / Doug Allen)
- **Engineering Cell Walls** (*Udaya Kalluri* / Shawn Mansfield / Debra Mohnen / Dominique Loque)
- **Breakthrough Technologies: Gene Expression and Editing** (*Vladimir Shulaev* / Kazuki Saito / George Lomonossoff / Jian-Kang Zhu)
- **Breakthrough Technologies: Chromosome Manipulation and Mutation** (*Gregory Copenhaver* / James Birchler / Luca Comai / Brande Wulff)
- **Translational Case Studies: Bottlenecks from Basic to Applied** (*Cathie Martin* / Peggy Lemaux / Oliver Yu / Katrina Cornish)
- **Translational Case Studies: From Lab to Commercial Products in the Field** (*Kenneth Davenport* / Marc-Andre D'Aoust / Stephen Temple)

GRS **Plant Metabolic Engineering**
Priming Plant Metabolism for the New Bioeconomy
Jul 18-19, 2015
Chair: Joshua R. Widhalm
Associate Chair: Andrew P. Klein

Polyamines

Polyamines and Their Metabolic Regulation in Biology and Disease
Jun 14-19, 2015
Waterville Valley Resort, Waterville Valley, NH
Chairs: Otto Phanstiel & Keiko Kashiwagi
Vice Chairs: Susan K. Gilmour & Alex R. Khomutov

- **Polyamine Metabolism and Human Disease** (*Robert Casero* / Steven Lipkin / Jan Pieter Abrahams / Keith Wilson)
- **Polyamines and Cell Signaling** (*Anthony Michael* / Manas Chattopadhyay / Ece Karatan / Paul Planet / Shinsuke Fujiwara)
- **Polyamines, Amino Acids and Translation** (*Myung-Hee Park* / Leonard Johnson / Sandro Valentini / Thomas Dever)
- **Polyamine Transport** (*Heather Wallace* / Laurence von Kalm / Colin Nichols / Igor Pottosin / Mark Bleackley)
- **Therapeutic Development** (*Patrick Woster* / Lyn-Marie Birkholtz / Margaret Phillips / T.J. Thomas)
- **Polyamines, Membranes and Cell Damage** (*Eugene Gerner* / Alfred Blume / Kazuei Igarashi / Jean-Luc Ravanat / Stephan Sigrist)

- **Polyamines in Cancer Development and Therapy**
  (*Keiko Kashiwagi* / Deborah Altomare / Christian Bailly / Tania Silva)
- **Polyamine Metabolism in Human Health and Cancers**
  (*Enzo Agostinelli* / Chinthalapally Rao / John Cleveland / David Feith / Jeff Gross)
- **Keynote Session: 40 Years of Medicinal Chemistry Research in Polyamines**
  (*Alex Khomutov* / Raymond Bergeron)

Polyamines
Role of Polyamines in Biology and Disease
Jun 13-14, 2015
Chair: Steven L. Holshouser
Associate Chair: Pinar Obakan

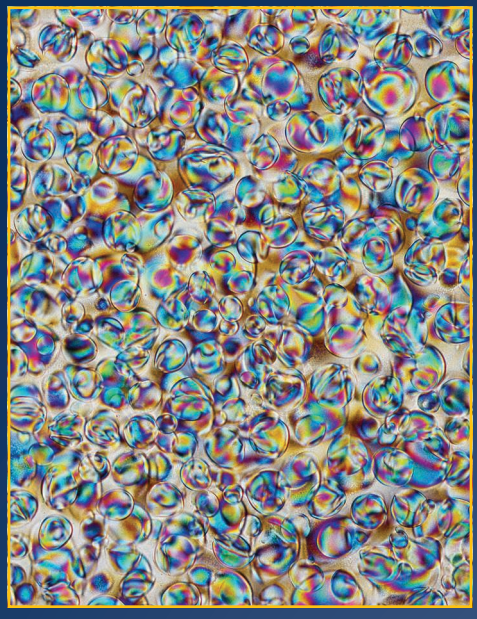
Polymers
Inventive Synthesis for Innovative Technologies
Jun 14-19, 2015
Mount Holyoke College, South Hadley, MA
Chair: Marc A. Hillmyer
Vice Chair: Matthew L. Becker

- **Device Applications**
  (*Yang Qin*, *Bryan Boudouris* / Lynn Loo / Joseph DeSimone)
- **Aqueous Systems**
  (*Eva Harth*, *Agostino Pietrangelo* / Heather Maynard / Nathan Gianneschi / Brent Sumerlin)
- **Biomaterials**
  (*Valerie Ashby*, *April Kloxin* / Kim Chaffin / Melissa Grunlan)
- **Olefin Polymerization**
  (*Garret Miyake*, *Lisa Baugh* / Lawrence Sita / Jerzy Klosin / Kyoko Nozaki)
- **New Synthesis Concepts**
  (*Emily Penzer*, *Luis Campos* / William Dichtel / Craig Hawker)
- **Porous and Responsive Functional Materials**
  (*Lei Fang*, *Andrew Boydston* / Malancha Gupta / Neil McKeown / Rint Sijbesma)
- **Functional Thin Films**
  (*Padma Gopalan*, *Christophe Sinturel* / Paula Hammond / Grant Willson)
- **Precision Structures**
  (*Nathaniel Lynd*, *Donghui Zhang* / Nicole Sampson / Jean Francois Lutz)
- **Functional Advanced Materials**
  (*Yan Xia*, *Kathryn Beers* / Robert H. Grubbs / Bryan Coughlin)

Polymers
Progress Towards Tomorrow's Materials
Jun 13-14, 2015
Chair: Sara A. Turner
Associate Chair: Joel M. Sarapas

Posttranslational Modification Networks
Gaining a Proteomic Understanding of Cellular Regulation Mechanisms in Animals and Plants
Jul 5-10, 2015
The Hong Kong University of Science and Technology, Hong Kong, China
Chairs: Zhiyong Wang & Alma L. Burlingame
Vice Chairs: Heribert Hirt & Lan Huang

- **Posttranslational Modifications in Cellular Regulation**
  (*Heribert Hirt* / Natalie Ahn / Peter Quail)
- **Phosphorylation and Signaling**
  (*Natalie Ahn* / Martin Larsen / Pedro Cutillas / Michael Sussman / Wolfram Weckwerth)
- **Protein Ubiquitination**
  (*Michael Sussman* / Xingwang Deng / Richard Vierstra / Joshua Baughman / Joshua Gendron)
- **Novel PTMs**
  (*Jyoti Choudhary* / Yingming Zhao / Xiaoyong Yang / Yiji Xia / Hong Zhang)
- **PTM Crosstalk and Networks**
  (*Chentao Lin* / Anne-Claude Gingras / Steven Huber / Namrata Udeshi)
- **Cell Signaling Networks**
  (*Ning Li* / Jun Qin / Chentao Lin / Waltraud Schulze / Yu-Ju Chen / Ning Li)
- **Evolution of PTM Networks**
  (*Lan Huang* / Pedro Beltrao / Steven Briggs)
- **PTMs in Disease and Immunity**
  (*Anne-Claude Gingras* / Feng Shao / Ileana Cristea / Frank Menke / Jyoti Choudhary)
- **Chromatin Modifications and Epigenetics**
  (*Ileana Cristea* / Benjamin Garcia / Jian-Kang Zhu / Steven Jacobsen)



Microscope image of a liquid crystalline polyamide and poly(ethylene glycol) composite under crossed polarizers. High performance polymers with anisotropic properties have a variety of applications from flexible electronics to membranes and fibers. Courtesy of Sara A. Turner and Stephanie R. Liffland (University of North Carolina at Chapel Hill) and T.J. Dingemans (TU Delft). Submitted by Sara A. Turner, Chair, Polymers GRS.

Preclinical Form & Formulation for Drug Discovery
Understanding Design and Delivery of Active Pharmaceuticals Including Biomolecules and Parenteral Drugs
Jun 7-12, 2015
Waterville Valley Resort, Waterville Valley, NH
Chairs: Robert Wenslow & Michael Pikal
Vice Chairs: Narayan Variankaval & Eric Munson

- **Keynote Session: Preclinical Form and Formulation for Drug Discovery**
  (*Michael Pikal* / Jennifer Dressman / Bruno Hancock)
- **Strategies for Overcoming Bioavailability Issues: Lipidic, Co-Crystals, Nanomilling**
  (*Gordon Amidon* / David Vodak / Shobha Bhattachar)
- **Amorphous Formulations: Delivery Routes and Theoretical Prediction of Stability (Including Computational Methods)**
  (*Patrick Connelly* / Kostantin Borisenko / Majed Fawaz)
- **Analytical Tools to Probe Form and Formulations**
  (*Karthik Nagapudi* / Robert Schurko / Simon Billinge / Chris Hartshorn)
- **Characterization of Lyophilization: Small Molecule and Biologics**
  (*Steven Nail* / Marcus Cicerone / Elizabeth Topp)
- **Parenteral Drug Development Technologies**
  (*Susan Herschenson* / Kim Woodrow / Tejal Desai / Robert Lee)
- **Biologics Formulation Development**
  (*Daan Crommelin* / Wim Jiskoot / David Volkin)
- **Tools to Predict Bioperformance: Assessing Developability**
  (*Riccardo Panicucci* / Keith Horspool)
- **Computation Solid State Chemistry: Simulation and Predictive Tools**
  (*Jamshed Anwar* / Lennart Linfors / Marcus Neumann / Dirk Zahn)

Preclinical Form & Formulation for Drug Discovery
Addressing Challenges in Drug Development Including Small Molecules and Biomolecules
Jun 6-7, 2015
Chair: Mehak Mehta
Associate Chair: Rui Fang

Proteins
From Fundamentals to Function
Jun 14-19, 2015
Holderness School, Holderness, NH
Chairs: Daniel P. Raleigh & Jane Clarke
Vice Chairs: Catherine A. Royer & Vijay S. Pande

- **Keynote Session: Technological Advances in Protein Science**
  (*Jane Clarke* / Xiaowei Zhuang / James Wells)
- **Recent Advances in Protein Science from Theory to Application**
  (*Vijay Pande* / Charles Brookes / Marius Clore / Bertrand Garcia-Morena / Lutz Jermutus / Amy Keating)
- **Evolution**
  (*Matthew Cordes* / Douglas Fowler / Eugene Shakhnovich / Matsuura Tomoaki)
- **Folding**
  (*C. Robert Matthews* / Bruce Bowler / Elizabeth Meiering / Emanuele Paci / Benjamin Schuler / Danny Hsu)
- **Design**
  (*Susan Marqusee* / William Degrado / Stephen Demarest)
- **Reversible and Irreversible Association**
  (*Josh Wand* / Danny Hatters / Birthe Kragelund / Jacqui Matthews / Rohit Pappu / Philipp Selenko)
- **Protein Interactions and Assembly**
  (*Matthew Chapman* / Colin Kleanthous / Yamuna Krishnan / Tom Muir)
- **Proteins in Action**
  (*Mark Stahl* / Vic Arcus / Karen Fleming / Wayne Fairbrother / Tanya Baker)
- **Keynote Session: Protein Folding and Proteostasis**
  (*Catherine Royer* / Jeffery Kelly / Judith Frydman)

Quantum Control of Light & Matter
Pushing Frontiers in Coherent Quantum Control and Quantum Technologies
Aug 2-7, 2015
Mount Holyoke College, South Hadley, MA
Chairs: Thomas G. Baumert & Lorenza Viola
Vice Chairs: Tobias Brixner & Tommaso Calarco

- **Quantum Interfering Pathways: From Proven Concepts to New Avenues / Young Investigator Presentations**
  (*Thomas Baumert* / Paul Brumer)
- **Quantum Chemistry and Biology, Multidimensional Spectroscopy**
  (*Marcus Motzkus* / Shaul Mukamel / Alan Aspuru-Guzik / Greg Engel / Birgitta Whaley)
- **Attosecond Control in Molecules and Plasmonic Systems**
  (*Nirit Dudovich* / Thomas Fennel / Hans Jakob Woerner)
- **Quantum Control for Quantum Information and Complex Systems**
  (*Raymond Laflamme* / Dietrich Leibfried / Markus Greiner / Mazyar Mirrahimi / Matthias Weidemueller)
- **Control of Open Quantum Systems and Thermodynamics**
  (*Ronnie Kosloff* / Francesco Ticozzi / Adolfo Del Campo)
- **Quantum Photonics**
  (*Hakan Tureci* / Robert Levis / Kjeld Eikema / Keith Nelson / Mohammad Hafazi)

- **Molecular Strong Field Control**
  (*Thomas Weinacht* / Eric Wells / Ilya Averbukh)
- **Optimal Quantum Control**
  (*Herschel Rabitz* / Matthias Wollenhaupt / Christiane Koch / Simone Montangero / Steffen Glaser)
- **Quantum Metrology and Sensing**
  (*Carlton Caves* / Aephraim Steinberg / Paola Cappellaro)

Radiation & Climate

Towards Understanding the Interactions Between Radiation, Clouds, Aerosol, Precipitation and Climate
Jul 26-31, 2015
Bates College, Lewiston, ME
Chairs: Bernhard Mayer & Eugene E. Clothiaux
Vice Chairs: David Turner & Dargan Frierson

- **Keynote Session: Key Outstanding Issues in Radiation and Climate**
  (*Stephen Klein* / Ulrike Lohmann / Bjorn Stevens)
- **Closing the Surface Energy Budget**
  (*Graeme Stephens* / Seiji Kato / Kevin Trenberth / Maike Ahlgrimm)
- **Remote Sensing of Warm Rain, Snow, and Cloud Properties**
  (*Matthew Lebsock* / Tristan L'Ecuyer / Gail Skofronick-Jackson)
- **Cloud Feedbacks, Rapid Adjustments, and Microphysical Parameterizations**
  (*Susan Van Den Heever* / Jerry Harrington / Hugh Morrison / Mark Zelinka)
- **Impact of Ice Crystal Microphysics on Ice Cloud Radiative Properties**
  (*Ping Yang* / Thomas Leisner / Bastiaan van Diedenhoven)
- **New Cloud Property Remote Sensing Techniques**
  (*Alexander Marshak* / Christine Chiu / Howard Barker / Tobias Zinner)
- **Cloud-Scale Processes**
  (*Graham Feingold* / Marat Khairoutdinov / Ruby Leung)
- **Frontiers in Modeling and Observational Studies of Aerosol Effective Radiative Forcing**
  (*Ralph Kahn* / Philip Stier / David Diner / Stephen Ghan)
- **The Future of Climate and Radiation / Selected Poster Presentations**
  (*Geeta Persad*)

Radiation & Climate
Understanding Climate Forcing, Feedback, and Response via Interactions Between Radiation, Clouds, Aerosol and Precipitation
Jul 25-26, 2015
Chair: Geeta G. Persad
Associate Chair: Matthew Igel

Red Cells

Emerging Concepts in Heath and Disease
Jun 28 - Jul 3, 2015
Holderness School, Holderness, NH
Chair: Luanne L. Peters
Vice Chair: Mitchell J. Weiss

- **Developmental Biology of Erythropoiesis**
  (*James Palis* / Mervin Yoder / James Palis)
- **Epigenetics and Chromatin Modification**
  (*Patrick Gallagher* / Emery Bresnick / Douglas Higgs / Laurie Steiner / Jennifer Trowbridge / Patrick Gallagher)
- **Transcriptional Control of Erythropoiesis**
  (*Andrew Perkins* / James Bieker / Gerd Blobel / Stuart Orkin / Andrew Perkins)
- **Erythropoiesis and Red Cell Production**
  (*Mohandas Narla* / Xuili An / Lionel Blanc / Sandrina Kinet / Harvey Lodish / Don Wojchowski / John Crispino)
- **Erythropoiesis: Terminal Erythroid Maturation**
  (*Theodosia Kalfa* / Saghi Ghaffari / Merov Socolovsky / Theodosia Kalfa)
- **Iron, Heme and the Red Cell**
  (*Nancy Andrews* / Janis Abkowitz / Jodie Babitt / Caroline Enns / Barry Paw / Clara Camaschella / Nancy Andrews)
- **Membrane Protein Structure and Function**
  (*Velia Fowler* / Philip Low / Jon Morow / Velia Fowler)
- **Red Cell Disorders**
  (*David Bodine* / Jeffrey Lipton / Vijay Sankaran / Len Zon / Stefano Rivella / David Bodine)
- **Red Cell Disorders: Infections**
  (*Cheryl Lobo* / Chetan Chitnis / Niraj Tolia / Carla Cerami / Cheryl Lobo)

Red Cells
Establishing a Research Career in Red Cell Biology
Jun 27-28, 2015
Chair: Vikram R. Paralkar
Associate Chair: Bryony J. Graham



Participants of the 2014 Membranes: Materials & Processes GRC at Colby-Sawyer College in New London, NH venture out for a hike during the afternoon free time.

Soft Condensed Matter Physics

Self-Assembly and Active Matter
Aug 9-14, 2015
Colby-Sawyer College, New London, NH
Chairs: Seth Fraden & Jean-Francois Joanny
Vice Chairs: Zvonimir Dogic & Michael Brenner

- **Soft Materials**
  (*Michael Rubinstein* / Masao Doi / Zhigang Suo)
- **Biomineralization**
  (*Elisabeth Charlaix* / Jeffrey Guasto / Lia Addadi / Peter Fratzl)
- **Outreach to Biology**
  (*Dave Weitz* / Jennifer Lippincott-Schwartz / Stanislas Leibler)
- **Self Assembly**
  (*Annie Colin* / Randy Kamien / Steve Granick / Michael Hagan)
- **Soft Matter: Active and Driven**
  (*Wilson Poon* / Sriram Ramaswamy / Yael Roichman)
- **Biological Active Matter**
  (*Cristina Marchetti* / Daniel Needleman / Kineret Keren / Lisa Manning)
- **Active Matter and Industry**
  (*Aparna Baskaran* / Michael Shelley / Patrick Doyle)
- **DNA Assembly**
  (*Robijn Bruinsma* / Daan Frenkel / Oleg Gang / Hendrik Dietz)
- **Biohydrodynamics**
  (*Paul Chaikin* / Raymond Goldstein)

Soft Condensed Matter Physics
Collective Phenomena in Soft Matter
Aug 8-9, 2015
Chair: Jing Yan
Associate Chair: Carl P. Goodrich

Spin Dynamics in Nanostructures

Nanoscale Spintronics with Magnons, Phonons, and Photons
Jul 26-31, 2015
The Hong Kong University of Science and Technology, Hong Kong, China
Chair: Gerrit E. W. Bauer
Vice Chair: Stuart Parkin

- **Spintronic Devices**
  (*Xiufeng Han*, *Yiran Chen* / Hideo Ohno / Alina Deac / Shinji Yuasa)
- **New Spintronic Materials**
  (*Claudia Felser* / Kin Fai Mak / Bart Van Wees / Yoshishige Suzuki / Charles Gould)
- **Spin Mechanics and Magnetometry**
  (*Sadamichi Maekawa* / Olivier Klein / Vincent Jacques / Hiroyuki Chudo)
- **Spin Caloritronics**
  (*Eiji Saitoh* / Sebastian Goennenwein / Jiang Xiao / Joseph Barker / Aakash Pushp)
- **Quantum Spintronics**
  (*Burkard Hillebrands* / Yasunobu Nakamura / Yaroslav Tserkovnyak / Rembertus Duine)
- **Fast Spintronics**
  (*Theo Rasing* / Roy Chantrell / Herrmann Duerr / Bert Koopmans / Samir Lounis)
- **Spin-Orbit Torques**
  (*Allan Macdonald* / Robert Buhrman / Roland Wiesendanger)
- **Magnetic Insulator Spintronics**
  (*Chris Hammel* / Arne Brataas / Felix Casanova / Bryan Hickey / Christian Back)
- **Strong Coupling**
  (*Xiang Rong Wang* / Hans Huebl / Yunshan Cao / Hong Tang)

Spin Dynamics in Nanostructures
Interplay of Spin, Charge and Lattice Dynamics
Jul 25-26, 2015
Chair: Yunshan Y. Cao
Associate Chair: Davide D. Bossini

Staphylococcal Diseases

Fundamental Knowledge Drives Translational Advances
Jul 12-17, 2015
Renaissance Tuscany Il Ciocco Resort, Lucca (Barga), Italy
Chairs: Simon Foster & Jos Van Strijp
Vice Chairs: Eric P. Skaar & Tammy L. Kielian

- **Keynote Session: What Lessons Can We Learn from Other Bacteria?**
  (*Emma Johnson*, *Andras Spaan* / Nassos Typas / Jan-Willem Veening)
- **Offensive Action: Staphylococcal Toxins**
  (*Francois Vandenesch* / Victor Torres / Michael Otto / Thomas Henry)
- **Is There Anything To Be Learned from Animal Models?**
  (*Arnold Bayer* / Steve Renshaw / Christopher Weidenmaier)
- **Defensive Action: Interaction with the Immune System**
  (*Suzan Rooijakkers* / Wolfgang Weninger / Rachel McLoughlin / Jean Pieters)
- **The Cell Cycle: Growth and Division**
  (*Angelika Grundling* / Mariana Pinho / Daniel Lopez)
- **Translational Aspects of Staphylococcal Diseases**
  (*Lloyd Miller* / Issac Chiu / Gabriel Nunez / Jay Kolls)
- **Imaging Pathogenesis**
  (*Dominique Missiakas* / James McNamara / Gootizen van Dam)
- **Antibiotics – The End of the Golden Era?**
  (*Steven Projan* / Kim Lewis / Dominique Monnet / Eszter Nagy)
- **Late-Breaking Topics / Selected Poster Presentations**
  (*Eric Skaar*, *Tammy Kielian*)

Staphylococcal Diseases
New Frontiers - Interact and Update
Jul 11-12, 2015
Chair: Andras N. Spaan
Associate Chair: Emma Johnson

Without the Gordon Research Conferences. . .

...there would hardly be a place for organized but unconstrained exchange of ideas and concepts among top scientists in the field.

(Robert Kostecki, Chair, 2014 Batteries GRC)

Stress Proteins in Growth, Development & Disease

From Protein Folding to Misfolding Disorders: The Importance of Maintaining Proteostasis over a Lifetime
Jul 5-10, 2015
Renaissance Tuscany Il Ciocco Resort, Lucca (Barga), Italy
Chair: Ursula Jakob
Vice Chair: Kevin Morano

- **Keynote Session: Protein Quality Control and Aging** (*Ursula Jakob, Kevin Morano* / Ulrich Hartl / Cynthia Kenyon)
- **Folding, Misfolding and Aggregation** (*Ulrich Hartl* / Judith Frydman / Elke Deuerling / Ellen Nollen / Sheena Radford)
- **Spatial Quality Control** (*Manajit Hayer-Hartl* / James Bardwell / Bernd Bukau / Thomas Nystrom)
- **Unfolded Protein Response Programs** (*Cynthia Kenyon* / Cole Haynes / Roberto Sitia / Luke Wiseman / Linda Hendershot)
- **Stress Proteins and Other Protective Mechanisms** (*Michel Toledano* / Johannes Buchner / Elizabeth Craig / James Shorter)
- **Changes in Protein Homeostasis During Development, Aging and Disease** (*Harm Kampinga* / Keith Blackwell / Ana-Maria Cuervo / Andrew Dillin / Vadim Gladyshev / Rick Morimoto)
- **Transcriptional and Translational Control of Stress Protein Expression** (*Gabriela Santoro* / Brian Freeman / Lea Sistonen / Jonathan Weismann)
- **Protein Triage and Degradation** (*Dennis Thiele* / Anne Bertolotti / Richard Gardner / Randolph Hampton / Thomas Langer)
- **Pharmacological Modulation of Proteostasis as a Therapeutic Approach** (*Jason Gestwicki* / Jeffrey Brodsky / Gabriela Chiosis / Jeffery Kelly)

String Theory & Cosmology

NEW!

New Ideas Meet New Experimental Data
May 31 - Jun 5, 2015
The Hong Kong University of Science and Technology, Hong Kong, China
Chair: Gary Shiu
Vice Chair: Ulf Danielsson

- **The Scientific Base for String Cosmology** (*Eva Silverstein* / Juan Maldacena / Slava Mukhanov)
- **Early Universe Theories: Top-Down Approaches** (*Savdeep Sethi* / Liam McAllister / Eva Silverstein / Thomas Van Riet)
- **Early Universe Theories: Bottom-Up Approaches** (*Koenraad Schalm* / Enrico Pajer / Misao Sasaki)
- **String Theoretical Models of Cosmology** (*Juan Maldacena* / Eric Bergshoeff / Joseph Conlon / Savdeep Sethi)
- **Late-Breaking Topics: New Results in Observational Cosmology** (*Gary Shiu*)
- **Frameworks and Models** (*Slava Mukhanov* / Daniel Baumann / Ben Wandelt / Lam Hui)
- **Large Scale Structure (LSS) and Other Probes** (*Ben Wandelt* / Neal Dalal / Uros Seljak)
- **Dark Matter and Dark Energy** (*Thomas Van Riet* / Sonia Paban / John Ellis / Hitoshi Murayama)
- **Testing String Theory Through Observational Cosmology** (*Liam McAllister* / Richard Easther / Koenraad Schalm)

Synthetic Biology

Advancing Biosystems Design
Jun 28 - Jul 3, 2015
Sunday River Resort, Newry, ME
Chair: Sven Panke
Vice Chair: Farren Isaacs

- **Genome Engineering** (*Farren Isaacs* / Anke Becker / Andrew Ellington / David Liu)
- **Mammalian Cell Engineering** (*June Medford* / Peng Yin)
- **Environmental Engineering** (*Vitor Martins Dos Santos* / Tobias Erb / June Medford)
- **Enabling Technologies** (*Anke Becker* / Mustafa Khammash)
- **Computational and Evolutionary Design** (*Andrew Ellington* / Douglas Densmore)
- **Systems Engineering for Industrial Applications** (*Tobias Erb* / Mattheos Koffas / Jay Keasling)
- **Systems Engineering and Chassis** (*Roy Bar-Ziv* / Vitor Martins Dos Santos / Eriko Takano)
- **Orthogonal Systems** (*Vincent Noireaux* / Floyd Romesberg)
- **Cell Free Biology** (*Sven Panke* / Roy Bar-Ziv / Takuya Ueda / Vincent Noireaux)

Three Dimensional Electron Microscopy

Breaking Barriers to Go Beyond Structure: Describing Functional States and Biological Context
Jun 21-26, 2015
Colby-Sawyer College, New London, NH
Chair: Eva Nogales
Vice Chair: Yifan Cheng

- **Biological Cutting Edge Methodologies Across Scales** (*Eva Nogales* / David Baker / Xiaowei Zhuang)
- **Image Analysis and Validation Strategies for Heterogeneous Samples** (*Helen Saibil* / Nikolaus Grigorieff / John Rubinstein)
- **Structure in the Cellular Context** (*Wolfgang Baumeister* / Elizabeth Villa / Daniela Nicastro)
- **Interpretation and Validation of Low-Medium Resolution Cryo-EM Structures** (*Hong-Wei Wang* / Gabriel Lander / Carolyn Moores)
- **Selected Poster Presentations: Recent Advances in Cryo-EM Technical Development** (*Edward Egelman*)
- **Strategies for Atomic Modeling of High-Resolution Cryo-EM Structures** (*Steve Harrison* / Paul Adams / Axel Brunger / Frank Dimaio / Simon Jennings / Alan Brown)
- **Improving Sample Preparation** (*Holger Stark* / Bridget Carragher / Robert Glaeser / Lori Passmore)
- **Development and Use of Correlative Methodologies** (*Grant Jensen* / Kay Gruenewald)
- **Selected Poster Presentations: Recent Advances in the Application of Cryo-EM Methodology** (*Yifan Cheng*)

Tissue Repair & Regeneration

Exploring Innovations in Tissue Repair and Regeneration: From Bench to Therapies
Jun 7-12, 2015
Colby-Sawyer College, New London, NH
Chair: Enrique Amaya
Vice Chair: Boris Hinz

- **Effects of Aging on Tissue Repair / Regeneration** (*Enrique Amaya* / Amy Wagers / Pura Munoz-Canoves / Bradley Olwin)
- **Organ Regeneration** (*Ralf Paus* / Stuart Forbes / Neil Chi / Clare Blackburn / Jeremy Duffield / Rick Livesey)
- **Nuclear Reprogramming and Dedifferentiation** (*Boris Hinz* / Penney Gilbert / Giacomo Cavalli / Kostas Kostarelos)
- **Model Organisms of Regeneration** (*Kerstin Bartscherer* / Peter Reddien / Michael Levin / Michalis Averof / James Godwin / Max Yun)
- **The Roles of Reactive Oxygen Species in Tissue Repair and Regeneration** (*T. Harshani Peiris* / Andrew Chisholm / Will Wood / Asma Nusrat)
- **Stem Cell Therapies for Repair / Regeneration** (*Michael Galko* / Peter Coffey / Thomas Reh / Graziella Pellegrini / Dennis Clegg / Steven Goldman)
- **Stem Cell Niche** (*Luisa Dipietro* / Valentina Greco / George Cotsarelis / Michael Brand)
- **Skin Repair / Cancer** (*Sabine Eming* / Marjana Tomic-Canic / Sabine Werner / Matthew Hardman / Malcolm Maden / Paul Martin)
- **lncRNAs and Progenitor Cells** (*Kimberly Mace* / Paola Arlotta / Daniel Lim / Edward Morrisey)

GRS **Tissue Repair & Regeneration**
Exploring Innovations in Tissue Repair and Regeneration: From Bench to Therapies
Jun 6-7, 2015
Chair: Tanuja H. Peiris

Topological & Correlated Matter

NEW!

Advances in Topological Phases of Matter in Crystalline Solids and Cold Atom Systems
Jun 28 - Jul 3, 2015
The Hong Kong University of Science and Technology, Hong Kong, China
Chairs: Tai-Kai Ng & N. Phuan Ong
Vice Chairs: Yong-Baek Kim & Yayu Wang

- **Keynote Session: Topological Phases of Matter** (*Patrick Lee* / Leon Balents)
- **The Majorana Bound State** (*Yong-Baek Kim* / Leo Kouwenhoven / Kam Law / Ali Yazdani)
- **Ultracold Atom Systems** (*Tin Lun Ho* / Victor Galitski / Qi Zhou / Tilman Esslinger)
- **Proximity Effects and Josephson Junctions on Topological States** (*Yayu Wang* / Zahid Hasan / Nadya Mason / Amir Yacoby / Rui-Rui Du)
- **Theoretical Advances** (*Naoto Nagaosa* / Andrei Bernevig / Liang Fu / Shuichi Murukami)
- **Topological Insulators and Topological Crystalline Insulators** (*Yong-Baek Kim* / Yong Chen / Vidya Madhavan / Laurens Molenkamp)
- **Quantum Anomalous Hall Effect** (*Tin Lun Ho* / Joseph Checkelsky / Kang Wang / Qikun Xue)
- **Physics of Dirac and Weyl Semimetals** (*Naoto Nagaosa* / Robert Cava / Yulin Chen / Xi Dai / Andrew Potter)
- **Future Directions of Research on Topological Matter / Late-Breaking Topics** (*Patrick Lee* / Yoshinori Tokura)

Tuberculosis Drug Discovery & Development

Challenges, Advances and Future Prospects in the Fight Against Tuberculosis
Jul 12-17, 2015
Melia Golf Vichy Catalan Business and Convention Center, Girona, Spain
Chairs: Sabine Ehrt & David Barros
Vice Chairs: Courtney C. Aldrich & Tanya Parish

- **Keynote Session: TB Treatment - The Way Ahead** (*David Barros* / Carl Nathan)
- **Physiology, Metabolism and Pathogenesis** (*Sabine Ehrt* / Michael Niederweis / Olivier Neyrolles / Bree Aldrich / Eric Rubin)
- **New Targets and Target Identification Approaches** (*David Sherman* / Valerie Mizrahi / Babak Javid / Gurdyal Besra)
- **Lessons Learned from Other Microbes** (*Clifton Barry* / David Pompliano / Katherine Young / Steven Kern)
- **Targeting *Mycobacterium tuberculosis* in the Host** (*Eric Rubin* / Philana Lin / Veronique Dartois / Anne Lenaerts)
- **"Omics" in TB Drug Discovery** (*Tanya Parish* / D. Branch Moody / Kyu Rhee / Robert Moritz)
- **New Strategies in TB Drug Discovery** (*David Olsen* / Richard Lee / Alfonso Mendoza / David Russell)
- **Hit to Lead Development** (*Courtney Aldrich* / Sophie Lagrange / Dickon Alley / Debrorah Hung / Philip Hipskind)
- **From Leads to Clinical Development** (*Debra Hanna* / Lawrence Geiter / Anna Upton / Wendy Marriner / Neil Schluger)

GRS **Tuberculosis Drug Discovery & Development**
New Strategies to Fight an Old Enemy
Jul 11-12, 2015
Chair: Nadine Ruecker
Associate Chair: Fraser Cunningham

Undergraduate Biology Education Research

NEW!

Investigating and Implementing Evidence-Based Reform
Jul 12-17, 2015
Bates College, Lewiston, ME
Chair: Gordon E. Uno
Vice Chair: Susan L. Elrod

- **Keynote Session: Connecting the Life Sciences to the Future of Education** (*Linnea Fletcher* / James Collins)
- **Contemporary Drivers of Biology, Biology Education, and Biology Education Reform** (*Anne Houtman* / Jay Labov / Charles Henderson / LaTanya Sharpe / Lee Zia)
- **The Impact of Biology Education Research on Shaping Current Educational Practices and Future Research** (*Mary Pat Wenderoth* / Erin Dolan / Michelle Smith / Tammy Long)
- **Maintaining and Broadening Participation in Biology** (*Tia McNair* / Jose Herrera / Muriel Poston)
- **Role of Societies, Funders, and Publishers in Driving and Implementing BER** (*Jacki Reeves-Pepin* / Cynthia Bauerle / Amy Chang / Susan Winslow)
- **Assessing Learning** (*April Maskiewicz* / Ross Nehm / Kathy Williams / Michelle Withers / David Hanauer)
- **Quantitative Science Concepts and Skills and Science Process Skills in Biology** (*John Jungck* / Chris Beck / Sam Donovan / Lou Gross)
- **Effective Faculty Development in Biology Education** (*Brad Williamson* / Gili Ad-Marbach / Deborah Allen / Diane Ebert-May / Cindy Lenhart)
- **Policy Implications for Biology Education Research and Reform** (*Stacey Kiser* / Shirley Malcom)

Viruses & Cells

From Molecular Mechanism to Pathogenesis and Prevention
Jun 21-26, 2015
Melia Golf Vichy Catalan Business and Convention Center, Girona, Spain
Chair: Sean P. Whelan
Vice Chair: Blossom Damania

- **Entry Mechanisms** (*Erica Sapphire* / Thijn Brummelkamp / Tom Kirchhausen / Robert Lamb / Jason Mercer)
- **Replication Mechanisms** (*Bert Semler* / Raul Andino / Ralf Bartenschlager / Stephen Cusack / Paula Traktman)
- **Transcription and Translation** (*Bryan Cullen* / Ian Goodfellow / Bernard Roizman / Benjamin Tenoever)
- **Host Components in Replication** (*Nihal Altan-Bonnet* / James Alwine / Wendy Barclay / Ileana Cristea / Clodagh O'Shea)
- **Host Response to Infection** (*Barbara Sherry* / Michael Diamond / Michael Malim / John Schoggins)
- **Viral Evasion Mechanisms** (*Marco Vignuzzi* / Michaela Gack / Jae Jung)
- **Pathogenesis** (*Julie Pfeiffer* / Adolfo Garcia-Sastre / Stephanie Karst / David Knipe)
- **Viral Oncogenesis** (*Blossom Damania* / Denise Galloway / Nancy Raab-Traub / Thomas Schulz / Linda Van Dyk)
- **Vaccines and Antivirals** (*Sean Whelan* / Heinz Feldmann / Karla Kirkegaard / John A. Young / Dong Yu)

Visualization in Science & Education

Grand Challenges in the Use of Visualization in Science and Education
Aug 2-7, 2015
Bates College, Lewiston, ME
Chairs: Bob Kolvoord & Katharina Scheiter
Vice Chairs: Mike Stieff & Ann F. Batiza

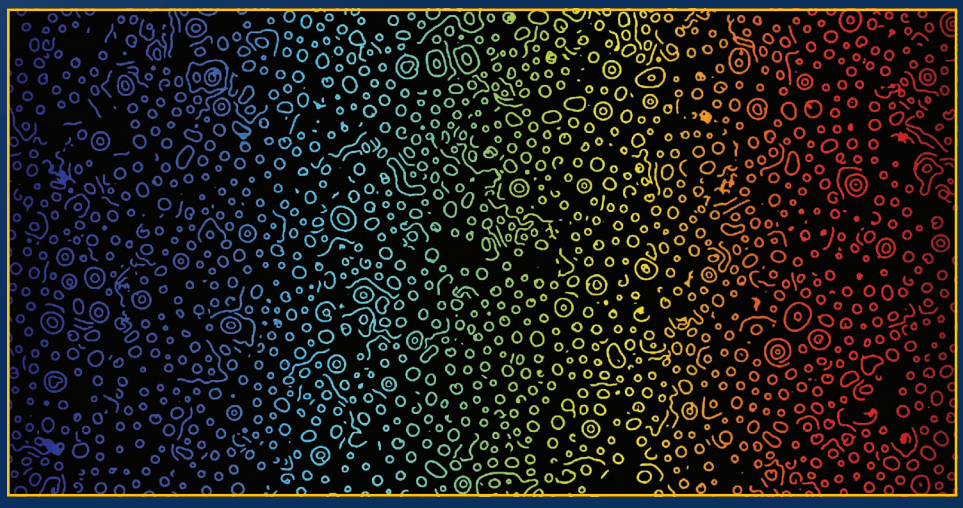
- **Challenges in Visualizing Big Data** (*Robert Hanson* / Nils Gehlenborg / Cesar Hidalgo)
- **Integrating Visualization in Education** (*Vetria Byrd* / Jennifer Frazier / David Klahr / Diana Sinton)
- **What Do Student-Constructed Visualizations Reveal About Misconceptions?** (*Mike Stieff* / Wouter van Joolingen / Michelle Wilkerson-Jerde)
- **Challenging Phenomena to Visualize** (*Brian Martin* / Jaymie Matthews / Hanchuan Peng / Chia Shen)
- **Assessing the Impact of Scientific Visualization** (*Martin Storksdieck* / Melanie Cooper / Margaret Evans)
- **Best Practices in Communicating Scientific Visualizations** (*Katharina Scheiter* / Ryan Wyatt / Jen Christiansen)
- **Applying Artistic Principles in Scientific Visualization / Late-Breaking Topics** (*Ann Batiza* / Addie Manis)
- **Latest Advances in Visualization** (*Sara Fabrikant* / Jason Leigh / Leilah Lyons)
- **The Impact of Technological Change on Visualization in Science and Education** (*Bob Kolvoord* / Brian Martin)

X-Ray Science

X-Ray Science Utilizing the Dramatic Increases in Peak and Average Brightness from Current/Planned Next Generation Accelerator Based X-Ray Sources
Jul 26-31, 2015
Stonehill College, Easton, MA
Chair: Chi-Chang Kao
Vice Chair: Hyunjung Kim

- **Non-Linear X-Ray Effects** (*Nina Rohringer* / Hitoki Yoneda / Filippo Bencievenga)
- **Strongly Correlated Electrons** (*Thomas Devereaux* / Nicholas Brookes / J.C. Seamus Davis / Andrea Cavalleri)
- **Inelastic X-Ray Scattering** (*Francesco Sette* / Alfred Baron / David Reis)
- **Biological Structure** (*Janos Hajdu* / Axel Brunger / Hideo Ago / David Agard)
- **Coherent Diffraction Imaging** (*Ian Robinson* / Daniel Shapiro / Pierre Thibault)
- **Development in Sources** (*Harald Reichert* / Efim Gluskin / Alexander Temnykh / Pantaleo Raimondi)
- **Advances in Electron Scattering/Microscopy** (*Robert Sinclair* / Yimei Zhu / Bradley Siwick)
- **Materials Under Extreme Conditions** (*Wendy Mao* / Justin Wark / Arianna Gleason / Sakura Pascarelli)
- **Keynote Session: Future Opportunities with Accelerator Based Light Sources** (*Helmut Dosch* / Gabriel Aeppli)

GRS **X-Ray Science**
X-Ray Science from Current and Planned Next Generation Accelerator Based X-Ray Sources
Jul 25-26, 2015
Chair: Ken R. Ferguson



Micron-sized silica Janus colloids with one hemisphere coated with metal swim like bacteria in an AC electric field, and link together to form meandering "snakes", which bite their own ends to form rotating rings. Courtesy of Jie Zhang, Jing Yan, and Steve Granick. Submitted by Jing Yan, Chair, Soft Condensed Matter Physics GRS.

By **Richard Dasheiff**

A career's twisting road

I wanted to be a physicist. When I was in elementary school, I corrected a teacher about the orbits of the planets. In high school, I told a teacher that we could directly image single atoms; she didn't believe me even after I showed her the journal article I saw it in. My parents were of two minds: proud of my scientific aptitude but, being of modest means and Jewish descent, hopeful their only son would become a "real" doctor someday, the medical kind. ¶ I enrolled in the University of Maryland (UMD), College Park, in 1969 and obtained two bachelor's degrees, in physics and astronomy, in 3 years. Michael A'Hearn, my astronomy adviser, told me he was content to add a tiny bit of knowledge to the world—prophetic words from the future team leader of Deep Impact, the space probe that blasted a hole in comet Tempel 1 35 years later. I decided that I, too, wanted to make a small contribution, in experimental physics.

In 1970, the Selective Service System held a lottery to determine the order in which men born in 1951—my birth year—would be called up for service in the Vietnam War. I won. My birthdate came up first. My physics adviser got a low number, too; he went abroad to medical school. With pressure and support from my father, I entered medical school at UMD. It kept me out of Vietnam. There were five other physics majors in my class.

Research was still my goal, so I worked in a neurobiology lab. After graduating, I went to Duke University Hospital for a combined residency and postdoc in neurology. For the next 30 years I was an academic neurologist, seeing patients, teaching, and doing basic research—the academic triad. I kept up with developments in physics (to which I yearned to return) by reading, especially *Science*. I learned that my physics adviser had gone into medical practice.

Retrospectively, I can see how good those decades were for medical research and researchers. Good ideas and valid protocols were rewarded with grant money, despite the high level of competition. Many hard-core scientists who had entered medicine to avoid the draft did important work.

I garnered an international reputation in my specialty, but my father never considered me a real doctor like the practitioners he saw in the cardiology and internal medicine clinics he frequented. Yet, before he passed away with a stroke in 2008, he made it clear he thought I'd had a good career. I agreed. Three years later, I retired.

My retirement didn't last long. My wife said I should get a job—she said I had too much energy—so I started filling in for absent neurologists in the field of stroke management. For 3 years, I have worked at hospitals in small towns across the United States, learning a new approach to medicine.



"Now I'm a real doctor, the kind my father so wanted me to be."

Medicine, it is said, is an art. The academic medicine I had practiced, though, is science. Everything you do for and to your patients is based on the best evidence, calculated for maximum efficacy, and reviewed and criticized by yourself and colleagues. It took me 3 years to stop looking at every problem as a possible publication, to stop answering every question with a PowerPoint presentation.

Now that I'm a real doctor, the kind my father so wanted me to be, I am practicing the art of medicine, although I still occasionally ask whether patients know the square root of two during mental-status exams; once I even found a patient who knew Ohm's law. My bedside manner has sharpened. I detect gratitude from my patients—a new type of satisfaction. It's an experience my father knew as a patient and wanted me to have on the other end. It took me 40 years, but here I am.

I haven't tried being a physicist yet, but careers are long, and only at the end can they be fully measured. ■

Richard Dasheiff is a neurologist and scientist who lives with his wife and two children in Dallas, Texas. For more on life and careers, visit www.sciencecareers.org. Send your story to SciCareerEditor@aaas.org.

ILLUSTRATION: ROBERT NEUBECKER

Downloaded from www.sciencemag.org on February 21, 2015

Published by AAAS